

Preface

Many regional and international environmental problems are a challenge to environmental analytical chemistry, and the understanding of relevant mechanisms is a key for the solution of environmental problems. To understand the interactions taking place in the environment, especially the intermediate interactions, analytical chemistry undoubtedly plays a central role and needs to be developed, although some progress has been made in recent years. Past experience and the present status reveal evidence that the development of analytical chemistry facilitates the understanding of environmental processes.

It is quite clear that further progress in this broad area of research will require an integrated understanding and continued communication across several disciplines. To facilitate this exchange and supported by the National Science Foundation of China (NSFC), Japan Society for Analytical Chemistry (JSAC) and Japan Analytical Instruments Manufacturers Association (JAIMA), 2002 China–Japan, and the China–Japan–Korea Symposia on Environmental Analytical Chemistry were successfully held in Beijing (2004) and Tokyo (2005). These symposia were very fruitful for all countries involved. Many new and exciting results were presented and some international cooperation research was carried out after the symposia. We brought together 33 papers from the symposium and another 5 relevant papers from outside in this special issue of Talanta.

Acknowledgements

We are grateful to the authors who submitted manuscripts for this special issue, and to the many reviewers to maintain the high quality of the papers. The Organizing Committee of the 2005 China–Japan–Korea Symposium on Environmental Analytical Chemistry wishes to thank the grant supports of NSFC, JSAC, JAIMA and Shimadzu Beijing Office, which made this symposium and special issue a success.

Guest Editor

Jin-Ming Lin^{a,b,*}

^a *Department of Chemistry, Tsinghua University,
Beijing 100084, China*

^b *Chinese Academy of Sciences, Research Center for
Eco-Environmental Sciences, No. 18, Shuangqing Road,
Haidian, Beijing 100085, China*

Guest Editor

Tsuneaki Maeda^c

^c *National Institute of Advanced Industrial Sciences and
Technology, Japan*

* Corresponding author. Tel.: +86 10 62841953;
fax: +86 10 62841953.

E-mail address: jmlin@mail.rcees.ac.cn

Available online 30 June 2006

Preparation and application of monolithic columns with narrow immobilized pH gradients

Guijie Zhu^{a,b}, Chun Yang^a, Lihua Zhang^{a,*}, Zhen Liang^a, Weibing Zhang^a, Yukui Zhang^{a,*}

^a Department of Biotechnology, Dalian Institute of Chemical Physics, Chinese Academy of Sciences, Dalian 116023, China

^b Graduate School of Chinese Academy of Sciences, Beijing 100039, China

Received 28 October 2005; received in revised form 5 December 2005; accepted 10 December 2005

Available online 19 January 2006

Abstract

Monolith with immobilized pH gradient (M-IPG) is a novel separation matrix for amphoteric substances, such as peptides and proteins. To improve the properties of the newly designed column, efforts were made to optimize the preparation procedure, including the concentrations of the monomers, glycidyl methacrylate (GMA) and ethylene glycol dimethacrylate (EDMA), as well as the kinds of porogens, which led to a monolith with improved permeability, uniformity and continuity. In addition, different diamines, including ethylenediamine, 1,3-diaminopropane, 1,4-diaminobutane and 1,5-diaminopentane, were subjected to aminate the polymer, and the last two exhibited excellent reactivity with epoxy on the polymer surface, which could obviously make the immobilization of pH gradient facilitated. Under the optimal conditions, a simple method to prepare M-IPG column with narrow pH gradient was developed with commercial carrier ampholytes (CAs) solution. Such columns were applied into the analysis of proteins and peptides, and showed the improved resolution compared to the traditional one with a wide pH distribution.

© 2005 Elsevier B.V. All rights reserved.

Keywords: Monolithic immobilized pH gradient; Column preparation; Narrow pH gradient

1. Introduction

Isoelectric focusing (IEF) is a high-resolution technique for the separation of amphoteric biomolecules. IEF with immobilized pH gradients (IPGs) is especially important in proteomics, where it serves as the first dimension in two-dimensional polyacrylamide gel electrophoresis (2D-PAGE) and contributes to the actual power in proteomic study. Capillary isoelectric focusing (CIEF), since firstly reported by Hjerten and Zhu [1], has become a widely used method for the separation of amphoteric compounds, in which carrier ampholytes (CAs) are used to establish a pH gradient and keep a sustaining current during focusing. Although helpful in focusing, carrier ampholytes always increase the current and then Joule heat during focusing. Furthermore, they could reduce UV detection sensitivity because of their high absorbance at low wavelengths. Therefore, it is attractive to perform both CIEF and preparative IEF without mobile CAs [2–7]. Therefore, immobilized pH gradient

(M-IPG) based on monolithic materials might be a good solution [8].

In 2D-PAGE, IPGs, with wide pH gradients can give an overview of the sample, and those with the narrow ones are used for more specialized and detailed research with improved resolution [9]. However, the latter gels are always expensive.

In this paper, a simple way to prepare narrow M-IPG columns from commercial CAs with wide pH range was developed. To achieve a commonly viable fabrication method, the preparation procedure was optimized, and such columns were successfully applied to the analysis of proteins and peptides, which showed higher resolution compared to those with a wide distribution of pH value. Just like IPGs this column could be used for more specialized and detailed research with improved resolution.

2. Materials and methods

2.1. Reagents and instrumentation

Glutaraldehyde (50% in water, Beijing Chemical Reagent Company, China), 1,4-butanediol (Fluka, Switzerland), cyclohexanol (Fluka, Switzerland), dodecanol (Fluka, Switzerland),

* Corresponding authors. Tel.: +86 411 84379720; fax: +86 411 84379560.
E-mail address: ykzhang@dicp.ac.cn (L. Zhang).

n-propanol (The Third Chemical Plant of Dandong, Liaoning, China), ampholine (pH 3.5–10.0, SIGAMA, Sweden), azobisisobutyronitrile (AIBN, The Fourth Shanghai Regent Plant, Shanghai, China), 3-methacryloxypropyltrimethoxysilane (γ -MAPS, 98%, Acros Organics, USA), GMA (Fluka, Switzerland), EDMA (Fluka, Switzerland), dimethyl sulfoxide (DMSO, Shenyang Chemical Reagent Plant, Shenyang, China) and sodium cyanoborohydride (CNBH_3Na , 95%, Acros Organics, USA) were used directly without further treatment. Other reagents were of analytical grade. Hemoglobin (Sino-American Biotechnology Co.), Carbonic anhydrase (MP, BIOMEDICALS, Germany) and peptide extract solutions (offered by Dalian Jintian Bioengineering Co. Ltd., Dalian, China) were filtered through 0.45 μm membranes before use. Capillaries (75 μm i.d., 375 μm o.d.) were purchased from Ruifeng Chromatographic Device Co. Ltd (Yongnian, Hebei, China).

Electrophoresis was performed on a set of TriSepTM-2000GV from Unimicro Technology (Shanghai, China) with a Data Module UV-vis detector and a CEC Control Module high-voltage power supply. A Workstation Echrom98 of Elite Co. (Dalian, China) was used for data acquisition and analysis.

2.2. Preparation of monolithic columns with narrow IPG

The pretreatment of capillaries was executed as previously described [8]. Briefly, a capillary was successively washed with HCl (1.0 mol/L), water, NaOH (1.0 mol/L), water, and ethanol for 20 min respectively, and then purged with nitrogen for 3 h. A solution of γ -MAPS (50% v/v in ethanol) was injected into the capillary and kept at room temperature for 24 h. Unreacted γ -MAPS was washed off using ethanol. A solution consisting of GMA, EDMA, AIBN, DMSO and 1,4-butanediol was degassed supersonically and injected into the pretreated capillary. With both ends sealed, the capillary was put in a water bath at 60 °C for 12 h. The monolith in the capillary was then washed with ethanol for 2 h, followed by water for another 1 h.

Simultaneously with the reaction in capillary, the same mixture was also polymerized in a vial to obtain sufficient amount of monolithic polymer for determining the pore volume and pore size using a mercury intrusion porosimetry (9310, MIC, USA), and also for the test of the polymer rigidity.

All the solutions used hereinafter were prepared in the mixed solvent of water and ethanol (1:1 v/v). The monolithic column was successively subjected to the diamine (1,4-diaminobutane or 1,5-diaminopentane, 1 mol/L), and then glutaraldehyde (5%). It should be pointed that it was very important to clean the monolith after each step of the reactions.

A monolithic column with narrow IPG was prepared according to the set-up shown in Fig. 1. At first, two capillaries were coated with polyacrylamide, and filled with 4% ampholine. A monolithic column that had been subjected to the diamine and the glutaraldehyde filled with electrolyte was then connected with the coated capillaries by Teflon tubes. Attention must be paid to avoid bubbles formed in the capillaries. After a focusing process, the two capillaries without polymers were removed. The monolithic column was kept at room temperature for 4 h and then reduced by NaCNBH_3 overnight.

2.3. Preparation of columns with wide IPG

The monolithic column prepared by the method mentioned in Section 2.2 was successively subjected to the following solutions: diamine (1,4-diaminobutane or 1,5-diaminopentane, 1 mol/L), glutaraldehyde (5%) and ampholine (4%) and then kept at room temperature for 4 h. After that a solution of NaCNBH_3 (25 mmol/L) was pumped through the column overnight. Finally a segment (~ 2 mm) of the outer polyimide covering on the capillary was removed to make a detection window.

2.4. CIEF in monolithic columns with IPG

Sample solutions were injected into the column from the anodic end to the detection window. Focusing was performed for several minutes till the current declined to about 10% of its original value. Consequently the focused zones in the column were pumped through the detection window by pressure.

3. Results and discussion

3.1. Preparation of columns with narrow IPG

3.1.1. Preparation method

According to the preparation protocol of monolithic columns with narrow IPG as shown in Fig. 1, the CAs were distributed along the three capillaries when the focusing was finished. Different pH ranges of the CAs were located in three capillaries, respectively. The CAs in the monolithic column established a middle pH part of the whole gradient. In principle, the pH gradient kept in the monolithic column could be in any range from pH 3 to 10 based on the lengths of the empty capillaries. The width of a narrow M-IPG should be proportion to the lengths of the involved capillaries. Additionally it was limited by the value of the available voltage as well as the properties of CAs involved. When the capillary at anodic end was 21 cm, and that at cathodic end was 19 cm, providing the gradient of ampholine in capillaries was even and linear, the left 30 cm length narrow IPG in our experiments was of a pH gradient from about 5.1 to 8.1.

3.1.2. Effects of the concentration and ratio of monomers

Due to the various viscosities, it should be pointed out that it is better to take liquid reagents according to their weights rather than volumes, which could improve the reproducibility of column preparation.

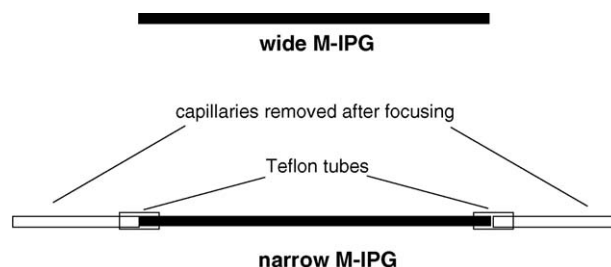


Fig. 1. Schematic diagram for the preparation of a narrow M-IPG.

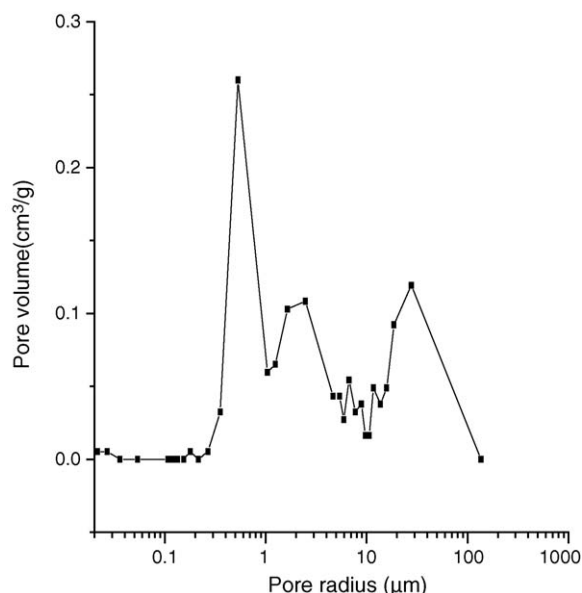


Fig. 2. Incremental pore volume per gram vs. pore radius.

Differing from the monolithic materials in CEC [11,12] and HPLC [13], the concentration of monomers in M-IPG columns should be as low as possible to exclusively exhibit the focusing capability. Another benefit of diluted monomers is the excellent permeability of the polymers. In addition, the low concentration could also weaken the non-specific interactions between samples and the separation media, and decline the risk of precipitation during focusing. After the systematic study, we found the total amount of monomers (GMA + EDMA) should be as low as 8–9% (weight ratio). Since GMA played a role of anchor to immobilize CAs, its amount in the solution greatly affected the property of M-IPG columns. Too little GMA was not able to immobilize enough CAs for focusing. On the contrary, too much GMA would result in exhausting amino groups of ampholine. In addition, the ratio of GMA and EDMA contributed much to the mechanical strength of the polymer. By comparison, the ratio of GMA/EDMA (w/w) should be in the range from 1/8 to 1/5. In our experiments, by adjusting the concentration and ratio of monomers, monolithic polymer with larger pore size and narrower pore size distribution could be obtained, as shown in Fig. 2.

3.1.3. Selection of the porogens

It is well known that the composition of porogens has great effects on the properties, especially the pore distribution of a monolithic polymer. Because M-IPG columns employ macroporous materials, it is convenient to utilize microscopic patterns to assess and compare the continuity and uniformity of polymers with different porogen systems. As shown in Table 1, *n*-propanol and cyclohexanol were not suitable to produce a monolithic column. Obviously the broken gel was not a good precursor for M-IPG because of the poor permeability and uniformity. Thus dodecanol was excluded from the preferential porogen. Although the uniformity of M-IPG was quite good,

Table 1
Effect of porogens on the microscopic patterns of the polymers

Porogens	Microscopic patterns of the polymers
Cyclohexanol	Good permeability and poor uniformity
<i>n</i> -Propanol	Good permeability and poor uniformity
Dodecanol	Broken gel
DMSO	Poor permeability and good uniformity
1,4-Butanediol	Poor permeability and very good uniformity
1,4-Butanediol/ <i>n</i> -propanol (1.04)	Good permeability but poor uniformity
1,4-Butanediol/cyclohexanol (0.94)	Little poor permeability but good uniformity
1,4-Butanediol/dodecanol (0.95)	Poor permeability and uniformity
1,4-Butanediol/DMSO (0.95)	Good permeability and uniformity

the permeability was rather poor when DMSO was selected as the porogen. As shown in Table 1, as *n*-propanol, dodecanol or cyclohexanol is selected in the binary porogen systems, the column indicated poor permeability, poor homogeneous appearance or both. In addition, we could see that 1,4-butanediol was very useful to improve the uniformity of the column but resulted in poor strength. Therefore, a binary porogen system with 1,4-butanediol and DMSO with a ratio from 1:1 to 2:1 was selected, which contributed greatly to the good permeability, uniformity and strength of the polymers, respectively.

3.1.4. Selection of the diamines

Generally, it takes hours, always overnight, for ammonia to react with epoxy groups due to the hydrophobic nature of the polymer surface. Diamines possess hydrocarbon chains that endue them with hydrophobic properties. Accordingly, they are ideal amination reagents. In our experiments, four diamines, ethylenediamine, 1,3-diaminopropane, 1,4-diaminobutane and 1,5-diaminopentane, were investigated to compare with ammonia, which was used in our previous work [8], about their reactivity with glutaraldehyde in solutions and epoxy groups on the polymer surface.

When treated with glutaraldehyde solution, the color of the aminated polymer changed to yellow, which could be used to judge the reaction. As shown in Table 2, the reactions of ammonia and ethylenediamine took place at lower speeds, and 1,3-diaminopropane showed the poorest reactivity. 1,4-diaminobutane and 1,5-diaminopentane reacted with glutaraldehyde rapidly. As a result, the substitution of ammonia by 1,4-diaminobutane or 1,5-diaminopentane could obviously reduce the reaction time in preparing M-IPG columns.

Table 2
Amination time of (di)amines on monolith

(Di) amines	Amination time
Ammonia	Overnight (>12 h)
Ethylenediamine	Overnight; no obvious color change
1,3-Diaminopropane	Over night; no change
1,4-Diaminobutane	1 h
1,5-Diaminopentane	1 h

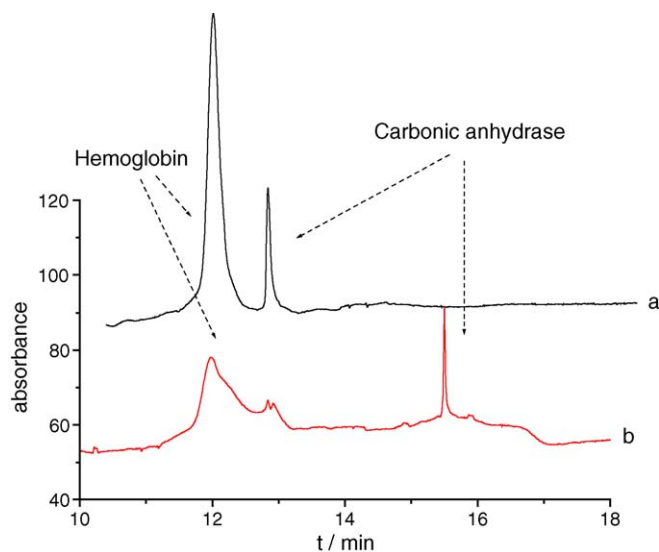


Fig. 3. Separation of hemoglobin and carbonic anhydrase with M-IPG. (a) Wide gradient column: 36 cm (26 cm effective length), catholyte: NaOH (20 mmol/L), anolyte: H_3PO_4 (20 mmol/L). (b) Narrow gradient column: 36 cm (29 cm effective length), catholyte: arginine (25 mmol/L), anolyte: glutamic acid (12.5 mmol/L); voltage: 12.3 kV, detection wavelength: 254 nm.

3.2. Properties of monolithic columns with narrow IPGs

Narrow IPGs, also known as zoom-in gels, are very important tools in 2D PAGE [10]. They can be used to further separate proteins overlapped within a gel spot. A narrow pH gradient provides a better resolving power than a wider one when they are of similar lengths. In the focusing of M-IPG, interested or suspicious peaks from wide gradient can be selected for further separation and study by a narrow one.

In our experiments, the properties of monolithic columns with narrow M-IPGs were studied by comparison with those with wide ones. Fig. 3 showed the separation of hemoglobin and carbonic anhydrase on such two kinds of columns with the same length under the same voltage value. From this figure, it could be seen that higher resolution could be obtained in narrow M-IPGs. In narrow M-IPGs the distance between two proteins was extended and the hemoglobin was further separated into two peaks instead of one peak in wide M-IPG. In Fig. 3b both the first and second peaks are hemoglobin. Because of containing multiple components the hemoglobin sample was separated in two peaks instead of one peak in wide M-IPG.

In addition, by manual sampling and propelling the focused zone, the resolution reproducibility of hemoglobin and carbonic anhydrase was better than 7% (R.S.D.) in three consecutive runs. All these results demonstrated that monolithic columns with narrow IPGs might be of great potential for the detailed study of interested proteins in proteome.

In addition, peptides extracted from soybean were also separated by monolithic columns with IPGs. Fig. 4a showed the results obtained on columns with wide distribution of pH gradient. The high peak associated with some small ones between 7 and 8 min might be basic components in the sample and could not stay in the segment of the capillary from the anodic end to the detection window after focusing, which could be described as

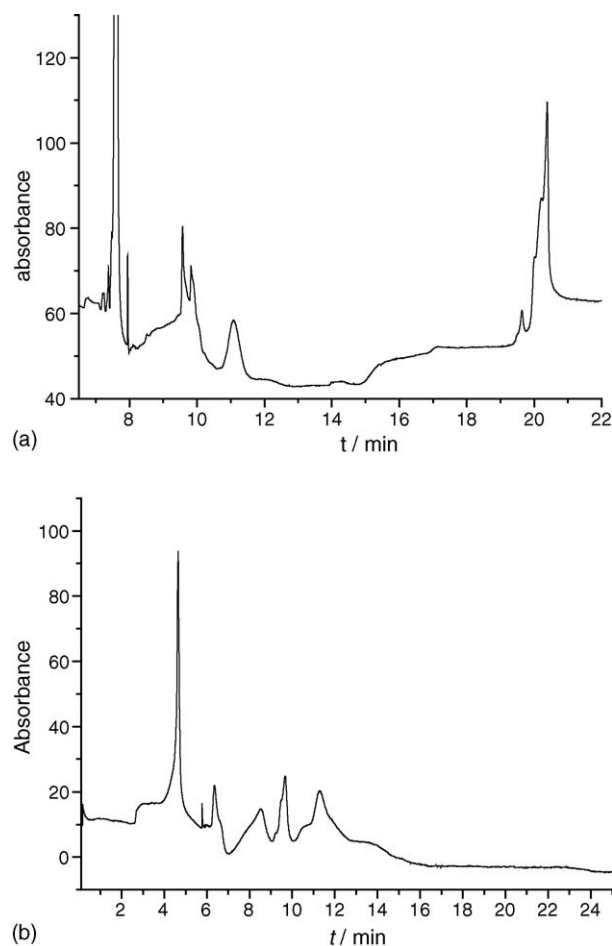


Fig. 4. Separation of peptides extracted from soybean with M-IPG. Column: 30 cm (22 cm effective length). (a) Catholyte: NaOH (20 mmol/L), anolyte: H_3PO_4 (20 mmol/L). (b) Catholyte: ammonia (pH 8), anolyte: acetic acid (pH 4); voltage: 10 kV; detection wavelength: 254 nm.

a process of pH gradient driving electrophoresis (PGDE) [14]. The peaks from 9 to 22 min were focused zones mechanically mobilized by a syringe after the voltage was turned off. Fig. 4b showed the separation results obtained on columns with narrow IPG. The peak from 4 to 5 min, as those from 7 to 8 min in Fig. 4a, were the basic species. The decreased peak number of the most basic components in (b) compared with those in (a) were the signals of transfer from a wide gradient to a narrow one.

The peaks from 19 to 21 min in Fig. 4a were acidic peptides, which were held in the M-IPG when H_3PO_4 (20 mmol/L) and NaOH (20 mmol/L) were used. When diluted acid (acetic acid pH 4) and base (ammonia pH 8) took the place of strong electrolytes, the acidic components went out of the column from the anode end during focusing. Thus the peaks of the acidic components disappeared in Fig. 4b. When strong electrolytes were used in focusing, the extremely basic or acidic analytes were confined to very narrow areas in the cathodic and anodic ends, and on the contrary, weak electrolytes always resulted in sample loss in the column. Thus when subjected to focusing in a narrow M-IPG, very acidic and basic species should be excluded from the column.

In the case of amphoteric compounds with p/s located within a narrow M-IPG, IEF often indicated improved resolution. The peaks from 9 to 12 min in Fig. 4a obtained by the wide gradient were further separated by the narrow M-IPG (6–12 min) in Fig. 4b. Obviously with the narrow pH gradients, more peaks appeared and higher resolution could be obtained.

4. Concluding remarks

The effects of monomers, porogens and diamines on the preparation of monolithic columns with immobilized pH gradient were studied systematically. Under the optimized conditions, a new method to prepare columns with narrow IPG was developed, and applied into the analysis of peptides and proteins, which showed higher resolution compared to the traditional one with a wide distribution of pH gradient. All the results demonstrated the potential of such columns into the selective and more detailed research of proteome.

Acknowledgements

This work was supported by the State Key Fundamental Research Program (2001CB51020 and 2004CB520804, The

Ministry of Science and Technology, People's Republic of China), Chinese Academy of Sciences and National Natural Science Foundation (20405104 and 20435020).

References

- [1] S. Hjerten, M.D. Zhu, J. Chromatogr. 346 (1985) 265–270.
- [2] T. Huang, X.-Z. Wu, J. Pawliszyn, Anal. Chem. 72 (2000) 4758–4761.
- [3] C.H. Lochmuller, S.J. Breiner, J. Chromatogr. 480 (1989) 293–300.
- [4] O. Sova, J. Chromatogr. 320 (1985) 15–22.
- [5] H. Rilbe, J. Chromatogr. 159 (1978) 193–205.
- [6] D. Hochstrasser, V. Augsburger, M. Funk, R. Appel, C. Pellegrini, A.F. Muller, Electrophoresis 7 (1986) 505–511.
- [7] N.I. Tracy, C.F. Ivory, Electrophoresis 25 (2004) 1748–1757.
- [8] C. Yang, G. Zhu, L. Zhang, W. Zhang, Y. Zhang, Electrophoresis 25 (2004) 1729–1734.
- [9] R. Wildgruber, A. Harder, C. Obermaler, G. Boauth, W. Weiss, S.J. Fey, P.M. Larsen, A. Gorg, Electrophoresis 21 (2000) 2610–2616.
- [10] A. Görg, W. Postel, S. Günther, Electrophoresis 9 (1988) 531–546.
- [11] H. Zou, X. Huang, M. Ye, Q. Luo, J. Chromatogr. A 954 (2002) 5–32.
- [12] E.F. Hilder, F. Svec, J.M.J. Fréchet, Anal. Chem. 76 (2004) 3887–3892.
- [13] C. Yang, Y. Wei, Q. Zhang, W. Zhang, T. Li, H. Hu, Y. Zhang, Talanta 66 (2005) 472–478.
- [14] C. Yang, W. Zhang, J. Duan, J. Zhang, Y.J. Zhang, Sep. Sci. 28 (2005) 76–78.

Microcolumn packed with YPA₄ chelating resin on-line separation/preconcentration combined with graphite furnace atomic absorption spectrometry using Pd as a permanent modifier for the determination of trace mercury in water samples

Hongmei Jiang, Bin Hu^{*}, Zucheng Jiang, Yongchao Qin

Department of Chemistry, Wuhan University, Wuhan 430072, PR China

Received 1 November 2005; received in revised form 10 February 2006; accepted 16 February 2006

Available online 24 March 2006

Abstract

A new method using a microcolumn packed with YPA₄ chelating resin as solid-phase extractor has been developed for the separation and preconcentration of trace Hg prior to its measurement by GFAAS with Pd as a permanent modifier. Various parameters such as the amount of the modifier, pH, sample flow rate, the concentration and volume of eluent have been studied in order to find the best conditions for the determination of mercury. The detection limit of the method (3σ) for Hg based on an enrichment factor of 100 was 0.2 ng ml^{-1} . A characteristic mass of 114 pg was obtained for mercury using Pd as a permanent modifier. The relative standard deviation was 2.8% at the 10 ng ml^{-1} level ($n=5$). The method has been applied to the determination of trace mercury in environmental water samples and the recoveries for the spiked samples are in the range of 91–105%.

© 2006 Elsevier B.V. All rights reserved.

Keywords: YPA₄ chelating resin; GFAAS; Hg; Water; Permanent modifier

1. Introduction

It is very clear that mercury and its compounds are highly toxic and readily released into the environment because of their high volatility and mobility [1,2]. Some poisonous hydrophobic compounds of mercury can cross biological membranes easily and concentrate in the blood and have an immediate and permanent effect on the brain and central nervous system [3]. The toxicological implications of the mercury content in the environment have encouraged the development of very selective and sensitive methods for its determination.

However, mercury is at such a low concentration in the environmental samples that the determination of mercury requires an enrichment step. Several approaches have been proposed for separation and preconcentration of trace mercury including solvent extraction [4], cloud point extraction [5], solid-phase extraction (SPE) [3,6–16]. Among these methods, SPE has

several advantages over the other separation/preconcentration techniques in view of: simpler operation, higher enrichment factor, reusability of the adsorbent and minimal costs due to low consumption of reagents and has found extensive application in trace analysis. Recent SPE studies are focusing on the development of new solid-phase extraction materials to improve the selectivity of the method. The most used solid-phase extraction materials are those derived from the incorporation of organic compounds on the surface of solid supports, which are mainly ion exchange resins [3,8], polyurethane foams [6,7,9], silica gel [10,11–13], cellulose [14,15], activated carbon [16]. Those organic compounds having sulfur donor atoms show strong affinity for soft metal ions, especially for mercury. For example, 6-mercaptopurine [3] immobilized on resin was used for determination of mercury and silver in environmental samples after batch preconcentration. 2-Aminoacetylthiophenol [10] functionalized amberlite XAD-2 was utilized for preconcentration of Cd(II), Hg(II), Ag(I), Ni(II), Co(II), Cu(II) and Zn(II) in tap water and river water. 2-Thiophenecarboxaldehyde [8] modified silica gel was used for preconcentration of ultratrace amounts of Hg(II) ions in spiked natural water samples prior

^{*} Corresponding author. Tel.: +86 27 87218764; fax: +86 27 68754067.
E-mail address: binhu@whu.edu.cn (B. Hu).

to the determination by hydride generation technique. Dithi-zone [12] and dithiocarbamate [13] derivatives loaded to silica gel has also been reported for selective extraction and preconcentration of Hg(II) ions. However, some of these solid-phase extraction materials suffer from a slow rate of uptake of metal ions and are unstable in acid medium such as dithiocarbamate salts.

Several analytical techniques, such as atomic absorption spectrometry (including flame atomic absorption spectrometry (FAAS), graphite furnace atomic absorption spectrometry (GFAAS), cold vapor atomic absorption spectrometry (CVAAS)) [3,4,7,8,12,15], atomic fluorescence spectrometry (AFS) [17], inductively coupled plasma optical emission spectrometry (ICP-OES) [10], inductively coupled plasma mass spectrometry (ICP-MS) [18], spectrophotometric measurements [5] and electrochemical analytical method have been applied to accurately determine trace mercury in various samples. CVAAS is one of the most widely used techniques for the selective determination of mercury in environmental, biological, clinical and industrial samples due to its excellent sensitivity [19]. Compared with CVAAS, the sensitivity of GFAAS is significantly lower than that of CVAAS and has rarely been used for the determination of mercury. However, GFAAS permits a higher sample throughput and requires less sample pretreatment. The main problem to limit the use of GFAAS for the determination of mercury is the high volatility of the element and its compounds. Therefore, thermal stabilization of mercury prior to its atomization is most important for avoiding losses of the analytes [20]. Several attempts have been made to overcome this obstacle such as adding various oxidizing agents and sulfur containing agents to prevent the reduction of mercury compounds, and more commonly, the use of platinum group metal (PGM) solutions as chemical modifiers. The last method has been proven to be very effective, but it has a drawback that the PGM modifier is progressively removed from the surface and must be applied before every atomization cycle. In recent years, using PGM which possess high boiling points as permanent modifiers has been successfully applied to the analysis of real samples in GFAAS leading to several benefits in comparison to conventional modifiers: increasing sample throughput with faster and simpler programs, reducing reagents blanks, preliminary elimination of unwanted modifier components, remarkably improvement in the tube lifetime, lowering analytical costs [21–27]. Moreover, it is compatible with in-line and in situ enrichment [21]. Pd, Rh, Ir, Au and Ru [2,19,20,24] have been successfully applied for mercury determination by GFAAS in different environmental samples. These metals were reduced on the inner of graphite surface as permanent modifiers by thermal or electrochemical processes. Notwithstanding permanent modifiers electrochemically deposited onto the graphite surface tube showed better long-term stability than thermally deposited for mercury determination, thermal deposition did not demand special equipment and can be employed easily by most laboratories [19,20]. Although electrodeposited Pd or Rh may be used as permanent modifiers, the sensitivity achieved was about two-fold less than with the same pre-reduced PGMs. Consequently, application of electrodeposited

PGM modifiers resulted in some losses of mercury, even under optimized experimental conditions [23]. Although using the high-melting PGM elements such as Ir, Rh or Ru as permanent modifiers, higher maximum pyrolysis temperature in comparison with those typical for Pd modifier can be obtained [25], the sensitivity for mercury determination with Rh or Ir modification was inferior than Pd alone was used [20]. With respect to the PGM chemical modifiers and permanent modification in GFAAS, Tsalev et al. [21] and Volynsky [23] have been critically reviewed.

A chelating resin (YPA₄) of aminoisopropylmercaptan type with a polythioether backbone, which the total contents of S and N in the resin are 24.89 and 7.82%, respectively, was found to have an excellent adsorption characteristic toward noble metals [28]. In our previous paper, chelating resin YPA₄ was used as both an adsorbent and a chemical modifier for electrothermal vaporization (ETV)–ICP-OES determination of Au, Pd, and Pt, in environmental and geological samples [29]. The purpose of this work was to present a sensitive, simple and rapid method to determine trace mercury in environmental water samples by a microcolumn packed with YPA₄ resin in combination with GFAAS using Pd as a permanent modifier. Experimental condition using Pd as permanent modifier was studied and optimized, and several parameters affected absorptive performance and capability of solid sorbent were evaluated. In the end, the developed method was applied for the determination of trace mercury in environmental water sample.

2. Experimental

2.1. Apparatus

The measurements were performed with a Hitachi 180-50 atomic absorption spectrometer (Japan) equipped with a heated graphite tube atomizer. A mercury hollow cathode lamp operated at 5 mA was utilized as the radiation source. Measurements were carried out in the integrated absorbance (peak area) mode at 253.7 nm, using a spectral band width of 2.6 nm. The heated programs employed for permanent modifier deposition and mercury determination are given in Table 1.

The pH values were controlled with a Mettler Toledo 320-S pH meter (Mettler Toledo Instruments (Shanghai) Co. Ltd.) supplied with a combined electrode. An HL-2 peristaltic pump (Shanghai Qingpu Instrument Factory, Shanghai, China) was employed to propel the sample, reagent and eluent. A minimum length of PTFE tubing with an i.d. of 0.5 mm was used for all connections in order to minimize the dead volume. A self-made PTFE microcolumn (20 mm × 2.0 mm i.d.), packed with YPA₄, was used in the manifold for separation/preconcentration.

2.2. Standard solution and reagents

Analytical grade reagents were used unless otherwise specified. Doubly distilled deionized water was used throughout. Plastic and glass containers and all other laboratory material that could come into contact with samples or standards

Table 1
Graphite atomizer temperature program

Parameter	Program 1 ^a			Program 2 ^b			
	Step			Step			
	1	2	3	Dry	Ash	Atomization	Clean
Temperature (°C)	110	130	800	110	200	1300	1800
Ramp time (s)	5	5	5	10	0	0	0
Hold time (s)	20	20	15	20	30	5	3

^a Used for thermal deposition of the modifier onto graphite surface [20].

^b Used for the determination of mercury.

were stored in 10% (v/v) nitric acid, and rinsed with double distilled deionized water prior to use. The stock solution for mercury (1 mg ml^{-1}) was prepared from HgCl_2 (The First Reagent Factory, Shanghai, China) which was dissolved in nitric acid. The stock standard solutions of Pd(II) (1 mg ml^{-1}) was prepared by dissolving of high-purity $\text{Pd}(\text{NO}_3)_2$ (The First Reagent Factory, Shanghai, China) in 0.1 mol l^{-1} nitric acid. Standard solutions were prepared by appropriate dilution of the stock solutions. The chelating resin YPA_4 was purchased from Department of Polymer Chemistry, in Wuhan University.

2.3. Preparation of YPA_4

The details on the chemical structure of YPA_4 was described in our previous publication [29]. YPA_4 with 140 mesh size was immersed in acetone and 1 mol l^{-1} HCl for 24 h, respectively, filtered and washed with double distilled deionized water, dried prior to storage for use for the adsorption of mercury.

2.4. Column preparation

A total of 50 mg of YPA_4 was filled into a PTFE microcolumn ($20 \text{ mm} \times 2.0 \text{ mm i.d.}$) plugged with a small portion of glasswool at both end. Before use, 5% thiourea + 1.0 mol l^{-1} HCl solution and doubly distilled deionized water were passed through the column in order to clean and condition it. Then, the column was conditioned to the desired pH with 0.1 mol l^{-1} NH_4Cl buffer solution.

2.5. General procedure

A 1 ml standard solution containing 100 ng Hg^{2+} at desired pH was sampled at a certain flow rate through a column prepared as stated above. The analyte trapped in the column was subsequently removed from the resin by 1 ml of tested eluent, and mercury in the effluents was analyzed by GFAAS. The column could be used repeatedly after regeneration with 5% thiourea + 1.0 mol l^{-1} HCl solution and double distilled deionized water, respectively. The recoveries of mercury were calculated from the ratio of the concentration found by GFAAS to that of the initial sample.

For the determination of optimum conditions (pH, flow rate, etc.), all experiments were performed according to the general procedure described above.

2.6. Treatment of the graphite tube with Pd as permanent modifier

Palladium permanent modifier was prepared following the procedure reported in literature [20]. Graphite tubes were pre-treated by pipetting $50 \mu\text{l}$ of a 1 mg ml^{-1} Pd standard solution into the tube, and submitting it to the temperature program 1 as shown in Table 1. This procedure was repeated four times, resulting in a total mass of $200 \mu\text{g}$ of Pd deposited on the tube wall.

2.7. Sample preparation

Lake water sample collected from East Lake, Wuhan, China, was filtered through a $0.45 \mu\text{m}$ membrane filter (Tianjin Jinteng Instrument Factory, Tianjin, China). Before use, the pH value was adjusted to 6.0 with 0.1 mol l^{-1} HCl and 0.1 mol l^{-1} $\text{NH}_3 \cdot \text{H}_2\text{O}$.

3. Results and discussion

3.1. Effect of permanent modifier

Palladium permanent modifier was prepared according to the above procedure, and the effect of the amount of Pd on the sensitivity for the determination of mercury was evaluated. Fig. 1 is the effect of Pd amount on the absorption signal of mercury. As could be seen, the analytical signal enhanced with the increase of deposited mass of Pd in the tube and then leveled off with further increasing a deposited mass of Pd from 100 to $200 \mu\text{g}$, when the deposited mass of Pd was larger than $200 \mu\text{g}$, the signal decreased slightly with continuing increase of the mass of Pd. In this work, $200 \mu\text{g}$ Pd was selected to be deposited on the inner wall of the graphite tube as a permanent modifier. Compared with that without Pd as permanent modifier, the sensitivity improved approximately five times.

After the preparation of Pd permanent modifier was accomplished, the electrothermal behaviors of Hg were studied. Fig. 2 is the effect of ashing temperature on the signal intensity of Hg. Under the temperature 200°C , no signal loss was found; however, the signal began to decrease when the ashing temperature exceeded 200°C , and with an increase of ashing temperature, the signal intensity reduced more, so the ashing temperature of 200°C was chosen in this work. The atomization temperature

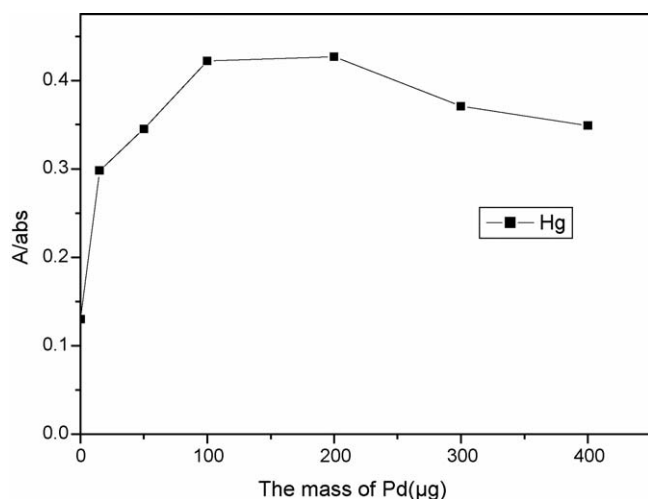


Fig. 1. Optimization of the mass of Pd for preparation of permanent modifier.

must be optimized in order to obtain the maximum analytical signals. Fig. 2 also showed the effect of the atomization temperature on the signal intensity of Hg. It can be seen that the absorption signal of mercury increased gradually with the increase of atomization temperature and the maximum absorption signal of mercury was obtained at 700 °C and this absorption maximum signal was kept constant with the further increase of atomization temperature to 1700 °C. In this work a temperature of 1300 °C was selected as the appropriate atomization temperature for Hg. The same tube could be used for at least 50 firings without any re-treatment.

3.2. Optimization of SPE parameters

Several parameters affected absorptive performance and capability of solid sorbent were examined, such as pH, sample flow rate, concentration and volume of eluent.

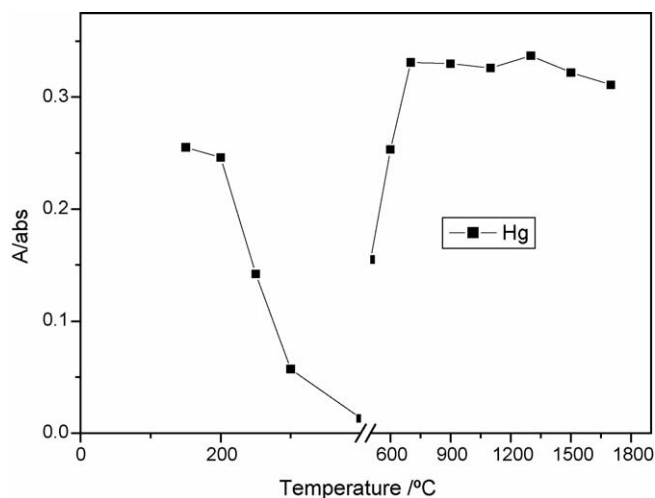


Fig. 2. Influence of the ashing and atomization temperature on the integrated absorbance of 100 ng Hg with 200 μg Pd as permanent modifier.

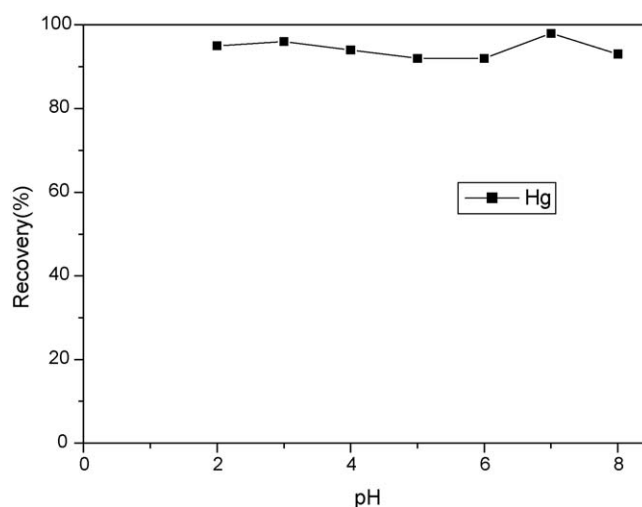


Fig. 3. Effect of pH on the recovery of Hg on YPA₄, Hg: 100 ng ml⁻¹.

3.2.1. Effect of pH on adsorption

The pH value plays an important role with respect to the adsorption of Hg²⁺ on YPA₄ chelating resin. In order to evaluate the effect of pH on the adsorption of mercury on YPA₄, the pH values of sample solutions were adjusted to a range of 2–8 with HCl or NH₃·H₂O. The result of the effect of pH on the recoveries of Hg²⁺ was shown in Fig. 3. It could be seen that Hg²⁺ was quantitative absorbed at the whole tested pH range. For the practical of environment samples, a pH of 6 was selected in the following work.

3.2.2. Effect of eluent concentration and volume

As a soft alkali containing sulfur functional groups, YPA₄ could form stable chelate with mercury that is a soft acid. To remove the mercury from YPA₄, a more soft alkali which can form a more stable chelate with mercury should be used. Thiourea was the just kind of alkali. In order to recover mercury retained in the column fast and quantitatively, a mixed solution of HCl and thiourea was used. Fig. 4 was the effect

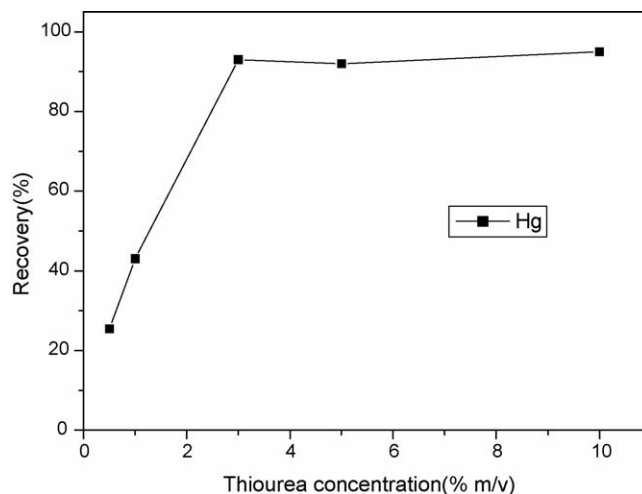


Fig. 4. Effect of thiourea concentration in elution solution on the recovery of Hg on YPA₄, Hg: 100 ng ml⁻¹, pH=6, HCl concentration: 1 mol l⁻¹.

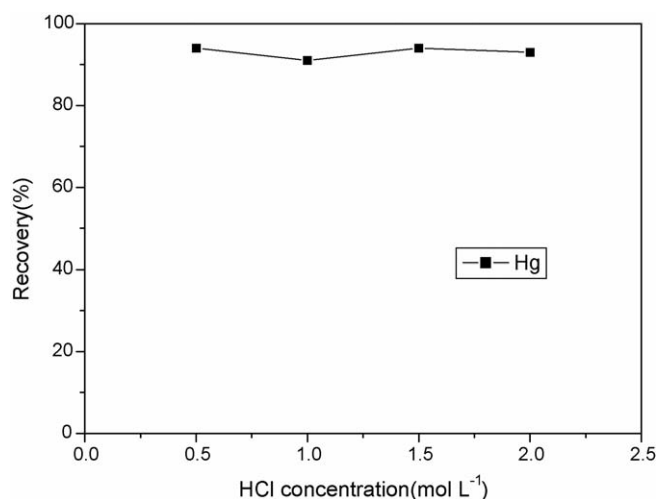


Fig. 5. Effect of HCl concentration in elution solution on the recovery of Hg on YPA₄. Hg: 100 ng ml⁻¹, thiourea concentration: 5% (m/v).

of thiourea concentration on the recovery of mercury by fixing the HCl concentration of 1 mol l⁻¹. It was found that the recovery of mercury increased with the increase in concentration of thiourea from 0.5 to 3% and then kept unchanged with the further increase in the thiourea concentration to 10%, a highest concentration tested. In the following experiments, 5% (m/v) thiourea was employed. By keeping the thiourea concentration at 5%, the effect of HCl concentration on the recovery of Hg was explored. As is shown in Fig. 5, Hg can be easily eluted in the whole HCl concentration studied. The HCl concentration of 1 mol l⁻¹ was chosen in this work.

Fig. 6 showed the effect of volume of the eluent on the recovery of Hg²⁺. As could be seen, 0.2 ml of mixture solution of 5% (m/v) thiourea and 1 mol l⁻¹ HCl could quantitatively desorb mercury.

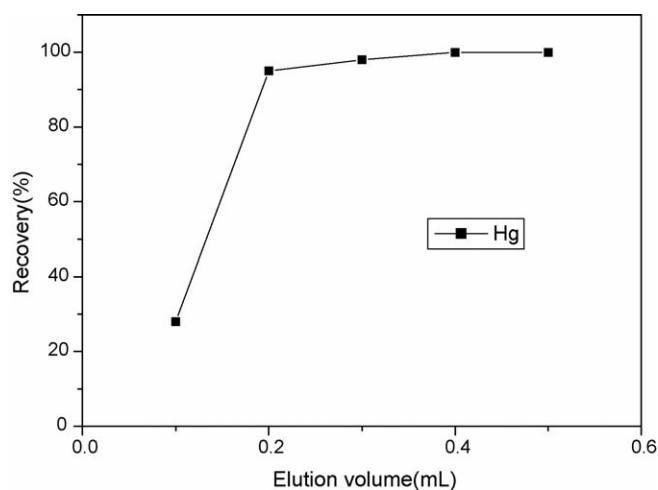


Fig. 6. Effect of elution volume on the recovery of Hg on YPA₄. Hg: 100 ng ml⁻¹, pH=6, HCl concentration: 1 mol l⁻¹, thiourea concentration: 5% (m/v).

3.2.3. Effect of flow rates of sample solutions

As the retention of element on the adsorbent depended upon the flow rate of the sample solution, its effect was examined under the optimum conditions (pH, eluent, etc.) by passing 1 ml of sample solution through the microcolumn with a peristaltic pump. The flow rates were adjusted in a range of 0.5–2.0 ml min⁻¹. As shown in Fig. 7, quantitative recoveries of Hg²⁺ was obtained at flow rates <1.2 ml min⁻¹. After the flow rate was over 1.2 ml min⁻¹, the recoveries of Hg²⁺ will decrease with the further increase of the flow rate due to a decrease in the adsorption kinetics at a high flow rate. Thus, a flow rate of 1.0 ml min⁻¹ was employed in this work.

3.2.4. Effect of the sample volume

In order to explore the possibility of enriching low concentrations of analyte from large volumes, the effect of sample volume on the retention of mercury was also investigated. For this purpose, a certain volume of sample solutions containing 100 ng Hg²⁺ was passed through the microcolumn with the optimum flow rate. As shown in Fig. 8, quantitative recoveries (>90%) were obtained for sample volumes of <27 ml. In this experiment, 25 ml of sample solution was adopted for the preconcentration of mercury from water sample, the retained mercury can be eluted with 5% thiourea + 1.0 mol l⁻¹ HCl, and a preconcentration factor of 100 is achieved by the concentration technique.

3.3. Adsorption capacity

The adsorption capacity was an important factor, because it determined how many YPA₄ was required to quantitatively concentrate mercury from a given solution. The capacity study used was adapted from that recommended by Maquieira et al. [30]. Under the selected experimental conditions, the static adsorption capacity of YPA₄ for Hg²⁺ was 38 mg g⁻¹.

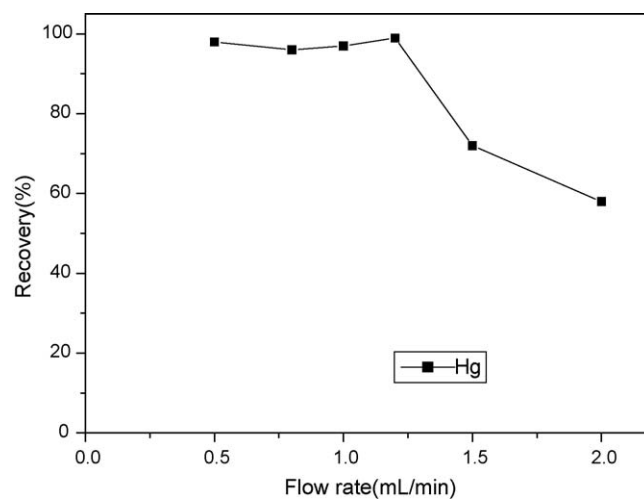


Fig. 7. Effect of flow rate on the recovery of Hg on YPA₄. Hg: 100 ng ml⁻¹, pH=6, eluent: 0.25 ml 1 mol l⁻¹ HCl + 5% (m/v) thiourea concentration.

Table 2
Comparison of limit of detection (LOD)

Method	LOD of instrument ^a	LOD of instrument ^b	LOD of method	Enrichment factor	Reference
YPA ₄ -Pd-GFAAS	571 pg –	114 pg 23 ng ml ⁻¹	1.5 pg 0.2 ng ml ⁻¹	100	This work
LLLE-GFAAS	52.92 ng ml ⁻¹	–	3.78 ng ml ⁻¹	14	[4]
Pd-CV-GFAAS	–	90 pg	90 pg	–	[3]
Pd-GFAAS	2400 pg	110 pg	110 pg	–	[20]
Pd-CV-GFAAS	–	93 pg	93 pg	–	[19]
Pd-GFAAS	–	55–60 pg	55–60 pg	–	[24]

LLLE: liquid–liquid–liquid extraction.

^a The graphite tube without permanent modifier.

^b The graphite tube using permanent modifier.

3.4. Interference effects

In order to demonstrate the selectivity of the developed micro-column separation and preconcentration system for the determination of mercury, the effect of alkali and alkaline earth metals (K⁺, Na⁺, Mg²⁺, Ca²⁺) and heavy metals (Cu²⁺, Co²⁺, Mn²⁺, Ni²⁺, Zn²⁺, Fe³⁺, Pb²⁺, Cd²⁺) on the measurement of 10 ng ml⁻¹ Hg²⁺, was investigated. The results showed that up to 4 µg ml⁻¹ of these heavy metal ions and at least 250 µg ml⁻¹ alkali and alkaline earth metals had no interferences with the determination of the mercury.

3.5. Limit of detection and precision

According to the definition of IUPAC, the limit of detection (LOD, 3σ) of this method was 0.2 ng ml⁻¹ with an enrichment factor of 100 and relative standard deviation (R.S.D.) was 2.8% ($C = 10 \text{ ng ml}^{-1}$, $n = 5$). A comparison of LOD obtained with several approaches for mercury determination by GFAAS is shown in Table 2. As could be seen, the presented method had a relative low limit of detection and was suitable for trace analysis in environmental samples. Preconcentration step combined

Table 3

Determination of Hg²⁺ in East Lake water and tap water ($n = 3$)

Sample	Added (ng ml ⁻¹)	Found (ng ml ⁻¹)	Recovery (%)
Lake water	0	2.77 ± 0.49	
	6	7.98 ± 0.75	91
	12	13.22 ± 0.25	90
Tap water	0	0.73 ± 0.035	
	2	2.88 ± 0.041	105
	6	6.41 ± 0.59	95

with permanent modification simultaneously dedicated to the improvement of the sensitivity.

3.6. Analysis application

The proposed method was applied to the determination of Hg in natural lake water sample (East Lake, Wuhan, China) and tap water, and the analytical results together with the recoveries by spiking Hg²⁺ to the water samples are listed in Table 3. As could be seen, the recoveries of 91–105% for the spiked samples were obtained. In order to establish the validity of the proposed procedure, the developed method was applied to the determination of the content of Hg²⁺ in certified reference material of GSBZ50016-90 environmental water. The determined value of $15.85 \pm 0.57 \text{ ng ml}^{-1}$ is coincided with the certified value of $14.8 \pm 1.4 \text{ ng ml}^{-1}$.

4. Conclusion

A new chelating resin YPA₄ was used as a solid sorbent to separate and preconcentrate trace Hg prior to the determination by GFAAS using Pd as permanent modifier. The developed method is simple, rapid, selective and sensitive and can be used for trace mercury determination in environmental samples.

Acknowledgment

Financial support from NCET, MOE of China is gratefully acknowledged.

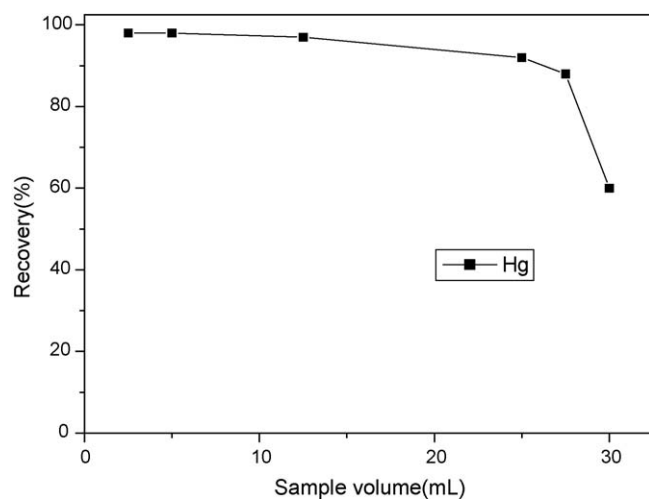


Fig. 8. Effect of sample volume on the recovery of Hg on YPA₄. Hg: 100 ng ml⁻¹, pH=6, eluent: 0.25 ml 5% (m/v) thiourea + 1 mol l⁻¹ HCl, flow rate: 1 ml min⁻¹.

References

- [1] B.C. Mondal, A.K. Das, *Anal. Chim. Acta* 477 (2003) 73.
- [2] E.M.M. Flores, B. Welz, A.J. Curtius, *Spectrochim. Acta Part B* 56 (2001) 1605.
- [3] B.C. Mondal, D. Das, A.K. Das, *Anal. Chim. Acta* 450 (2001) 223.
- [4] J.L. Capelo, C.D. dos Reis, C. Maduro, A. Mota, *Talanta* 64 (2004) 217.
- [5] M. Garrido, M.S.D. Nezio, A.G. Lista, M. Palomeque, B.S.F. Band, *Anal. Chim. Acta* 502 (2004) 173.
- [6] M.F. El-Shahat, E.A. Moawed, M.A.A. Zaid, *Talanta* 59 (2003) 851.
- [7] M.A.H. Hafez, I.M.M. Kenawy, M.A. Akl, R.R. Lashein, *Talanta* 53 (2001) 749.
- [8] E.M. Soliman, M.B. Saleh, S.A. Ahmed, *Anal. Chim. Acta* 523 (2004) 133.
- [9] G.A. Zachariadis, A.N. Anthemidis, M. Karpouzi, J.A. Stratis, *J. Anal. Atom. Spectrom.* 18 (2003) 1274.
- [10] Y. Guo, B. Din, Y. Liu, X.J. Chang, S.M. Meng, J.H. Liu, *Talanta* 62 (2004) 209.
- [11] P.K. Jal, S. Patel, B.K. Mishra, *Talanta* 62 (2004) 1005.
- [12] M.E. Mahmouda, M.M. Osmana, M.E. Amerb, *Anal. Chim. Acta* 415 (2000) 33.
- [13] M.E. Mahmoud, *Anal. Chim. Acta* 398 (1999) 297.
- [14] K. Zih-Perényi, A. Lasztity, Zs. Horvath, A. Lévai, *Talanta* 47 (1998) 673.
- [15] M.Q. Yu, D.W. Sun, W. Tian, G.P. Wang, W.B. Shen, N. Xu, *Anal. Chim. Acta* 456 (2002) 147.
- [16] A.M. Starvin, T.P. Rao, J. Hazard. Mater. B 113 (2004) 75.
- [17] H. Bagheri, A. Gholami, *Talanta* 55 (2001) 1141.
- [18] S.E. Long, W.R. Kelly, *Anal. Chem.* 74 (2002) 1477.
- [19] R.G.M. Moreno, E. de Oliceira, J.J. Pedrotti, P.V. Olivera, *Spectrochim. Acta Part B* 57 (2002) 769.
- [20] E. Bulska, W. Kandler, A. Hulanicki, *Spectrochim. Acta Part B* 51 (1996) 1263.
- [21] D.L. Tsalev, V.I. Slaveykova, L. Lampugnani, A. D'Ulivo, R. Georgieva, *Spectrochim. Acta Part B* 55 (2000) 473.
- [22] D.L. Tsalev, A.D. Ulivo, L. Lampugnani, M. di Marco, R. Zamboni, *J. Anal. Atom. Spectrom.* 10 (1995) 1003.
- [23] A.B. Volynsky, *Spectrochim. Acta Part B* 59 (2004) 1799.
- [24] A.F. da Silva, B. Welz, A.J. Curtius, *Spectrochim. Acta Part B* 57 (2002) 2031.
- [25] A. Volynsky, V. Krivan, *J. Anal. Atom. Spectrom.* 12 (1997) 333.
- [26] E.C. Lima, F. Barbosa Jr., F.J. Krug, *Anal. Chim. Acta* 409 (2000) 267.
- [27] E.C. Lima, J.L. Brasil, H.D.P. Santos, *Anal. Chim. Acta* 484 (2003) 233.
- [28] S.H. Dong, W.X. Tang, Y.H. Hu, *Acta Polym. Sinica* 2 (1990) 142.
- [29] Y.W. Wu, Z.C. Jiang, B. Hu, J.K. Duan, *Talanta* 63 (2004) 585.
- [30] A. Maquieira, H. Elmahadi, R. Puchades, *Anal. Chem.* 66 (1994) 3632.

Preparation and adsorption properties of crosslinked polystyrene-supported low-generation diethanolamine-typed dendrimer for metal ions

Changmei Sun^{a,b}, Rongjun Qu^{a,b,*}, Chunnuan Ji^b, Chunhua Wang^b, Yanzhi Sun^b,
Zhongwen Yue^b, Guoxiang Cheng^a

^a School of Materials Science and Engineering, Tianjin University, Tianjin 300072, China

^b School of Chemistry and Materials Science, Yantai Normal University, Yantai 264025, China

Received 31 October 2005; received in revised form 15 January 2006; accepted 15 January 2006

Available online 17 February 2006

Abstract

Two novel chelating resins, polystyrene supported G1.0 diethanolamine-typed dendrimer (PS-DEA) and G2.0 diethanolamine-typed dendrimer (PS-(DEA)₂), were prepared by anchoring low-generations diethanolamine-typed dendrimer into crosslinked polystyrene in this paper. Fourier transform-infrared spectra (FTIR), scanning electron microscopy (SEM) and elemental analysis were employed to character their structures. The results of adsorption for metal ions showed that the resins had good adsorption capacities for Cu²⁺, Ag⁺ and Hg²⁺, especially PS-DEA for Cu²⁺. The adsorption kinetics and adsorption isotherms of PS-DEA for Cu²⁺ and PS-(DEA)₂ for Hg²⁺ were studied. The results showed that the adsorption kinetics of the two resins can be modeled by pseudo second-order rate equation wonderfully and Langmuir and Freundlich equations could well interpret the adsorption of PS-(DEA)₂ for Hg²⁺ and PS-DEA for Cu²⁺, respectively. The adsorption mechanism of the resins for Cu²⁺ was confirmed by X-ray photoelectron spectroscopy (XPS).

© 2006 Elsevier B.V. All rights reserved.

Keywords: Polymer-supported low-generation dendrimer; Preparation; Adsorption; Metal ions

1. Introduction

Recently, the removal and recovery of heavy metal ions from industrial wastewater has been a significant concern in all industrial branches owing to economic and environmental factors. As an effective method, chelating resins are widely used to remove heavy metal ions in the waste stream [1–6]. The chelate resin is very important for metal ion complexation due to their hydrophilicity, accessibility and high capacity. Among chelating resins, the most popular ones are those containing polyamines, guanidyl group, and aminopyridine. These chelating resins containing nitrogen atoms have good adsorption capacity and adsorption selectivity for divalent transition metal ions.

Dendrimers [7–12] are currently attracting great attention due to their unusual and tunable chemical and physical properties, and the wide range of potential applications. An important fea-

ture of dendrimers is the presence of internal, dynamic cavities, often containing moieties capable of coordinating metal ions.

The diethanolamine (DEA) molecule contains two hydroxyl groups and one N atom. If it were anchored to the crosslinked polystyrene beads in form of dendrimer, the novel chelating resins obtained could be expected to possess hydrophilic nature and good adsorption capacity for metal ions. So in this paper, we designed and synthesized two novel chelating resins by anchoring low-generations diethanolamine-typed dendrimer into crosslinked polystyrene by a novel method. The study of the adsorption properties of the resins for metal ions showed that both the resins had good adsorption capacities for Cu²⁺, Ag⁺ and Hg²⁺.

2. Experimental

2.1. Materials

Commercial macroporous chloromethylpolystyrene beads (chlorobeads, PS-Cl), chlorine content 19.85%, were purchased from Chemical Factory of Nankai University of China.

* Corresponding author. Tel.: +86 535 6673982; fax: +86 535 6672574.
E-mail address: qurongjun@eyou.com (R. Qu).

Diethanolamine was purchased from Aldrich Chemical Co., USA. Other reagents were analytical-grade chemical products and used without further purification. Before using, pyridine was redistilled after dried by potassium hydrate and benzene was dried by magnesium sulfate. Aqueous solutions containing metal ions at various concentrations (10^{-2} – 10^{-3} M) were prepared from metal salts and controlled by titration with a standard ethylenediamine tetraacetic acid (EDTA) solution.

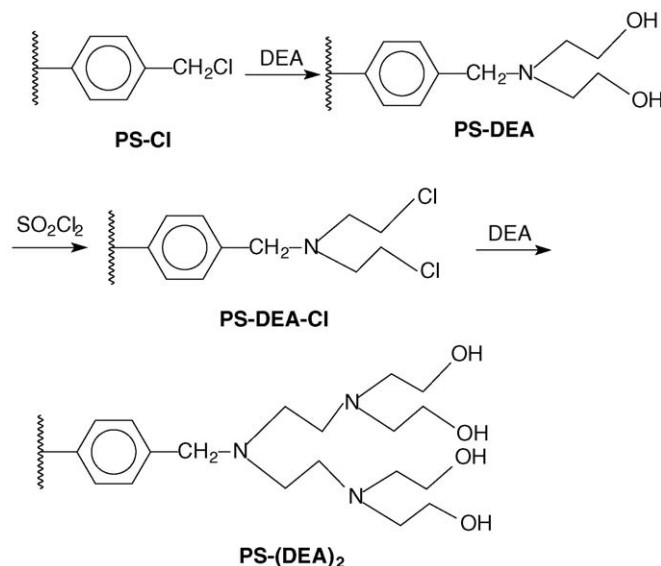
2.2. Instruments

Infrared spectra were recorded on a MAGNA-IR 550(series II) Fourier transform-infrared spectrometer, Nicolet Co., USA, test conditions: potassium bromide pellets, scanning 32 times, resolution is 4 cm^{-1} . The content of S and N elementary analyses were performed on an Elementar VarioEL III instrument, Elementar Co., Germany. The shapes and surface morphology of the resins were examined on a JSF5610LV scanning electron microscope, JEOL Co., Japan. XPS spectra were collected on PHI 1600ESCA system, Perkin-Elmer Co., USA, test conditions: Mg K α (1253.6 eV), power 200.0 W, resolution 187.85 eV.

2.3. Preparation of the resins

The PS-Cl beads (about 15 g) were swollen in 100 ml of ethanol for more than 2 h. Then 50 ml of diethanolamine was added and the mixture was magnetically stirred at 35°C for 3 h. After this, 30 ml of tetrahydrofuran was added. In order to make the reaction more complete, after 17 h, the temperature was raised to 50°C and the reaction lasted for another 12 h. Finally, the product was filtered off and washed with NaOH water solution, distilled water and ethanol successively. Then it was transferred to Soxhlet's extraction apparatus for reflux-extraction in 95% ethanol for 10 h and then was dried under vacuum at 50°C over 48 h. The product obtained was polystyrene supported G1.0 diethanolamine-typed dendrimer (PS-DEA). Elemental analysis (%): N, 4.686. The content of N functional group is calculated to be 3.347 mmol g^{-1} resin.

A 5.5 g of PS-DEA were swollen in the mixture of 50 ml benzene and 5 ml pyridine for 5 h at room temperature and another 1 h at 90°C . After cooling down to room temperature, the mixture was placed in ice-water bath. With magnetically stirring, 20 ml of thionyl chloride was added dropwise within 10–15 min. Then the temperature was raised to 60°C for 7 h. After this, the beads were filtered off and washed with distilled water, ethanol and hydrochloric acid. Then the product was transferred to Soxhlet's extraction apparatus for reflux-extraction in 95% ethanol for 10 h and was dried under vacuum at 50°C over 48 h. The product obtained in this step was abbreviated to be PS-DEA-Cl in this paper. The PS-DEA-Cl beads obtained were swollen in 50 ml of ethanol and then 40 ml of diethanolamine was added. With magnetically stirring, the reaction lasted 1 h at 10°C , 4 h at 25°C , 17 h at 50°C and another 3 h at 80°C . Then the product was filtered off and washed with distilled water and ethanol. Finally, it was transferred to Soxhlet's extraction apparatus for reflux-extraction in 95% ethanol for 10 h and then was dried



Scheme 1. The synthesis route of PS-DEA and PS-(DEA)₂.

under vacuum at 50°C over 48 h. The product obtained was polystyrene supported G2.0 diethanolamine-typed dendrimer (PS-(DEA)₂). Elemental analysis (%): N, 6.435. The content of N functional group is calculated to be 4.596 mmol g^{-1} resin. The synthesis routine to the resins was shown schematically in Scheme 1.

2.4. Adsorption procedure

In a thermostat-cum-shaking assembly, batch adsorption experiments were carried out by shaking 0.05 g of resin with 20 ml of an aqueous solution of metal ions of the desired concentration, pH, and temperature in 50 ml Pyrex glass tube. At predetermined time intervals, the solutions in the specified tubes were separated from the adsorbent. The concentration of metal ions was decided by titration method. The adsorption amounts were calculated according to the following Eq. (1), the coefficient of distribution for the metal ion was calculated according to Eq. (2) and the utilization ratio of N was calculated from Eq. (3).

$$Q = \frac{(C_0 - C)V}{W} \quad (1)$$

$$D = \frac{V}{W} \left(\frac{C_0}{C} - 1 \right) \quad (2)$$

$$\frac{Q}{N} = \frac{Q_0}{N\%} \quad (3)$$

where Q is the adsorption amount (mmol/g), C_0 and C the initial and concentrations of metal ions in solution when the contact time is t , respectively (mmol/ml), V the volume (ml), W the weight of resin beads (g), D the coefficient of distribution (ml/g), Q/N the utilization ratio of N, Q_0 the saturation adsorption (mmol/g), and $N\%$ is the content of N functional group (mmol/g).

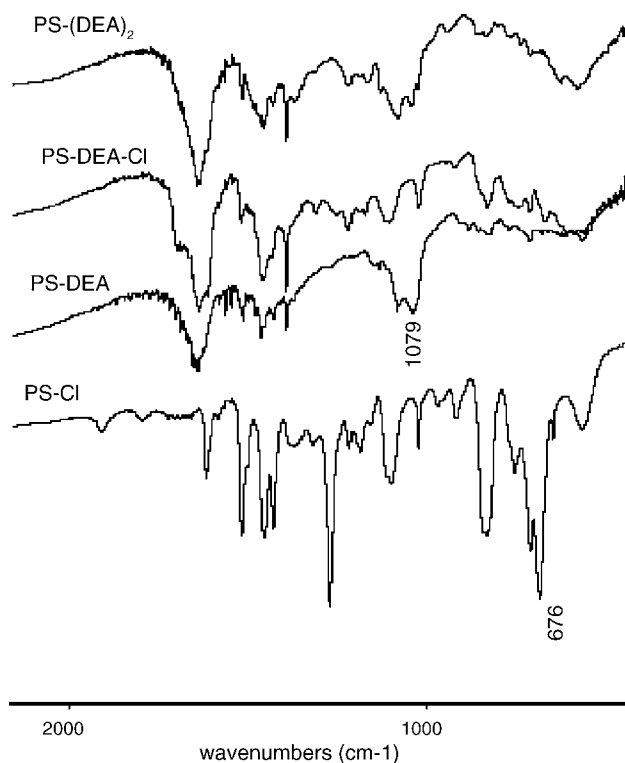


Fig. 1. FTIR spectra of PS-Cl, PS-DEA, PS-DEA-Cl and PS-(DEA)₂ resins.

3. Results and discussion

3.1. Infrared spectra characterization

Fig. 1 shows the infrared spectra of PS-Cl, PS-DEA, PS-DEA-Cl and PS-(DEA)₂ resins. By comparison with the curve of PS-Cl, the characteristic peak of at 676 cm⁻¹ almost disappears in the curve of PS-DEA, and a new broad peak appears at 1079 cm⁻¹, which is the characteristic peak of C–O bond, indicating that DEA groups have been introduced into the polymeric matrix successfully. The characteristic peak of C–O bond disappeared after PS-DEA reacted with thionyl chloride, while it appeared again after PS-DEA-Cl reacted with diethanolamine as can be seen in the curves of PS-DEA-Cl and PS-(DEA)₂, respectively, which confirmed that the expected reaction really occurred.

3.2. SEM observations of the resins

The SEM images in Fig. 2 visually show the morphological differences of the surface of PS-Cl, PS-DEA and PS-(DEA)₂ resins. Compared with the PS-Cl resin, the amount of pores on the surface of PS-DEA and PS-(DEA)₂ resins increased obviously because of the introduction of the –N(C₂H₄OH)₂ groups. It's implied that the macroporous structure of PS-Cl resin had not been damaged after the reaction and those pores which collapsed when the resin was dried under vacuum condition reopened after the polar groups –N(CH₂CH₂OH)₂ were introduced into the polymer matrix. The existence of macropores would provide convenient diffusion channels for metal ions into the interior

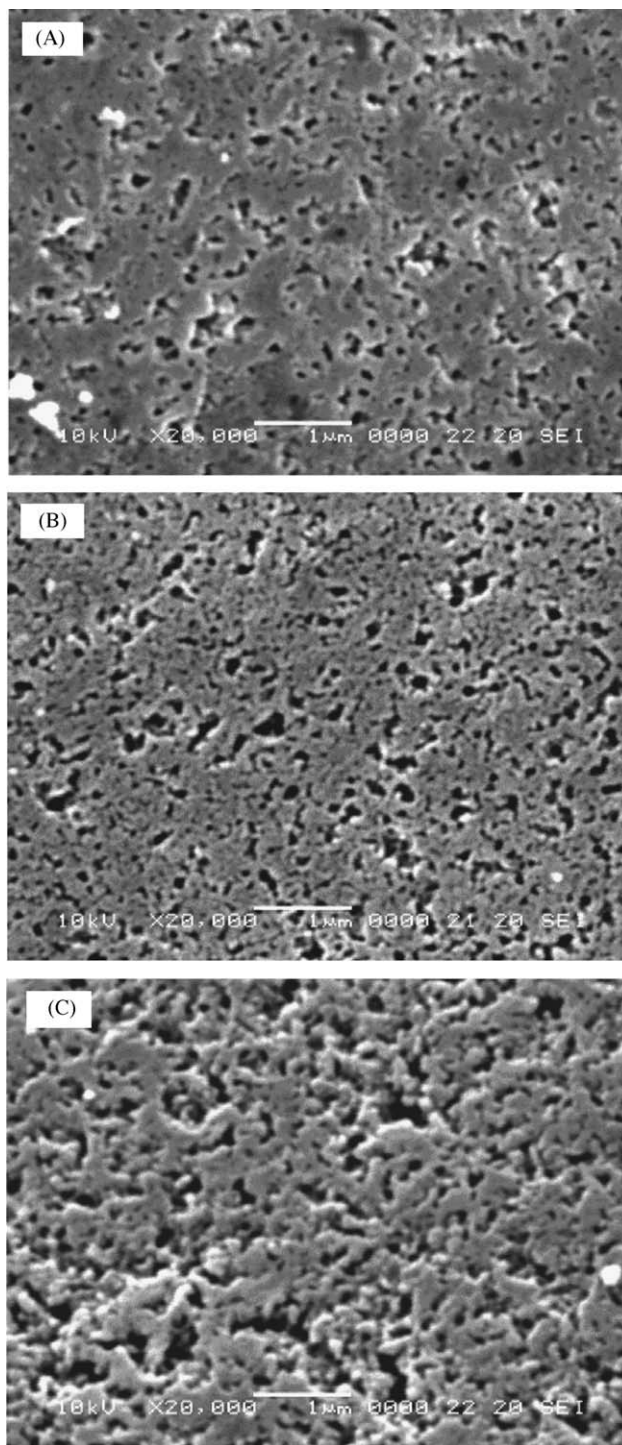


Fig. 2. The SEM images of (A) PS-Cl, (B) PS-DEA, and (C) PS-(DEA)₂ resins.

of the resins if they were used in adsorption of metal ions in aqueous solution.

3.3. Adsorption for metal ions

Fig. 3 shows the utilization ratio of N (*Q/N*) and the saturation adsorption capacities of PS-DEA and PS-(DEA)₂ resins for Ag⁺, Cu²⁺, Ni²⁺, Cd²⁺, Hg²⁺, Zn²⁺ and Pb²⁺. Obviously, the PS-DEA and PS-(DEA)₂ resins have better adsorption capacity

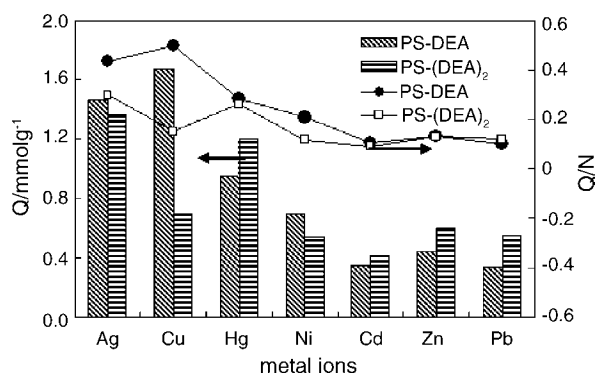


Fig. 3. The utilization ratio of N and saturation adsorption capacities of PS-DEA and PS-(DEA)₂ resins for metal ions at 25 °C.

for Ag⁺, Cu²⁺ and Hg²⁺ ions than for Ni²⁺, Cd²⁺, Zn²⁺ and Pb²⁺ ions, especially PS-DEA for Cu²⁺. Besides, it also can be seen from Fig. 3 that, generally, the Q/N of PS-DEA is higher than that of PS-(DEA)₂ resin, which probably because that the functional groups in PS-(DEA)₂ resin are so bulky that the complex formed blocked some pore canals and the metal ions couldn't diffuse into the resin to coordinate with the inner functional groups. Thus it can be seen that more N content didn't mean the better adsorption capacity for metal ions, that is, the increasing generation of dendrimer which was introduced into the PS matrix is not always beneficial to the adsorption properties. Another phenomenon that should be noticed is that the Q/N of PS-(DEA)₂ resin for Hg²⁺ is the highest among the several metal ions and the saturation adsorption capacity can reach about 1.2 mmol/g. So in the following part, the adsorption of PS-DEA for Cu²⁺ and PS-(DEA)₂ for Hg²⁺ are selected to be studied in detail.

The adsorption of PS-DEA for Cu²⁺ at pH 1.78–5.6 was studied at 25 °C. Within pH 1.78–4.50, the distribution coefficient D increased with the increasing pH value. It's probably because that the N atoms can easily be protonized at lower pH condition and lose coordination capacity. Also, the experiment showed that at higher pH condition (>5.0), Cu(OH)₂ precipitation appeared and the adsorption system became opaque.

3.4. Adsorption kinetics

A study of adsorption kinetics is desirable as it provides information about the mechanism of adsorption, which is important for efficiency of the process. The adsorption kinetics of PS-DEA for Cu²⁺ and PS-(DEA)₂ for Hg²⁺ at different temperature was studied in this part. The results showed that adsorption equilibriums of PS-DEA for Cu²⁺ were all established in 8 h and the adsorption rates increased with the increasing temperature (see the values of k_2 in Table 1), while the saturation adsorption capacities didn't increase with the increasing temperature as we expected. A possible explanation for this is that the diffusion rate of Cu²⁺ is enhanced by increasing temperature, so Cu²⁺ can approach and contact with the resin much faster at higher temperature. Consequently, the complexes quickly formed on the surface and outer layer of the resin at high temperature prevent the Cu²⁺ from diffusing into the inside of the resin, so the value of adsorption capacities at highest temperature is not the largest.

Table 1

Parameters of pseudo second-order kinetic models of PS-DEA for Cu²⁺ and PS-(DEA)₂ for Hg²⁺

Temperature (°C)	Pseudo second-order model of PS-DEA for Cu ²⁺			Pseudo second-order model of PS-(DEA) ₂ for Hg ²⁺		
	k_2	Q_0	R^2	k_2	Q_0	R^2
5	0.18	1.85	0.9912	2.78	1.03	0.9997
15	0.37	1.63	0.9955	1.90	1.08	0.9991
35	1.99	1.36	0.9994	2.36	1.16	0.9996

Deferring from those of PS-DEA for Cu²⁺, the adsorption equilibriums of PS-(DEA)₂ for Hg²⁺ were established in about 2 h, which were much faster than those of PS-DEA for Cu²⁺.

Successful application of the adsorption demands innovation of cheap, easily available and abundant adsorbents of known kinetic parameters, and adsorption characteristics. Adsorption kinetics can be modeled by several models [13], including pseudo first-order Lagergren equation and pseudo second-order rate equation given below as Eqs. (4) and (5), respectively.

$$\log(Q_0 - Q) = \log Q_0 - \frac{k_1}{2.303}t \quad (4)$$

$$\frac{t}{Q} = \frac{1}{k_2 Q_0^2} - \frac{1}{Q_0}t \quad (5)$$

where k_1 is the rate constant of pseudo first-order adsorption (h⁻¹), k_2 (g/mmol) the rate constant of pseudo second-order adsorption, Q_0 and Q are the adsorption amount at equilibrium and at time t , respectively.

Both the models were used to fit the kinetics curves and the results showed that pseudo second-order model was more suitable since the values of R^2 could be regarded as a measure of the goodness-of-fit of experimental data on the kinetic models [14]. The straight-lines of pseudo second-order kinetic model are showed in Fig. 4. The parameters calculated according to the model are listed in Table 1. It can be seen that the values of k_2 of PS-DEA for Cu²⁺ at the three temperatures are higher than

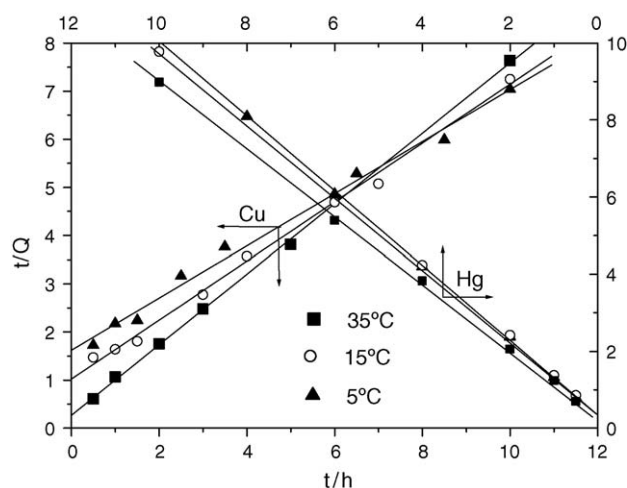


Fig. 4. The pseudo second-order kinetic models of PS-DEA for Cu²⁺ and PS-(DEA)₂ for Hg²⁺.

those of PS-(DEA)₂ for Hg²⁺, implying that the adsorption rate of PS-(DEA)₂ for Hg²⁺ is faster than that of PS-DEA for Cu²⁺.

Deferring from that of PS-(DEA)₂ for Hg²⁺, the effect of temperature on the adsorption of PS-DEA for Cu²⁺ is orderly, that is, the adsorption rate constant k increases with the increasing temperature. According to Arrhenius equation, $\ln k_2 = -E_a/RT + \ln A$, plotting $\ln k_2$ against $1/T$, a straight line can be obtained. The apparent activation energy of adsorption E_a calculated from the linear slope is 52.67 kJ mol⁻¹. This low activation energy as compared to these of typical chemical reaction of 65–250 kJ mol⁻¹ implies that the adsorption of PS-DEA for Cu²⁺ is a facile procedure.

The thermodynamic parameters such as change in standard free energy (ΔG), enthalpy (ΔH), and entropy (ΔS) are determined by using Eqs. (6) and (7),

$$\Delta G = \Delta H - T\Delta S \quad (6)$$

$$\log D = \frac{\Delta S}{R} - \frac{\Delta H}{2.303RT} \quad (7)$$

where D is the distribution ratio, T the solution temperature (K), and R is the gas constant. ΔH and ΔS are calculated from the slope and intercept of van't Hoff plots of $\log D$ versus $1/T$. The results are listed in Table 2.

It can be seen that the adsorption process is spontaneous with the negative values of ΔG . The ΔH being negative value justifies that the adsorption of PS-DEA for Cu²⁺ is an exothermal process in nature. The positive value of ΔS shows increased disorder at the solid–solution interface during the adsorption of PS-DEA for Cu²⁺.

3.5. Isothermal adsorption

The adsorption isotherms were studied and the data were analyzed with Langmuir (8) and Freundlich (9) equations, respectively. Then, Figs. 5 and 6 were obtained.

$$\frac{C}{Q} = \frac{1}{bQ_0} + \frac{C}{Q_0} \quad (8)$$

$$\ln Q = \ln K_F + \frac{1}{n} \ln C \quad (9)$$

where Q is the adsorption capacity (mmol/g), C the equilibrium concentration of metal ions (mmol/ml), Q_0 the saturated adsorption capacity (mmol/g), b an empirical parameter, n the Freundlich constant, and K_F the binding energy constant reflecting the affinity of the resin to metal ions. As we know, the Langmuir equation is applicable to homogeneous adsorption,

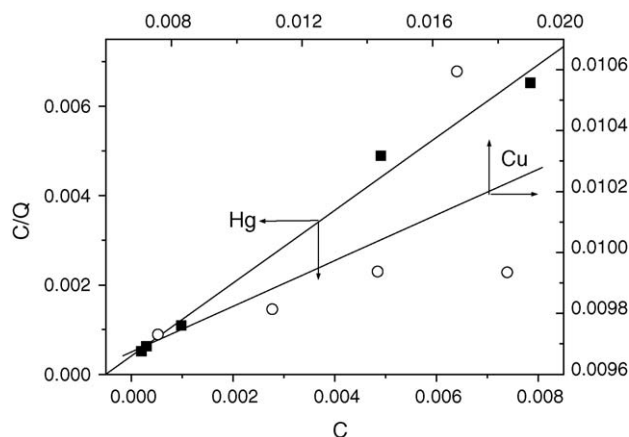


Fig. 5. The Langmuir isotherms of PS-DEA for Cu²⁺ and PS-(DEA)₂ for Hg²⁺ at 25 °C.

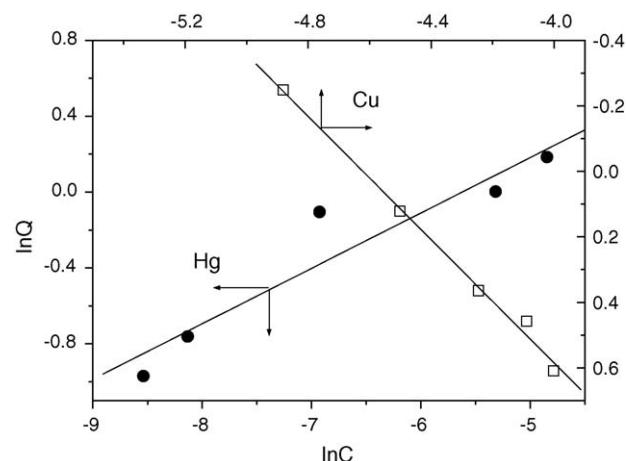


Fig. 6. The Freundlich isotherms of PS-DEA for Cu²⁺ and PS-(DEA)₂ for Hg²⁺ at 25 °C.

where the adsorption of each sorbate molecule onto the surface had equal adsorption activation energy. While, the Freundlich equation is employed to describe heterogeneous systems and reversible adsorption and is not restricted to the formation of monolayer.

The parameters for the two isotherms obtained from Figs. 5 and 6 are presented in Table 3. It can be seen that in the case of PS-DEA for Cu²⁺, the regression coefficient R^2 obtained from Freundlich model is much higher than that from Langmuir model, suggesting the nonapplicability of Langmuir model to this system. On the contrary, the Langmuir model is better than Freundlich model to fit the adsorption isotherm of PS-(DEA)₂

Table 2
The thermodynamic parameters of PS-DEA for Cu²⁺

Temperature (°C)	D	ΔG (kJ mol ⁻¹)	ΔH (kJ mol ⁻¹)	ΔS (kJ mol ⁻¹)	E_a (kJ mol ⁻¹)
5	103.63	-5.9	-2.2	13.3	52.67
15	100.14	-6.0			
25	97.88	-6.2			
35	93.50	-6.3			

Table 3
Langmuir and Freundlich parameters of PS-DEA for Cu²⁺ and PS-(DEA)₂ for Hg²⁺ at 25 °C

	Freundlich parameters			Langmuir parameters		
	K_F	$1/n$	R^2	Q_0	b	R^2
PS-DEA for Cu ²⁺	77.61	0.94	0.9938	20.73	5.16	0.3705
PS-(DEA) ₂ for Hg ²⁺	5.17	0.29	0.9019	1.23	1977.87	0.9892

Table 4
The binding energy (eV) of the adsorption of PS-DEA and PS-(DEA)₂ for Cu²⁺

Resins	N 1s	Cu 2p
PS-DEA	399.39	
PS-DEA-Cu	398.66, 400.62	932.91
PS-(DEA) ₂	399.49	
PS-(DEA) ₂ -Cu	398.37, 400.09	933.17
Cu(SO ₄) ₂		935.20

for Hg²⁺, implying that the adsorption mechanism for Cu²⁺ and Hg²⁺ are not the same.

3.6. Adsorption mechanism of PS-DEA and PS-(DEA)₂ for Cu²⁺

In order to compare the adsorption mechanism of the two resins reasonably, the same absorbed metal ion should be chosen. Table 4 shows the XPS data of PS-DEA and PS-(DEA)₂ before and after adsorption for Cu²⁺. It can be seen that the N 1s binding energy of PS-DEA increased from 399.39 to 400.62 eV after the adsorption for Cu²⁺, meaning that N is an electron donor. Meanwhile, a new N 1s peaks appears at 398.66 eV, which probably because that a part of N atoms are set free from the hydrogen bonds (N···H···O) in PS-DEA resin after the adsorption for Cu²⁺. The similar phenomenon can also be seen in PS-(DEA)₂ resin. The Cu 2p binding energies of PS-DEA and PS-(DEA)₂ both decrease compared with that of Cu(SO₄)₂, meaning that Cu atom is an electron acceptor.

4. Conclusion

Two novel chelating resins, PS-DEA and PS-(DEA)₂, were prepared by anchoring low-generations diethanolamine-typed dendrimer into crosslinked polystyrene in this paper. FTIR, SEM and elemental analysis were employed to character their structures. The adsorption for several metal ions was studied. The results showed that the resins had good adsorption capacities for Cu²⁺, Ag⁺ and Hg²⁺, especially PS-DEA for Cu²⁺. And more content of functional group didn't mean the better adsorption capacity for metal ions. The adsorption kinetics and adsorption

isotherms of PS-DEA for Cu²⁺ and PS-(DEA)₂ for Hg²⁺ were studied. The results showed that the adsorption kinetics of the two resins can be modeled by pseudo second-order rate equation wonderfully and Langmuir and Freundlich equations could well interpret the adsorption of PS-(DEA)₂ for Hg²⁺ and PS-DEA for Cu²⁺, respectively. The XPS results showed that N atoms were that main electron donors to coordinate with Cu²⁺ in both PS-DEA and PS-(DEA)₂ resins.

Acknowledgements

The work was supported by the Postdoctoral Science Foundation of China (No. 2003034330), the Science Foundation for mid-youth elite of Shandong Province, the Nature Science Foundation of Shandong Province (No. Y2005F11), the Nature Science Foundation of Yantai Normal University (No.032912, 20052901, 042920), Educational Project for Postgraduate of Yantai Normal University (No. YD05001), and Applied Project of Educational Bureau of Shandong Province (No. J05D03, J04B02).

References

- [1] R.R. Navarro, K. Sumi, N. Fuiji, M. Matsumura, Water Res. 30 (1996) 2488.
- [2] M.I. Delacour, E. Gailiez, M. Bacauet, M. Morcellte, J. Appl. Polym. Sci. 73 (1999) 899.
- [3] S. Ridvan, A. Tuncel, A. Denizli, J. Appl. Polym. Sci. 83 (2002) 2467.
- [4] N.K. Bozena, J.B. Orola, W.T. Andrzej, A. Wieslaw, React. Funct. Polym. 42 (1999) 213.
- [5] R.J. Qu, C.H. Wang, C.N. Ji, C.M. Sun, X.R. Sun, G.X. Cheng, J. Appl. Polym. Sci. 95 (2005) 1558.
- [6] R.J. Qu, C.P. Liu, W.J. Ruan, L. Sun, Q.J. Liu, Chin. J. Mater. Res. 13 (1999) 51.
- [7] J.M.J. Frychet, D.A. Tomalia, Angew. Chem. 115 (2003) 2314.
- [8] S. Hecht, J.M.J. Frychet, Angew. Chem. 113 (2001) 76.
- [9] R. Touzani, H. Alper, J. Mol. Catal. A: Chem. 227 (2005) 197.
- [10] T. Endo, T. Yoshimur, K. Esumi, J. Colloid Interf. Sci. 286 (2005) 602.
- [11] J.H. Bu, Q.Y. Zheng, C.F. Chen, Z. T. Tetrahedron 61 (2005) 897.
- [12] N.Y. Lee, W.J. Jang, S.H. Yu, J. Im, S.K. Chung, Tetrahedron Lett. 46 (2005) 6063.
- [13] S. Wang, H. Li, J. Hazard. Mater. B 126 (2005) 71.
- [14] A. Saeed, M. Iqbal, M.W. Akhtar, J. Hazard. Mater. B 117 (2005) 65–73.

Method development for the analysis of polybrominated diphenyl ethers, polychlorinated biphenyls, polychlorinated dibenzo-*p*-dioxins and dibenzo-furans in single extract of sediment samples

Hanxia Liu^{a,b}, Qinghua Zhang^a, Maoyong Song^a,
Guibin Jiang^a, Zongwei Cai^{a,b,*}

^a State Key Laboratory of Environmental Chemistry and Ecotoxicology, Research Center for Eco-Environmental Sciences,
Chinese Academy of Sciences, Beijing 100085, PR China

^b Dioxin Analysis Laboratory, Hong Kong Baptist University, Kowloon, Hong Kong, China

Received 31 October 2005; received in revised form 29 November 2005; accepted 29 November 2005

Available online 6 January 2006

Abstract

A comprehensive method was developed for quantitative analysis of polybrominated diphenyl ethers (PBDEs), polychlorinated biphenyls (PCBs) and polychlorinated dibenzo-*p*-dioxins and dibenzo-furans (PCDD/Fs) in one single extract of environmental samples. The sample preparation procedure included two fractionation steps using silver nitrate silica chromatography to separate PBDEs from PCBs and PCDD/Fs and florisil column to separate PCBs from PCDD/Fs. Acidic silica, acidic alumina and gel permeation chromatography (GPC, for PCBs) or activated carbon column (for PCDD/Fs) were used for further clean-up. The sample extracts were analyzed by using high-resolution gas chromatography/high-resolution mass spectrometry. The entire method was validated from the analysis of mixed standards of PBDEs, PCBs and PCDD/Fs ($n = 3$); the analysis of certified reference biota (WMF-01). The method was applied for the analysis of 10 sediment samples collected from Haihe River and Dagu Drainage River in Tianjin City. No significant PBDEs pollution was found in the areas.

© 2005 Elsevier B.V. All rights reserved.

Keywords: PBDEs; PCBs; PCDD/Fs; AgNO₃ silica gel chromatography; Sediments

1. Introduction

Polybrominated diphenyl ethers (PBDEs), polychlorinated biphenyls (PCBs) and polychlorinated dibenzo-*p*-dioxins and dibenzo-furans (PCDD/Fs) have been of great concern due to their toxicity and potential health risks [1–5]. However, most of the currently available methods involve two or three individual sample preparation procedures followed by instrument analysis, which is time and solvent consuming. Thus, a rapid and reliable procedure for the simultaneous sample preparation for PBDEs, PCBs and PCDD/Fs is needed.

Separation of PBDEs from PCBs and PCDD/Fs is difficult and vital in the simultaneous sample preparation procedure and consequent gas chromatography/mass spectrometry (GC/MS)

analysis because the compounds often have co-elution problem on various types of GC-column with the same isobaric ions [6–9]. Multi-layer silica column has been used to separate PBDEs from PCBs and PCDD/Fs. In the multi-layer silica column, silver nitrate silica was found to play an important role in the separation procedure. It was reported that PBDEs could not be separated from PCBs and PCDD/Fs by using the multi-layer silica column if the layer of acidic silica was overloaded with sample extracts due to the severe matrix effect on separation efficiency [6]. In these cases, a new multi-layer silica column was needed to clean the sample prior to the separation of PBDEs, which not only affected the recovery but also spent much more time and solvent. In this study, investigation was conducted to use silver nitrate silica to replace the multiple-layer silica to separate PBDEs from PCBs and PCDD/Fs after the clean-up by individual acidic silica and acidic alumina column chromatography. Further clean-up of the PCBs and PCDD/Fs fractions were achieved by using GPC and active carbon col-

* Corresponding author. Tel.: +852 3417070; fax: +852 34117348.
E-mail address: zwcai@hkbu.edu.hk (Z. Cai).

umn chromatography, respectively. The method was validated through the analysis of mixed standards and certified reference tissue sample (WMF-01) and applied for the determination of PBDEs along with PCBs and PCDD/Fs in sediment samples collected from Haihe River and Dagou Drainage River in Tianjin City.

2. Materials and methods

2.1. Chemicals

All solvents were absolute grade and were purchased from Tedia. Silica gel (0.063–0.100 mm) was obtained from Merck. Bio-Beams SX-3 was purchased from Bio-Rad. Standard solutions of PCDD/Fs (1613-LCS (Labeled Compound Stock Solution), 1613-ISS (^{13}C -1, 2, 3, 4-TCDD and ^{13}C -1, 2, 3, 7, 8, 9-HxCDD Internal Standard Spiking Solution) and 1613-PAR (Native PCDD/Fs, Precision and Recovery Stock Solution)), PCBs (WP-LCS (WHO ^{13}C -PCBs Surrogate Spiking Solution), WP-ISS (WHO ^{13}C -PCBs, Internal Standard Solution), MXP) and PBDEs (^{13}C -labeled MBDE-MXC, MBDE-139-IS) were obtained from Wellington Laboratories. Certified reference material WMF-01 (reference fish tissue for organic contaminant analysis) was also obtained from Wellington Laboratories. Ten sediment samples were collected from Haihe River and Dagou Drainage River in Tianjin City of China in November 15–16, 2003. Detailed sample collection and extraction procedures were described elsewhere [10,11].

2.2. Sample preparation and purification

Freeze-dried environmental sediment samples were spiked with ^{13}C -labeled surrogate standards prior to a 24-h Soxhlet extraction with 1:1 dichloromethane (DCM):hexane. After the extraction, acidic silica was added to remove lipid in the tissue samples. The extract was concentrated by using a rotary evaporator, and the residue was dissolved in 7 ml hexane in the vial. Eight millilitres of concentrated sulphuric acid was added and the vial was shaken and then allowed to stand for an hour. The above extraction, concentration and acidic treatment steps were not needed during the development of the chromatographic clean-up procedure, for which a solution of mixed chemical standards was used. The organic layer in the vial was sequentially subjected to acidic silica gel, acidic alumina, silver nitrate (AgNO_3) silica (10%, w/w) for the separation of PBDEs from PCBs and PCDD/Fs and florisil for the separation of PCBs and PCDD/Fs. Activated carbon chromatography columns and gel permeation chromatography (GPC) were used for further clean-up of PCBs and PCDD/Fs, respectively. The activated carbon column was packed by using a glass pipette from bottom to top with glass wool, 0.15–0.2 ml silica gel, 0.35–0.4 ml 18% activated carbon/celite 545 mixture, 0.15–0.2 ml silica gel and glass wool. The GPC was packed with pre-swollen and washed Bio-Beads SX-3 corresponding to 30 g dry material by using 1:1 DCM:hexane as the solvent. The eluted sample was collected in three fractions, which were concentrated to dryness. Then, ^{13}C -labeled internal standards, WP-ISS (for PCBs), MBDE 139

(for PBDEs) and 1613-ISS (for PCDD/Fs), were added prior to the GC injection.

2.3. Instrumental analysis

The instrument analysis of PBDEs, PCDD/Fs and PCBs was performed on an Agilent 6890 gas chromatography coupled with an Autospec Ultima mass spectrometer operating with EI source in SIM mode. Two microliters of sample extract was injected with splitless mode into a DB-5MS fused silica capillary column (60 m \times 250 μm i.d. \times 0.25 μm film thickness) with helium as carrier gas. The details of the MS analysis and quality control are described in the EPA methods 1614-draft, 1613B and 1668A.

3. Results and discussion

3.1. Method development

3.1.1. Separation of PBDEs from PCBs and PCDD/Fs by using silver nitrate silica column

The key work of the method development for the analysis of PBDEs, PCBs and PCDD/Fs in one single sample was to separate PBDEs from PCBs and PCDD/Fs in the sample extract. Martínez et al. reported that separation of PBDEs from PCBs could be achieved by using neutral silica as absorbents [12]. Therefore, separation of PBDEs from PCBs and PCDD/Fs were investigated on neutral silica column (9 mm i.d., 8 cm). Different silica gel activation processes, baked at 170 °C for at least 24 h and baked at 550 °C for 6 h and keep in 170 °C for at least 24 h, were investigated. The results showed that neutral silica under the current conditions could not effectively separate PBDEs from PCDD/Fs and PCBs. Neutral silica baked at 550 °C for 6 h is less adsorptive than the one baked at 170 °C. The different results of separation efficiency between our experiments and that reported by Martínez et al. may be due to the difference of characteristics of the silica sorbents or their preparation procedure.

AgNO_3 silica was then selected for the separation of PBDEs from PCBs and PCDD/Fs. The results showed that the orders of elution depended on the levels of chlorination or bromination of the compounds, but in different patterns. For PCBs and PCDD/Fs, mono-CBs and 2,3,7,8-TCDD were the last eluted congeners, respectively; while mono-BDEs were first eluted out of the AgNO_3 silica column among the PBDEs. Therefore, in order to separate PBDEs from PCBs and PCDD/Fs, the separation of BDE-28 from PCB-28 and 2,3,7,8-TCDD, which are the first or the last elution congeners among our target compounds, was the most difficult. Chromatograms of 2,3,7,8-TCDD/F, PCB-28 and BDE-28 in different fractions were presented in Fig. 1. As shown in Fig. 1, 100% 2,3,7,8-TCDD and PCB-28 were eluted in the first 80 ml hexane, and 90% of 2,3,7,8-TCDD was eluted in 90 ml hexane, while BDE-28 was only detected in the 6% DCM in hexane eluting solvent, indicating that a complete separation of PBDEs from PCBs and PCDD/Fs was achieved. Therefore, 100 ml of hexane was selected to elute PCBs and PCDD/Fs, followed by 40 ml of 6% DCM in hexane for the elution of PBDEs.

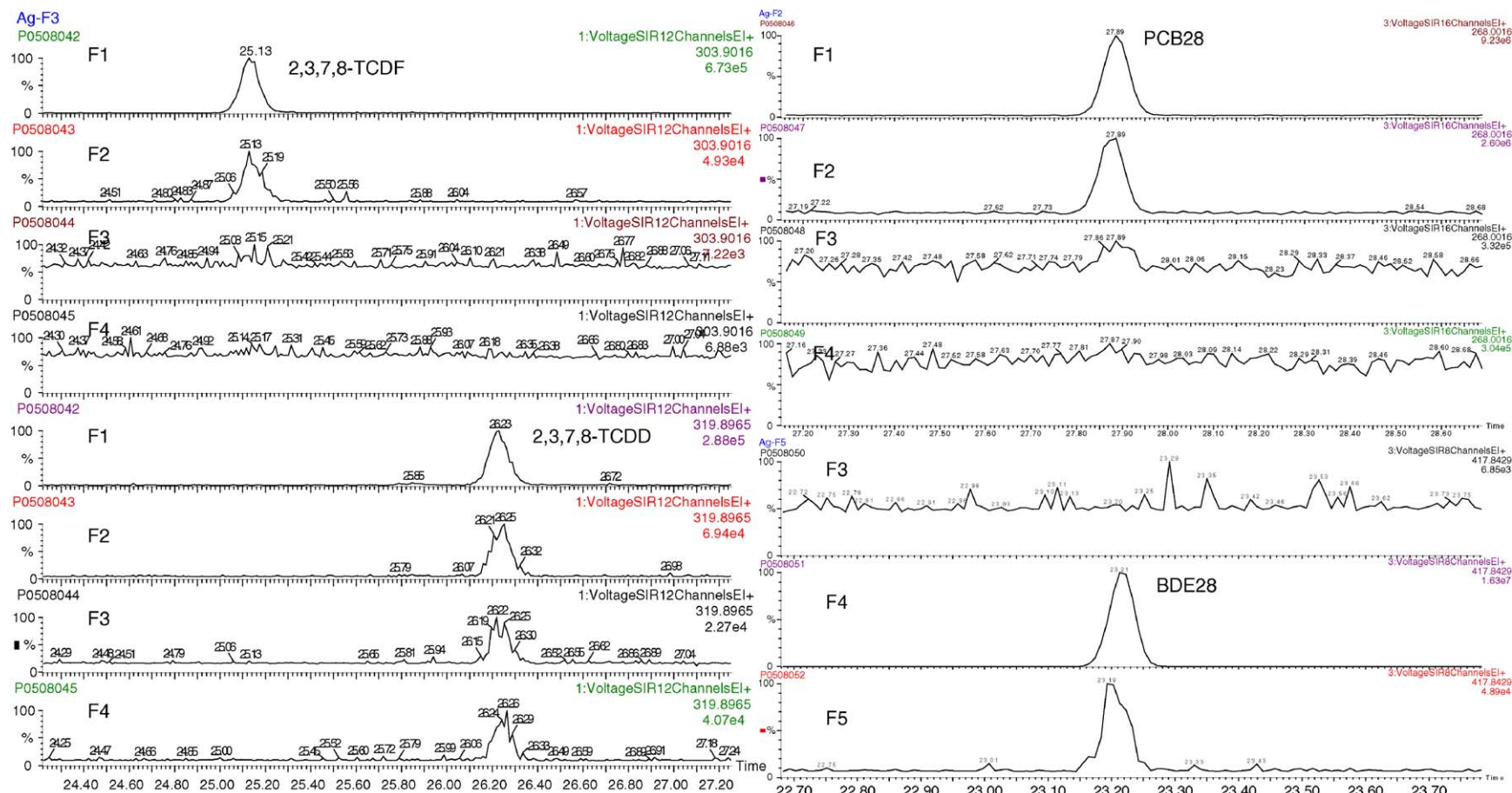


Fig. 1. GC/MS chromatograms of 2,3,7,8-TCDD/F, PCB-28 and BDE-28 in different fractions separated on the AgNO₃ silica column. F1 represents the fraction eluted by using 60 ml hexane. F2 and F3 were the fractions eluted with additional 20 and 30 ml hexane, respectively. F4 represents the fraction eluted by 40 ml 6% DCM in hexane, and F5 was with additional 20 ml of 6% DCM in hexane.

Table 1

Recoveries and relative standard deviation (R.S.D.) ($n = 3$) of PCBs, PCDD/Fs and PBDEs from the analysis of the standard mixture of 1613-LCS, WHO-LCS, MXP and MBDE-LCS

Compounds	#1	#2	#3	Average	R.S.D.
¹³ C-BDE-15	62	43	44	50	22
¹³ C-BDE-28	87	74	81	81	8
¹³ C-BDE-47	125	117	116	119	4
¹³ C-BDE-99	79	79	78	79	1
¹³ C-BDE-153	88	87	84	86	2
¹³ C-BDE-154	98	98	98	98	0
¹³ C-BDE-183	66	62	61	63	4
IS ¹³ C-2378-TCDF	83	65	58	69	18
IS ¹³ C-12378-PeCDF	80	67	65	71	12
IS ¹³ C-23478-PeCDF	82	72	61	72	15
IS ¹³ C-123478-HxCDF	90	75	60	75	20
IS ¹³ C-123678-HxCDF	89	72	60	74	19
IS ¹³ C-234678-HxCDF	88	75	60	74	18
IS ¹³ C-123789-HxCDF	80	72	57	70	17
IS ¹³ C-1234678-HpCDF	78	73	61	71	13
IS ¹³ C-1234789-HpCDF	71	70	60	67	9
IS ¹³ C-2378-TCDD	67	63	53	61	11
IS ¹³ C-12378-PeCDD	79	71	59	70	15
IS ¹³ C-123478-HxCDD	92	80	60	77	21
IS ¹³ C-123678-HxCDD	89	81	57	76	22
IS ¹³ C-1234678-HpCDD	82	73	58	71	17
IS ¹³ C-OCDD	66	62	52	60	12
¹³ C-CB-77	100	88	94	94	6
¹³ C-CB-81	99	90	96	95	5
¹³ C-CB-105	80	90	100	90	11
¹³ C-CB-114	82	87	100	89	11
¹³ C-CB-118	66	84	93	81	17
¹³ C-CB-123	79	89	100	90	12
¹³ C-CB-126	76	79	90	82	9
¹³ C-CB-156	84	89	97	90	8
¹³ C-CB-157	85	89	100	91	8
¹³ C-CB-167	89	87	94	90	4
¹³ C-CB-169	90	88	96	91	5
¹³ C-CB-189	96	89	100	95	6
¹³ C-CB-28	34	60	72	56	35
¹³ C-CB-52	52	68	74	65	17
¹³ C-CB-101	70	72	80	74	7
¹³ C-CB-153	83	79	86	83	4
¹³ C-CB-180	65	84	87	79	15
¹³ C-CB-194	62	77	74	71	12
¹³ C-CB-206	61	76	83	73	16
¹³ C-CB-209	112	144	151	136	15

3.1.2. Further separation and purification of fractions containing PCBs and PCDD/Fs

The separation of PCBs and PCDD/Fs was studied by using different chromatography columns with various solvent mixtures. Florisil chromatography column was found simpler and more efficient, which is accord with previous reports [6,13,14]. Eight centimetres of florisil was filled in the 9 mm i.d. glass column. Thirty-five milliliters of 6% DCM in hexane was selected to elute PCBs, followed by 150 ml of 100% DCM for the elution of PCDD/Fs.

A gel permeation chromatography column was used to remove high molecular weight interferences in the fraction of PCBs. After loading the sample extract containing PCBs, high molecular weight interferences were removed in the first 84 ml

Table 2

Data on PBDEs, PCBs and PCDD/Fs obtained from the analysis of the Certified Reference Material (WMF-01)

Compounds	Measured (pg/g)	Certified (pg/g)	Z-score
BDE-28	3243	3124 ± 290	0.41
BDE-47	123287	123200 ± 24800	0.00
BDE-99	37377	37500 ± 220	0.03
BDE-100	40733	35870 ± 14500	0.34
BDE-153	14165	17040 ± 8000	0.36
BDE-154	18535	19790 ± 2880	0.44
BDE-183	392	532 ± 400	0.35
CB-77	2425	2233 ± 720	0.27
CB-81	154	201 ± 58	0.80
CB-105	60933	49050 ± 14200	0.84
CB-114	4846	3523 ± 1670	0.79
CB-118	154207	130100 ± 32500	0.74
CB-123	4719	4233 ± 2620	0.19
CB-126	848	739 ± 260	0.42
CB-156	17472	14890 ± 5020	0.51
CB-157	4225	3488 ± 870	0.85
CB-167	9351	9750 ± 3090	0.13
CB-169	92	76 ± 30	0.54
CB-189	2263	2016 ± 611	0.40
2378-TCDF	13.75	13.10 ± 4.9	0.13
12378-PeCDF	0.07	1.53 ± 1.4	1.04
23478-PeCDF	7.61	7.15 ± 2.2	0.21
123478-HxCDF	0.27	0.86 ± 1.0	0.59
123678-HxCDF	0.30	0.51 ± 0.7	0.30
234678-HxCDF	0.31	0.68 ± 1.2	0.31
123789-HxCDF	0.05	0.25 ± 0.4	0.50
1234678-HpCDF	0.30	1.01 ± 1.9	0.37
1234789-HpCDF	0.03	0.30 ± 0.5	0.54
OCDF	0.72	1.38 ± 2.1	0.31
2378-TCDD	14.39	13.10 ± 4.4	0.29
12378-PeCDD	3.01	2.72 ± 1.3	0.22
123478-HxCDD	0.03	0.22 ± 0.3	0.63
123678-HxCDD	0.77	0.88 ± 0.4	0.28
123789-HxCDD	0.03	0.27 ± 0.4	0.59
1234678-HpCDD	0.39	0.59 ± 0.7	0.29
OCDD	4.83	3.91 ± 6.2	0.15

of 1:1 DCM:hexane, and PCBs were then eluted with additional 30 ml of 1:1 DCM:hexane. It was found that GPC was efficient for removing the chemicals that interfered with the quantification of PCBs, which is consist with the literature reports [15–17].

Further clean-up for the PCDD/Fs fraction was achieved by using the carbon column chromatography. The sample extract was loaded with 1:1 DCM:cyclohexane and the PCDD/Fs were eluted with 30 ml toluene.

Table 3

Background contamination of PCBs and PBDEs in method blanks ($n = 5$)

Congeners	Average (pg/sample)	R.S.D. (%)
PCB-77	0.21	17.5
PCB-105	2.82	19.3
PCB-118	6.30	17.8
BDE-47	6.94	12.4
BDE-99	3.43	20.5
BDE-153	ND	–

Table 4

Concentrations of PCBs, PCDD/Fs, and PBDEs detected in sediment samples from Haihe River and Dagou Drainage River (pg/g dw)

Name	H1	H2	H3	H6	H7	H8	H9	H10	N1	N3
BDE-15	28.4	40.3	37.4	50.2	19.5	50.0	829.8	363.7	1480.4	9985.6
BDE-17	2.7	2.0	5.3	5.3	2.3	9.8	3.3	1.6	31.7	7.4
BDE-28	12.6	10.1	28.8	16.9	8.1	28.9	17.2	6.7	168.1	201.3
BDE-47	45.1	67.8	158.5	30.3	24.7	69.7	17.4	8.2	756.4	23.0
BDE-49	14.4	13.2	40.0	19.7	9.1	30.4	10.3	4.0	281.3	9.6
BDE-66	10.4	8.6	22.0	8.1	6.9	18.4	2.5	1.0	88.5	3.1
BDE-71	0.7	0.5	1.1	1.2	0.4	2.0	0.3	0.1	2.3	0.3
BDE-77	2.3	1.7	3.6	2.1	1.4	5.7	0.5	0.2	13.3	0.5
BDE-85	1.4	2.5	1.8	1.9	2.0	3.3	0.4	0.1	40.4	1.8
BDE-99	31.2	59.9	183.7	25.5	29.2	26.5	8.8	4.2	983.1	15.8
BDE-100	7.9	22.4	43.4	6.0	5.0	5.4	2.8	1.1	198.3	4.7
BDE-119	0.4	0.4	0.8	0.3	0.2	0.9	0.1	0.1	0.6	0.4
BDE-126	6.4	5.0	8.0	5.9	1.6	16.9	0.6	0.3	12.3	10.0
BDE-138	3.2	1.9	4.1	2.5	2.0	7.7	0.9	0.6	9.8	2.5
BDE-153	18.9	29.9	1.2	29.4	24.6	18.4	4.1	2.1	308.1	6.6
BDE-154	7.0	16.0	19.0	9.2	4.9	4.9	2.0	1.0	113.7	2.4
BDE-183	49.9	19.1	61.0	137.9	48.0	64.2	18.6	5.3	487.5	26.5
Total-PBDEs	242.9	301.3	619.5	352.3	189.8	362.9	919.5	400.4	4975.8	10301.7
CB-77	31.5	112.5	186.3	357.2	173.5	53.2	29.9	13.1	235.0	121.7
CB-81	1.3	1.4	5.8	19.0	1.8	2.6	0.6	0.3	14.7	2.3
CB-105	34.7	48.6	230.6	504.6	84.1	102.7	26.5	11.6	256.8	98.3
CB-114	2.2	2.4	11.1	14.7	2.3	4.2	1.3	0.7	17.4	3.5
CB-118	75.4	102.9	429.1	1094.0	145.9	159.0	99.5	45.9	407.4	633.9
CB-123	3.8	3.8	21.3	44.1	6.7	10.5	5.7	4.5	19.5	73.2
CB-126	2.9	4.6	8.1	31.6	5.1	11.5	5.0	1.7	15.6	30.6
CB-156	9.3	16.0	72.7	156.5	25.8	73.4	13.7	6.5	54.5	62.8
CB-157	3.0	4.8	16.5	53.8	7.3	36.7	5.5	2.3	15.0	29.8
CB-167	4.2	7.4	26.4	66.7	10.9	51.5	9.8	4.0	24.9	57.0
CB-169	0.7	1.0	1.4	8.5	1.4	4.0	0.8	0.3	22.6	2.7
CB-189	1.4	3.1	5.2	32.1	3.5	37.7	5.3	2.0	11.1	22.2
CB-28	381.0	568.4	3591.1	5009.1	1092.8	535.6	294.1	172.3	5767.1	456.5
CB-52	151.0	215.0	727.6	1831.1	342.5	244.7	166.4	121.0	1403.2	247.0
CB-101	89.8	114.8	560.4	1318.1	221.1	361.4	186.7	82.0	725.2	790.5
CB-138	90.5	117.3	622.9	1236.2	209.7	406.5	106.3	59.4	437.4	278.4
CB-153	87.5	118.8	610.4	1533.9	253.7	437.6	186.2	84.0	500.4	577.9
CB-180	28.0	43.7	163.1	712.0	96.9	444.6	100.0	38.0	205.6	313.5
CB-209	31.4	60.9	200.8	933.5	156.8	495.3	1522.8	242.3	225.5	7187.7
Total-PCBs	1029.5	1547.4	7490.6	14956.4	2841.7	3472.5	2766.0	891.7	10358.7	10989.4
2378-TCDF	2.1	1.8	3.5	4.2	1.7	3.5	1.6	0.9	7.2	3.4
12378-PeCDF	2.1	2.0	0.9	1.7	0.5	5.5	1.3	0.3	8.6	4.9
23478-PeCDF	2.2	0.7	1.8	1.4	0.9	7.3	0.7	0.4	2.1	0.3
123478-HxCDF	3.6	6.6	6.5	13.6	4.7	76.5	17.9	7.4	37.8	125.3
123678-HxCDF	2.1	2.0	0.6	5.1	1.6	24.3	2.4	0.1	5.7	15.1
234678-HxCDF	1.5	1.9	0.9	3.9	1.4	21.5	3.2	1.4	6.2	35.0
123789-HxCDF	0.3	0.7	1.3	0.1	0.1	0.1	0.1	0.1	0.2	0.2
1234678-HpCDF	5.9	10.5	13.3	28.7	9.6	335.0	25.5	8.6	37.1	423.4
1234789-HpCDF	1.0	2.6	1.5	6.0	2.2	54.1	6.1	2.1	7.4	98.9
OCDF	7.8	19.3	25.9	69.5	23.9	721.9	141.2	47.0	71.6	3119.6
2378-TCDD	0.4	0.7	0.9	0.5	0.1	0.5	0.5	0.3	0.1	1.8
12378-PeCDD	0.1	0.4	0.8	0.1	0.1	0.1	0.9	0.5	0.2	0.2
123478-HxCDD	0.4	0.9	0.9	2.7	0.8	11.0	17.9	5.7	12.3	74.4
123678-HxCDD	0.3	2.3	0.9	13.1	5.3	61.6	12.6	3.8	13.0	141.3
123789-HxCDD	0.6	1.4	0.9	7.5	2.0	32.9	7.0	2.3	9.8	41.7
1234678-HpCDD	8.7	60.0	69.6	199.8	57.9	1056.6	271.2	80.8	215.0	3091.8
OCDD	63.4	333.1	326.7	984.1	317.2	5360.6	2928.6	992.3	2171.6	54147.4
Total-PCDD/Fs	102.7	446.7	457.1	1342.0	429.8	7773.1	3438.6	1153.8	2605.8	61324.7

3.2. Method validation

Method performance was evaluated by triplicate analyses of mixed standards including MBDE-MXC, 1613-LCS MXP and WP-LCS. The average recoveries and relative standard deviation (R.S.D.) of PBDEs, PCDD/Fs and PCBs are listed in Table 1. The results met the acceptance criteria specified in the US-EPA methods 1614-draft (25–150%), 1613B (17–185%) and 1668A (25–150%).

CRM sample (WMF-01) was analyzed to validate the developed single analysis method for the PBDEs, PCBs and PCDD/Fs. The results were satisfied with Z -score ≤ 1 for all congeners. The recoveries of PBDEs, PCBs and PCDD/Fs were 91–110, 64–101 and 78–101%, respectively, which again met the criteria specified in US-EPA method 1614-draft, 1668A and 1613B. Congener-specific concentrations of three groups of chemicals in WMF-01 are summarized in Table 2 and compared with the certified values.

3.3. Quantitative analysis of sediment samples

The method was applied for the analysis of 10 sediment samples collected from Haihe River and Dagou Drainage River in Tianjin City. Seventeen 2,3,7,8-substituted chlorinated congeners of PCDD/Fs, 12 WHO toxic congeners of PCBs, 6 indicator PCBs (PCB-28, -52, -101, -138, -153 and -180) and PCB-209 as well as 17 PBDEs (BDE-15, -17, -28, -47, -49, -66, -71, -77, -85, -99, -100, -119, -126, -138, -153, -154 and -183) were quantitatively determined. The background contamination of PCBs and PBDEs in method blanks is listed in Table 3. Concentrations of PBDEs, PCBs and PCDD/Fs determined in the sediment samples were listed in Table 4. Average recoveries for PCBs, PCDD/Fs and PBDEs are 45–92, 67–79 and 64–110%, respectively, which met the criteria specified in US-EPA methods 1668A, 1613 and 1614-draft.

The obtained results indicated that sediments from Haihe River were contaminated with PBDEs, PCBs and PCDD/Fs. The concentrations of PBDEs, PCBs and PCDD/Fs in the sediments from Haihe River were 189.8–10301.7 pg/g dry weight (dw), 891.7–14956.4 pg/g dw and 102.7–61324.7 pg/g dw, respectively. Serious PCDD/Fs pollution was found in Dagou Drainage River that is a municipal waste water discharging river. The detected profiles of PCDD/Fs show that the production of pentachlorophenol (PCP) or PCP-Na in this area may be the principal pollution source of PCDD/Fs, which is in accord with previously reported data [10]. The levels of PCBs and PCDD/Fs in site H10 were lower, compared to the results obtained from the previous sediment samples collected in July 2003. The difference in concentration may be due to the different sampling time because the samples analyzed in this study were collected during the flood season and the previously reported data referred to the samples collected in November. The contamination of PBDEs was investigated in this area for the first time. The results indicate that the contamination levels of PBDEs

were low in Haihe River and Dagou Drainage River in Tianjin City.

4. Conclusion

A more convenient and stable sample preparation procedure has been developed to allow the determination of PBDEs, PCBs and PCDD/Fs in one single environmental sample. Silver nitrate silica was successfully used to separate PBDEs from PCBs and PCDD/Fs. The entire method was validated through the analysis of WMF-01 certified reference fish tissue. The performance of the method is satisfied. The method was applied to analyze sediment samples. Contamination levels of PBDEs were first reported for the sediment sample collection areas, along with PCBs and PCDD/Fs levels compared with the data reported previously.

Acknowledgements

This work is jointly supported by National Basic Research Program of China (2003CB415001) and the State Hi-tech. Development Plan (2002AA601011). Jiang and Cai would also like to acknowledge the Distinguished Young Scholar Award of the National Science Foundation of China (20329701).

References

- [1] E. Eljarrat, A. De La Cal, D. Larrazabal, B. Fabrellas, A.R. Fernandez-Alba, F. Borrull, R.M. Marce, D. Barcelo, *Environ. Pollut.* 136 (2005) 493.
- [2] G. Falcó, A. Bocio, J.M. Llobet, J.L. Domingo, *Food Chem. Toxicol.* 43 (2005) 1713.
- [3] A. Fernandes, S. White, K. D'Silva, M. Rose, *Talanta* 63 (2004) 1147.
- [4] S. Litten, D.J. Mcchesney, M.C. Hamilton, B. Fowler, *Environ. Sci. Technol.* 37 (2003) 5502.
- [5] C. Pirard, E. De Pauw, J.-F. Focant, *J. Chromatogr. A* 998 (2003) 169.
- [6] H. Liu, Q. Zhang, Z. Cai, A. Li, Y. Wang, G. Jiang, *Anal. Chim. Acta*, in press.
- [7] E. Eljarrat, A. de la Cal, D. Barcelo, *J. Chromatogr. A* 1008 (2003) 181.
- [8] E. Eljarrat, D. Barcelo, *Trends Anal. Chem.* 23 (2004) 727.
- [9] M. Alaei, in: R. Clement, B. Burk (Eds.), *Proceedings of the Fourth Biennial International Conference on Monitoring and Measurement of the Environment*, Toronto, 2002, p. 309.
- [10] Q. Zhang, Study on characteristics of dioxin-like compounds in Taihu Lake and Haihe River basin in Tianjin, Ph.D. Thesis, Chinese Academy of Sciences, Beijing, 2004, p. 87.
- [11] R. Yang, A. Lv, J. Shi, G. Jiang, *Chemosphere* 61 (2005) 347.
- [12] A. Martínez, M. Ramil, R. Montes, D. Hernanz, E. Rubí, I. Rodríguez, R. Cela Torrijos, *J. Chromatogr. A* 1072 (2005) 83.
- [13] E. Aries, D.R. Anderson, N. Ordsmith, K. Hall, R. Fisher, *Chemosphere* 54 (2004) 23.
- [14] L. Ramos, L.M. Hernandez, M.J. Gonzalez, *J. Chromatogr. A* 759 (1997) 127.
- [15] L.G.M.Th. Tuinstra, W.A. Traag, J.A. van Rhijn, P.F.V.D. Spreng, *Chemosphere* 29 (1994) 1859.
- [16] R. Lega, G. Ladwig, O. Meresz, R.E. Clement, G. Crawford, R. Salemi, Y. Jones, *Chemosphere* 34 (1997) 1705.
- [17] K. Saito, A. Sjödin, C.D. Sandau, M.D. Davis, H. Nakazawa, Y. Matsuki, D.G. Patterson, *Chemosphere* 57 (2004) 373.

Subcellular distribution of rare earth elements and characterization of their binding species in a newly discovered hyperaccumulator *Pronephrium simplex*

Ying Lai, Qiuquan Wang*, Limin Yang, Benli Huang

Department of Chemistry and the MOE Key Laboratory of Analytical Sciences, Xiamen University, Xiamen 361005, China

Received 31 October 2005; received in revised form 17 December 2005; accepted 22 December 2005

Abstract

Subcellular distribution of rare earth elements (REEs, including 14 lanthanides and yttrium) in a newly discovered REE hyperaccumulator, *Pronephrium simplex* (*P. simplex*), was determined by a chemical sequence extraction followed by ICP-MS analysis. Results showed that most REEs are associated with cell wall and proteins, and REEs concentration in the proteins, $2899.5 \mu\text{g g}^{-1}$, is much higher than those in the cell wall; in the chloroplast of *P. simplex*, REEs distribute almost equally in chloroplast membrane and thylakoid, while most REEs in the thylakoid are binding with photosystem II (PS II); a new REE-binding peptide in the lamina of *P. simplex*, which can accumulate REEs up to $3000 \mu\text{g g}^{-1}$ and has higher affinity with light REEs, was characterized, indicating that its molecular mass is 5073 Da, and may have β -sheet structure; isoelectrofocusing electrophoretic photograph indicated that it is acidic peptide with IP of 3.7. Such information should be useful for understanding of both the storage and physiological role of REEs in *P. simplex* and further studies on the phytoremediation of REEs contaminated environments.

© 2006 Published by Elsevier B.V.

Keywords: Hyperaccumulator; Fern; Rare earth elements; Protein; Chloroplast; Photosystem II

1. Introduction

Rare earth elements (REEs) have been widely used in agricultural activities, and the resulted environmental contamination and accumulation in food chain would grow rapidly in the next few decades [1]. Phytoremediation, a technique using plant hyperaccumulator to remove contamination from soil and water, is a good choice as it is safe and cost-effective. Although the hyperaccumulators of other heavy metals were intensively studied [2], less attention was paid to REE-hyperaccumulator. REEs are very likely to exist in certain special forms in plants, and play important role in regular physiological activities. However, there always have been controversial opinions on whether REE can enter into plant cells and influence their physiological activities. Nagahashi et al. [3] have reported that the casparian strip could provide effective barrier to apoplastic movement of lanthanum. Moreover, in early stage many researchers believed that

although REEs could bind to the surface of cells, they could not pass the membrane and enter into the cell [4]. Recently, scientists discovered that low level of REE could easily pass across the membrane with the help of some carriers, such as protein, hormone, etc. [5–7]. Our previous study by electrospray ionization mass spectrometry (ESI-MS) showed that lanthanum could not only pass across cell wall but also enter into chlorophyll-*a* and form a double decker sandwich like complex in spinach under the stress of La^{3+} [8]. The results from Shan and co-workers [9,10] and Wei et al. [11] also showed that although most of REEs were deposited on cell wall, the rest of REEs could indeed enter into the interior, some even enter into the chloroplast of *Dicranopteris dichotoma* (*D. dichotoma*), a famous REE-hyperaccumulator. However, great difference was found between the results from different researchers concerning REEs distribution in the cell of *D. dichotoma* [9,11,12]. Different fractionation methods might be responsible for the great difference. Furthermore, researches on the mechanism of REE hyperaccumulation at molecular level is too few compared to those of other heavy metals, although the results obtained are somewhat inspiring [13–15]. Guo et al. [13] discovered two REE binding

* Corresponding author. Tel.: +86 592 218 1796; fax: +86 592 218 1796.
E-mail address: qqwang@xum.edu.cn (Q. Wang).

proteins from *D. dichotoma* by size exclusion chromatography (SEC) and neutron activation analysis (NAA), one of them has the molecular mass of about 8.0×10^5 Da and the other less than 12,400 Da. Wang et al. [14] found one REE binding peptide of 2208 Da from the same plant through ICP-MS and MALDI-MS analysis.

Most recently, a new REE-hyperaccumulator, *Pronephrium simplex* (*P. simplex*), which can accumulate REEs up to 1.2 mg g^{-1} dry lamina mass, was discovered in Nanjing natural reservation of semi-tropical rain forest of China [15]. In the present work, a chemical sequence extraction combined with ultracentrifuge fractionation and ICP-MS analysis was proposed to investigate the subcellular distribution of REEs in *P. simplex*. A possible REE binding peptide in its laminae was recognized by size exclusion chromatography coupled with ICP-MS, and characterized by ESI-MS, isoelectrofocusing electrophoresis (IEF) and IR.

2. Experimental

2.1. Instrumentation

Beckman Avanti™ J-25 refrigerated centrifuge and Hitachi SCP 55H refrigerated ultracentrifuge were used for subcellular component fractionation. An ELAN DRC II ICP-MS (Perkin-Elmer SCIEX, USA) was used for the determination of REEs. The working conditions were shown in Table 1.

ESI-MS was performed on Bruker ESQUIRE-LC™ ion trap MS (Bremen, Germany). IEF was performed on DYY-10C electrophoresis apparatus with DYCZ-27B electrophoresis tank (Beijing Liu Yi instrument plant, China). Avater 360 FT-IR spectrometer (Nicolet, USA) was used to obtain the IR spectrum of REE binding peptide.

2.2. Reagents and samples

REE oxides (purity >99.9999%) were obtained from Changchun Institute of Applied Chemistry of Chinese Academy of Science. 2-Mercaptoethanol was purchased from



Fig. 1. The photograph of *P. simplex* in Nanjing natural reservation of semi-tropical rain forest, Fujian province of China (north latitude: $24^{\circ}56'20''$; east longitude: $117^{\circ}11'30''$).

Sigma, sodium dodecylsulfonate (SDS) from TCI (Japan), phenylmethylsulfonyl fluoride (PMSF), Triton X-100 and 2-(*N*-morpholino) ethane sulfonic acid (MES, ultra pure) from AMESCO, dithioerythritol (DTT) (>99.0%), acrylamide (>99.9%), bis-acrylamide (>99.9%), nonidet P-40 (NP-40), urea (>99.5%), tetraethylethylenediamine (TEMED) (>99.0%) and ammonium persulphate (>98.0%) from BBI (Canada), isoelectric focusing calibration kit Broad PI (pH 3.0–10.0) and Ampholine™ (pH 3.5–10) from Amersham (Sweden). All other reagents were at least of AR or BR grade.

P. simplex is a short creeping fern that grows in forest or on stream banks at low altitudes distributing mainly in China, Viet Nam and Japan (Ryukyu Islands). *P. simplex* and its host soil were collected from Nanjing natural reservation of semi-tropical rain forest, Fujian province of China (north latitude: $24^{\circ}56'20''$; east longitude: $117^{\circ}11'30''$). The photograph of this fern is shown in Fig. 1.

2.3. Cell fractionation of *P. simplex* lamina

Cell fractionation method I adopted the protocol described by Shan et al. [9]. The finally resulted precipitation by this method was designated as crude proteins and further subject to SEC-ICP-MS analysis using the conditions described in our previous work [15]. The separated REE binding peptide was further characterized by ESI-MS, IEF and IR spectrum. Cell fractionation method II adopted the protocol described by Wei et al. [11] with slight modifications.

Cell fractionation method III was established according to published references [12,16]. Detailed procedures are: (1) 10 g Fern laminae were ground to powder under liquid N_2 , dried in shade, and extracted with ether for 8 h (soxhlet extraction) to get crude lipids; (2) the resulted residue I was extracted with 150 mL boiling water for 3.5 h (repeat three times), combine

Table 1
Working conditions of ELAN DRC II ICP-MS

Parameter	Setting value
Nebulizer gas	0.96 L min^{-1}
Auxiliary gas	1.2 L min^{-1}
Plasma gas	15 L min^{-1}
Makeup gas	0.18 L min^{-1}
Lens voltage	6.6 V
ICP RF power	1100 W
Analog stage voltage	−1750 V
Pulse stage voltage	1050 V
Sample flush	20 s
Read delay	15 s
Est. reading time	8.48 s
Replicate	3
Detect isotopes	^{89}Y , ^{139}La , ^{140}Ce , ^{141}Pr , ^{143}Nd , ^{147}Sm , ^{153}Eu , ^{155}Gd , ^{159}Tb , ^{161}Dy , ^{165}Ho , ^{166}Er , ^{169}Tm , ^{172}Yb , ^{175}Lu

all the solutions and centrifuge at $800 \times g$ for 10 min; (3) the supernatant obtained from step 2 was concentrated to 50 mL with rotary evaporator under reduced pressure, then 250 mL ethanol was added and placed overnight, the resulted precipitation is crude polysaccharides; (4) the residue obtained from step 2 was extracted with 100 mL 0.1 mol L^{-1} NaOH at 80°C for 2 h (repeat two times), combine all the solutions and centrifuge at $10,000 \times g$ for 10 min. The resulted supernatant is crude proteins, and the residue is cellulose and pectin, which are the main components of cell wall. The crude polysaccharides obtained was further extracted with chloroform–normal butyl alcohol (4:1) for seven times to remove proteins and finally got purer polysaccharides. The chloroplast of *P. simplex* was extracted and fractionated by using the procedures previously proposed [17].

2.4. Determination of REEs by ICP-MS

All fractions obtained from lamina tissue or chloroplast fractionation were dried at 105°C for 24 h, weighed, and digested by $\text{HNO}_3\text{--HClO}_4$ (5:1) for the determination of REEs content by ICP-MS. Proteins and all other soluble fractions were also digested and diluted to an appropriate volume for ICP-MS determination. Protein concentration was determined by G-250 method [18].

REEs content in the soil sample was determined by ICP-MS after dried and ground and digested with the mixture of $\text{HNO}_3/\text{HF}/\text{HClO}_4$ (5:1:1). Bioavailable REEs in the host soil were obtained by extracting with 0.11 mol L^{-1} acetic acid [19].

2.5. Determination of the isoelectric point of REE binding peptide by IEF

The method proposed by He et al. [20] was modified to determine the IP of the REE binding peptide obtained. The ampholyte, AmpholineTM, of pH 3.5–10 was adopted for building the pH gradient. The migration conditions for isoelectric focusing were modified as follows: at beginning 200 V for 30 min, then gradually ramped to 1000 V and kept constant for 15 h; and then ramped to 1100 V and kept for 1 h. Finally, the focusing gels were stained with Coomassie blue R-250.

3. Results and discussion

3.1. Comparison of three cell fractionation methods and determination of REEs contents in different subcellular fractions of *P. simplex* lamina

The results shown in Table 2 indicated that large amount of REEs are binding with cell walls, which coincides with those in literatures [9,11,12]. However the exact values of REEs contents in the cell walls obtained from the three methods are quite different. As far as methods I and II are concerned, in order to retain the biological activity of biomolecules as much as possible, all the experiments are conducted under very mild conditions, resulting in low extraction efficiency. However, it is inapplicable to improve extraction efficiency only by increas-

Table 2

$\sum \text{REE}$ of subcellular fractions obtained by methods I–III ($\mu\text{g g}^{-1}$ fresh lamina weight)^a

	$\sum \text{REE}^b$	% ^c
Method I		
Cell wall	381.5	88.6
Cell debris	1.53	0.35
Crude proteins	7.36	1.7
Free amino acids and pigments	40.1	9.3
Lamina	430.5	
Method II		
Cell wall	394.2	94.9
Organelle	4.3	1.03
Cell membrane	1.8	0.43
Soluble fraction	15.3	3.68
Lamina	415.6	
Method III		
Crude lipids	11.7	2.6
Crude polysaccharides	2.1	0.47
Crude proteins	131.6	28.8
Cellulose and pectin	310.9	68.1
Lamina	456.2	

^a Three measurements for each sample, R.S.D. < 5%.

^b $\sum \text{REE}$ is the sum of the concentrations of 15 REEs.

^c % means the percentage of $\sum \text{REE}$ in each fraction of lamina to that of the whole lamina.

ing the solvent amount and extraction times. A relatively violent method should be therefore established to make extraction more efficient and quantificational. Based on such a consideration, a scheme of chemical sequence treatment was adopted, which extracts lipid by ether, gets total polysaccharides through boiling water, obtains total proteins by dilute base, and the finally resulted residue are the main components, cellulose and pectin of cell wall. The results obtained indicated that about 68% REEs are located in the cell wall of *P. simplex*. It is well known that pectin acid in cell wall is a kind of polygalacturonic acid, and most of its carboxyl groups have not been esterified, they can therefore provide many binding sites for metal ions. It has been proved that large amount of Ca is stored in cell wall as calcium pectinate to reinforce the cell wall. Since the ratio of charge to ionic radius of REE is higher than that of calcium, REEs may have higher intensity to bind with pectin acid [21,22]. It might be inferred that most REEs are deposited as REE–pectin acid complexes in cell wall when they translocate in the plant. However, about 30% REEs can still pass across the cell wall and bind with proteins. It is very likely that REE could regulate and control the physiologic function of the hyperaccumulator, *P. Simplex*, through the interactions with certain proteins. As for polysaccharide and lipid, they have much lower REE content, and cannot be the main reason of REE hyperaccumulation.

The distribution patterns of REEs in the subcellular components of *P. simplex* lamina obtained by cell fractionation method III, the host soil (H-soil) and the bioavailable fraction of the host soil (BAF-H-soil) are shown in Fig. 2 as Masuda–Coryell diagrams [23,24]. BAF-H-soil present light REE enrichment pattern ($\sum \text{LREE}/\sum \text{HREE} = 3.33$) compared with that of H-soil (1.91). All the subcellular components present light REE enrichment pattern, especially the protein fraction (4.51), sug-

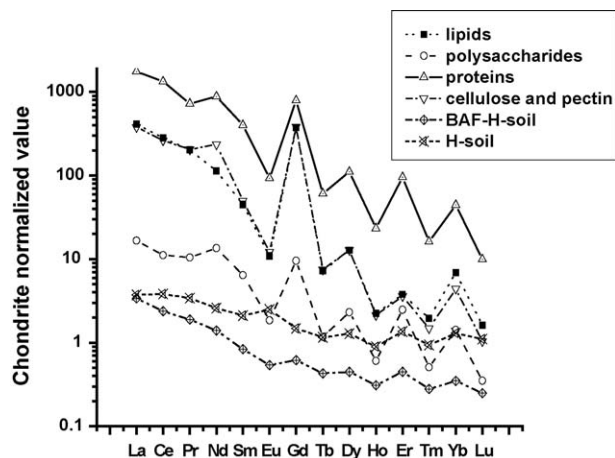


Fig. 2. Chondrite normalized REE patterns of subcellular components, host soil (H-soil) and bioavailable fraction of host soil (BAF-H-soil) of *P. simplex*.

gesting selective uptake of light REEs by this fern. Furthermore, the amount of light REEs such as La, Ce, Pr and Nd account for 84.9% of total REEs in the protein fraction, indicating that light REEs may have much stronger intensity to bind with the proteins than heavy ones. REEs concentration in different subcellular components listed in Table 3 also indicated that proteins have much higher intensity to accumulate REEs than those of the others. If REEs deposition in cell wall is passive and uncontrollable to some extent, accumulation of REEs by the proteins in *P. simplex* should be an initiative behavior.

3.2. REE distribution in the chloroplast of *P. simplex* laminae

Chloroplast is the organelle where photosynthesis occurs in green plant cells. It is surrounded by double membranes. Inside the inner membrane is thylakoid, which contains photosystem I (PS I) and photosystem II (PS II) [25,26]. The cooperation of these two systems makes the whole photosynthesis. It is well known that suitable amount of REEs can improve the photosynthesis of green plants; the binding sites of REEs in chloroplast are thus attracting more and more attention for understanding REE functions during plant growing. Karukstis et al. [27] showed that REE ion could interact with the membrane of thylakoid by electrostatic attraction, since the mutual attraction exists between the negative charged membrane and the positive charged REE ion under physiological conditions [28]. PS II is suggested to be another important existing place for REEs, the negatively charged carboxyl groups of aspartic acid and glutamic acid in

Table 3
REE contents in biological molecules of *P. simplex* laminae ($\mu\text{g g}^{-1}$ dry weight)^a

	$\sum \text{REE}^b$ ($\mu\text{g g}^{-1}$)
Crude lipids	620.6
Polysaccharides (deproteinization)	32.5
Crude proteins	2899.5
Cellulose and pectin	672.9

^a Three measurements for each sample, R.S.D. < 5%.

^b $\sum \text{REE}$ is the sum of the concentrations of 15 REEs.

Table 4

REEs content ($\mu\text{g mg}^{-1}$ chl's chloroplast)^a in subcomponents of chloroplast

	$\sum \text{REE}^b$	% ^c
Chloroplast	10.4	100
Chloroplast membrane	4.9	46.6
Thylakoid	5.6	53.4
PS I ^d	0.66	6.4
PS II	4.9	47.1

^a REEs content in subcomponents of chloroplast containing 1 mg chlorophyll.

^b The sum of the concentrations of 15 REEs.

^c % means the percentage of $\sum \text{REEs}$ in each fraction of chloroplast to that of the whole chloroplast.

^d Soluble fraction rich of PS I.

PS II could provide possible binding sites for REEs under physiological pH condition [29]. Ono [30] reported that lanthanides could replace the functional calcium presenting in the photosynthetic oxygen-evolving center (OEC) of PS II. Kruk et al. [31] proposed that the 33 kDa protein of PS II contained one lanthanide low-affinity binding site. We also observed that in lanthanum cultured spinach, lanthanum could not only partly replacing magnesium in the chlorophyll, but also share the common binding sites of PS II proteins together with the inorganic cofactors of calcium and manganese [17]. In order to get further understanding of the influence of REEs on photosynthesis, the chloroplast of *P. simplex* was fractionated and REEs concentration in each fraction was determined. Results were shown in Table 4.

In the chloroplast of *P. simplex*, 46.6% REEs associate with chloroplast membrane and 53.4% REEs are located in thylakoid. Nearly half (47.1%) of the total amount of REEs in the chloroplast is associated with PS II in the thylakoid, while only 6.4% REEs is found in the fraction of PS I. All these results indicated that the main compartment of REE influencing photosynthesis of *P. simplex* is PS II.

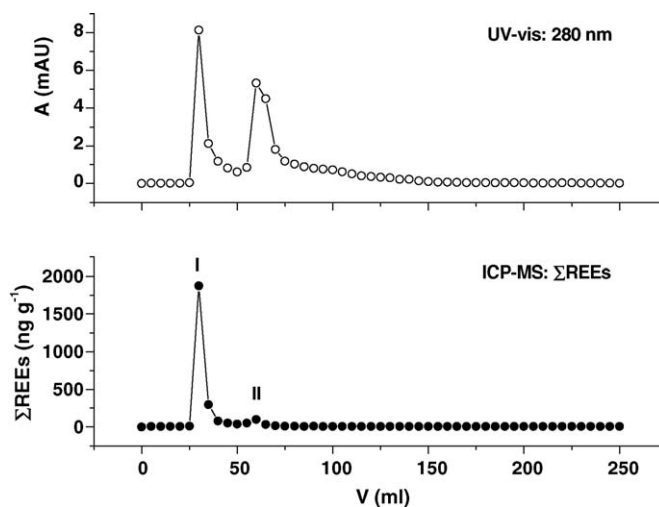


Fig. 3. Elution profiles of *P. simplex* proteins with Sephadex G-25 coupled to ICP-MS detection; stationary phase, Sephadex G-25; column, 10 mm i.d. \times 500 length mm; mobile phase, 50 mM Tris-HCl (pH 8.0); flow rate, 1 ml min⁻¹; column temperature (298 \pm 1)K. The working conditions of ICP-MS were described in Table 1.

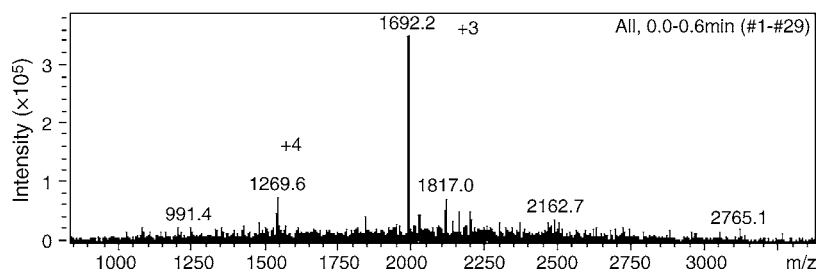


Fig. 4. ESI-MS spectrum of REE binding peptide in *P. simplex*.

3.3. Preliminary characterization of REE binding peptide in *P. simplex*

Since the protein fraction of *P. simplex* laminae has the highest REEs content, one dominating REE binding peptide (protein I in Fig. 3) was separated and determined by SEC-ICP-MS from the Tris–HCl extractable proteins of *P. simplex*, and further characterized by ESI-MS, IEF and IR spectrum. The preference for light REEs of this peptide might partly explain light REEs enrichment in *P. simplex*. ESI-MS spectrum shown in Fig. 4 indicated that the calculated molecular mass of the peptide is 5073 Da that is in accordance with our previous result obtained by MALDI–TOF-MS.

Furthermore, it could be calculated from IEF photograph that the isoelectric point of this peptide is about 3.7. It has been proved by amino acid analysis with HPLC that the peptide contains much more acidic amino acids such as glutamic acid and aspartic acid than basic amino acids such as arginine and lysine [15]. What worthy of note is that this acidic peptide may be negatively charged under physiological pH condition, which makes it possible to provide binding sites for REEs. IR spectrum showed that the amide I band of this peptide is around 1632 cm^{-1} , indicating that the peptide may contain β -sheet structure according to empirical rule [32].

4. Conclusion

The proposed chemical sequence extraction combined with ultracentrifuge fractionation and ICP-MS analysis could provide reliable subcellular distribution of REEs in *P. simplex* laminae. Cellulose and pectin, proteins are the main storage of REEs in *P. simplex*; PS II is found to be the main compartment of REEs in the chloroplast of *P. simplex*, giving the evidence that REEs participate in the photosynthetic process of the plant; the REE-binding peptide characterized in the lamina of *P. simplex* offers a clue to understand the hyperaccumulation of REEs by *P. simplex*. Moreover, this is also important for the phytoremediation of REE-contaminated environment by this fern and more possible transgenic hyperaccumulators of high biomass in the future.

Acknowledgements

This work was financially supported by National Basic Research Program of China (No. 2003CCA00500) and National Natural Science Foundation of China (Nos. 20535020,

20475046 and 20175019). We are also grateful to Dr. Zhenji Li of Department of Biology, Xiamen University, and Mr. Guozhong Lin of Nanjing National Natural Reservation of semi-tropical rain forest for helping us in sampling *P. simplex*. We appreciate the comments of anonymous referees on this paper.

References

- [1] A.A. Volokh, A.V. Gorbunov, S.F. Gundorina, B.A. Revich, M.V. Frontasyeva, C.S. Pal, Sci. Total Environ. 95 (1990) 141.
- [2] D.E. Salt, R.D. Smith, I. Raskin, Annu. Rev. Plant Physiol. Plant Mol. Biol. 49 (1998) 643.
- [3] G. Nagahashi, W.W. Thomson, R.T. Leonard, Science 183 (1974) 670.
- [4] G.X. Xu, Rare Earth, vol. 2, 2nd edn., Metallurgical industry publishing house, Beijing, 1995, p. 491 (in Chinese).
- [5] Y. Cheng, B. Chen, J. Lu, K. Wang, J. Inorg. Biochem. 69 (2) (1998) 1.
- [6] P. Yang, H.Z. Du, S.W. Xue, Chin. Sci. Bull. 47 (2002) 1518.
- [7] S.W. Mo, H.L. Chen, N. Liu, Y.P. Yu, J.N. Jin, J. Sichuan Univ. (Nat. Sci. Edn.) 35 (1998) 875 (in Chinese).
- [8] Q.Q. Wang, Y. Lai, L.M. Yang, B.L. Huang, Anal. Sci. 17 (2001) 789.
- [9] X.Q. Shan, H.O. Wang, S.Z. Zhang, H.F. Zhou, Y. Zheng, H. Yu, B. Wen, Plant Sci. 165 (2003) 1343.
- [10] X.P. Wang, X.Q. Shan, S.Z. Zhang, B. Wen, Anal. Bioanal. Chem. 376 (2003) 913.
- [11] Z.G. Wei, F.S. Hong, M. Yin, H.X. Li, F. Hu, G.W. Zhao, J.W.C. Wong, Microchem. J. 80 (2005) 1.
- [12] Z.Y. Zhang, Y.Q. Wang, J.X. Sun, F.L. Li, Chin. Rare Earth 21 (3) (2000) 42 (in Chinese).
- [13] F.Q. Guo, Y.Q. Wang, J.X. Sun, H.M. Chen, L. Xu, G.Y. Cao, J. Radioanal. Nucl. Ch. 18 (3) (1996) 133.
- [14] H. Wang, X.Q. Shan, S.Z. Zhang, Anal. Bioanal. Chem. 376 (2003) 49.
- [15] Y. Lai, Q.Q. Wang, W.W. Yan, L.M. Yang, B.L. Huang, J. Anal. At. Spectrom. 20 (2005) 751.
- [16] Y.Q. Wang, F.Q. Guo, L. Xu, H.M. Chen, J.X. Sun, G.Y. Cao, Nucl. Techniq. 22 (3) (1999) 160 (in Chinese).
- [17] W.W. Yan, L.M. Yang, Q.Q. Wang, Chin. Sci. Bull. 50 (2005) 1714.
- [18] M.M. Bradford, Anal. Biochem. 72 (1976) 248.
- [19] T. Serife, K. Senol, E. Latif, Anal. Chim. Acta 413 (2000) 33.
- [20] Z.X. He, S.Z. Zhang, Electrophoresis, Science Press, Beijing, 1999, p.155 (in Chinese).
- [21] L.H. Rao, Mineral Nutrition of Plant and its Diagnosis, Agriculture Press, Beijing, 1993, p. 5 (in Chinese).
- [22] X.M. Xie, L. Xu, J.B. Cai, L.X. Zha, B.X. Huang, Chin. Rare Earth 20 (1) (1999) 61 (in Chinese).
- [23] A. Masuda, J. Earth Sci. Nagoya Univ. 10 (1962) 173.
- [24] C.G. Coryell, J.W. Chase, J.W. Winchester, J. Geophys. Res. 68 (1963) 559.
- [25] B. Anderson, J.M. Anderson, Biochim. Biophys. Acta 593 (1980) 427.
- [26] J.M. Anderson, FEBS Lett. 124 (1981) 1.

- [27] K.K. Karukstis, M.Y. Kao, D.A. Savin, R.A. Bittker, K.J. Kaphengst, C.M. Emetarom, N.R. Naito, D.Y. Takamoto, *J. Phys. Chem.* 99 (1995) 4339.
- [28] H.Y. Nakatani, J. Barber, J.A. Forrester, *Biochim. Biophys. Acta* 504 (1978) 215.
- [29] Y. Yamamoto, S. Nakayama, C.L. Cohn, D.W. Krogmann, *Arch. Biochem. Biophys.* 255 (1987) 156.
- [30] T. Ono, *J. Inorg. Biochem.* 82 (2000) 85.
- [31] J. Kruk, K. Burda, M. Jemioła-Rzeminska, K. Strzalka, *Biochemistry* 42 (2003) 14862.
- [32] J.G. Wu, *Recent Techniques and Application of Fourier Transform Infrared Spectrum*, vol. 2, 1st ed., Scientific and Technical Documents Publishing House, 1994, p. 193 (in Chinese).

PVC matrix membrane sensor for fluorescent determination of phosphate

Xucong Lin^a, Xiaoping Wu^a, Zenghong Xie^{a,*}, Kwok-Yin Wong^b

^a Institute of Food Safety and Environmental Monitoring, Department of Chemistry, Fuzhou University, Fuzhou, Fujian 350002, China

^b Department of Applied Biology and Chemical Technology, The Hong Kong Polytechnic University, Hunghom, Kowloon, Hong Kong, China

Received 31 October 2005; received in revised form 22 December 2005; accepted 20 January 2006

Available online 3 March 2006

Abstract

A novel polyvinyl chloride (PVC) matrix membrane sensor responsive to inorganic phosphate ion was described. The working pH range is 4.0–6.0 and the response time is about 7.5 min. Under the optimum condition, the sensor displayed a good linear response for H_2PO_4^- anion over the concentration range 6.00–15.00 $\mu\text{g/ml}$ with a limit detection of 0.02 $\mu\text{g/ml}$. The life span of membrane sensors is 90–120 days, and it could be used for 60 times with several supplements of the fluorescent probe. Applied for the determination of phosphate at levels of 8.00–12.00 $\mu\text{g/ml}$ in artificial seawater, the recoveries ranged from 96.6% to 103.8%, and the relative standard deviation was less than 4%.

© 2006 Elsevier B.V. All rights reserved.

Keywords: PVC membrane sensor; Phosphate; Fluorescent determination

1. Introduction

The determination of inorganic phosphate is especially important in the field of environmental and food analysis. The role of phosphate in eutrophication of seawater, as well as the influence of excess intake of phosphate in food products upon human health [1], is well known. Development of accurate methods for the determination of phosphate in situ is one of current topics of analytical chemistry [2].

In general, phosphate determination was based on the molybdenum blue method of Fiske and Subbarow, which was both complicated and time consuming [3]. Enzyme sensors or amperometric biosensors and ion-selective electrodes for phosphate based on the formation of glucose-phosphate or potential response on the alloy electrode had been developed [4,5]. Based on the liquid-membrane electrodes, coated-wire electrodes, heterogeneous membrane electrodes and metal electrodes, various potentiometric phosphate electrodes had been studied during the past decade [6–8]. In addition, several sensors for phosphate detection were also described with a series of enzymes such as pyruvate oxidase, acid phosphatase, maltose phosphatase and glucose oxidase, etc. [9–12]. However, it was unsuited to apply in situ at seawater due to the instability of electrode and invalidation

of enzyme at high salinity. A rapid and simple alternative is the use of optic sensors. Optic sensors with fluorescence detection as a new method for environmental monitoring draw a great attention recently [13]. It was sensitive and well suited for real-time analysis, and various optic sensors have been designed for H^+ , CO_2 , O_2 and so on. However, there were few available methods for measuring inorganic anions, and few fluorescence sensors for phosphate anions were reported [14–17].

Aluminum–Morin (Al–Morin) was a perfect fluorescent probe relying on an inherent quenching property of ionic analytes. It has been well used in the detection of phosphate in our previous work and good results were obtained [18]. PVC membrane was transparent and stable in water, and well used in various applications. It cannot mix well with Al–Morin solution directly. By combining with some techniques to modify PVC membrane matrix, Al–Morin indicators can be well immobilized and the leakage of Al–Morin in hydrophilic matrix such as polyvinyl alcohol (PVA) is also well solved; therefore, a reliable PVC sensor matrix may be formed. To our knowledge, so far the applications of PVC–Al–Morin technique to the analysis of phosphate in seawater have not been reported.

In this work, a fluorescent PVC sensing membrane was formed via a simple pretreatment of extracting Al–Morin probe from the acid solutions with pentyl alcohol, and the characteristics of PVC sensing membranes were investigated for the determination of seawater. It is proved to be a very simple, sen-

* Corresponding author. Tel.: +86 591 87893229.

E-mail address: zhxie@fzu.edu.cn (Z. Xie).

sitive and reliable technique for the determination of phosphate anion in water.

2. Experimental

2.1. Apparatus

Fluorescent spectra were recorded with a fluorescence spectrophotometer 970-CRT (Shanghai, China) at 25 °C. HAC–NaAc buffer solutions were calibrated by a pH meter pH-3C (Shanghai, China). Mixture for membranes was stirred by a vortex mixer QL-901 (Jiangshu, China). The devices for preparation and measure membranes are developed in our lab.

2.2. Reagents

All reagents were of analytical reagent-grade and deionized doubly distilled water was used throughout. Polyvinyl chloride (SG-5 D737, Fuzhou); tri-butyl-phosphate (TBP) (A.R. Shanghai); Aluminum–Morin, composed of $\text{AlCl}_3 \cdot 6\text{H}_2\text{O}$ (A.R. Shanghai) and Morin (A.R. Germany), were extracted with pentyl alcohol (A.R. Shanghai).

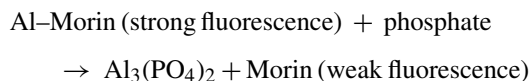
2.3. Membrane preparation

A 1.0×10^{-3} mol/l Al–Morin was prepared with the 1:1 alcohol–water solution. Using 5.0 ml of pentyl alcohol, Al–Morin probe was extracted under the acidic condition (pH 3.0–4.0). Mixing 1.0 ml of Al–Morin pentyl alcohol solution, 2.0 ml of PVC tetrahydrofuran (THF) solution with 0.10 ml of TBP, the mixture was injected into the devices (50.0 mm \times 25.0 mm \times 20.0 mm) for the sensitive membranes after air bubble suspending inside was removed with ultrasonic. Polymerization was carried out over 12 h to form transparent PVC membranes in the room temperature.

3. Results and discussion

3.1. Fluorescent response to phosphate

Based on the reaction between phosphate and Al–Morin, while H_2PO_4^- being added, the highly fluorescent complex Al–Morin was destroyed to produce $\text{Al}_3(\text{PO}_4)_2$ and Morin. Due to the weak fluorescence of $\text{Al}_3(\text{PO}_4)_2$ and Morin, the fluorescence of the reaction system was quenched distinctly. The reaction equilibrium was shown by the formula:



With the increase in concentration of H_2PO_4^- from 1.00 $\mu\text{g/ml}$ to 17.00 $\mu\text{g/ml}$, the reaction of phosphate to Al(III) was improved, which caused the extent of fluorescence quenching aggravating accordingly (shown in Fig. 1). The extent of fluorescence quenching had a good linear relationship with the concentration of H_2PO_4^- , which can be used to measure phosphate in water directly.

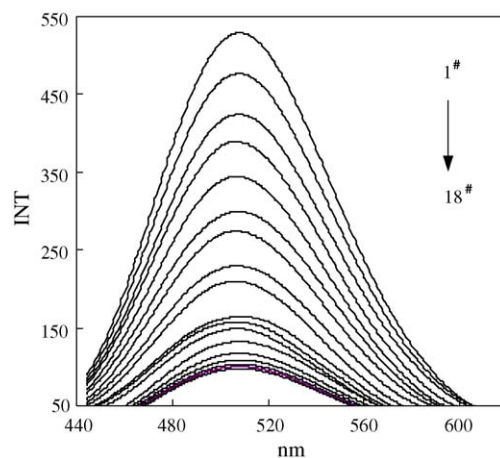


Fig. 1. The fluorescence spectra of the membrane quenched by different concentrations of phosphate $\text{C}_{\text{H}_2\text{PO}_4^-}$: 1#, 0.00 $\mu\text{g/ml}$; 2#, 1.00 $\mu\text{g/ml}$; 3#, 2.00 $\mu\text{g/ml}$; 4#, 3.00 $\mu\text{g/ml}$; 5#, 4.00 $\mu\text{g/ml}$; 6#, 5.00 $\mu\text{g/ml}$; 7#, 7.00 $\mu\text{g/ml}$; 8#, 8.00 $\mu\text{g/ml}$; 9#, 9.00 $\mu\text{g/ml}$; 10#, 0.00 $\mu\text{g/ml}$; 11#, 11.00 $\mu\text{g/ml}$; 12#, 12.00 $\mu\text{g/ml}$; 13#, 13.00 $\mu\text{g/ml}$; 14#, 14.00 $\mu\text{g/ml}$; 15#, 15.00 $\mu\text{g/ml}$; 16#, 16.00 $\mu\text{g/ml}$; 17#, 17.00 $\mu\text{g/ml}$; 18#, 18.00 $\mu\text{g/ml}$; $\lambda_{\text{Ex}} = 424$ nm, $\lambda_{\text{Em}} = 510$ nm, $S = 2$, pH 5.0.

3.2. Effect of pH

The effect of pH values on the fluorescent intensity of Al–Morin was investigated and the results are shown in Fig. 2. A small bulge happens to the surface layer of PVC membrane when pH is less than 4.0, and the fluorescence is strongest and changes distinctly at 510 nm. When pH was higher than 7.0, the fluorescence wavelength will shift to 530 nm, and the fluorescence intensity became weak and PVC membrane got stiff. When pH ranged from 4.0 to 6.0, the fluorescence was moderate with little change at the 524 nm.

3.3. Effect of the PVC precursor content

Thickness of membranes depended on the contents of PVC precursor, and had a tremendous impact on response time and sensitivity. For the determination of H_2PO_4^- at the level of 5.00 $\mu\text{g/ml}$, the response time of membranes composed of 1.60 g PVC in 50.0 ml THF was 750 s. In this case, the viscosity of membrane is too serious to respond to phosphate rapidly, though

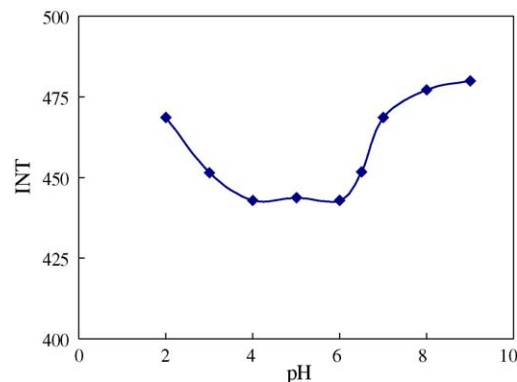


Fig. 2. The pH dependence on the fluorescence response of the membrane: $\lambda_{\text{Ex}} = 424$ nm, $\lambda_{\text{Em}} = 510$ nm, $S = 25.0$, pH 5.0.

the ratio of $\Delta F_0/F$ of quenching is 0.25 (ΔF_0 is the change of the fluorescence intensity and F is value of the fluorescence intensity). Response time of membranes made up of 2.00 g PVC in 50.0 ml THF is 600 s with a $\Delta F_0/F$ of 0.18. With the thickness adding, the response is weakened. The longest response time is that of membranes composed of 5.62 g PVC in 50.0 ml THF, which is more than 1000 s. Therefore, 2.00 g PVC in 50.0 ml THF is the optimal concentration of PVC for membrane.

3.4. Effect of Al–Morin and TBP

The dosage of plasticized reagent TBP and Al–Morin solvent in pentyl alcohol was an important parameter for fabrication of a perfect sensitive membrane, which has an obvious effect on detective limit and sensitivity. The transparent degree of membranes and the sensitivity were low with a small amount of TBP and Al–Morin. A great amount of TBP and Al–Morin leads to obvious viscosity and fragility, even a negative fluorescent restraint. In this experiments, the optimized dosage of TBP and Al–Morin has been optimized to fabricate high quality sensitive membranes (Table 1). It shows that the optimal dosage of TBP is 0.10 ml and that of Al–Morin is 1.00 ml.

3.5. Response time

Response time not only depended on the diffusion of phosphate between solution and the sensitive membrane, but also on the reaction between phosphate and the indicator immobilized in PVC membrane. When the concentration of phosphate is low, the response time to reach the equilibrium at low concentration was less than that in high concentration of phosphate. In the buffer solution (pH 5.0), the response time on concentration was changed from 380 s to 250 s, when the concentration of phosphate ranged from 9.00 $\mu\text{g/ml}$ to 11.00 $\mu\text{g/ml}$, and reached the highest at 450 s when phosphate was at 5.00 $\mu\text{g/ml}$.

3.6. Measure of phosphate

With the model of $I_{MF}/I_F = (K_{MF} \times K_e)/K_F \times [M]$ (K_{MF} and K_F are the fluorescence emission ratios of MF and F, respectively, K_e is the equilibrium constant of M and F, M is the analyte, and F is some fluorescent complex or material), the ratio of fluorescence quenching F_0/F had a linear relationship with the

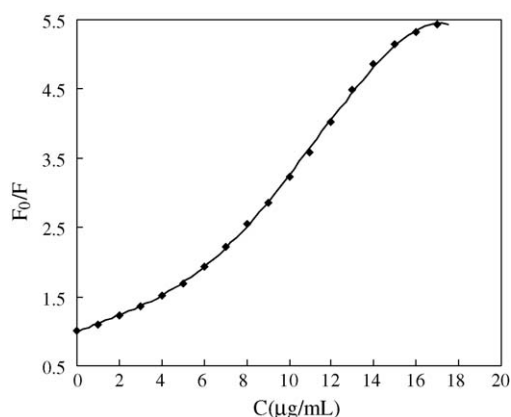


Fig. 3. The curve of correlation of F_0/F with the different concentrations of H_2PO_4^- : $\lambda_{\text{Ex}} = 424 \text{ nm}$, $\lambda_{\text{Em}} = 510 \text{ nm}$, $S = 25.0$, pH 5.0.

concentration of M. In our work, the M was phosphate and F was Al–Morin. Based on this model, a good relationship of the ratio of fluorescent quenching (F_0/F) with the quantity of H_2PO_4^- ranging from 6.00 ppm to 15.00 ppm was obtained (Fig. 3). The limit of detection ($3\delta/k$) was 0.02 $\mu\text{g/ml}$.

3.7. Stability and reversibility

After being marinated in water for 60 days, composite membrane was still stable, and the leak fluorescent intensity of Al–Morin in the blank reagent was 0–2.857. Measured for 20 times, F_0/F is stable, and the relative standard deviation is 0.07%. Marinated in the buffer solution (pH 5.0) for 10 h, composite membrane is also stable without obvious leakage. Scanned within 5400 s at several times, the fluorescence intensities were 566.8, 568.1, and 564.2, respectively. It indicated that the membrane had an ability to restrain the leakage of fluorescent combination in aqueous solution.

Reaction with phosphate decreased the amount of Al–Morin immobilized in the PVA/PVC composite membrane. Via marinated in $1.0 \times 10^{-3} \text{ mol/l}$ Al–Morin for 2 min or 3 min and washed with water, Al–Morin immobilized in the matrix was supplied and maintained constant. The response of sensitive membrane upon consecutive cycles of the switch between phosphate and Al–Morin fluorescent complex is reversible (shown in Fig. 4). The fluorescence intensity of sensitive matrix had recovered and the extent of fluorescence quenching of PVC membrane

Table 1
Effect of TBP and Al–Morin

Type	PVC* (ml)	Al–Morin (ml)	TBP (ml)	Membrane
Effects of TBP	2.00	0.00	0.00	White, opacity, crisp
	2.00	0.00	0.05	Transparent, frangible
	2.00	0.00	0.10	Transparent, pliable
	2.00	0.00	0.15	Transparent, obvious viscosity, frangible
	2.00	0.00	0.20	Transparent, obvious viscosity, frangible
Effects of Al–Morin	2.00	≥ 2.00	0.10	White, opacity
	2.00	1.50	0.10	Transparent, dim
	2.00	≤ 1.00	0.10	Transparent, lustrous

* 2.00 g PVC in 50.0 ml THF.

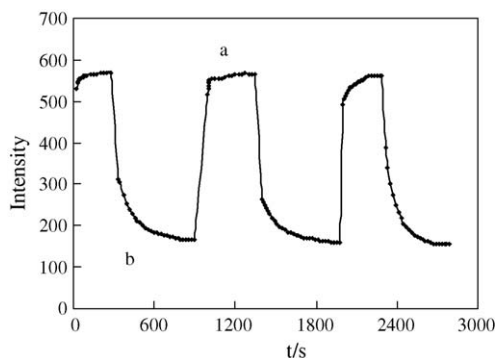


Fig. 4. Fluorescence reproducibility of the PVC membrane: response of the membrane upon consecutive cycles of the switches between phosphate and Al-Morin fluorescent reagent: (a) supplied with Al-Morin and (b) fluorescence quenched by phosphate.

was identical mostly, which demonstrated that this fluorescent matrix has a good recovery for the fluorescent intensity quenched by phosphate.

3.8. Life of membrane sensor

Stored in dryness, PVC sensitive membrane is stable for 90–120 days. In weak acidic solution, PVC membrane maintains stability for 30 days and is sensitive to phosphate ($C \leq 18.00 \mu\text{g/ml}$) after it has been measured in seawater sample for 18 times. By several supplements of fluorescent reagent, sensitive membranes can be used for 60 times, with the relative standard deviation of measure being less than 3%. Its appropriate life is more than 600 min.

3.9. Effect of coexistent ions

Interference of several coexistent ions has been studied (Figs. 5 and 6). It showed that coexistent ions have a little negative effect on PVC sensitive membrane, and the ratio of $\Delta F_0/F$ was less than 0.07. Cationic ions such as Ni^{2+} , Zn^{2+} and so on have an ability to inhabit the formation of Al-Morin immobilized in membrane, which accelerated the fluorescent quenching.

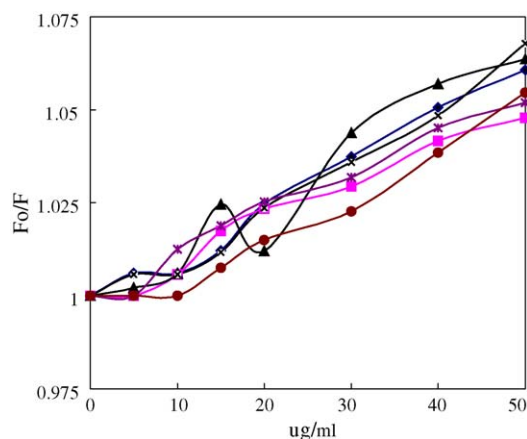


Fig. 5. Effect of the amount of coexisting cations on F_0/F of the membrane: (■) Ca^{2+} ; (×) Zn^{2+} ; (▲) Fe^{3+} ; (◆) Mg^{2+} ; (✱) Mn^{2+} , Ni^{2+} .

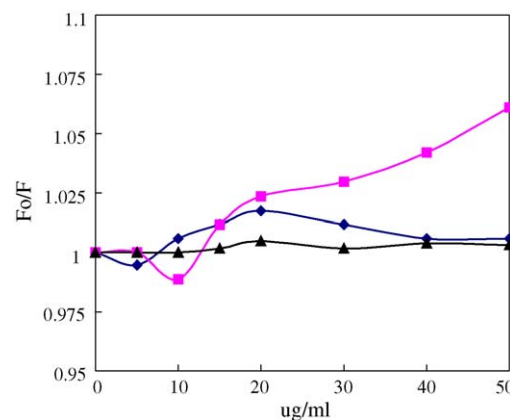


Fig. 6. Effect of coexisting anions on F_0/F of the membrane: (■) CO_3^{2-} ; (◆) SO_4^{2-} ; (▲) CH_3COO^- .

Effects of ions such as CO_3^{2-} and SO_4^{2-} were less than 0.05 ($\Delta F_0/F$), with the relative deviation of measure being less than 3%. All of Ca^{2+} , Zn^{2+} , Fe^{3+} , Mg^{2+} , Mn^{2+} , and Ni^{2+} that have no obvious disturbance at the concentration of $30 \mu\text{g/ml}$, $25 \mu\text{g/ml}$, $25 \mu\text{g/ml}$, $30 \mu\text{g/ml}$, $35 \mu\text{g/ml}$, and $40 \mu\text{g/ml}$ and concentrations of CO_3^{2-} , AC^- , and SO_4^{2-} were more than $50 \mu\text{g/ml}$, respectively.

3.10. Effect of salinity

Different salinities (S) are controlled with different concentrations of Ca^{2+} and Mg^{2+} . In simulated seawater whose salinity ranges from 5.0 to 50.0, the fluorescence intensity is kept constant and has no noticeable change with the variety of salinity, which ranges from 610.973 to 611.428. But when salinity was more than 30.0, the concentration of Mg^{2+} is so high that it has a negative effect on the fluorescence intensity. As a result, the optimal salinity of samples resembled to real seawater and existed within the range from 20.0 to 30.0.

4. Samples analysis

Analysis of H_2PO_4^- in simulated samples (pH 5.0, $S = 25.0$), and the results are shown in Table 2. Under the optimum condition, the sensor displayed a good linear response for H_2PO_4^- anion over the concentration range $6.00\text{--}15.00 \mu\text{g/ml}$ with a limit detection of $0.02 \mu\text{g/ml}$. Applied for the determination of phosphate at levels of $8.00\text{--}12.00 \mu\text{g/ml}$ in artificial seawater, the recoveries ranged from 96.6% to 103.8%, and the relative standard deviation was less than 4%.

Table 2
Analytical result of simulated seawater samples

Samples	H_2PO_4^- concentration/ppm		Recovery (%)
	Added	Found (mean \pm S.D. ^a)	
x ₁	8.00	7.81 \pm 0.18	97.62
x ₂	10.00	9.66 \pm 0.32	96.60
x ₃	12.00	12.45 \pm 0.47	103.81

The mean of three determinations.

^a S.D. = standard deviation.

5. Conclusion

A novel polyvinyl chloride (PVC) matrix membrane sensor responsive to phosphate ion has been presented. The leakage of Al–Morin in hydrophilic matrix, which acted as the bottleneck of membrane sensor, was well solved. Based on fluorescence quenching of Al–Morin probe, the sensor is sensitive to trace phosphate in water, and easy to be prepared rapidly. It is available for application, although the need for supplements of Al–Morin was a limitation in terms of practicability.

Acknowledgements

This work was supported by Program for New Century Excellent Talents in University (NCET-04-0612), National Natural Science Foundation of China (Grants 20305004 and 20575012), National High Technology Research and Development Program of China (2004AA639720), and Natural Science Foundation of Fujian Province, China (2005Y015, D0410010).

References

- [1] E. Watanabe, H. Endo, K. Toyama, *Biosensors* 3 (1988) 297.

- [2] K. Robards, I.D. McKelvie, R.L. Benson, et al., *Anal. Chim. Acta* 287 (1994) 147.
[3] N. Conrath, B. Grundig, St. Huwel, K. Cammann, *Anal. Chim. Acta* 309 (1995) 47.
[4] S.O. Engblom, *Biosens. Bioelectron.* 13 (1998) 981.
[5] S. Kalayc, G. Somer, G. Ekmekci, *Talanta* 65 (2005) 87.
[6] P.G. Veltsistas, M.I. Prodromidis, C.E. Efstathiou, *Anal. Chim. Acta* 502 (2004) 15.
[7] S.A. Glazier, M.A. Arnold, *Anal. Chem.* 63 (1991) 754.
[8] G.C. Petrucell, *Anal. Commun.* 33 (1996) 227.
[9] Y. Su, M. Mascini, *Anal. Lett.* 28 (1995) 1359.
[10] H. Mohammadi, A. Amine, A. Ouarzane, M. El Rhazi, *Microchim. Acta* 149 (2005) 251.
[11] N. Conrath, B. Grundig, *Anal. Chim. Acta* 309 (1995) 47.
[12] S. Huwel, L. Haalck, N. Conrath, *Enzyme Microb. Technol.* 21 (1997) 413.
[13] M.E. Padilla-Tosta, J.M. Lloris, R. Martínez-Máñez, et al., *Inorg. Chem. Commu.* 3 (2000) 45.
[14] M.M.G. Antonisse, B.H.M. Snellink-Ruel, J.F.J. Engbersen, et al., *Sens. Actuators B* 47 (1998) 9.
[15] V.K. Gupta, R. Ludwig, S. Agarwal, *Anal. Chim. Acta* 538 (2005) 213.
[16] M.M.F. Choi, P. Hawkins, *Sens. Actuators B* 90 (2003) 211.
[17] M.R. Ganjali, F. Mizani, M. Salavati-Niasari, *Anal. Chim. Acta* 481 (2003) 85.
[18] Z.H. Xie, X.C. Lin, G.N. Chen, *Chem Res. Chin. Univ.* 19 (2003) 201.

Improved detectability in pharmacokinetic study of tibolone by gas chromatography-high resolution mass spectrometry with selected ion monitoring

Junghyun Son^a, Ju-Yeon Moon^a, Seol-A Kim^{a,b}, Young-Dae Cho^{a,b}, Jong-Dae Kim^{a,b}, Dong-Hyun Kim^a, Man Ho Choi^{a,*}

^a Life Sciences Division, Korea Institute of Science and Technology, 39-1 Hawolok-dong, Seongbuk-ku, Seoul 136-791, South Korea

^b Department of Chemistry, Kyung Hee University, Seoul 130-701, South Korea

Received 31 October 2005; received in revised form 3 February 2006; accepted 3 February 2006

Available online 7 March 2006

Abstract

A combination of high resolution mass spectrometry (HRMS) and gas chromatography has been used to improve sensitivity and selectivity in pharmacokinetic study of tibolone. The study was undertaken in 12 healthy volunteers after oral administration of 2.5 mg tibolone tablet and plasma concentrations of two major metabolites, 3 α -hydroxytibolone (3 α OHT) and 3 β -hydroxytibolone (3 β OHT), were analyzed first by gas chromatography–mass spectrometry (GC–MS). Pharmacokinetic parameters AUC_{0–12h} (13.70 ± 4.01 ng h ml^{–1}), C_{max} (3.89 ± 1.00 ng ml^{–1}), and T_{max} (1.83 ± 0.55 h) for 3 α OHT were initially measured by GC–MS. The AUC_{0–12h} of 3 β OHT concentration was 5.5-folds higher than that of 3 α OHT. Improved results in detectability were obtained by GC–HRMS analysis of two metabolites with the same samples. The previously undetected metabolites, 3 α OHT and 3 β OHT, in samples collected at 15 and 24 h in GC–MS system were successfully detected by GC–HRMS analysis and could be calculated pharmacokinetic parameters as well. But, no significant pharmacokinetic parameters were found in two analytical runs. The limit of quantification for HRMS analysis in selected ion monitoring mode of 3 α OHT and 3 β OHT as trimethylsilyl derivatives down to 0.02 ng ml^{–1}, while their recovery rates varied in the range of 82.5–108.0%. This method demonstrated a good overall accuracy and precision as 90.1–102.3% and 1.6–11.4%, respectively. This method could potentially have implications for pharmacokinetic study or clinical trial of rapidly metabolized drugs.

© 2006 Elsevier B.V. All rights reserved.

Keywords: Pharmacokinetic; GC–HRMS; Tibolone; Trimethylsilylation

1. Introduction

Tibolone, (7 α ,17 α)-17-hydroxy-7-methyl-19-norpregn-5(10)-en-20-yn-3-one, is a synthetic steroid which mimics the activity of estrogen and progesterone, and tissue-specific drug for relief of estrogen-deficiency and prevention of osteoporosis [1,2]. It is rapidly metabolized into three major metabolites, which all contribute to the pharmacological effects, and extensively absorbed in human after oral administration (Fig. 1). Two of these, 3 α -hydroxytibolone (3 α OHT) and 3 β -hydroxytibolone (3 β OHT), have estrogenic activity while tibolone and its Δ^4 -isomer have predominantly progestogenic

and androgenic activities [3,4]. Due to rapid metabolism, the plasma concentrations of each compound are very low and some of the pharmacokinetic parameters could not reliably be measured or were determined from amount sampling [4–6].

In many studies, tibolone and its metabolites, which have been present at trace levels, were assayed by liquid chromatography with unit resolution mass spectrometry. As an efficient method in pharmacokinetic and drug metabolism studies, accelerator mass spectrometry (AMS) has been proposed and it brings attomolar sensitivity which can be reduced radiation [7–9]. However, the major problems associated with the AMS approach may still premature in biomedical and clinical applications and this method provided insufficiently chemical structure of analytes in a single run, while gas chromatographic–mass spectrometric (GC–MS) method have been the key technique to assay steroid molecules as their

* Corresponding author. Fax: +82 2 958 5081.

E-mail address: mh.choi@kist.re.kr (M.H. Choi).

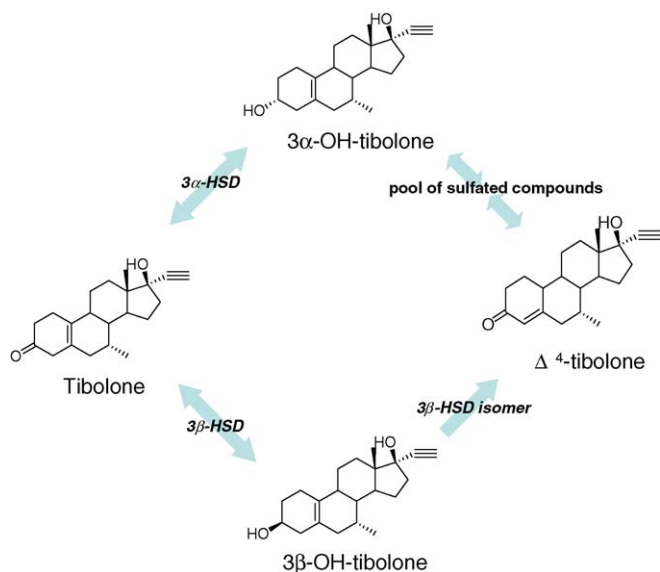


Fig. 1. Tibolone and its metabolites measured in previous pharmacokinetic studies. 3 α -HSD: 3 α -hydroxysteroid dehydrogenase; 3 β -HSD: 3 β -hydroxysteroid dehydrogenase.

suitable volatile derivatives [10–13]. Trimethylsilyl (TMS) derivatization is mainly employed for this purpose [12,13], and a mixture of *N*-methyl-*N*-trifluorotrimethylsilylaceta-mide, ammonium iodide, and dithioerythritol has been routinely used because of its rapid and high reactivity even toward carbonyl ketone group. The GC analysis combined with high resolution mass spectrometry (GC-HRMS) is also not affected by interfering substances because combination of selected ion monitoring with HRMS (HR/SIM-MS) at resolution of 4000 provides high selectivity for xenobiotic drugs. In the literature, HRMS analysis has been successfully applied to metabolism studies [14–16], but not to the pharmacokinetic study to date.

In continuation of our steroid analysis work, the present study was undertaken to initially validate using GC/SIM-MS, but it has inadequate selectivity and sensitivity for long-term or trace-dosing pharmacokinetic studies. The HRMS method, therefore, was employed and tested on future potential as an alternative approach in pharmacokinetic study. This was done in order to establish qualitative and quantitative data for bioavailability of tibolone over a wide period of time.

2. Experimental

2.1. Chemicals and spiked samples

Two metabolites of tibolone, 3 α OHT and 3 β OHT, were purchased from Toronto Research Chemicals (North York, ON, Canada). Ethisterone as an internal standard was obtained from Steraloids (Newport, RI, USA). Methanol and methyl *tert*-butylether (MTBE; HPLC grade) were purchased from Burdick & Jackson (Muskegon, MI, USA). *N*-Methyl-*N*-(trimethylsilyl)trifluoroacetamide, dithioerythriol, and ammonium iodide were purchased from Sigma (St. Louis, MO, USA).

Each stock solution of 3 α OHT, 3 β OHT, and ethisterone was prepared at the concentrations of 1.0 mg ml⁻¹ in methanol as their free forms. These solutions were used to prepare working solutions of various concentrations in methanol and kept below 4 °C using amber vials. The working solution of internal standard was prepared by diluting a stock solution at 200 ng ml⁻¹. The calibration curves were obtained using seven calibration points, i.e. spiked plasma samples prepared by addition of the stock solution to blank human plasma, giving final concentrations of 0.1, 0.2, 0.5, 1.0, 2.0, 5.0, and 10 ng ml⁻¹.

2.2. Drug administration and sample collection

After having undergone a thorough medical examination, 12 healthy male volunteers participated in the study. Informed consent forms were signed according to institutional guidelines. This study was also approved by the Human Subjects Committee of Kyung Hee University, and was conducted at the Kyung Hee Medical Center. Tibolone tablet (2.5 mg) was orally administered to each volunteer with 200 ml water and then the blood sample was collected at 0, 0.5, 1, 1.5, 2, 3, 4, 6, 8, 10, 12, 15, and 24 h post-dose. Plasma was harvested after centrifugation and stored at -20 °C.

2.3. Sample preparation

Fifty micro-liter of internal standard solution (200 ng ml⁻¹) was spiked to each sample (2 ml) to make final concentrations of 5.0 ng ml⁻¹ and 5.0 ml MTBE was added, and then vortexed for 30 s. The samples were centrifuged for 5 min at 2500 rpm and organic layer was separated by placing it in a dry ice-acetone bath (-30 °C). Ether extracts were evaporated to dryness under a stream of nitrogen gas. The extracts were further dried in vacuum desiccator over phosphorus pentoxide and potassium hydroxide for 30 min. After trimethylsilylation with 50 μ l MSTFA/NH₄I/DTE (500:4:2, v/w/w) for 30 min at 60 °C, the sample prepared was injected (2 μ l) into the GC-MS and GC-HRMS systems.

2.4. Validation of the analytical method

The calibration curves for 3 α OHT and 3 β OHT in plasma were generated by plotting the peak area ratios for analyte to an internal standard versus the concentrations in the standard-spiked plasma samples by least-squares linear regression. The calibration curves were obtained using seven calibration standards, and each standard was prepared in triplicate. The intra-day coefficient of variation (CV) and accuracy of the method were evaluated by the analysis of five plasma samples spiked to make final concentrations of 0.1, 0.2, 0.5, 1.0, 2.0, 5.0, and 10 ng ml⁻¹. The CV and accuracy for inter-day assay were assessed at the concentrations of 0.2, 1.0, and 10 ng ml⁻¹, and repeated for five different days over a 3-week period without particular care for measuring the reproducibility of the present method in the same manner as described for plasma sample.

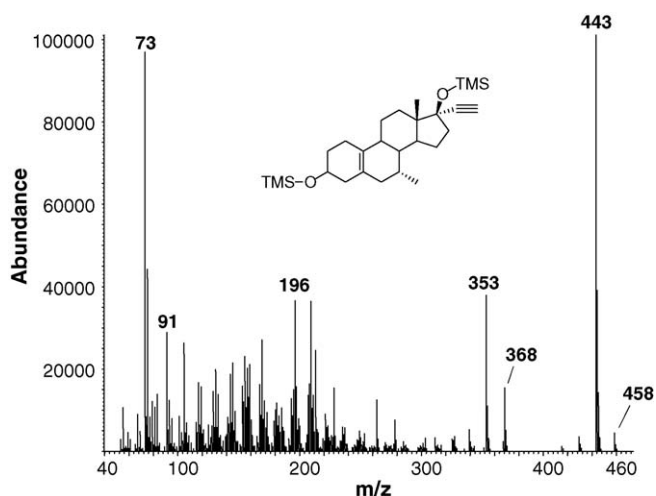


Fig. 2. Electron-impact mass spectrum of 3 α -hydroxytibolone as its TMS derivative obtained in the scanning mode at a rate of 0.48 scans/s with a mass range of m/z 50–480.

2.5. Instrumental conditions

GC–MS analyses in selected ion monitoring (SIM) modes were performed with an Agilent 6890 plus gas chromatograph interfaced to an Agilent 5973 mass selective detector (GC–MSD; Avondale, PA, USA) and JMS-700 high resolution mass spectrometer (Jeol; Tokyo, Japan). Samples were first analyzed by GC–MSD through a Ultra-2 capillary column (Agilent; 25 m \times 0.2 mm, 0.33 μ m) in the split-injection mode (10:1)

at 280 $^{\circ}$ C, and the oven temperature was initially 200 $^{\circ}$ C and raised to final temperature of 320 $^{\circ}$ C (6 min) at 20 $^{\circ}$ C min $^{-1}$. Helium, as a carrier gas, was set to a column head pressure of 100 kPa (column flow: 1.2 ml min $^{-1}$ at 200 $^{\circ}$ C). The electron energy was 70 eV and the ion source temperature was 230 $^{\circ}$ C. SIM experiments were performed by monitoring the fragment ions, $[M + 2TMS - CH_3]^+$ (m/z 443 for 3 α OHT and 3 β OHT) and $[M + 2TMS]^+$ (m/z 456 for internal standard).

The GC–HRMS analysis was also performed with an Agilent 6890 plus GC and an Ultra-1 capillary column (Agilent; 17 m \times 0.2 mm, 0.11 μ m) with a helium head pressure of 45.8 kPa. The temperatures of interface and reservoir were 280 and 80 $^{\circ}$ C, respectively, and the initial column temperature was 200 $^{\circ}$ C for 2 min, increasing at a rate of 5 $^{\circ}$ C min $^{-1}$ to 260 $^{\circ}$ C and at a rate of 20 $^{\circ}$ C min $^{-1}$ to 310 $^{\circ}$ C and held for 3.5 min. Electron energy and accelerator voltage were 60 eV and 10 kV, respectively. The HR/SIM experiments at resolution 4000 were performed by monitoring the fragment ions, $[M + 2TMS - CH_3]^+$ (m/z 443.2796 for 3 α OHT and 3 β OHT) and $[M + 2TMS]^+$ (m/z 456.2880 for internal standard).

2.6. Data analysis

Pharmacokinetic parameters were calculated based on the concentration in plasma represented two major metabolites of tibolone, 3 α OHT and 3 β OHT. The area under the plasma concentration-time curve (AUC) was determined by a non-compartmental method using WinNolin (Version 3.1; Scientific Consulting, Lexington, KY, USA) with trapezoidal method.

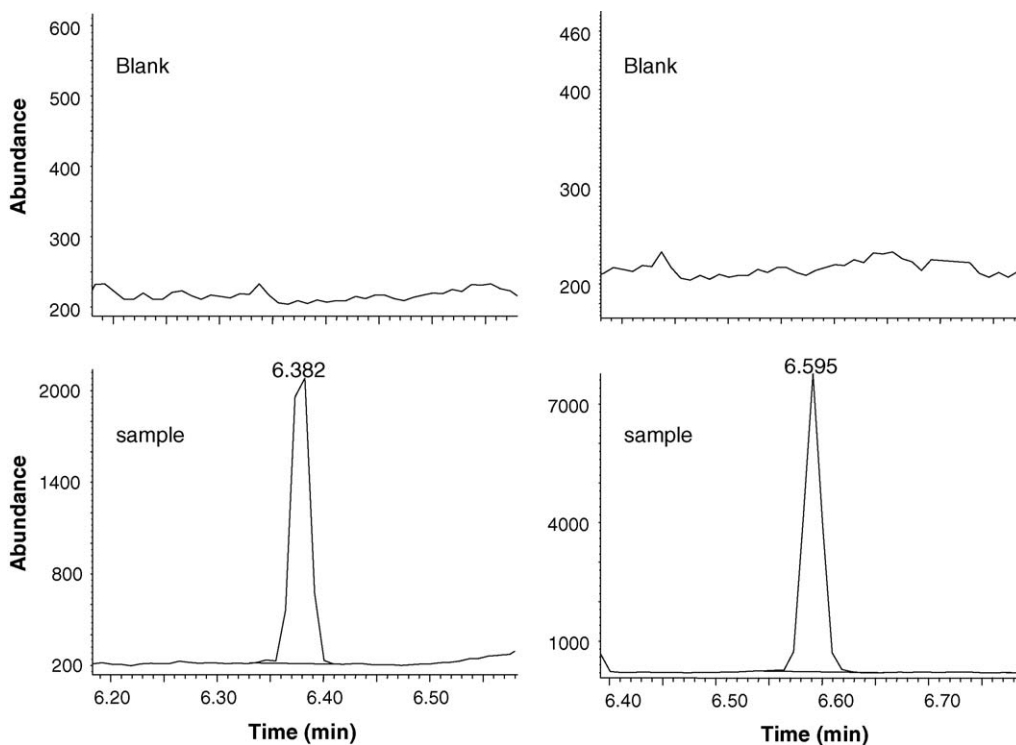


Fig. 3. GC/SIM–MS analyses of 3 α -hydroxytibolone (left panel) and 3 β -hydroxytibolone (right panel) at time-point 1 h after administration of tibolone tablet (2.5 mg). Two steroids were monitored at m/z 443 through an Ultra-2 capillary column (25 m \times 0.2 mm \times 0.33 μ m). The oven temperature was initially 200 $^{\circ}$ C and raised to final temperature of 320 $^{\circ}$ C (6 min) at 20 $^{\circ}$ C min $^{-1}$.

Maximum plasma concentration (C_{\max}) and the corresponding T_{\max} were reported as observed.

3. Results and discussion

3.1. Sample preparation and GC–MS properties of analytes

Under the present extraction with MTBE, three analytes (3 α OHT, 3 β OHT, and ethisterone as an internal standard) were more efficiently recovered than other organic solvents tested, such as acetone, *n*-hexane, and diethylether (data not shown). Dried extract was then trimethylsilylated to improve volatility and GC–MS properties [12,13]. The main advantage of TMS derivatization in steroid analysis is the formation of intense molecular ion or $[M-CH_3]^+$ ion, so that interferences are less likely to be encountered in SIM analysis. Mass spectral patterns of 3 α / β -OHT and ethisterone as their TMS derivatives show strong $[M-CH_3]^+$ ion and molecular ion, and fragmentation patterns also associated with M-90 $[M-Si(CH_3)_3OH]^+$ and M-105 $[M-Si(CH_3)_3OH-CH_3]^+$ mostly like any other TMS derivatives (Fig. 2). In GC/SIM-MS analysis with these intense peaks, 3 α OHT and 3 β OHT were selectively detected without any significant interference (Fig. 3).

3.2. Validation of the method

The standard calibration curves obtained from spiked human plasma containing 3 α OHT and 3 β OHT were linear over the range of 0.1–10 ng ml⁻¹ while the correlation coefficient was greater than 0.9998. The typical calibration curves for 3 α OHT and 3 β OHT were given by the equations, $y = 0.1703x - 0.0037$, and $y = 0.1025x - 0.0022$, respectively, where y indicates the peak area ratio and x represents the concentration of two metabolites of tibolone in ng ml⁻¹ concentration. The intra- and inter-day variations of 3 α OHT and 3 β OHT in plasma were acceptable with good precision and accuracy values, as listed in Table 1. The intra-day coefficients of variation were less than 9.7%, and the intra-day accuracies were between 94.6 and 102.3% within the concentration range of the calibration curves in plasma. The inter-day coefficients of variation did not exceed 11.4%, and its

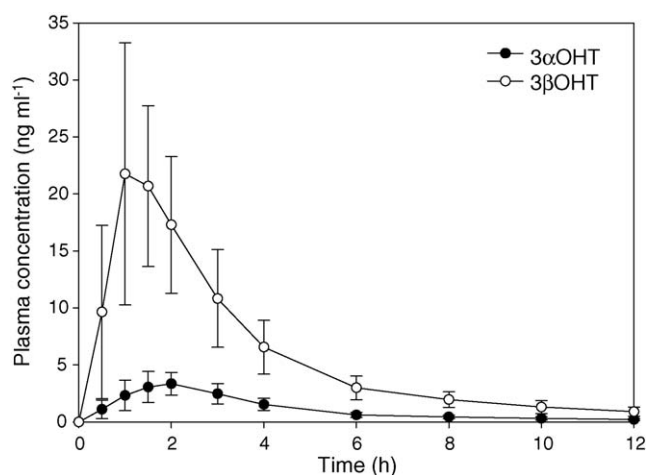


Fig. 4. Plasma concentration-time profiles of 3 α -hydroxytibolone and 3 β -hydroxytibolone following administration of tibolone (2.5 mg). Data are the mean \pm S.D. of 12 volunteers.

accuracies were between 90.1 and 102.0%. The limit of quantification (LOQ) for 3 α OHT and 3 β OHT were set to 1.0 ng ml⁻¹, which is the lowest concentration of the analyte that can be measured with a coefficient of variation and accuracy less than 15%, while 2 ml of plasma sample was analyzed by GC/SIM-MS.

The recovery test for 3 α OHT and 3 β OHT was also determined in plasma at three different concentrations spiked. After sample preparation, the values obtained for 3 α OHT at 0.2, 1.0 and 10 ng ml⁻¹ were 93.4, 107.7, and 96.6%, respectively, while 3 β OHT was recovered with 82.5, 108.0, and 92.7%, indicating that the matrix effects were minimized.

3.3. Pharmacokinetic parameters from healthy volunteers

The plasma samples were taken with 12 time points within 24 h post-dosing of tibolone tablet (2.5 mg), and 3 α OHT and 3 β OHT as major metabolites of tibolone were analyzed from 12 healthy volunteers. Two metabolites were not detectable after 12 h post-dosing and some plasma could not be measured even at 12 h. Important pharmacokinetic parameters, AUC_{0–12h}, C_{\max} , and T_{\max} of 3 α OHT and 3 β OHT were calculated by

Table 1
Method validation for GC/SIM-MS analysis of 3 α -hydroxytibolone and 3 β -hydroxytibolone in human plasma

Concentration added (ng ml ⁻¹)	Intra-day			Inter-day		
	Concentration found ^a (ng ml ⁻¹)	CV (%)	Accuracy (%)	Concentration found ^a (ng ml ⁻¹)	CV (%)	Accuracy (%)
3 α -Hydroxytibolone						
0.2	0.20 \pm 0.01	6.7	98.6	0.18 \pm 0.02	11.4	92.2
1.0	0.95 \pm 0.06	6.5	94.6	1.02 \pm 0.03	2.8	101.8
10.0	10.20 \pm 0.90	8.3	102.3	10.10 \pm 0.47	4.6	101.5
3 β -Hydroxytibolone						
0.2	0.20 \pm 0.02	9.7	100.0	0.20 \pm 0.02	10.7	102.0
1.0	0.95 \pm 0.02	1.6	95.0	0.90 \pm 0.03	2.8	90.1
10.0	10.20 \pm 0.55	5.4	101.5	9.90 \pm 0.66	6.7	99.2

Analyzed on an Ultra-2 (25 m \times 0.2 mm, 0.33 μ m) fused silica capillary column in SIM mode and relative voltage of electron multiplier set to 400 V higher than that in the scanning mode for each ion monitored.

^a Data are expressed as mean \pm S.D.

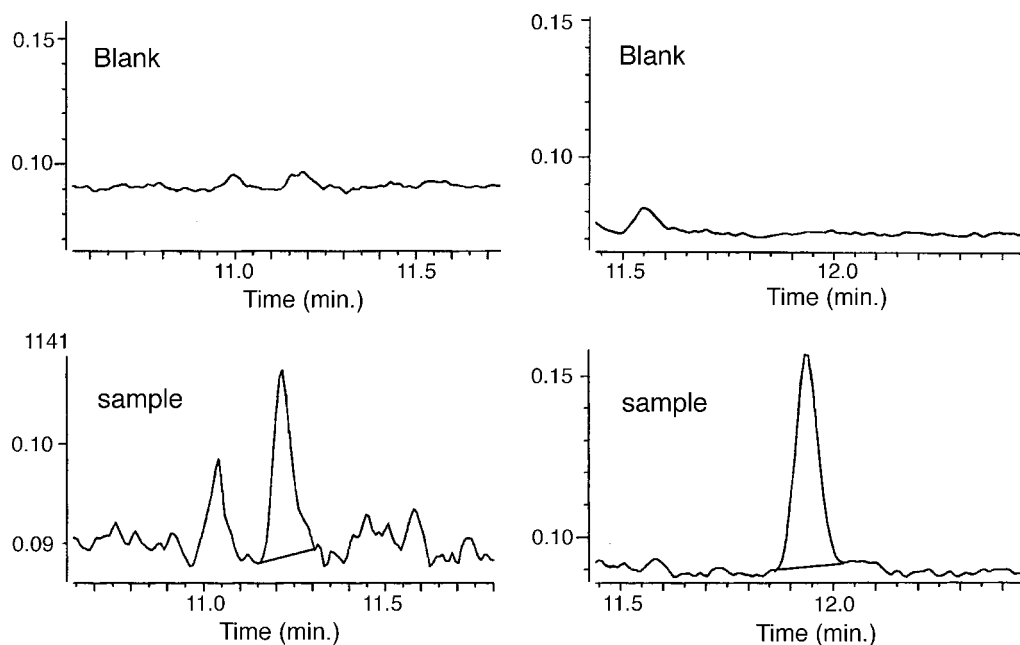


Fig. 5. Representative GC-HR/SIM-MS of 3 α -hydroxytibolone (left panel) and 3 β -hydroxytibolone (right panel) at time point 24 h after administration of tibolone tablet (2.5 mg). Two steroids were monitored at m/z 443.2796 with resolution 4000.

GC/SIM-MS analysis, and The plasma concentration-time profiles of 3 α OHT and 3 β OHT are shown in Fig. 4. A remarkable difference was noted between two metabolites. The AUC_{0-12h} of 3 β OHT concentration was 5.5 times higher than that of 3 α OHT and the results are not correspond with data obtained from post-menopausal women that no significant differences between 3 α OHT and 3 β OHT were found [4]. In addition, C_{max} of 3 β OHT was 6.5 times higher than that of 3 α OHT, whereas T_{max} was 40% lower in 3 β OHT.

Our goal was to evaluate an analytical method that is the selective and sensitive analysis in pharmacokinetic study to realize long-term and trace-dosing studies. The GC-HR/SIM-MS analysis, therefore, was conducted with the same samples and the previously undetected 3 α OHT and 3 β OHT in samples of time points at 12, 15, and 24 h in GC-SIM/MS system were measured their concentrations by HRMS analysis. In the 24-h time point, one could measurable while 2 ml of plasma was prepared (Fig. 5). The pharmacokinetic parameters of 3 α OHT and 3 β OHT were similar in GC-SIM/MS and GC-HR/SIM-MS analyses. Long-term kinetic information is needed to accurately calculate elimination rates of the drugs with slow turnover rates, and the GC-HRMS method was successfully applied with acceptable sensitivity of 0.02 ng ml^{-1} as LOQ because they provided better signal-to-noise values without additional sample purification steps.

4. Conclusion

The major advantages of the present method are the efficient recovery of 3 α OHT and 3 β OHT from human plasma samples using liquid-liquid extraction with methyl *tert*-butylether

as the extraction solvent and the subsequent TMS derivatization to enhance the GC-MS properties. The present method was capable to measure down to 1.0 ng ml^{-1} (GC/SIM-MS) and 0.02 ng ml^{-1} (GC-HR/SIM-MS) with excellent peak shapes, higher responses, and shorter analysis time. Especially, GC-HR/SIM-MS method may applicable to the analytical technique for trace analysis in human subjects. The small blood volumes required enable studies, which might be measurable from only finger-prick blood volumes.

Acknowledgement

We thank Prof. Kyung Tae Lee (College of Pharmacy, Kyung Hee University) for the kind donation of plasma samples.

References

- [1] T.E. Vogelvang, M.J. van der Mooren, V. Mijatovic, *Treat. Endocrinol.* 3 (2004) 105.
- [2] A. Sadarangani, A.M. Salgado, S. Kato, M. Pinto, A. Carvajal, C. Monso, G.I. Owen, P. Vigil, *Biol. Res.* 38 (2005) 245.
- [3] R.M.E. Vos, S.F.M. Krebbers, C.H.J. Verhoeven, L.P.C. Delbressine, *Drug Metabol. Dispos.* 30 (2002) 106.
- [4] C.J. Timmer, H.A.M. Verheul, D.P. Doorstam, *Br. J. Clin. Pharmacol.* 54 (2002) 101.
- [5] C.H.J. Verhoeven, R.M.E. Vos, L.P.C. Delbressine, *Eur. J. Drug Metabol. Pharmacokinet.* 27 (2002) 1.
- [6] C.J. Timmers, J.A.M. Huisman, *Pharmacotherapy* 22 (2002) 310.
- [7] S.R. Dueker, Y. Lin, B.A. Buchholz, P.D. Schneider, M.W. Lamé, H.J. Segall, J.S. Vogel, A.J. Clifford, *J. Lipid Res.* 41 (2000) 1790.
- [8] G. Lappin, R.C. Garner, *Nat. Rev. Drug Discov.* 2 (2003) 233.
- [9] M.H. Choi, P.L. Skipper, J.S. Wishnok, S.R. Tannenbaum, *Drug Metabol. Dispos.* 33 (2005) 714.

- [10] M.H. Choi, B.C. Chung, W. Lee, U.C. Lee, Y. Kim, *Rapid Commun. Mass Spectrom.* 13 (1999) 376.
- [11] M.H. Choi, K.R. Kim, B.C. Chung, *Analyst* 125 (2000) 711.
- [12] M.H. Choi, B.C. Chung, *Analyst* 126 (2001) 306.
- [13] M.H. Choi, Y.S. Yoo, B.C. Chung, *J. Invest. Dermatol.* 116 (2001) 57.
- [14] C.M. Gross, I.M. Davis, R.F. Arrendale, J. Jersey, J. Amin, *J. Pharm. Biomed. Anal.* 12 (1994) 195.
- [15] M. Machnik, H. Geyer, S. Horning, A. Breidach, P. Delahaut, W. Schänzer, *J. Chromatogr. B* 723 (1999) 147.
- [16] A.L. Ham, A. Ranasinghe, E.J. Morinello, J. Makamura, P.B. Upton, F. Johnson, J.A. Swenberg, *Chem. Res. Toxicol.* 12 (1999) 1240.

Review

A review of current activities of analytical separation in Korea in 2004

Dong-Sun Lee*

Department of Chemistry, Seoul Women's University, Seoul 139-774, Republic of Korea

Received 30 October 2005; received in revised form 1 February 2006; accepted 1 February 2006

Available online 10 March 2006

Abstract

This review gives a quick overview of the current Korean research activities and trends in the field of analytical science with specific focus on the use of analytical separation techniques. In this review, the current standing and central trends, emerging techniques in the Korean community of analytical separation researchers are emphasized.

© 2006 Elsevier B.V. All rights reserved.

Keywords: Research activities; Separation; Analytical science; Korea; 2004

Contents

1. Introduction	43
2. Publication data analysis	43
3. Presentation data analysis	44
4. Methodology	45
5. Analytes and matrix	45
6. Trends and emerging technology	46
Acknowledgements	46
References	46

1. Introduction

The purpose of this review is to inform a quick overview of the current Korean research activities and trends in the field of analytical science. Particularly, this review focuses on the use of analytical separation techniques. In this review, the current standing and central trends, emerging techniques in the Korean community of analytical separation researchers are emphasized.

Indeed, there is a positive correlation between the estimation of the number of papers published in the commonly recognized journals throughout the world and the relative level or range of research works in the specific area of the science in the selected country. Unfortunately, there is no detailed report on the publication and presentation data for the study of analytical chemistry for many years in Korea.

Therefore, publication papers contributed to the 17 international [1–10] and the seven Korean journals [11–14] for 1 year in 2004 were surveyed, and presentation data in the four national meetings [15–18] were also analyzed. Then, methodology, analytes and matrix, trends and emerging techniques were briefly reviewed with emphasis on the field of analytical separation.

This survey has indicated that the slow increase in the number of papers published in the international journals did not coincide with the significant increase in the national journals. However, major analytical techniques in Korea are being or will soon be influenced by the international main streams and the introduction of newly developed instrumentations or devices. The focus has shifted rapidly from research on conventional mature separation techniques to a far broader range of advanced techniques.

2. Publication data analysis

We first investigated publication data contributed to the international or Korean journals for 1 year in 2004. It is not an

* Tel.: +82 2 970 5654; fax: +82 2 070 5972.E-mail address: dslee@swu.ac.kr.

Table 1

Numbers of research papers published in the international journals related to analytical separation by Korean authors in 2004

International journals related to analytical separation	Domestic affiliation	Foreign affiliation	Total	Ratio (%)
<i>Anal. Chem.</i>	12	24	36	25.5
<i>Chromatographia</i>	13	0	13	9.2
<i>J. Chromatogr. A</i>	9	4	13	9.2
<i>Rapid Commun. Mass Spectrom.</i>	9	4	13	9.2
<i>Anal. Biochem.</i>	7	5	12	8.5
<i>Anal. Chim. Acta</i>	5	6	11	7.8
<i>Electrophoresis</i>	6	4	10	7.1
<i>Anal. Sci. (Japan)</i>	4	3	7	5.0
<i>Anal. Bioanal. Chem.</i>	2	3	5	3.5
<i>Talanta</i>	5	0	5	3.5
<i>Analyst</i>	1	2	3	2.1
<i>J. Am. Soc. Mass Spectrom.</i>	2	1	3	2.1
<i>J. Sepa. Sci.</i>	3	0	3	2.1
<i>Anal. Lett.</i>	2	0	2	1.4
<i>Eur. J. Mass Spectrom.</i>	0	2	2	1.4
<i>J. Mass Spectrom.</i>	1	1	2	1.4
<i>J. Chromatogr. Sci.</i>	1	0	1	0.7
Total	82	59	141	

exhaustive literature survey about every application of analytical techniques. Table 1 lists a total number of 141 papers; most correspond to scientific contributions published within the last 1 year in the 17 well-known international scientific journals related to analytical separation. *Anal. Chem.*, *Chromatographia*, *J. Chromatogr. A*, *Rapid Commun. Mass Spectrom.*, and *Anal. Biochem.* were top five publication media. Then, *Anal. Chim. Acta*, *Electrophoresis*, *Anal. Sci.*, *Anal. Bioanal. Chem.*, and *Talanta* were followed. Among the 141 papers, 82 papers (corresponding to 58.2%) were contributed by domestic affiliations and other 59 papers by foreign affiliations.

Two hundred and fourteen analytical papers corresponding to 17.7% among the total 1209 papers in the seven selected Korean journals in 2004 are summarized in Table 2. It is widely recognized that the Bulletin of the Korean Chemical Society (*Bullet. Korean Chem. Soc.*) is one of the representative journals in Korea, and *Anal. Sci. Technol.* is contributing a significant percentage of publications in the analytical field. The Korean Chemical Society (KCS), The Korean Society of Analytical Sci-

Table 2

Numbers of analytical research papers published in the seven selected Korean journals in 2004

Society (established year/members)	Journal	Analytical papers (Total papers)
The Korean Chemical Society (1951, 4663)	<i>Bulletin (Eng.) J. Korean Chem. Soc.</i>	54 (429) 10 (93)
The Korean Society of Analytical Science (1988, 990)	<i>Anal. Sci. Technol.</i>	70 (70)
The Pharmaceutical Society of Korea (1951, 2745)	<i>Arch. Pharm. Res. (Eng.) Yakhakheoji</i>	22 (214) 6 (66)
Korean Society of Food Science & Technology (1968, 3100)	<i>Food Sci. Biotechnol. (Eng.) Korean J. Food Sci. Technol.</i>	16 (168) 36 (169)
Total		214 (1209)

ence (KOANAL), The Pharmaceutical Society of Korea (PSK), and The Society of Food Science and Technology (KOSFOST) are four major societies for the contribution and the dissemination of analytical science in the nation. Recently, electronic submission systems by computer were introduced to the most scientific societies.

3. Presentation data analysis

Without any doubt, the world of analytical separation is changing rapidly in Korea as well as advanced countries. We experienced these changes as we looked over the symposia, oral presentations, and poster sessions. This is presentation data analysis at a glance to help in understanding on the current standing of analytical separation in Korea. Nowadays, more and more research projects deal with separation techniques in analytical sciences, a fact that is verified by the increasing number of presentation data in the four national meetings of the KCS and KOANAL. As can be seen in Table 3, topics related to separation varied from 43.4 to 34.9% among the total 221 and 346 presentations given in these meetings. Koichi Tanaka, Nobel Laureate from Shimadzu Corp. was invited to the 94th National Meeting of the KCS (October 21, 2004. Jeju) for a plenary lecture. At this meeting he presented special talk entitled "The Origin and the Future of Macromolecule Ionization by Laser Irradiation".

Table 3

Presentations at the particular annual meetings in 2004

Conference meeting	Symposium or key note	Poster (oral)	Total	Separation
The 93rd National Meeting of the KCS (April 22–23, 2004. Seoul) Analytical Chemistry Division	13	99	112	55
The 94th National Meeting of the KCS (October 21–22, 2004. Jeju) Analytical Chemistry Division	7	102	109	41
Sub-total	20	201	221	96 (43.4%)
The 32nd Meeting of the Korean Society of Analytical Sciences (May 27–28, 2004. Jeju Univ.)	7	168 (17)	192	70
The 33rd Meeting of the Korean Society of Analytical Sciences (November 18–19, 2004. Choongmu Marina)	10	130 (14)	154	51
Sub-total	17	198 (31)	346	121 (34.9%)

Table 4

Distribution of methodology of research papers published in the international journals related to analytical separation by Korean authors in 2004

Methodology	No. of papers	Ratio (%)
LC–MS (tandem), LC, MALDI-TOF-MS	45	31.9
CE, isoelectric focusing, electrophoresis, chip	26	18.4
Electrochemistry, ion selective electrode, sensor	20	14.2
GC–MS (tandem), GC, sample preparation	11	7.8
FFF, SFE, other separation	9	6.4
Immunoassay, ELISA	9	6.4
Fluorometry, fluorescent nanosensor, biosensor	6	4.3
Miscellaneous	6	4.3
ICP-MS, ICP-AES, AES	4	2.8
NMR	3	2.1
Surface plasmon resonance	2	1.4
Total	141	100.0

4. Methodology

The listings in Tables 4 and 5 are general groupings of the journals, oral and/or poster sessions including that particular methodology and application. The commonly used analytical methods discussed here do not include the overall field of analytical science such as spectrometry and electro-analytical method. Separations are increasingly becoming important for fundamental and applied research. On one hand of international level, liquid chromatography–mass spectrometry (LC–MS), matrix assisted laser desorption ionization-time-of-flight mass spectrometry (MALDI-TOF-MS), capillary electrophoresis (CE), Chip, gas chromatography–mass spectrometry (GC–MS), GC, field flow fractionation (FFF) and supercritical fluid chromatography (SFC) were major methodology corresponding to 62% of total 141 papers, as shown in Table 4. On the other hand, on a national level, GC–MS, GC, high resolution GC–high resolution MS (HRGC–HRMS), LC–MS, LC, electrospray ionization MS (ESI-MS), atmospheric pressure ionization MS (API-MS), flow

Table 5

Distribution of methodology of research papers published in the “Analytical Science & Technology” (Korean) in 2004

Methodology	No. of papers	Ratio (%)
GC–MS (tandem), GC, HRGC-HRMS	18	25.7
LC–MS (tandem), LC, ESI-MS, API-MS, ion exchange, size exclusion chromatography	13	18.6
Miscellaneous	8	11.4
Neutron activation analysis, isotopic radio activity	6	8.6
Other separation	4	5.7
Spectrometry, laser spectrometry	4	5.7
Solvent extraction	3	4.3
ICP-MS, ICP-AES	3	4.3
Flow injection analysis	2	2.9
CE	2	2.9
Raman spectrometry	2	2.9
Fluorometry	2	2.9
Electrochemical analysis	2	2.9
NMR	1	1.4
Total	70	100.0

Table 6

Distribution of methodology of research papers presented at the 93rd national meeting of the KCS (April 22–23, 2004, Seoul), Analytical Chemistry Division

Session	Methodology	No. of papers	Ratio (%)
Symposium	Bioassay on microscale	6	
	New trends and challenges in analytical technologies	7	
	Sub-total	13	11.6
Poster	Miscellaneous	55	49.1
	CE–MS, CE	15	13.4
	LC–MS	13	11.6
	GC–MS	11	9.8
	Lab-on-a-chip	3	2.7
	MALDI-TOF-MS	1	0.9
	SFC	1	0.9
Total		112	100.0

injection analysis (FIA), and other separation corresponding to more than 60% over the total 70 papers contributed in *Anal. Sci. Technol.* in last 1 year as shown in Table 5.

Meanwhile, in the spring national meeting of the KCS, last year, CE–MS, CE was top method (Table 6). And LC–MS, LC, then GC–MS, GC were the next frequent methods of choice. In the case of October meeting, GC–MS or GC was first one, then LC–MS, LC, CE–MS, CE were followed (Table 7).

We can see that through the year, the focus has shifted from research on conventional mature separation techniques to a far broader range of advanced techniques. MS has rapidly become a common tool for analytical separation in many areas.

5. Analytes and matrix

The broad range of analytical topics was reported. There has also been increasing interest in the specific bio-samples dealing with proteomics, genomics, and metabolomics. International level, drugs, proteins or biological and environmental samples are characterized as the top three among the criterion of analyte and sample matrix in all aspects (Table 8). On a national level, metals and environmental samples were top two analytes and matrix (Table 9). From these results it would appear that there is some evidence that the presence of environmental and

Table 7

Distribution of methodology of research papers presented at the 94th national meeting of the KCS (October 21–22, 2004, Jeju), Analytical Chemistry Division

Session	Methodology	No. of papers	Ratio (%)
Symposium	Current status and prospects of new analytical technologies	7	
Poster	Miscellaneous	66	60.6
	GC–MS	15	13.8
	LC–MS	10	9.2
	CE–MS, CE	7	6.4
	MALDI-TOF-MS	4	3.7
	MALDI-TOF-MS	1	0.9
	SFC	1	0.9
Total		109	100.0

Table 8

Distribution of analyte and matrix of research papers published in the international journals related to analytical separation by Korean authors in 2004

Analyte and matrix	No. of papers	Ratio (%)
Miscellaneous	22	15.6
Drugs	21	14.9
Protein, peptide, proteomics	19	13.5
Cell, bacteria, virus, pathogen	10	7.1
Environmental, PAH, phenols, VOC, Nox	9	6.4
Bio-sample, blood, albumin, bilirubin, Metalbolomics	8	5.7
DNA, nucleotide	8	5.7
Amino acid	7	5.0
Enzyme	5	3.5
Material, polymer, nanotube	4	2.8
Metal	4	2.8
Natural product, plants	4	2.8
Saccharide	4	2.8
DO, BOD	3	2.1
Electrolyte, ion	3	2.1
Hormone	3	2.1
Pesticide, fungicide	3	2.1
Cytochrome <i>c</i>	2	1.4
Food	2	1.4
Total	141	100.0

Table 9

Distribution of analyte and matrix of research papers published in the "Analytical Science & Technology" (Korean) in 2004

Analyte and Matrix	No. of papers	Ratio (%)
Metal, elements	19	27.1
Environmental, VOC, phenols, bisphenols, dioxins, PCB, PAH	17	24.3
Miscellaneous	11	15.7
Material, polymer	6	8.6
Drugs	5	7.1
Natural product, plants	5	7.1
Bio-sample, blood, urine, metabolite, gene	4	5.7
Enzyme	1	1.4
Protein	1	1.4
Food	1	1.4
Total	70	100.0

bio-scientific needs enhances the importance of analytical separation. Probably these data is helpful in understanding on the current standing and the important role of analytical separation in Korea.

6. Trends and emerging technology

Most of attention is devoted to the separation topic, which represents almost more than half the total published papers and is covered with application of GC–MS (tandem), LC–MS (tandem), MALDI-TOF-MS, and CE–MS. From these results we concluded that MS has rapidly become a common tool for analytical separation in many areas. This hyphenated combination ensures more reliable detection, identity confirmation and quantification of target analytes as well as the identification of unknowns.

Analytical instrumentation has, over the past 30 years, undergone a remarkable transformation. And it is going through increases in throughput through miniaturization, parallelization, integration, and automation. The latest research has expanded to single cell or unimolecule levels. Bioactive substance such as DNA and proteins, chiral medicines, environmental poisons have been chosen more and more as analytical objects.

Major analytical techniques in Korea are being or will soon be influenced by the international main streams and the introduction of newly developed instrumentations or devices. There is increasing demand for faster, simpler and more economic analytical methods that represent a real alternative to the highly manipulative multi-step procedures still in use in many laboratories. The increase in the number of papers in the use of advanced analytical methods by some experts does not mean that they can make all aspects of analytical methods. Still there are lots of problems in the development of analytical methodology.

In the current stage, basic efforts and challenges are rare to develop and to build new innovative analytical instrumentations in Korea. However, I hope and confident that our young scientists can discover their target goal in the nearest future. For all research activities, it is important to emphasize that innovative ideas, well-educated skillful experts, steady efforts, financial supports and special actions by international collaborations with experts are essentially required for the further advance in the fields of analytical separation.

Acknowledgements

This review was presented at 2005 China–Japan–Korea Symposium on Environmental Analytical Chemistry of JAIMA Conference (September 1–2, 2005, Makuhari Messe, Chiba, Japan). The author acknowledge to Professor Hiroshi Nakamura (Tokyo Science University), Emeritus Professor Toshiyuki Hobo (Tokyo Metropolitan University), and Dr. Tsuneaki Maeda (AIST) for inviting me to JAIMA Conference.

References

- [1] <http://pubs.acs.org/journals/ancham/index.html>.
- [2] <http://www.sciencedirect.com/science/journal/00032697>.
- [3] <http://www.sciencedirect.com/science/journal/00032670>.
- [4] <http://www.rsc.org/Publishing/Journals/an/index.asp>.
- [5] <http://link.springer.de/link/service/journals/00216/>.
- [6] <http://www3.interscience.wiley.com/cgi-bin/jhome/76510662>.
- [7] <http://www.j-chrom-sci.com/>.
- [8] <http://www.wiley-vch.de/publish/en/journals/alphabeticIndex/2027/>.
- [9] <http://www.sciencedirect.com/science/journal/00399140>.
- [10] <http://www3.interscience.wiley.com/cgi-bin/jhome/4849>.
- [11] <http://www.kcsnet.or.kr/>.
- [12] Anal. Sci. Technol. 15 (6) (2004).
- [13] <http://www.psk.or.kr/home/kor/>.
- [14] <http://www.kosfost.or.kr/>.
- [15] Program and Abstract, The 93rd National Meeting of the Korean Chemical Society.
- [16] Program and Abstract, The 94th National Meeting of the Korean Chemical Society.
- [17] Program and Abstract, The 32nd National Meeting of the Korean Society of Analytical Science.
- [18] Program and Abstract, The 33rd National Meeting of the Korean Society of Analytical Science.

Determination of estrogens in water by HPLC–UV using cloud point extraction

Ling Wang^{a,b}, Ya-Qi Cai^a, Bin He^a, Chun-Gang Yuan^a,
Da-Zhong Shen^b, Jing Shao^a, Gui-Bin Jiang^{a,*}

^a State Key Laboratory of Environmental Chemistry and Ecotoxicology, Research Center for Eco-Environmental Sciences,
Chinese Academy of Sciences, P.O. Box 2871, 100085 Beijing, PR China

^b School of Chemistry and Chemical Engineering, Shandong University, Jinan 250100, PR China

Received 30 October 2005; received in revised form 12 January 2006; accepted 13 January 2006

Available online 17 February 2006

Abstract

A method based on cloud point extraction was developed to determine four kinds of estrogens: estriol (E3), estradiol (E2), estrone (E1), and progesterone (P) in water by high performance liquid chromatography separation and ultraviolet detection (HPLC–UV). The non-ionic surfactant Triton X-114 was chosen as extractant solvent. The parameters affecting extraction efficiency, such as concentrations of Triton X-114 and Na₂SO₄, equilibration temperature, equilibration time and centrifugation time were evaluated and optimized. Under the optimum conditions, preconcentration factors of 99 for E3, 73 for E2, 152 for E1 and 86 for P were obtained for 10 mL water sample. The detection of limitation was 0.23 ng mL⁻¹ for E3, 0.32 ng mL⁻¹ for E2, 0.25 ng mL⁻¹ for E1 and 5.0 ng mL⁻¹ for P. The proposed method was successfully applied to the determination of trace amount of estrogens in wastewater treatment plant (WWTP) effluent water and exposure water with 10 ng mL⁻¹ E2 for toxicological study in our lab. For the case of WWTP effluent water samples, no estrogen was found. The accuracy of the proposed method was tested by recovery measurements of spiked samples and good recoveries of 81.2–99.5% were obtained.

© 2006 Published by Elsevier B.V.

Keywords: Estrogens; Cloud point extraction; Triton X-114; Non-ionic surfactant; HPLC–UV

1. Introduction

The detection of natural and synthetic estrogens in water [1,2] has attracted great interest in the research community and the general public because of their potential adverse ecological effects. Exposure to environmental estrogens has given rise to decreased sperm counts, increased testicular, prostate, breast cancer, and to reproductive disorders in human males [3]. Relatively large amounts of natural and synthetic reproductive hormones enter various environments via several pathways such as the sewage treatment plant (STP) effluent outfalls. The large amounts of animal wastes and biosolids applied to agricultural fields might flow into nearby bodies of water or infiltrate through the soil into groundwater [4]. Cattle and poultry manure have been reported as a source of the environmental loadings of 17 β -estradiol [1].

Naturally occurring estrogens include estradiol and its most common metabolites and/or precursors: estrone and/or estriol. Progesterone is considered as a hormone balancer. Their physicochemical properties were listed in Table 1. The concentrations of estrogens in the environment are about several sub-ng to thousands of ng L⁻¹ level [4,5]. The most widely used methods for analyzing these estrogens are chromatographic techniques such as gas chromatography (GC) or high performance liquid chromatography (HPLC), but their sensitivity and selectivity limit their direct use for determination of these contaminants at a very low concentration level in environmental samples with complex matrix. Therefore, a sample pretreatment step prior to chromatographic analysis is usually necessary, such as liquid–liquid extraction (LLE) and solid-phase extraction (SPE). Unfortunately, all of these methods require a large sample volume and time-consuming. In particular, the traditional liquid–liquid extraction method is also dangerous to analysts because of the large volume of volatile organic solvent required. So in the last decades, the green liquid–liquid extraction method cloud point extraction (CPE) has been employed in analytical chemistry to

* Corresponding author. Tel.: +86 10 6284 9334; fax: +86 10 6284 9179.
E-mail address: gbjiang@mail.reces.ac.cn (G.-B. Jiang).

Table 1
Physicochemical properties of estrogens^a

Chemical name	Molecular weight	Water solubility (mg/L, 25 °C)	Vapour pressure (mmHg)	log K_{ow}
Estrone (E1)	270.4	30	1.4×10^{-7}	3.13
17 β -Estradiol (E2)	272.4	3.6 ^b	1.3×10^{-8}	4.01
Estriol (E3)	288.4	441	1.97×10^{-10}	2.45
Progesterone (P)	314.4	8.81	1.3×10^{-6}	3.87

^a Data from SRC PhysProp Database.

^b Tested at 27 °C.

preconcentrate organic compounds [6–8] and metal ions [9–11]. Compared with the traditional organic liquid–liquid extraction, cloud point extraction requires a very small amount of relatively nonflammable and nonvolatile surfactants that are friendly to the environment. Another important merit is that no analytes are lost because it is unnecessary to evaporate the solvents. Using appropriate conditions such as temperature, concentration of surfactant, and equilibration time, the solution containing the surfactant becomes turbid and separates two phases: a surfactant-rich phase (at a very small volume) and a larger volume of aqueous solution phase (bulk amount) with a diluted surfactant concentration, which approximates to its critical micelle concentration (CMC). The hydrophobic analytes of the solution are extracted into the surfactant-rich phase. Compared to the initial solution volume, the surfactant-rich phase volume is very small, thus a high enrichment factor can be obtained. As a promising alternative to traditional solvent extraction, CPE, especially the extraction of environmental pollutants is still at its initial stage. Only a few reports can be found on the extraction of polycyclic aromatic hydrocarbons (PAH) [12–14] and polychlorinated biphenyls (PCBs) [15] and dibenzofurans (PCDFs) [16], polychlorinated dibenzop-dioxins (PCDDs) [14], pesticides [16], vitamins [17] and other organic compounds such as chlorinated phenols [18]. All these indicate that cloud point extraction have great analytical potential as an effective enrichment method. But no reports have been published about how to extract estrogens from the water.

In the present study, a method was developed for analyzing the trace level determination of estrogens in water by CPE using Triton X-114 as the extraction solvent. The instrument is a high performance liquid chromatography coupled with an UV detector.

2. Experimental

2.1. Reagents

All reagents used were HPLC grade, and purified water from a Milli Q system was used throughout the experiments. Estroil, 17 β -estradiol, estrone and progesterone were obtained from Sigma–Aldrich, USA. Standard stock solutions (1000 μ g/mL) containing these compounds were prepared by dissolving an appropriate amount of these compounds in methanol. Working solutions were prepared daily by an appropriate dilution of the stock solutions. The non-ionic surfactant TritonX-114 (Acros Organics, New Jersey, USA) was used without further

purification. Na₂SO₄ (Beijing Chemical Factory, PR China) was prepared immediately before each experiment.

The vessels used for trace analysis were washed with methanol and purified water before usage.

2.2. Instrumentation

The HPLC system used includes an Agilent 1100 series binary pump, an Agilent 1100 series VWD detector and a Rheodyne 7225i injector. The separations were performed on an Inertsil ODS-C18 column (250 mm \times 4.6 mm, particle size, 5 μ m). Acetonitrile and water were used as mobile phase with the gradient program as follows: 0–4.5 min, 45:55; 5.0–20 min 75:25, acetonitrile:water, v/v, and 1 mL min^{−1} was selected as the flow rate of the mobile phase. The VWD detector settings were as follows, 0–10 min, 200 nm, for E3, E2, E1, 11–20 min, and 240 nm for progesterone. A personal computer equipped with an Agilent Chemstation program for LC systems was used to acquire and process chromatographic data. Peak area was used as the analytical measurement. A thermostatic bath (TB-85 Thermo Bath, Shimadzu, Japan), maintained at the desired temperature, was used to obtain cloud point preconcentration. Centrifugation with calibrated centrifugal tubes (Beijing Medicinal Instrument company, PR China) was used to accelerate the phase separation process. Easypure deionized water was used in this study (Model D7382-33, Barnstead Thermolyne Corporation, Dubuque, IA, USA). An Agilent syringe was used for injecting the sample into the loop. Twenty microliters were chosen as the injecting volume.

2.3. Cloud point procedure

For the extraction and preconcentration of estrogens, an aliquot of 10 mL of sample solution containing the analytes with 0.25% (w/v) of TritonX-114 and 0.4 M Na₂SO₄, were kept for 60 min in the thermostatic bath at 45 °C. Then the phase separation was accelerated by centrifugation for 5 min at 3500 rpm. After phase separation, the bulk aqueous phase was removed and the volume of the two phases was measured. Then, 20 μ L of the remaining surfactant-rich phase was directly injected in the HPLC loop for subsequent analysis.

2.4. Extraction of estrogens in real samples

Sample 1: Fishes were kept in the exposure water with 10 ng mL^{−1} E2 for toxicological study in our lab. Theoretically,

E2 may degrade into E1 and CO₂ in short time. This exposure water was determined after 24 h.

Sample 2: The effluent water from Gaobeidian (waste water treatment factory) WWTP (Beijing, China).

The real water samples were filtered through a 0.45 μm pore-size membrane filter to remove the suspended particular matter and detected within 48 h after receiving them from WWTP (protected by adding 1% formaldehyde to the water). A 10 mL real water sample was submitted to the cloud point extraction procedure using 0.25% TritonX-114 and 0.4 M Na₂SO₄. After phase separation, 20 μL of surfactant-rich phase was directly injected to the injection loop for the analysis. Standard solutions containing 10, 10, 10, 50 ng mL⁻¹ of E3, E2, E1 and P were added to a 10 mL real water for the recovery test, respectively.

3. Results and discussion

TritonX-114 with a cloud point temperature of 23 or 24 °C [19,20] is one of the most commonly used non-ionic surfactants in the cloud point extraction [20]. There are several different parameters that can influence the extraction efficiency. They were investigated in our experiments. However, it is found that the preconcentration factor is independent of the initial concentration [21].

3.1. Effect of the concentration of surfactant

The theoretical preconcentration factor depends on the concentration of surfactant. For its low cloud point temperature and high density, Triton X-114 was chosen as the extractant solvent, and phase separation was facilitated by centrifugation [22]. The effect of the concentration of surfactant was examined in our study and the result was shown in Fig. 1. From Fig. 1, it can be found that when the concentration of surfactant in solution varies in the range 0.20–2.0%, the highest extraction efficiency is at 0.25%. In this experiment, when the concentration of surfactant is below 0.25%, it always suspends in the bulk solution and is

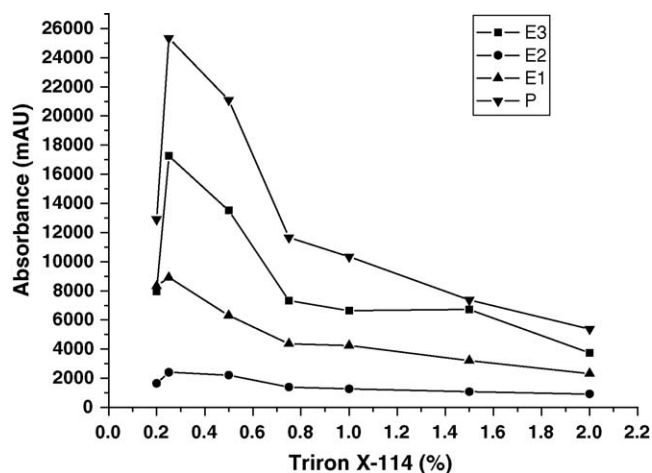


Fig. 1. Extraction effect of the estrogens as a function of Triton X-114 concentration: (■) estriol; (◆) estradiol; (▲) estrone; (▼) progesterone.

very difficult to separate into two phases. Based on these experiment results, 0.25% TritonX-114 was adopted as the optimum amount to achieve best analytical signals and highest extraction efficiency.

3.2. Effect of equilibration time

The equilibration time can affect the preconcentration factor of the surfactant [15], therefore, study on the determination of the optimum equilibration time was carried out to obtain appropriate recovery percentages for the analytes. Triton X-114 surfactant exhibits a similar behavior for all the estrogens under the given concentration range. Fig. 2 shows an increase in the extraction efficiency within the initial 20 min, then slight decrease in the following 30 min and increase again at 60 min, which is similar to the result of other research [20]. As a consequence, 60 min was adopted as the optimum equilibration time.

3.3. Effect of concentration of Na₂SO₄

The addition of salt to the solution can influence the extraction process. For most non-ionic surfactant, the presence of salts may facilitate phase separation since they increases the density of the aqueous phase [23]. Available electrolytes can also change the cloud point temperatures of non-ionic surfactant. The relevant electrolytes are usually in high concentrations (exceeding 0.1 M) [24]. The salting-in and salting-out effects can be used to interpret the electrolyte effects on the cloud points of non-ionic surfactant [25]. To study the influence of the electrolyte, different concentrations of Na₂SO₄, ranging from 0 to 0.7 M were added to the solution. The results are in concordance with other studies. The final surfactant-rich phase volume was not noticeably influenced by the increased ionic strength [25]. When the concentration is higher than 0.4 M, the surfactant-rich phase will be on the surface of the solution, which will make it more difficult to separate the extraction solvent into two phases and the accuracy and reproducibility probably were not satisfactory. As

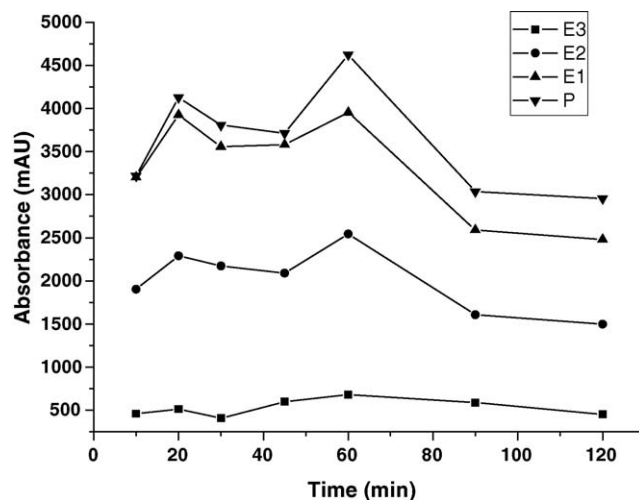


Fig. 2. Effect of the equilibration time on the extraction efficiency: (■) estriol; (◆) estradiol; (▲) estrone; (▼) progesterone.

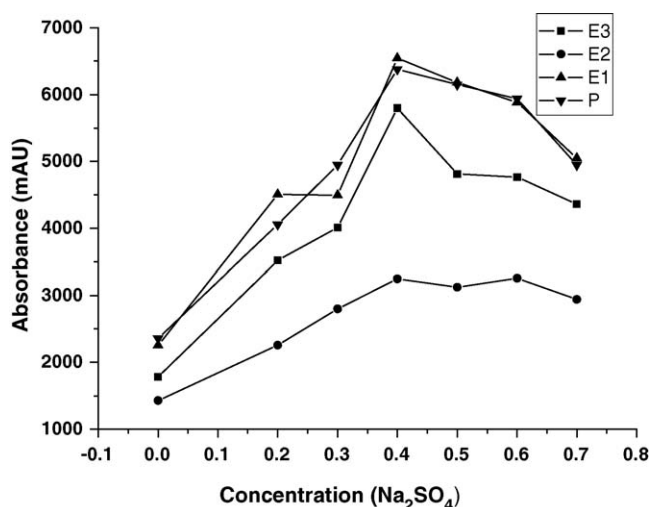


Fig. 3. Effect of the ionic strength on the extraction efficiency: (■) estriol; (◆) estradiol; (▲) estrone; (▼) progesterone.

shown in Fig. 3, the extraction effect is best when the concentration is 0.4 M.

3.4. Effect of the equilibration temperature

When the cloud point extraction procedure was processed at equilibration temperature of the surfactant, the best extraction effect was achieved [26]. Thus, it is necessary to examine the effect of temperature on cloud point extraction. If the temperature is lower than the cloud point, two phases cannot be formed. Higher temperature leads to the decomposition of estrogens. In order to employ the lowest possible equilibration temperature to the efficient separation of phases, the equilibration temperature was examined. Theoretically, the optimal equilibration temperature of the extraction occurs when the equilibration temperature is 15–20 °C greater than the cloud point temperature of surfactant [26]. Fig. 4 shows the effects of equilibration temperature on the extraction efficiency. The maximum signals were obtained at

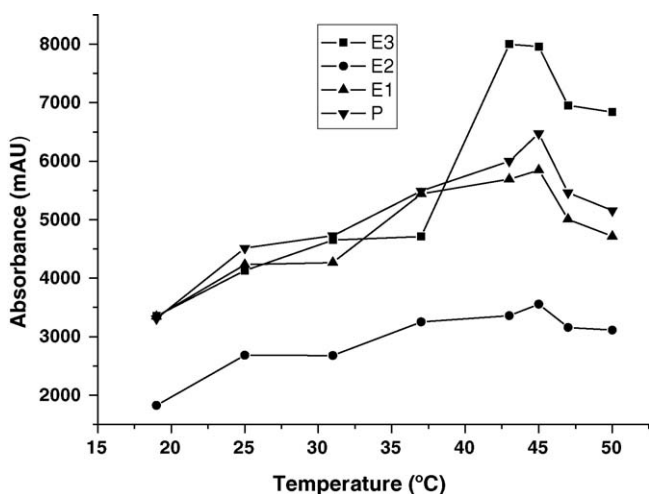


Fig. 4. Effect of temperature on the extraction efficiency: (■) estriol; (◆) estradiol; (▲) estrone; (▼) progesterone.

Table 2

Analytical characteristics of the method

Analyte	Enrichment factor	Detection limit ^a (ng mL ⁻¹)	R.S.D. (%)	R ²	Linear range (ng mL ⁻¹)
Estriol	99	0.23	8.5	0.9973	1–51.6
Estradiol	73	0.32	12	0.996	1–90
Estrone	152	0.25	8.1	0.9961	1–192
Progesterone	86	5.0	10.1	0.9994	50–1600

^a Limit of detection defined as three times the signal-to-noise ratio.

temperatures between 37–50 °C. Therefore 45 °C was selected as the working equilibration temperature.

3.5. Effect of centrifugation time

The effect of centrifugation time on phase separation was studied in the range 2–20 min at 3500 rpm. The results showed that 5 min was enough to get a complete phase separation. So a centrifugation time of 5 min was selected as optimum.

3.6. Characteristics of analytical method

Table 2 shows some characteristics of the proposed method. The linearity of the four estrogen compounds was in the range 1.0–51.6 ng mL⁻¹ for E3, 1–90 ng mL⁻¹ for E2, 1–192 ng mL⁻¹ for E1 and 50–1600 ng mL⁻¹ for P, respectively. The detection limits based on three levels of the background signal to noise were 0.23 ng mL⁻¹ for E3, 0.32 ng mL⁻¹ for E2, 0.25 ng mL⁻¹ for E1 and 5 ng mL⁻¹ for P, respectively. Fig. 5 is the comparison of chromatograms before enrichment and after enrichment.

3.7. Analysis of real samples

In order to validate the accuracy and precision of the proposed method under the selected conditions, WWTP effluent water sample, exposure water in our lab and spiked samples

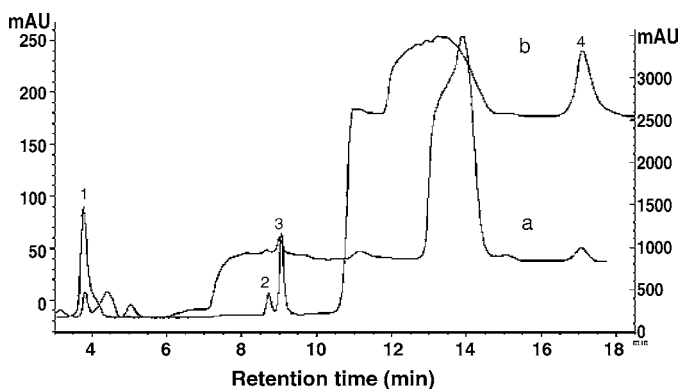


Fig. 5. Chromatograph of a standard solution (a) standard solution in the bulk aqueous before enrichment (left). (b) Standard solution in the enrichment-phase (right). Experimental conditions: Triton X-114 is 0.25% and 0.4 M for Na₂SO₄, equilibration temperature is 45 °C, equilibration time is 60 min.

Table 3
Determination and recoveries of four analytes spiked water samples

Water sample	Added (ng mL ⁻¹)	Found ^a (ng mL ⁻¹)	Recovery ^b (%)
WWTP effluent water			
E3	–	nd	–
	10.0	9.9	99.0 ± 8.5
E2	–	nd	–
	10.0	8.1	81.2 ± 11.5
E1	–	nd	–
	10.0	9.8	98.0 ± 8.1
P	–	nd	–
	50.0	46.1	92.1 ± 10.1
Exposed water in our lab (E2: 10 ng mL ⁻¹)			
E3	–	nd	–
	10.0	9.9	99.5 ± 10.1
E2	–	5.6	–
	10.0	15.4	99.0 ± 12.0
E1	–	nd	–
	10.0	9.8	98.0 ± 10.5
P	–	nd	–
	50.0	49.5	99.0 ± 11.5

^a Mean for three determinations.

^b Mean and standard deviation for three determinations. nd: not detected.

had been tested. The results are shown in Table 3. In all cases the spiked recoveries were satisfied, showing no obvious matrix interferences.

4. Conclusion

The cloud point technique was applied as an effective method for the extraction of four kinds of estrogens (estriol, estradiol, estrone, progesterone) in aqueous samples. Using HPLC technique coupled with UV detector, the concentration of Triton X-114 is 0.25% and 0.4 M for Na₂SO₄, equilibration temperature is 45 °C, equilibration time is 60 min and centrifugation time is 5 min. The high recoveries and precision showed the optimal experimental condition were satisfied. In conclusion, the proposed method is a simple, rapid, and effective method for the simultaneous determination of four kinds of estrogens with their very low concentration in environmental water.

Acknowledgements

This work was jointly supported by the National Basic Research Program of China (2003CB415001) and National Natural Science Foundation of China (20137010).

References

- [1] D. Kolpin, E. Furlong, M. Meyer, E.M. Thurman, S. Zaugg, L. Barber, H. Buxton, *Environ. Sci. Technol.* 36 (2002) 1202.
- [2] M.J. López de Alda, D. Barceló, *J. Chromatogr. A* 892 (2000) 391.
- [3] R. Liu, J.L. Zhou, A. Wilding, *J. Chromatogr. A* 1022 (2004) 179–189.
- [4] M.J. López de Alda, D. Barceló, *Fresenius J. Anal. Chem.* 371 (2001) 437.
- [5] W. Roger, Giese, *J. Chromatogr. A* 1000 (2003) 401.
- [6] S.Y. Yuan, C. Liu, C.S. Liao, B.V. Chang, *Chemosphere* 49 (2002) 1295.
- [7] I. Casero, D. Sicilia, S. Rubio, D. Pérez-Bendito, *Anal. Chem.* 71 (1999) 4519.
- [8] R. Carabias-Martínez, E. Rodríguez-Gonzalo, J. Domínguez-Alvarez, J. Hernández-Méndez, *Anal. Chem.* 71 (1999) 2468.
- [9] J.R. Chen, K.C. Teo, *Anal. Chim. Acta* 434 (2001) 325.
- [10] J.L. Manzoori, G. Karim-Nezhad, *Anal. Chim. Acta* 484 (2003) 155.
- [11] Ch.G. Yuan, G.B. Jiang, Y.Q. Cai, B. He, J.F. Liu, *Atom. Spectrom.* 25 (2004) 170.
- [12] A. Rodenbrock, K. Selber, M.R. Egmond, M.R. Kula, *Bioseparation* 9 (2000) 269.
- [13] A. Collén, J. Persson, M. Linder, T. Nakari-Setälä, M. Penttilä, F. Tjerneld, U. Sivars, *Biochim. Biophys. Acta* 1569 (2002) 139.
- [14] S.R. Sirimanne, J.R. Barr, D.G. Patterson, L. Ma, *Anal. Chem.* 68 (1996) 1556.
- [15] A. Eiguren-Fernández, Z. Sosa-Ferrera, J.J. Santana-Rodríguez, *Anal. Chim. Acta* 358 (1998) 145.
- [16] A. Eiguren-Fernández, Z. Sosa-Ferrera, J.J. Santana-Rodríguez, *Analyst* 124 (1999) 487.
- [17] C. García-Pinto, J.L. Pérez-Pavón, B. Moreno-cordero, *Anal. Chem.* 64 (1992) 2334.
- [18] T. Saitoh, W.L. Hinze, *Anal. Chem.* 63 (1991) 2520.
- [19] K. Toerne, R. Rogers, R.V. Wandruszka, *Langmuir* 16 (2000) 2141.
- [20] B. Delgado, V. Pino, J.H. Ayala, V. González, A.M. Afonso, *Anal. Chim. Acta* 518 (2004) 165.
- [21] J.L. Li, B.H. Chen, *J. Colloid Interf. Sci.* 263 (2003) 625.
- [22] F. Shemirani, M. Baghdadi, M. Ramezani, M.R. Jamali, *Anal. Chim. Acta* 534 (2005) 163.
- [23] R. Carabias-Martínez, E. Rodríguez-Gonzalo, B. Moreno-Cordero, J.L. Rez-Pavon, C. García-Pinto, E. Fernandez Laespada, *J. Chromatogr. A* 902 (2000) 251.
- [24] M.K. Purkait, S.S. Vijay, S. DasGupta, S. De, *Dyes and Pigments* 63 (2004) 151.
- [25] V. Pino, J.H. Ayala, A.M. Afonso, V. González, *J. Chromatogr. A* 949 (2002) 291.
- [26] R.P. Frankewich, W.L. Hinze, *Anal. Chem.* 66 (1994) 944.

Spectral assignments to the light emissions of fluorescent organic small molecules in aqueous medium

Shao Fen Chen, Yuan Fang Li, Cheng Zhi Huang*

College of Chemistry and Chemical Engineering, and Key Laboratory of Eco-Environments of Three Gorges Reservoir Region under PRC National Education Ministry, Southwest University, Chongqing 400715, China

Received 30 October 2005; received in revised form 16 January 2006; accepted 20 January 2006
Available online 10 March 2006

Abstract

Spectrofluorometric identifications of artificial organic dyes have important environmental significance, but both scattered light signals and the fluorescence signals were twins in fluorospectroscopy, and the light scattering signals are always the interference sources of spectrofluorometry. In order to investigate the relationship between the light scattering and fluorescence in the spectrofluorometric measurements, herein we discuss the scattered light and fluorescence emission properties of organic small molecules (OSMs) using Lignin Pink (LP) in neutral medium as an example. With the help of UV–vis measurements, and starting from three-dimensional light emission measurements, scattered light and fluorescence emissions could be assigned. Investigations by increasing LP concentration showed that the light emission at 282.0 and 344.0 nm could be attributed to the resonance light scattering (RLS) signals and that at 420.0 and 570.0 nm are composed of both RLS and fluorescence emissions, respectively. UV–vis measurements showed that LP does not have the tendency of aggregation, and the strong RLS signals should be ascribed to the large hydrodynamic diameter of LP itself in aqueous medium, supported by dynamic light scattering (DLS) measurements.

© 2006 Published by Elsevier B.V.

Keywords: Lignin Pink (LP); Organic small molecules (OSMs); Resonance light scattering (RLS); UV–vis absorption; Fluorescence

1. Introduction

Artificial organic dyes have important environmental effects, and most of them have low biodegradable ability and potential toxicity [1], which can cause water pollution and affect growths of aquatic organism and microbes, etc. Especially some azo dyes, such as Tropaeolin O, have toxicity to aquatic microbial populations and lead to the decrease of biomass [2]. These azo dyes also are high carcinogenic that can decompose and produce aromatic amine, then change the structure of DNA, which result in human pathological changes and induce cancer. About 100 years ago, Fuchsin dye was confirmed to have connection with the cancer of male bladder. The Sudan Red was also thought to have the character of carcinogenicity and mutagenicity recently. In order to identify their roles physiologically and environmentally played, one has applied optical techniques. Of these optical techniques, spectrofluorometry has great potential and has shown high promise. However, fluores-

cence and scattered light signals are twins in spectrofluorometry since the appearance of light scattering is unavoidable in any medium, and the scattered light signals always act as interference roles, reducing the determination sensitivity in spectrofluorometry. Efforts have been made to reduce the interference effects of scattered light emission such as low-temperature frozen and magnetic field-resolved techniques [3]. On the other hand, the scattered light signals could have been useful for detecting the size and distribution of particles in colloid, polymer and pharmaceutical sciences. By simultaneously scanning the excitation and emission monochromators of a common spectrofluorometer with $\lambda_{\text{ex}} = \lambda_{\text{em}}$, a resonance light scattering (RLS) technique has been constructed [4,5] and it has proved that this technique is a new sensitive spectroscopic tool because the RLS measurement and enhanced RLS signals could be measured when the wavelength of the light beam for excitation is close to the absorption region of the aggregation or assembly species. These enhanced RLS signals have been successfully applied to characterize the aggregation and assembly of biological and chemical species [4–8] and quantify the nucleic acids [9,10], proteins [11,12], drugs [13], bacteria [14,15] and environment contaminations [16], etc.

* Corresponding author. Tel.: +86 23 68254659; fax: +86 23 68254000.
E-mail address: chengzhi@swu.edu.cn (C.Z. Huang).

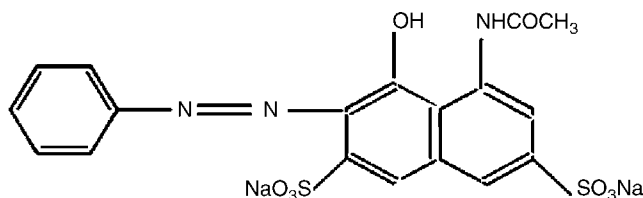


Fig. 1. The molecular structure of Lignin Pink.

In fact, the signals are very complex measured by the RLS mode, namely by simultaneously scanning the excitation and emission monochromators of the spectrofluorometer by keeping $\lambda_{\text{ex}} = \lambda_{\text{em}}$. The signals obtained by RLS mode are connected not only with the molecule absorption, the size of assemblies [17,18], excitation wavelength and emission wavelength, but also with the slit width of spectrofluorometer [19]. It has been reported that the signals obtained by RLS mode not only include the Rayleigh scattering, but also the Tyndall scattering [20,21], etc. In our experiments we observed that the signals by RLS mode contain fluorescence signals for some species, particularly organic small molecules (OSMs) with small Stokes shift, whose excitation and emission spectra are overlapped. Considering that OSMs are very important acting as binding guest to probe the biomolecules and environmental acceptors, herein we take the anion dye Lignin Pink (LP) as an example since LP is mostly applied to the dyeing of lignin and chitosan, and try to discuss components of the light emission signals in the synchronous RLS scanning mode of the excitation and emission monochromators of the spectrofluorometer.

2. Experimental

2.1. Apparatus

A Hitachi F-4500 spectrofluorometer (Tokyo, Japan) was used to record the scattered light and fluorescence emissions, while a Hitachi UV-3010 spectrophotometer (Tokyo, Japan) was used to measure the absorption spectra. A N5 PCS submicron particles size analyzer (Beckman-Coulter, Miami, USA) was employed to determine the size (hydrodynamic diameter) based on dynamic light scattering (DLS) and a PHS-3C digital pH meter (Shanghai Dazhong Analytical Instruments Plant, Shanghai) was used to measure the pH values of the aqueous solutions. A QL-901 vortex mixer (Haimen Qilinbei'er Instrumental Ltd., Haimen, PRC) was employed to blend the solutions in volumetric flasks.

2.2. Reagents

A $1.0 \times 10^{-2} \text{ mol L}^{-1}$ stock solutions of Lignin Pink (LP, the molecular structure is showed in Fig. 1) were prepared by dissolving the commercial powder (Shanghai Chemical Reagents Co., China) into doubly distilled water, and working solutions of 1.0×10^{-3} , 1.0×10^{-4} and $1.0 \times 10^{-5} \text{ mol L}^{-1}$ were prepared by diluting the stock solution directly. Britton-Robinson buffer solution was used to control the acidity of the system. All reagents were of analytical grade without further purification. Water used throughout was doubly distilled.

2.3. Procedure

Appropriate volume of LP working solution was placed in a 10-mL volumetric flask, and then 1.0 mL of BR buffer solution was added in. The mixture was vortexed and diluted to 10.0 mL with doubly distilled water and then mixed thoroughly. The RLS spectra were directly obtained by simultaneously scanning the excitation and emission monochromators of the F-4500 spectrofluorometer with $\lambda_{\text{ex}} = \lambda_{\text{em}}$ from 220.0 to 700.0 nm. Both the excitation and emission slit widths were kept as 10.0 nm and the PMT voltage was 400 V for RLS measurements. The fluorescence emission spectra, on the other hand, were obtained by keeping the slit widths 10.0 nm for both excitation and emission and the PMT voltage 700 V considering that the fluorescence emission is much weaker than light scattering one. The absorption spectrum was made against buffer solutions with slit width 0.5 nm using the cell of 0.2-cm length. The size (hydrodynamic diameter) distribution was measured by N5 PCS submicron particle analyzer at a 90° scattering angle in a stable ambient of 20.0°C by taking the viscosity and the refractive index values of 1.002 centipoises and 1.333, respectively. The hydrodynamic diameter of the particles given directly by computer is calculated via the Stokes Einstein equation.

3. Results and discussion

3.1. Three-dimensional emissions of LP

Using 3D function of F-4500 spectrofluorometer, we could get the light emission mapping of LP in aqueous solution including fluorescence and scattered light emissions (Fig. 2). It can be seen that there are four “hilltops” (A, B, C and D regions in Fig. 2a) across the straight line of $\lambda_{\text{ex}} = \lambda_{\text{em}}$ over the region of 220.0–700.0 nm (Fig. 2a), and there are six lower “hilltops” centered at E (282.0, 420.0), F (282.0, 570.0), G (344.0, 420.0), H (344.0, 570.0), M (420.0, 588.0) and N (570.0, 588.0) in the expression way of (λ_{ex} , λ_{em}) with the unit of nanometer. These “hilltops” correspond to the broken Rayleigh scattering line following $\lambda_{\text{ex}} = \lambda_{\text{em}}$ in contour plot (A, B, C and D regions in Fig. 2b), and also to the “fingerprint” regions (E, F, G, H, M and N) which display the features of fluorescence emissions of LP at 420.0 and 570.0 nm when excited at 282.0 nm, at 420.0 and 570.0 nm when excited at 344.0 nm, at 588.0 nm when excited at 420.0 nm, and at 588.0 nm when excited at 570.0 nm. Owing to too much weaker than the scattered light signals, these fluorescence “hilltops” of fluorescence (E, F, G, H, M and N in Fig. 2a) are more flat in 3D plot. In order to further understand the information of the light emission mapping, we can investigate the features of scattered light and fluorescence emissions, respectively.

3.2. RLS features of LP

The straight line following $\lambda_{\text{ex}} = \lambda_{\text{em}}$ in Fig. 2b could be available by RLS mode, that is, the light scattering signals following $\lambda_{\text{ex}} = \lambda_{\text{em}}$ straight line could be available by simultaneously scanning the excitation and emission monochromators of the

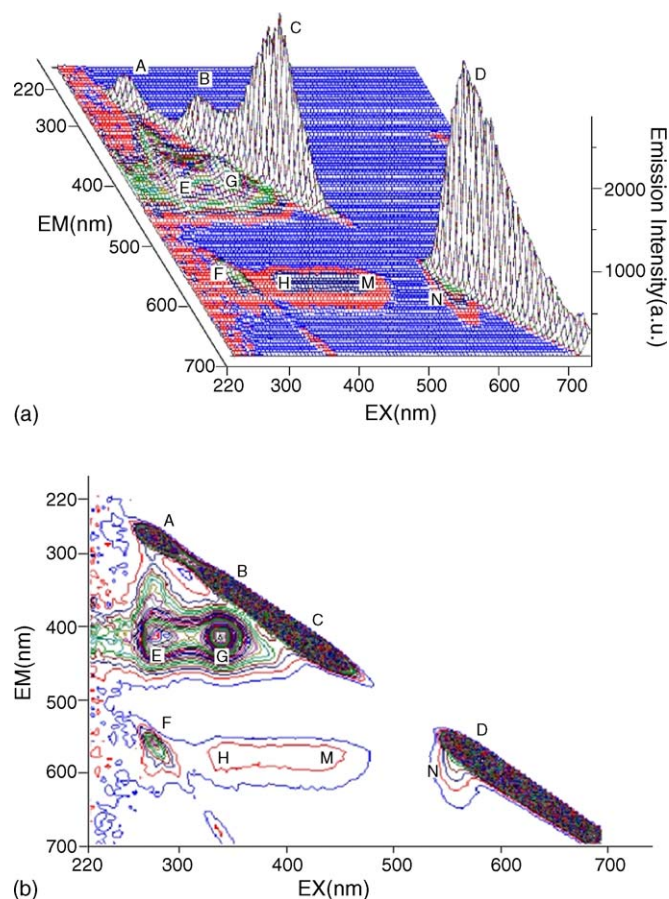


Fig. 2. Mapping of the light emission of LP in aqueous medium. Concentrations: LP, $3.0 \times 10^{-4} \text{ mol L}^{-1}$; pH 7.0; slit width: 10 nm; left, 3D plot; right, contour plot.

spectrofluorometer by keeping $\lambda_{\text{ex}} = \lambda_{\text{em}}$. Fig. 3 displays the RLS spectra characterized at 282.0, 344.0, 420.0, and 570.0 nm, corresponding to the hilltops of A, B, C and D regions in Fig. 2a. It could be seen that the RLS spectral features of LP change with its concentration and these changes take regular patterns. When LP lowers than $1.0 \times 10^{-5} \text{ mol L}^{-1}$, the feature peaks of LP are not apparent, and the shapes of peaks are similar to that of buffer solutions with the exception of higher scattering intensities (Fig. 3a); when LP ranges from 2.0×10^{-5} to $9.0 \times 10^{-4} \text{ mol L}^{-1}$ there are four peaks characterized at 282.0, 344.0, 420.0 and 570.0 nm, respectively. In spite of this, there still have variations in this concentration range. The peak intensity at 282.0 nm almost does not change, while the peaks at 344.0, 420.0 and 570.0 nm increase with increasing LP concentration from 2.0×10^{-5} to $7.0 \times 10^{-5} \text{ mol L}^{-1}$. Furthermore, the peak of 570.0 nm has red-shift tendency, and there are three isoscattering points at 335.2, 456.8 and 554.0 nm (Fig. 3b), respectively. On the other hand, the RLS intensities at 282.0, 344.0 and 420.0 nm decrease with increasing LP from 1.0×10^{-4} to $9.0 \times 10^{-4} \text{ mol L}^{-1}$, and the intensity at peak of 570.0 nm still increases with continuing red-shift tendency (Fig. 3c). Furthermore, the peaks at 282.0, 344.0 and 420.0 nm disappear when LP is higher than $1.0 \times 10^{-3} \text{ mol L}^{-1}$, and peak at 570.0 nm continues increasing and being red-shifted (Fig. 3d).

The variation of RLS spectra with LP increasing is interesting. Considering that RLS signals are directly related to the formation of large particles and could be used for the assignments of aggregation [4–8], we measured molecular absorption spectra and fluorescence emission spectra in order to investigate whether the variation of RLS spectra results from the aggregation or not.

3.3. The molecular absorption and fluorescence emission spectra of LP

Fig. 4 shows that LP has four absorption peaks characterized at 230.0, 310.0, 504.0 and 530.0 nm, and all the absorbance at these wavelengths have good linear relationships with LP concentrations, indicating that Beer's law is obeyed, and no aggregations occur in the medium. Therefore, the strong RLS signals are not resultant from the aggregation.

Fig. 5 displays the fluorescence emission features of LP, corresponding to G and H fingerprint regions in Fig. 2. When LP excited at 344.0 nm, there are two emissions. One is very strong located at 420.0 nm while the other is weak located at 570.0 nm. Both of them get increased with the red shift of 570.0 nm emission (Fig. 5a and b) when increasing LP until $1.0 \times 10^{-4} \text{ mol L}^{-1}$. When LP increasing up to $3.0 \times 10^{-3} \text{ mol L}^{-1}$, however, its fluorescence emissions are close to zero, which probably is due to the self-absorption of LP at high concentration [22].

3.4. Correlation among RLS, fluorescence and absorption spectra of LP

The arrows indicated position in Fig. 4 displays the relationships between RLS and absorption spectra of LP. There are good inversion relationships between the RLS spectra and the absorption spectra [23], that is, strong absorption corresponds to the weak RLS signals, while the characteristic RLS peaks at 282.0, 344.0, 420.0 and 570.0 nm nearly correspond to the troughs of absorption (please see the arrows indicated A, B, C, and D in Fig. 4). As questioned above, the RLS intensities decrease at 282.0, 344.0 and 420.0 nm but increase at 570.0 nm with increasing LP. The reason is that the absorptions at 282.0, 344.0 and 420.0 nm increase with increasing LP (Fig. 4), which makes the signals of RLS decrease due to the internal filtering effects. The RLS intensities at 570.0 nm, however, increase throughout with increasing LP since the absorption background is very low, which does not have any negative effect on RLS.

The emission at 420 and 570 nm obtained by simultaneously scanning the excitation and emission monochromators of the spectrofluorometer with $\lambda_{\text{ex}} = \lambda_{\text{em}}$ should include RLS and fluorescence emission. From Fig. 2 (b), we observed the overlapped fluorescence and RLS signals for 420 and 570 nm, so we think there exist synchronous fluorescence for 420 and 570 nm. And Figs. 3 and 5 show that the RLS and fluorescence intensities have the identical trends at 420 nm, namely, both of which are increased with increasing LP until $1.0 \times 10^{-4} \text{ mol L}^{-1}$, then decrease and disappear finally with the further increasing LP. These fluorescence intensities changes also are adapt

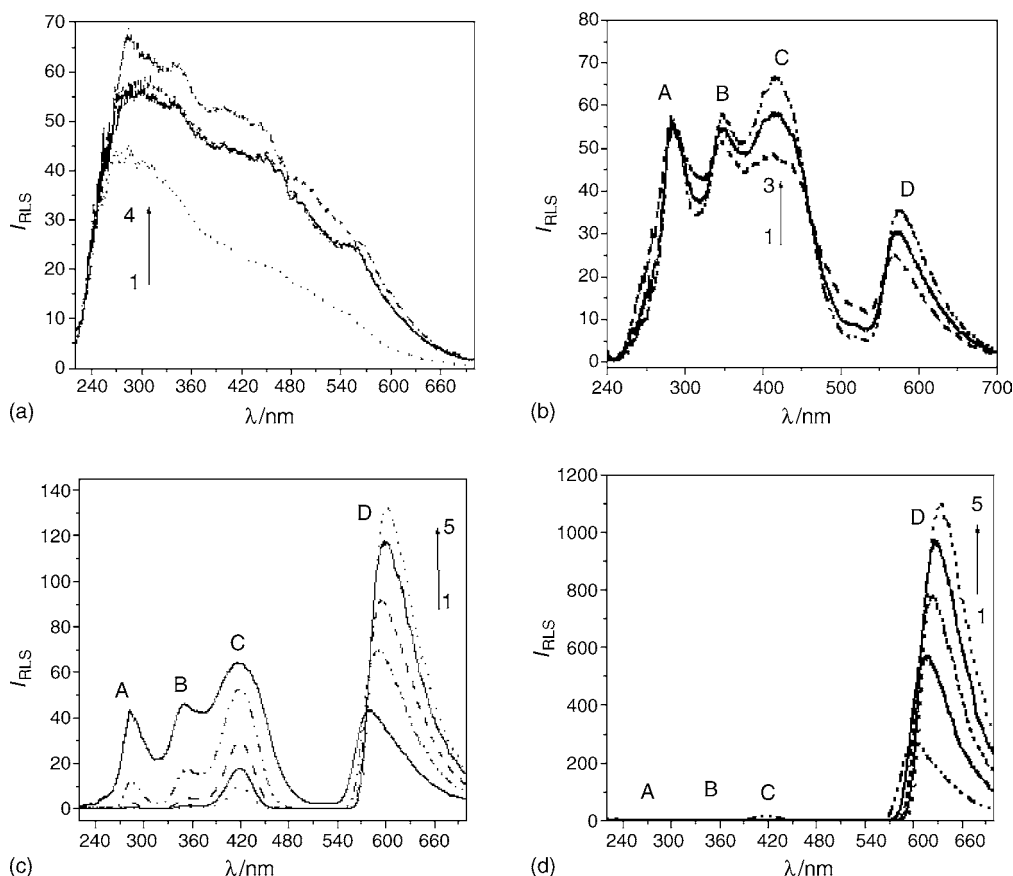


Fig. 3. RLS spectra of LP. A, B, C and D correspond to the “hilltops” in Fig. 2. Concentrations (mol L^{-1}): LP, a (curves 1–4): 0.0, 1.0×10^{-6} , 5.0×10^{-6} , 1.0×10^{-5} ; b (curves 1–3): 3.0×10^{-5} , 5.0×10^{-5} , 7.0×10^{-5} ; c (curves 1–5): 1.0×10^{-4} , 3.0×10^{-4} , 5.0×10^{-4} , 7.0×10^{-4} , 9.0×10^{-4} ; d (curves 1–5): 1.0×10^{-3} , 3.0×10^{-3} , 5.0×10^{-3} , 7.0×10^{-3} , 1.0×10^{-2} ; pH 7.0.

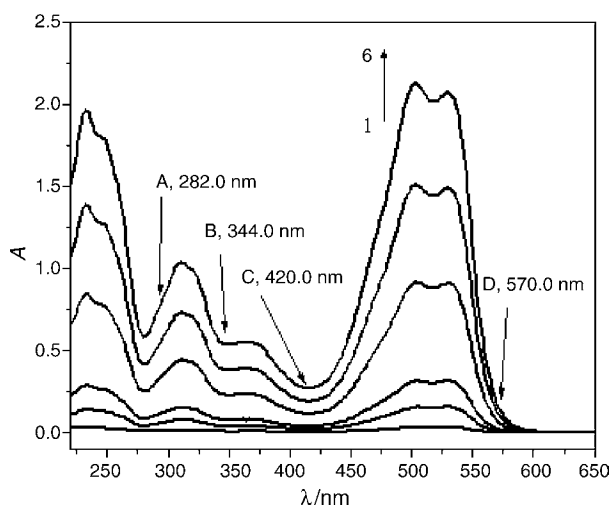


Fig. 4. Absorption spectra of LP. Concentrations (mol L^{-1}): LP, (curves 1–6): 1.0×10^{-5} , 5.0×10^{-5} , 1.0×10^{-4} , 3.0×10^{-4} , 5.0×10^{-4} , 7.0×10^{-4} ; pH 7.0. The linear regression equations (c , mol L^{-1}) could be obtained of $A_{230} = 0.040 + 28.98c$ ($n = 10$, $r = 0.9991$), $A_{310} = 0.008 + 14.62c$ ($n = 10$, $r = 0.9999$), $A_{504} = 0.021 + 29.87c$ ($n = 10$, $r = 0.9998$), and $A_{530} = 0.048 + 28.27c$ ($n = 10$, $r = 0.9995$) over the range of 1.0×10^{-5} to $1.5 \times 10^{-3} \text{ mol L}^{-1}$ at the wavelengths of 230.0, 310.0, 504.0 and 530.0 nm, respectively.

to 570.0 nm, but there exist some differences between 420.0 and 570.0 nm. The later one has a red-shift tendency for both fluorescence and RLS. We suppose the reason that signals of 420.0 and 570.0 nm are composed of both scattered light and fluorescence emissions and that major contribution to the signals of 420 nm is fluorescence emission, and that to the signals of 570.0 nm is light scattering emission. The red shifting of fluorescence and scattering may be due to the internal filtration effect of molecule absorption.

In order to discuss the internal filtration effect of molecular absorption on scattering, which makes the RLS intensity decrease, we could introduce the correction factor $A(\lambda)$ [24] to correct the RLS spectra in order to reduce the effect of internal filtration of molecular absorption:

$$A(\lambda) = \left[\frac{2.303A}{1 - 10^{-A}} \right]^2 \quad (1)$$

Then we obtained the corrected RLS spectra:

$$I_{\text{Corr}}(\lambda) = A(\lambda)I_{\text{ms}}^{\text{Abs}} \quad (2)$$

where $I_{\text{Corr}}(\lambda)$ is the RLS intensity after compensation and $I_{\text{ms}}^{\text{Abs}}$ is the apparent RLS intensity (namely, the measured RLS intensity directly from the spectrofluorometer). By introducing the correction factor $A(\lambda)$ for apparent RLS spectra of LP (Fig. 3c), we obtained the corresponding corrected RLS spectra (Fig. 6).

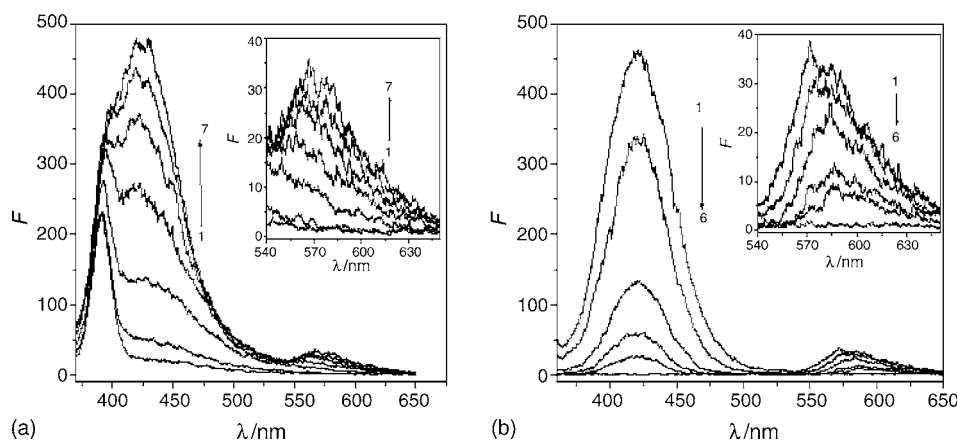


Fig. 5. Fluorescence emissions of LP excited at 344.0 nm, corresponding to G and H fingerprint regions in Fig. 2. Concentrations (mol L^{-1}): LP, a (curves 1–7): 0.0, 1.0×10^{-6} , 1.0×10^{-5} , 3.0×10^{-5} , 5.0×10^{-5} , 7.0×10^{-5} , 1.0×10^{-4} ; b (curves 1–6): 3.0×10^{-4} , 5.0×10^{-4} , 7.0×10^{-4} , 9.0×10^{-4} , 1.0×10^{-3} , 3.0×10^{-3} ; pH 7.0. The insets in (a) and (b) are the signals magnification from 540.0 to 650.0 nm, respectively.

It is clear that the corrected RLS intensity is much stronger than the apparent RLS intensity (Fig. 3c) that could be directly determined by using the spectrofluorometer. However, the shape of spectrum at 420 nm is abnormal, which demonstrates that most of the signals at 420 nm are fluorescence emissions. The reason for spectral abnormality is that we have taken parts of fluorescence signals for scattering signals during RLS spectra correction. After RLS spectra correction, the peak located at 570.0 nm still has a red-shifting tendency, demonstrating that the RLS signals contain parts of fluorescence since the red-shift tendency of fluorescence emission results from hydrophobicity to hydrophilicity [25]. From these results we could explain that the shift of RLS spectra is mainly due to molecule absorption, and may be partly related to fluorescence, which results in the distortion of spectra.

3.5. Mechanism of the strong RLS emission of LP

We determined the distribution of hydrodynamic diameter of LP molecules with different concentration. It was found

that the RLS signals fluctuate greatly when LP is lower than $1.0 \times 10^{-3} \text{ mol L}^{-1}$, and the hydrodynamic diameter distribution could be available over the range of 330.0–500.0 nm. When LP ranges from 1.0×10^{-3} to $1.0 \times 10^{-2} \text{ mol L}^{-1}$, on the other hand, the hydrodynamic diameters keep constant and the value is about 300 nm (Fig. 7). It should be noted that the hydrodynamic diameter is inconsistent with the trim size of LP molecule and these data just represent a trend. Because the hydrodynamic diameter of LP obtained via the Stokes Einstein equation is based on assuming spherical LP molecule, but the LP molecule is not spherical. These results demonstrate that LP has not aggregation tendency, and the strong RLS signals should be ascribed to the large hydrodynamic diameters due to the freedom of the molecular movements. Too concentrated LP, for example, ranging from 1.0×10^{-3} to $1.0 \times 10^{-2} \text{ mol L}^{-1}$, has very low RLS signals due to the confinements of the molecular movements. The increasing RLS intensity with LP concentration could be understood since the intensity depends on both the size and number of scatterers [17,18].

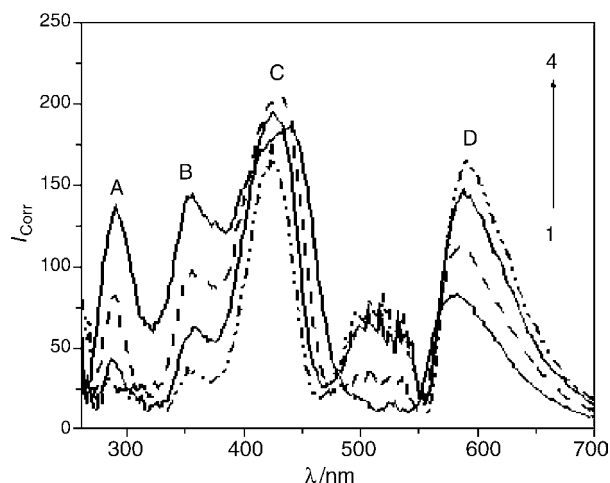


Fig. 6. Corrected RLS spectra of LP. Concentrations (mol L^{-1}): LP (curves 1–4): 3.0×10^{-4} , 5.0×10^{-4} , 7.0×10^{-4} , 9.0×10^{-4} ; pH 7.0.

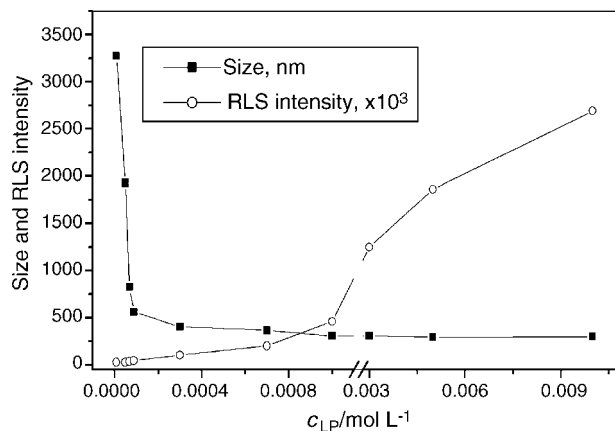


Fig. 7. Variation of sizes and RLS intensity with increasing LP concentration as measured by dynamic light scattering (DLS) technique. The determination angle is 90° . pH 7.0.

3.6. Environmental factors affecting the light emission of LP

We tested the effect of pH on the RLS spectra, fluorescence spectra and absorption spectra of LP. The results showed that the intensities of absorption and RLS almost remain stable during the pH from 1.81 to 9.50, and then decrease as pH is higher than 9.50 with blue-shifting tendency. On the other hand, the fluorescence change is different from the trends of absorption and RLS with pH. The intensities of fluorescence decrease with pH from 3.3 to 7.0, then keep constant during the pH from 7.0 to 9.6, finally decrease in higher pH medium. These changes, which may be relative to the molecule structure of LP, are different from the spectrum changes of Rhodamine B with the pH variations [21].

LP has a strong conjugated structure, and molecule inner hydrogen bond between the hydroxyl group and the hydrogen atom of acetilamino group, which prompts the rigidity of molecule, making LP molecule be fluorescent. At low pH, the nitrogen atom of acetilamino group may combine with proton, destroying the molecule inner hydrogen bond and weakening the fluorescence intensity. With the pH increasing, the combining of the nitrogen atom in acetilamino group with proton becomes weak, and then the nitrogen atom in acetilamino group can interact with the hydrogen in hydroxyl group, forming hydrogen bond, and strengthening the fluorescence intensity. As the pH ranges from 7.0 to 9.6, the system reach equilibrium, and therefore, the fluorescence intensities remain constant. With further pH increasing, the hydroxyl group leaves off the proton, weakening the rigidity of molecule and lessening fluorescence intensities.

4. Conclusion

By investigating the fluorescence and scattered light emission properties of Lignin Pink in aqueous medium, we could conclude that the RLS variations of LP are not due to its self-aggregation but from the large hydrodynamic diameter of the LP itself, and that the scattering spectra is related to the particle size, molecule structure, fluorescence and absorption, etc. The scattering spectra, available through RLS mode, hold complicated information, not only the Rayleigh scattering but also the dynamic light scattering from the free movements of the

molecular because of the acute fluctuation of RLS data at wide slit width. Therefore we could distinguish the scattered light emission signals in different systems, especially for those small organic molecules (OSM) with fluorescence emission.

Acknowledgements

All authors herein are grateful to the supports from the National Natural Science Foundation of China (NSFC No: 20425517), and the Municipal Science and Technology Committee of Chongqing.

References

- [1] K.T. Chung, S.E. Stevens, *Environ. Toxicol. Chem.* 12 (1993) 2121.
- [2] G.B. Michaels, D.L. Lewis, *Environ. Toxicol. Chem.* 4 (1985) 45.
- [3] L.J. Yu, Y.Q. Li, W. Sui, *Spectrosc. Spec. Anal.* 819 (2002) 22.
- [4] R.F. Pasternack, C. Bustamante, P.J. Collings, A. Giannetto, E.J. Gibbs, *J. Am. Chem. Soc.* 115 (1993) 5393.
- [5] R.F. Pasternack, P.J. Collings, *Science* 269 (1995) 935.
- [6] G.D. Luca, A. Romeo, L.M. Scolaro, *J. Phys. Chem. B* 109 (2005) 7149.
- [7] P. Kubat, K. Lang, Z. Zelinger, V. Kral, *Chem. Phys. Lett.* 395 (2004) 82.
- [8] D.M. Togashi, S.M.B. Costa, A.J.F.N. Sobral, A.M.d'A.R. Gonsalves, *J. Phys. Chem. B* 108 (2004) 11344.
- [9] C.Z. Huang, K.A. Li, S.Y. Tong, *Anal. Chem.* 68 (1996) 2259.
- [10] C.Z. Huang, K.A. Li, S.Y. Tong, *Anal. Chem.* 69 (1997) 514.
- [11] C.X. Yang, Y.F. Li, C.Z. Huang, *Chin. J. Anal. Chem.* 31 (2003) 148.
- [12] Y.J. Chen, J.H. Yang, X. Wu, T. Wu, Y.X. Luan, *Talanta* 58 (2002) 869.
- [13] X.L. Hu, S.P. Liu, H.Q. Luo, *Acta Chim. Sin.* 61 (2003) 1287.
- [14] Z.H. Liao, Y.H. Luo, Z.L. Jiang, J.Y. Xie, *Anal. Testing Tech. Inst.* 9 (2003) 65.
- [15] M.M. Yang, Z.L. Jiang, *Spectrosc. Spec. Anal.* 22 (2002) 204.
- [16] D. Wang, H.Q. Luo, N.B. Li, S.P. Liu, *J. Southwest. China. Norm. Univ. (Nat. Sci. Ed)* 29 (2004) 1005.
- [17] J. Yguerabide, E.E. Yguerabide, *Anal. Biochem.* 262 (1998) 137.
- [18] J. Yguerabide, E.E. Yguerabide, *Anal. Biochem.* 262 (1998) 157.
- [19] Y.J. Wei, PhD Dissertation, Peking University, Beijing, 1997.
- [20] Z.P. Li, K.A. Li, S.Y. Tong, *Talanta* 51 (2000) 63.
- [21] Y.J. Wei, Z.M. Kang, C.G. Liu, R.J. Lan, H.Y. Wang, *Spectrosc. Spec. Anal.* 24 (2004) 1659.
- [22] G.Z. Chen, *The Analytical Method of Fluorescence*, Science Press, Beijing, 1990, p. 134.
- [23] C.Q. Ma, Y. Liu, K.A. Li, S.Y. Tong, *Chin. Sci. Bull.* 44 (1999) 682.
- [24] C.Z. Huang, Y.F. Li, C.X. Yang, *Chin. J. Anal. Chem.* 29 (2001) 832.
- [25] J.X. Lu, G.Z. Zhang, Z.N. Huang, P. Zhao, *Acta. Chim. Sin.* 60 (2002) 967.

Interference-free determination of fluoroquinolone antibiotics in plasma by using excitation–emission matrix fluorescence coupled with second-order calibration algorithms

Dong-Mei Fang, Hai-Long Wu*, Yu-Jie Ding, Le-Qian Hu, A-Lin Xia, Ru-Qin Yu

State Key Laboratory of Chemo/Biosensing and Chemometrics, College of Chemistry and Chemical Engineering, Hunan University, Changsha 410082, China

Received 29 October 2005; received in revised form 23 December 2005; accepted 13 January 2006

Available online 21 February 2006

Abstract

Fluoroquinolones or so-called second-generation quinolones, in particular, ofloxacin (OFL), norfloxacin (NOR), and enoxacin (ENO), with therapeutic advantages possess strongly overlapped fluorescence spectra. In this paper, two strategies were proposed for simultaneous direct determination of OFL, NOR and ENO in plasma by combining fluorescence excitation–emission matrix (EEM) with second-order calibration based on the alternating trilinear decomposition algorithm (ATLD) and parallel factor analysis (PARAFAC). The results showed that both algorithms could solve the problem of serious fluorescence spectral overlapping of the sought-for analytes even in the presence of uncalibrated interferents. However, ATLD has advantages of being insensitive to overestimated component number and fast convergence. The results by using ATLD with an estimated component number of five were reasonably acceptable for clinical analysis. The average recoveries of OFL, NOR and ENO in synthetic samples were 99.7 ± 2.4 , 101.5 ± 2.4 and $97.3 \pm 3.8\%$, respectively; the average recoveries of OFL, NOR and ENO in complex plasma were 94.3 ± 2.6 , 85.6 ± 3.3 and $103.3 \pm 3.0\%$, respectively.

© 2006 Elsevier B.V. All rights reserved.

Keywords: Excitation–emission fluorescence; Alternating trilinear decomposition; Parallel factor analysis; Second-order calibration; Fluoroquinolones; Plasma

1. Introduction

Quinolones are important synthetical antibiotics with antibacterial activity. They have been widely used in therapy of different kinds of infectious diseases. The quinolones fluorinated in 6 or 8 position of the main ring are called fluoroquinolones. These second-generation quinolones have important therapeutic advantages of relatively high antibacterial activity. Ofloxacin (OFL), norfloxacin (NOR), and enoxacin (ENO) are basic fluoroquinolone medicaments. Since they have similar structures with heavily overlapped fluorescence spectra, it is difficult to determine them using traditional methods without separation. Muñoz de la Peña et al. [1] used the parallel factor model approach to treat the three-way fluorescence data to determine fluoroquinolone antibiotics in human serum. Espinosa-Mansilla et al. [2] utilized PLS for fluorescence data analysis to deter-

mine fluoroquinolone antibiotics in urine. The determination of quinolones has been reported also by Zhang et al. [3].

With the increasing popularity of modern hyphenated instruments capable of generating three-dimensional arrays, particularly when the data follow the so-called trilinear model [4], the decomposition of a three-dimensional cube of data built with response matrices measured for different samples used to be unique, allowing spectral profiles as well as relative concentrations of individual sample components to be extracted directly. This property has been referred to as the “second-order advantage” [5,6], which has been the subject of much current in chemometric research. Moreover, high-order data are particularly suitable for quantitative analysis of complex multicomponent samples. Two types of algorithms have been reported in chemical literatures for decomposition of three-way data arrays. The first type is to resolve the array by directly performing an eigenanalysis, with the well-known examples of generalized rank annihilation method (GRAM) [7–9] and the direct trilinear decomposition (DTLD) [10–12] method. The second type aims at fitting a trilinear model to the data by utilizing an iter-

* Corresponding author. Tel.: +86 731 8821818; fax: +86 731 8821818.
E-mail address: hlwu@hnu.cn (H.-L. Wu).

ative procedure. This type of method is exemplified by parallel factor analysis (PARAFAC) [13] and alternating trilinear decomposition (ATLD) [14]. In practical application, when estimated component number is inaccurate compared to the actual component number, DTLTD could possibly provide imaginary solutions. PARAFAC algorithm is actually an alternating least-square algorithm which is sensitive to the number of estimated factors used in calculation. Another annoying characteristic of PARAFAC is its slow convergence rate. On the other hand, ATLD is a fast iterative trilinear decomposition algorithm and has the capacity of being insensitive to the number of estimated factors chosen in calculation.

It has been proved that the utilization of fluorescence excitation–emission data matrix of the analytes as analytical signal is a viable way to increase the spectral information useful and disposable for a model. In this paper, we utilized the property of “mathematical separation” to displace “chemical separation” with the help of trilinear decomposition for second-order calibration. Through the treatment of three-way EEM fluorescence data by both ATLD and PARAFAC algorithms, fluoroquinolones in complex plasma samples were determined simultaneously. The proposed method avoids a series of separation procedures and gives satisfactory results.

2. Theory

2.1. Trilinear model for second-order calibration

The trilinear model for second-order calibration can be given by

$$x_{ijk} = \sum_{n=1}^N a_{in} b_{jn} c_{kn} + e_{ijk} \quad (i = 1, \dots, I; j = 1, \dots, J; k = 1, \dots, K) \quad (1)$$

where N denotes the number of factors, which should be considered as a total number of detectable species, including the components of interest and background as well as uncalibrated interferent (s). x_{ijk} is the element of three-way data array \mathbf{X} ($I \times J \times K$) with a component number of N . a_{in} is the element (i, n) of an $I \times N$ matrix \mathbf{A} with relative excitation spectra of the N species. b_{jn} is the element (j, n) of an $J \times N$ matrix \mathbf{B} with relative emission spectra of the N species. c_{kn} is the element (k, n) of an $K \times N$ matrix \mathbf{C} with relative concentrations of the N species in K samples, and e_{ijk} is the i, j and k th residual error element of three-way residual array \mathbf{E} ($I \times J \times K$).

2.2. PARAFAC algorithm

The PARAFAC model was developed by Carroll and Chang [15] under the name canonical decomposition (CANDECOMP) and by Harshman [13] under the name PARAFAC. This algorithm is based on a least-squares minimization. The disadvantage of the PARAFAC is that it requires a precise estimation of the number of components in the mixtures and being slow in convergence.

2.3. ATLD algorithm

A novel algorithm called alternating trilinear decomposition was proposed by Wu et al. [14] to overcome the aforementioned disadvantages, which can be described as follows. It uses the alternating least-squares principle, Moore–Penrose generalized inverse based on singular value decomposition (SVD) and alternating iterative strategy to improve the performance of trilinear decomposition, making a loss function to reach a minimum.

The loss function is defined as the sum of squares of residual error [7] as follows:

$$\sigma_1 = \sum_{i=1}^I \left\| \mathbf{X}_{i..} - \mathbf{B} \text{diag}(\mathbf{a}_{(i)}) \mathbf{C}^T \right\|_F^2 \quad (2)$$

$$\sigma_2 = \sum_{j=1}^J \left\| \mathbf{X}_{.j.} - \mathbf{C} \text{diag}(\mathbf{b}_{(j)}) \mathbf{A}^T \right\|_F^2 \quad (3)$$

and

$$\sigma_3 = \sum_{k=1}^K \left\| \mathbf{X}_{..k} - \mathbf{A} \text{diag}(\mathbf{c}_{(k)}) \mathbf{B}^T \right\|_F^2 \quad (4)$$

where σ_1, σ_2 and σ_3 can be considered equivalent to each other owing to the cyclic symmetry property of the trilinear model [14]. $\|\cdot\|_F$ indicates the Frobenius matrix norm, that is, $\|\mathbf{A}\|_F^2$ is the trace of the matrix $(\mathbf{A}^T \mathbf{A})$. $\mathbf{X}_{i..}$, $\mathbf{X}_{.j.}$ and $\mathbf{X}_{..k}$ are the i th horizontal slice matrix of size $J \times K$, the j th lateral slice matrix of size $K \times I$, and the k th frontal slice matrix of size $I \times J$, respectively. $\text{diag}(\cdot)$ denotes the diagonal matrices with elements equal to the i, j and k th rows of matrices \mathbf{A} – \mathbf{C} , respectively.

ATLD algorithm minimizes alternately one of the above-mentioned loss functions over \mathbf{A} for fixed \mathbf{B} and \mathbf{C} , over \mathbf{B} for fixed \mathbf{A} and \mathbf{C} and over \mathbf{C} for fixed \mathbf{A} and \mathbf{B} . From the updated \mathbf{A} – \mathbf{C} based on the alternating least-squares principle, one can get the relative excitation matrix \mathbf{A} , the relative emission matrix \mathbf{B} and the relative concentration matrix \mathbf{C} as follows:

$$\mathbf{a}_{(i)}^T = \text{diag}(\mathbf{B}^+ \mathbf{X}_{i..} (\mathbf{C}^T)^+), \quad i = 1, \dots, I \quad (5)$$

$$\mathbf{b}_{(j)}^T = \text{diag}(\mathbf{C}^+ \mathbf{X}_{.j.} (\mathbf{A}^T)^+), \quad j = 1, \dots, J \quad (6)$$

and

$$\mathbf{c}_{(k)}^T = \text{diag}(\mathbf{A}^+ \mathbf{X}_{..k} (\mathbf{B}^T)^+), \quad k = 1, \dots, K \quad (7)$$

where $\text{diag}(\cdot)$ denotes a column N -vector composed by diagonal elements of a square matrix. The superscript $+$ denotes the Moore–Penrose generalized inverse, e.g. $\mathbf{A}^+ = (\mathbf{A}^T \mathbf{A})^{-1} \mathbf{A}^T$. In each iteration cycle, \mathbf{A} and \mathbf{B} are normalized to unit length columnwise.

When second-order calibration model is applied, the relevant subjects which should be taken into account are: (a) how model uniqueness can be assessed, (b) how to estimate the number of corresponding spectral components, (c) how to identify specific components from the information provided by the model and

(d) how to calibrate the model in order to obtain real concentration for a particular analyte in an unknown sample. In this paper, after finishing the iterative procedure, the final concentration estimates in unknown samples may be obtained by a plot of relative concentration contributions of each component of interest versus its standard concentrations in the reference samples, similar to a calibration curve plot for one component, or by regression of relative concentration contributions of each component of interest against its standard concentrations.

3. Experimental

3.1. Apparatus

All of fluorometric measurements were carried out on F-4500 fluorescence spectrophotometer (HITACHI) fitted with a xenon lamp and interfaced to a 486 personal computer. In all cases, 1.00 cm quartz cell was used. All computer programs were written in Matlab and all calculations were carried out on a PC under the Windows 2000 operating system.

3.2. Reagents

All solvents used were of analytical grade. Ofloxacin, norfloxacin, and enoxacin were purchased from National Institute for Control of Pharmaceutical and Biological Products in Changsha. Stock solutions with $100 \mu\text{g mL}^{-1}$ of ofloxacin, norfloxacin, and enoxacin were prepared by dissolving of appropriate amount in 0.1 mol L^{-1} NaOH. A sodium acetate/acetic acid buffer solution of pH 4.0 was employed. The stock solution with 0.1 mol L^{-1} sodium dodecil sulfate (SDS) was also prepared. The water used was doubly distilled.

The plasma was purchased from the Blood Center in Changsha.

3.3. Analytical methodology

Working solutions were obtained from diluting the stock solutions.

Simultaneous determinations of OFL, NOR and ENO in plasma were done in 12 samples. The concentrations of these species are listed in Table 1. No. 1–7 samples were used as calibration set and No. 8–12 samples as test set. All samples contained a concentration of $1.2 \times 10^{-2} \text{ mol L}^{-1}$ of SDS and an acetic acid/acetate buffer (pH 4.0). Simultaneous determination of OFL, NOR and ENO in plasma was performed by adding appropriate amount of plasma in standard analyte solutions and using these solutions as samples.

3.4. Parameters

The excitation wavelengths were set from 250.0 to 340.0 nm at an interval of 5.0 nm, and the emission wavelength varied from 363.0 to 501.0 nm with an interval of 3.0 nm. Slit width was 5.0/5.0 nm. The scan rate was 1200 nm/min.

Table 1

Concentrations of synthetic samples containing ofloxacin (OFL), norfloxacin (NOR) and enoxacin (ENO)

Sample	<i>c</i> ($\mu\text{g mL}^{-1}$)		
	OFL	NOR	ENO
1	0.0400	0.0000	0.0000
2	0.0000	0.0160	0.0000
3	0.0000	0.0000	0.0800
4	0.0120	0.0160	0.0400
5	0.0240	0.0120	0.0800
6	0.0360	0.0160	0.1200
7	0.0480	0.0200	0.1600
8	0.0160	0.0120	0.0800
9	0.0200	0.0200	0.1600
10	0.0240	0.0160	0.1200
11	0.0280	0.0160	0.1200
12	0.0400	0.0200	0.0400

3.5. Data array

The effect of Rayleigh and Raman scatterings in all response matrices was roughly compensated just by subtracting the average response matrix of three blank solutions. Thus a $47 \times 19 \times 12$ data array was assembled.

4. Results and discussion

4.1. Influence of pH

Since the three analytes are weak acids, their fluorescence spectra depend on the degree of protonation. The degree of overlapping was reported to be minimal at pH 4.0 [1,2]. Zhang et al. [3] studied the correlation between protonation and tautomerism and luminescence characteristics of quinolone in detail. So the optimum pH was fixed at 4.0, by using a sodium acetate/acetic acid buffer solution.

4.2. Influence of the concentration of SDS

The use of SDS, which is a kind of surfactant, is to stabilize the fluorescence intensity of analytes. According to the literatures [1,2], we choose SDS at an optimum concentration of $1.2 \times 10^{-2} \text{ mol L}^{-1}$, which could make the fluorescence intensity stable.

4.3. Linear range

Referring to the literatures [1–3], the linear ranges of OFL, NOR and ENO were 0–80, 0–25 and 0–300 $\mu\text{g L}^{-1}$, respectively. We prepared the working solutions according to the linear range of the analytes.

4.4. Three-way fluorescence spectrum of 0.2 mL of plasma

Fig. 1 shows a three-dimensional plot of EEM fluorescence for human plasma. One notices from the plasma spectrum that there exist some interferents beside the analytes of interest. Since

Table 2

Determination of ofloxacin (OFL), norfloxacin (NOR) and enoxacin (ENO) in synthetic samples by using EEM fluorescence and ATLD algorithm ($N=5$)

No.	Predicted concentrations ($\mu\text{g mL}^{-1}$)			Recoveries (%)		
	OFL	NOR	ENO	OFL	NOR	ENO
8	0.0157	0.0121	0.0803	97.9	100.6	100.4
9	0.0191	0.0193	0.1530	95.5	96.4	95.6
10	0.0240	0.0167	0.1152	100.2	104.3	96.0
11	0.0286	0.0165	0.1244	102.0	103.0	103.7
12	0.0412	0.0212	0.0364	102.9	103.2	91.0
Average recoveries (%)				99.7 ± 2.4	101.5 ± 2.4	97.3 ± 3.8

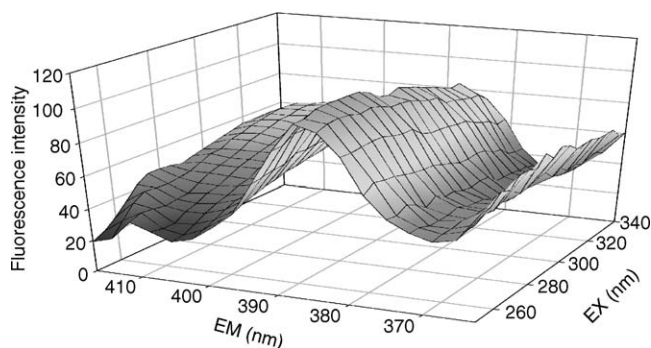


Fig. 1. Three-dimensional plot of fluorescence spectrum for 0.2 ml of plasma.

the main advantage of second-order calibration is that it allows concentration information of an individual component to be extracted even in the presence of any number of uncalibrated constituents, ATLD and PARAFAC algorithms are proposed to resolve three overlapping analytes of interest in the possible presence of interferents even with strong fluorescence. This

method presented satisfactory results and had advantages over other traditional methods.

4.5. Simultaneous determination of OFL, NOR and ENO

The recoveries OFL, NOR and ENO in synthetic samples and in plasma samples by using ATLD with an estimated number of factors of 5 are given in Tables 2 and 3, respectively. When the estimated component number is set to 5, the correlation coefficients of OFL, NOR and ENO by regressing relative concentrations with actual concentrations in calibration set are 0.9978, 0.9954 and 0.9997, respectively; the correlation coefficients of OFL, NOR and ENO in plasma are 0.9974, 0.9979 and 0.9982, respectively.

Table 4 shows the recoveries of OFL, NOR and ENO in plasma samples by using PARAFAC with the component number of 5. Only when the component number is chosen as 5, the relative concentration profiles, excitation spectra and emission spectra can be resolved correctly. This shows PARAFAC is sensitive to the component number. The correlation coefficients of

Table 3

Determination of ofloxacin (OFL), norfloxacin (NOR) and enoxacin (ENO) in plasma samples by using EEM fluorescence and ATLD algorithm ($N=5$)

NO.	Predicted concentrations in plasma ($\mu\text{g mL}^{-1}$)			Recoveries in plasma (%)		
	OFL	NOR	ENO	OFL	NOR	ENO
8	0.0149	0.0095	0.0807	93.2	79.1	100.8
9	0.0196	0.0174	0.1726	98.2	86.9	107.9
10	0.0225	0.0144	0.1275	93.6	90.3	106.2
11	0.0251	0.0134	0.1203	89.6	83.8	100.2
12	0.0388	0.0176	0.0406	97.1	87.9	101.4
Average recoveries (%)				94.3 ± 2.6	85.6 ± 3.3	103.3 ± 3.0

Table 4

Determination of ofloxacin (OFL), norfloxacin (NOR) and enoxacin (ENO) in plasma samples by using EEM fluorescence and PARAFAC algorithm ($N=5$)

No.	Predicted concentrations in plasma ($\mu\text{g mL}^{-1}$)			Recoveries in plasma (%)		
	OFL	NOR	ENO	OFL	NOR	ENO
8	0.0142	0.0129	0.0838	88.9	107.2	104.8
9	0.0196	0.0203	0.1690	98.1	101.4	105.7
10	0.0214	0.0167	0.1213	89.2	104.1	101.1
11	0.0242	0.0165	0.1245	86.4	103.0	103.7
12	0.0362	0.0206	0.0341	90.6	102.9	85.3
Average recoveries (%)				90.6 ± 3.0	103.7 ± 1.5	100.1 ± 5.9

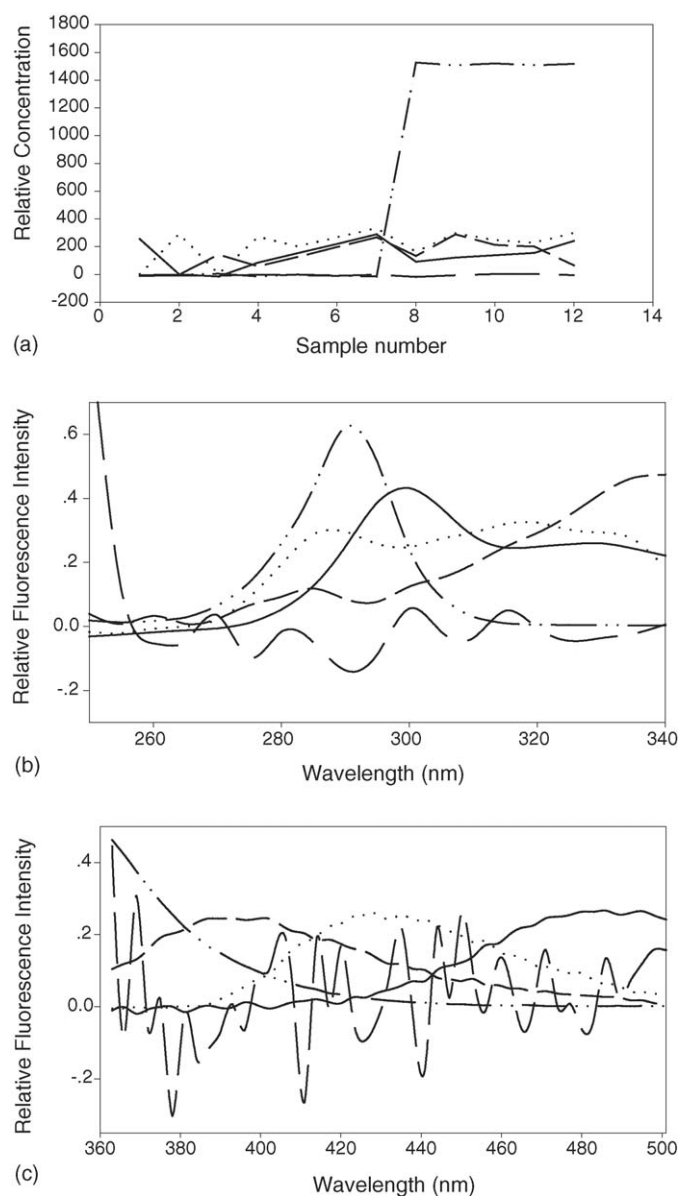


Fig. 2. Relative concentration profiles, excitation and emission spectra of ofloxacin (OFL), norfloxacin (NOR), enoxacin (ENO) and plasma. (a) Relative concentration profiles; (b) emission spectra; (c) excitation spectra of ofloxacin (solid line), norfloxacin (dotted line), enoxacin (dash line), plasma (dash double-dotted line) and background (long dash line) calculated with ATLD ($N=5$).

OFL, NOR and ENO in plasma are 0.9974, 0.9994 and 0.9978, respectively.

The relative concentration profiles, the excitation and emission spectra can be obtained from PARAFAC and ATLD. Fig. 2 shows the relative concentration profiles, the excitation and emission spectra for factor number of five by using ATLD. It was obviously found that in the plasma there existed serious interference.

Comparing the predicted concentrations by using PARAFAC and ATLD, it shows that a satisfactory resolution capacity is obtained by the application of both second-order calibration algorithms in a complex matrix as human plasma. However,

in this case, one can get more satisfactory resolution capacity by applying of ATLD than PARAFAC (Tables 3 and 4). For OFL and ENO, ATLD gave better prediction results than PARAFAC, though for NOR, PARAFAC gave better prediction results than ATLD according to the average recoveries and deviations. Moreover, applying PARAFAC algorithm to such three-way array data requires the knowledge of correct component number to obtain correct relative excitation spectra and emission spectra and relative concentration profiles, and the iterative numbers is rather high. ATLD shows a faster convergence than PARAFAC and eliminates the uncertainty associated with factor number estimation. These results demonstrate that the ATLD algorithm is preferred to determine simultaneously analytes in complex matrix with some advantages over the PARAFAC algorithm.

5. Conclusions

In this paper, three-way fluorescence excitation–emission matrix (EEM) data array treated by alternating trilinear decomposition (ATLD) and parallel factor analysis (PARAFAC) algorithms for second-order calibration has been utilized to simultaneously determine fluoroquinolones with heavily overlapped spectra. This work demonstrated that the combination of EEM and second-order calibration algorithms is a powerful tool for direct quantitative analysis of fluoroquinolones in plasma. The results showed that the ATLD algorithm could rapidly solve the problem of serious fluorescence spectral overlapping of the analytes with uncalibrated interferents and was insensitive to an overestimation of component number as compared to PARAFAC.

Acknowledgements

The authors would like to thank the National Nature Science Foundation of China for financial support (Grant Nos. 20475014, 20375012 and 20435010) and the Chinese Ministry of Education for Excellent Young Teachers Program.

References

- [1] A. Muñoz de la Peña, A. Espinosa Mansilla, D. González Gómez, A.C. Olivieri, H.C. Goicoechea, *Anal. Chem.* 75 (2003) 2640.
- [2] A. Espinosa-Mansilla, A. Muñoz de la Peña, F. Salinas, D. González Gómez, *Talanta* 62 (2004) 853.
- [3] L.T. Zhang, W.N. Liu, Z.X. Zhou, *J. Hebei Med. Univ.* 19 (1998) 319.
- [4] R. Bro, *Chemom. Intell. Lab. Syst.* 38 (1997) 149.
- [5] B.R. Kowalski, M.B. Seasholtz, *J. Chemom.* 5 (1991) 129.
- [6] K.S. Booksh, B.R. Kowalski, *Anal. Chem.* 66 (1994) 782A.
- [7] B.E. Wilson, E. Sanchez, B.R. Kowalski, *J. Chemom.* 8 (1989) 493.
- [8] E. Sanchez, B.R. Kowalski, *Anal. Chem.* 58 (1986) 496.
- [9] K. Faber, A. Lorber, B.R. Kowalski, *J. Chemom.* 11 (1997) 95.
- [10] E. Sanchez, B.R. Kowalski, *J. Chemom.* 4 (1990) 29.
- [11] K.S. Booksh, Z. Lin, Z. Wang, B.R. Kowalski, *Anal. Chem.* 66 (1994) 2561.
- [12] M. Gui, S.C. Rutan, A. Agbodjan, *Anal. Chem.* 67 (1995) 3293.
- [13] R.A. Harshman, *UCLA Working Papers in Phonetics* 16 (1970) 1.
- [14] H.L. Wu, M. Shibukawa, K. Oguma, *J. Chemom.* 12 (1998) 1.
- [15] J. Carroll, J. Chang, *Psychometrika* 35 (1970) 283.

Analysis of environmental pollutants metabolized from pesticides using capillary electrophoresis with multiphoton-excited fluorescence detection

Sheng Chen, Youzhi Xu, Yanhua Bi, Wei Du, Bi-Feng Liu*

The Key Laboratory of Biomedical Photonics of MOE – Hubei Bioinformatics and Molecular Imaging Key Laboratory, Department of Systems Biology, College of Life Science and Technology, Huazhong University of Science and Technology, Wuhan 430074, China

Received 29 October 2005; received in revised form 22 November 2005; accepted 24 November 2005

Available online 4 January 2006

Abstract

Multiphoton-excited fluorescence by diode laser of continuous wave was uniquely developed for capillary electrophoresis to determine aniline species metabolized from pesticides. To achieve 2-photon excitation fluorescence, derivatization procedure was performed using fluorescein isothiocyanate (FITC). The concentration ratio of FITC to the analytes was discussed for quantitative analysis. Several parameters that influenced separation quality of capillary zone electrophoresis were investigated, such as applied voltage, buffer pH value and concentration, etc. Under the optimized conditions, four pesticide residues were completely separated and determined within 4 min, with detection limit down to zeptomole level (calculated detection volume: 45.0 aL). Quantitative analyses exhibited excellent linear dynamic relationship in the range of about two orders of magnitude. The established method was further validated by testing spiked lake water sample.

© 2005 Elsevier B.V. All rights reserved.

Keywords: Capillary electrophoresis; Multiphoton-excited fluorescence; Pesticide metabolites; Aniline species

1. Introduction

Due to rapid development of two decades, capillary electrophoresis (CE) has currently been recognized as a powerful technique for analysis [1]. It features high performance, low sample/reagent requirement and low time consumption that make its widespread use in far-reaching areas such as chemistry, biology, environment, medicine and pharmaceuticals. In present, using CE to analyze environmental sample is a very hot topic [2,3]. Different CE separation modes such as capillary zone electrophoresis (CZE), micellar electrokinetic chromatography (MEKC) and capillary electrochromatography (CEC) of open tube or monolithic column have been involved, coupling with various detection schemes including ultraviolet (UV), laser induced fluorescence (LIF), electrochemistry and mass spectrometry (MS), etc. UV detection shows great popularity in this field because of its good applicability to environmental compounds of a wide range. For those species that are transparent in UV–vis light range, for example, inorganic cations, deriva-

tization can be conveniently employed [4]. MS also gets quite interesting, owing to its capability for identifying unknown compounds. However, detection limit is not so encouraging. LIF represents the highest sensitivity among all these detection methods. Single molecules level has been achieved with LIF. Usually, derivatization procedure is required, since compounds are seldom natively fluorescent.

Global environmental problem becomes a more and more crucial issue. Thousands upon thousands of man-made chemicals are released into nature. Many of them and corresponding metabolic residues are accumulated that greatly threatens the environment where we live in. Pesticide, for instance, is such a kind of organic toxin. Hence, to monitor these compounds is undoubtedly vital. Picó et al. [5] presented an extensive review on determining pesticide residues using CE. Special concern has been given to provide comprehensive coverage of procedures that are of real use, such as various approaches to trace enrichment or improved detection systems. Regan et al. [6] compared CZE, MEKC and cyclodextrin-modified MEKC methods for the separation of pesticides and other endocrine disrupting chemicals. CEC [7,8] was also applied as an efficient means for pesticides and metabolic residues analysis, either in monolithic column [7] or open tubular format [8]. Recently Chicharro

* Corresponding author. Tel.: +86 27 8779 2170; fax: +86 27 8779 2203.
E-mail address: bfliu@mail.hust.edu.cn (B.-F. Liu).

et al. [9] described a MEKC method for analyzing the pesticide residues in environmental waters. Simultaneous UV and electrochemical detection were performed. But the detection sensitivity was relatively low. Wall and El Rassi [10] developed a MEKC separation method with LIF detection of pesticides metabolites. Detection of limit of sub-nM was eventually accomplished.

Recently, we demonstrated a novel detection method, continue-wave based multiphoton-excited (MPE) fluorescence with diode laser for CE [11]. A detection limit of zepto-mole has been readily achieved for rhodamine species, which exhibited good prospect in various application fields coupling with CE separation. In this article, we reported a CE method for separating environmental pollutants metabolized from the pesticides, with this newly designed detection scheme. Several aniline residues were analyzed as their derivatives of fluorescein isothiocyanate (FITC). The derivatization ratio of FITC to analyte was optimized for quantitation. Several CE parameters that influenced separation resolution such as voltage, pH value and concentration of buffer were investigated in detail. Under the optimized conditions, four aniline species were completely separated within 4 min, with detection limit in mass of zepto-mole level. Further work was performed to analyze real-world environmental sample of lake water.

2. Experimental

2.1. Apparatus and procedure

Analyses were carried out on a home-built system as described previously [11] (Fig. 1), which consists of an inverted fluorescence microscope (CK40, Olympus, Japan), a laser source, a detection unit of end-column format and a high voltage supply (0–30 kV) for electrophoresis (Shanghai Nuclear Research Institute, China). In brief, a laser beam from a diode laser (808 nm/1 W; Institute of Semiconductor, Beijing, China) was reflected by a dichroic mirror (E625SP, Chroma, USA), and focused into capillary column with an oil objective (100×, NA1.25, Olympus, Japan). The excited fluorescence was then

collected using the same objective to a photo multiplier tube (PMT R5070, Hamamatsu, Japan), thru E625SP and a low-pass filter (BG18, Newport, USA). The PMT current was converted and amplified into a voltage, and acquired with an A/D converter (homemade). Program for data acquisition was locally written in Borland C++. The collimator of diode laser was manufactured in laboratory.

To achieve end-column detection, a special cathodic reservoir was designed due to the very short working distance of oil objective with ultra high numerical aperture, in which a thin glass chip of 150 mm thickness was employed as the bottom of the reservoir so that the laser could be easily focused into the outlet end of separation capillary. Samples were introduced at the anodic side by siphoning (15 cm for 5 s). Prior to use, the new capillary (54 cm in length, Polymicro, USA) was flushed with 1 M NaOH, H₂O for 15 min, respectively, following with the buffer solution for 30 min at room temperature. Every five injections, the rinse cycle was repeated to ensure reproducibility.

2.2. Chemicals

Aniline species such as *p*-toluidine, aniline, *p*-ethoxyaniline, *p*-phenylenediamine and FITC were obtained from Sigma-Aldrich (MO, USA). All other reagents were of analytical grade. Water purified by the Milli-Q system (Millipore, USA) was used for the preparation of all solutions.

2.3. Sample preparation

Stock solutions of aniline species were prepared at a concentration of 1×10^{-2} M in 10 mM borate buffer (pH 9.0). FITC was dissolved in acetone at a concentration of 1×10^{-2} M. For derivatization, amino acids and FITC (over amount) solutions were mixed. The mixture was then placed in a dark area over night at room temperature.

Real-world water sample was collected from East Lake (Wuhan, China). It was filtered through 0.45 μm membrane prior

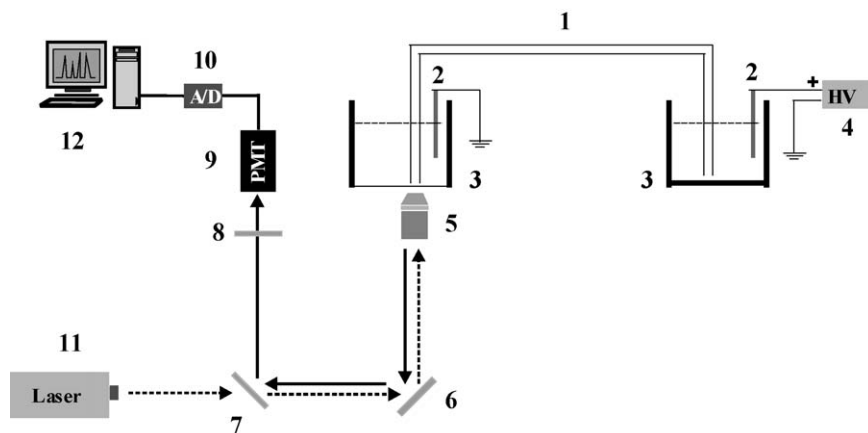


Fig. 1. Schematic description of CE-MPE instrument. (1) Capillary for separation; (2) Pt electrode; (3) buffer reservoir; (4) high voltage supply; (5) 100× objective; (6) reflector; (7) dichroic mirror; (8) short-pass filter; (9) PMT; (10) A/D converter; (11) diode laser; (12) computer.

to use. Derivatization procedure was performed following the same way as the standards.

3. Results and discussion

3.1. Two-photon excitation fluorescence

MPE was firstly predicted by Göppert-Mayer [12] and were experimentally proven in 1960 [13]. However, wide application of MPE in biology became true until 1990 when MPE-based laser scanning microscopy was invented [14]. Recently MPE has been introduced into CE as a mode of LIF detection by Shear and his colleagues [15–17]. Because of ultra-low detection background and detection volume (aL), extremely low mass detection limit about zeptomole level could be achieved.

In theory, for a n -photon process, the probability of MPE (ϕ_n) was determined by several parameters of incident light including average power (P_{av}^n), pulse width (τ) and repeating frequency (f), etc., as described in Eq. (1) [18]:

$$\phi_n = \frac{\xi \sigma_n}{(\hbar \omega)^n F^n} \frac{P_{ave}^n}{(\tau f)^{n-1}} \quad (1)$$

where $\hbar \omega$, F , σ and ξ represent energy of a photon, area of focus, photon absorption section of molecule and waveform factor, respectively. Usually, MPE is achieved with pulsed laser of f-second that is definitely very expensive. With advancement of laser technology, diode laser of high energy becomes available, and is very cheap. Thus, we constructed a continuous wave-based MPE system with diode laser of low cost for CE detection.

3.2. Optimization of derivatization procedure

To achieve MPE fluorescence detection, the analyte should have fluorescence potential. Nevertheless, the aniline species metabolized from pesticides were not natively fluorescent. Thus, derivatization procedure was necessary. The laser line employed in this work was 808 nm. In theory, energy was enough for 2-photon excitation of any compound whose excitation wavelength was longer than 404 nm. FITC has been widely used for efficiently labeling amine species. And its 2-photon excited fluorescence was proven in previous study. As a consequence, FITC was chosen to tag the four aniline analytes.

For obtaining stable derivatization to guarantee reliable quantitation, excessive amount of derivatization reagent was required as suggested by Refs. [10,19]. Here, different concentration ratios of FITC to the analyte were attempted. It was found that the fluorescence intensity increased with the increase of the derivatization ratio as illustrated in Fig. 2. When the ratio was over 5, the intensity showed relatively constant for all the four analytes. Thus, a derivatization ratio of 7 was chosen for further experiments. It was interesting for *p*-phenylenediamine that two derivatization products were realized at low ratio value, because there were two NH_2 -groups in molecular structure. But only one product would be obtained in case that the derivatization ration was over 5 where both NH_2 -groups were saturated, as depicted in Fig. 3.

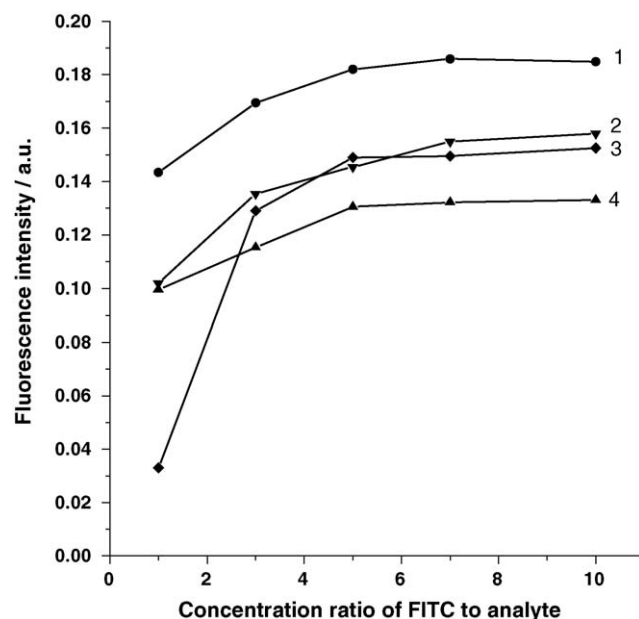


Fig. 2. Effect of concentration ratio of FITC to analyte on derivatization. Derivatization conditions: 10 mM borate buffer (pH 9.5) at room temperature over night. Curve identity: (1) *p*-toluidine; (2) *p*-ethoxyaniline; (3) *p*-phenylenediamine; (4) aniline.

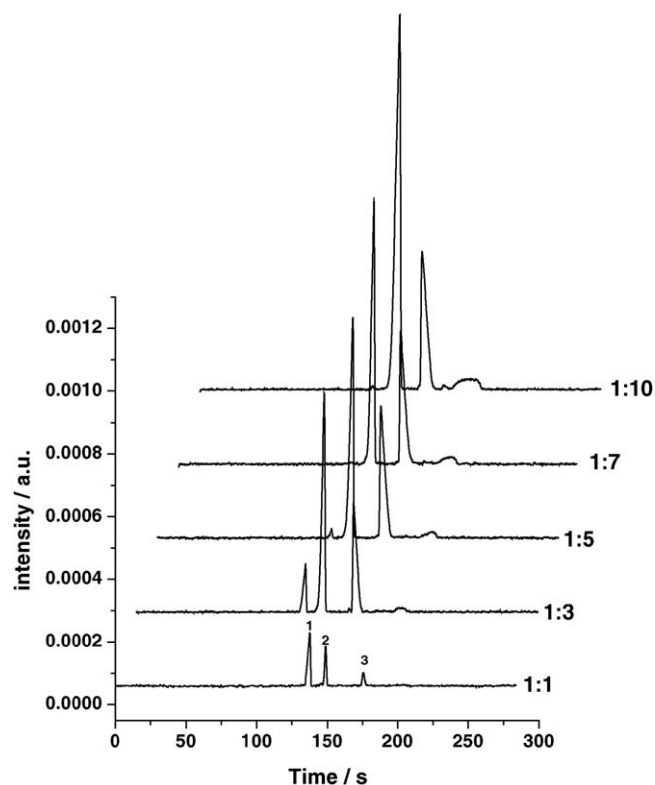


Fig. 3. Effect of concentration ratio of FITC to *p*-phenylenediamine on derivatization. Conditions were the same as in Fig. 1. Peak identity: (1) *p*-phenylenediamine-FITC; (2) FITC; (3) *p*-phenylenediamine-(FITC)₂.

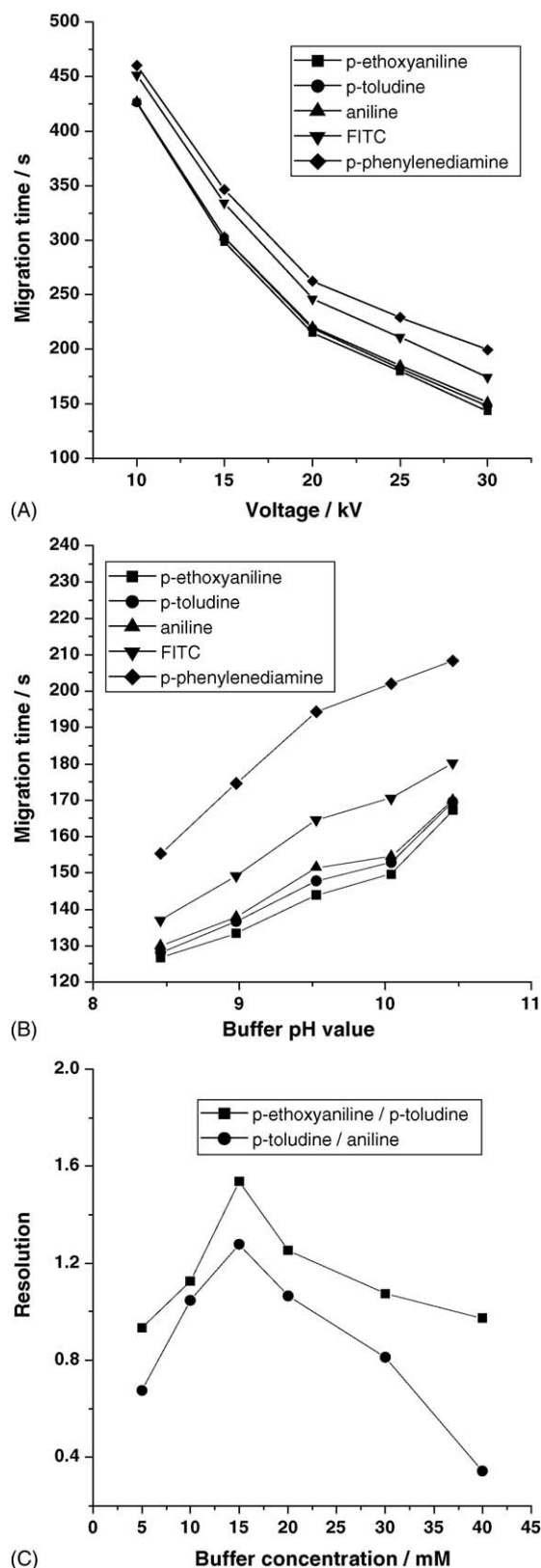


Fig. 4. Influence of parameters on CE separation of aniline species and FITC. (A) Voltage. Buffer condition: 15 mM borate solution (pH 9.5); (B) buffer pH value. Other buffer condition: 15 mM borate solution. Separating voltage: 30 kV; (C) buffer concentration. Other buffer condition: pH 9.5 borate solution. Separating voltage: 30 kV.

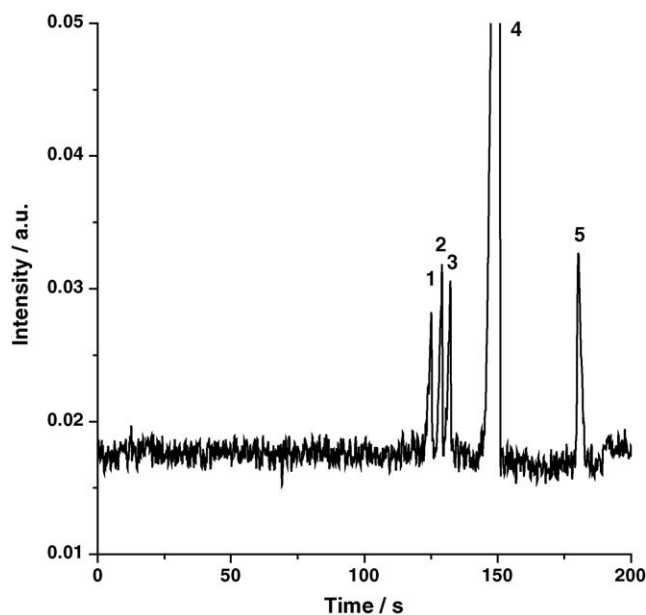


Fig. 5. Electropherogram of standard aniline species and FITC by CZE-MPE method. Separation conditions: buffer: 15 mM borate solution (pH 9.5), separating voltage: 30 kV, injection: siphoning at 15 cm for 5 s. Peak identity: (1) p-ethoxyaniline (57.55 μ M); (2) p-toluidine (102.75 μ M); (3) aniline (80.25 μ M); (4) FITC; (5) p-phenylenediamine (85.50 μ M).

3.3. Optimization of CZE separation

Several key parameters governed the quality of CZE separation, such as separating voltage, buffer pH value, concentration and species, and buffer additive as well. Here, the former three factors were discussed in this study. Increasing separating voltage significantly shortened separation time as shown in Fig. 4A. The separation resolution was also improved at meanwhile. Consequently, a voltage of 30 kV was selected for separation. Buffer pH was varied from 8.5 to 10.5 to search out the best value for separation. Fig. 4B described the tendency of the migration behaviors of the four analytes and FITC with the shift of buffer pH. And a pH value of 9.5 was finally decided. As for buffer concentration, 15 mM was believed to be the best according to the resolutions of two peaks pairs (Fig. 4C). Higher concentration would lead to Joule-heating effect that could cause peak broadening, while we used a voltage of 30 kV for separation.

Under the optimized conditions as investigated above, The four aniline residues were completely resolved by CZE mode together with FITC as shown in Fig. 5.

3.4. Quantitation

Calibration curves were established from nine concentration levels of sample that exhibited a linear dynamic range of about two orders of magnitude between logarithm of peak heights and sample concentrations (see Table 1 for details). Detection limits were also calculated, based on a peak height of three times the baseline noise as shown in Table 1. The detection volume was calculated as recommended by a Ref. [20].

Table 1
Quantitative data

Species	Calibration curve, $Y = AX + B$	γ	Linear range (μM)	R.S.D. (%) ($n = 8$)	Detection limit	
					Concentration (μM)	Mass (μmole)
<i>p</i> -Toluidine	$Y = 0.840X + 4.586$	0.9832	685–6.42	3.49	1.60	72.00
Aniline	$Y = 0.809X + 4.694$	0.9893	535–5.02	2.68	1.25	56.25
<i>p</i> -Ethoxyaniline	$Y = 1.008X + 6.349$	0.9958	385–7.22	2.12	1.86	83.70
<i>p</i> -Phenylenediamine	$Y = 0.698X + 2.932$	0.9837	555–5.20	2.86	2.60	117.0

Y : logarithm of peak height; X : logarithm of sample concentration; calculated detection volume: 45.0 aL [20].

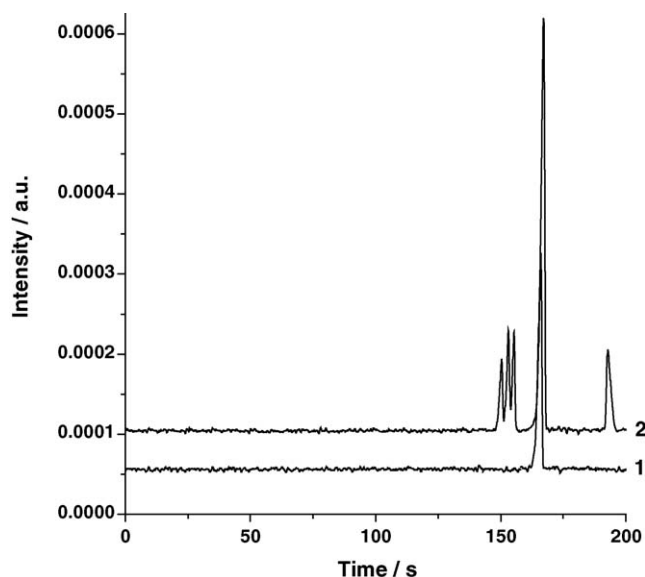


Fig. 6. Electropherograms of lake water sample and spiked lake water sample. (1) Lake water; (2) spiked lake water. Separation conditions were the same as in Fig. 4. Peak identity were the same as in Fig. 4.

3.5. Lake water analysis

To test our method for real-world sample applicability, lake water was analyzed. The sample treatment was described in experimental section. No pollution from the four aniline species was found as shown in Fig. 6. For further validating our established approach, the water sample was spiked with the standards. Recoveries for *p*-toluidine, aniline, *p*-ethoxyaniline, *p*-phenylenediamine were found to be $98.6 \pm 1.6\%$, $98.1 \pm 1.3\%$, $99.1 \pm 1.5\%$ and $96.4 \pm 2.2\%$, respectively ($n = 3$).

4. Conclusion

In this article, we demonstrated a CZE method to determine pesticide residues, uniquely coupling with multiphoton-excited fluorescence by diode laser of continuous wave. Derivatization and separation conditions were investigated in detail. Four aniline species were completely separated and detected within 4 min. Although the detection limit in mass was down to zepto-

mole level, it should be stated that the sensitivity in concentration was not so encouraging as conventional LIF detection scheme. On/off-line concentration method, e.g., solid micro-extraction, sample stacking, sweeping or pH-junction, etc., would be very useful to improve the sensitivity in concentration, which was also under our further consideration.

Acknowledgements

The authors gratefully acknowledge the financial supports from National Natural Science Foundation of China (Grant Nos.: 20405006, 30570468), and Program for Distinguish Young Scientist of Hubei Province (2004ABB004).

References

- [1] W.W.C. Quigley, N.J. Dovichi, Anal. Chem. 76 (2004) 4645.
- [2] Y. Pico, Encyclopedia of Analytical Science, Elsevier, 2005, pp. 362–374.
- [3] E. Dabek-Zlotorzynska, H. Chen, L. Ding, Electrophoresis 24 (2003) 4128.
- [4] B.-F. Liu, L.-B. Liu, J.-K. Cheng, J. Chromatogr. A 834 (1999) 277.
- [5] Y. Picó, R. Rodríguez, J. Mañes, TrAC 22 (2003) 133.
- [6] F. Regan, A. Moran, B. Fogarty, E. Dempsey, J. Chromatogr. A 1014 (2003) 241.
- [7] M. Bedair, Z. El Rassi, J. Chromatogr. A 1013 (2003) 47.
- [8] T. O'Mahony, V.P. Owens, J.P. Murrihy, E. Guihen, J.D. Holmes, J.D. Glennon, J. Chromatogr. A 1004 (2003) 181.
- [9] M. Chicharro, A. Zapardiel, E. Bermejo, A. Sanchez, R. Gonzalez, Electroanalysis 16 (2004) 311.
- [10] W. Wall, Z. El Rassi, Electrophoresis 22 (2001) 2312.
- [11] S. Chen, B.-F. Liu, L. Fu, T. Xiong, T. Liu, Z. Zhang, Z.-L. Huang, Q. Lu, Y.-D. Zhao, Q. Luo, J. Chromatogr. A, in press.
- [12] M. Göppert-Mayer, Ann. Phys. 9 (1931) 273.
- [13] W. Kaiser, C.G.B. Garrett, Phys. Rev. Lett. 7 (1961) 229.
- [14] W. Denk, J.H. Strickler, W.W. Webb, Science 248 (1990) 73.
- [15] M.L. Gostkowski, J.B. McDoniel, J. Wei, T.E. Curey, J.B. Shear, J. Am. Chem. Soc. 120 (1998) 18.
- [16] M.J. Gordon, E. Okerberg, M.L. Gostkowski, J.B. Shear, J. Am. Chem. Soc. 123 (2001) 10780.
- [17] M.L. Plenert, J.B. Shear, Proc. Natl. Acad. Sci. U.S.A. 100 (2003) 3853.
- [18] P.E. Hanninen, E. Soini, S.W. Hell, J. Microsc. 176 (1994) 222.
- [19] B.-F. Liu, L. Zhang, Y.-T. Lu, J. Chromatogr. A 918 (2001) 401.
- [20] W.R. Zipfel, R.M. Williams, W.W. Webb, Nat. Biotechnol. 21 (2003) 1369.

Gold nanoparticle/alkanedithiol conductive films self-assembled onto gold electrode: Electrochemistry and electroanalytical application for voltammetric determination of trace amount of catechol

Lei Su, Lanqun Mao *

Center for Molecular Science, Institute of Chemistry, the Chinese Academy of Sciences, Beijing 100080, China

Received 29 October 2005; received in revised form 10 January 2006; accepted 13 January 2006

Available online 20 February 2006

Abstract

This paper describes novel electrochemical properties of gold nanoparticles/alkanedithiol conductive films and their electroanalytical applications for voltammetric determination of trace amount of one kind of environmental pollutants, catechol. The conductive films are prepared by closely packing 12-nm diameter gold nanoparticles (Au-NPs) onto Au electrodes modified with the self-assembled monolayers (SAMs) of alkanedithiols (i.e., $\text{HS}(\text{CH}_2)_n\text{SH}$, $n = 3, 6, 9$). The assembly of the Au-NPs onto the SAM-modified electrodes essentially restores the heterogeneous electron transfer between Au substrate and redox species in solution phase that is almost totally blocked by the SAMs and, as a result, the prepared Au-NP/SAM-modified electrodes possess a good electrode reactivity without a remarkable barrier toward the heterogeneous electron transfer. Moreover, the prepared Au-NP/SAM-modified electrodes are found to exhibit a largely reduced interfacial capacitance, compared with bare Au electrode. These electrochemical properties of the Au-NP/SAM-modified electrodes essentially make them very useful for electroanalytical applications, which is illustrated by voltammetric determination of trace amount detection of environmental pollutant, catechol.

© 2006 Elsevier B.V. All rights reserved.

Keywords: Alkanedithiol; Catechol; Electron transfer; Gold nanoparticles; Interfacial capacitance

1. Introduction

Considerable attention has been drawn on the synthesis, characterization and applications of Au-NPs because of their distinct chemical and physical properties from the bulk Au [1–3]. Attempt so far on electrochemistry of the Au-NPs has revealed that such kind of metal nanoparticles possess excellent electrochemical properties that are very attractive for fundamental electrochemical investigations and electroanalytical applications, for example, electrocatalysis [4–6], biosensors [7], and protein electrochemistry [8–10]. In most cases, the Au-NPs are confined onto electrode substrates through the formation of one-, two- or three-dimensional Au-NP architectures, e.g., by layer-by-layer assembling [11] or entrapping Au-NPs within polymers containing functional groups [12,13].

The SAMs of alkanedithiols terminated with thiol or amino groups are particularly useful for preparing Au-NP-modified

electrodes because the prepared Au-NP/SAM-modified electrodes exhibit good stability and controllable surface coverage of the Au-NPs [12–14]. The latter property is remarkable since it enables the prepared Au-NP/SAM-modified electrode to possess tunable electrode dimensions [15–19]. For instance, when the Au-NPs are sparsely confined onto the insulating films self-assembled onto electrode substrates, the diffusion layer of the Au-NPs (or their clusters) can be separated, depending on the time scale (i.e., scan rate) used and, as a consequence, the electrode resembles a micro-sized electrode array. Accordingly, the electrode covered with almost closely packed Au-NPs (or their coalescences), of which the diffusion layers are totally overlapped each other over the time scale frequently used, essentially functions as a macro-sized electrode electrochemically [20–22]. A close survey of the literature reveals that much effort has been made on the electrochemistry and electrochemical applications of the Au-NPs-based micro-sized electrode array possibly because of its excellent electrochemical features; little attention has been drawn on the Au-NPs-based macro-sized electrode, although the electrochemical properties of such kind of electrode is also fundamentally interesting and practically useful

* Corresponding author. Tel.: +86 10 62646525; fax: +86 10 62559373.
E-mail address: lqmao@iccas.ac.cn (L. Mao).

and the electrode is readily prepared, without a need for concise control of surface coverage of the Au-NPs.

In this study, we investigate electrochemistry of Au-NP/SAM conductive films prepared by closely packing 12-nm diameter Au-NPs onto the SAMs of $\text{HS}(\text{CH}_2)_n\text{SH}$ ($n = 3, 6, 9$) confined onto bare Au electrode, aiming at understanding the electrochemical properties of such kind of electrodes and establishing a new electroanalytical method for trace amount determination of environmental pollutant, such as catechol. As will be demonstrated, very different from the Au-NP/SAM-modified electrodes with a limited coverage of the Au-NPs, behaving micro-sized electrode array, the electrodes prepared here possess the same electrode activity as a macro-sized Au bulk electrode. Moreover, we find that such kind of electrodes exhibit a largely reduced capacitance, compared with bare Au. These intrinsic electrochemical properties of the Au-NP/alkanedithiol-modified electrodes are envisaged to be useful for voltammetric determination of trace amount of redox-active environmental pollutant, such as catechol.

2. Experimental

2.1. Chemicals

1,3-Propanedithiol ($\text{HS}(\text{CH}_2)_3\text{SH}$), 1,6-hexanedithiol ($\text{HS}(\text{CH}_2)_6\text{SH}$), 1,9-nonanedithiol ($\text{HS}(\text{CH}_2)_9\text{SH}$) and hydrogen tetrachloroaurate(III) hydrate ($\text{HAuCl}_4 \cdot 3\text{H}_2\text{O}$) were purchased from Sigma–Aldrich. Hydroxylamine, potassium ferricyanide, catechol and other chemicals of at least analytical reagent were obtained from Beijing Chemical Corporation (Beijing, China). Colloidal Au nanoparticles were prepared by citrate reduction of HAuCl_4 in aqueous solution [23]. The prepared Au colloidal nanoparticles were characterized with transmission electron microscopy (Fig. 1A) and UV–vis spectrometry (Fig. 1B). As can be seen from Fig. 1, the prepared colloidal Au-NPs have an average diameter of ca. 12 nm and exhibit an absorption at ca. 520 nm, characteristic of the absorption of the Au-NPs of this size [24,25].

2.2. Electrode pretreatment and modifications

Gold electrodes (0.18 cm in diameter, Bioanalytical Systems Inc.) were polished with alumina powder (1.0 and 0.05 μm) and sonicated in acetone and twice distilled water (each for 3–5 min). The electrodes were then electrochemically cleaned by consecutively cycling the potential between -0.2 and $+1.6$ V at 0.5 V/s in 0.5 M H_2SO_4 solution until a cyclic voltammetric characteristic of a clean Au electrode was obtained. The surface roughness factor (f) of bulk Au electrodes was calculated to be close to 3.0 ($f = Q/Q_{\text{ref}}$, Q is the electric charge for the Au surface oxide determined by integrating reduction peak of the surface oxide in a cathodic scan in 0.5 M H_2SO_4 , and Q_{ref} , is the reference electric charge of $400 \mu\text{C}/\text{cm}^2$ for polycrystalline Au [26]).

SAMs of alkanedithiols $\text{HS}(\text{CH}_2)_n\text{SH}$ ($n = 3, 6, 9$) were prepared by immersing the cleaned Au electrodes into ethanol solution containing $\text{HS}(\text{CH}_2)_n\text{SH}$ (10 mM) for more than 24 h at room temperature. The electrodes ($\text{HS}(\text{CH}_2)_n\text{SH}$ -modified Au)

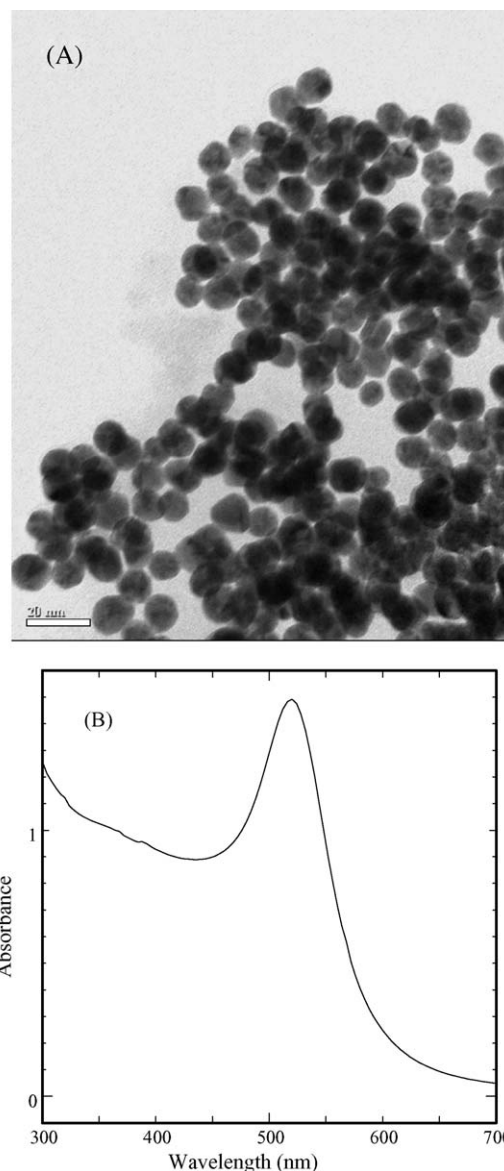


Fig. 1. Typical TEM images (A) and absorption spectrum (B) of the colloidal Au-NPs prepared in this study. Scale bar in (A), 20 nm.

were then thoroughly rinsed with ethanol and doubly distilled water and dried with N_2 gas before electrochemical measurements. For confining Au-NPs onto the SAM-modified electrodes, the SAM-modified electrodes were first immersed into the colloidal Au solution for 12 h. After being rinsed with doubly distilled water, the electrodes were then immersed into 0.5 mM Au^{3+} /hydroxylamine mixture for 5 min for further seeding the Au-NPs onto the electrode surface. Finally, the electrodes (Au-NP/SAM-modified electrodes) were immersed into absolute ethanol at ca. 50°C for 5 min before use.

2.3. Instruments and measurements

Electrochemical measurements were performed with electrochemical analyzer (CHI 660A, CH Instruments) in 0.10 M phosphate buffer (pH 7.0). $\text{HS}(\text{CH}_2)_n\text{SH}$ -modified and Au-NP/ $\text{HS}(\text{CH}_2)_n\text{SH}$ -modified Au electrodes were used as working

electrode, an Ag/AgCl (saturated KCl) electrode as reference electrode and an Au coil as counter electrode. TEM images were obtained with HITACHI 9000 electron microscope (Hitachi, Tokyo, Japan). Absorption spectrum was recorded with a Tech-comp UV-8500 spectrophotometer (Shanghai, China).

3. Results and discussion

3.1. Electrochemical properties of the $\text{HS}(\text{CH}_2)_n\text{SH}$ -modified electrodes

In order to clarify the electrochemical properties of the Au-NP/SAM-modified Au electrodes, we first studied the electrochemical behavior of the $\text{HS}(\text{CH}_2)_n\text{SH}$ -modified electrodes (without assembly of the Au-NPs). Fig. 2 displays cyclic voltammograms (CVs) for 1.0 mM $\text{Fe}(\text{CN})_6^{3-}$ redox couple at bare and the $\text{HS}(\text{CH}_2)_n\text{SH}$ -modified Au electrodes. At bare Au electrode (solid line), a pair of well-defined redox peaks was recorded with a peak-to-peak separation (ΔE_p) of ca. 60 mV (at 100 mV/s), characteristic of the reversible redox process of the $\text{Fe}(\text{CN})_6^{3-}$ couple [27]. At the $\text{HS}(\text{CH}_2)_3\text{SH}$ -modified electrode a reversible voltammetry was also recorded for the $\text{Fe}(\text{CN})_6^{3-}$ couple with ΔE_p of ca. 60 mV (at 100 mV/s) (dotted line), which was almost identical with that recorded at bare Au electrode. This suggests that the electrode activity of the $\text{HS}(\text{CH}_2)_3\text{SH}$ -modified electrode is essentially equivalent to that of bare Au electrode, probably due to the combined consequences of a pinhole effect and little kinetics barrier of the thin monolayer of $\text{HS}(\text{CH}_2)_3\text{SH}$ [28–31]. Contrarily, no voltammetric peaks were recorded at the $\text{HS}(\text{CH}_2)_{6,9}\text{SH}$ -modified electrodes in the potential window employed (dashed and dot-dashed lines, overlapped in Fig. 2).

It has been reported that compact and pinhole-free SAMs could be formed onto the Au substrate with alkanethiols with a long hydrocarbon chain due to the formation of strong Au–S

bond and the strong hydrophobic interactions between the hydrocarbon chains and that the formed SAMs can effectively suppress the heterogeneous electron transfer between Au substrate and redox species in solution phase [28–31]. Therefore, the suppressed CVs responses at the $\text{HS}(\text{CH}_2)_{6,9}\text{SH}$ -modified electrodes indicate that such kinds of the SAMs are compact and essentially pinhole-free. The blocked effect of the SAMs of the $\text{HS}(\text{CH}_2)_{6,9}\text{SH}$ on the heterogeneous electron transfer was further characterized with electrochemical impedance spectroscopy (EIS) (data not shown). We found that, consistent with the voltammetric behavior obtained above, the charge transfer resistance (R_{ct}) of the $\text{Fe}(\text{CN})_6^{3-}$ couple at the $\text{HS}(\text{CH}_2)_{6,9}\text{SH}$ -modified electrodes was several orders of magnitude larger than those at bare and $\text{HS}(\text{CH}_2)_3\text{SH}$ -modified Au electrodes.

Fig. 3 shows typical CVs of bare and $\text{HS}(\text{CH}_2)_n\text{SH}$ -modified Au electrodes in 0.10 M phosphate buffer containing no redox species. At bare Au electrode (solid line), a pair of slight and broad peaks was recorded at ca. 0.25 V, characteristic of the adsorption of solution species onto Au surface. The tailed cathodic peak commencing at 0.05 V was attributed to the reduction of the dissolved oxygen. Contrarily, only largely reduced charge current was recorded at the $\text{HS}(\text{CH}_2)_n\text{SH}$ -modified Au electrodes (dotted, dashed, and dot-dashed lines). The slight difference in charge current between the $\text{HS}(\text{CH}_2)_n\text{SH}$ -modified electrodes (inset, Fig. 3) reflects the difference in the interfacial capacitance, which is dependent on the length of hydrocarbon chain of the alkanedithiols used, as predicted by Helmholtz theory, in which the double-layer interface was considered as an ideal capacitor and the capacitance could be presented as below [28–31].

$$C^{-1} = d_m / \varepsilon_0 \varepsilon_m A$$

where d_m is the distance from the bulk electrode surface to the terminal plane of the SAMs, and here equals the thickness of the SAMs; ε_0 is the permittivity of the free space, ε_m the dielectric constant of the SAMs, and A is the real surface area.

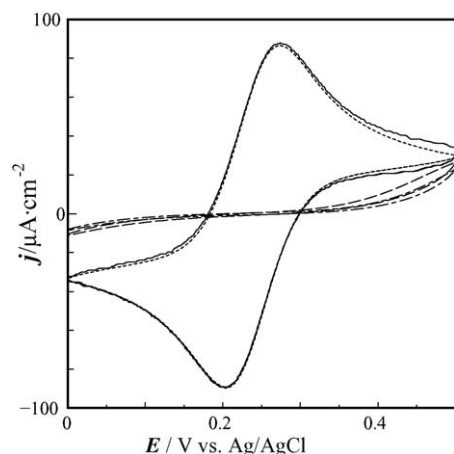


Fig. 2. Typical CVs at bare Au (solid line) and Au electrodes modified with the SAM of $\text{HS}(\text{CH}_2)_3\text{SH}$ (dotted line), $\text{HS}(\text{CH}_2)_6\text{SH}$ (dashed line), or $\text{HS}(\text{CH}_2)_9\text{SH}$ (dot-dashed line) in 0.10 M phosphate buffer (pH 7.0) containing 1.0 mM $\text{Fe}(\text{CN})_6^{3-}$. Scan rate, 0.1 V/s. The solid and dotted lines, dashed and dot-dashed lines are almost overlapped.

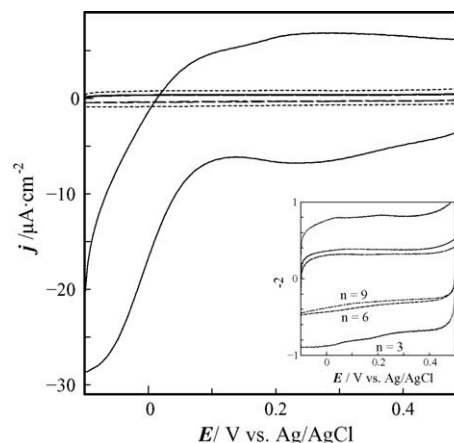


Fig. 3. CVs of bare Au electrode (solid line) and Au electrodes modified with the SAM of $\text{HS}(\text{CH}_2)_3\text{SH}$ (dotted line), $\text{HS}(\text{CH}_2)_6\text{SH}$ (dashed line), or $\text{HS}(\text{CH}_2)_9\text{SH}$ (dot-dashed line) in 0.10 M phosphate buffer (pH 7.0). Scan rate, 0.1 V/s. The dashed and dot-dashed lines are almost overlapped. Inset: enlarged CVs of the SAM-modified electrodes obtained under the same conditions.

3.2. Electron transfer properties of the Au-NP/HS(CH₂)_nSH-modified electrodes

It has been reported that the blocked heterogeneous electron transfer by the SAM could be restored by assembling the Au-NPs onto the SAM and the reversibility of redox couples (e.g., Fe(CN)₆^{3−}) at the Au-NP/HS(CH₂)_nSH-modified electrodes varies with surface coverage of the Au-NPs and, in turn, the reversibility of the electrode reaction could be used to probe the surface coverage of the Au-NPs [14,32]. Fig. 4 compares CVs obtained at Au-NP/SAM-modified electrodes before and after being further seeded with Au-NPs in 0.10 M phosphate buffer containing 1.0 mM Fe(CN)₆^{3−}. Without being seeded with Au-NPs, the Au-NP/HS(CH₂)₆SH-modified electrode exhibits a large ΔE_p (ca. 150 mV, at 100 mV/s) for the Fe(CN)₆^{3−} couple even the HS(CH₂)₆SH-modified electrode was immersed in colloidal Au solution for a long time (more than 12 h) for the assembly of Au-NPs. This reflects that it is relatively difficult to achieve a high coverage of the Au-NPs only by immersing the SAM-modified electrode into Au colloidal solution. This is possibly due to the repulsive interaction between the surface-confined Au-NPs and free Au-NPs in solution [33]. In order to obtain a high surface coverage of the Au-NPs onto the SAM-modified electrodes and thus to prepare Au-NP/SAM conductive films, the Au-NPs were further seeded onto the Au-NP/SAM-modified electrodes with the method detailed in Section 2. As shown in Fig. 4, after being further seeded with Au-NPs, the Au-NP/HS(CH₂)₆SH-modified Au electrode exhibits a reversible process for the Fe(CN)₆^{3−} couple (dashed line), suggesting that the electron transfer process blocked with the SAMs of HS(CH₂)₆SH (Fig. 2, dashed line) was clearly restored upon the Au-NPs layer onto the SAM-modified electrodes. The reversibility of the Fe(CN)₆^{3−} couple at the Au-NP/HS(CH₂)₆SH-modified electrode ($\Delta E_p = \sim 60$ mV, dashed line) was dramatically improved even to the same level as that at bare Au electrode (Fig. 4, solid line) and better than that at

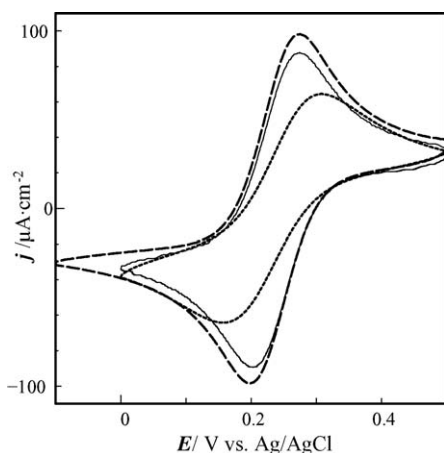


Fig. 4. CVs at bare Au (solid line), the Au-NP/HS(CH₂)₆SH-modified Au electrodes before (dotted line) and after (dashed line) being further seeded with Au-NPs in 0.10 M phosphate buffer (pH 7.0) containing 1.0 mM Fe(CN)₆^{3−}. Scan rate, 0.1 V/s.

the Au-NP/HS(CH₂)₉SH-modified electrode ($\Delta E_p = \sim 90$ mV, not shown). The former observation confirms that the Au-NP/HS(CH₂)₆SH film exhibit no remarkable barrier to the heterogeneous electron transfer kinetics, resembling a macro-sized bare Au electrode, while the latter one is indicative of a distance-dependent and hence tunable feature of electron transfer properties at the Au-NP/HS(CH₂)_nSH-modified electrodes. The prepared Au/HS(CH₂)_nSH-modified electrodes were found to be relatively stable for voltammetric measurements. For example, the redox peak currents of Fe(CN)₆^{3−} redox couple were found to be almost identical after continuously cycling the electrodes for 30 cycles.

The restored electron transfer and its distance-dependent feature at the Au-NP/HS(CH₂)_nSH-modified electrodes were further confirmed by EIS as displayed in Fig. 5. As demonstrated above, at the HS(CH₂)₃SH-modified electrode, the charge transfer is fast enough (as fast as that at bare Au electrode) and thus the assembly of the Au-NPs onto such an electrode did not further increase the electron transfer rate. This could be evident from almost the same charge transfer resistance (R_{ct}) of the Fe(CN)₆^{3−} redox couple at the HS(CH₂)₃SH-modified (dotted line) and Au-NP/HS(CH₂)₃SH-modified electrodes (dashed line), of which both are very close to that at bare Au electrode (solid line). The R_{ct} at the Au-NP/HS(CH₂)₆SH-modified electrode is essentially close to that at bare Au electrode (Fig. 5, inset), again indicating that the Au-NP/HS(CH₂)₆SH-modified electrode possesses the same electrode activity as a macro-sized electrode. The R_{ct} at the Au-NP/HS(CH₂)₉SH-modified electrode (dot-dashed line) is larger than those at the Au-NP/HS(CH₂)_{3,6}SH-modified electrodes, confirming the distance-dependent feature of the charge transfer properties at the Au-NP/HS(CH₂)_nSH-modified electrodes. Even so, the R_{ct} at the Au-NP/HS(CH₂)₉SH-modified electrode is much smaller than those at the HS(CH₂)_{6,9}SH-modified electrodes (without

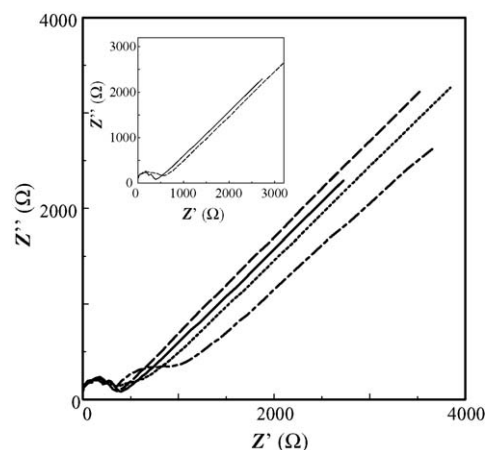


Fig. 5. Nyquist plots of bare (solid line), HS(CH₂)₃SH-modified (dotted line), Au-NP/HS(CH₂)₃SH-modified (dashed line), and Au-NP/HS(CH₂)₉SH-modified (dot-dashed line) Au electrodes in 0.10 M phosphate buffer (pH 7.0) containing 1.0 mM Fe(CN)₆^{3−}. Inset displays Nyquist plots of bare (solid line) and Au-NP/HS(CH₂)₆SH-modified (dashed line) Au electrodes for a clear comparison. EIS conditions, potential, 0.24 V; alternative voltage, 5 mV; frequency range, 100 kHz to 0.1 Hz.

the assembly of the Au-NPs) (i.e., more than $10^6 \Omega$), again indicative of the restoration of electron transfer upon the assembly of the Au-NPs. The restored heterogeneous electron transfer by the assembly of Au-NPs onto the SAM-modified electrodes is very similar to the case of carbon nanotubes as demonstrated in our recent work [34].

Previous reports have demonstrated that the electron transfer between the monolayer-protected Au-NPs and the bare electrode proceeds through electron hopping with the intervening monolayer as tunneling bridges and that the electron transfer rate constant is several orders of magnitude faster than those through redox polymers [35] and than Au–alkanethiol–Fc tunnel junctions [36] and varies exponentially with the core edge-to-edge spacing as expected for an electron tunneling reaction [37,38]. Similarly, the Au-NPs attached onto the SAMs of alkanedithiols may be considered to function as a relay in the process of electronic communication between bare Au and the redox species in solution phase [22]. As a result, in the case of the SAMs with a short hydrocarbon chain (e.g., $n = 6$), the flux of electron transfer restored can well satisfy Nernstian equilibrium, resulting in a good reaction reversibility and a low charge transfer resistance at the electrode, e.g., Au-NP/HS(CH₂)₆SH-modified electrode as described above (Figs. 4 and 5). Whereas, in the case of the SAM with a longer hydrocarbon chain (e.g., $n = 9$), the charge transfer rate could be decreased substantially, leading to relatively sluggish charge transfer kinetics and thus a quasi-reversibility as well as a large charge-transfer resistance at this type of electrode (Fig. 5).

3.3. Interfacial capacitance of the Au-NP/HS(CH₂)_nSH-modified electrodes

Fig. 6 compares the CVs obtained at the HS(CH₂)_nSH-modified (dotted, dashed and dot-dashed lines) and Au-NP/HS(CH₂)_nSH-modified (solid lines) electrodes in 0.10 M phosphate buffer in the absence of the redox species. As

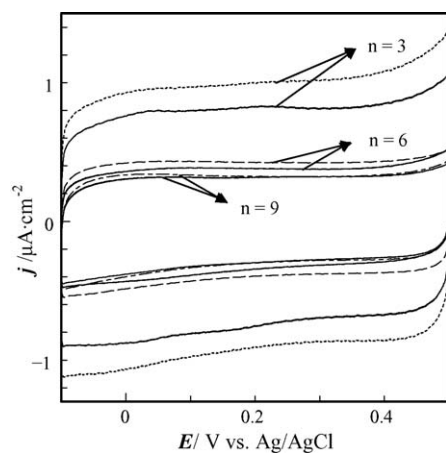


Fig. 6. CVs obtained at the HS(CH₂)_nSH-modified (solid lines) and Au-NP/HS(CH₂)_nSH-modified Au electrodes in 0.10 M phosphate buffer (pH 7.0). $n = 3$ (dotted line), $n = 6$ (dashed line), and $n = 9$ (dot-dashed line) as indicated in the figure. Scan rate, 0.1 V/s.

described above, the formation of SAMs of alkanedithiols onto bare Au electrodes largely reduces the interfacial capacitance (Fig. 3). The assembly of the Au-NPs onto the SAM-modified electrodes was not found to restore the interfacial capacitance reduced by the SAMs, i.e., the capacitances of the Au-NP/HS(CH₂)_nSH-modified electrodes remain much smaller than that of bare Au electrode as displayed in Figs. 3 and 6. The largely reduced interfacial capacitance of the Au-NP/SAM-modified Au electrodes demonstrated here, combined with the restored electron transfer, substantially makes them particularly useful for electroanalytical applications, such as voltammetric determination of trace amount of redox species as demonstrated below.

3.4. Electroanalytical applications

Fig. 7 shows typical CVs of the Fe(CN)₆^{3−} redox couple at bare (A) and Au-NP/HS(CH₂)₆SH-modified (B) Au electrodes. At bare Au electrode, the faradiac response for the Fe(CN)₆^{3−} redox couple was not clearly distinguished unless the concentration of such species was increased to 40 μM (A), suggesting that the detection limit of bare Au electrode is in a level of 10^{-5} M, consistent with literature values [39]. The detection limit of such a redox couple was greatly improved

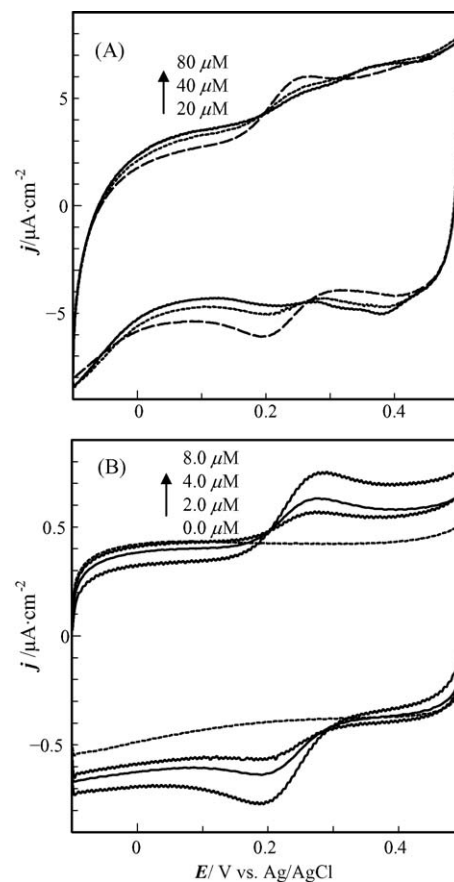


Fig. 7. CVs at bare (A) and Au-NP/HS(CH₂)₆SH-modified (B) Au electrodes in 0.10 M phosphate buffer (pH 7.0) containing Fe(CN)₆^{3−} redox couple with various concentrations (indicated in the figures). Scan rate, 0.1 V/s.

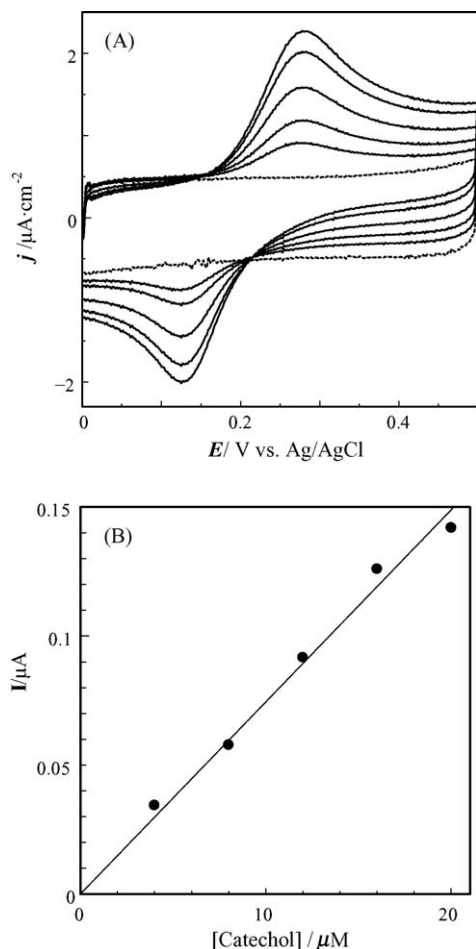


Fig. 8. (A) CVs at the Au-NP/HS(CH₂)₆SH-modified Au electrode in 0.10 M phosphate buffer (pH 7.0) containing catechol with various concentrations of (from inner to outer) 0.0, 4.0, 8.0, 12.0, 16.0 and 20.0 μM. Scan rate, 0.05 V/s. (B) Plot of the reduction peak current against the concentration of catechol.

at the Au-NP/HS(CH₂)_nSH-modified Au electrodes as shown in Fig. 7B. For example, the faradiac response for Fe(CN)₆³⁻ was even clearly recorded with a concentration as low as 2.0 μM. This indicates that the reduced capacitance of the Au-NP/HS(CH₂)_nSH-modified Au electrodes substantially make them useful for trace amount detection of the redox species, such as environmental pollutant, catechol, as shown in Fig. 8. As shown, the faradiac response for 4.0 μM catechol was even recorded without clearly overlapping with the charging current noise. The peak current increased linearly with the concentration of catechol as displayed in Fig. 8B with a linear equation of $I (\mu\text{A}) = 5.36 \times 10^{-3} + 7.08 \times 10^{-3} \times C (\mu\text{M})$ with correlation coefficient of 0.994.

4. Conclusion

We have demonstrated the novel electrochemical properties and potential electroanalytical applications of gold nanoparticles/alkanedithiol-modified electrodes prepared by closely packing 12-nm diameter gold nanoparticles onto bulk Au with self-assembled monolayers of alkanedithiols. The pre-

pared Au-NP/SAM-modified electrodes possess excellent electrode activity without a barrier to heterogeneous electron transfer between the bulk Au and redox species in solution phase. In addition, the Au-NP/SAM-modified electrodes show a very small interfacial capacitance. This demonstration may offer a new insight into interfacial electrochemistry of the metallic nanoparticles anchored onto the insulating films and could provide a new platform for electrochemical investigations and electroanalytical applications, such as for voltammetric determination of trace amount of environmental pollutants.

Acknowledgements

We gratefully acknowledge the financial support from National Natural Science Foundation of China (Grant Nos. 20375043, 20435030 and 20575071) and Chinese Academy of Sciences (Grant No. KJCX2-SW-H06).

References

- [1] M.C. Daniel, D. Astruc, *Chem. Rev.* 104 (2004) 293.
- [2] I. Willner, E. Katz, *Angew. Chem. Int. Ed.* 43 (2004) 6042.
- [3] T.K. Sau, C.J. Murphy, *J. Am. Chem. Soc.* 126 (2004) 8648.
- [4] C.R. Raj, T. Okajima, T. Ohsaka, *J. Electroanal. Chem.* 543 (2003) 127.
- [5] M.S. El-Deab, T. Ohsaka, *J. Electroanal. Chem.* 553 (2003) 107.
- [6] M.M. Maye, Y.B. Lou, C. Zhong, *Langmuir* 16 (2000) 7520.
- [7] X. Luo, J. Xu, Y. Du, H. Chen, *Anal. Biochem.* 334 (2004) 284.
- [8] K.R. Brown, A.P. Fox, M.J. Natan, *J. Am. Chem. Soc.* 118 (1996) 1154.
- [9] S. Liu, H. Ju, *Electroanalysis* 15 (2003) 1488.
- [10] J. Feng, G. Zhao, J. Xu, H. Chen, *Anal. Biochem.* 342 (2005) 280.
- [11] A.N. Shipway, M. Lahav, R. Gabai, I. Willner, *Langmuir* 16 (2000) 8789.
- [12] S. Bharathi, M. Nogami, S. Ikeda, *Langmuir* 17 (2001) 1.
- [13] J. Jia, B. Wang, A. Wu, G. Cheng, Z. Li, S. Dong, *Anal. Chem.* 74 (2002) 2217.
- [14] K.R. Brown, L.A. Lyon, A.P. Fox, B.D. Reiss, M.J. Natan, *Chem. Mater.* 12 (2000) 314.
- [15] W. Cheng, S. Dong, E. Wang, *Anal. Chem.* 74 (2002) 3599.
- [16] M.D. Musick, D.J. Peña, S.L. Botsko, T.M. McEvoy, J.N. Richardson, M.J. Natan, *Langmuir* 15 (1999) 844.
- [17] K. Šulík, C. Amatore, K. Holub, V. Mareček, W. Kutner, *Pure Appl. Chem.* 72 (2000) 1483.
- [18] R. Bilewicz, M. Majda, *J. Am. Chem. Soc.* 113 (1991) 5464.
- [19] E. Sabatani, I. Rubinstein, *J. Phys. Chem.* 91 (1987) 6663.
- [20] M. Lu, X.H. Li, B.Z. Yu, H.L. Li, *J. Colloid. Interf. Sci.* 248 (2002) 376.
- [21] T. Baum, D. Bethell, M. Brust, D.J. Schiffrin, *Langmuir* 15 (1999) 866.
- [22] S.L. Horswell, I.A. O'Neil, D.J. Schiffrin, *J. Phys. Chem. B* 107 (2003) 4844.
- [23] G. Frens, *Nature* 241 (1973) 20.
- [24] A. Doron, E. Katz, I. Willner, *Langmuir* 11 (1995) 1313.
- [25] K.R. Brown, D.G. Walter, M.J. Natan, *Chem. Mater.* 12 (2000) 306.
- [26] J.C. Hoogvliet, M. Dijkema, B. Kamp, W.P.V. Bennekoum, *Anal. Chem.* 72 (2000) 2016.
- [27] A.J. Bard, L.R. Faulkner, *Electrochemical Methods: Fundamentals and Applications*, 2nd ed., John Wiley and Sons Inc., New York, 2001.
- [28] M.D. Porter, C.E.D. Chidsey, *J. Am. Chem. Soc.* 109 (1987) 3559.
- [29] C. Miller, P. Cuendet, M. Grätzel, *J. Phys. Chem.* 95 (1991) 877.
- [30] C. Miller, M. Grätzel, *J. Phys. Chem.* 95 (1991) 5225.
- [31] U.K. Sur, R. Subramanian, V. Lakshminarayanan, *J. Colloid. Interf. Sci.* 266 (2003) 175.
- [32] D. Bethell, M. Brust, D.J. Schiffrin, C. Kiely, *J. Electroanal. Chem.* 409 (1996) 137.

- [33] K.C. Grabar, P.C. Smith, M.D. Musick, J.A. Davis, D.G. Walter, M.A. Jackson, A.P. Guthrie, M.J. Natan, *J. Am. Chem. Soc.* 118 (1996) 1148.
- [34] L. Su, F. Gao, L. Mao, *Anal. Chem.*, Revised.
- [35] J.S. Facci, R.H. Schmehl, R.W. Murray, *J. Am. Chem. Soc.* 104 (1982) 4959.
- [36] C.E.D. Chidsey, *Science* 251 (1991) 919.
- [37] S. Chen, R.W. Murray, *J. Phys. Chem. B* 103 (1999) 9996.
- [38] S. Chen, R. Pei, *J. Am. Chem. Soc.* 123 (2001) 10607.
- [39] J. Wang, *Analytical Electrochemistry*, 2nd ed., John Wiley and Sons Inc., 2000 (Chapter 1).

Fragmentation study and analysis of benzoylurea insecticides and their analogs by liquid chromatography–electrospray ionization–mass spectrometry

Xia Yang^a, Yan Xia^b, Xun Liao^a,
Yumin Zuo^b, Yiping Liao^{a,*}, Huwei Liu^{a,*}

^a The Key Lab of Bioorganic Chemistry and Molecular Engineering, Ministry of Education, Institute of Analytical Chemistry, College of Chemistry and Molecular Engineering, Peking University, Beijing 100871, China

^b College of Chemistry and Chemical Engineering, Nankai University, Tianjin 300071, China

Received 28 October 2005; received in revised form 15 January 2006; accepted 15 January 2006

Available online 17 February 2006

Abstract

Two insecticides, diflubenzuron and hexaflumuron, and their analogs have been separated by liquid chromatography (LC) and their fragmentation mechanisms were studied by electrospray ionization–ion trap mass spectrometry (ESI–MSⁿ) in both positive- and negative-ion modes. Sequential product ion fragmentation experiments were performed in order to explain the degradation pathways and identify their predominant fragment ions. It was indicated that the characteristic fragmentations are the loss of neutral molecules such as HF, HNO₂, and HCl to form stable ring structure or the cleavage of the acyl amine to form conjugated structure. Furthermore, the separation and determination of two benzoylurea (BU) insecticides and their analogs in the water samples from Weiming Lake have been described by LC–ESI–MS in negative mode. By the use of deprotonated molecule for quantitative analysis at low capillary exit voltage, low detection limits, good linearity and reproducibility for standard solutions were presented.

© 2006 Elsevier B.V. All rights reserved.

Keywords: LC–ESI–MS; Benzoylurea; Fragmentation; Determination

1. Introduction

Benzoylurea (BU) insecticides act as powerful insect growth regulators (IGRs) which interfere with chitin synthesis in target pests and cause death. BU insecticides have many attractive properties such as high selectivity, high biological activity, rapid degradation in soil and water and the acute low toxicity for animals. Diflubenzuron and hexaflumuron are two important benzoylurea insecticides, which coexist with their analogs in the environment. The demands placed on current regulatory monitoring programs require the development of increasingly sophisticated analytical techniques, which are capable of qualitatively and quantitatively determining these BU insecticides and their analogs at trace levels.

There are many analogs of diflubenzuron and hexaflumuron in the environment, which may be the byproducts in the process of synthesis, such as 1-(4-bromophenyl)-3-(2,6-difluorobenzoyl)urea (compound 1), 1-(2-nitrophenyl)-3-(2,6-difluorobenzoyl)urea (compound 2), 1-(2,4-dinitrophenyl)-3-(2,6-difluorobenzoyl)urea (compound 3), 1-(3,5-dichloro-4-(1,1,2,2-tetrafluoroethoxy)phenyl)-3-(2,6-dichlorobenzoyl)urea (compound 4) (Fig. 1).

Different techniques have been applied to the analysis of these compounds. BU insecticides have been analyzed by gas chromatography (GC) with both electronic capture and mass spectrometry detection, but complex derivatization processes are required due to their thermostability [1–3]. Diflubenzuron has also been analyzed by packed-capillary supercritical fluid chromatography–mass spectrometry (SFC–MS) with electron-capture negative ionization (ECNI), using carbon dioxide as mobile phase, but the detection limits are not as low as high performance liquid chromatogra-

* Corresponding authors. Tel.: +86 10 62754976; fax: +86 10 62751708.
E-mail address: hwliu@pku.edu.cn (H. Liu).

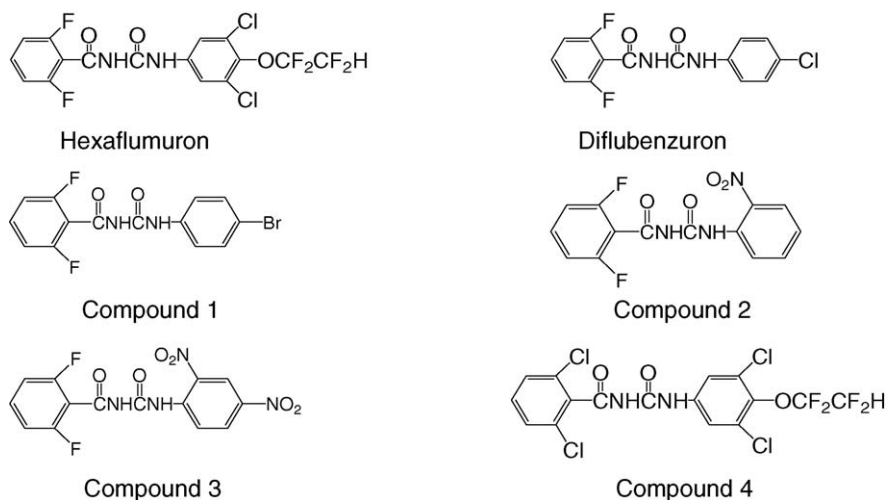
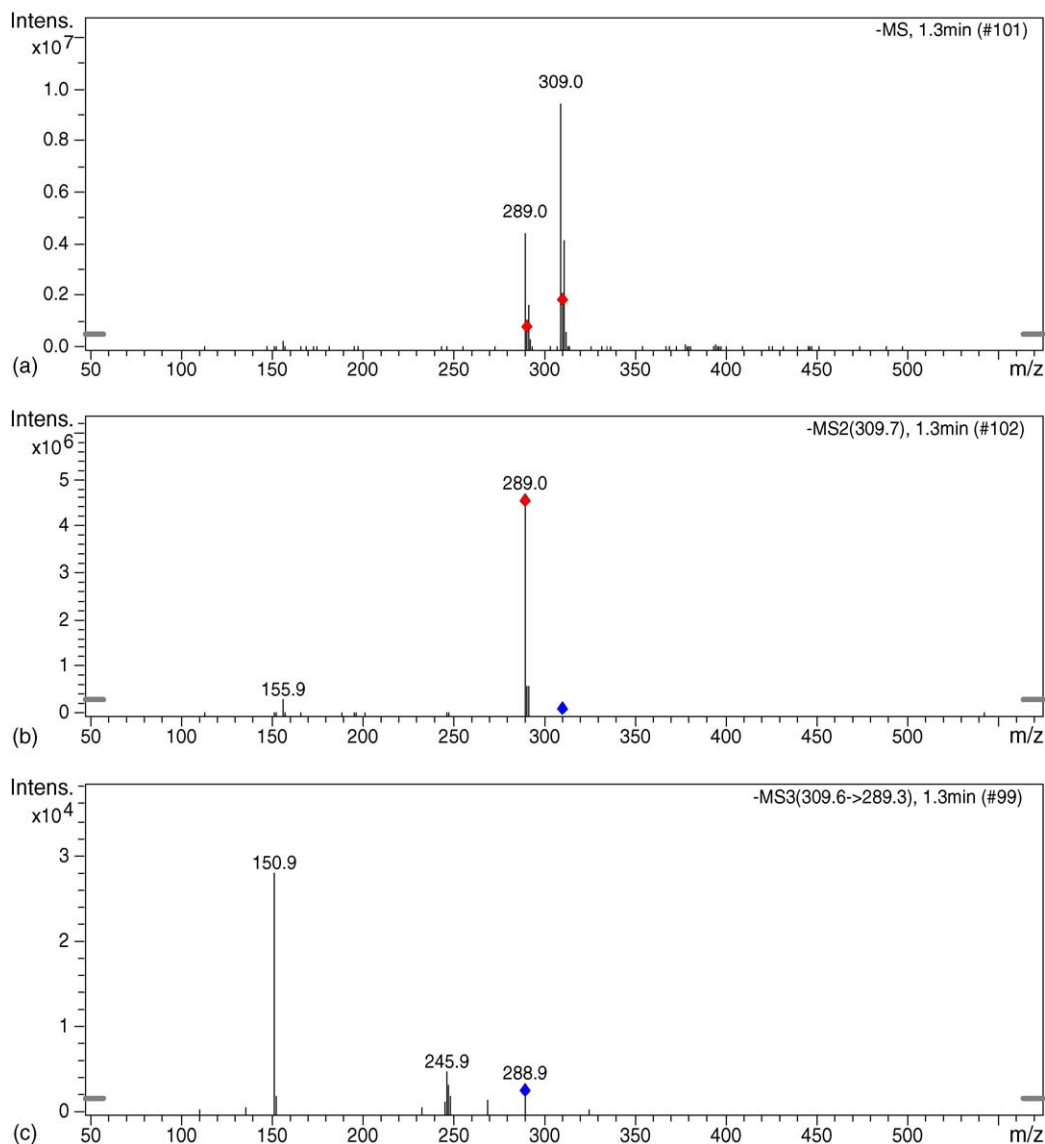
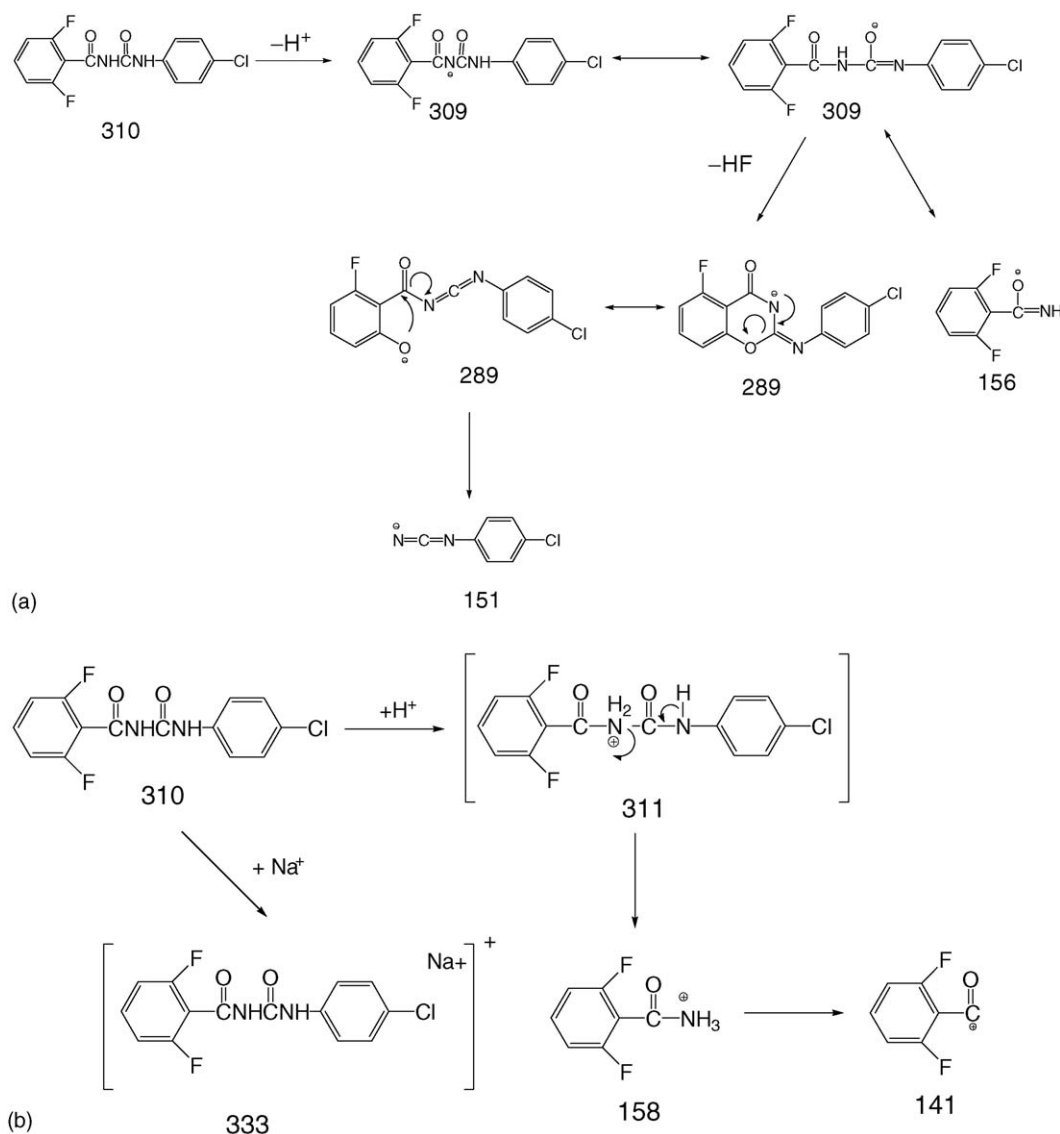


Fig. 1. Structures of hexaflumuron, diflubenzuron and their four analogs.

Fig. 2. (–)-ESI- MS^3 spectra of diflubenzuron: (a) MS of diflubenzuron; (b) MS^2 of m/z 309; (c) MS^3 of m/z 309 \rightarrow 289.



Scheme 1. Proposed ESI-MS fragmentation processes for diflubenzuron. (a) (–)-ESI conditions; (b) (+)-ESI conditions.

phy (HPLC) because of the lower acceptable sample introduction volume [4]. For this reason, HPLC with ultraviolet (UV) detectors [5–8], electrochemical [9] detectors and even the photochemical-spectrofluorimetric method [10] have been used to determine these BU insecticides in some matrices.

LC/MS provides an ideal system for the analysis of BU insecticides [11–15]. This system has advanced in reliability and ruggedness to the point where industrial and regulatory laboratories can now use these systems for routine analysis [16]. The complicated environmental samples will require a comprehensive structural elucidation, which can be directly and conveniently achieved by ion trap MS^n analysis. The elucidation of the mass spectral fragmentations of diflubenzuron, hexaflumuron and their analogs will facilitate the identification of unknown BU compounds based on common fragmentation pattern observed

under varying ionization conditions. Up to now, few studies have used MS^n to study fragmentation pathways of BU insecticides. Valenzuela et al. [14] determined three BU insecticide residues in citrus fruits using LC/atmospheric pressure chemical ionization-mass spectrometry (APCI-MS). From the negative-ion mass spectrometry, they got the main ions $[M - H]^-$, the secondary fragment ions $[M - H - HF]^-$ and other fragment ions. However, they did not provide the details of fragmentation ions and mechanism by MS^n .

In this paper, we present the investigation of the fragmentation mechanism of diflubenzuron, hexaflumuron and their analogs using electrospray ionization-ion trap MS (ESI- MS^n)—in both positive- and negative-ion modes. Furthermore, the separation and determination of six benzoylurea compounds were studied by LC-ESI-MS in negative mode, obtaining the best specificity and sensitivity for their detection.

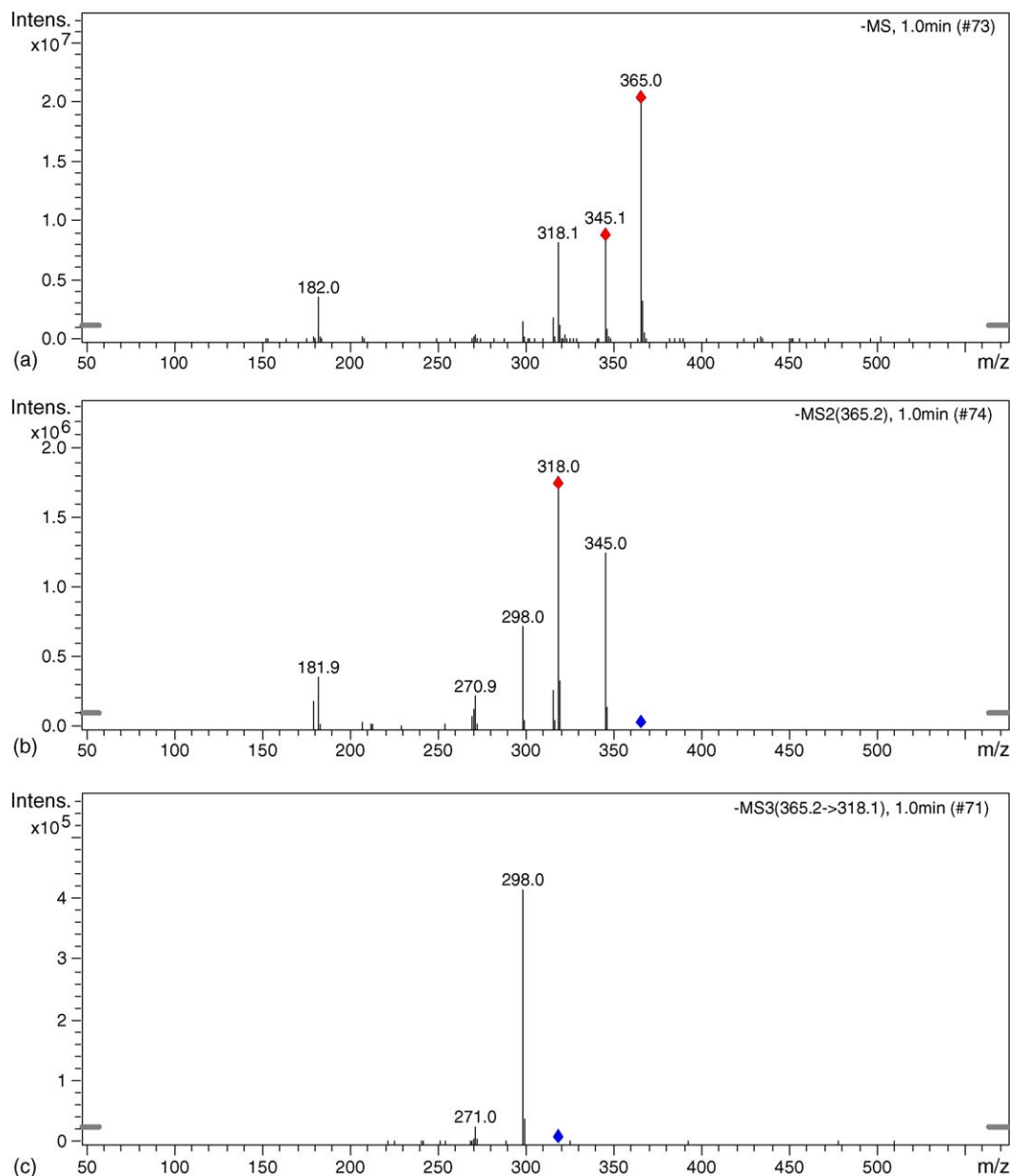


Fig. 3. (–)-ESI-MS³ spectra of compound 3: (a) MS of compound 3; (b) MS² of m/z 365; (c) MS³ of m/z 365 → 318.

2. Experimental

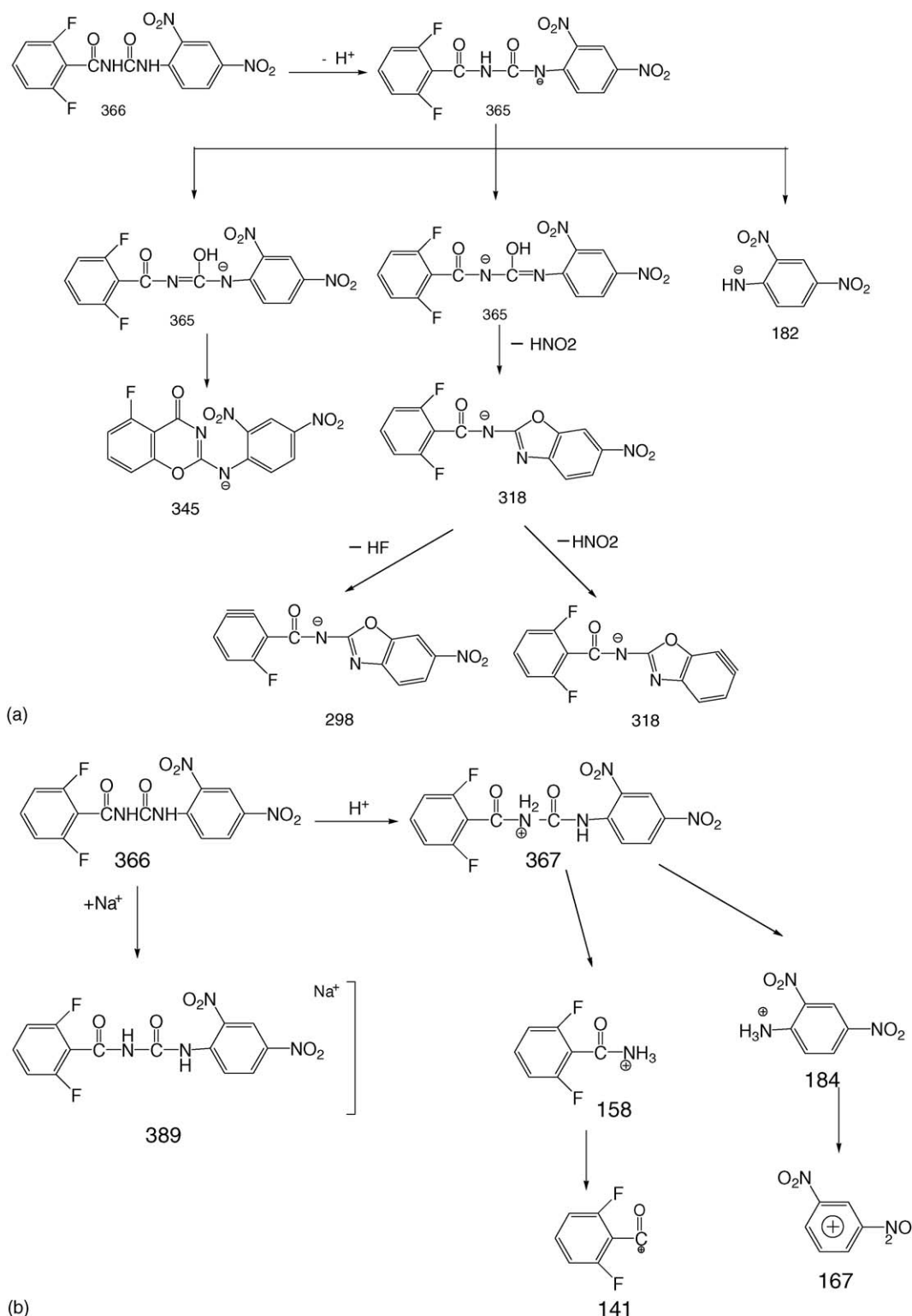
2.1. Reagents

Ammonium formate (>99.9) was purchased from Sigma–Aldrich Inc. (USA); both acetonitrile and methanol from Dima Technology Inc. (USA) were of HPLC grade. Dichloromethane of analytical grade was obtained from Beijing Chemical Factory (Beijing, China). Diflubenzuron, hexaflumuron and their analogs were synthesized by the authors at College of Chemistry and Chemical Engineering of Nankai University, Tianjin, China.

2.2. Preparation of standard solutions and samples

The calibration standards at concentrations of 0.004, 0.02, 0.1, 0.2, 0.4, 0.8 and 1.0 $\mu\text{g/ml}$ were prepared in acetonitrile–water (30:70).

Spiked water samples for recovery determination were prepared by the addition of an appropriate amount of a standard stock solution (10 $\mu\text{g/ml}$) to Weiming Lake water (100 ml). Extraction of the BU compounds were based on the method reported by Valenzuela et al. [14]. Weiming Lake water (10 ml) was diluted with 30 ml of pure water and the compounds were extracted on a SPE cartridge containing unendcapped C18 sor-



Scheme 2. Proposed ESI-MS fragmentation processes for compound 3. (a) (–)-ESI conditions; (b) (+)-ESI conditions.

bent, which was preconditioned with 3 ml of methanol and 3 ml of water. Diluted lake water sample (1 ml) was passed through the cartridge under manual positive pressure. After the enrichment step the cartridge was rinsed with 2 ml of water and 10 ml of air with the syringe. BU compounds were eluted with 5 ml of

dichloromethane, and then the eluate was evaporated to dryness with air at 50 °C. A 0.5 ml of acetonitrile was added and thoroughly mixed in an ultrasonic bath for 2 min. The extract was filtered through 0.45 μ m and 2 μ l was injected into the LC/MS system.

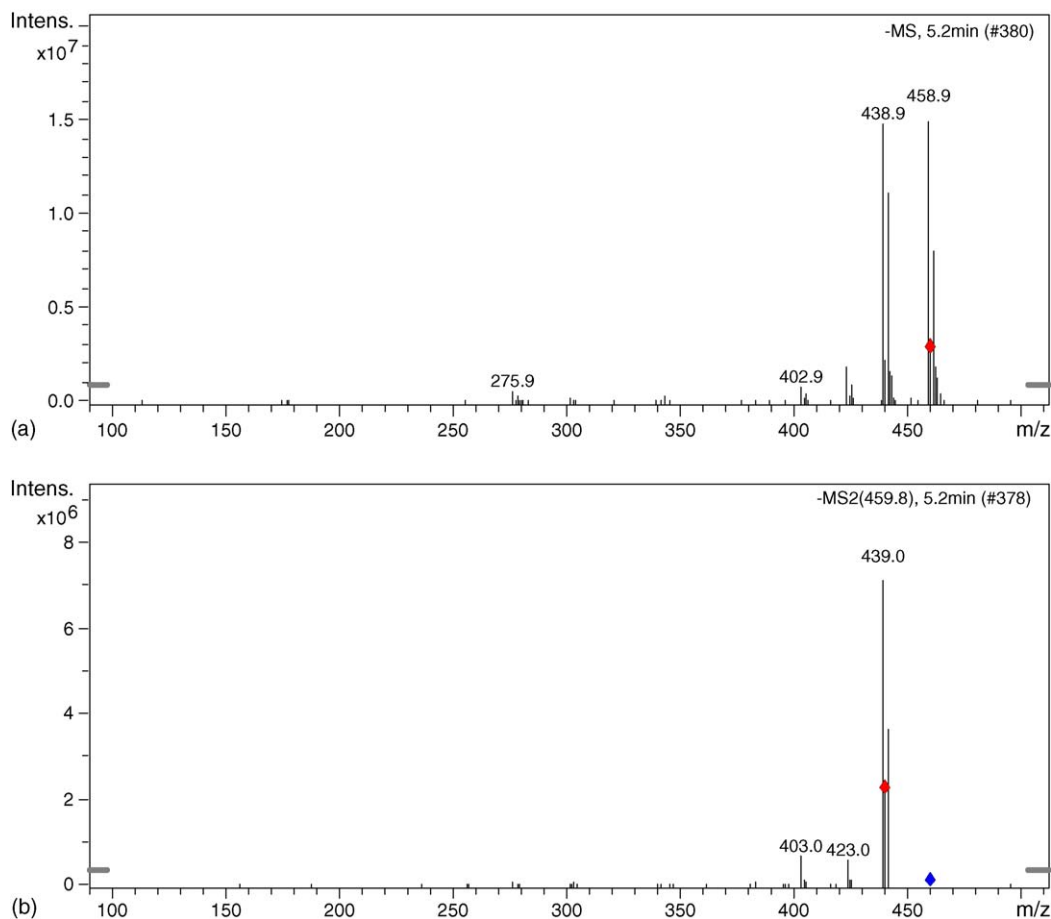
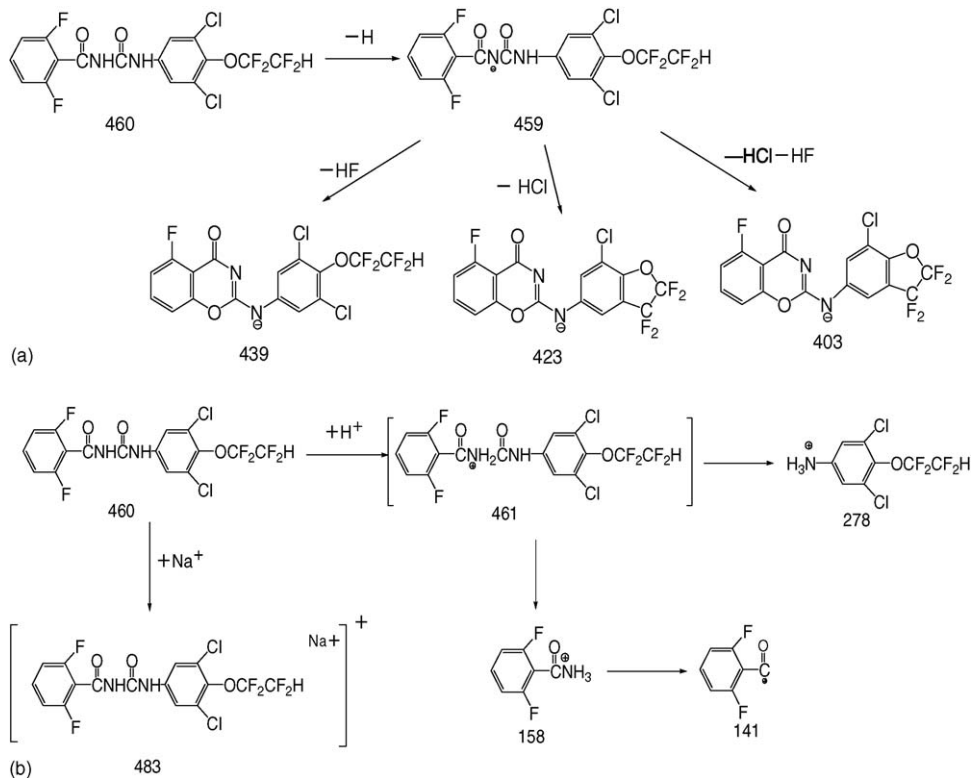


Fig. 4. (–)-ESI-MS² spectra of hexaflumuron: (a) MS of hexaflumuron; (b) MS² of m/z 460.



Scheme 3. Proposed ESI-MS fragmentation processes for hexaflumuron. (a) (–)-ESI conditions; (b) (+)-ESI conditions.

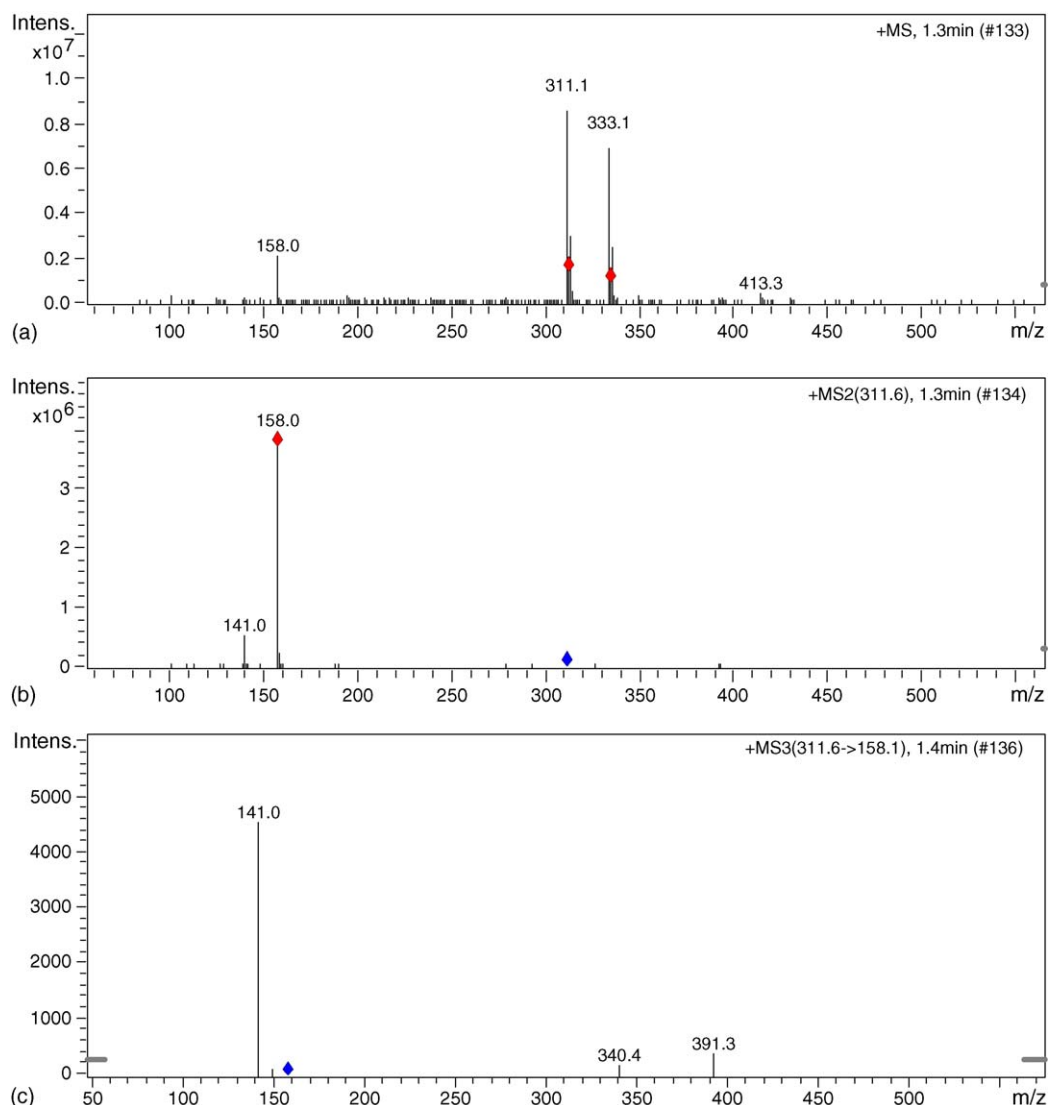


Fig. 5. (+)-ESI-MS³ spectra of diflubenzuron: (a) MS of diflubenzuron; (b) MS² of m/z 311; (c) MS³ of m/z 311 \rightarrow 158.

2.3. Chromatographic conditions

An Agilent 1100 series LC system (Agilent Technologies, Palo Alto, CA, USA) was used with a Venusil XBP C18 column (2.1 mm \times 50 mm i.d., 5 μ m) (Agila Technologies, USA). The solvents used as mobile phase were acetonitrile and water with 5 mM ammonium formate. The gradient selected for LC/ESI-MS at a flow rate of 0.3 ml/min was 48% acetonitrile, which was then increased to 85% in 5 min. The column temperature was 25 °C.

2.4. Mass spectrometry

The LC system was coupled on-line to LC/MSD Trap XCT ion-trap mass spectrometer (Agilent Technologies, CA, USA) equipped with an ESI or an APCI source operating in positive- or negative-ion mode. For the fragmentation experiments with

ESI source, sample solutions eluted from LC column were introduced into the ion source via a metal ESI needle set at high voltage (± 3.5 kV) and a heated capillary at 300 °C. The other instrument conditions were as follows: nebulizer pressure, 50.0 psi; drying gas (N₂) flow-rate, 10.0 l/min, and drying gas temperature, 325 °C. The ultra scan mode was utilized in the scan range of 100–560 m/z . MS^{*n*} experiments were carried out in AutoMS^{*n*} operation mode. The isolation and fragmentation width were 4.00 m/z , and the fragmentation amplitude was set to 1 V.

3. Results and discussion

3.1. Fragmentation study

As well known, ESI is a soft ionization technique with little fragmentation of molecule. To detect abundant fragment ions,

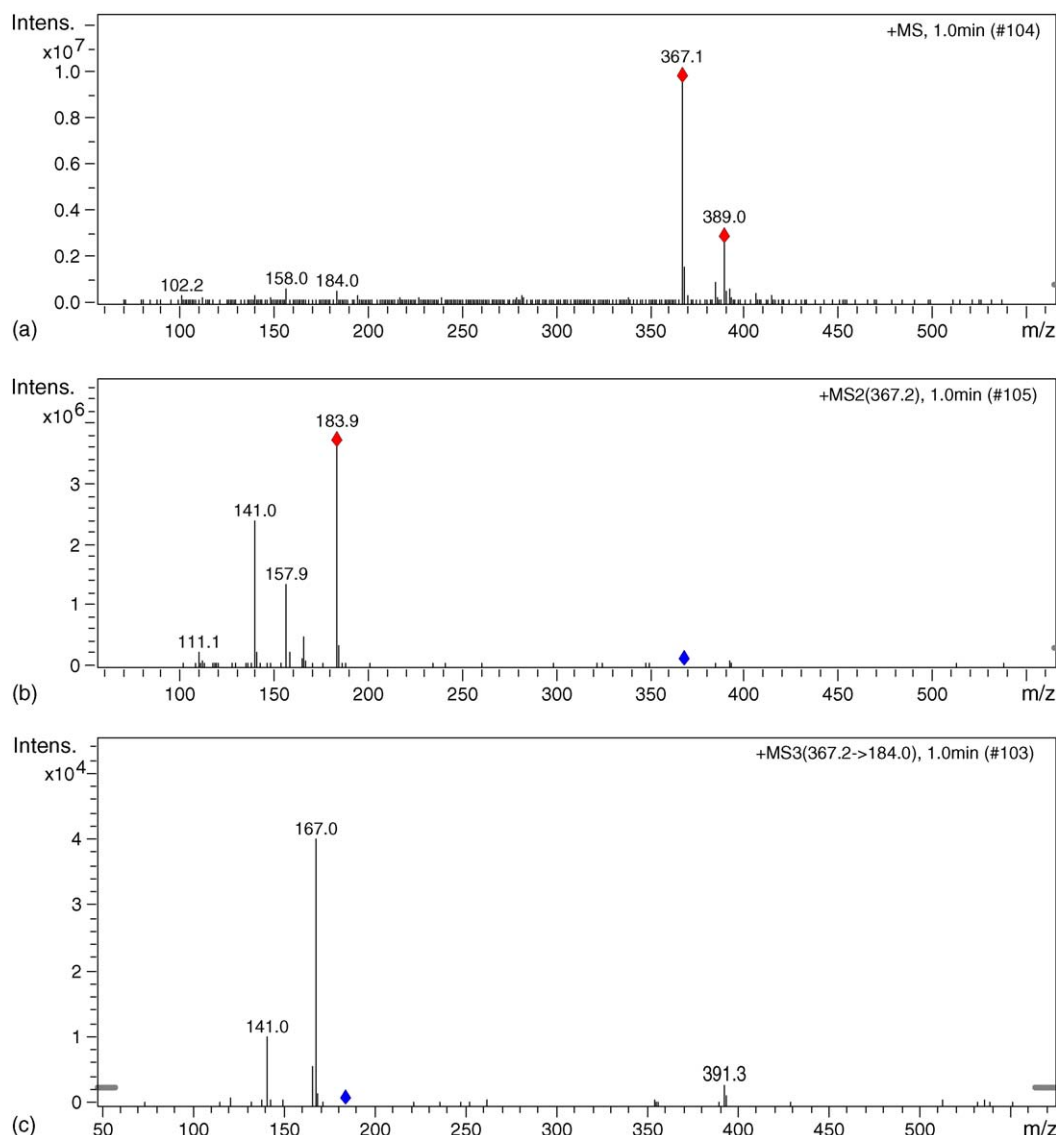


Fig. 6. (+)-ESI-MS³ spectra of compound 3: (a) MS of compound 3; (b) MS² of m/z 367; (c) MS³ of m/z 367 \rightarrow 184.

collision-induced dissociation (CID) has to be optimized by changing the capillary exit voltages (CapEx). This voltage can generate enough energy to break bonds by accelerating ions into collisions with molecules of the drying gas [17]. Because the skimmer voltage is fixed, the content of fragmentation can be enhanced by increasing the CapEx. In this work, the sequential product ion fragmentation behaviors of BU compounds under both the positive- and negative-ion mode of ESI were investigated in detail.

3.1.1. Negative-ion mode

Fig. 2(a) shows the negative-ion ESI-MS spectrum of diflubenzuron. The main peak at m/z 309 is assigned to the deprotonated ion $[M - H]^-$. In addition, another peak is also observed at m/z 289. In order to further explore the correlation between the fragmentation patterns and structural features of

these compounds, MS² and MS³ spectra were acquired for the $[M - H]^-$ ions of all six compounds. Fig. 2(b) shows the MS² of $[M - H]^-$, and the mass differences between the precursor ion at m/z 309 and the product ions at m/z 289 and 156 are 20 and 153 Da, respectively, corresponding to the neutral HF and C₇H₄NOC₂Cl. The MS³ data m/z 151 showed in Fig. 2(c) is obtained by resonance with the molecule of m/z 289 and then loss of a lactone structure. The fragmentation mechanism of diflubenzuron is proposed in Scheme 1(a). For the compound 3, the fragmentation of m/z 345 is also resulted from the precursor ion $[M - H]^-$ via a loss of neutral HF. However, the fragment ion detected at m/z 182, which is observed in the MS² spectrum of the deprotonated molecule, originates from the cleavage of the acyl amine close to the nitro-substituted phenyl ring. Because of the electron withdrawing effect of *o*- and *p*-nitryl, this pair of electrons on the nitrogen is stabilized. It is also due to the loss

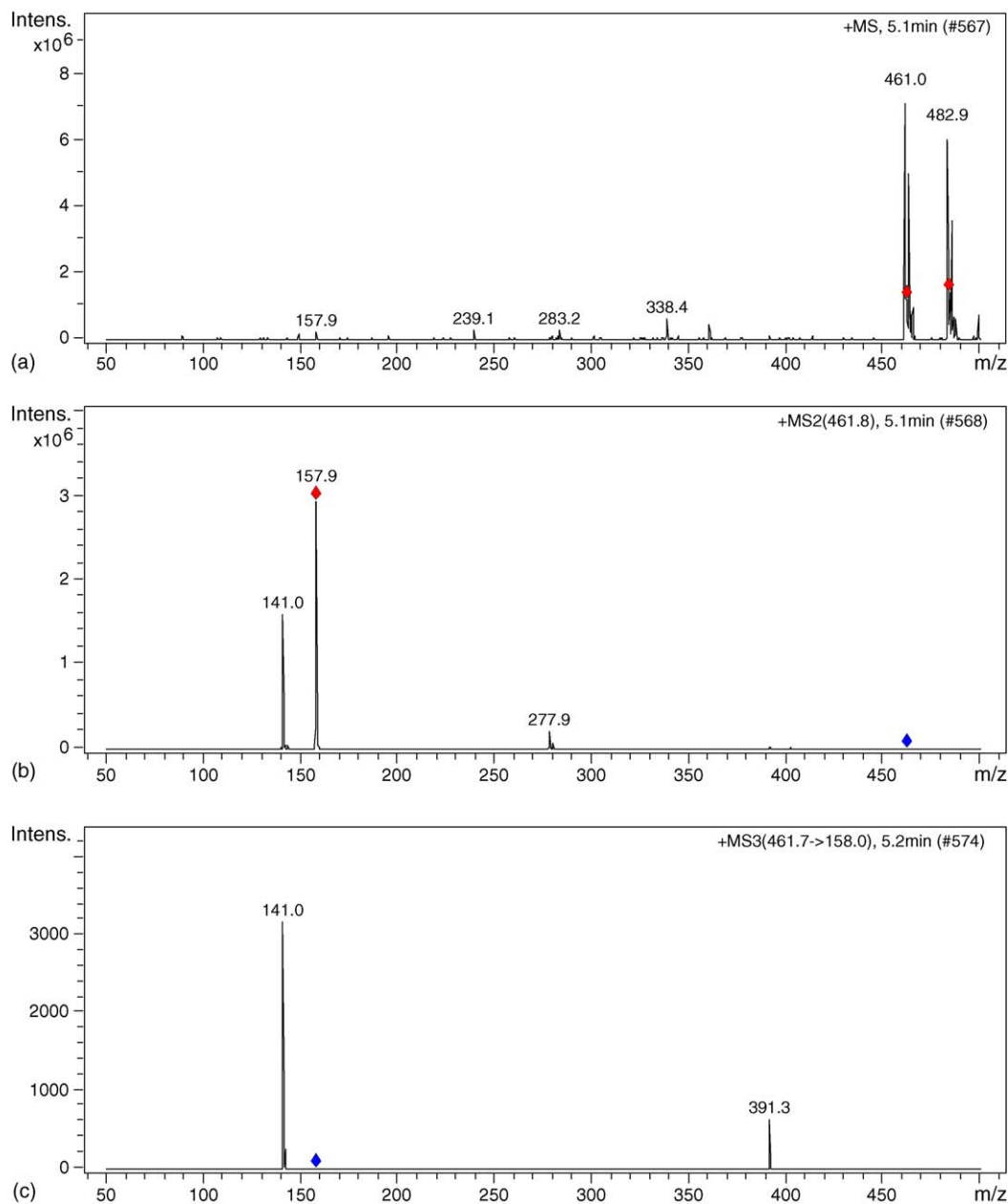


Fig. 7. (+)-ESI-MS³ spectra of hexaflumuron: (a) MS of hexaflumuron; (b) MS² of m/z 461; (c) MS³ of m/z 461 \rightarrow 158.

of neutral HNO₂, a stable five-member ring is formed (Fig. 3 and Scheme 2(a)). In a similar fashion, the fragment ions at m/z 439, 423 and 403 observed in mass spectra of hexaflumuron (Fig. 4) can be explained to be the losses of HF and HCl, and the proposed fragmentation mechanism is showed in Scheme 3(a).

In addition, the results proved that fragment ions resulted from APCI-MS of negative-ion mode are mostly similar to those from ESI with the same mode, which was also referred in some literatures [14,18].

3.1.2. Positive-ion mode

The positive-ion ESI-MS³ spectrum of diflubenzuron, hexaflumuron and compound 3 are presented in Figs. 5–7, respec-

tively. All of six compounds gave the protonated species $[M+H]^+$, and $[M+Na]^+$ after ionization in the electrospray source. Taking compound 3 for example, the resulting protonated species, $[M+H]^+$, at m/z 367 loses the isocyanate portion (209 Da) to give a species at m/z 158. This is followed by loss of the neutral species NH₃ (17 Da), leading to a ion at m/z 141. Moreover, another fragment ion resulting from $[M+H]^+$ is at m/z 184, originating from the cleavage of the right acyl amine, and then by loss of the neutral species NH₃ (17 Da), obtaining a species at m/z 167 (Scheme 2(b)). The mass fragmentation of other five compounds is very similar to that of compound 3 (Scheme 1(b) and Scheme 3(b)). The spectra of diflubenzuron (MH⁺ = 311 Da) and hexaflumuron (MH⁺ = 461 Da) show main fragment ions at m/z 158 followed by m/z 141 and another main

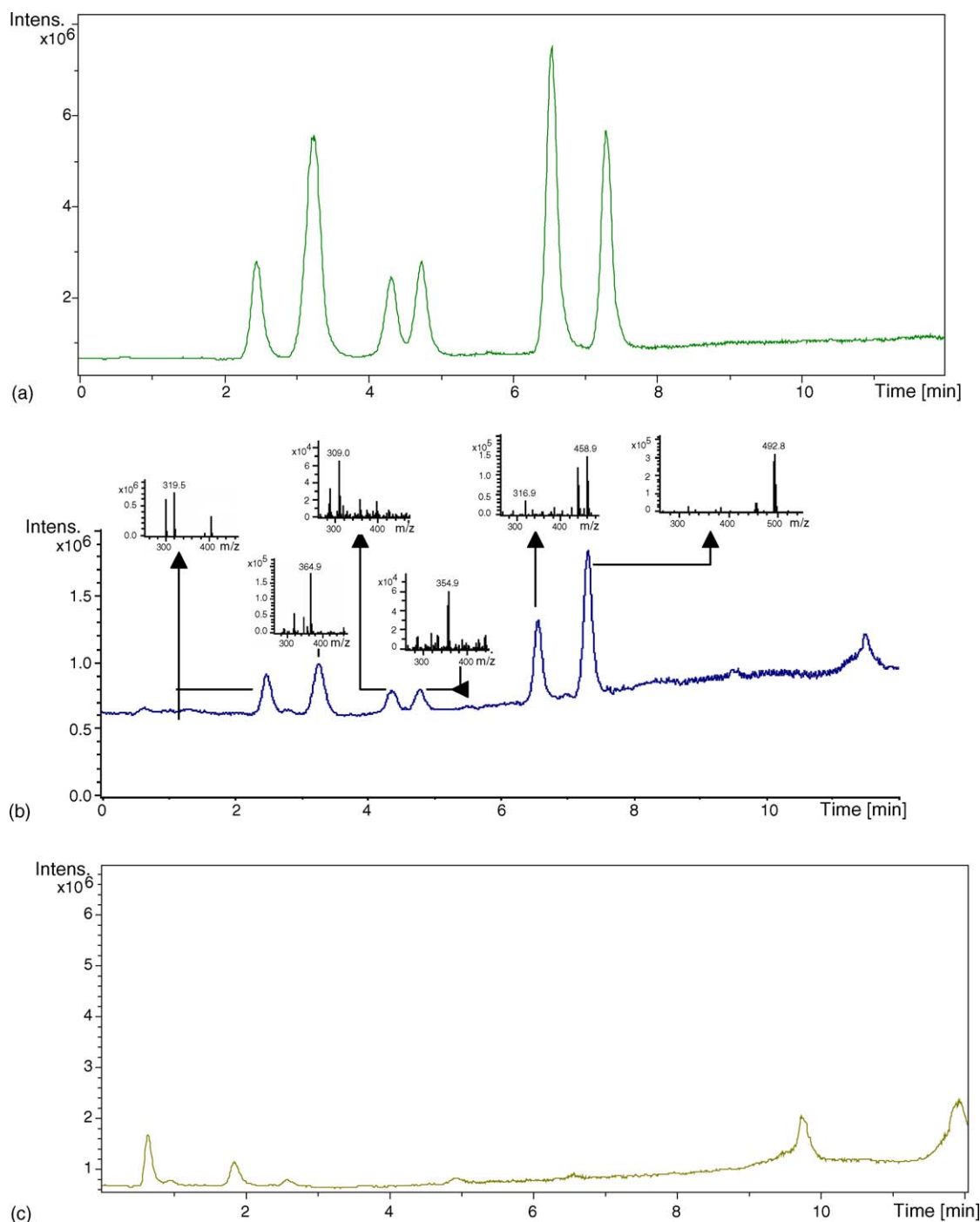


Fig. 8. (a) Total ion chromatogram (TIC) of 20 µg/ml standard solution; (b) TIC of 0.5 µg/ml spiked lake water sample; (c) TIC of blank sample.

fragment ion of hexaflumuron at m/z 278 is obtained due to the loss of the neutral group ($C_8H_3NO_2F_2$).

Table 1 shows the relative abundances of ions for these BU compounds obtained at different CapEx voltages of positive-ion mode. Using the selected value (125 and 160 V), the molecular cation $[M+H]^+$ was always the base peak. However, higher CapEx voltage (190 V) caused increasing fragmentation and the fragment ions formed the base peak of the spectrum, with the exception of hexaflumuron, compounds 2 and 3. In a similar way, increasing of the CapEx voltage caused a concomitant increase

of the relative abundances of fragment ions in the negative-ion mode (Table 2). It is noteworthy that when using 125 V as CapEx voltage, the molecular anion $[M-H]^-$ was the base peak, except for hexaflumuron. At lower potential, little fragment ions were produced for structure identification, and at higher potential, high response for each molecular ion cannot be obtained. So, a CapEx voltage at 95 V in negative-ion mode was found to be the most appropriate in order to obtain high response for quantitative analysis with deprotonated molecule $[M-H]^-$.

Table 1
Main fragments of the BU compounds obtained at different CapEx voltages in positive-ion mode

Mode	Compound	M_w	Fragment ions	Assignment	Relative abundance (%)		
					125 V	160 V	190 V
ESI+	Diflubenzuron	310	311	$[M+H]^+$	100	100	59
			333	$[M+Na]^+$	69	80	97
			158	$[M+H-C_7H_4NOCl]^+$	15	24	100
			141	$[M+H-C_7H_4NOCl-NH_3]^+$	<1	<1	9
ESI+	Compound 1	354	355	$[M+H]^+$	100	100	23
		356	357	$[M+H]^+$	93	95	23
			377	$[M+Na]^+$	40	54	34
			379	$[M+Na]^+$	42	55	28
			158	$[M+H-C_7H_4NOCl]^+$	35	95	100
			141	$[M+H-C_7H_4NOCl-NH_3]^+$	<1	5	8
ESI+	Compound 2	321	322	$[M+H]^+$	100	100	100
			344	$[M+Na]^+$	10	12	28
			360	$[M+K]^+$	3	3	2
			158	$[M+H-C_7H_4N_2O_3]^+$	6	11	57
			139	$[M+H-C_8H_3NO_2F_2]^+$	5	8	12
ESI+	Compound 3	366	367	$[M+H]^+$	100	100	100
			389	$[M+Na]^+$	20	27	33
			158	$[M+H-C_7H_3N_3O_5]^+$	<1	6	18
			141	$[M+H-C_7H_3N_3O_5-NH_3]^+$	<1	3	11
			184	$[M+H-C_8H_3NO_2F_2]^+$	<1	4	8
			167	$[M+H-C_8H_3NO_2F_2-NH_3]^+$	<1	<1	<1
ESI+	Hexaflumuron	460	461	$[M+H]^+$	100	100	100
			483	$[M+Na]^+$	49	46	92
			158	$[M+H-C_9H_3O_2F_4Cl_2N]^+$	<1	4	9
			141	$[M+H-C_9H_3O_2F_4Cl_2N-NH_3]^+$	<1	<1	15
			278	$[M+H-C_8H_3NO_2F_2]^+$	<1	<1	<1
ESI+	Compound 4	494	495	$[M+H]^+$	100	100	34
			517	$[M+Na]^+$	46	55	16
			190	$[M+H-C_9H_3O_2F_4Cl_2N]^+$	<1	10	100
			173	$[M+H-C_9H_3O_2F_4Cl_2N-NH_3]^+$	<1	<1	25
			278	$[M+H-C_8H_3NO_2Cl_2]^+$	<1	<1	<1

Table 2
Main fragments of the BU compounds obtained at different CapEx voltages in negative-ion mode

Mode	Compound	M_w	Fragment ions	Assignment	Relative abundance (%)		
					125 V	160 V	190 V
ESI−	Diflubenzuron	310	309	$[M-H]^-$	100	100	100
			289	$[M-H-HF]^-$	39	47	66
			156	$[M-H-C_7H_4NOCl]^-$	2	3	1
			151	$[M-H-HF-C_7H_3O_2F]^-$	<1	<1	1
ESI−	Compound 1	356	355	$[M-H]^-$	100	100	100
		354	353	$[M-H]^-$	88	78	83
			335	$[M-H-HF]^-$	24	30	39
			333	$[M-H-HF]^-$	27	28	42
			156	$[M-H-C_7H_4NOCl]^-$	1	1	1
ESI−	Compound 2	321	320	$[M-H]^-$	100	100	33
			300	$[M-H-HF]^-$	99	99	100
			137	$[M-H-C_8H_3NO_2F_2]^-$	16	44	65
			162	$[M-H-HF-C_7H_3O_2F]^-$	<1	<1	2
ESI−	Compound 3	366	365	$[M-H]^-$	100	100	100
			345	$[M-H-HF]^-$	32	42	61
			318	$[M-H-HNO_2]^-$	37	41	49
			298	$[M-H-HNO_2-HF]^-$	5	8	15
			182	$[M-H-C_8H_3NO_2F_2]^-$	16	18	46
			271	$[M-H-2HNO_2]^-$	1	2	1

Table 2 (Continued)

Mode	Compound	M_w	Fragment ions	Assignment	Relative abundance (%)		
					125 V	160 V	190 V
ESI–	Hexaflumuron	460	459	$[M - H]^-$	87	78	58
			439	$[M - H - HF]^-$	100	100	100
			423	$[M - H - HCl]^-$	16	12	10
			403	$[M - H - HF - HCl]^-$	2	5	9
ESI–	Compound 4	494	493	$[M - H]^-$	100	100	100
			457	$[M - H - HF]^-$	12	19	18

Table 3

Calibration curve, detection limit, recovery, and R.S.D. of intraday and interday

Compound	Linear equation	R	LOD (ng/ml)	Recovery (%)	R.S.D. (%)	
					intraday	interday
Diflubenzuron	$Y = 6337.8X - 21204$	0.9993	7	76.4	1.04	4.6
Compound 1	$Y = 759.60X + 13006$	0.9996	12	86.0	1.82	2.8
Compound 2	$Y = 2185.2X - 12535$	0.9949	10	96.7	1.62	4.7
Compound 3	$Y = 24137X - 63703$	0.9968	2	75.4	0.78	1.1
Hexaflumuron	$Y = 10847X + 4348.9$	0.9993	2.2	77.0	2.17	1.2
Compound 4	$Y = 20403X + 39099$	0.9990	2	89.1	1.82	1.6

3.2. LC–ESI–MS study of diflubenzuron, hexaflumuron and their analogs

Diflubenzuron, hexaflumuron and their analogs were separated using a 50 mm \times 2.1 mm i.d. C₁₈ LC column (5 μ m) and a binary gradient mobile phase comprising ACN and water with 5 mM ammonium formate over a period of 10 min at a flow rate of 0.3 ml/min. The injection volume was 2 μ l. The use of this column with small inner diameter and short length at low flow rate shortened the separation time and reduced the consumption of mobile phase. Extracted ion chromatogram in negative-ion mode was used to obtain the highest sensitivity for quantitative analysis. The mass-to-charge (m/z) values of $[M - H]^-$ for six compounds are as follows: m/z 309 (diflubenzuron), m/z 355 (compound 1), m/z 320 (compound 2), m/z 365 (compound 3), m/z 459 (hexaflumuron), m/z 493 (compound 4).

Each of the BU compound was chromatographed at an initial concentration of 1 μ g/ml using ESI–MS detection, then followed by serial dilution down to the limits of detection as reported in Table 3. Calibration curves for standard samples in acetonitrile and water were found to be linear in the range between 10 and 1000 ng/ml, and the correlation coefficient between peak area and concentration for these compounds were satisfactory (0.994–0.999). LC–ESI–MS of a mixture of six BU compounds is given in Fig. 8(a), showing complete baseline resolution of six analytes.

Table 3 also lists the repeatability of peak area, indicating that the relative standard deviation (R.S.D.) was 1.0–2.2% within 1 day, and 1.0–4.7% for day-to-day repeatability.

Based on the calibration, Weiming Lake water samples spiked with 1 μ g/ml of six BU compounds, respectively, were extracted and analyzed by LC/ESI–MS. Fig. 8(b) and (c) present the chromatograms of extracts of a spiked lake water sample and a blank

sample. It can be seen that no peak was detected between 2 and 8 min for blank sample. The recovery was calculated to be 75–97% for six BU compounds.

4. Conclusions

The structures of fragment ions proposed for BU compounds were supported by ESI–MS³ data. Certain characteristic fragmentations have been shown to be the loss of neutral molecules such as HF, HNO₂ and HCl to form stable ring structure or the cleavage of the acyl amine to form conjugated structure. The data provide useful information on the structure of these compounds and can be used in the characterization of such BU compounds.

This LC–ESI–MS method was shown to be feasible for the analysis of diflubenzuron, hexaflumuron and their analogs in groundwater, which relies for quantitation on the deprotonated molecule of them. The main advantages over the LC/UV method previously described are that the sensitivity is improved and the analytes can be unambiguously identified in the samples at low levels.

Acknowledgements

We thank Mr. D. Wen and Mr. F. Gao at Peking University for their helpful suggestions. This work was supported by NSFC (Grand no. 20575003).

References

- [1] J.K. Mensah, E. Lundanes, T. Greibrokk, B. Holen, J. Chromatogr. A 765 (1997) 85.
- [2] H.J. Stan, P. Klaffenbach, Fresenius J. Anal. Chem. 339 (1991) 40.
- [3] M.J. Wimmer, R.R. Smith, J.P. Jones, J. Agric. Food Chem. 39 (1991) 280.
- [4] C. Brede, E. Lundanes, J. Chromatogr. A 712 (1995) 95.

- [5] T. Tomsej, J. Hajslova, J. Chromatogr. A 704 (1995) 513.
- [6] A. Balinova, J. Chromatogr. A 823 (1998) 11.
- [7] G.E. Miliadis, N.G. Tsiropoulos, P.G. Aplada-Sarlis, J. Chromatogr. A 835 (1999) 113.
- [8] A.I. Valenzuela, R. Lorenzini, M.J. Redondo, G. Font, J. Chromatogr. A 839 (1999) 101.
- [9] E. Rodriguez, R.J. Barrio, A. Goicolea, Anal. Chim. Acta 384 (1999) 63.
- [10] M.D. Gil-Garcia, Talanta 53 (2001) 915.
- [11] K.A. Barnes, R.J. Fussell, J.R. Startin, S.A. Thorpe, S.L. Reynold, Rapid Commun. Mass Spectrom. 9 (1995) 1441.
- [12] C. Molina, G. Durand, D. Barcelo, J. Chromatogr. 29 (1995) 113.
- [13] K.A. Barnes, R.J. Fussell, J.R. Startin, M.K. Pegg, S.A. Thorpe, S.L. Reynold, Rapid Commun. Mass Spectrom. 11 (1997) 117.
- [14] A.I. Valenzuela, Y. Pico, G. Font, Rapid Commun. Mass Spectrom. 14 (2000) 572.
- [15] A.G. Frenich, M.D.G. Garcia, F.J. Arrebola, J.L.M. Vidal, M.M. Galera, T. Lopez, Chromatographia 52 (2000) 569.
- [16] J.D. Vargo, Anal. Chem. 70 (1998) 2699.
- [17] M. Rodriguez, D.B. Orescan, Anal. Chem. 70 (1998) 2710.
- [18] K.A. Barnes, J.R. Startin, S.A. Thorpe, S.L. Reynolds, R.J. Fussell, J. Chromatogr. A 712 (1995) 85.

Determination of polybrominated diphenyl ethers in soil from e-waste recycling site

Zongwei Cai^{a,*}, Guibin Jiang^b

^a Department of Chemistry, Hong Kong Baptist University, Kowloon Tong, Hong Kong SAR, China

^b Research Center for Eco-environmental Sciences, the Chinese Academy of Sciences, Beijing, China

Received 27 October 2005; received in revised form 10 January 2006; accepted 13 January 2006

Available online 17 February 2006

Abstract

Soil samples collected from an electronic waste recycling site were prepared by using Soxhlet extraction and multiple-step column chromatographic clean-up. Gas chromatography/ion trap mass spectrometry method was developed to determine polybrominated diphenyl ethers (PBDEs) in the sample extracts. The method performance was evaluated by the recovery of ¹³C-labeled internal standards and by analyzing quality assurance and quality control samples. Relative error and relative standard deviation obtained from the analysis of duplicated samples and spiked matrix were better than 10%. PBDEs were detected in the field soil samples collected from an e-wastes disposal site at levels from low parts-per-billions to 600 parts-per-billions.

© 2006 Elsevier B.V. All rights reserved.

Keywords: PBDEs; e-Waste; Soil; GC–ion trap MS

1. Introduction

Polybrominated diphenyl ethers (PBDEs) are anthropogenic chemicals that have been extensively used as flame retardants in furniture, building materials and electronic components. PBDEs can be released into the environment, persistent with a high bioaccumulation potential and thus affect human health. The flame retardant have been detected with significant levels in environmental [1–3] and biological [4,5] samples. Recent toxicological studies suggested that several PBDEs and/or their metabolites might have disrupted the endocrine system [6,7]. Thus, trace analysis of PBDEs is important.

Illegal recycling operations of electronic wastes (e-wastes) have been reported to cause severe environmental pollution of PBDEs [8–10]. The hazardous e-wastes smuggled from Western countries into the illegal recycling sites in China included computers, electronic appliances and transformer carcasses. In the e-waste sites, recycling operations consist of toner sweeping, dismantling electronic equipment, selling computer monitor

yokes to copper recovery corporations, plastic chipping and melting, burning wires to recover copper, melting circuit boards over open fires and using acid chemical strippers to recover gold and other metals. In an e-waste recycling site in Taizhou city, Zhejiang Province in China, for example, most of the wastes get processed in large-scale dismantling yards where thousands of labourers sit all day wielding chisel and hammer, breaking down the electronic equipment, although it has been declared that it is illegal to work on waste computers, monitors and televisions and that all work must be done in permitted facilities. These e-waste activities cause severe damage to the environment and expose the workers and local residents to toxic chemicals through inhalation, dermal exposure and oral intake of contaminated foods. The contamination of PBDEs is one of the most concerned problems because the e-wastes contain significant levels of flame retardants made of various PBDEs products [9,10]. However, little information on the PBDE congener profiles and concentrations in the environment around the e-waste recycling site has been reported. This study aims to apply a capillary gas chromatography/ion trap mass spectrometry method for analyzing PBDEs in soil samples collected from the e-waste disposal site. Various contamination sources of PBDEs were discussed based on the obtained analytical results.

* Corresponding author. Tel.: +852 34117070; fax: +852 34117348.
E-mail address: zwcai@hkbu.edu.hk (Z. Cai).

Table 1

Concentrations of native and ^{13}C -labeled PBDEs in calibration standard solutions ($\text{pg}/\mu\text{L}$)

Compounds	CS ^a -1	CS-2	CS-3	CS-4	CS-5	^{13}C -labeled PBDE
BDE-3	1.0	5.0	20	100	400	100
BDE-15	1.0	5.0	20	100	400	100
BDE-28	1.0	5.0	20	100	400	100
BDE-47	1.0	5.0	20	100	400	100
BDE-99	1.0	5.0	20	100	400	100
BDE-139	1.0	5.0	20	100	400	100
BDE-153	1.0	5.0	20	100	400	100
BDE-154	1.0	5.0	20	100	400	100
BDE-183	1.0	5.0	20	100	400	100

^a Calibration standard.

2. Experimental

2.1. Chemical reagents and standard solutions

Chemicals used in this study were analytical or higher grade. The PBDE standard solutions were purchased from Wellington Laboratories (Ontario, Canada). Cleaned sand was purchased from Fluka (Milwaukee, USA) and used for method development. A set of 5 PBDE calibration standard solutions (CS-1–CS-5) contained 19 native PBDEs and 10 ^{13}C -labeled PBDEs. The concentrations of mono- to hepta-brominated diphenyl ethers ranged from 1 to 400 $\text{pg}/\mu\text{L}$ while the ^{13}C -labeled standards were maintained constantly at 100 $\text{pg}/\mu\text{L}$ (Table 1).

2.2. Sample preparation and analysis

Cleaned sand was spiked with known levels of PBDE standards prior to the sample preparation for evaluating method accuracy and precision. Environmental soil samples were collected from six sampling points around an approximate 30-m² disposal site of e-wastes. The samples were thoroughly mixed and ground prior to the sample preparation. One gram of each of the sand and field soil sample was mixed with 10 g anhydrous sodium sulphate and 5 g of acid washed copper powder. After 1 ng of ^{13}C -labeled PBDE internal standard was added, the sample was Soxhlet extracted with a solvent containing hexane and acetone (1:1, v/v) for 12 h. The sample was cleaned-up with columns of acidic silica gel and activated neutral alumina for the GC/MS/MS analysis. One microliter of the sample extract was injected into a DB-5 column (60 m, 0.25 mm i.d., 0.25 μm film thickness) with injector temperature of 280 °C and splitless injection mode on a ThermoQuest Trace GC/PolarisQ ion trap mass spectrometer. The column temperature was programmed from 110 °C (1 min) to 180 °C at rate of 8 °C/min; from 180 °C (1 min) to 280 °C at 2 °C/min and finally hold for 10 min at 280 °C. Ion trap was used for the electron impact ionization (EI) MS/MS analysis. The MS source temperatures, source energy and emission current were set at 250 °C, 70 eV and 250 mA. Collision-induced dissociation (CID) experiments were conducted on selected precursor ions for the PBDE congeners. The ion trap MS parameters included isolation width (1.0 amu), isolation time (8 ms), excitation time (15 ms), resonant excitation voltage (1.00 V), and q -value (0.45).

3. Results and discussion

Sample preparation procedure for PBDEs in solid samples was performed by using Soxhlet extraction and column chromatographic clean-up [11]. Quantitative recoveries (more than 65%) were achieved for the sample preparation procedure, except for the mono-BDE congener (BDE-3) which had an average recovery of 40%. BDE-3 has relatively low boiling point, which might result in losses during the concentration procedure. Nevertheless, low recovery should not affect the method accuracy and precision because isotope dilution GC–MS technique is applied. The accuracy and precision of the method were evaluated by analyzing the cleaned sand samples spiked with known amount PBDEs. The obtained relative errors and relative standard deviations were less than 30% ($n = 6$) when the added PBDE levels were 1 parts-per-billion (ppb). Calibration standards were analyzed under the optimized MS/MS parameters. Linear calibration was obtained within the range of 1–400 pg for the PBDE congeners. For the ion trap MS/MS analysis, the most intensive ion peak of each PBDE congener was selected as the parent ion [9,10]. The selected parent ions were isolated in the ion trap and fragmented by using tandem mass spectrometry. MS/MS spectra of all analytes were recorded, from which a characteristic ion was selected as quantitative ion. The quantitative ions were selected based on the criteria of peak intensity and ion specificity as well as potential interference from other compounds. The $[M - \text{COBr}]^+$ fragment ion was observed as the base peak for PBDEs with *ortho*-substituted bromine, while the fragmentation ion with the loss of Br_2 ($[M - \text{Br}_2]^+$ ion) was the base ion for non-*ortho* substituted congeners. Identification of the PBDEs in soil samples was performed with the criteria of chromatographic retention time, selected characteristic ion and bromine isotope ratio.

Method detection limits obtained with the developed sample preparation procedure and with the optimized GC–MS parameters ranged from 0.008 to 0.1 ng/g (dry weight) for the targeted PBDEs when 10 g of soil were analyzed. Limits of quantitation was defined as five times of the method detection limits,

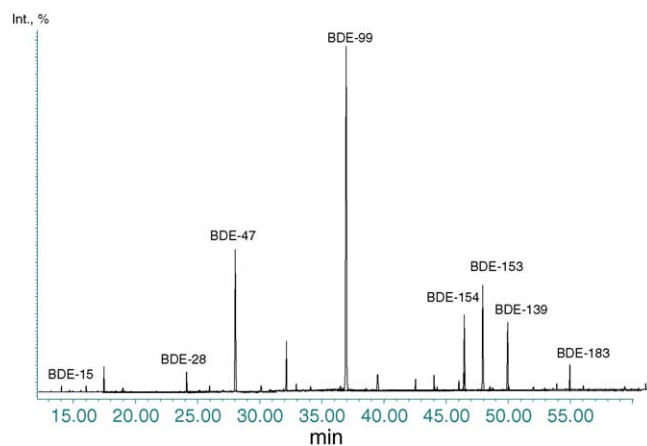


Fig. 1. Total ion chromatogram from the GC–ion trap MS analysis of the sample extract of soil 6. BDE-3 was not detected. Peaks of other PBDEs were observed, but not identified due to the unavailability of standards.

Table 2
Levels (ppb) of PBDEs detected in the soil samples (dried weight)

Congener	Blank	Soil 1	Soil 2	Soil 3	Soil 4	Soil 5	Soil 6	Soil 6-dup	Spiked soil ^a
BDE-3	nd ^b	nd	nd	nd	nd	nd	nd	nd	4.50 ± 0.19
BDE-15	nd	0.60	0.69	0.81	0.76	0.78	0.92	0.89	5.17 ± 0.40
BDE-28	nd	4.10	5.22	5.37	5.18	4.41	5.78	5.25	4.85 ± 0.31
BDE-47	nd	206	195	264	220	213	204	199	4.46 ± 0.30
BDE-99	nd	520	502	534	578	599	579	530	5.20 ± 0.43
BDE-139	nd	26.1	32.4	41.8	30.7	33.0	46.0	42.5	5.09 ± 0.21
BDE-153	nd	68.0	70.3	82.4	69.8	76.9	77.2	72.9	4.80 ± 0.16
BDE-154	nd	42.0	39.2	48.5	54.9	52.3	57.1	54.5	4.51 ± 0.38
BDE-183	nd	10.4	12.7	14.3	13.0	11.2	12.2	11.4	4.76 ± 0.11

^a Spiked levels of PBDEs were 5 ppb in soil blank matrix ($n = 3$).

^b nd = not detected.

i.e., 0.04–0.5 ng/g. The developed method was applied for the determination of PBDEs in soil sample collected from the e-waste site located in Taizhou, Zhejiang Province in China. Fig. 1 shows the total ion chromatogram obtained from the GC–ion trap MS analysis of the sample extract of the soil 6 collected from the e-waste deposit site. BDE-3 was not detected. Peaks of other PBDEs were observed, but not identified due to the unavailability of standards. Isotope dilution MS technique was applied for the PBDE quantitation. Relative response factors of the native PBDEs to the corresponding ¹³C-labeled internal standards were measured and used to quantify the PBDE levels in the samples. Only the PBDEs, whose ¹³C-labelled internal standards were available (Table 1), were quantitatively analyzed. The recoveries of the ¹³C-labeled internal standards were better 60% with relative standard deviation ranging from 8 to 26%. The developed method was applied to determine PBDEs in six soil samples collected from an e-waste recycling site. Table 2 lists the quantitative results of the detected PBDE congeners. Both individual and averaged concentrations of the PBDEs are presented for the soil samples. Because the soil samples were collected from the sampling points around the same e-wastes disposal site, the detected PBDE levels were similar with a standard deviation of less than 30%. The data indicated that the PBDEs existed in the soil samples with concentrations ranging from sub-ppb to about 600 ppb (dry weight). Mono-BDE (BDE-3) was not detected in the collected soil samples. BDE-15 (di-BDE) was detected at concentrations from 0.60 to 0.92 ppb in the soil samples. The average concentration of the tri-BDE (BDE-28) was 5.01 ppb with a standard deviation of 0.62. Other PBDE congeners detected in the soils were BDE-47, BDE-99, BDE-139, BDE-153, BDE-154, and BDE-183, whose averaged levels varied from 12.3 to 552 ppb. Tetra- (BDE-47), penta- (BDE-99) and hexa-BDE (BDE-139, BDE-153, BDE-154), were the predominant isomers and its congener pattern was similar to a commercial penta-BDE formulation [12]. Thus, the high levels of the PBDE congeners probably resulted from the commercial penta-BDE product used in the fire retardants because the soil samples were collected in the vicinity of a site for the e-wastes disposal. Uncontrolled disposal and recycling have apparently resulted in the soil contamination with the PBDEs.

The quality assurance and quality control (QA/QC) included the sample analysis of matrix blank, spiked matrix and duplicated samples (Table 2). Recovery of the ¹³C-labelled internal standards was again better than 60% for the QA/QC samples. No PBDEs were detected in the matrix blank. The variation between the duplicated samples (soil 6) was less than 10% for all targeted PBDEs. Results from the analysis of three spiked matrix blanks indicated that the method had good accuracy and precision with relative error and relative standard deviation of less than 10% ($n = 3$).

Acknowledgements

The authors would like to thank the financial support from Faculty Research Grant (FRG/01-02/II-34) of Hong Kong Baptist University and the Environment and Conservation Fund (ECF-13/2004). We would also like to acknowledge the National Distinguished Young Scholar Award from the National Science Foundation of China (#20329701) and the Support from the CAS International Partnership Project.

References

- [1] B. Strandberg, N.G. Dodder, I. Basu, R.A. Hites, *Environ. Sci. Technol.* 35 (2001) 1078.
- [2] S. Lacorte, M. Guillaumon, E. Martinez, P. Viana, D. Barcelo, *Environ. Sci. Technol.* 37 (2003) 892.
- [3] K. Hartonen, S. Bøwardt, S.B. Hawthorne, M.-L. Riekkola, *J. Chromatogr. A* 774 (1997) 229.
- [4] M. Alae, D.B. Sergeant, M.G. Ikonou, J.M. Luross, *Chemosphere* 44 (2001) 1489.
- [5] J.W. Choi, T.S. Fujimaki, K. Kitamura, S. Hashimoto, H. Ito, N. Suzuki, S. Sakai, M. Morita, *Environ. Sci. Technol.* 37 (2003) 817.
- [6] J.R. Fowles, A. Fairbrother, L. Baecher-Steppan, N.I. Kerkvliet, *Toxicology* 86 (1994) 49.
- [7] I. Meerts, J.J. van Zanden, E. Luijckx, I. van Leewen-Bol, G. Marsh, E. Jakobsson, A.A. Bergman, A. Brouwer, *Toxicol. Sci.* 56 (2000) 95.
- [8] G. Soderstrom, S. Marklund, *Environ. Sci. Technol.* 36 (2002) 1959.
- [9] D. Wang, Z. Cai, G. Jiang, A. Leung, M.H. Wong, R.W.K. Wong, *Chemosphere* 60 (2005) 810.
- [10] D. Wang, Z. Cai, G. Jiang, M.H. Wong, W.K. Wong, *Rapid Commun. Mass Spectrom.* 19 (2005) 83.
- [11] T. Hyotylainen, K. Hartonen, *Trends Anal. Chem.* 21 (2002) 13.
- [12] C. de Wit, *Chemosphere* 46 (2002) 583.

LC–MS analysis of antifouling agent Irgarol 1051 and its decyclopropylated degradation product in seawater from marinas in Hong Kong

Zongwei Cai^{a,*}, Yun Fun^a, Wai-Tang Ma^a,
Michael Hon-Wah Lam^b, James Tsui^a

^a Department of Chemistry, Hong Kong Baptist University, Hong Kong, China

^b Department of Biology and Chemistry, City University of Hong Kong, Hong Kong, China

Received 26 October 2005; received in revised form 16 January 2006; accepted 20 January 2006

Available online 28 February 2006

Abstract

A method for the trace analysis of antifouling agent Irgarol 1051 and its decyclopropylated degradation product in seawater was developed by using reversed-phase LC–MS with quadrupole time-of-flight mass spectrometry detection. Atrazine-*d*₅ was used as the internal standard for the LC–MS determination. Irgarol 1051 and the major degradation product were detected at trace levels in seawater samples collected from several marinas in Hong Kong. The water samples were pre-concentrated by solid-phase extraction with a polystyrene-divinylbenzene cartridge. Quadrupole time-of-flight tandem mass spectrometry in positive ion electrospray ionization was used for the identification and quantitation. The recoveries of Irgarol 1051 and degradation product were >85%. Method detection limits were 0.2 ng l^{−1} and 0.8 ng l^{−1} for the antifouling agent and the decyclopropylated degradation product, respectively.

© 2006 Elsevier B.V. All rights reserved.

Keywords: Irgarol 1051; Decyclopropylated degradation product; Seawater; Solid-phase extraction; LC–MS

1. Introduction

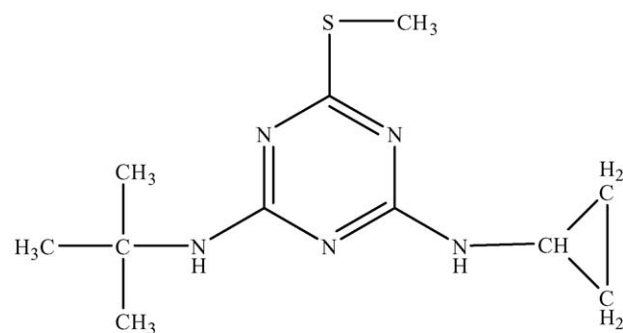
Irgarol 1051 (2-methylthio-4-tertbutylamino-6-cyclopropyl-amino-s-triazine) (Fig. 1) is a recently developed herbicide and has been used as an alternative to tributyltin biocide agent in antifouling paints [1]. This compound is used in tin-free antifouling paint formulations [2]. These paints are applied to the hulls of ships and boats to prevent the growth of bacteria, microalgae, mussels and other invertebrates. Although Irgarol 1051 is not highly toxic to fish and crustacean species, the antifouling agent has demonstrated extremely high toxicity to plant species. It has been reported that Irgarol 1051 is a potent inhibitor of photosynthesis in marine and fresh water alga [3]. It was reported that the antifouling agent could inhibit photosynthesis in corals at concentrations of 100 ng l^{−1} [3]. Earlier studies reported that chronic toxicity of Irgarol 1051 to selected algal and periphy-

ton communities was observed in the concentration range of 0.6–5.9 μg l^{−1} and 0.06–0.25 mg l^{−1}, respectively [4–6].

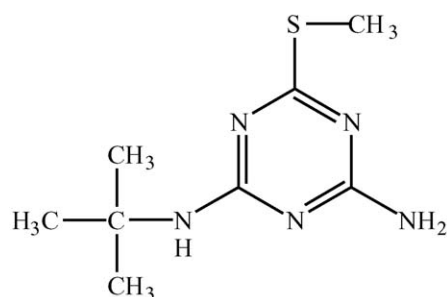
Irgarol 1051 and its major degradation product, the decyclopropylated compound (2-methylthio-4-tertbutylamino-6-amino-s-triazine) (Fig. 1) have been detected in aquatic environments [7–12]. Photodegradation of Irgarol 1051 has been proposed as the most possible mechanism for the formation of the decyclopropylated degradation product [3,7,9,13–15]. The degradation product is generally less toxic to aquatic phytoplankton but more toxic to root elongation of terrestrial plants than Irgarol 1051 [4,5]. The main pathway of Irgarol 1051 entering into the environment is its direct release from the paint surface of boats [8]. Thus, levels of the antifouling agent are high in those areas with high yachting activity and low water exchange rate [9]. In some marinas, the concentration is sufficiently high to pose a risk to aquatic life.

Irgarol 1051 has been frequently detected in seawater alone with its decyclopropylated degradation product [3,9]. Levels of Irgarol 1051 in water were reported ranging from 1 ng l^{−1} to 4000 ng l^{−1}. Recently, Irgarol 1051 was detected in a pilot

* Corresponding author. Tel.: +852 34117070; fax: +852 34117348.
E-mail address: zwcai@hkbu.edu.hk (Z. Cai).



Irgarol 1051 (m.w. 253)



Decyclopropylated degradation product (m.w. 213)

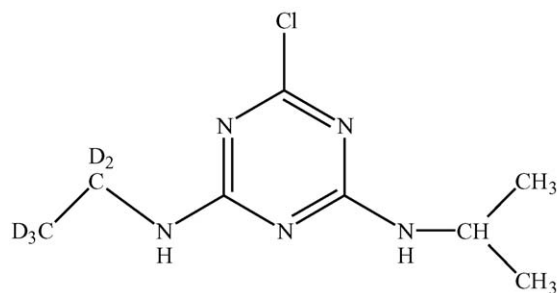
Atrazine- d_5 (m.w. 220)

Fig. 1. Structures of Irgarol 1051, its major degradation product and the internal standard atrazine- d_5 .

monitoring study carried out in the coastal Mediterranean area of Catalonia at ng l^{-1} levels [9,10]. Determination of Irgarol 1051 and its degradation products often involves sample pre-concentration and instrument analysis. Liquid–liquid extraction using dichloromethane [16] and solid-phase extraction (SPE) [10] have been reported. The polymeric stationary phase (polystyrene-divinylbenzene) is known to be more suitable for compounds with high polarity [10,17]. Several instrumental analytical methods have been developed for the detection of Irgarol 1051 and its degradation products, including gas chromatography coupled with mass spectrometry (GC–MS) [16], high performance liquid chromatography with UV (LC–UV) and mass spectrometry (LC–MS) [18,19]. However, only a few applications using LC–MS have been reported. LC coupled with MS provides capability of both chromatography detection and MS identification. The technique has been applied for structural elucidation of a wide range of molecules including environmental degradation products and metabolites [17,20–22]. This paper

describes method development for the determination of Irgarol 1051 and its decyclopropylated degradation product by using a polymeric SPE cartridge for highly efficient extraction and LC–MS detection with quadrupole time-of-flight (Q–TOF) mass spectrometry.

2. Experiment

2.1. Chemicals and reagents

The SPE cartridge with polymeric phase (polystyrene-divinyl benzene, 200 mg) was purchased from Isolute (Mid Glamorgan, UK). The internal standard atrazine- d_5 (2-chloro-4-ethylamino-6-isopropylamino-1,3,5-triazine- d_5) (Fig. 1) was obtained from Crescent Chemical Co. Inc. (Augsburg, Germany). Standards of Irgarol 1051 and its decyclopropylated degradation product were provided by Dr. Michael Lam, Department of Biology and Chemistry, City University of Hong Kong. Standard solutions containing Irgarol 1051 and the decyclopropylated degradation product with concentrations ranging from 1 ng ml^{-1} to 1000 ng ml^{-1} as well as the internal standard atrazine- d_5 at 50 ng ml^{-1} were separately prepared in methanol. HPLC-grade organic solvents acetonitrile and methanol were obtained from Acros Organics (New Jersey, USA). Ammonium acetate was from (Barcelona, Spain). Deionized water was generated from a Milli-Q system (Waters). All standard solutions were stored at 4°C until use.

2.2. Water sampling

Surface seawater samples were collected from five marina stations located in Hong Kong: Pak Sha Wan, Ma Liu Shui, Tsim Sha Tsui, Central and Aberdeen Typhoon Shelter. Five liters of the seawaters was collected in 2.5-l precleaned amber glass bottles and kept at 4°C in the dark until analysis. Prior to the SPE extraction, the water samples were filtered through a glass fiber filter ($0.45 \mu\text{m}$) in order to remove the suspended particles [23]. Each sample was analyzed in duplicate with sample volume of 500 ml and the averaged results were reported. A seawater sample was collected from a remote area (approximately 75 km south of the Hong Kong Island). After the sample was analyzed inter-day and intra-days ($n = 18$) and confirmed to contain no detectable Irgarol its decyclopropylated degradation product, it was used as a reference seawater sample for method development including recovery, accuracy and precision experiments.

2.3. Solid-phase extraction

Solid-phase extraction was conducted with reversed-phase polymeric cartridge (polystyrene-divinylbenzene) with a water flow rate of about 10 ml min^{-1} under a water vacuum pump. Recovery tests were conducted by using 100 ml and 500 ml standard water containing the two analytes at 50 ng l^{-1} and 10 ng l^{-1} , respectively. Sample volume of 500 ml was used for the SPE extraction for experiments of accuracy and precision as well as the real water sample analysis. After the sample extraction, the

cartridge was aspirated for 10 min to remove water residues. The cartridge was then eluted twice with 2 ml methanol at a flow rate of 1 ml min^{-1} , and the extracts were collected in a 10-ml glass tube. The extract was evaporated to dryness with a stream of dry nitrogen at 35°C and reconstituted with $100 \mu\text{l}$ acetonitrile containing 50 ng ml^{-1} of atrazine- d_5 as internal standard for the LC–MS analysis (Ma et al. [17]). The above same extraction procedure was applied for the recovery tests using silica-bonded C_{18} cartridges (360 mg and 1 g, Waters Corporation, Milford, USA) and one phenyl cartridge (200 mg, Alltech, Deerfield, USA).

The SPE recovery was determined by analyzing standard water samples that were prepared with both deionized water and the reference seawater. Five nanograms each of Irgarol and the decyclopropylated degradation product was fortified into 100 ml and 500 ml of the individual water, giving a fortified concentration of 50 ng l^{-1} and 10 ng l^{-1} , respectively. After the SPE extraction, 5 ng atrazine- d_5 was added to the sample extract and used as the internal standard for LC–MS analysis.

2.4. LC–MS analysis

LC–MS analysis with electrospray ionization (ESI) was performed on an Agilent HP1100 capillary HPLC system (San Francisco, USA) interfaced with a quadrupole time-of-flight mass spectrometer (Q-TOF MS) (QSTAR Pulsar i, Applied Biosystem, Canada). A reversed-phase C_{18} column (Waters Symmetry, $2.1 \text{ mm} \times 100 \text{ mm}$, $3.5 \mu\text{m}$) was used for the separation of Irgarol 1051 and its degradation product. The flow rate was $200 \mu\text{l min}^{-1}$ and the sample injection volume was $5 \mu\text{l}$ for calibrations standards and seawater sample extracts. A gradient program with mobile phase A (5 mM ammonium acetate) and B (acetonitrile) was used. The initial composition of mobile phase was 80% A for 0.5 min and then decreased within 7 min to 20% A where it was kept for 10 min. The MS parameters were optimized for the analytes. It was observed that both Irgarol 1051 and its major degradation products showed a higher response under positive ion mode of electrospray, which is similar to other triazine compounds (Ferrer and Barcelo [12]). Full-scan data over a mass range from 100 amu to 350 amu was acquired from the ESI-MS analysis. The optimized experimental parameters involved the ionspray gas temperature (400°C), ionspray voltage (5500 V), focusing potential (150 V) and declustering potential (50 V). Identification of Irgarol 1051 and its degradation product in the seawater samples was performed based on the detection of their $[M+H]^+$ ions (m/z 254.1439 for Irgarol 1051 and m/z 214.1126 for the degradation product) with accurate mass assignment and the comparison of retention times with those of the corresponding authentic standards. Quantitation was based on internal standard method, in which the $[M+H]^+$ ion peak ratios of the analytes related to atrazine- d_5 m/z 221.1330 were used.

Calibration standard solutions of Irgarol 1051 and the decyclopropylated degradation product with concentrations ranging from 10 ng ml^{-1} to 1000 ng ml^{-1} as well as the internal standard at 50 ng ml^{-1} . With the injection volume of $5 \mu\text{l}$, the on-column amount of the calibration standards ranged from 50 pg to 5000 pg for the analytes, while the injection amount of the internal stan-

dard was kept as 250 pg. The peak area ratios of the analytes to the internal standard were calculated for each calibration point. The calibration curves were used for the quantitative analyses of Irgarol 1051 and the decyclopropylated degradation product in samples for method development and in real sample extracts. Levels of the analytes detected in the seawater samples were found within the dynamic calibration range. Instrument detection limits were determined by analyzing the diluted standard solutions with lowest amounts of the analytes on-column when peaks were detected with signal-to-noise ratio better than 3. Method detection limits were calculated from the instrument detection limits by considering the volumes of original water sample and volumes of final sample extract and injection. Accuracy and precision data were achieved with double LC–MS analyses of four 500-ml standard samples of both deionized water and reference seawater containing Irgarol 1051 and the major degradation product at 10 ng l^{-1} .

3. Results and discussion

3.1. Method development

The LC–MS detection of Irgarol 1051 and its decyclopropylated degradation product was based on the criteria of chromatographic retention time and accurate mass of corresponding $[M+H]^+$ ions. Under the LC–MS conditions, the retention time of Irgarol 1051 and the decyclopropylated degradation product was $12.08 \pm 0.02 \text{ min}$ and $9.94 \pm 0.02 \text{ min}$, respectively, when the calibration standard solutions were analyzed ($n=6$). The $[M+H]^+$ ions of Irgarol 1051 at m/z 254.1427 and the degradation product at m/z 214.1116 were detected with mass accuracy of less than 10 ppm when the measured values were compared to the theoretical masses of the corresponding protonated molecular ions. The two analytes as well as the internal standard atrazine- d_5 (retention time 10.15 min) can be separated not only chromatographically but also with their different $[M+H]^+$ ions masses.

Calibration curves obtained from the analyses of standard solutions showed good linearity ($R^2 > 0.99$) for Irgarol 1051 and its decyclopropylated degradation product over the concentration range of 10–1000 ng/ml with the injection volume of $5 \mu\text{l}$. The regression equation was $y = 2.96x + 0.056$ and $y = 0.56x + 0.028$ for Irgarol 1051 and its decyclopropylated degradation product, respectively, where y is the peak area ratio of the analyte to the internal standard and x is the concentration of the analyte. The calibration standards were analyzed together with the samples for method development and real seawater samples.

Recoveries of Irgarol 1051 and its decyclopropylated degradation product were examined for solid-phase extraction (SPE) procedures using the C_{18} and polymeric cartridges. The obtained data indicated that the C_{18} and phenyl cartridges had poor recovery for both analytes ($<45\%$), while the polymeric (polystyrene-divinylbenzene) cartridge provided quantitative recoveries. The spiked samples using the deionized water gave similar recovery as those using the reference seawater, while the tests with 100 ml water (50 ng l^{-1}) generally had 5–10% better recovery

Table 1

SPE and LC–MS method development for the determination of Irgarol 1051 and its decyclopropylated degradation product in seawater

Compound	MDL ^a (ng l ⁻¹)	Deionized water				Reference seawater			
		Recovery ^b (%)		Relative error ^c (%)	R.S.D. ^d (%)	Recovery (%)		Relative error (%)	R.S.D. (%)
		100 ml	500 ml	500 ml	500 ml	100 ml	500 ml	500 ml	500 ml
Irgarol 1051	0.2	90.1 ± 2.5	91.6 ± 5.9	-13.7	8.3	93.2 ± 4.9	89.0 ± 8.9	-10.2	11.3
Degradation product	0.8	92.1 ± 2.7	90.9 ± 3.7	-9.4	7.1	90.2 ± 3.4	86.7 ± 5.7	-6.4	9.8

^a MDL, method detection limits.^b Six recovery test samples were analyzed with water volume of 100 ml (50 ng l⁻¹) and 500 ml (10 ng l⁻¹).^c Relative error was obtained from the averaged results of four standard water samples with double LC–MS analyses (*n* = 8).^d R.S.D., relative standard deviation (*n* = 8).

than those with 500 ml water (10 ng l⁻¹). Recovery for water volume lower than 100 ml was not examined because the method with lower volume of water sample might not have suitable detection limits for the real sample analysis. Although larger water volume (>500 ml) may increase the total amount of the analytes being concentrated, break through may occur during the SPE extraction, resulting in poor recovery. In contrast to the C₁₈ and phenyl cartridges that did not provide quantitative recoveries, the polymeric cartridge gave good recoveries ranging from 85% to 95% for Irgarol 1051 and its decyclopropylated degradation product in both deionized and seawater (Table 1). Thus, the SPE procedure with the polymeric cartridge was selected for the field sample analysis.

The LC–MS method appears to have better sensitivity for Irgarol 1051 than its decyclopropylated degradation product. Instrument detection limit, defined as a signal-to-noise ratio more than 3, was determined by analyzing a series of diluted standard solutions. The instrument detection limits were 5 pg and 20 pg on-column injection for Irgarol 1051 and the decyclopropylated degradation product, respectively. Assuming the analytes were quantitatively recovered during the sample preparation, the corresponding method detection limits were 200 pg l⁻¹ and 800 pg l⁻¹ (or 0.2 ng l⁻¹ and 0.8 ng l⁻¹), respectively, because 500 ml water was extracted and only 5 µl out of the final 100 µl sample extract was injected. It should be noted that the matrix effect and interference background were not taken into account for the estimation of the method detection limits. Nevertheless, the results from experiments of recover, accuracy and precision by using both deionized water and reference seawater indicated that matrix effects were not significant under the current conditions (Table 1). Increasing injection volume might potentially lower the method detection limits. Background levels from matrix, however, may be significantly increased for the LC–MS analysis because of the 5000-fold enrichment during the sample preparation. Sample enrichment is an important process for the trace analysis. SPE has been demonstrated as a promising pre-concentration technique for water analysis. However, the salt background and the relatively high polarity of the analytes posted a unique challenge on the SPE extraction and instrument analysis. Thus, application of more sensitive LC–MS technique is more preferable in order to further decrease the method detection limits. A triple quadrupole mass spectrometry with multiple reaction monitoring (MRM) mode would provide several folds

high sensitivity than Q-TOF MS. The limited duty cycle of any TOF MS analyzer for the ESI ion sources that produce continuous ion beams provides much worse quantitative detection limits than quadrupole instrument, for which the duty cycle is much more effective. Nevertheless, the current method with the available Q-TOF MS provided the needed detection limits of low ng l⁻¹ levels with satisfied method performance for the determination of Irgarol 1051 and its decyclopropylated degradation product in the marine water samples.

For the determination of method accuracy and precision, four standard water samples prepared by both deionized water and reference seawater with the concentration of Irgarol and the decyclopropylated degradation product at 10 ng l⁻¹ were extracted by the established polymeric SPE procedure and analyzed twice by LC–MS. The obtained results listed in Table 1 indicate that under the current conditions of sample preparation and LC–MS analysis, the method performance was comparable when analyzing Irgarol 1051 than its decyclopropylated degradation product in deionized water or the reference seawater. The developed SPE extraction and internal standard analytical method provided good accuracy with relative error <15%. The precision of the method given as relative standard deviation (R.S.D.) was also less than 15% (*n* = 8).

3.2. Analysis of seawater samples

Seawater samples from five marina stations in Hong Kong (Pak Sha Wan, Ma Liu Shui, Tsim Sha Tsui, Central and Aberdeen Typhoon Shelter) were analyzed in order to assess the presence of Irgarol 1051 and its degradation products. Irgarol 1051 and its decyclopropylated degradation product were identified based on criteria of the chromatographic retention time and the exact mass of $[M+H]^+$ ion (Fig. 2). Fig. 2 shows an extracted mass chromatogram for Irgarol 1051 (12.08 min), the decyclopropylated degradation product (9.97 min) and atrazine-d₅ (10.22 min) obtained from the analysis of the seawater sample collected from the station of Pak Sha Wan. The detection was further confirmed by MS–MS analyses (Fig. 3). The confirmation criteria for the positive detection of Irgarol 1051 and its decyclopropylated degradation product, therefore, included MS–MS analysis and exact mass measurement for both parent and fragment ions. Although the MS–MS spectra were quite simple, major fragment ions at *m/z* 198.0825 and *m/z* 158.0512 were

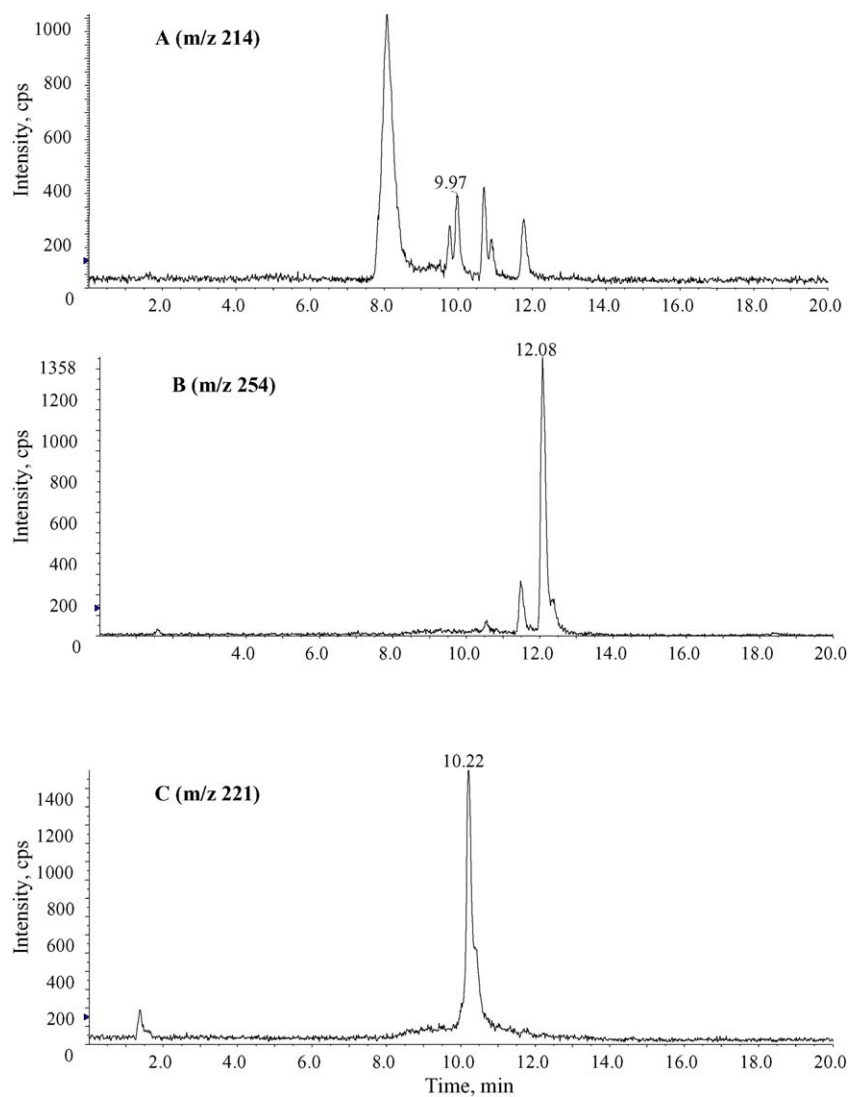


Fig. 2. Extracted ion chromatograms at m/z 214 for the decyclopropylated degradation product (A), m/z 254 (B) for Irgarol 1051 and m/z 221 for atrazine- d_5 (C) obtained from the analysis of a seawater sample taken from Pak Sha Wan. The sample injection volume was 5 μ l.

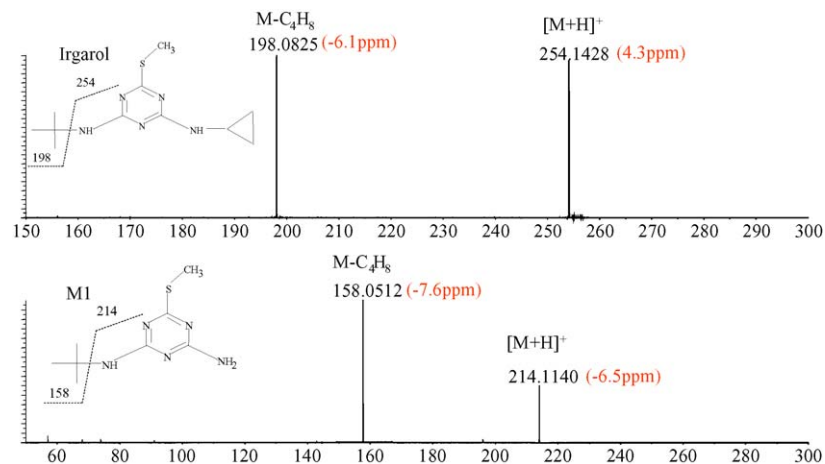


Fig. 3. MS-MS spectra of Irgarol 1051 (upper) and its decyclopropylated degradation product (lower) detected in seawater sample taken from Pak Sha Wan. The MS-MS fragmentation and exact mass measurement confirmed the detection.

Table 2

Levels of Irgarol 1051 and its decyclopropylated degradation product detected in surface seawater samples collected from five marina stations in Hong Kong

Station	Irgarol 1051 (ng l ⁻¹)	Degradation product (ng l ⁻¹)
Pak Sha Wan ^a	11.2 ± 0.5 ^b	18.6 ± 1.5
Ma Liu Shui	8.8 ± 0.2	10.1 ± 0.5
Tsim Sha Tsui	6.6 ± 0.2	7.8 ± 0.5
Central	6.5 ± 0.1	10.1 ± 0.9
Aberdeen Typhoon Shelter	5.7 ± 0.3	6.9 ± 0.6

^a The Pak Sha Wan station is a yachting marina.

^b The data were averaged from two duplicated sample analyses ($n = 4$).

detected for Irgarol 1051 and its decyclopropylated degradation product, respectively (Fig. 3). The measured exact masses of the characteristic fragment ions that were resulted from the loss of the tertbutyl moiety were detected with mass difference of less than 10 ppm, compared to their theoretical values.

Irgarol 1051 and its major degradation products were detected in all collected surface seawater samples. Their levels were determined by using the established internal standard method. The analytical results that were averaged from two duplicated sample analyses ($n = 4$) with deviation of less than 10% for all field samples are listed in Table 2. The obtained data indicated that the seawater was contaminated with trace levels of Irgarol and its decyclopropylated degradation product. The highest levels of the pollutants were detected in the samples taken at Pak Sha Wan where a yacht club is located. Other four marina stations closed to ports and cruise line terminals appeared to contain relatively lower concentrations of Irgarol and its degradation product probably because these stations are more involved with operations of larger ships. It is known that Irgarol 1051 is restricted to be used in antifouling paint for boats with length of >25 m (Konstantinou and Albanis [9]). Higher level of Irgarol 1051 was detected in the seawater samples collected in Pak Sha Wan probably because more small-size boats exist in the marina of yacht club. The obtained data also indicate that the decyclopropylated degradation product found in the collected seawater were at a higher concentrations than Irgarol 1051. This is probably due to the relatively high degradation rate of Irgarol 1051 into the decyclopropylated product in the surface seawater. Other degradation products such as possible deisopropylated and hydroxylated metabolites were not detected in the seawater samples.

4. Conclusion

Solid-phase extraction with a polymeric cartridge (polystyrene-divinylbenzene) provided quantitative recovery for extracting Irgarol 1051 and its decyclopropylated degradation product from seawater. The developed LC–MS

method with Q-TOF MS detection in positive ion electrospray ionization can be applied to determine the antifouling agent and the degradation product in water at low ng l⁻¹ levels with good accuracy and precision. The analytical method has been successfully used to analyze Irgarol 1051 and the decyclopropylated degradation product in surface seawater samples collected from five marina stations in Hong Kong.

Acknowledgement

This work was supported by earmarked grants (HKBU2017/02P) obtained from RGC, University Grants Committee of Hong Kong.

References

- [1] K.V. Thomas, J. Chromatogr. A 825 (1998) 29–35.
- [2] I. Ferrer, D. Barcelo, J. Chromatogr. A 854 (1999) 197–206.
- [3] H. Okamura, T. Watanabe, I. Aoyama, M. Hasobe, Chemosphere 46 (2002) 945–951.
- [4] H. Okamura, T. Aoyama, T. Takami, T. Maruyama, Y. Suzuki, M. Matsumotos, I. Katsuyama, J. Hamada, T. Beppu, O. Tanaka, R.J. Maguire, D. Liu, Y.L. Lau, G.J. Pacepavicius, Mar. Pollut. Bull. 40 (2000) 754–763.
- [5] B. Dahl, H. Blanck, Mar. Pollut. Bull. 32 (1996) 342–350.
- [6] H. Okamura, I. Aoyama, D. Liu, R.J. Maguire, G.J. Pacepavicius, Y.L. Lau, Water Res. 34 (2000) 3523–3530.
- [7] G. Gatidou, A. Kotrikla, N.S. Thomaidis, T.D. Lekkas, Anal. Chim. Acta 505 (2004) 153–159.
- [8] K.V. Thomas, M. McHugh, M. Waldock, Sci. Total Environ. 2939 (2002) 117–127.
- [9] I.K. Konstantinou, T.A. Albanis, Rev. Environ. Int. 30 (2004) 235–248.
- [10] I. Ferrer, D. Barcelo, J. Chromatogr. A 926 (2001) 221–228.
- [11] I. Ferrer, B. Ballesteros, Environ. Sci. Technol. 31 (1997) 3530–3535.
- [12] I. Ferrer, D. Barcelo, Analysis 26 (1998) 118–122.
- [13] D. Liu, R.J. Maguire, Y.L. Lau, G.J. Pacepavicius, H. Okamura, I. Aoyama, Water Res. 31 (1997) 2363–2369.
- [14] V.A. Sakkas, D.A. Lambropoulou, T.A. Albanis, J. Photochem. Photobiol. A Chem. 147 (2002) 135–141.
- [15] G.A. Penuela, I. Ferrer, D. Barcelo, J. Environ. Anal. Chem. 78 (2000) 25–40.
- [16] M.A. Gough, J. Fothergill, J.D. Hendrie, Mar. Pollut. Bull. 28 (1994) 613–620.
- [17] W.T. Ma, K. Steinbach, Z. Cai, Anal. Bioanal. Chem. 378 (2004) 1828–1835.
- [18] H. Okamura, I. Aoyama, D. Liu, J. Maguire, G.J. Pacepavicius, Y.L. Lau, J. Environ. Sci. Health B 34 (1999) 225–238.
- [19] K. Martinez, I. Ferrer, D. Barcelo, J. Chromatogr. A 879 (2000) 27–37.
- [20] Z. Cai, T. Qian, R.N.S. Wong, Z.H. Jiang, Anal. Chim. Acta 492 (2003) 283–293.
- [21] T. Qian, Z. Cai, R.N.S. Wong, N.K. Mak, Z.H. Jiang, J. Chromatogr. B 816 (2005) 223–232.
- [22] K.H. Lam, M.H.W. Lam, P.K.S. Lam, T. Qian, Z. Cai, H. Yu, R.Y.H. Chenug, Mar. Pollut. Bull. 49 (2004) 356–367.
- [23] W.T. Ma, Z. Cai, G.B. Jiang, Rapid Commun. Mass Spectrom. 17 (2003) 2707–2712.

Optical biosensor for the determination of BOD in seawater

Yaqi Jiang^a, Lai-Long Xiao^a, Li Zhao^a, Xi Chen^{a,b,*},
Xiaoru Wang^a, Kwok-Yin Wong^c

^a Department of Chemistry and Key Laboratory of Analytical Sciences of the Ministry of Education,
College of Chemistry and Chemical Engineering, Xiamen University, Xiamen 361005, China

^b State Key Laboratory of Marine Environmental Science, Xiamen University, Xiamen 361005, China

^c The Hong Kong Polytechnic University, Hunghom, Kowloon, Hong Kong, China

Received 25 October 2005; received in revised form 24 November 2005; accepted 26 November 2005

Available online 14 February 2006

Abstract

An automatic sensing system was developed using an optical BOD sensing film. The sensing film consists of an organically modified silicate (ORMOSIL) film embedded with an oxygen-sensitive Ru complex. A multi-microorganisms immobilization method was developed for the BOD sensing film preparation. Three different kinds of microorganisms, *Bacillus licheniformis*, *Dietzia maris* and *Marinobacter marinus* from seawater, were immobilized on a polyvinyl alcohol ORMOSILs. After preconditioning, the BOD biosensor could steadily perform well up to 10 months. The linear fluctuant coefficients (R^2) in the range of 0.3–40 mg L⁻¹ was 0.985 when a glucose/glutamate BOD standard was applied. The reproducible response for the BOD sensing film could be obtained within $\pm 2.3\%$ of the mean value in a series of 10 samples in 5.0 mg L⁻¹ BOD standard GGA solution. The effects of temperature, pH and sodium chloride concentration on the two microbial films were studied as well. The BOD sensing system was tested and applied for the BOD determination of seawater.

© 2006 Elsevier B.V. All rights reserved.

Keywords: Optical BOD biosensor; ORMOSILs; Seawater

1. Introduction

Since the progressive environmental pollution problems over the world, the need for environmental monitoring and pollution control is greater than ever. The rapid, easy-to-operate, low cost determination methods, which can operate on line (even in situ) will be highlighted. In the measurement of biodegradable organic compounds and pollutants of surface and seawater, the biochemical oxygen demand (BOD) is one of the most important and widely used parameter. Generally, the authorized BOD₅ method, which is defined as the biochemical oxygen demand of waste samples measured over 5 days at 20 °C, must last 5 days under specified standard incubation and skill of the operator to get reproducible results, is not suitable for in situ determination [1,2]. Numerous BOD biosensors [3–15] have been developed since Karube et al. [10] firstly reported a BOD biosensor based on Clark dissolved oxygen electrode immobi-

lized microorganisms in 1977. Up to now, most of the BOD biosensors are still based on the immobilization of a microbial layer on an amperometric oxygen electrode [3–10]. However, they still remain some limitations such as (a) the depletion of oxygen occurring during BOD measurement using a sensor based on the Clark electrode and (b) the microorganisms immobilized in current BOD sensors are not able to be applied in the samples containing a higher concentration of salt such as seawater. During the past decade, some considerations are focused on fiber optical chemical sensors for the determination of oxygen due to rapid performance, no oxygen consumption and less toxicity [11–15]. Although most of the BOD sensors previously reported have been designed for long-term use, and even commercialized, it seems that the performance of these sensors is still not satisfactory for the on-line environmental monitoring of seawater since the rapid and highly steady measurement of BOD is necessary in the marine environment.

In our laboratory, effort has been made to develop optical BOD sensors based on the luminescence quenching of Ru complexes immobilized in the sensing film. Organically modified

* Corresponding author. Tel.: +86 592 2184530.
E-mail address: xichen@xmu.edu.cn (X. Chen).

silicates (ORMOSILs)–PVA was used as a matrix to immobilize different kinds of seawater bacteria and domestic bacilli. The microbial film was laid over an oxygen film and the complex film was placed into a sample cell for BOD measurement [15]. In the present study, the response characteristics of a novel immobilized microbial membrane based on ORMOSILs–PVA were examined. The response time, reproducibility, linear range and the effects of temperature, pH and the sodium chloride concentration in the sample were evaluated. Furthermore, an automatic optical BOD sensing system was setup to develop a biosensor for rapid and stable in situ determination of the BOD in seawater.

2. Experimental

2.1. Apparatus

An automatic optochemical BOD sensing system was employed for acquiring the changes of fluorescence intensity. The system consociates some function parts as: (1) sampling part, including sampling peristaltic pump and valves for sample distribution; (2) controlling part, including a industrial manipulative computer and software; (3) measurement part, including a sensing detection cell and constant temperature controller; (4) light to current conversion part, including an optical fiber and a PMT. The sensing film was placed in the middle of the detection cell when temperature was kept constant by a temperature controller with a precision of $\pm 0.2^\circ\text{C}$. An excitation light with the wavelength of 495 nm from a blue LED was directed onto the sensing layer at an angle of, typically, 45° . The emission fluorescence was filtrated by a cut-off filter with a half bandwidth of 10 nm at 580 nm, and transferred by an optical fiber to detection unit equipped with a R928 PMT (Hamamatsu, Japan).

The experimental results were then processed by the software installed in the BOD system.

2.2. Chemicals and BOD standard solution

The oxygen-sensing indicator, $[\text{Ru}(\text{Ph}_2\text{phen})_3](\text{ClO}_4)_2$ (Ph_2phen = 4,7-diphenyl-1,10-phenanthroline), was synthesized and purified in the laboratory of Department of Applied Biology and Chemical Technology, Hong Kong Polytechnic University. Dimethyldimethoxysilane (DiMe-DMOS) was obtained from Fluka AG (Buchs, Switzerland). Tetramethoxysilane (TMOS) and poly(vinyl acetate) (PVA) were purchased from Aldrich (Milwaukee, WI, USA). A PVA–ORMOSILs material containing 8% (w/w) PVA solution and 1:1.2 TMOS:DiMe-DMOS (v/v), was prepared for the multi-microorganisms immobilization. The buffer solution $0.067 \text{ mol L}^{-1} \text{ KH}_2\text{PO}_4\text{--Na}_2\text{HPO}_4$ buffer (pH 7.4) was selected for BOD measurements. The standard BOD solution was prepared by adding 0.0750 g glucose and 0.0750 g L^{-1} glutamic acid (GGA) into 100 mL phosphate buffer solution (pH 7.4), and used as the standard BOD solution ($1000 \pm 185 \text{ mg L}^{-1}$) [16]. The seawater samples were taken from the area around Xiamen University and filtrated by $10 \mu\text{m}$ isopore membrane filters (Millipore, USA) before determination. All other chemicals were of analytical grade and the distilled water was used throughout.

2.3. Microorganisms

Three microorganisms, *B. licheniformis*, *D. maris* and *M. marinus*, were selected and applied for BOD sensing film. *D. maris* and *M. marinus* were selected and obtained directly from seawater of Yantai, north of China. *B. licheniformis* was obtained from freshwater and cultured in seawater (Fig. 1).

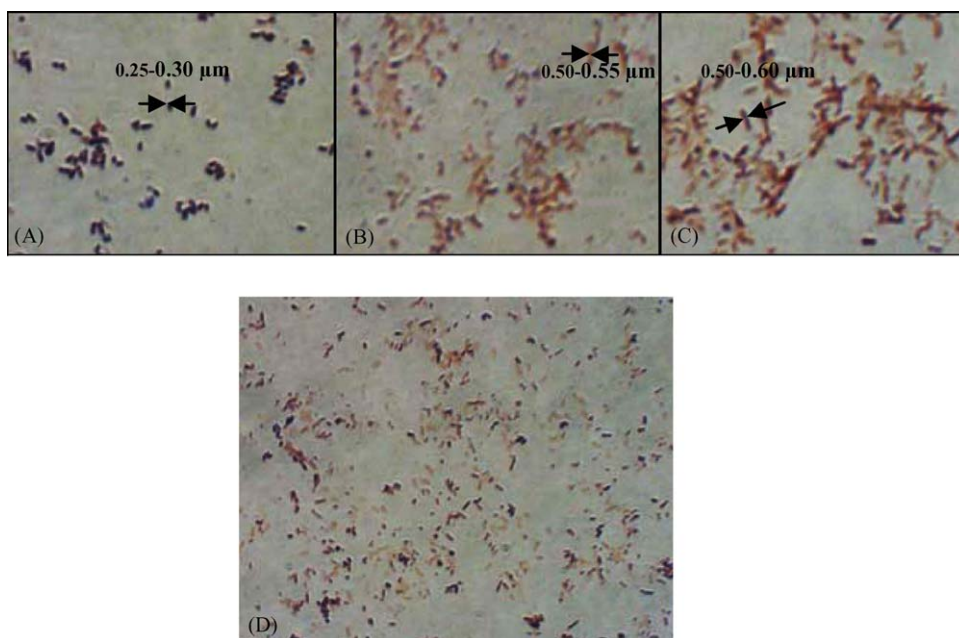


Fig. 1. Microscope pictures of the microorganisms for BOD application. (A) *Marinobacter marinus*, (B) *Dietzia maris*, (C) *Bacillus licheniformis* and (D) multi-microorganisms (amplificatory times: 3000).

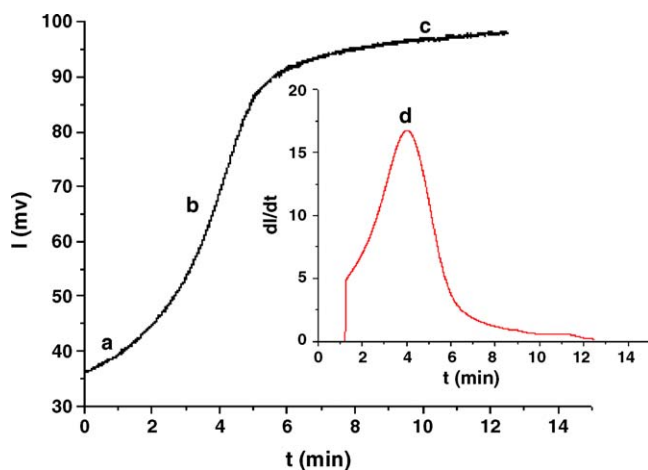


Fig. 2. Typical response of the BOD sensor when exposed to a standard BOD solution. Experimental conditions: constant temperature, 35 °C; pH of buffer, 7.4; concentration of NaCl, 3.2%; concentration of BOD, 5 mg L⁻¹. Film immobilized with sieved bacteria from seawater was used.

2.4. BOD sensing film preparation

In the preparation of oxygen sensing film, a detail description was presented in the reference [15]. ORMOSILs were prepared by mixing TMOS, DiMe-DMOS and 0.01 mol L⁻¹ HCL (1:1.2:1.5 v/v/v) for the microorganisms immobilization. The precursors were stirred at 60 °C for 1 h. 200 µL of microorganisms (*B. licheniformis*:*D. maris*:*M. marinus*, 1:2:1 w/w/w) in solution was mixed with 200 µL 8% (w/w) PVA and 200 µL ORMOSILs. After the mixture of sol was spread onto an optical oxygen-sensing film produced. The measurement signal is reproducible within a mean value of $\pm 12\%$ in a series of 10 pieces of BOD sensing film in 10 mg L⁻¹ BOD standard GGA solution.

2.5. Experimental procedure

The BOD sensing film was inserted into a black and airtight detection cell in which sample solutions were kept motionless in all measurements. The temperature of the detection cell was maintained at 35 °C. When the temperature of the sample solution (20 mL) reached at 35 °C, the detection cell was overturned by the manipulate program, and the solution was added into the detection cell. The output of the sensing film increased gradually and then reached a steady state after a few minutes. The typical response is presented in Fig. 2. Experiment results showed that there was a linear relationship between the maximal changing rate of fluorescence intensity (dI/dt) and the BOD value.

3. Results and discussion

3.1. BOD measurement mode

In the BOD measurement, the immobilized microorganisms have the processes of endogenous and active respiration. A typ-

ical optical response of the BOD sensing film was presented in Fig. 2. As shown in Fig. 2a, the initial steady-state output of the sensor represented the endogenous respiration state of the immobilized microorganisms. When the sample solution was added into the cell, the consumption of the dissolved oxygen surrounding the microbial film started and the output of the sensor increased gradually accordingly (Fig. 2b). After a while, the microorganisms stepped into an active respiration state, decomposing various organic substances, leading to the rapid consumption of the oxygen surrounding the microbial film and resulting in the prompt increase of the output of the fluorescence intensity. When the balance of the consuming and diffusion rates of oxygen on the microbial film appeared, the immobilized microorganisms put up the steady endogenous respiration state again and the output came into a steady state by degrees (Fig. 2c).

There are two measuring techniques available for the above BOD sensing response, the steady-state method (SSM) and the initial-rate (DTM) [17,18]. In SSM, a steady-state current or fluorescent intensity could be obtained at the beginning representing equilibrium between the oxygen diffusion and the endogenous respiration rate of the immobilized bacteria. The current or fluorescent intensity difference (ΔI) between the two steady states corresponded to the BOD value of the sample. The response time was around 9 min followed by 20 min recovery time. In the DTM, the rate of change of the current or fluorescent intensity (dI/dt), which reflects acceleration of the bacterial respiration rate, was used for estimating the BOD value of samples to a certain extent. This method normally provided a 4 min response time followed by a recovery time less than 10 min for BOD measurement. The experiment results showed that there was a linear relationship between the maximal mutative velocity of fluorescence intensity (dI/dt) and BOD values (Fig. 2b).

3.2. PVA–ORMOSILs material for microorganism's immobilization

PVA is a kind of non-toxic and hydrophilic materials and is capable of maintaining the maximum microbial activity. In the study, PVA has been applied to immobilize microbial cells for BOD biosensing films. In Fig. 3, PVA/ORMOSILs is evenly spread in the network shape on an oxygen ORMOSILs film. A crosslinking of DiMe-DOMS and TMOS are considered to be dispersed homogeneously in the PVA matrix through hydrogen bonds [19]. The content of PVA has an obvious effect on the physical characteristics of the microorganism film. The increase of the DiMe-DMOS concentration can enhance the response and the flexibility of the microbial sensing layer. However, the further improved hydrophobicity cannot guarantee enough solubility for PVA in the ORMOSILs matrix and then lengthen the response time. Under our preparation conditions, the optimized volume ratio of DiMe-DMOS to TMOS was 1.2 to 1 (v/v). Furthermore, a concentration of 8% PVA in ORMOSILs was selected since the percentage of PVA arrives at 10% (PVA/ORMOSILs v/v), the film begins to dilate and flake away from oxygen film.

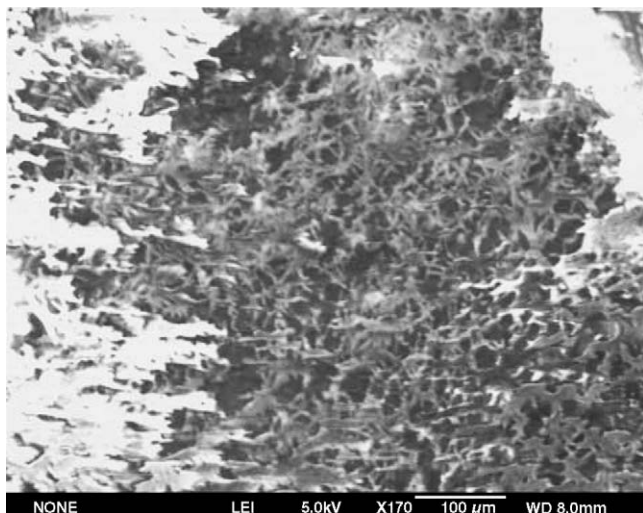


Fig. 3. FE-SEM images of an PVA/OROSILs on oxygen sensing film.

3.3. Effect of temperature, pH and co-exciting substances

The suitable temperature is found to be around 35 °C. As shown in Fig. 4, although the response intensity increased rapidly and the response time shortened sharply till 50 °C, the lifetime of the BOD sensing film was shortened since the microorganism became inactive easily at a higher temperature and the reduction of oxygen concentration in the solution. As a result, in order to prolong the lifetime of the bacteria, a temperature of 35 °C was selected in studying the films of sieved bacteria from seawater.

As the pH of seawater is around 7–8, the influences of pH on BOD response were investigated from pH 6.0 to 8.5. The fluorescent response increases until pH 7 and remains constant above that. Since the mobilized microorganisms are cultured or sieved by seawater, they present high assimilation efficiency to BOD and adapt the application to seawater. Therefore, the BOD

sensor can be employed to detect the BOD value of different seawater samples. In subsequent experiments, the pH of samples was adjusted to 7.9 using phosphate buffer.

In the application of BOD measurement in seawater, chloride ion is the most common component of seawater with an average concentration of 3.2%. Generally, chloride concentration greatly affects the activity of microorganisms. Most biosensors immobilized with limnetic microorganisms are not suitable for seawater application since the response intensity decreases sharply with the increase of chloride ion concentration. In our study, the response intensity only decreased by 15% when the concentration of chloride ion was higher than 4%. The result indicated that the BOD sensor is able to tolerate the inhibition effect of high salt concentrations in seawater on microorganism respiration.

The effect of coexisting compounds is another essential factor for BOD sensing film. The experiments were performed to test the effects of most metal ions at a concentration of 1 mg L⁻¹ on the fluorescent intensities in 5 mg L⁻¹ GGA solution. The experimental results showed that except silver and lead cations, the prepared BOD sensing films were almost independent to those ions owing to their high hydrophobic surface.

3.4. Effect of different cell concentrations of the microbial layer

A higher cell density in a microbial layer can be applied to achieve a better signal response even for very low BOD. However, as shown in Fig. 5, it is obvious that sensing film containing higher cell concentration is more sensitive but has a smaller dynamic range and a longer response time when the volume of multiple microorganisms is beyond 200 μL (44 mg L⁻¹ for each microorganism, 1:2:1 w/w/w). It is due to the higher oxygen consumption by the cells through the endogenous respiration [20].

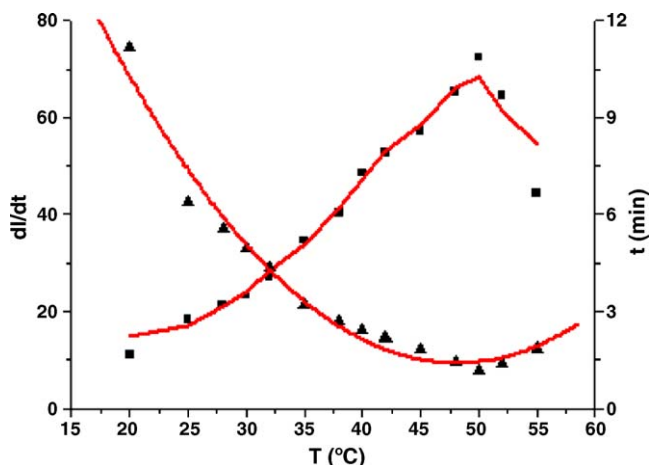


Fig. 4. Effect of temperature on the sensor response. Experimental conditions: constant temperature, 35 °C; pH of buffer, 7.9; GGA concentration, 10 mg L⁻¹; concentration of NaCl, 3.2%. (▲) Effect of temperature on the sensor response time; (■) effect of temperature on the change of velocity of the fluorescence intensity (dl/dt).

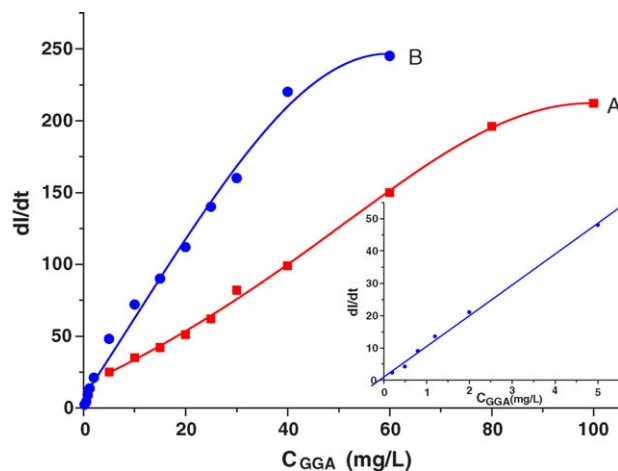


Fig. 5. Linear responses of BOD sensing films to different concentration microorganisms immobilization. Film immobilized with microorganisms solution, 0.1 mL (A) and 0.2 mL (B). Experimental conditions: constant temperature, 35 °C; pH of buffer, 7.9; concentration of NaCl, 3.2%; inset: linearity of (B) at low BOD concentration.

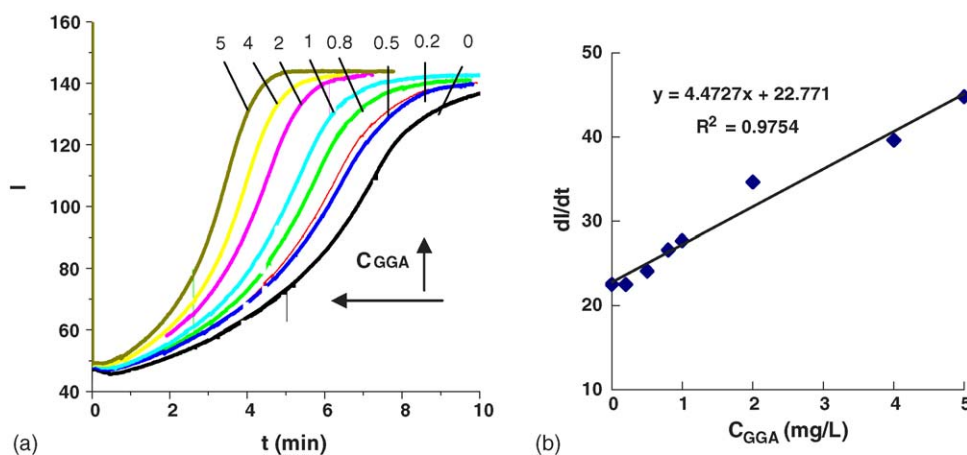


Fig. 6. Response curve (a) and response linearity (b) of co-immobilized sensing film from 0 to 5 mg L⁻¹ GGA solution BOD value increased: (1) 0 mg L⁻¹, (2) 0.2 mg L⁻¹, (3) 0.5 mg L⁻¹, (4) 0.8 mg L⁻¹, (5) 1 mg L⁻¹, (6) 2 mg L⁻¹, (7) 4 mg L⁻¹ and (8) 5 mg L⁻¹. Conditions: T , 35 °C; pH, 7.8; NaCl, 3.2%.

3.5. Characters of BOD sensing film

In the experiment, the fluorescent intensity from BOD sensing film was increased with solutions containing higher concentration of GGA. A linear relationship between BOD standard GGA concentration and change of velocity of the fluorescence intensity (dI/dt) was observed in the range of 0.2–40 mg L⁻¹ GGA solution. The detection limit of the sensor is 0.1 mg L⁻¹. As shown in Fig. 6, a typical response time for 5 mg L⁻¹ BOD standard GGA solution is about 3.2 min.

In the BOD sensing application, the films generally needed reactivation before used. The stability of the sensors was determined after they had been immersed in the GGA solution (BOD of 100 mg L⁻¹) at pH 7.9 and 35 °C. After 1 month's storage, the initial fluorescence response of the films decreased by 10% compared with the newly made films, but the response to BOD remained the same if the sensing film was reactivated well. Experimental result demonstrated that the BOD sensing films could be stored up to 10 months without significant deterioration. However, the films had to be reactivated for 1 day in GGA solutions (BOD of 100 mg L⁻¹) before use, in order to achieve the best sensitivity, stability and reproducibility.

3.6. Application for BOD determination of seawater

The automatic BOD system was set on a ship for pollution investigation of seawater. The system could be controlled by an individual industrial manipulative computer that installed in the system or a main computer system on the ship by an S-232 mode as well (Fig. 7). The processes including the reactivation of BOD sensing film, the calibration of the linearity of dI/dt and BOD concentration, keeping a constant temperature, sampling and the determination data transportation to the main controlling computer, could be performed automatically. Seawater samples from different sampling places were pumped into a tank on the ship, and then flowed through a membrane filter with a pore size of 50 μ m. Before testing, a 20 mL water sample was stored and pre-heated in the measurement cell. The cell turned down to begin the measurement as soon as the temperature reached 35 °C. The BOD detection results have been compared with those of the Chinese Standard Process for BOD₅ (GB 7488-87), and are listed in Tables 1 and 2.

From the determination results of BOD, it could be found that the sample pH value almost kept at 7.9. There are obvious differences of BOD concentration between cleaning seawater area such as swimming place and the living area around Xiamen

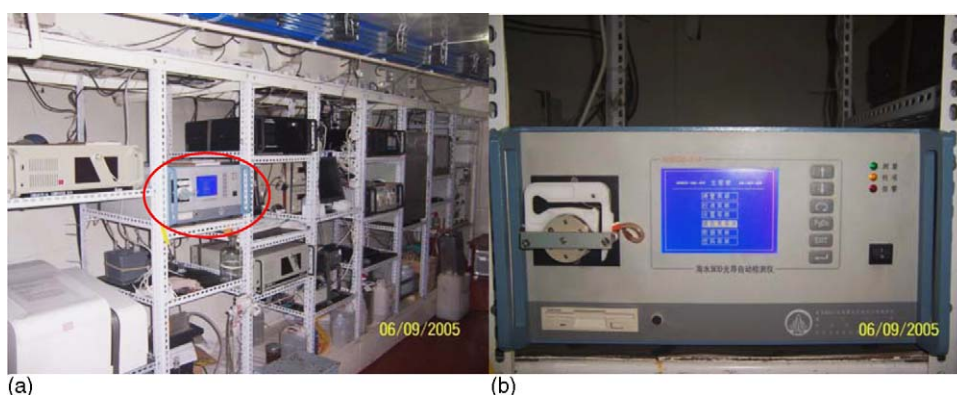


Fig. 7. Automatic BOD system for seawater pollution investigation. (a) BOD system was set on the investigation ship; (b) view of BOD system.

Table 1

BOD determination results from a living area around Xiamen University (118°05'53.0" E, 24°26'05.0" N; $n=6$)

Date	Sample	Testing result (mg L ⁻¹)	GB BOD ₅ (mg L ⁻¹)	pH
2004/3/11	Tide seawater	3.82 ± 0.09	3.5 ± 0.2	7.90
	Refulgent seawater	4.33 ± 0.17	4.5 ± 0.4	
2004/3/24	Tide seawater	3.68 ± 0.19	3.6 ± 0.2	7.88
	Refulgent seawater	4.68 ± 0.11	4.2 ± 0.3	
2004/4/12	Tide seawater	2.76 ± 0.09	2.9 ± 0.3	7.90
	Refulgent seawater	4.79 ± 0.09	5.3 ± 0.4	
2004/5/13	Tide seawater	3.67 ± 0.08	3.8 ± 0.3	7.92
	Refulgent seawater	4.32 ± 0.16	4.5 ± 0.4	
2004/5/18	Tide seawater	3.16 ± 0.07	3.0 ± 0.4	7.87
	Refulgent seawater	4.23 ± 0.10	4.3 ± 0.4	
2004/5/28	Tide seawater	3.22 ± 0.16	3.5 ± 0.4	7.90
	Refulgent seawater	4.10 ± 0.06	3.9 ± 0.2	
2004/6/12	Tide seawater	3.16 ± 0.10	3.0 ± 0.4	7.91
	Refulgent seawater	2.44 ± 0.13	2.5 ± 0.2	
2004/9/14	Tide seawater	2.57 ± 0.11	2.8 ± 0.2	7.90
	Refulgent seawater	3.83 ± 0.04	3.7 ± 0.4	

Table 2

BOD determination results from a swimming site around Xiamen University (118°06'32.1" E, 24°25'53.4" N; $n=6$)

Date	Sample	Testing result (mg L ⁻¹)	GB BOD ₅ (mg L ⁻¹)	pH
2004/3/11	Tide seawater	2.12 ± 0.15	2.0 ± 0.2	7.90
	Refulgent seawater	3.48 ± 0.16	3.2 ± 0.2	
2004/3/24	Tide seawater	2.34 ± 0.09	2.1 ± 0.2	7.87
	Refulgent seawater	3.68 ± 0.09	3.3 ± 0.3	
2004/4/12	Tide seawater	2.09 ± 0.17	2.3 ± 0.2	7.89
	Refulgent seawater	3.26 ± 0.12	3.0 ± 0.2	

University. The results indicated that some organic pollutants were let from residential area. Moreover, the BOD concentration of refulgent seawater became higher than that of tide seawater, further confirmed that the increase of the BOD value was caused by the wastewater from the living area.

4. Conclusions

An automatic BOD system with a novel optical BOD sensing film immobilizing multi-microorganisms was successfully applied for the BOD determination of seawater. Some factors such as measurement temperature, pH, co-existing substance, sodium chloride, which affected the BOD determination, were studied. The minimum measurable BOD by this system was 0.1 mg L⁻¹, and the response time was only 3.2 min for 5 mg L⁻¹ BOD. The study results showed that the BOD system exhibits its advantages in the determination of low BOD, and is suitable to evaluate the complicated seawater samples without being dramatically affected by sodium chloride and other ions. The determination results obtained from actual seawater demonstrate a good correlation with those obtained from conventional BOD₅ analysis.

Since the rapid and on-line monitoring of BOD is of major concern when surveying water pollution, the new technologies using optical fiber will lead to improved BOD sensors. For a BOD system's commercial viability, the robustness, simplicity, rapidity and cost considerations of the BOD system are other challenging areas of research.

Acknowledgements

This research work was financially supported by the Natural Scientific Foundation of Fujian (D0410001) and the Science and Technology Project of Fujian Province (2003Y005-5, 2005I-030), which are gratefully acknowledged.

References

- [1] APHA, American Public Health Association Standard methods, 17th ed., American Public Health Association, Washington, DC, 1989.
- [2] Japanese Industrial Standards Committee, JISK 0102, Japanese Standards Association, Tokyo, 1989.
- [3] C. Preininger, I. Klimant, O.S. Wolfbeis, Anal. Chem. 66 (1994) 1841.
- [4] G.J. Chee, Y. Nomura, I. Karube, Anal. Chim. Acta 379 (1999) 185.
- [5] K. Riedel, R. Renneberg, M. Kuhn, F. Scheller, Appl. Microbiol. Biotechnol. 28 (1988) 316.
- [6] Y. Sakai, N. Abe, S. Takeuchi, F. Takahashi, J. Ferment. Bioeng. 80 (1995) 300.
- [7] S.B. Jonnalagadda, S. Nadupalli, Talanta 64 (2003) 18.
- [8] K. Catterall, K. Morris, C. Gladman, H.J. Zhao, N. Pasco, R. John, Talanta 55 (2001) 1187.
- [9] D.D. Chen, Y.B. Cao, B.H. Liu, J.L. Kong, Anal. Bioanal. Chem. 372 (2002) 737.
- [10] I. Karube, T. Matsunaga, S. Mitsuda, S. Suzuki, Biotechnol. Bioeng. 19 (1977) 1535.
- [11] C. Preininger, I. Klimant, O.S. Wolfbeis, Anal. Chem. 66 (1994) 1841.
- [12] X.M. Li, F.C. Ruan, W.Y. Ng, K.Y. Wong, Sens. Actuators B 21 (1994) 143.
- [13] G.J. Chee, Y. Nomura, K. Ikebuburo, I. Karube, Biosens. Bioelectron. 15 (2000) 371.

- [14] I. Klimant, O.S. Wolfbeis, *Anal. Chem.* 67 (1995) 3160.
- [15] Y.J. Dai, L. Lin, P.W. Li, X. Chen, X.R. Wang, K.Y. Wong, *Int. J. Environ. Anal. Chem.* 84 (2004) 607.
- [16] Japanese Industrial Standards Committee, JISK 3602, Japanese Standards Association, Tokyo, 1990.
- [17] Z. Yang, H. Suzuki, S. Sasaki, S. McNiven, I. Karube, *Sens. Actuators B* 45 (1997) 217.
- [18] J. Liu, B. Mattiasson, *Water Res.* 36 (2002) 3786.
- [19] H. Schmidt, *J. Non-cyst. Solids* 112 (1989) 418.
- [20] I. Klimant, O.S. Wolfbeis, *Anal. Chem.* 67 (1995) 3160.

Electrochemiluminescent behaviors of alkaloids and tris(2,2'-bipyridine) ruthenium in organically modified silicate film

Li Zhao^a, Ying Tao^a, Xiaoqing Yang^b, Liyan Zhang^c, Munetaka Oyama^d, Xi Chen^{a,*}

^a Department of Chemistry and Key Laboratory of Analytical Sciences of the Ministry of Education, College of Chemistry and Chemical Engineering, Xiamen University, Xiamen 361005, China

^b College of Foreign Languages and Cultures, Xiamen University, Xiamen 361005, China

^c Department of Chemical and Material Engineering, Longyan College, Longyan 364000 Fujian, China

^d Division of Creative Research, International Innovation Center, Kyoto University, Sakyo-ku, Kyoto 606-8501, Japan

Received 25 October 2005; received in revised form 22 November 2005; accepted 24 November 2005

Available online 18 January 2006

Abstract

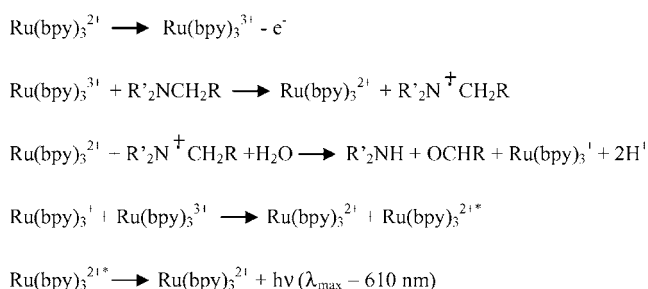
Electrogenerated chemiluminescences (ECLs) of alkaloids, such as berberine, trigonelline, allantoin and betaine, were studied in an aqueous alkaline buffer solution (pH 9.5), based on tris(2,2'-bipyridine)ruthenium(II) [Ru(bpy)₃²⁺] immobilized in organically modified silicates (ORMOSILs) film on a glassy carbon electrode (GCE). The immobilized Ru(bpy)₃²⁺ showed good electrochemical and photochemical activities. In a flow system, the eluted alkaloids were oxidized on the modified GCE, and reacted with immobilized Ru(bpy)₃²⁺ at the potential of +1.50 V (versus Ag/AgCl). The luminescence with λ_{max} 610 nm was caused by a reaction of electrolytically formed Ru(bpy)₃³⁺ with an oxidized amine group to generate Ru(bpy)₃²⁺*. The determination limit was 5 × 10⁻⁶ mol L⁻¹, 8 × 10⁻⁶ mol L⁻¹, 2.0 × 10⁻⁵ mol L⁻¹ and 5.0 × 10⁻⁵ mol L⁻¹ for berberine, trigonelline, allantoin and betaine at S/N 3, respectively. In addition, the factors affecting the determination of the four alkaloids were also studied.

© 2005 Elsevier B.V. All rights reserved.

Keywords: Electrogenerated chemiluminescence; Alkaloids; Tris(2,2'-bipyridine) ruthenium; ORMOSILs; Chinese medicines

1. Introduction

The electrogenerated chemiluminescence (ECL) method using tris(2,2'-bipyridine) ruthenium(II) [Ru(bpy)₃²⁺] and amine-containing compounds has received considerable attention during the past decade due to its low detection limit and wide linear working range with relatively simplified optical setup [1–6]. Generally, the amino group present in amine produces a secondary amine following by a dealkylation process in the presence of water. The intermediates of neutral amine radical have sufficient energy to react with Ru(bpy)₃²⁺ or Ru(bpy)₃³⁺ to yield excited state Ru(bpy)₃²⁺* and hence to produce light emission. The reaction processes are as follows [1]:



Scheme 1. ECL reaction processes of amine and Ru(bpy)₃²⁺.

While Ru(bpy)₃²⁺ ECL as a detection is of advantage in some applications, Ru(bpy)₃²⁺ is required to be delivered into the reaction cell continuously, which causes the reagent expense and Ru(bpy)₃²⁺ waste in operation. Large amounts of Ru(bpy)₃²⁺ are required when solution phase ECL is used for routine HPLC or FIA analysis. An approach by immobilizing Ru(bpy)₃²⁺ at an electrode arises to minimize the amount of Ru(bpy)₃²⁺ expended. In the immobilization of Ru(bpy)₃²⁺, several methods

* Corresponding author. Tel.: +86 592 2184530; fax: +86 592 2184530.
E-mail address: xichen@xmu.edu.cn (X. Chen).

have been reported including Langmuir–Blodgett [7,8], self-assembled techniques [9,10], Nafion films [11,12] and sol–gel [13–15] techniques. Compared with the ordinary sol–gel material, organically modified silicates (ORMOSILs) are more attractive in the incorporation of chromophoric materials owing to their better stability, optical transparency, flexibility, permeability and porosity. Thus, ORMOSILs provide a good matrix to entrap chemiluminescent reagents [16,17]. Recently, great attention has been paid to the method of employing ORMOSILs to create a matrix for the immobilization of $\text{Ru}(\text{bpy})_3^{2+}$ [18], and a glassy carbon electrode (GCE) modified with an immobilization of $\text{Ru}(\text{bpy})_3^{2+}$ in ORMOSILs film has been applied to the determination of methamphetamine in scout cases [19].

Berberine, trigonelline, allantoin and betaine (Fig. 1) belong to the alkaloid family and have various pharmaceutical applications. Berberine and allantoin are well-known for their antibacterial and antiphlogistic effect, and are taken as main effective compositions in some Chinese medicines [20,21]. The study of trigonelline is also attractive because it can be used for some anticancer drug [22]. The determination of these compounds in biological fluids or botanic drugs has always been of great importance for the evaluation of their effects. There are several analytical techniques available to determine these compounds. Although chromatographic methods, including gas chromatography–mass spectrometry (GC–MS) [23], high performance liquid chromatography (HPLC) [24,25] and electrokinetic chromatography (EKC) [26], are the most current methods for their analysis, the procedures are lengthy and often involve derivatization methods to convert the analytes to detectable form.

In this work, we report experimental results in using tetramethoxysilane (TMOS) and dimethyldimethoxysilane (DiMe-DiMOS) as co-precursor to immobilize poly(*p*-styrenesulfonate) (PSS), and then $\text{Ru}(\text{bpy})_3^{2+}$ on GCE via ion-association. We

found that luminescence was generated from the ORMOSILs modified GCE, which was caused by the ECL reaction between berberine, trigonelline, allantoin or betaine with the immobilized $\text{Ru}(\text{bpy})_3^{2+}$. The factors influencing the ECL intensity of these alkaloids are discussed. The commercial software (Gaussian 98 package) was applied to the calculation of ionization potentials (IPs) of the N atom for these alkaloids ECL comparison. The relationships between IPs and luminescence intensities are also studied.

2. Experimental

2.1. Reagents

Berberine, trigonelline, allantoin and betaine were purchased from Bio-product Institute of Chinese Medicine (Beijing, China). $\text{Ru}(\text{bpy})_3\text{Cl}_2 \cdot 6\text{H}_2\text{O}$, $\text{Si}(\text{OCH}_3)_4$ (TMOS) and $(\text{CH}_3)_2\text{Si}(\text{OCH}_3)_2$ (DiMe-DiMOS) were obtained from Fluka AG (Buchs, Switzerland) and used as received. Poly(*p*-styrenesulfonate) (PSS) was purchased from Aldrich (Milwaukee, WI, USA). All other chemicals were of guaranteed grade. The water used throughout was purified with a Millipore system (Millipore Co., USA). The stock solution (10 mmol mL^{-1}) and working solutions of the four alkaloids were prepared by carrier solution.

2.2. Fabrication of the modified electrode

Glassy carbon electrode (GCE, BAS Co., Ltd. Tokyo, Japan) was polished with 1, 0.3 and $0.1 \mu\text{m}$ $\alpha\text{-Al}_2\text{O}_3$, respectively, rinsed thoroughly with water between each polishing step, sonicated in water successively and then allowed to dry at room temperature.

In a typical procedure of ORMOSILs, TMOS was mixed with DiMe-DiMOS ([DiMe-DiMOS]:[TMOS] 1.2:1, v/v),

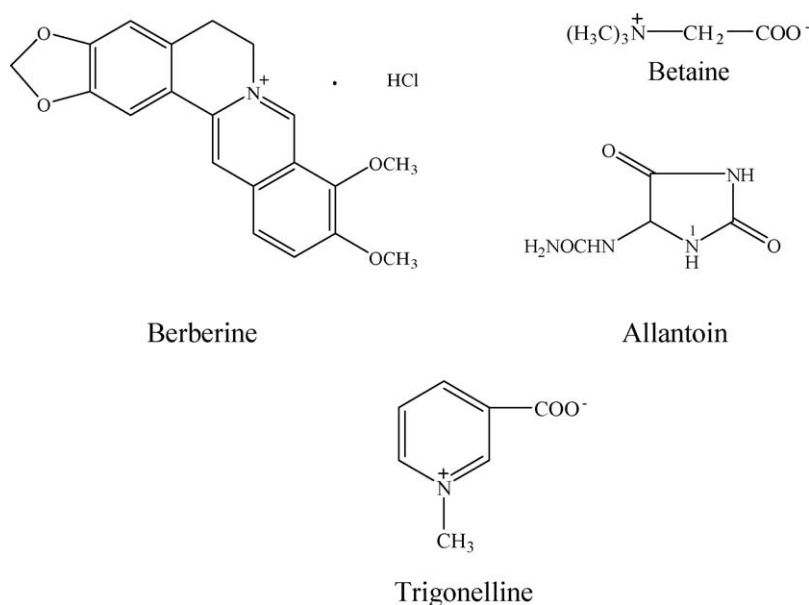


Fig. 1. Chemical structures of alkaloids.

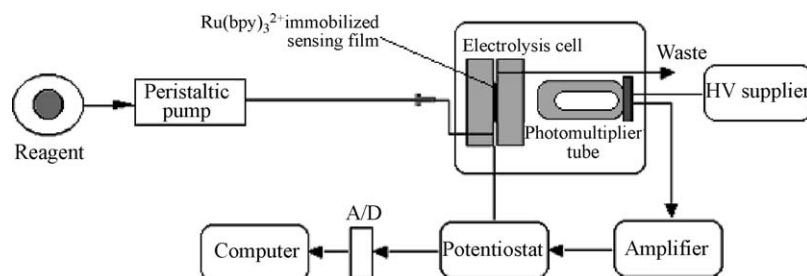


Fig. 2. Experimental setup for immobilized $\text{Ru}(\text{bpy})_3^{2+}$ ECL.

0.01 mol L^{-1} HCl and PSS. The mixture was stirred and heated at 60°C in a water bath for about 1 h until a thick solution resulted and was subsequently stored at room temperature for 10 min.

An aliquot ($6 \mu\text{L}$) of the solution was dropped onto the GCE surface and allowed to dry in the dark for 24 h. The aged ORMOSILs modified electrode was then immersed in 1 mmol L^{-1} $\text{Ru}(\text{bpy})_3^{2+}$ aqueous solution (pH 8.0) for about 0.5 h. $\text{Ru}(\text{bpy})_3^{2+}$ was immobilized in the ORMOSILs film by producing an ion-association complex with PSS. The modified GCE was washed thoroughly with water and stored in the ambient state. The thickness of the film was estimated to be $2 \mu\text{m}$ via SEM.

2.3. Electrochemical, ECL apparatus and procedures

Electrochemical measurements were performed with a CHI 800 Electrochemical Analyzer (CHI Co., Shanghai, China). A standard three-electrode arrangement was employed with a platinum auxiliary electrode and an Ag/AgCl reference electrode. The ORMOSILs-modified GCE was used as a working electrode.

The main body of the thin layer electrolysis flow cell was constructed from two pieces of Diflon blocks separated by a $50 \mu\text{m}$ thick Teflon spacer. The volume of the thin layer cell was about $1.5 \mu\text{L}$. A three-electrode system was used for potentiostatic control of the electrolytic system. The working electrode was an ORMOSILs-modified glassy carbon disk (22.1 mm^2). The counter electrode was set at the outlet with a stainless-steel pipe, and the reference electrode was Ag/AgCl (saturated KCl solution) [19]. The CHI 800 Electrochemical Analyzer taken as potentiostat was used for electrolysis. ECL intensity was observed through an IFFM-D FIA Luminescence Analyzer (Ruimai Co., China).

As shown in Fig. 2, a flow injection system equipped with a Rheodyne 7125 sample injector (Cototi, CA, USA, $20 \mu\text{L}$) and an injection loop of $20 \mu\text{L}$ was used. All the pH measurements were made with a Delta 320A pH-meter (Mettler Toledo Instruments-Shanghai Co., Shanghai, China). The measurement of ECL spectra was carried out with a set of cut-off filters from 450 to 650 nm (Aopu Optics, Beijing, China).

To calculate the ionization potentials (IPs) of these compounds, we used the hybrid B3LYP density functional method [27,28] as implemented in the Gaussian98 package [29], as well as the standard 6-31G* basis set for all atoms. Geometry

optimizations on both the neutral and ionized compounds were performed using analytical gradients and the Berny algorithm with no constrained degrees of freedom. The theoretical IP was defined as the difference in the total energies of the cationic and neutral compounds, i.e., $\text{IP} = E_{\text{total}}(\text{cation}) - E_{\text{total}}(\text{neutral})$.

3. Result and discussion

3.1. Electrochemical and ECL characters of the film immobilized $\text{Ru}(\text{bpy})_3^{2+}$

Typically, TMOS, DiMe-DMOS and 0.01 mol L^{-1} HCl (1:1.2:2, v/v) were selected for the ORMOSILs film preparation and $\text{Ru}(\text{bpy})_3^{2+}$ immobilization. The color of the ORMOSILs obtained was transparent and the texture rubbery. The percent of pores with sizes ranging from 0.8 to 2.0 nm for the ORMOSILs film was about 47.8% (vol%) [30]. The calculation result by HYPERCHEM software showed the molecular size of $\text{Ru}(\text{bpy})_3^{2+}$ reagent had a diameter of about 2.0 nm . It indicated that the ORMOSILs film using TMOS–DiMe-DMOS precursors contained more than 47.8% silica cages with a suitable size for $\text{Ru}(\text{bpy})_3^{2+}$ embedding. Although a shorter response time could be achieved when spin-coating was applied to the $\text{Ru}(\text{bpy})_3^{2+}$ film preparation, the weaker ECL response of the film led to worse detection limits for alkaloids due to its smaller capacity for $\text{Ru}(\text{bpy})_3^{2+}$. In this experiment, an ORMOSILs film with a thickness of about $2 \mu\text{m}$ was prepared by dip-coating so that a higher ECL intensity change could be obtained (Fig. 3).

The electrochemical behaviors of $\text{Ru}(\text{bpy})_3^{2+}$ immobilized in ORMOSILs films was investigated by using cyclic voltammetry (CV) and chronocoulometry (CC) since the applied potential affects ECL characters of $\text{Ru}(\text{bpy})_3^{2+}$ and coexisting

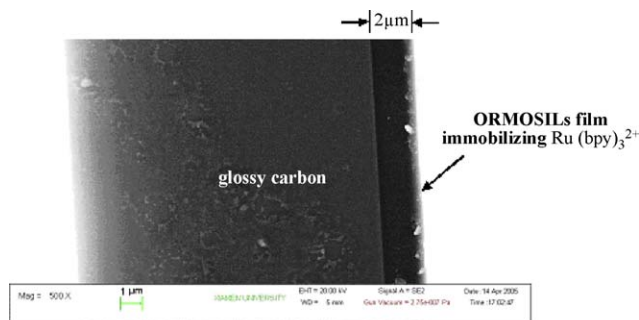


Fig. 3. SEM image of a typical ormosils film on GCE.

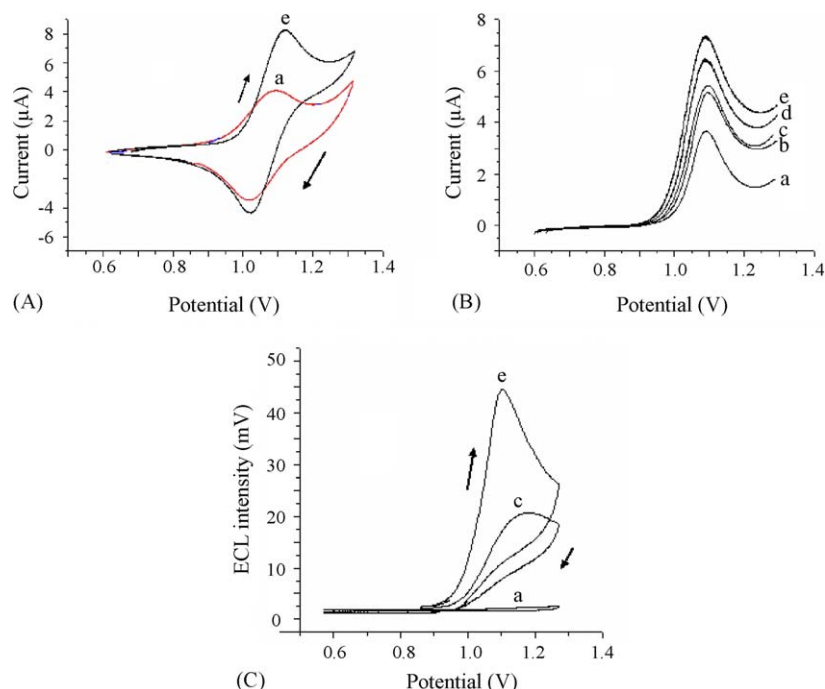


Fig. 4. Cyclic voltammograms (A), line scan voltammetry responses (B) and ECL curves during the CV of (C) on the glassy carbon electrode immobilized $\text{Ru}(\text{bpy})_3^{2+}$ in a buffer solution containing various kinds of alkaloids. (a) Buffer solution ($0.1 \text{ mol L}^{-1} \text{ KH}_2\text{PO}_4\text{--NaOH}$ buffer, pH 9.5), (b) buffer solution + $5.0 \times 10^{-4} \text{ mol L}^{-1}$ betaine, (c) buffer solution + $5.0 \times 10^{-4} \text{ mol L}^{-1}$ allantoin, (d) buffer solution + $1.0 \times 10^{-4} \text{ mol L}^{-1}$ trigonelline and (e) buffer solution + $1.0 \times 10^{-4} \text{ mol L}^{-1}$ berberine.

compounds. As shown in Fig. 4A, the CVs of $\text{Ru}(\text{bpy})_3^{2+}$ immobilized in ORMOSILs film in 0.1 mol L^{-1} phosphate buffer (pH 9.5) and the buffer solution containing berberine were performed. Analogously to the CV behaviors of $\text{Ru}(\text{bpy})_3^{2+}$ in aqueous solution, a pair of redox waves appeared with an oxidation peak at 1.10 V and a reduction peak appeared at 1.02 V , which was attributed to the one-electron redox reaction of $\text{Ru}(\text{bpy})_3^{2+}$. The potential between oxidation and reduction peak was about 80 mV , which showed a good electrochemical reversibility of $\text{Ru}(\text{bpy})_3^{2+}$ immobilized in the ORMOSILs film. Fig. 4B indicates that in the line scan voltammetry responses, the anodic current obviously increased in the presence of various kinds of alkaloids in the positive direction potential scan. The anodic current intensity at $+1.10 \text{ V}$ was changed from $3.65 \mu\text{A}$ for $\text{Ru}(\text{bpy})_3^{2+}$ to $5.18 \mu\text{A}$ for betaine, $5.95 \mu\text{A}$ for allantoin, $6.45 \mu\text{A}$ for trigonelline and $7.38 \mu\text{A}$ for berberine addition. It offers an evidence that oxidized $\text{Ru}(\text{bpy})_3^{2+}$ immobilized in the ORMOSILs film would react with alkaloids in an alkaline buffer solution. The addition of alkaloids in buffer solution obviously increased the oxidation rate of $\text{Ru}(\text{bpy})_3^{2+}$ in the ORMOSILs film on the GCE, resulting in the increase of ECL intensity. In Fig. 4C, typical ECL signal changes with the change of applied potential for allantoin and berberine has been presented. It is obvious that the ECL intensity of $\text{Ru}(\text{bpy})_3^{2+}$ was increased when alkaloids were added, which showed the same trend and order as the change of their oxidation changes as Fig. 4B. The experimental results indicated that the apparent diffusion coefficient (D_{app}) of $\text{Ru}(\text{bpy})_3^{2+}$ immobilized in film could be estimated according to the description of Anson et al. [31]. A

pulse with applied potentials between 0.6 and 1.2 V and the wavelength of 250 nm was selected for chronocoulometry experiment. D_{app} with $7.6 \times 10^{-10} \text{ cm}^2 \text{ s}^{-1}$ was obtained from the experimental result of chronocoulometry curve (Fig. 5) and Cottrell equations (Eqs. (1) and (2)).

$$i(t) = \frac{nFAD^{1/2}C}{\pi^{1/2}t^{1/2}} \quad (1)$$

$$Q(t) = \frac{2nFAD^{1/2}Ct^{1/2}}{\pi^{1/2}} \quad (2)$$

Furthermore, the apparent velocity coefficient (K_s) of $\text{Ru}(\text{bpy})_3^{2+}$ immobilized in film was estimated to be 0.56 s^{-1} (298 K) according to the cyclic voltammetry results [32].

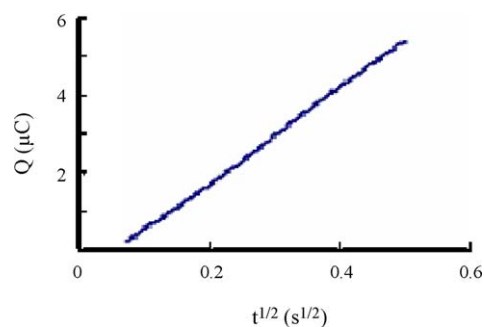


Fig. 5. Chronocoulometry curve of Q vs. $t^{1/2}$ $\text{Ru}(\text{bpy})_3^{2+}$ immobilized on a GCE buffer solution: $0.1 \text{ mol L}^{-1} \text{ KH}_2\text{PO}_4\text{--NaOH}$ – $0.2 \text{ mol L}^{-1} \text{ KNO}_3$ buffer, pH 9.5.

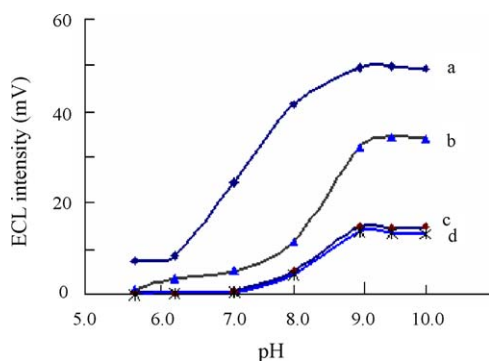


Fig. 6. Effect of pH on alkaloids ECLs. Experimental conditions: concentration of samples: $1.0 \times 10^{-4} \text{ mol L}^{-1}$ for trigonelline and berberine, $5.0 \times 10^{-4} \text{ mol L}^{-1}$ for allantoine and betaine; volume of injection sample; $20 \mu\text{L}$; applied voltage: $+1.5 \text{ V}$; PMT voltage: -900 V ; carrier solution: $0.1 \text{ mol L}^{-1} \text{ KH}_2\text{PO}_4\text{--NaOH}$ – $0.2 \text{ mol L}^{-1} \text{ KNO}_3$ (pH 9.5); flow rate: 0.5 mL min^{-1} .

ECL intensity at the $\text{Ru}(\text{bpy})_3^{2+}$ modified GCE (22.1 mm^2) in a flow injection system was measured as a function of the applied potential. Volumes of sample solution ($20 \mu\text{L}$) containing $1.0 \mu\text{g mL}^{-1}$ berberine, trigonelline, $5.0 \mu\text{g mL}^{-1}$ allantoine and betaine were injected into a carrier stream containing $0.1 \text{ mol L}^{-1} \text{ KH}_2\text{PO}_4\text{--NaOH}$ buffer, pH 9.5. The flow stream was stopped as soon as the alkaloids arrived on the surface of the modified GCE, which was held at a set of linearly increasing potential from $+0.6 \text{ V}$ (versus Ag/AgCl). As shown in Fig. 6, the ECL intensity was clearly observed when the applied potential was over $+1.0 \text{ V}$. Upon the oxidation of $\text{Ru}(\text{bpy})_3^{2+}$, an ECL signal increased rapidly to a maximum of $+1.10 \text{ V}$. The shapes of the CVs of the alkaloids on the $\text{Ru}(\text{bpy})_3^{2+}$ modified GCE was similar to those of ECLs curves, indicating that luminescence of $\text{Ru}(\text{bpy})_3^{2+}$ was caused by the reaction between the reducing intermediate and $\text{Ru}(\text{bpy})_3^{3+}$ to produce excited state [33,34]. Based on the He et al. [1] study, the electrochemical oxidation potential of amines (E_p versus NHE) was around $+1.0$ to $+1.6 \text{ V}$ for tertiary, secondary or primary amine, respectively. At the applied potential of $+1.5 \text{ V}$, the electrochemical oxidation of a tertiary amine for berberine, trigonelline, allantoine and betaine produced a radical cation as shown in Scheme 1, and the radical cation then reacted with oxidized $\text{Ru}(\text{bpy})_3^{3+}$ to produce light emission at the wavelength of 610 nm .

3.2. Effect of pH and electrolytes in the carrier solution

ECL signals of $\text{Ru}(\text{bpy})_3^{2+}$ and amines could be obtained in a wide pH range from 4.0 to 9.0 [35–37]. The experimental results showed that ECL responses of the alkaloids were highly dependent on the carrier solution pH. Very weak ECL signals were obtained before the pH of the carrier solution reached 6.0 (Fig. 6). Strong luminescence in the medium of $\text{Ru}(\text{bpy})_3^{2+}$ was observed in the pH ranging from 9.0 to 10.0 for the alkaloids. With further increase of the pH, the ECL intensity declined slightly. In addition, noise increased greatly at higher pH. The pH of carrier solution was kept at 9.5 for the analytical application.

ECL intensity is known to be highly dependent on the concentration and species of electrolyte in the carrier solution due to the electrolytic efficiency [2,38]. Generally, the luminescence intensity of $\text{Ru}(\text{bpy})_3^{2+}$ was increased by changing the supporting electrolyte in the order $\text{NO}_3^- > \text{CH}_3\text{COO}^- \approx \text{F}^- > \text{CH}_3\text{O}^- \approx \text{Cl}^- > \text{Br}^-$ [19]. ECL intensity was also affected by different kinds of buffer solution at pH 9.5. Among them, a buffer solution with the concentration of $0.1 \text{ mol L}^{-1} \text{ NaOH--K}_2\text{HPO}_4$ containing $0.2 \text{ mol L}^{-1} \text{ KNO}_3$ (pH 9.5) was selected since a brighter luminescence and stable responses were obtained. A lower flow rate of reagent might cause larger background signal by the observation of brighter luminescence. The optimal flow rate was estimated to be 0.5 mL min^{-1} .

3.3. ECLs comparison of alkaloids

In general, the ECL reaction of $\text{Ru}(\text{bpy})_3^{2+}$ and amines involves a charge-transfer process [39]. The first ionization potential (IP) for the alkyl amines generally decreases in the order of primary > secondary > tertiary [40]. According to experimental results, the ECL intensity of alkaloid increases in the order of berberine > trigonelline > allantoine > betaine, which shows a reversed order of IP (Table 1). Although berberine, trigonelline, allantoine and betaine are all tertiary amines, their ECL intensity is obviously different. IP values can primarily reflect the general trend of luminescence intensity for this same type amine. The conjugated group around N atom will affect the radical formed through either electro-donating or conjugation effects, which therefore have an important role to play in determining the alkaloids ECL efficiency. Larger conjugated

Table 1
Comparison of ionization potentials and relative ECL responses of alkaloids and amines

Compound	ECL intensity (mV)	Ionization potential (eV) ^a	ECL optimum potential (V vs. Ag/AgCl)	Detection limit ($\mu\text{mol L}^{-1}$)
Berberine	46	7.10 (N)	+1.08	5.0
Trigonelline	32	7.19 (N)	+1.10	8.0
Allantoine	15	7.50 (₁ N)	+1.06	20
Betaine	12	7.56 (N)	+1.11	50
$\text{C}_3\text{H}_7\text{NH}_2$	2	8.30	+1.15	–
$(\text{C}_3\text{H}_7)_2\text{NH}$	6	7.54	+1.10	–
$(\text{C}_3\text{H}_7)_3\text{N}$	71	6.84	+1.17	–

All ECL intensities were obtained in $0.1 \text{ mol L}^{-1} \text{ NaOH--K}_2\text{HPO}_4$ buffer solution pH 9.5, applied potential $+1.50 \text{ V}$ (Ag/AgCl), concentration of alkaloid, berberine and trigonelline, $1.0 \times 10^{-4} \text{ mol L}^{-1}$, allantoine and betaine $5.0 \times 10^{-4} \text{ mol L}^{-1}$, propylamine $1.0 \times 10^{-3} \text{ mol L}^{-1}$, dipropylamine $5.0 \times 10^{-4} \text{ mol L}^{-1}$, concentration of tripropylamine: $5.0 \times 10^{-5} \text{ mol L}^{-1}$.

^a B3LYP/6-31 G(d) calculation method was applied to N IP calculation.

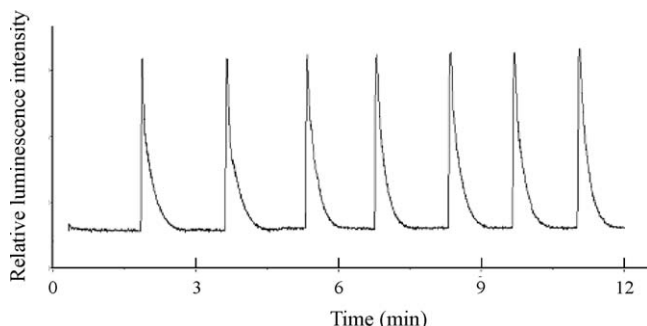


Fig. 7. Typical ECL responses of berberine. Experimental conditions are the same as Fig. 6. Concentration of berberine: $1.0 \times 10^{-4} \text{ mol L}^{-1}$.

group stabilizes the N radical formed and gives stronger ECL response, which makes a lower IP value of compound. This is supported by the fact that berberine with the largest conjugated group makes the brightest light emission. In the comparison of the alkaloid ECL intensity, the IP value of 7.10 eV for berberine was changed to 7.19 eV for trigonelline, and the ECL response of trigonelline was about 30% less than that of berberine. Moreover, the luminescence intensity of allantoin (IP 7.50 eV) or betaine (IP 7.56 eV) was less than that of 10% ECL intensity of berberine.

3.4. Flow injection analysis and stability of modified electrode

According to the best experimental condition as 0.1 mol L^{-1} NaOH– K_2HPO_4 (pH 9.5), 0.2 mol L^{-1} KNO_3 carrier solution and a flow rate of 0.5 mL min^{-1} , a typical flow injection recording of $1.0 \times 10^{-4} \text{ mol L}^{-1}$ berberine is shown in Fig. 7. Under the condition, the calibration curves were linear from $8 \times 10^{-4} \text{ mol L}^{-1}$ to $5 \times 10^{-2} \text{ mol L}^{-1}$ for allantoin and betaine, $1 \times 10^{-5} \text{ mol L}^{-1}$ to $3 \times 10^{-3} \text{ mol L}^{-1}$ for berberine and trigonelline. The determination limit was $5 \times 10^{-6} \text{ mol L}^{-1}$, $8 \times 10^{-6} \text{ mol L}^{-1}$, $2.0 \times 10^{-5} \text{ mol L}^{-1}$ and $5.0 \times 10^{-5} \text{ mol L}^{-1}$ for berberine, trigonelline, allantoin and betaine at S/N 3, respectively. Both berberine and trigonelline showed good reproducibility with R.S.D. values well below 3% at $1.0 \times 10^{-4} \text{ mol L}^{-1}$.

Typically, the ORMOSILs film modified GCE was stored in 0.1 mol L^{-1} NaOH– K_2HPO_4 buffer solution at pH 9.5 at room temperature. Generally, the modified GCE did not need to be reactivated before ECL measurement. The modified GCE was ready for use after obtaining six signals with a S.D. less than 5%. Experimental results demonstrated that the modified GCE could be stored up for one month without significant deterioration. The initial ECL response for $1.0 \times 10^{-4} \text{ mol L}^{-1}$ berberine decreased by 5% compared with the newly-made ORMOSILs film if the modified GCE was stored in the buffer solution at 4°C for 1 month.

4. Conclusions

This study identified that the ORMOSILs material used TMOS and DiMe-DMOS as co-precursor is suitable to pro-

vide an effective means to prepare composite films for the immobilization of the ECL reagent, $\text{Ru}(\text{bpy})_3^{2+}$. From the CV and ECL results, the ORMOSILs film modified GCE immobilized $\text{Ru}(\text{bpy})_3^{2+}$ showed good electrochemical and ECL activities. The modified GCE was applied to the detection of some alkaloids such as berberine, trigonelline, allantoin and betaine in a flow injection system, and exhibited a variety of good performance characteristics including higher sensitivity, short response time, good stability and long application life. Moreover, ECL emission of alkaloid was affected by its conjugated group around N atom, and IP calculation values could provide a general trend of ECL intensity for the alkylamines. These results suggest that it may be possible to extend the ECL applications to alkaloids analysis based on the proposed $\text{Ru}(\text{bpy})_3^{2+}$ modification method on GCE electrode.

Acknowledgements

We express our sincere thanks to the National Nature Scientific Foundation of China (No. 20375033), the Science and Technology Project of Fujian Province (2005I-030) and Japan Society for Promotion of Science (JSPS) for their financial support of this research.

References

- [1] L. He, K.A. Cox, N.D. Danielson, *Anal. Lett.* 232 (1990) 195.
- [2] A.W. Knight, G.M. Greenway, *Analyst* 121 (1996) 101R.
- [3] X.P. Wu, F.X. Huang, J.P. Duan, G.N. Chen, *Talanta* 65 (2005) 1279.
- [4] X. Chen, Y. Tao, L. Zhao, Z.H. Xie, G.N. Chen, *Luminescence* 20 (2005) 109.
- [5] X. Chen, C.Q. Yi, M.J. Li, X. Lu, Z. Li, P.W. Li, X.R. Wang, *Anal. Chim. Acta* 466 (2002) 79.
- [6] G.N. Chen, L. Zhang, R.E. Lin, Z.C. Yang, J.P. Duan, H.Q. Chen, D.B. Hibbert, *Talanta* 50 (2000) 1275.
- [7] X. Zhang, A.J. Bard, *J. Phys. Chem.* 92 (1988) 5566.
- [8] C.J. Miller, P. McCord, A.J. Bard, *Langmuir* 7 (1991) 2781.
- [9] Y.S. Obeng, A.J. Bard, *Langmuir* 7 (1991) 195.
- [10] Y. Sato, K. Uosaki, *J. Electroanal. Chem.* 384 (1995) 57.
- [11] L.L. Shultz, J.S. Stoyanoff, T.A. Nieman, *Anal. Chem.* 68 (1996) 349.
- [12] T.M. Downey, T.A. Nieman, *Anal. Chem.* 64 (1992) 261.
- [13] M.M. Collinson, B. Novak, S.A. Martin, J.S. Taussing, *Anal. Chem.* 72 (2000) 2914.
- [14] H.Y. Wang, G.B. Xu, S.J. Dong, *Analyst* 126 (2001) 1095.
- [15] H.Y. Wang, G.B. Xu, S.J. Dong, *Electroanalysis* 14 (2002) 853.
- [16] M.M. Collinson, J. Taussig, S.A. Martin, *Chem. Mater.* 11 (1999) 2594.
- [17] M.M. Collinson, S.A. Martin, *Chem. Commun.* (1999) 899.
- [18] J.K. Lee, S.H. Lee, M. Kim, H. Kim, D.H. Kim, W.Y. Lee, *Chem. Commun.* (2003) 1602.
- [19] C.Q. Yi, Y. Tao, B. Wang, X. Chen, *Anal. Chem. Acta* 541 (2005) 75.
- [20] K.J. Zhu, T. Li, *China Pharma.* 9 (2000) 22.
- [21] R. Zhang, Y. Wan, D.H. Zhang, *J. Nanchang Univ. (Eng. Tech.)* 19 (1997) 81.
- [22] Y.M. Ma, J.X. Fu, *Shanxi Forest Tech.* 1 (1997) 75.
- [23] H.A. Weber, M.K. Zart, A.E. Hodges, H.M. Molloy, B.M. O'Brien, L.A. Moody, A.P. Clark, R.K. Harris, D. Overstreet, C.S. Smith, *J. Agric. Food Chem.* 51 (2003) 7352.
- [24] C. Yu, Y.C. Hong, H. Zhang, *Chin. J. Chromatogr.* 12 (1994) 37.
- [25] M. Czauderna, J. Kowalczyk, *J. Chromatogr. B* 744 (2000) 129.
- [26] H. Okamoto, A. Uetake, R. Tamaya, T. Nakajima, K. Sagara, Y. Ito, *J. Chromatogr. A* 929 (2001) 133.
- [27] C. Lee, W. Yang, R.G. Parr, *Phys. Rev. B* 37 (1989) 785.

- [28] M.J. Frisch, G.W. Trucks, H.B. Schlegel, G.E. Scuseria, et al., Gaussian 98 (Rev. A 10), Gaussian, Inc., Pittsburgh, PA, 2001.
- [29] J.A. Holeman, N.D. Danielson, *Anal. Chim. Acta* 277 (1993) 55.
- [30] X. Chen, L. Lin, P.W. Li, Y.J. Dai, X.R. Wang, *Anal. Chim. Acta* 506 (2004) 9–15.
- [31] F.C. Anson, *Anal. Chem.* 36 (1964) 975.
- [32] E. Laviron, *J. Electroanal. Chem.* 101 (1979) 19.
- [33] N.E. Tokel, A.J. Bard, *J. Am. Chem. Soc.* 94 (1972) 2862.
- [34] I. Rubinstein, C.R. Martin, A.J. Bard, *Anal. Chem.* 55 (1983) 1580.
- [35] K. Uchikura, M. Kirasawa, *Anal. Sci.* 7 (1991) 971.
- [36] K. Uchikura, M. Kirasawa, A. Sugh, *Anal. Sci.* 9 (1993) 121.
- [37] J.L. Leland, M.J. Powell, *J. Electrochem. Soc.* 137 (1990) 3127.
- [38] X. Chen, M. Sato, Y.J. Lin, *Microchem. J.* 58 (1998) 13.
- [39] J.B. Noffsinger, N.D. Danielson, *Anal. Chem.* 59 (1987) 865.
- [40] I. Rubinstein, A.J. Bard, *J. Am. Chem. Soc.* 103 (1981) 512.

Determination of carbamates in nature water based on the enhancement of electrochemiluminescent of $\text{Ru}(\text{bpy})_3^{2+}$ at the multi-wall carbon nanotube-modified electrode

Zhenyu Lin, Guonan Chen*

The MOE Key Laboratory of Analysis and Detection Technology for Food Safety, and Department of Chemistry, Fuzhou University, Fuzhou, Fujian 350002, China

Received 25 October 2005; received in revised form 4 December 2005; accepted 5 December 2005

Available online 19 January 2006

Abstract

A multi-wall carbon nanotube (MWNT)/Nafion composite film-modified electrode was developed in this paper, and its chemical and electrochemiluminescent (ECL) behavior of tris(2,2'-bipyridyl)ruthenium ($\text{Ru}(\text{bpy})_3^{2+}$) on this electrode has been investigated in detail. It has been also found that some carbamates were able to enhance the ECL intensity of $\text{Ru}(\text{bpy})_3^{2+}$ greatly at this modified electrode. Based on which, a sensitive and simple method for determination of pirimicarb, methomyl, aldicarb and carbofuran were developed, and the proposed method has been applied to determine the carbamates in the nature water.

© 2005 Published by Elsevier B.V.

Keywords: Electrochemiluminescent; Multi-wall carbon nanotube; Modified electrode tris(2,2'-bipyridyl)ruthenium; Carbamate

1. Introduction

Since the discovery of carbon nanotube [1], it has been attracted much interest all over the world. It is a kind of inorganic material with a nanostructure, which is promising as an immobilization substance because of its significant mechanical strength, high surface area, excellent electrical conductivity and good chemical stability [2]. It has been used in many fields, such as nanoelectric device [3–5], composite materials [6], atomic force microscope probes [7], field-emission devices [8], gas and chemical sensors [9,10] and lithium ion storage [11]. Generally, carbon nanotubes exist in two forms: single-wall carbon nanotube (SWNT) and multi-wall carbon nanotube (MWNT) [12]. The subtle electronic behaviors of carbon nanotube revealed that they have the ability to promote electron-transfer reactions when they were used as an electrode material. Scanning tunneling spectroscopy (STS) measurement indicated that the MWNT has a relatively higher electrical conductivity than the SWNT [13]. Gooding et al. reported the electrochemical properties of protein at carbon nanotube-modified electrodes [14]. Many other

workers have applied the carbon nanotube-modified electrodes in the analytical applications. Dong and co-workers had studied electrochemiluminescent (ECL) on SWNT-modified electrode [15–17]. However, no attention has been paid to the electrochemiluminescent behavior at a MWNT-modified electrode.

Nafion film has been widely used for modification of electrode and for construction of biosensors and chemical sensors [18], and has been also used as an effective ion-exchanger for tris(2,2'-bipyridyl)ruthenium ($\text{Ru}(\text{bpy})_3^{2+}$). However, the rate of charge transfer in the pure Nafion film is lower. Our experiments showed that use of MWNT/Nafion composite film for modification of the carbon electrode would increase the charge-transfer rate greatly, based on which the ECL behavior of $\text{Ru}(\text{bpy})_3^{2+}$ on a multi-wall carbon nanotube-modified electrode was investigated in detail in this paper.

Carbamate pesticides have become increasingly important in recent years, due to their broad spectrum of activity, relatively rapid disappearance and generally low mammalian toxicity. But they are inhibitor of acetylcholinesterase, and considered toxic to human beings [19]. There were many methods to detect the carbamates, such as fluorescence [20], ultraviolet (UV) [21] and mass spectrometry (MS) [22]. These methods have some disadvantages, such as lower sensitivity and tedious procedure or expensive equipments.

* Corresponding author. Tel.: +86 591 87893315; fax: +86 591 83713833.
E-mail address: gnchen@fzu.edu.cn (G. Chen).

The ECL of $\text{Ru}(\text{bpy})_3^{2+}$ has been attracted much attention as a sensitive and selective detection method in analytical chemistry because of its excellent stability and ability to produce with a good quantum yield [23]. In this paper, based on the fact that some carbamates can enhance the ECL intensity of $\text{Ru}(\text{bpy})_3^{2+}$, a simple and sensitive method has been established to determine some carbamates, such as pirimicarb, methomyl, aldicarb and carbofuran. The proposed method has been applied to determine carbamates in the nature water.

2. Experimental

2.1. Apparatus

ECL intensity versus potential was measured by using a BPCL Ultra-Weak Chemiluminescence Analyzer controlled by a personal computer with BPCL program (Institute of Biophysics, Chinese Academy of Sciences) in conjunction with a CH Instruments model 660a electrochemical analyzer (Shanghai Chenghua instrument Co., China). The electrochemical analyzer was used for controlling waveforms and potentials. A block diagram of this system is shown in Fig. 1.

A conventional three-electrode system was used for the electrolytic system, including a modified glassy carbon electrode as a working electrode, a platinum wire as the counter electrode and Ag/AgCl (saturated KCl) electrode as the reference electrode. A commercial 3 ml cylindroid glass cell was used as ECL cell, and it was placed directly in the front of the photomultiplier tube.

Normal phase NH_2 solid-phase extraction (SPE) cartridges were provided by the Waters Tech. The cartridge contains 500 mg adsorbent.

2.2. Chemicals

$\text{Ru}(\text{bpy})_3\text{Cl}_2 \cdot 6\text{H}_2\text{O}$ was obtained from Sigma Chemical Company and used without further purification. The MWNT

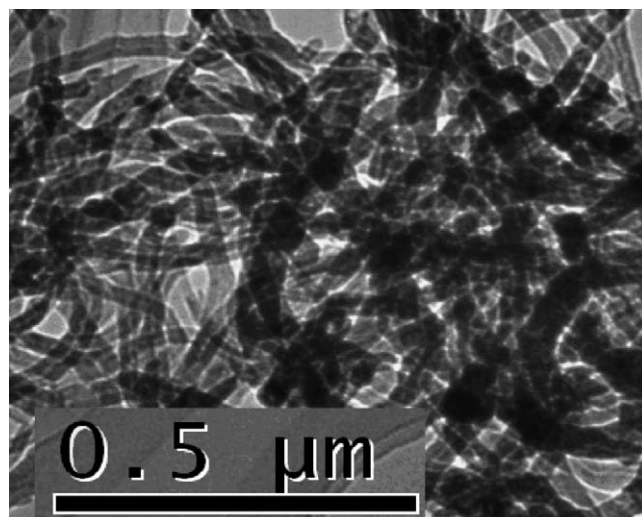


Fig. 2. TEM image of MWNTs-DMF suspension (200 kV JEOL JEM-2010).

was obtained from Shenzhen Nanotech Port Co. Ltd. and purified according to the literature method [24], and the TEM image of the MWNT is shown in Fig. 2. Pirimicarb and aldicarb were obtained from the laboratories of Dr. Ehrenstorfer GmbH. Methomyl and carbofuran were obtained from the State Pesticide Product Supervision & Testing Center (Beijing, China). All the other chemicals were of analytical grade. Ultra-pure water (Millipore) was used throughout.

2.3. Preparation of MWNT-Nafion/GC electrode and immobilized with $\text{Ru}(\text{bpy})_3^{2+}$

The GC was pretreated before use by polishing their surfaces with aqueous slurries of alumina powders (average particle diameters: 1.0 and 0.3 μm $\alpha\text{-Al}_2\text{O}_3$) on a polishing microcloth and then rinsed with water and sonicated in acetone. MWNT/Nafion composite film was then prepared by dropping 10 μl suspension (1 mg MWNT were dispersed in 10 ml Nafion ethanol solution) onto the GC (5 mm i.d.) electrode surface and the solvent was evaporated in the air. The modified electrodes were then dipped into the phosphate buffer solution (PBS; 0.2 mol/l, pH 7.0) containing 1×10^{-4} mol/l of $\text{Ru}(\text{bpy})_3^{2+}$ for 16 h, and then rinsed by ultra-pure water for 3 min.

2.4. Sample preparation

For SPE assays, each cartridge was conditioned with 3 ml of dichloromethane, 3 ml of methanol and two times of 3 ml of ultra-pure water. After loaded with the water samples, column was washed twice with 3 ml of ultra-pure water, followed by vacuum dry for 2 min. Subsequently, the elution was performed with 1 ml of methanol/acetonitrile (50/50, v/v) for three times, then followed by evaporation to dryness under a gentle stream of nitrogen.

The dry residues obtained from the SPE assays were redissolved with 0.2 ml buffer solution.

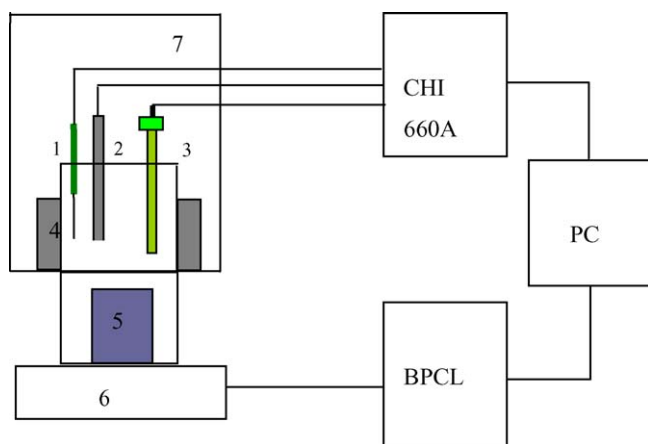


Fig. 1. A block diagram of the ECL detection system. (1) Counter electrode, (2) working electrode, (3) reference electrode, (4) jacket for localization, (5) photomultiplier tube, (6) base frame and (7) detection chamber. BPCL, CL detector; PC, computer controller and data processing system.

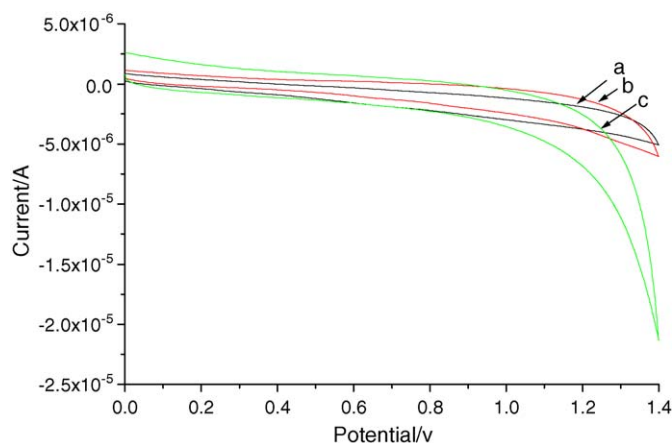


Fig. 3. CV curves of different electrodes at the phosphate buffer solution. Phosphate buffer solution: 0.2 mol/l (pH 7.0); scan rate: 0.1 V/s. (a) Bare GC electrode, (b) pure Nafion-modified electrode and (c) MWNT/Nafion composite film-modified electrode.

3. Results and discussion

3.1. Electrochemical and ECL behavior of MWNT/Nafion composite film-modified electrode

Fig. 3 shows the cyclic voltammetry of different kinds of electrodes in the phosphate buffer solution (pH 7.0). From Fig. 3, it can be found that the current obtained at the pure Nafion-modified electrode has no apparent difference, but at MWNT/Nafion composite film, the current was found to be greatly increased, which can be attributed to the electrocatalysis of the MWNT.

Fig. 4 shows the cyclic voltammograms of the MWNT/Nafion composite film-modified electrode and the pure Nafion-modified electrode in phosphate buffer solution (pH 7.0). It can be known from Fig. 4 that the oxidation current obtained at the MWNT/Nafion composite film-modified electrode is much greater than that of pure Nafion-modified electrode, which can

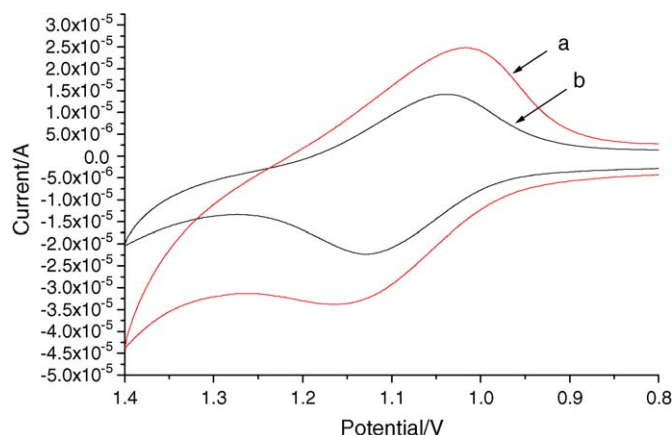


Fig. 4. CV behavior of the MWNT/Nafion composite film-modified electrode immobilized with $\text{Ru}(\text{bpy})_3^{2+}$. Phosphate buffer solution: 0.2 mol/l (pH 7.0); scan rate: 0.1 V/s. Both electrodes have been immersed in $\text{Ru}(\text{bpy})_3^{2+}$ solution for 16 h before measurement. (a) MWNT-Nafion/GC immobilized with $\text{Ru}(\text{bpy})_3^{2+}$ and (b) the pure Nafion-modified electrode.

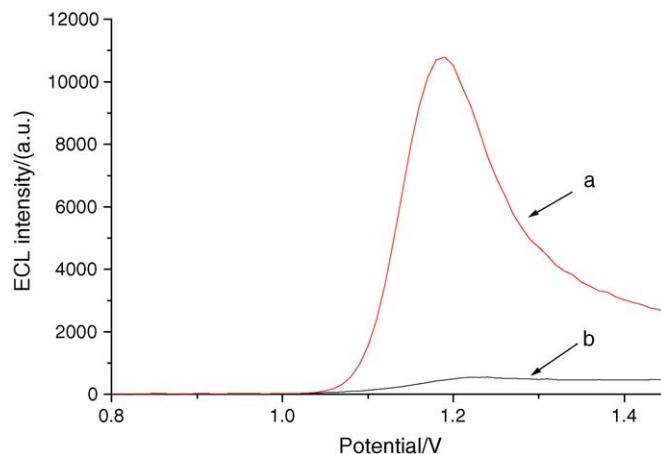


Fig. 5. ECL intensity of MWNT/Nafion composite film-modified electrode (a) and pure Nafion-modified electrode (b); scan rate: 0.1 V/s; PBS buffer solution: 0.2 mol/l (pH 7.0). Both electrodes have been immersed in 1×10^{-4} mol/l $\text{Ru}(\text{bpy})_3^{2+}$ for 16 h.

be attributed to the electronic conduction of MWNT and also to the adsorption of $\text{Ru}(\text{bpy})_3^{2+}$ by MWNT. The oxidation potentials of $\text{Ru}(\text{bpy})_3^{2+}$ at both electrodes are basely the same.

The ECL behavior of $\text{Ru}(\text{bpy})_3^{2+}$ on the pure Nafion-modified electrode and MWNT/Nafion composite film-modified electrode has been investigated and the results are shown in Fig. 5. From Fig. 5, we can know that the ECL intensity of $\text{Ru}(\text{bpy})_3^{2+}$ on the pure Nafion-modified electrode is much lower than that on the MWNT/Nafion composite film-modified electrode. The reasons for the better performance of the carbon nanotube electrode for an ECL reaction maybe attributed to the dimensions of carbon nanotube (of the tubes, the channels that are inherently present in the tubes), the electronic structure and the topological defects present on the tube surface [25]. Therefore, the MWNT can provide the more effective area of the electrode, and can act as a promoter to enhance the electrochemical reaction.

3.2. The reproducibility of MWNT/Nafion-modified GCE

The MWNT/Nafion-modified film is stable on the surface of the electrode. As shown in Fig. 6, when the electrode was repetitively cycled at 100 mV/s for seven times, the ECL intensity was changed within 5%. When the modified electrode has been store at 4 °C for 2 weeks, the chemical and ECL behavior of modified electrode was not found much change.

3.3. Enhancement of ECL intensity of $\text{Ru}(\text{bpy})_3^{2+}$ at MWNT-Nafion/GC electrode by carbamates

Our preliminary experiments showed that some carbamates could greatly enhance the ECL intensity of $\text{Ru}(\text{bpy})_3^{2+}$ at the MWNT/Nafion-modified GCE. Fig. 7 shows the enhancement of ECL intensity of $\text{Ru}(\text{bpy})_3^{2+}$ when 0.1 $\mu\text{mol/l}$ different kind of carbamates (pirimicarb, methomyl, aldicarb and carbofuran) are added into the buffer solution. The possible mechanism for this enhanced ECL reaction can be described in Fig. 8. $\text{Ru}(\text{bpy})_3^{2+}$

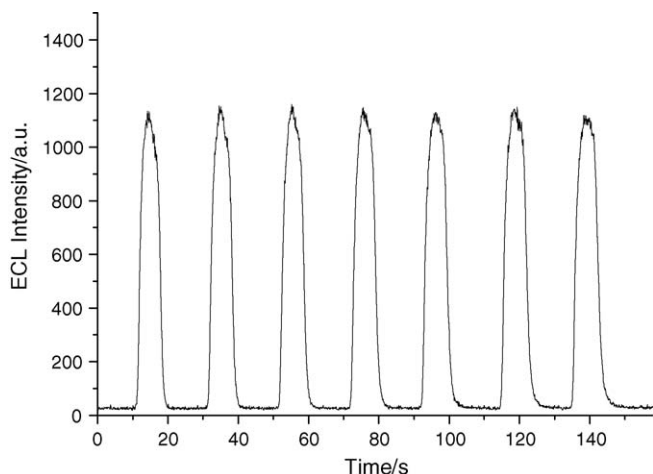


Fig. 6. The reproducibility of MWNT/Nafion modified GCE; scan rate: 0.1 V/s; PBS buffer solution: 0.2 mol/l (pH 6.0). Electrode has been immersed in 1×10^{-4} mol/l $\text{Ru}(\text{bpy})_3^{2+}$ for 16 h.

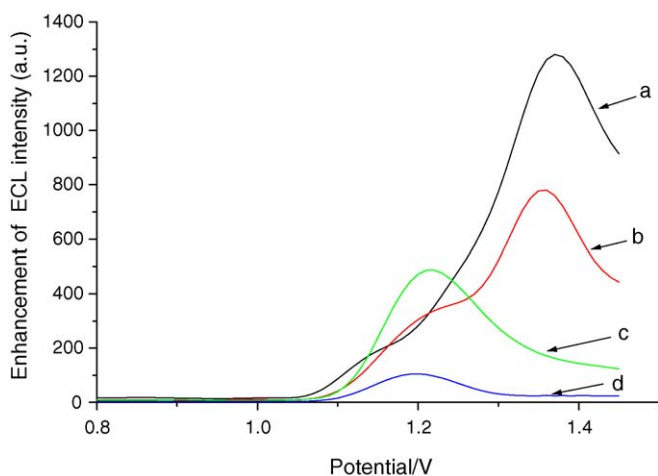


Fig. 7. The enhancement of ECL on MWNT/Nafion composite film-modified electrode by carbamates. PBS buffer solution: 0.2 mol/l (pH 6.0). (a) 0.1 $\mu\text{mol/l}$ pirimicarb, (b) 0.1 $\mu\text{mol/l}$ methomyl, (c) 0.1 $\mu\text{mol/l}$ aldicarb and (d) 0.1 $\mu\text{mol/l}$ carbofuran. LSV, 0.8–1.45 V. Scan rate: 0.1 V/s, electrode has been immersed in 1×10^{-4} mol/l $\text{Ru}(\text{bpy})_3^{2+}$ for 16 h.

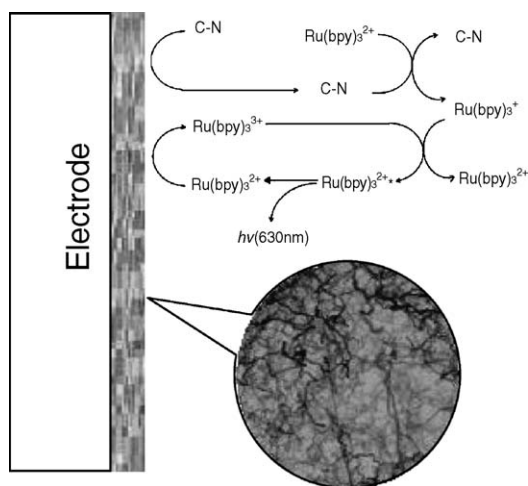


Fig. 8. The proposed mechanism for the ECL reaction of $\text{Ru}(\text{bpy})_3^{2+}$ with a carbamate C–N= carbamate, the marked is the membrane of the Nafion contains CNTs.

was first oxidized to give $\text{Ru}(\text{bpy})_3^{3+}$ at the electrode, and the carbamate(C–N) loses a proton to form the strongly reducing intermediate C–N^* . C–N^* further reacts with $\text{Ru}(\text{bpy})_3^{3+}$ to produce $\text{Ru}(\text{bpy})_3^{2+}$, and then $\text{Ru}(\text{bpy})_3^{2+}$ reacts with $\text{Ru}(\text{bpy})_3^{3+}$ to form $\text{Ru}(\text{bpy})_3^{2+*}$. When $\text{Ru}(\text{bpy})_3^{2+*}$ goes back to $\text{Ru}(\text{bpy})_3^{2+}$ it emits the light.

3.4. Selection of reaction medium

It is well known that the medium plays an important role in ECL reaction. The effect of the buffer components on the ECL was examined by using acetate buffer, phosphate buffer, borate buffer and BR buffer solution under the same pH 7.0. It was found that the maximum enhanced ECL signal for pirimicarb could be obtained in phosphate buffer solution, and the similar results could be also obtained for methomyl, aldicarb and carbofuran. Therefore, PBS was selected in subsequent work.

Carbamate pesticides were easily oxidized in the alkaline solution, so the pH of the buffer solution was preferred to be lower than 7.0. It was observed that the background ECL intensity of $\text{Ru}(\text{bpy})_3^{2+}$ increased greatly with pH, and the net ECL intensity enhancements (ΔI) reached a maximum value and was kept constant in the range of pH 5.5–6.5, so pH 6.0 was chosen subsequently.

3.5. Effect of the immobilized $\text{Ru}(\text{bpy})_3^{2+}$

The amount of the $\text{Ru}(\text{bpy})_3^{2+}$ immobilized in the MWNT/Nafion film also has an important effect on the ECL intensity. The immobilization of $\text{Ru}(\text{bpy})_3^{2+}$ in the film can be controlled by the immerge time or the concentration of $\text{Ru}(\text{bpy})_3^{2+}$ solution. However, it was found that the longer immerge time was favorable to obtain a uniform and dense film. Therefore, the immerge time was held at 16 h, and changed the concentration of $\text{Ru}(\text{bpy})_3^{2+}$ solution to examine the enhanced ECL intensities. It was found that the enhanced ECL intensity was increased with the concentration of $\text{Ru}(\text{bpy})_3^{2+}$ in the range of 1.0×10^{-5} to 1.0×10^{-3} mol/l, but the background ECL intensity was quite high when the $\text{Ru}(\text{bpy})_3^{2+}$ concentration was higher than 1.0×10^{-4} mol/l and a significant increase in the noise amplitude of the base line was observed, which would increase the detection limit. Therefore, 1.0×10^{-4} mol/l $\text{Ru}(\text{bpy})_3^{2+}$ solution was used for all subsequent experiments.

3.6. Analytical application

The calibration curves were obtained under the optimized condition and the results are shown in Table 1. It can be known from Table 1 that the regression equations revealed a linear relationship between the concentration of carbamate and the ECL intensity in a wide range, the detection limits are 2.0×10^{-9} , 1.8×10^{-8} , 1.2×10^{-7} and 1.7×10^{-7} mol/l, respectively.

The developed method has been used for the spiked nature water, and the results are shown in Table 2. The spiked water sample was treated according to the procedure described in Section 2.4.

Table 1

Linear relationships of enhanced ECL intensity with the concentration of carbamates

Pesticide	Linear range (mol/l)	Linear regression equation (C , mol/l)	Correlation coefficient (R)	Detection limit $S/N=3$, mol/l
Pirimicarb	8.0×10^{-9} to 1.0×10^{-6}	$I_{\text{ECL}} = 6.24 \times 10^9 C + 25.3$	0.9924	2.0×10^{-9}
Methomyl	3.0×10^{-8} to 3.0×10^{-6}	$I_{\text{ECL}} = 5.76 \times 10^8 C + 35.4$	0.9916	1.8×10^{-8}
Aldicarb	3.0×10^{-7} to 4.0×10^{-6}	$I_{\text{ECL}} = 3.45 \times 10^7 C - 15.4$	0.9934	1.2×10^{-7}
Carbofuran	5.0×10^{-7} to 7.0×10^{-6}	$I_{\text{ECL}} = 2.97 \times 10^7 C - 29.8$	0.9948	1.7×10^{-7}

Table 2

Average recoveries of three assay using ECL method for carbamates in the laboratory-spiked ultra-pure water samples

Pesticide	Added (mol/l)	Recovery (%)
Primicarb	1.0×10^{-7}	95.7
Methomyl	1.0×10^{-7}	107.4
Aldicarb	1.0×10^{-6}	86.1
Carbofuran	1.0×10^{-6}	83.2

4. Conclusions

The MWNT/Nafion composite film-modified electrode was developed in this paper, and it was found to be able to enhance the ECL of $\text{Ru}(\text{bpy})_3^{2+}$ greatly. We also found that some carbamate pesticides could enhance the ECL of $\text{Ru}(\text{bpy})_3^{2+}$, based on which, a sensitive, simple and quick method for determination of carbamates, such as pirimicarb, methomyl, aldicarb and carbofuran has been established. The proposed method had been applied to determine the spiked nature water. In order to apply this method for determination of the multi-residual carbamate pesticides, a capillary electrochromatography (CEC) system coupled with ECL detection is being developed in this laboratory.

Acknowledgements

This project was financially supported by the National Nature Sciences Funding of China (20575011) and the Science Foundation of State Education Department (20040386002).

References

- [1] S. Iijima, Nature 314 (1991) 56–59.
- [2] G.C. Zhao, L.I. Zhang, X.W. Wei, Z.S. Yang, Electrochem. Commun. 5 (2003) 825–829.
- [3] C.T. White, T.N. Todorov, Nature 393 (1998) 240–242.
- [4] S.J. Tans, A.R.M. Verschuere, C. Dekker, Nature 393 (1998) 49–52.
- [5] P.G. Collins, A. Zettl, H. Bando, A. Thess, R.E. Smalley, Science 278 (1997) 100–103.
- [6] J. Hone, M.C. Llaguno, M.J. Biercuk, A.T. Johnson, B. Batlogg, J.E. Fischer, Appl. Phys. A 74 (2002) 339–343.
- [7] S.S. Wong, A.T. Woolley, E. Joselevich, C.L. Cheung, C.M. Lieber, J. Am. Chem. Soc. 120 (1998) 8558–9557.
- [8] K. Yu, Z. Zhu, Q. Li, W. Lu, Appl. Phys. A 77 (2003) 811–817.
- [9] R.H. Baughman, C.X. Cui, A.A. Zakhidov, Z. Lqbal, J.N. Barisci, G.M. Spinks, G.G. Wallace, A. Mazzoldi, D. De Rossi, A.G. Rinzler, O. Jaschinski, S. Roth, M. Kertesz, Science 284 (1999) 1340–1344.
- [10] J. Wang, M. Musameh, Anal. Chem. 75 (2003) 2075–2079.
- [11] G.Q. Ning, F. Wei, G.H. Luo, Q.X. Wang, Y.L. Wu, H. Yu, Appl. Phys. A 78 (2004) 955–959.
- [12] W.S. Huang, W.B. Hu, J.C. Song, Talanta 61 (2003) 411–416.
- [13] C. Wang, M. Waje, X. Wang, J.M. Tang, R.C. Haddon, Y. Yan, Nano Lett. 4 (2) (2004) 345–348.
- [14] J.J. Gooding, R. Wibowo, J.Q. Liu, W.R. Yang, D. Losic, S.N. Orbons, F.J. Mearns, J.G. Shapter, D.B. Hibber, J. Am. Chem. Soc. 125 (2003) 9006–9007.
- [15] K.B. Wu, S.S. Hu, J.J. Fei, W. Bai, Anal. Chem. Acta 489 (2003) 215–221.
- [16] F.H. Wu, G.C. Zhao, X.W. Wei, Electrochem. Commun. 4 (2002) 690–694.
- [17] Z.H. Guo, S.J. Dong, Anal. Chem. 76 (2004) 2683–2688.
- [18] J. Wang, M. Musameh, Y.H. Lin, J. Am. Chem. Soc. 125 (2003) 2408–2409.
- [19] T. Mahasiko, Y. Kenji, N. Taketoshi, J. Agric. Food Chem. 52 (2004) 727–735.
- [20] A. De Kok, M. Hiemstra, C.P. Vreeker, Chromatographia 24 (1987) 469–476.
- [21] N. Zhou, X.Q. He, W.B. Xu, Chin. J. Anal. Chem. 23 (2) (1995) 237.
- [22] B. Sara, C. Roberta, D.C. Antonio, N. Manuela, T. Davide, J. Agric. Food Chem. 52 (2004) 665–671.
- [23] H.Y. Wang, G.B. Xu, S.J. Dong, Anal. Chem. Acta 480 (2003) 285–290.
- [24] S.C. Tsang, Y.K. Chen, P.J.F. Harris, M.L.H. Green, Nature 372 (1994) 159–162.
- [25] P.J. Britto, K.S.V. Santhanam, P.M. Ajayan, Bioelectrochem. Bioenerg. 41 (1996) 121–125.

Determination of lead in environmental water by a backward light scattering technique

Ke Jun Tan, Cheng Zhi Huang*, Yu Ming Huang

College of Chemistry and Chemical Engineering, Southwest University, Chongqing 400715, PR China

Received 23 October 2005; received in revised form 7 December 2005; accepted 12 December 2005

Available online 18 January 2006

Abstract

An optical fiber assembly developed in our laboratory, which is based on detecting backward light scattering (BLS) signals, is now applied to detect the lead content in environmental samples. Due to effectively eliminating the interference of reflected light, this BLS signals based detection assembly can be used to determine analyte directly. In HAc–NaAc buffer medium (pH 4.8), the interaction of lead and sodium tetraphenylboron (TPB) in the presence of polyethylene glycol (PEG) yields large particles of ternary complex, resulting in strong enhanced backward light scattering (BLS) signals characterized at 371 nm. By measuring the BLS signals with the homemade optical fiber assembly coupled with a common spectrofluorometer, we found that the enhanced BLS intensity is proportional to lead content over the range of 0.03–1.0 $\mu\text{g ml}^{-1}$ with the limit of determination (LOD) of 2.6 ng ml^{-1} . Three artificial water samples containing various coexistent substances were detected with the recovery of 90.1–107.5%. Standard addition method was used to detect the lead content in drink tap water, and found that the lead is hardly to detect due to too low content. Prior enrichment should be made in order to detect river water samples, and it was found that the content of lead in Jialing River at Bebei Dock is about 14 ng ml^{-1} , identical to the results using inductively coupled plasma atomic emission spectrometry (ICP-AES).

© 2005 Published by Elsevier B.V.

Keywords: Backward light scattering (BLS); Lead; Environmental analysis

1. Introduction

Recent studies of resonance light scattering (RLS) have led to widespread interests as a simple, sensitive and cost-effective alternative for quantitative analysis in biochemical, pharmaceutical and environmental applications since it has become extensively applicable in the quantification of nucleic acids [1–4], proteins [5,6], metallic ions [7], surfactant [8,9] and drugs [10,11], etc. Coupled with total internal reflected at liquid/liquid interface, the RLS technique has much improved in terms of sensitivity and selectivity [12–15]. By imaging single particle, RLS imaging technique has been applied successfully for the determination of proteins based on the aggregation of organic dyes [16]. These measurements of light scattering signals, however, are based on detecting the signals at right angle, and the scattered light both in forward and backward, which are much stronger than that at right angle, have been neglected

for analytical purposes according to the Rayleigh scattering law [17,18].

The scattered light intensity by a spherical particle illuminated by a monochromatic light beam can be expressed as [17,18],

$$I = \frac{8\pi^4 r^6 n_{\text{med}}^4 I_0}{d^2 \lambda_0^4} \left| \frac{m^2 - 1}{m^2 + 2} \right|^2 (1 + \cos^2 \beta) \quad (1)$$

where r is the particle radius, n_{med} the refractive index of the medium surrounding the particle, I_0 the intensity of incident monochromatic light, d the distance between the particle and the position where the scattered light is detected, m the relative refractive index of the bulk particle material and β is scattering angle which is decided by the detection direction and the forward direction of the incident beam. That is, light scattering properties of a particle depend on size, composition, shape, homogeneity, bathing medium refractive index, and the scattering angle. Considering the scattering angle, Eq. (1) could be written concisely as

$$I = K(1 + \cos^2 \beta) \quad (2)$$

* Corresponding author. Tel.: +86 2368254659; fax: +86 2368254000.
E-mail address: chengzhi@swu.edu.cn (C.Z. Huang).

where

$$K = \frac{8\pi^4 r^6 n_{\text{med}}^4 I_0}{d^2 \lambda_0^4} \left| \frac{m^2 - 1}{m^2 + 2} \right|^2 \quad (3)$$

which is a constant related to the intensity of the incident beam and the refractive index of medium. As Eq. (2) demonstrates, the scattered light intensity is greatly dependent on the scattering angle β . The scattered light intensity (I) is two times greater in the forward direction ($\beta = 0^\circ$) or backward direction ($\beta = 180^\circ$) than that at right angles to the incident beam ($\beta = 90^\circ$).

Backward light scattering (BLS) spectroscopy is widely used in biomedical and physical sciences. It has been demonstrated that BLS can provide structural and functional information about the tissue, such as the size distribution and density of epithelial nuclei [19,20]. The BLS signals coupled with biomedical imaging has been used to probe the structure of living epithelial cells in situ exempting the experimental procedures of tissue preparation or removal [21]. Backman reported an optical probe technique based on BLS spectroscopy that is able to detect pre-cancerous and early cancerous changes in cell-rich epithelia [22]. BLS signals, however, was not used to direct quantification for analytical purpose for the interference of reflected light. In our former reports, we have proved that detecting BSL signals could result high sensitivity in the detection of nucleic acids and proteins [23]. Later on, we make an optical assembly based on BLS signals detections [24], which can effectively eliminate the interference of reflected light by adjusting the height of solution surface and the incident angle θ , resulting in the scattering signals of analyte that could be measured distinctly. By coupling common spectrofluorometer with our above homemade BLS optical assembly, we herein developed a BLS technique by simultaneously scanning the excitation and emission monochromator of the spectrofluorometer without wavelength difference of the two monochromator. Since the interference of reflected light was eliminated effectively, the scattering signals of analyte could be measured distinctly, and result in a high sensitivity of analyte.

Lead is a common environmental contaminant. Low-level lead exposure can lead to a number of adverse health effects [25]. In the past few years, it has witnessed a large number of reports on the detection of lead ions [26–34]. This research interest is strongly related to the analytical significance of trace lead ion found in environmental and biological processes. Current methods for lead detection, such as atomic absorption spectrometry [35–37], inductively coupled plasma mass spectrometry [38–40], and anodic stripping voltammetry [41,42], often require sophisticated equipment or suffer from narrow linear range. Simple and inexpensive determination methods of Pb ion are important in the fields of environmental monitoring, clinical toxicology, wastewater treatment, and industrial process monitoring. In order to identify the applications, we apply our homemade BLS assembly in this work to detect the lead content in water with a limit of detection of 2.6 ng ml^{-1} and R.S.D. of 3.7%.

2. Experimental

2.1. Apparatus

BLS spectra and intensities measurements were conducted on a Hitachi F-2500 spectrofluorometer (Tokyo, Japan) coupled with our homemade optical fiber assembly (Fig. 1 illustrates the setup) by simultaneously scanning the excitation and emission monochromator of the spectrofluorometer with $\Delta\lambda = 0$. pH values were measured with a pH-3C pH meter (Shanghai, China). An MVS-1 vortex mixer (Beide Scientific Instrumental Ltd., Beijing, China) was used to blend the solutions.

For comparison, TPS-7000 ICP single track scanning emission spectrometer (Purkinje General Instrument Co., Ltd., Beijing) was used to determine lead contents in river water samples with the instrumental parameters of 40 MHz frequency of the high-frequency generator, 1 kW incident power, 10 mm observe height, 6501 h^{-1} plasma gas (Ar) flow rate, 101 h^{-1} auxiliary gas (Ar) flow rate, 6501 h^{-1} coolant gas (Ar) flow rate, 0.1 s integral time, 5 number of replicates, 650 V negative high voltage, 0.2 MPa carrier gas (Ar) pressure, and 0.0012 nm step distance.

2.2. Reagents

$5.0 \times 10^{-3} \text{ mol l}^{-1}$ working solution of sodium tetraphenylboron (TPB, Shanghai Chemical Reagent Co., Ltd., 99.0%) and polyethylene glycol with the average molecular mass of 570–660 (PEG 600, Shanghai Chemical Reagent Purchasing Station, Shanghai) are prepared by dissolving the commercial products in doubly distilled water.

HAc–NaAc buffer solutions were used to control the acidity of the aqueous solutions. Working solution of lead was $18 \mu\text{g ml}^{-1}$ and was prepared by dissolving lead nitrate (Beibei Chemical Reagent Factory, Chongqing) in doubly distilled water. All reagents were of analytical reagent grade without further purification. Doubly distilled water was used throughout.

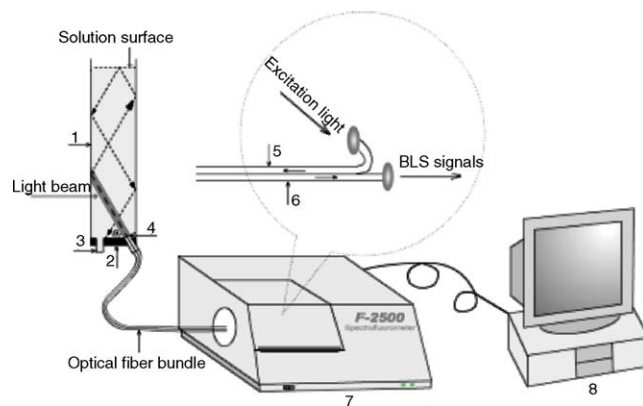


Fig. 1. Backward light scattering signals detection system. 1, Optical probe; 2, pedestal; 3, leaking orifice; 4, optical fiber entrance; 5, optical fiber for excitation light transmission; 6, optical fiber for BLS signals transmission; 7, F-2500 spectrofluorometer; 8, computer.

2.3. Sample pretreatments

In order to enrich and separate lead in the water sample, absorbent cotton was employed. The pretreatment of the absorbent cotton was mainly according to ref. [43]. At first, absorbent cotton was dried for 1 h in a 30 °C electrothermal incubator and stored in desiccator for the preparation of sulfhydryl cotton. Prior place 20 ml of thioglycolic acid in 500-ml wide-necked bottle, and add in turn 12 ml of acetic anhydride, 8 ml of acetic acid, and two drops of concentrated sulfuric acid, then immediately mixed uniformly. After that, 4 g prior prepared absorbent cotton was added and soaked for 16 h at 70–80 °C in thermostatted chamber. After taking the wide-necked bottle out and cooling to room temperature, washed the cotton with water to neutrality, spread it out on filter paper and dried it at 40–50 °C in electro thermal incubator for 1 h. The treated absorbent cotton was stored in brown bottle for later use.

Separation and enrichment of sample were conducted according to ref. [44]. One thousand milliliters of water sample was filtered two times with 0.15 μm filter paper and then the pH was adjusted the to 5.5 with diluted hydrochloric acid. After that, the lead should be enriched by sulfhydryl cotton column with a 2 ml min^{-1} flow speed. Lead was eluted from sulfhydryl cotton by 10 ml 1 mol l^{-1} hydrochloric acid and then heated at 70 °C in thermostatted chamber for 1 h to drive redundant hydrochloric acid off and then diluted to 10 ml with doubly distilled water and mixed. Concentrated by 100 times enrichment lead sample was obtained.

2.4. Procedure

Appropriate volume of sample or working solution of lead nitrate was placed in a 25-ml volumetric flask, and then 2.0 ml of buffer solution (pH 4.8) was added. After vortexed, 0.50 ml of PEG working solution was added. The mixture was vortexed again, and 1.0 ml of TPB working solution was added. After vortexed once more, the mixture was diluted to 25 ml with doubly distilled water and mixed thoroughly, then transferred into our homemade BLS optical assembly that was coupled to F-2500 spectrofluorometer. The BLS spectra were obtained by scanning simultaneously the excitation and emission monochromators of the spectrofluorometer from 300 to 600 nm with $\lambda_{\text{ex}} = \lambda_{\text{em}}$, using a slit width of 10.0 nm for both excitation and emission monochromator.

3. Results and discussion

3.1. Spectral characteristics of the interaction

In order to detect effectively the BLS signals, we designed an optical assembly as displayed in Fig. 1. Optical probe 1 is a hard-glass cylinder, and on its pedestal 2 a leaking orifice 3 being made so that waste solution could be flow out. Excited incident light beam from light source Xe lamp of spectrofluorometer transmits through optical fiber 5 to solution. The BLS signals produced from the particles in the solution under the excitation of the incident light beam could be collected and reach to the

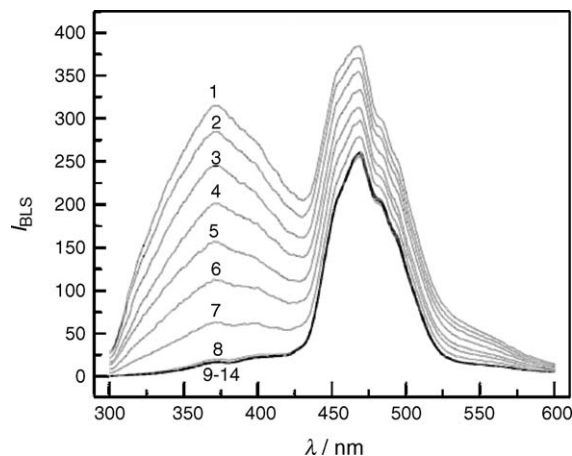


Fig. 2. BLS spectra of Pb^{2+} -PEG-TPB. Curves 1–8: Pb^{2+} -PEG-TPB; 9, Pb^{2+} ; 10, PEG; 11, Pb^{2+} -PEG; 12, TPB; 13, Pb^{2+} -TPB, 14, TPB-PEG, c_{PEG} ($\times 10^{-4} \text{ mol l}^{-1}$): 1–8, 1.0; 9, 0; 10, 4.0; 11, 1.0; 12, 0; 13, 0; 14, 1.0; c_{TPB} ($\times 10^{-4} \text{ mol l}^{-1}$): 1–8, 2.0; 9, 0; 10, 0; 11, 0; 12, 8.0; 13, 2.0; 14, 2.0; $c_{\text{Pb}^{2+}}$ (ng ml^{-1}): 1, 1008; 2, 864; 3, 720; 4, 576; 5, 432; 6, 288; 7, 144; 8, 0; 9, 3600; 10, 0; 11, 3600; 12, 0; 13, 3600; 14, 0. pH 4.8; $\lambda = 371 \text{ nm}$.

PMT detection element of the spectrofluorometer through the light transmission of the optical fiber 6.

Fig. 2 displays the BLS spectral features of Pb^{2+} , PEG, TPB, Pb^{2+} -PEG, Pb^{2+} -TPB, TPB-PEG and Pb^{2+} -PEG-TPB. It can be seen that the BLS signals of Pb^{2+} , PEG, TPB, Pb^{2+} -PEG, Pb^{2+} -TPB, TPB-PEG have a characteristic at 469 nm, which should be ascribed to the strong emission of Xe lamp [45]. A new characteristic band at 371 nm could be observed concerning the ternary complex of Pb^{2+} -PEG-TPB, and the BLS intensity (I_{BLS}) at this wavelength gets increased with increasing lead concentration. This can be due to the formation of ternary complex since TPB can combine with Pb^{2+} , and Pb^{2+} can interact with PEG by electrostatic attraction, resulting in the formation of large particles of ternary complex. As shown in Fig. 2, there are two peaks in BLS spectra from 300 to 600 nm, but that at 371 nm is very sensitive with the increasing of lead concentration comparing with that at 469 nm. So all BLS signals were measured at 371 nm in order to determine lead content in this test.

3.2. Optimization of analytical procedure

Fig. 3 shows the pH effects on the I_{BLS} of ternary complex Pb^{2+} -PEG-TPB. The I_{BLS} of Pb^{2+} -PEG-TPB varies a very little over the pH range of 3.6–5.6 in HAc–NaAc medium, while that of Pb^{2+} -PEG-TPB dropped sharply out of this range. Selecting pH 4.8 as the optimal acidity in this test controlled using 2.0 ml buffer.

Effects of the PEG concentrations on the I_{BLS} of the ternary complex of Pb^{2+} with PEG and sodium tetraphenylborate were investigated. As Fig. 4 shows, the I_{BLS} of Pb^{2+} -PEG-TPB gets increased with increasing PEG content, indicating that PEG participates the formation of ternary complex. I_{BLS} of Pb^{2+} -PEG-TPB get increased sharply when the concentration of PEG initially get increased $0.3 \times 10^{-4} \text{ mol l}^{-1}$. When c_{PEG}

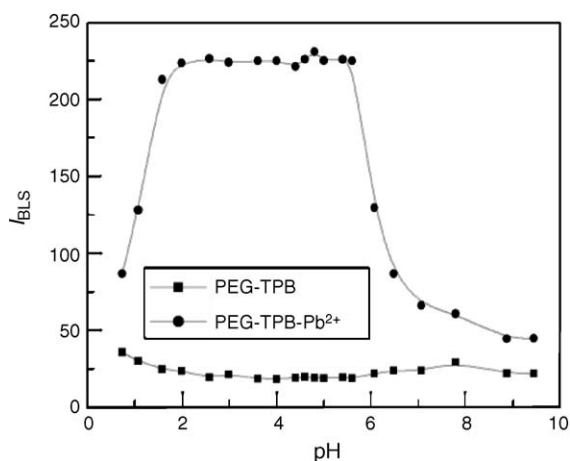


Fig. 3. Dependence of I_{BLS} on pH of the medium. c_{PEG} : $1.0 \times 10^{-4} \text{ mol l}^{-1}$; c_{TPB} , $2 \times 10^{-4} \text{ mol l}^{-1}$; $c_{Pb^{2+}}$, 720 ng ml^{-1} ; $\lambda = 371 \text{ nm}$.

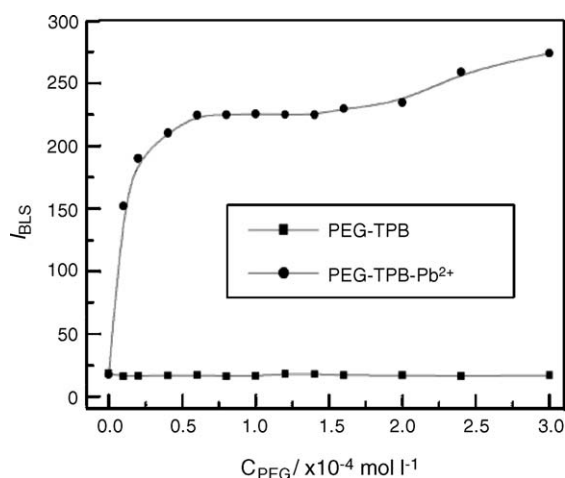


Fig. 4. Dependence of I_{BLS} on the PEG concentrations. c_{TPB} : $2.0 \times 10^{-4} \text{ mol l}^{-1}$; $c_{Pb^{2+}}$, 720 ng ml^{-1} . pH 4.8; $\lambda = 371 \text{ nm}$.

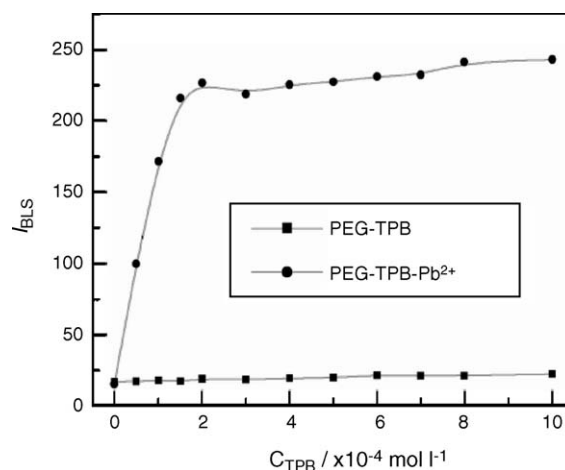


Fig. 5. Dependence of I_{BLS} on TPB concentrations. c_{PEG} , $1.0 \times 10^{-4} \text{ mol l}^{-1}$; $c_{Pb^{2+}}$, 720 ng ml^{-1} . pH 4.8; $\lambda = 371 \text{ nm}$.

is $0.6 \times 10^{-4} \text{ mol l}^{-1}$, I_{BLS} gets the maximum. If c_{PEG} is further increased until $1.4 \times 10^{-4} \text{ mol l}^{-1}$, the I_{BLS} was almost a constant, and if over $1.4 \times 10^{-4} \text{ mol l}^{-1}$, the I_{BLS} gets increase again. The experimental results indicated that PEG serves as both a component to form ternary complex and a reagent to stabilize the system.

Fig. 5 shows that effects of the TPB concentrations on the formation of ternary complex of Pb^{2+} with PEG and sodium tetraphenylborate. No enhanced BLS signals could be observed without TPB addition. When c_{TPB} gets increased to $2.0 \times 10^{-4} \text{ mol l}^{-1}$, the BLS intensity gets increased sharply and then I_{BLS} being a constant with continue addition of TPB.

3.3. Tolerance of coexisting foreign substances

Given a tolerance level of 10%, the influences of coexisting foreign substances including common metal ions, sugars and surfactants have been examined and listed in Table 1. Metal

Table 1
Tolerance levels of coexisting foreign substances

Foreign substances	Concentration ($\mu\text{g ml}^{-1}$)	Change of I_{BLS} , (%)	Foreign Substances	Concentration ($\mu\text{g ml}^{-1}$)	Change of I_{BLS} , (%)
$\text{Na}^+ (\text{Cl}^-)$	4600	0.6	$\text{Eu}^{3+} (\text{Cl}^-)$	0.061	4.7
$\text{Mg}^{2+} (\text{Cl}^-)$	48.62	2.6	$\text{Ba}^{2+} (\text{Cl}^-)$	0.06	10.3
$\text{Cd}^{2+} (\text{Cl}^-)$	44.96	−8.1	$\text{Al}^{3+} (\text{K}^+, \text{SO}_4^{2-})$	0.03	−0.2
$\text{Ni}^{2+} (\text{Cl}^-)$	40	−5.2	$\text{Cl}^- (\text{Na}^+)$	7100	0.6
$\text{K}^+ (\text{Cl}^-)$	15.6	−0.7	$\text{NO}_3^- (\text{Na}^+)$	1240	0.4
$\text{Cu}^{2+} (\text{SO}_4^{2-})$	12.71	−6.8	$\text{SO}_4^{2-} (\text{Na}^+)$	576	−2.4
$\text{Zn}^{2+} (\text{NO}_3^-)$	10.71	−3.8	$\text{F}^- (\text{Na}^+)$	0.76	2.6
$\text{Cr}^{3+} (\text{Cl}^-)$	8.32	6.4	$\text{PO}_4^{3-} (\text{Na}^+)$	0.30	−0.3
$\text{La}^{3+} (\text{NO}_3^-)$	2.78	−2.4	Citric acid	3.36	4.2
$\text{Co}^{2+} (\text{Ac}^-)$	2.36	−1.6	EDTA	0.09	−8.0
$\text{Ca}^{2+} (\text{Cl}^-)$	1.6	7.4	Glycerin	400	−3.3
$\text{Hg}^{2+} (\text{Cl}^-)$	1.48	7.3	Lactose ^a	40	6.7
$\text{Fe}^{3+} (\text{SO}_4^{2-})$	1.12	3.2	Tween 80	0.64	9.9
$\text{NH}_4^+ (\text{Cl}^-)$	1.8	3.6	SLS	1.15	0.4
$\text{Se}^{4+} (\text{Cl}^-)$	0.40	0.8	SDBS	0.70	−3.7
$\text{Ag}^+ (\text{NO}_3^-)$	0.32	9.0			

^a $\times 10^{-6} \text{ mol l}^{-1}$. $c_{Pb^{2+}}$: $0.36 \mu\text{g ml}^{-1}$, c_{PEG} , $1.0 \times 10^{-4} \text{ mol l}^{-1}$; c_{TPB} , $2.0 \times 10^{-4} \text{ mol l}^{-1}$. pH 4.8; $\lambda = 371 \text{ nm}$.

Table 2
Analytical parameters

TPB ^a	Linear regression equation c ($\mu\text{g ml}^{-1}$)	Linear range ($\mu\text{g ml}^{-1}$)	Correlation coefficient (r)	LOD (ng ml^{-1})
2.0	$\Delta I = 6.05 + 300.5c$	0.03–1.0	0.9984	2.6
4.0	$\Delta I = 28.17 + 231.6c$	0.06–1.8	0.9915	6.2

^a TPB concentration is expressed as $\times 10^{-4} \text{ mol l}^{-1}$. c_{PEG} , $1.0 \times 10^{-4} \text{ mol l}^{-1}$, pH 4.8; $\lambda = 371 \text{ nm}$.

Table 3
Determination results for artificial samples

Sample	Main interferences ^a	Found ^{b,c} (ng ml^{-1})	Recovery range ^c (%)	R.S.D. ^c (%)
1	Cd^{2+} , Ni^{2+} , Zn^{2+} , glycerin	173.5	90.1–102.0	4.9
2	La^{3+} , Ni^{2+} , K^{+}	186.1	99.4–107.5	3.2
3	Cr^{3+} , Se^{4+} , Ca^{2+} , Eu^{3+} , lactose	178.4	97.5–103.8	2.6

^a Concentrations ($\mu\text{g ml}^{-1}$): Cd^{2+} , 4.5; Ni^{2+} , 2.0; Zn^{2+} , 1.1; La^{3+} , 1.4; K^{+} , 7.8; Cr^{3+} , 1.7×10^{-2} ; Se^{4+} , 1.0×10^{-2} ; Ca^{2+} , 1.6×10^{-2} ; Eu^{3+} , 3.0×10^{-3} ; glycerin, 40; lactose, 18.

^b The desirous value of $c_{\text{Pb}^{2+}}$ is 180 ng ml^{-1} .

^c The results were obtained from five measurements. c_{PEG} , $1.0 \times 10^{-4} \text{ mol l}^{-1}$; c_{TPB} , $2.0 \times 10^{-4} \text{ mol l}^{-1}$. pH 4.8; $\lambda = 371 \text{ nm}$.

ions such as Na^{+} , Ni^{2+} , Mg^{2+} and Cd^{2+} can be allowed at very high concentration. Especially, Na^{+} could be allowed at $4600 \mu\text{g ml}^{-1}$, and glycerin could be allowed $400 \mu\text{g ml}^{-1}$. On the contrary, some cation and anion were allowed at very lower concentration levels. Owing to combine with TPB, K^{+} can be allowed only $15.6 \mu\text{g ml}^{-1}$, while EDTA, PO_4^{3-} and citric acid can be allowed a very lower concentration levels due to combining with lead. Therefore, for a simple sample, lead can be

determined directly. For sophisticated sample, however, all interferences of coexisting foreign substances could be eliminated by separation and enrichment of lead with sulphhydryl cotton.

3.4. Calibration curve and sample detection

Under the optimum condition defined, the relationships of I_{BLS} and the concentration of lead were investigated. The analytical parameters for the determination of lead were shown in Table 2. Experiments showed that the linear ranges and the sensitivities of lead were affected by the concentration of TPB. The linear ranges were extended with increasing the TPB concentration, but the limit of detection gets higher accordingly.

To test the present assay, artificial samples, tap water and river water were detected. Three artificial samples containing metal ions, glycerin and lactose were determined, and the results were given in Table 3. It can be seen that the recovery ranges from 90.1 to 107.5%, and R.S.D. is lower than 4.9%. While three tap water samples, taking from our laboratory, were determined without any pretreatment and the recovery tests were also conducted (Table 4). The recoveries of standard addition are in the range of 95.0–105.1% with the R.S.D. lower than 3.7%. The results in Table 4 indicate that lead is hardly detected in the tap water due to its too low content. In such case, we considered detecting two environmental samples. Sampling from Jialing River in Beibei Dock flow region, two real samples separated and enriched with the sulphhydryl cotton considering that serious interference to the lead determination and too lower concentration level of lead in samples [43,44]. As Table 5 shows, the detection results by BLS method were in identical to that with ICP-AES values. The relative standard deviation is less than 3.7%. Compared to the results of ICP-AES assay, the results of this method seems much more satisfactory.

Table 4
The recoveries of standard addition of lead in tap water

Sample ^a	Found ($n = 5$, ng ml^{-1})	Average ($n = 5$, ng ml^{-1})	R.S.D. (%)	Recovery (%)
1	176.4, 180.2, 175.0, 189.2, 188.7	181.9	3.7	98.0, 100.1, 97.2, 105.1, 104.8
2	178.9, 170.9, 183.3, 181.2, 175.0	177.9	2.8	99.4, 95.0, 101.8, 100.7, 97.2
3	179.4, 181.4, 183.9, 187.9, 181.9	182.9	1.8	99.7, 100.8, 102.2, 104.4, 101.0

^a Lead concentrations of all three tap water samples are hardly detected by the present BLS method without separation and enrichment. The concentration of added Pb^{2+} is 180 ng ml^{-1} . c_{PEG} : $1 \times 10^{-4} \text{ mol l}^{-1}$; c_{TPB} : $2 \times 10^{-4} \text{ mol l}^{-1}$. pH 4.8; $\lambda = 371 \text{ nm}$.

Table 5
Determination of lead in environmental samples

Sample	Present BLS assay ^a		R.S.D. (% , $n = 5$)	ICP-AES assay ^b	
	Found (ng ml^{-1})	Average ($n = 5$, ng ml^{-1})		Found (ng ml^{-1})	R.S.D. (% , $n = 5$)
1	15.8, 15.3, 15.7, 14.4, 15.8	15.4	3.7	13.0	3.4
2	13.0, 14.3, 13.6, 13.5, 13.8	13.6	3.6	12.0	1.7

The environmental water samples were taking from Jialing River at Beibei Dock.

^a c_{PEG} , $1.0 \times 10^{-4} \text{ mol l}^{-1}$; c_{TPB} , $2.0 \times 10^{-4} \text{ mol l}^{-1}$. pH 4.8; $\lambda = 371 \text{ nm}$.

^b $\lambda = 220.353 \text{ nm}$, step distance: 0.0012 nm , number of replicates: five.

4. Conclusion

Lead in environmental water was determined sensitively with present BLS method. It can be seen that this proposed BLS detection assembly is a simple, and has a high sensitivity. We believe that the BLS detection assembly, if combining to a laser light source, will become more sensitive and sufficiently general for various biochemical, pharmaceutical and environmental analysis. Considering that BLS could serve as a new principle to construct a sensitive light scattering detector, which may be applied to analytical chemistry, environmental chemistry, biochemistry and medicine fields, it is reasonable to expect that BLS technique should be widely applicable and worthy of further exploration.

Acknowledgments

We thank the National Natural Science Foundation of China (NSFC, 20425517) and the Municipal Science and Technology Committee of Chongqing.

References

- [1] C.Z. Huang, K.A. Li, S.Y. Tong, *Anal. Chem.* 68 (1996) 2259.
- [2] C.Z. Huang, K.A. Li, S.Y. Tong, *Anal. Chem.* 69 (1997) 514.
- [3] Z.P. Li, K.A. Li, S.Y. Tong, *Talanta* 55 (2001) 669.
- [4] X.Y. Du, S. Sasaki, H. Nakamura, I. Karube, *Talanta* 55 (2001) 93.
- [5] C.Z. Huang, Y.F. Li, J.G. Mao, D.G. Tan, *Analyst* 123 (1998) 1401.
- [6] H. Zhong, J.J. Xu, H.Y. Chen, *Talanta* 67 (2005) 749.
- [7] Y.K. Zhao, Q.E. Cao, Z.D. Hu, Q.H. Xu, *Anal. Chim. Acta* 388 (1999) 45.
- [8] C.X. Yang, Y.F. Li, C.Z. Huang, *Anal. Bioanal. Chem.* 374 (2002) 868.
- [9] Z. Yang, Z.F. Liu, S.P. Liu, H.Q. Luo, L. Kong, *J. Southwest Norm. Univ. (Nat. Sci. Ed.)* 29 (2004) 773.
- [10] S.P. Liu, H.Q. Luo, N.B. Li, Z.F. Liu, W.X. Zheng, *Anal. Chem.* 73 (2001) 3907.
- [11] L. Kong, S.P. Liu, X.J. Zhou, *J. Southwest Norm. Univ. (Nat. Sci. Ed.)* 28 (2003) 252.
- [12] P. Feng, W.Q. Shu, C.Z. Huang, Y.F. Li, *Anal. Chem.* 73 (2001) 4307.
- [13] P. Feng, C.Z. Huang, Y.F. Li, *Anal. Biochem.* 308 (2002) 83.
- [14] W. Lu, C.Z. Huang, Y.F. Li, *Analyst* 27 (2002) 1392.
- [15] W. Lu, C.Z. Huang, Y.F. Li, *Anal. Chim. Acta* 475 (2003) 151.
- [16] C.Z. Huang, Y. Liu, Y.H. Wang, H.P. Guo, *Anal. Biochem.* 321 (2003) 236.
- [17] J. Yguerabide, E.E. Yguerabide, *Anal. Biochem.* 262 (1998) 137.
- [18] J. Yguerabide, E.E. Yguerabide, *Anal. Biochem.* 262 (1998) 157.
- [19] J.R. Mourant, I.J. Bigio, J. Boyer, R.L. Conn, T. Johnson, T. Shimada, *Laser Surg. Med.* 17 (1995) 350.
- [20] L.T. Perelman, V. Backman, M. Wallace, G. Zonios, R. Manoharan, A. Nusrat, S. Shields, M. Seiler, C. Lima, T. Hamano, I. Itzkan, J. Van Dam, J.M. Crawford, M.S. Feld, *Phys. Rev. Lett.* 80 (1998) 627.
- [21] R. Gurjar, V. Backman, L.T. Perelman, I. Georgakoudi, K. Badizadegan, I. Itzkan, R.R. Dasari, M.S. Feld, *Nat. Med.* 7 (2001) 1245.
- [22] V. Backman, M.B. Wallace, L.T. Perelman, J.T. Arendt, R. Gurjar, M.G. Müller, Q. Zhang, G. Zonios, E. Kline, T. McGillican, S. Shapshay, T. Valdez, K. Badizadegan, J.M. Crawford, M. Fitzmaurice, S. Kabani, H.S. Levin, M. Seiler, R.R. Dasari, I. Itzkan, J. Van Dam, M.S. Feld, *Nature* 406 (2000) 35.
- [23] Y.H. Wang, H.P. Guo, K.J. Tan, C.Z. Huang, *Anal. Chim. Acta* 521 (2004) 109.
- [24] C.Z. Huang, K.J. Tan, *PR China Patent* 200510020225.4, 2005.
- [25] H.L. Needleman, *Human Lead Exposure*, CRC Press, Boca Raton, FL, 1992.
- [26] S. Deo, H.A. Godwin, *J. Am. Chem. Soc.* 122 (2000) 174.
- [27] C.T. Chen, W.P. Huang, *J. Am. Chem. Soc.* 124 (2002) 6246.
- [28] J. Li, Y. Lu, *J. Am. Chem. Soc.* 122 (2000) 10466.
- [29] T. Hayashita, D. Qing, M. Minagawa, J.C. Lee, C.H. Ku, N. Teramae, *Chem. Commun.* 17 (2003) 2160.
- [30] M. Telting-Diaz, E. Bakker, *Anal. Chem.* 74 (2002) 5251.
- [31] T. Pan, O.C. Uhlenbeck, *Nature* 358 (1992) 560.
- [32] W.S. Xia, R.H. Schmehl, C.J. Li, J.T. Mague, C.P. Luo, D.M. Guldi, *J. Phys. Chem. B* 106 (2002) 833.
- [33] A.S. Templeton, T.P. Trainor, S.J. Traina, A.M. Spormann, G.E. Brown Jr., *Proc. Natl. Acad. Sci. U.S.A.* 98 (2001) 11897.
- [34] J. Liu, Y. Lu, *Chem. Mater.* 16 (2004) 3231.
- [35] D.I. Bannon, C. Murashchik, C.R. Zapf, M.R. Farfel, J.J. Chisolm Jr., *Clin. Chem.* 40 (1994) 1730.
- [36] J.E. Tahan, V.A. Granadillo, R.A. Romero, *Anal. Chim. Acta* 295 (1994) 187.
- [37] O. Acar, *Talanta* 65 (2005) 672.
- [38] S.K. Aggarwal, M. Kinter, D.A. Herold, *Clin. Chem.* 40 (1994) 1494.
- [39] H.W. Liu, S.J. Jiang, S.H. Liu, *Spectrochim. Acta B* 54 (1999) 1367.
- [40] H.M. Al-Swaidan, *Talanta* 43 (1996) 1313.
- [41] B.J. Feldman, J.D. Osterloh, B.H. Hata, A. D'Alessandro, *Anal. Chem.* 66 (1994) 1983.
- [42] P.J.S. Barbeira, N.R. Stradiotto, *Talanta* 44 (1997) 185.
- [43] H.Y. Du, B. Yang, B.W. Wang, *J. Fushun Pet. Inst.* 15 (1995) 32.
- [44] B.Z. Qiao, Y. Yang, W. Tian, *Chin. J. Health Lab. Tech.* 10 (2000) 425.
- [45] Y.F. Li, C.Z. Huang, X.H. Huang, M. Li, *Anal. Chim. Acta* 429 (2001) 311.

A flow-based enzyme-linked immunosorbent assay on a polydimethylsiloxane microchip for the rapid determination of immunoglobulin A

Hizuru Nakajima^a, Maiko Yagi^a, Yuki Kudo^a,
Tatsuro Nakagama^a, Takuya Shimosaka^b, Katsumi Uchiyama^{a,*}

^a Faculty of Urban Environmental Sciences, Tokyo Metropolitan University, 1-1 Minamiohsawa, Hachioji, Tokyo 192-0397, Japan

^b National Metrology Institute of Japan (NMIJ), National Institute of Advanced Industrial Science and Technology (AIST),
Tsukuba Central 3, Umezono, Tsukuba, Ibaraki 305-8563, Japan

Received 28 October 2005; received in revised form 17 December 2005; accepted 22 December 2005

Available online 10 February 2006

Abstract

A flow-based enzyme-linked immunosorbent assay (ELISA) on a polydimethylsiloxane (PDMS) microchip has been developed for the rapid determination of immunoglobulin A (IgA). The analytical principle of this integrated method is the same as the conventional sandwich-type ELISA. A primary antibody (anti-IgA) was adsorbed on the surface of a PDMS microchannel, and then an antigen (IgA) and a secondary antibody (anti-IgA HRP labeled) were reacted successively. The resulting antigen–antibody complex, fixed on the surface of the microchannel, was detected using Amplex® Red and a fluorescent imaging system. The calibration curve of the IgA standard solution was linear in the range of 0–50 ng/mL at the flow rate of 10 μ L/min. This flow rate corresponds to the reaction time of 4.8 s. Compared to the conventional assay on a 96-well microtiter plate, the present assay on the microchip dramatically shortened the reaction time necessary for the enzyme–substrate reaction from 30 min to 4.8 s, i.e., to 1/375. The amounts of the reagent and sample were also reduced to 1/100 compared to the 96-well microtiter plate.

© 2006 Elsevier B.V. All rights reserved.

Keywords: Microchip; ELISA; Rapid determination; Immunoglobulin A; Saliva; Stress

1. Introduction

It has been reported that the concentration of cortisol [1–7] chromogranin A [7–8] amylase [9] and immunoglobulin A (IgA) [10–12], etc., in human saliva changes with exposure to stress. Therefore, the measurement of these concentrations may allow the objective evaluation of stress. Enzyme-linked immunosorbent assay (ELISA) has been a primary choice for the determination of IgA because of its high selectivity and sensitivity. The conventional ELISA on a 96-well microtiter plate, however, needs a long analysis time and many expensive reagents.

To overcome these drawbacks, the integration of immunoassay into a microchip seems to be effective. The mean diffusion time of a molecule is proportional to the square of the dis-

tance. Therefore, the diffusion time of molecules in a very small microchannel is extremely short. This effect allows for a rapid test in immunoassay [13]. There are many examples of microchip-based immunoassays. For example, Eteshola and Leckband [14] demonstrated the feasibility of ELISA on a microchip. Kitamori and co-workers [15] developed a bead-bed immunoassay system on a microchip and applied it to the determination of human secretory immunoglobulin A and carcinoembryonic antigen for cancer diagnosis [16]. Similarly, Uchiyama et al. [17] evaluated the dioxin toxicity using immunoassay method on a bead-bed microchip. In order to perform a pumpless assay, Lai et al. [18] developed a compact disk-like microfluidic platform and applied ELISA and protein–ligand binding assays [19].

In our previous paper [20] we reported the possibility of ELISA on a microchip for the rapid determination of IgA in human saliva. The analytical principle of this integrated method is the same as the conventional sandwich-type ELISA.

* Corresponding author. Tel.: +81 426 77 2830; fax: +81 426 77 2821.
E-mail address: uchiyama-katsumi@c.metro-u.ac.jp (K. Uchiyama).

In the paper, we showed that the reaction time necessary for an enzyme–substrate reaction was shortened from 30 to 5 min due to size effects of the microchip. However, accurate control of the reaction time was very difficult, which critically affected the reproducibility. On this point, a flow-based integrated system seems to be superior to our previous method because the reaction time can be simply controlled by the flow rate.

In this paper, we report a flow-based analytical system for the rapid determination of IgA, which is based on a sandwich ELISA using a polydimethylsiloxane (PDMS) microchip.

2. Experimental

2.1. Chemicals

All reagents used in this study were of analytical reagent grade, unless otherwise stated. For the chip fabricate, a blank mask plate coated with a thin layer of 50 nm Cr/Cr₂O₃ (DUFR-2506 (p)-L) was obtained from ULVAC Equipment Sales Inc. (Tokyo, Japan). A positive type photoresist (PMER P-RZ300) and developer solution (PMER P-1S) were both obtained from Tokyo Ohka Kogyo (Kawasaki, Japan). Cerium(IV) diammonium nitrate, perchloric acid, nitric acid and hydrofluoric acid were purchased from Wako Pure Chemical Industries (Osaka, Japan). Acetone and ammonium fluoride were obtained from Kanto Chemicals (Tokyo, Japan). PDMS microfluidic devices were fabricated by curing the prepolymer components of Sylgard 184 (Dow Corning, MI, USA) on a template. Human IgA ELISA quantitation kit was obtained from Bethyl Laboratories Inc. (Montgomery, TX, USA). Bovine serum albumin (BSA) was purchased from Calbiochem (San Diego, CA, USA). 10-Acetyl-3,7-dihydroxyphenoxazine (Amplex[®] Red) was obtained from Molecular Probes (Eugene, OR, USA). Hydrochloric acid, hydrogen peroxide solution (30%) and tris(hydroxymethyl)aminomethane were purchased from Wako Pure Chemical Industries (Osaka, Japan). Sodium hydrate, sodium dihydrogenphosphate, disodium hydrogenphosphate, sodium hydrogen carbonate and sodium carbonate were obtained from Kanto Chemicals (Tokyo, Japan). Water was purified on a Milli-Q system (Nihon Millipore, Tokyo, Japan). The Tris buffer was prepared from tris(hydroxymethyl)aminomethane and hydrochloric acid. The phosphate buffer was prepared from dihydrogenphosphate and disodium hydrogenphosphate. The carbonate buffer was prepared from sodium hydrogen carbonate and sodium carbonate. All buffers were filtered through a 0.45 µm membrane filter (JHWPO 4700, Nihon Millipore, Tokyo, Japan) and degassed with an aspirator before use.

2.2. Fabrication of master glass template

The master glass channel template, that is, the mold of the PDMS microchannel was prepared using photolithography and a wet-chemical etching procedure as previously reported [21–24]. Briefly, the blank mask plate was coated with a thin layer of PMER P-RZ300 positive photoresist using a spin coater (K-359 S-1, Kyowa Riken, Japan) at 600 rpm for 2 min, and then

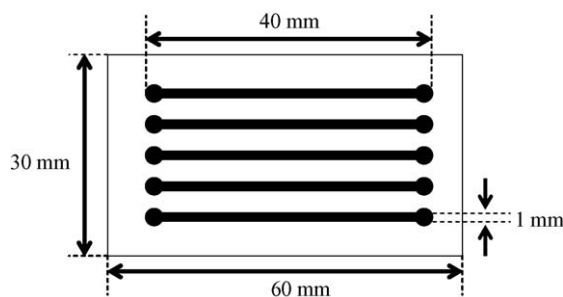


Fig. 1. Design of channel network used to prepare PDMS microchip.

it was baked in an oven at 85 °C for another 15 min. A serpentine channel design (made using Illustrator 10 and printed out on positive film by Kodak Co., Ltd., Tokyo, Japan) (Fig. 1) was transferred onto the mask plate by exposure to a long-wavelength ultraviolet lamp (FL15BLB, Toshiba, Tokyo, Japan) for about 2 min, followed by developing in PMER P-1S solution for about 1 min. The template with the channel design was then further baked at 85 °C for 15 min. The Cr/Cr₂O₃ layer was then removed with a mixture of 17% (w/v) cerium(IV) diammonium nitrate and 5% (v/v) perchloric acid solution to define the channel on the mask plate. After rinsing in 2 M HNO₃ for 5 min, a positive relief channel was obtained by etching the glass in 1 M NH₄F/1 M HF solution using an incubator (SN-M40S, NISSIN, Tokyo, Japan) at 25 °C for 22 min to produce a relief channel height of about 20 µm. After silanizing in 5% (v/v) trimethylchlorosilane/toluene for 24 h at room temperature, the master glass template was kept in a clean box before use.

2.3. Fabrication of PDMS microchip

First, an adhesive cellulose tape was fenced around the glass template and then 10 PEEK tubes (1/16 in. o.d., ca. 10 mm long) were placed on the glass template using water-soluble glue to define the reservoirs. A 10:1 weight mixture of the PDMS prepolymer and curing agent was thoroughly mixed. The mixture was degassed with a vacuum pump and then 3.5 g of the mixture was poured onto the glass template with positive relief to form the channel, while 1.5 mL of the mixture was spin-coated (1000 rpm, 2 min) on a slide glass (76 mm × 52 mm, 0.8–1.0 mm thick, S9111, Matsunami Glass Ind., Ltd, Osaka, Japan). After curing at 60 °C for 1 h, the PDMS mold with negative relief was peeled off and then the two pieces were immediately brought together. The mold was placed in an oven at 120 °C for 4 h for complete bonding. Finally, the 10 PEEK tubes (0.13 mm i.d., 1/16 in. o.d., 50 mm long) were mounted in the device for sample installation and exhaust.

2.4. Apparatus

Fig. 2 shows a schematic diagram of the analysis system used in this study. The system consisted of a microflow pump (MP 680, GL Sciences, Tokyo, Japan), a syringe pump (PHD2000, Harvard Apparatus, Holliston, MA, USA), five 1 mL gastight syringes (Hamilton, Reno, NV, USA), an injection valve (9725, Rheodyne, Cotati, CA, USA) equipped with a 100 µL sample

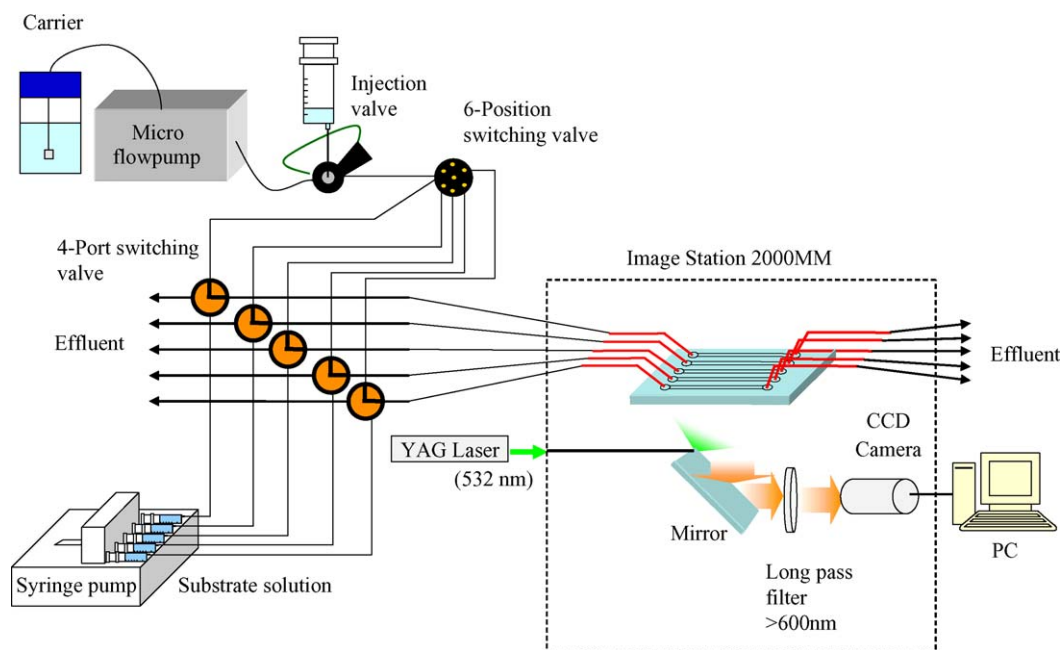


Fig. 2. Schematic diagram of the analysis system.

loop, a six-position switching valve (9060, Rheodyne, Cotati, CA, USA), five 4-port switching valves (V-101L, Upchurch Scientific Inc., Oak Harbor, WA, USA), a fluorescence imaging device (Image Station 2000 MM, Kodak, Rochester, NY, USA) with an IS2000MM filter (em600WA) and a DPSS 532 nm laser (Intelite Inc., Genoa, NV, USA). The data analysis was carried out using 1D image analysis software (KODAK, Rochester, NY, USA) on a PC.

2.5. Flow-based microchip immunoassay

The substrate solution was flowed into the microchannel by the syringe pump, while other solutions were introduced into the microchannel via the injection valve. The carrier solution was a 50 mM Tris–HCl buffer (pH 8.0) containing 0.14 M NaCl. The flow rate of the carrier solution was adjusted to 20 $\mu\text{L}/\text{min}$. The inner walls of all the flow channels between the injection valve and the microchip were washed with 1 M sodium hydrate, water, 1 M hydrochloric acid and water, in that order, and then blocked by a BSA solution (10 mg/mL in 50 mM carbonate buffer (pH 9.6)) for 30 min to prevent non-specific adsorption of the protein, followed by washing with the carrier solution. To clean the inner surface of the microchannel, all the microchannels were washed with 1 M sodium hydrate, water, 1 M hydrochloric acid and water, in that order, before use.

First, the microchannels were filled with the primary antibody solution (20 $\mu\text{g}/\text{mL}$ in 50 mM carbonate buffer (pH 9.6)), and then incubated for 60 min to allow adsorption of the primary antibody onto the surface of the PDMS microchannel. After the incubation, the chip was connected to the apparatus, and then the carrier solution was flushed through the microchannels for 1 min to remove any unadsorbed primary antibody. Next, the BSA solution (10 mg/mL in 50 mM Tris–HCl buffer (pH 8.0) containing 0.14 M NaCl) was introduced into the microchan-

nels, and then the liquid flow was stopped for 30 min to allow blocking of the microchannels. Thereafter, the microchannels were washed with the carrier solution for 2 min to remove any unadsorbed BSA. Next, the antigen standards (0–50 ng/mL in 50 mM Tris–HCl buffer (pH 8.0) containing 0.14 M NaCl and 10 mg/mL BSA) were injected into the individual microchannels, and then the liquid flow was stopped for 60 min to allow the reaction of the primary antibody with the antigen. Thereafter, the microchannels were washed with the carrier solution for 2 min. Next, the secondary antibody (anti-hIgA HRP labeled) solution (100 ng/mL in 50 mM Tris–HCl buffer (pH 8.0) containing 0.14 M NaCl and 10 mg/mL BSA) was introduced into the microchannels, and then the liquid flow was stopped for 60 min to allow the reaction of the primary antigen with the secondary antibody. Thereafter, the microchannels were washed with the carrier solution for 2 min to remove any unreacted secondary antibody. Finally, a substrate solution (0.1 mM Amplex[®] Red containing 2 mM hydrogen peroxide and 0.1 M phosphate buffer (pH 7.4)) was flowed into the microchannels by the syringe pump at the flow rate of 0.1–20 $\mu\text{L}/\text{min}$, and then the enzyme turnover was monitored by the fluorescence imaging system.

3. Results and discussion

3.1. Comparison of enzyme–substrate reaction times on 96-well microtiter plate with that on microchip

All the reactions were performed on the surface of the microchannel. At first, the anti-hIgA was physically adsorbed onto the hydrophobic PDMS surface. The hIgA standard solution was then introduced to complete the immune reaction of the anti-hIgA/hIgA binding on the surface of the microchannel. The complex was then reacted with the second anti-IgA labeled with HRP followed by the introduction of the Amplex[®] Red

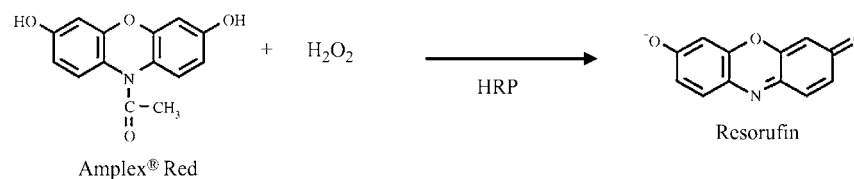


Fig. 3. Chemical structure of Amplex® Red and its conversion to resorufin.

solution using the syringe pumps. The enzyme–substrate reaction was simply achieved by controlling the pumps. As shown in Fig. 3, the Amplex® Red reacts with hydrogen peroxide, in combination with HRP, to produce the highly fluorescent oxidation product, resorufin. The amount of the produced resorufin was measured using the fluorescence imaging device.

The time course of the enzyme–substrate reaction was examined. Figs. 4 and 5 show the time course of the enzyme–substrate reaction using the conventional 96-well microtiter plate assay and microchip assay. In the conventional 96-well microtiter plate assay, the enzyme–substrate reaction was proportional to the reaction time before 1 h and reached equilibrium after 4 h. On the other hand, the enzyme–substrate reaction was proportional to the reaction time before 1.6 min and reached equilibrium after 8 min during the microchip assay. These results indicate that the microchip assay shortens the enzyme–substrate reaction time.

This effect is probably due to an increase in the specific interfacial area and a reduction in the diffusion distance. An increase in the specific interfacial area means that the reaction field increases. The specific interfacial area of the 50 μ L substrate solution in the 96-well microtiter plate (6.5 mm in diameter) was estimated to be 13 cm^{-1} , whereas that of the microchannel (1 mm \times 40 mm \times 20 μ m) was 1020 cm^{-1} . Therefore, the specific interfacial area of the microchannel was 80 times greater than that of the 96-well microtiter plate. The increase in the reaction rate would occur due to the increased reaction field.

In the conventional 96-well microtiter plate assay, the liquid depth was 1.5 mm, whereas that of the microchannel was

20 μ m. Therefore, the diffusion distance in the microchannel was 75 times shorter than that of the 96-well microtiter plate. The mean diffusion time of a molecule is proportional to square of the diffusion distance [13]. Thus, the diffusion time of the substrate and the product molecule in the microchannel would be 5600 times shorter than the conventional 96-well microtiter plate.

3.2. Preparation of calibration curve

We examined the reaction time to prepare the calibration curve of IgA. Fig. 6 shows the time course of enzyme–substrate reaction on the microchip assay. The fluorescence intensity increased with an increase in the reaction time of the enzyme–substrate reaction because the formation of resorufin increases with an increase in the reaction time. Moreover, the fluorescence intensity increased with an increase in the concentration of IgA. A slight increase in the fluorescence intensity from the blank microchannel was also observed. This is due to the self-oxidation of Amplex® Red into resorufin or the non-specific adsorption of the secondary antibody. Fig. 7 and Table 1 show the calibration curve of IgA. The calibration curve of IgA standard solution was linear in the range of 0–50 ng/mL over the reaction time of 4.8 s (under the flow rate of 10 μ L/min). The slope of the calibration curve increased with an increase in the reaction time. However, the relative standard deviation (R.S.D.)

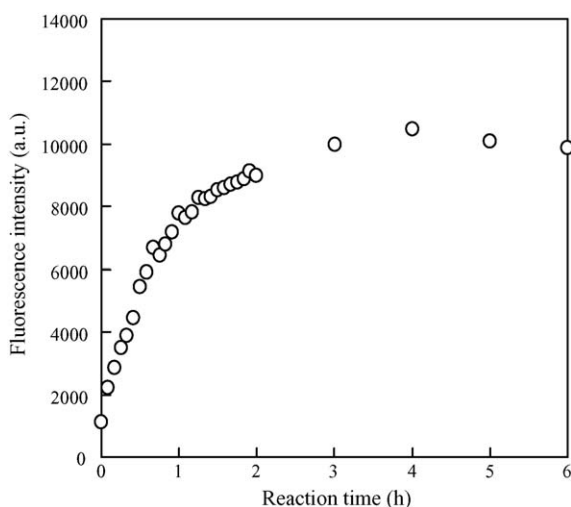


Fig. 4. Time course of enzyme–substrate reaction using conventional 96-well microtiter plate assay. Conditions: IgA concentration, 50 ng/mL; substrate volume, 50 μ L; exposure time, 30 s.

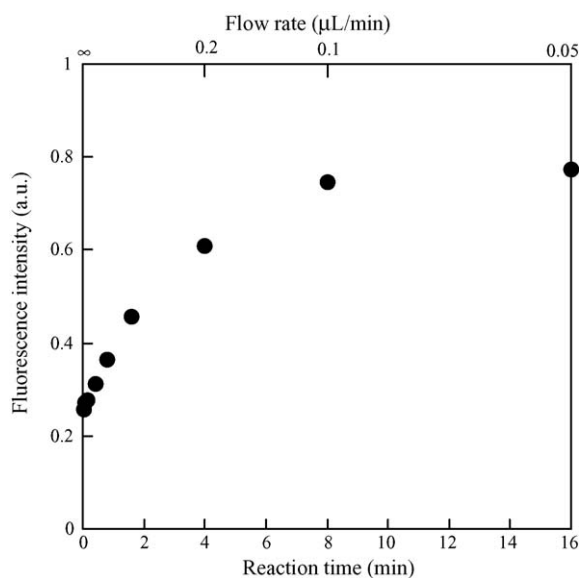


Fig. 5. Time course of enzyme–substrate reaction using microchip assay. Conditions: IgA concentration, 50 ng/mL; substrate volume, 0.8 μ L; exposure time, 90 s.

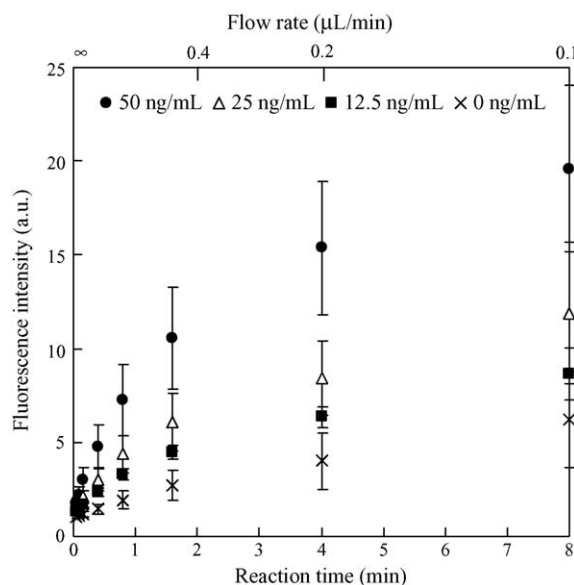


Fig. 6. Time course of enzyme–substrate reaction using microchip assay. Conditions: exposure time, 90 s. The numbers in the figure denote the concentration of IgA.

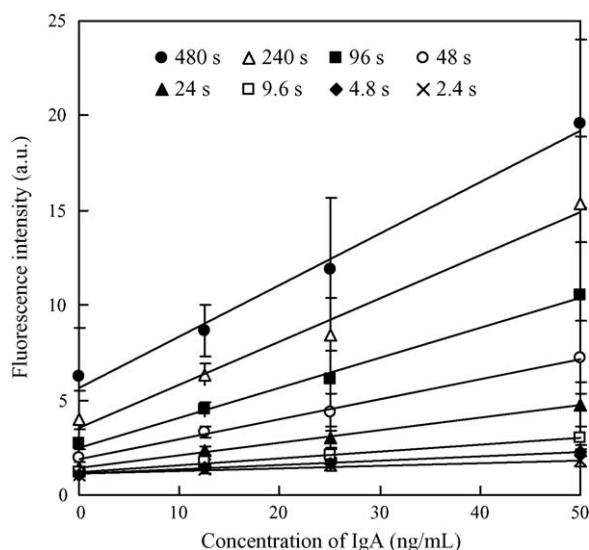


Fig. 7. Calibration curve of IgA. Conditions: exposure time, 90 s. The numbers in the figure denote the reaction time.

Table 1
Calibration curve of IgA

Flow rate (μL/min)	Reaction time (s)	Regression line	Correlation coefficient
0.1	480	$y = 0.2710x + 5.669$	0.9909
0.2	240	$y = 0.2278x + 3.552$	0.9854
0.5	96	$y = 0.1574x + 2.512$	0.9937
1	48	$y = 0.1057x + 1.899$	0.9972
2	24	$y = 0.0656x + 1.462$	0.9980
5	9.6	$y = 0.0366x + 1.208$	0.9982
10	4.8	$y = 0.0229x + 1.101$	0.9966
20	2.4	$y = 0.0141x + 1.133$	0.9322

x: concentration of IgA (ng/mL), y: fluorescence intensity.

value showed high values (20%<) over the reaction time of 24 s (at the flow rate of 2 μL/min).

Based on these results, we decided that the reaction time for the enzyme–substrate reaction was 4.8 s. The conventional assay on a 96-well microtiter plate needs 30 min for the enzyme–substrate reaction [25]. Therefore, this result indicates that the flow-based microchip ELISA shortens the reaction time necessary for the enzyme–substrate reaction by 1/375. The amounts of the reagent and sample were also reduced to 1/100 compared to the conventional 96-well microtiter plate assay.

4. Conclusion

In this paper, we presented a flow-based ELISA on a PDMS microchip for the rapid determination of IgA. The analytical principle of this method is the same as that for the conventional sandwich-type ELISA. Compared with the conventional 96-well microtiter plate assay, the microchip assay dramatically shortened the reaction time necessary for the enzyme–substrate reaction. We are now investigating the shortening of the reaction time necessary for the antigen–antibody reaction. The combination of the “Photochemical Patterning of Protein on Inner Wall of Microchannel” [26–28] and the “Integration of detection system” [23,24] with this developed assay will allow an on-site multi-immunoassay.

Acknowledgements

This study was partially supported by a grant-in-aid for scientific research on priority areas “Evolution of environmental, health and safety and development of educational program” from the Japanese Ministry of Education, Culture, Sports, Science and Technology (MEXT) and the Ministry of Economy, Trade and Industry for a regional consortium project.

References

- [1] K. Vedhara, J. Miles, P. Bennett, S. Plummer, D. Tallon, E. Brooks, L. Gale, K. Munnoch, C. Schreiber-Kounine, C. Fowler, S. Lightman, A. Sammon, Z. Rayter, J. Farndon, *Biol. Psychol.* 62 (2003) 89.
- [2] S.K. Chiu, C.P. Collier, A.F. Clark, K.E. Wynn-Edwards, *Clin. Biochem.* 36 (2003) 211.
- [3] R. Yehuda, S.L. Halligan, R.K. Yang, L.S. Guo, I. Makotkine, B. Singh, D. Pickholtz, *Life Sci.* 73 (2003) 349.
- [4] B.A.G. Jonsson, B. Malmberg, A. Amilon, A.H. Garde, P. Orback, *J. Chromatogr. B.* 784 (2003) 63.
- [5] A. Sgoifo, F. Braglia, T. Costoli, E. Musso, P. Meerlo, G. Ceresini, A. Troisi, *Neurosci. Biobehav.* 27 (2003) 179.
- [6] L. Anfossi, C. Tozzi, C. Giovannoli, C. Baggiani, G. Giraudi, *Anal. Chim. Acta* 468 (2002) 315.
- [7] H. Nakane, *R&D Rev. Toyota CRDL* 34 (3) (1999) 17.
- [8] H. Nakane, *R&D Rev. Toyota CRDL* 38 (2) (2003) 50.
- [9] N. Enberg, H. Alho, V. Loimaranta, M. Lenander-Lumikari, *Oral Surg. Oral Med. Oral Pathol.* 92 (2001) 292.
- [10] H. Nakane, *R&D Rev. Toyota CRDL* 32 (3) (1997) 112.
- [11] R. Deinzer, C. Kleineidam, R. Stiller-Winkler, H. Idel, D. Bachg, *Int. J. Psychophysiol.* 37 (2000) 219.
- [12] M.R. Reid, L.T. Mackinnon, P.D. Drummond, *J. Psychosom. Res.* 51 (2001) 721.
- [13] K. Uchiyama, H. Nakajima, T. Hobo, *Anal. Bioanal. Chem.* 379 (2004) 375.

- [14] E. Eteshola, D. Leckband, *Sens. Actuators B* 72 (2001) 129.
- [15] K. Sato, M. Tokeshi, H. Kimura, T. Ooi, M. Nakao, T. Kitamori, *Anal. Chem.* 72 (2000) 1144.
- [16] K. Sato, M. Tokeshi, H. Kimura, T. Kitamori, *Anal. Chem.* 73 (2001) 1213.
- [17] K. Uchiyama, M. Yang, T. Sawazaki, H. Shimizu, S. Ito, *Sens. Actuators B* 103 (2004) 200.
- [18] S. Lai, S. Wang, J. Luo, L.J. Lee, S.-T. Yang, M.J. Madou, *Anal. Chem.* 76 (2004) 1832.
- [19] L.G. Puckett, E. Dikici, S. Lai, M. Madou, L.G. Bachas, S. Daunert, *Anal. Chem.* 76 (2004) 7263.
- [20] H. Nakajima, H. Masuda, S. Ishino, T. Nakagama, T. Shimosaka, K. Arai, Y. Yoshimura, K. Uchiyama, *Bunseki Kagaku* 54 (2005) 817.
- [21] W. Xu, K. Uchiyama, T. Shimosaka, T. Hobo, *Chem. Lett.* 34 (2000) 762.
- [22] W. Xu, K. Uchiyama, T. Shimosaka, T. Hobo, *J. Chromatogr. A* 907 (2001) 279.
- [23] Y. Guo, K. Uchiyama, T. Nakagama, T. Shimosaka, T. Hobo, *Electrophoresis* 26 (2005) 1843.
- [24] K. Miyaki, Y. Guo, T. Shimosaka, T. Nakagama, H. Nakajima, K. Uchiyama, *Anal. Bioanal. Chem.* 382 (2005) 810.
- [25] Bethyl Laboratories Human IgA ELISA quantitation kit Product Information.
- [26] H. Nakajima, T. Fukuda, M. Takizawa, T. Shimosaka, T. Hobo, K. Uchiyama, *Trans. Mater. Res. Soc. Jpn.* 29 (2004) 947.
- [27] H. Nakajima, S. Ishino, H. Masuda, T. Shimosaka, T. Nakagama, T. Hobo, K. Uchiyama, *Chem. Lett.* 34 (2005) 358.
- [28] H. Nakajima, S. Ishino, H. Masuda, T. Nakagama, T. Shimosaka, K. Uchiyama, *Anal. Chem. Acta* (2006), in press.

The chemiluminescence mechanism of 3,4-bis(3-indolyl)-1H-pyrrole-2,5-dione, and the characteristics of chemiluminescence developed in the reaction with $\text{CH}_3\text{CN}-\text{H}_2\text{O}_2-\text{NaOH}$

Manabu Nakazono, Akihiro Uesaki, Kiyoshi Zaitso*

Graduate School of Pharmaceutical Sciences, Kyushu University, 3-1-1 Maidashi, Higashi-ku, Fukuoka 812-8582, Japan

Received 20 October 2005; received in revised form 6 December 2005; accepted 6 December 2005

Available online 18 January 2006

Abstract

The chemiluminescence (CL) mechanism of 3,4-bis(3-indolyl)-1H-pyrrole-2,5-dione (IPD) was investigated using liquid chromatography electrospray ionization mass spectrometry (LC–ESI–MS) of the products formed after the IPD CL reaction. We found that IPD produced strong CL via the decomposition of dioxetane formed after oxidation of the maleimide and indole moieties in the presence of CH_3CN , H_2O_2 and NaOH. The IPD CL was used for evaluating the antioxidant effect on curcumin and epigallocatechin gallate.

© 2005 Elsevier B.V. All rights reserved.

Keywords: Chemiluminescence; Dioxetane; Singlet oxygen; Curcumin; Epigallocatechin gallate

1. Introduction

We have focused on the number of chemiluminescence (CL) moiety in the structure of a molecule to develop highly sensitive CL reagents. Various indole derivatives were synthesized, and the CL characteristics were evaluated [1]. MaCapra and Chang reported that indole derivatives emitted light via dioxetane [2]. Recently, we found that the CL intensity of 3,4-bis(3-indolyl)-1H-pyrrole-2,5-dione (IPD) which had two indolyl groups in the structure was 124-fold stronger than that of indole in the presence of CH_3CN , H_2O_2 and NaOH [3]. It was reported that singlet oxygen ($^1\text{O}_2$) was produced by mixing CH_3CN , H_2O_2 and NaOH (Fig. 1) [4]. As described above, we measured the CL caused by the efficient $^1\text{O}_2$ generation system, $\text{NaOCl}-\text{H}_2\text{O}_2$ [5] to give an additional evidence that the IPD CL is due to $^1\text{O}_2$.

Using liquid chromatography electrospray ionization mass spectrometry (LC–ESI–MS), we investigated the IPD CL mechanism by analyzing the molecular ions of the products formed after the IPD CL reaction. Furthermore, to apply IPD CL to the evaluation of the antioxidant effect, we measured the CL intensities of IPD in the presence of curcumin (diferuloylmethane) or

epigallocatechin gallate (EGCG) which have a $^1\text{O}_2$ -quenching effect, a neuroprotective effect and an anticancer effect [6–8].

2. Experimental

2.1. Reagents

3,4-Bis(3-indolyl)-1H-pyrrole-2,5-dione (IPD) was prepared by the reported method [9]. NaClO (5% aqueous solution), NaOH and H_2O_2 (30% aqueous solution) were purchased from Wako Pure Chemical Industries (Osaka, Japan). Curcumin was purchased from BIOMOL Research Laboratories (Pennsylvania, USA). EGCG was obtained from MITSUI NORIN (Shizuoka, Japan). All other chemicals and solvents were of analytical reagent grade.

2.2. Apparatus

Lumat LB 9501 (Berthold, Wildbad, Germany) was used to measure the CL with a round-bottom glass tube (75 mm × 12 mm i.d.). Reversed phase HPLC was conducted using an LC 2695 separation module (Waters, Osaka, Japan). A TSK-gel ODS-80TsQA (5 μm , 4.6 mm i.d. × 250 mm, Tosoh, Tokyo) column was used, and the column oven was operated at 45 °C. A 2996 photodiode array (PDA) detector was used for detection. ESI-

* Corresponding author. Tel.: +81 92 642 6596; fax: +81 92 642 6601.
E-mail address: zaitso@phar.kyushu-u.ac.jp (K. Zaitso).

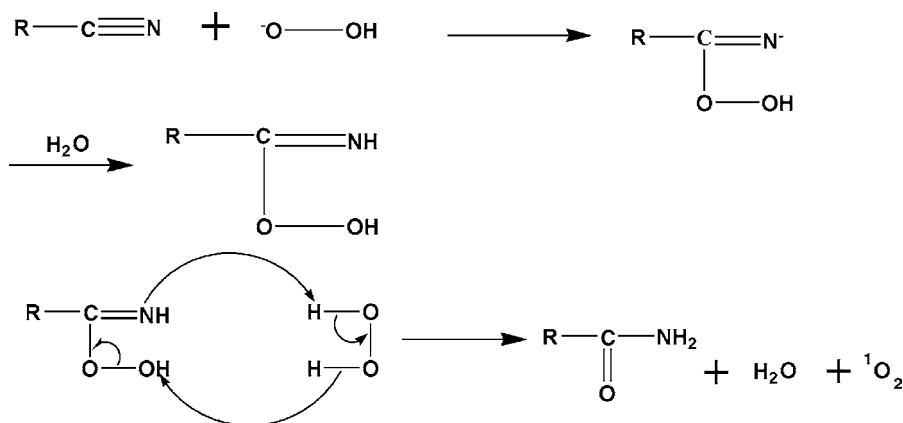


Fig. 1. Production of ${}^1\text{O}_2$ in the presence of CH_3CN , H_2O_2 and NaOH .

MS measurements were taken by a ZQ MS detector (capillary voltage: 3 kV, negative ion mode).

2.3. The LC–ESI–MS measurement for the determination of the CL mechanism of IPD

To 200 μL of a 0.1 mmol L^{-1} IPD in CH_3CN was added 100 μL of 20 mmol L^{-1} NaOH . After allowing the solution to stand for 25 s, the CL reaction was initiated by the addition of 100 μL of 250 mmol L^{-1} H_2O_2 . After allowing the solution to stand for 20 min, 50 μL of the mixture solution was subjected to HPLC (20–25% CH_3CN gradient for 10 min and then 25–75% CH_3CN gradient for 15 min containing 1% aqueous HCOOH and 10 mM aqueous $\text{CH}_3\text{COONH}_4$, flow rate: 0.7 mL/min).

2.4. The CL measurement of IPD in the presence of $\text{NaClO}-\text{H}_2\text{O}_2$

To 100 μL of a 10 mmol L^{-1} H_2O_2 was added 100 μL of 10 mmol L^{-1} NaClO . After allowing the solution to stand for 10 s, the mixture was added 100 μL of 10 mmol L^{-1} NaOH . After allowing the solution to stand for 20 s, the CL reaction was initiated by the addition of 100 μL of 100 mmol L^{-1} IPD in CH_3OH using the automatic injection system in the luminometer. The CL emissions were measured for 5 min. The integral photon counts were used to estimate the CL intensities.

2.5. The CL measurement of IPD in the presence of curcumin and EGCG

To 200 μL of a 0.1 mmol L^{-1} IPD in CH_3CN were added 50 μL of 0.1–5 mmol L^{-1} curcumin or EGCG in CH_3CN and 100 μL of 20 mmol L^{-1} NaOH . After standing for 20 s, the CL reaction was initiated by the addition of 100 μL of 250 mmol L^{-1} H_2O_2 using the automatic injection system in the luminometer. The CL emissions were measured for 5 min (curcumin) or 10 min (EGCG), and the integral photon counts were used for estimating the CL intensities.

3. Results and discussion

3.1. The CL mechanism of IPD

The HPLC chromatogram of the products after IPD CL development is shown in Fig. 2. Each compound (I–III) was stable for 5 h after the CL reaction of IPD. The ESI–MS spectra of I–III peaks in the HPLC chromatogram were showed in Fig. 3. Negative ions, 187.3 (retention time (Rt): 16.07 min), 372.3 (Rt: 21.67 min) and 358.4 (Rt: 23.50 min)) were observed. It was thought that each negative ion, 187.3, 372.3 or 358.4 showed the molecular ion of I, II or III, respectively (Fig. 3). The negative ion of asterisk peak component (Rt: 3.95 min) in Fig. 2 was 383.0. The peak component may be a decomposed compound of IV in Fig. 4. However, we could not give an accurate structure. Thus, the oxidation of the double bond in the maleimide moiety of IPD proceeds, and indole-3-glyoxylamine (I) and indole-3-glyoxylic acid should be produced (Fig. 4). The oxidation of the double bond in the maleimide moiety of IPD and OH addition in the imide proceeds, and II should be produced (Fig. 4). The double bond at the 2,3 position in one of the two indole moieties of IPD is oxidized, and III should be produced (Fig. 4). This indicated that

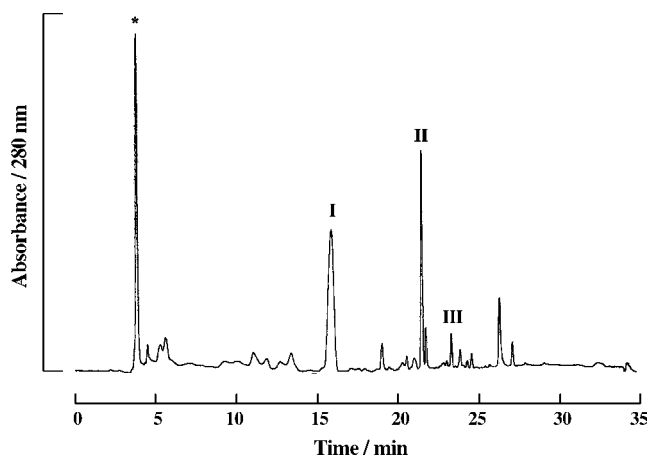


Fig. 2. HPLC chromatogram of the products after IPD CL development. Asterisk peak component (Rt: 3.95 min) may be a decomposed compound of IV in Fig. 4.

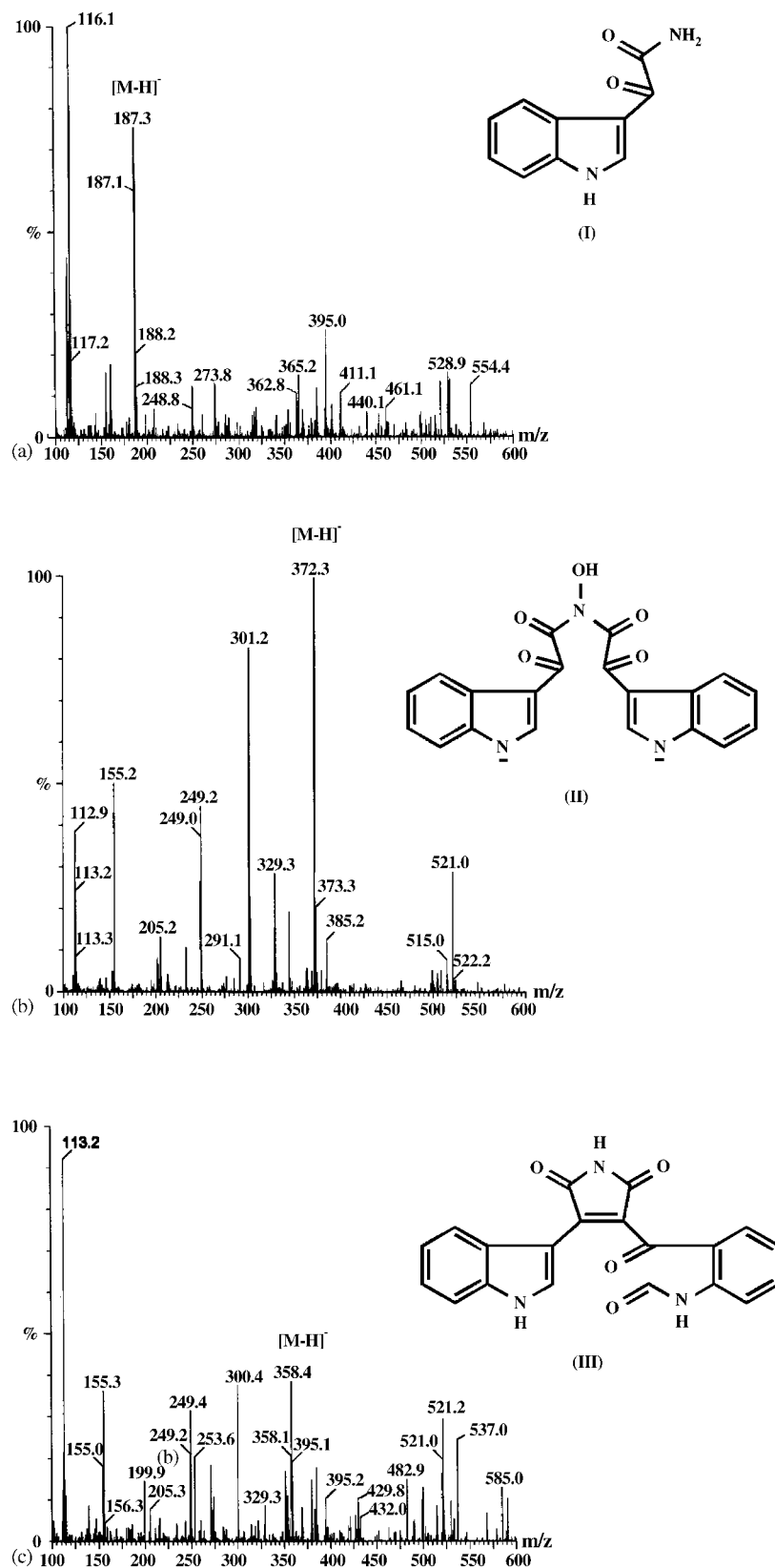


Fig. 3. The ESI-MS spectra of **I–III** peaks in the HPLC chromatogram: (a) **I**; (b) **II**; (c) **III**.

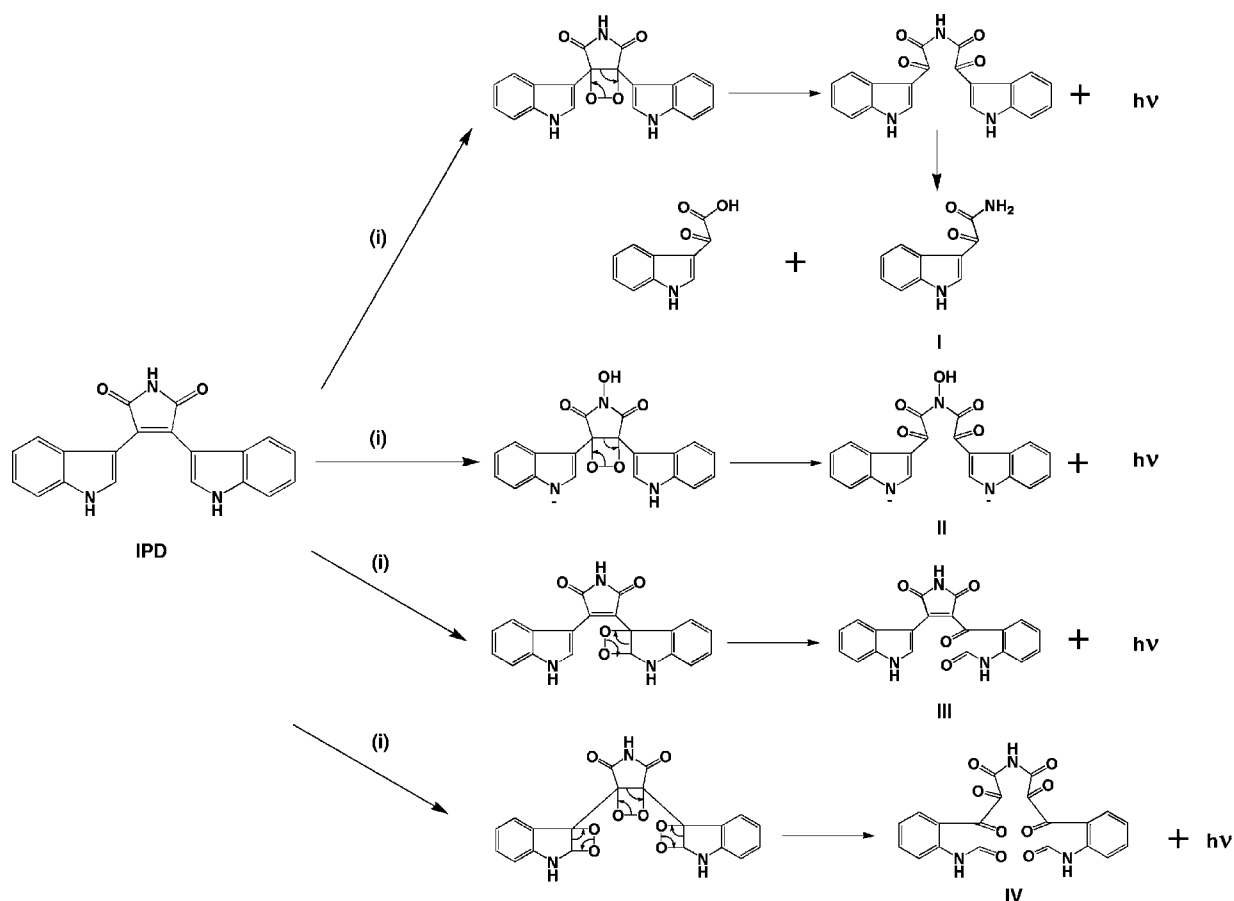


Fig. 4. The possible CL mechanism of IPD: (i) H_2O_2 , NaOH, CH_3CN .

IPD might emit light via at least three CL reactions simultaneously.

3.2. The CL characteristics of IPD in the presence of $\text{NaClO-H}_2\text{O}_2$

IPD did not emit light in the presence of 10 mM H_2O_2 (Fig. 5, curves 5 and 6). Curves 1 and 3 showed the CL due to the oxidation by $^1\text{O}_2$ in the presence and absence of NaOH. This indicated that the CL intensity of IPD due to the oxidation by $^1\text{O}_2$ increased in an alkaline medium. IPD also emitted light by NaClO in the presence and absence of NaOH (Fig. 5, curves 2 and 4). The CL intensity of IPD due to only $^1\text{O}_2$ was the CL intensity obtained by subtracting curve 2 from curve 1. From these results, we found that $^1\text{O}_2$ has a great effect on the IPD CL intensity.

3.3. Antioxidant effect of curcumin and EGCG on IPD CL

The structure of curcumin and EGCG is shown in Fig. 6. The CL intensities of IPD decreased with an increase of the concentration in the range of 0.1–1 mM curcumin or 1–5 mM EGCG (Figs. 7 and 8). From a comparison of the decrease in IPD CL intensities in the presence of 1 mM curcumin and EGCG, the antioxidant effect of curcumin was 2.6-fold stronger than that of EGCG. The IPD CL in CH_3CN might be utilized for the evaluation of antioxidants having $^1\text{O}_2$ -quenching activity.

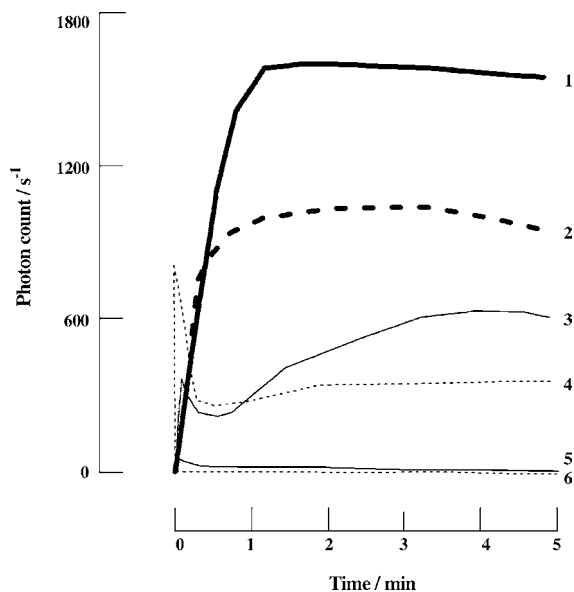


Fig. 5. The CL development of IPD by $^1\text{O}_2$ oxidation. The concentration of IPD in each CL reaction was 0.1 mM in CH_3OH : (1) $[\text{H}_2\text{O}_2] = 10$ mM, $[\text{NaClO}] = 10$ mM, $[\text{NaOH}] = 10$ mM; (2) $[\text{NaClO}] = 10$ mM, $[\text{NaOH}] = 10$ mM; (3) $[\text{H}_2\text{O}_2] = 10$ mM, $[\text{NaClO}] = 10$ mM; (4) $[\text{NaClO}] = 10$ mM; (5) $[\text{H}_2\text{O}_2] = 10$ mM, $[\text{NaOH}] = 10$ mM; (6) $[\text{H}_2\text{O}_2] = 10$ mM.

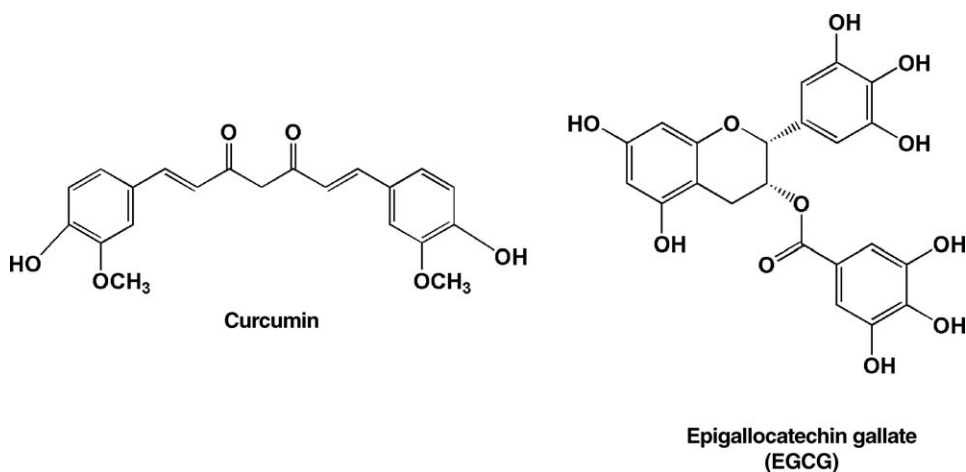


Fig. 6. Structure of curcumin and epigallocatechin gallate (EGCG).

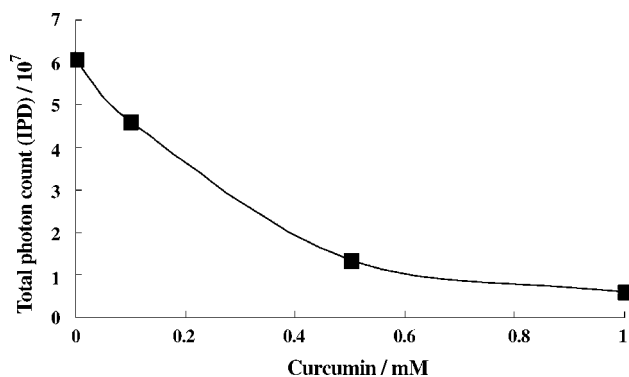


Fig. 7. The CL development of IPD in the presence of curcumin: [IPD] = 0.1 mM, [NaOH] = 20 mM, and [H₂O₂] = 250 mM.

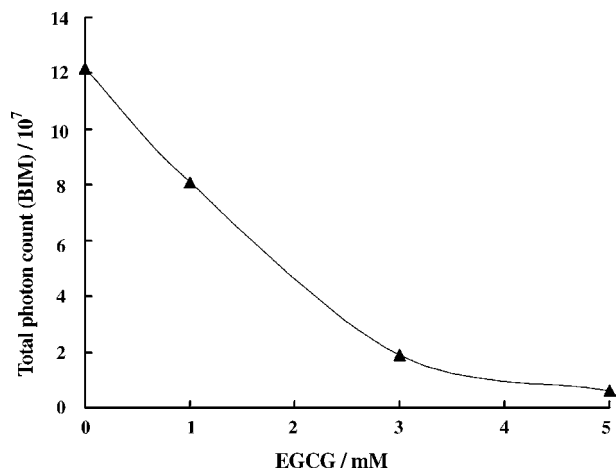


Fig. 8. The CL development of IPD in the presence of EGCG: [IPD] = 0.1 mM, [NaOH] = 20 mM, and [H₂O₂] = 250 mM.

4. Conclusions

From the LC–ESI–MS of the products of IPD CL, it was found that the decomposition of dioxetane formed after the oxidation of the maleimide and indole moieties proceeded in the IPD CL. IPD may emit light via at least three CL reactions simultaneously. We found that curcumin has a stronger antioxidant effect than that of EGCG by evaluating the decrease in the IPD CL intensity.

Acknowledgements

This work was supported by the Japan Society for the Promotion of Science (No. 17590034). The authors would like to thank Waters (Osaka, Japan) for the LC–ESI–MS measurements in the CL mechanism determination of IPD.

References

- [1] N. Sugiyama, M. Akutagawa, Bull. Chem. Soc. Jpn. 40 (1967) 240.
- [2] F. MaCapra, Y.C. Chang, J. Chem. Soc. Chem. Commun. (1966) 522.
- [3] M. Nakazono, M. Asechi, K. Zaito, Biolum. Chemilum., Prog. Perspect. (2005) 175.
- [4] E. Mckeown, W.A. Waters, Nature 203 (1964) 1063.
- [5] A.M. Held, D.J. Halko, J.K. Hurst, J. Am. Chem. Soc. 100 (1978) 5732.
- [6] K.C. Das, C.K. Das, Biochem. Biophys. Res. Commun. 295 (1) (2002) 62.
- [7] M. Thiagarajan, S.S. Sharma, Life Sci. 74 (8) (2004) 969.
- [8] C.S. Young, Nature 389 (1997) 134.
- [9] G. Zhu, S.E. Conner, X. Zhou, C. Shih, T. Li, B.D. Anderson, H.B. Brooks, R.M. Campbell, E. Considine, J.A. Dempsey, M.M. Faul, C. Ogg, B. Patel, R.M. Schultz, C.D. Spencer, B. Teicher, S.A. Watkins, J. Med. Chem. 46 (2003) 2027.

Homogeneous time-resolved fluoroimmunoassay of 3,5,3'-triiodo-L-thyronine in human serum by using europium fluorescence energy transfer

Guilan Wang^a, Jingli Yuan^{a,*}, Xiaodan Hai^a, Kazuko Matsumoto^b

^a Department of Analytical Chemistry, Dalian Institute of Chemical Physics, Chinese Academy of Sciences, Dalian 116023, China

^b Department of Chemistry, Waseda University, Shinjuku-ku, Tokyo 169-8555, Japan

Received 19 October 2005; received in revised form 29 November 2005; accepted 29 November 2005

Available online 6 January 2006

Abstract

A sensitive homogeneous time-resolved fluoroimmunoassay method for 3,5,3'-triiodo-L-thyronine (T3) based on the fluorescence resonance energy transfer (FRET) from a fluorescent Eu³⁺ complex, {[4,6-dichloro-1,3,5-triazin-2-yl)amino-biphenyl-4''-yl]-2,2':6',2''-terpyridine-6,6''-diyl}bis(methylenitrilo) tetrakis(acetate)-Eu³⁺ (DTBTA-Eu³⁺) ($\lambda_{\text{ex,max}} = 335 \text{ nm}$, $\lambda_{\text{em,max}} = 615 \text{ nm}$), to an organic fluorescence dye Cy5 has been developed. The new assay system combined the use of DTBTA-Eu³⁺-labeled T3-bovine serum albumin (BSA) conjugate and Cy5-labeled anti-T3 monoclonal antibody for a competitive-type immunoassay. After the competitive reactions of DTBTA-Eu³⁺-labeled T3-BSA and T3 sample with Cy5-labeled anti-T3 antibody, the T3 concentration was measured with a time-resolved mode by monitoring the sensitized emission of Cy5 derived from FRET in a homogeneous format. The method gives the detection limit of 0.26 ng/ml. The coefficient variations of the method are less than 2.0% and the recoveries are in the range of 80–111% for serum sample measurement. The concentrations of T3 in 30 human serum samples were determined, and the results were compared with those of the independently determined by a radio-immunoassay method. A good correlation was obtained with a correlation coefficient of 0.989.

© 2005 Elsevier B.V. All rights reserved.

Keywords: Homogeneous immunoassay; 3,5,3'-Triiodo-L-thyronine; Europium; Fluorescence resonance energy transfer

1. Introduction

3,5,3'-Triiodo-L-thyronine (T3) is one of thyroid hormones. Its daily production is about 30 μg , in which about 20% is produced by the direct synthesis and secretion of the thyroid gland and about 80% by peripheral conversion of L-thyroxine (T4) in extrathyroidal tissues [1]. It has been known that the serum concentration level of T3 is very low (reference interval, 0.7–2.1 ng/ml) [2], and some heterogeneous immunoassay methods including radio immunoassay (RIA) [3,4], enzyme immunoassay (EIA) [5], chemiluminescent immunoassay [6,7] and electrochemiluminescent immunoassay [8], have been developed for the determination of T3 in human serum samples. Although these methods have been developed, however, the current methods are tedious and time-consuming because

the methods require immobilization of the antigen and the separation of the reaction solution. Recently, a homogeneous enzyme immunoassay method for the determination of T3 was developed by Karapitta et al. [2], but this method is still time-consuming over 2 h per assay.

Time-resolved fluoroimmunoassay (TR-FIA) technique using fluorescent lanthanide complexes as labels has been widely used for highly sensitive detections of various biomolecules [9–13]. By using fluorescence resonance energy transfer (FRET) between a fluorescent lanthanide label and an organic fluorescence label, some homogeneous TR-FIA and DNA hybridization assay methods have been successfully developed [14–20]. However, the method has not been widely used due to its lower sensitivity compared with heterogeneous one. Other homogeneous fluorescence immunoassay methods, such as a liposome-trap-release based method [21], and a pH-sensitive polymer based method [22], have also been developed recently. These methods have provided new strategies for designing the sensitive homogeneous assay platforms.

* Corresponding author. Tel.: +86 411 84379660; fax: +86 411 84379660.
E-mail address: jingliyuan@yahoo.com.cn (J. Yuan).

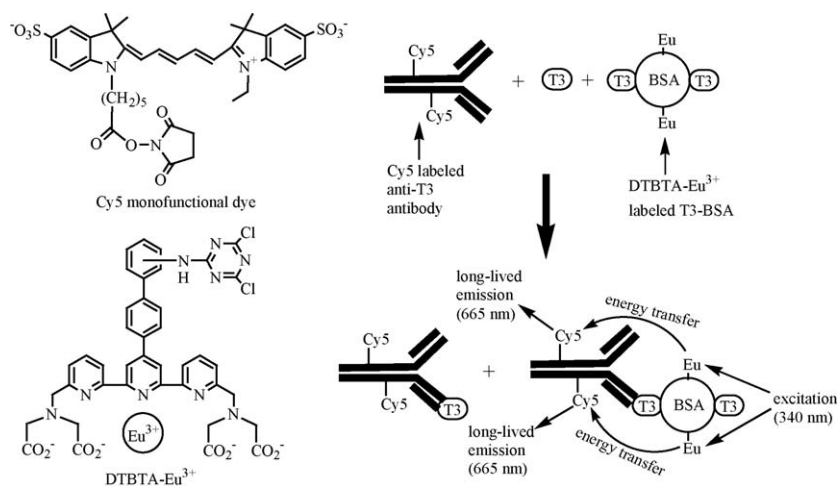


Fig. 1. Structures of donor-acceptor pair for FRET and principle of the homogeneous TR-FIA for T3.

In the present work, a sensitive homogenous TR-FIA method for the determination of T3 in human serum samples based on FRET was developed by using a newly synthesized Eu³⁺ complex DTBTA-Eu³⁺ (structure see Fig. 1) [23] as a donor and an organic fluorescence dye Cy5 as an acceptor. The principle of the method is shown in Fig. 1. In the competitive immunoassay system, due to the formation of the immune complex of Cy5-labeled antibody-DTBTA-Eu³⁺-labeled T3-BSA, Cy5 and DTBTA-Eu³⁺ come close to each other, thus resulting in the energy transfer from Eu³⁺ complex to Cy5. Compared with the fluorescence lifetime of Cy5, the emission lifetime of Cy5 in the energy transfer system is greatly long since the fluorescence lifetime of the donor is very long (>1.0 ms). By measuring the sensitized and long-lived emission of Cy5 with time-resolved mode, the interferences from the direct emission of Cy5 excited by ultraviolet light and the emission from the donor can be avoided, since the former is short-lived, which can be suppressed by time-resolved fluorescence measurement, and the latter is minimal at measurement wavelength [14,16,18]. Therefore, the concentrations of T3 in samples can be directly detected without any immobilization and separation steps. The detection results of T3 in human serum samples have demonstrated that the new method has the advantages of high sensitivity, easy to perform and less time-consuming (less than 1 h).

2. Experimental

2.1. Labeling of anti-T3 monoclonal antibody with Cy5

After dialyzing 0.5 ml of anti-T3 monoclonal antibody (0.6 mg/ml, OEM Concepts Co.) twice at 4 °C against 3 l of water, 140 µl of 0.5 M carbonate buffer of pH 9.1 and 60 µl (1 mg/ml) of Cy5 monofunctional reactive dye (Amersham Life Science, Inc.) were added to the solution. After the solution was stirred at room temperature for 30 min, the labeled antibody was separated from the unreacted dye by a Sephadex G-50 column with 0.05 M NH₄HCO₃ of pH 8.0 as eluent. The labeling ratio of Cy5 to antibody (Cy5/antibody) was calculated by the method given in the Cy5 monofunctional

dye product specification by measuring the absorbance of the labeled antibody solution at 650 and 280 nm (labeling ratio = [Cy5]/[antibody], in which [Cy5] = A_{650 nm}/250,000, [antibody] = (A_{280 nm} - 0.05A_{650 nm})/170,000). The labeling ratio is 1.3. The Cy5-labeled antibody was stored at 4 °C, and diluted by 0.05 M Tris-HCl buffer of pH 7.8 containing 0.2% BSA, 0.9% NaCl and 0.1% NaN₃ before use in immunoassay.

2.2. Labeling of T3-BSA conjugate with DTBTA-Eu³⁺

The europium complex fluorescence label, DTBTA-Eu³⁺, was synthesized according to a previous method [23]. Preparation of T3-BSA conjugate and its labeling with DTBTA-Eu³⁺ are described in the following.

After 0.6 mg T3 (Sigma) and 6 mg BSA (Sigma) were dissolved in 3.6 ml of 0.1 M phosphate buffer of pH 7.1, 0.1 ml of 1% glutaraldehyde was added. The solution was stirred at room temperature for 1 h, and further incubated at 4 °C for 24 h. To the solution was added 2 mg NaBH₄, and the solution was stirred at room temperature for 2 h. After dialyzing twice for 24 h at 4 °C against 3 l of saline solution, to 0.5 ml of T3-BSA conjugate solution (BSA concentration is ~0.8 mg/ml) were added 200 µl of 0.5 M carbonate buffer of pH 9.1 and 230 µg of DTBTA-Eu³⁺. The solution was stirred at room temperature for 3 h, and then the DTBTA-Eu³⁺-labeled T3-BSA conjugate was separated from the unreacted label by a Sephadex G-50 column with 0.05 M NH₄HCO₃ of pH 8.0 as eluent. The labeling ratio of DTBTA-Eu³⁺ to T3-BSA (DTBTA-Eu³⁺/T3-BSA) was estimated by using the absorbance of the solution at 335 nm and the molar extinction coefficient of free DTBTA-Eu³⁺ (3.11 × 10⁴ M⁻¹ cm⁻¹) to be ~6.5. By changing the amount of DTBTA-Eu³⁺ used for the labeling reaction (1200, 800, 460 and 120 µg, respectively), several kinds of DTBTA-Eu³⁺-labeled T3-BSA conjugates with different labeling ratio (22, 19, 12 and 4.0, respectively) were also prepared. The DTBTA-Eu³⁺-labeled T3-BSA conjugates were stored at 4 °C, and diluted by 0.05 M Tris-HCl buffer of pH 7.8 containing 0.2% BSA, 0.9% NaCl and 0.1% NaN₃ before use in immunoassay.

2.3. Homogeneous TR-FIA of T3 in human serum samples

Human serum samples obtained from healthy people were stored at -30°C before use. A series of T3 standard solutions were prepared by diluting 1.00 mg/ml T3 solution with 0.05 M Tris–HCl buffer of pH 7.8 containing 5% BSA, 0.9% NaCl and 0.1% NaN_3 .

To a 1.5 ml tube, 60 μl of the Cy5-labeled antibody, 7.5 μl of the DTBTA- Eu^{3+} -labeled T3-BSA and 200 μl of T3 standard solution or human serum were added and incubated at 37°C for 45 min. After the reaction, a 90 μl solution was used for time-resolved fluorescence measurement on a Perkin-Elmer Victor 1420 Multilabel Counter with measurement conditions of excitation wavelength, 340 nm; emission wavelengths, 665 and 615 nm; delay time, 75 μs ; window time (counting time), 200 μs . (It was confirmed by experiments that the conditions of 75 μs delay time and 200 μs window time are optimal for the measurement. The emission of unreacted Cy5-labeled antibody can be fully suppressed by the measurement of 75 μs delay time, which allows the prolonged emission of Cy5 in FRET system to be measured.)

2.4. RIA of T3 in human serum samples

The results of T3 concentrations in 30 human serum samples determined by a clinical RIA method were obtained from the Clinical Analysis Center, Dalian Medical University.

3. Results and discussion

3.1. Evaluation of the assay method

The present method is based on the FRET from a Eu^{3+} complex DTBTA- Eu^{3+} to an organic dye Cy5 in a competitive immunoassay format. As shown in Fig. 1, the amino-reactive groups in two fluorescence labels, (4,6-dichloro-1,3,5-triazin-2-yl)amino group in DTBTA- Eu^{3+} and *N*-hydroxysuccinimide ester group in Cy5, make the labels be easily conjugated to T3-BSA conjugate and anti-T3 antibody by the formations of stable covalent bonds between the labels and the proteins, respectively. The high stabilities of the labeled proteins allow them to be long-term stored, and also ensure the fluorescence labels not to be dissociated in the assay process.

Fig. 2 shows the emission spectrum of DTBTA- Eu^{3+} and the absorption and emission spectra of Cy5. The absorption spectrum of Cy5 has good spectral overlapping on the emission peaks of the Eu^{3+} complex, which indicates the DTBTA- Eu^{3+} complex and Cy5 as a donor–acceptor pair for FRET is satisfied. It is also noteworthy that the emission intensity of the Eu^{3+} complex at 665 nm, the emission maximum wavelength of Cy5, is very weak. This spectrum feature shows that the measurement of the sensitized emission of Cy5 at 665 nm in a FRET system does not be greatly affected by the donor's emission.

After the competitive immune reactions of Cy5-labeled anti-T3 antibody with T3 sample and DTBTA- Eu^{3+} -labeled T3-BSA in a homogeneous solution, the FRET from the Eu^{3+} complex to Cy5 occurs by the formation of the immune complex, Cy5-

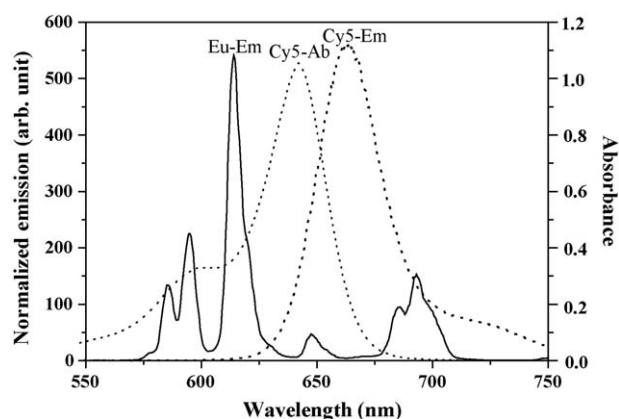


Fig. 2. Emission spectrum of DTBTA- Eu^{3+} (Eu-Em) and absorption and emission spectra of Cy5 (Cy5-Ab, Cy5-Em).

labeled antibody-DTBTA- Eu^{3+} -labeled T3-BSA (the amount of this complex is inversely related to the amount of T3). Since the emission lifetime of Cy5 in such a FRET system is greatly prolonged, the T3 concentration in the sample can be directly determined by measuring the long-lived Cy5 emission with time-resolved mode. According to Refs. [14,15,19], the effect of high variation in absorbance of different samples at excitation wavelength can be corrected by using the ratio of the fluorescence intensities of acceptor emission and donor emission as the final signal. Therefore, the ratio of Cy5 emission at 665 nm to the Eu^{3+} emission at 615 nm, $I_{665\text{ nm}}/I_{615\text{ nm}} \times 10^3$, was used as the final fluorescence signal in the assay system.

3.2. Assay conditions

First, the effect of the antibody concentration {the molar concentration of antibody was calculated by using the equation $[\text{antibody}] = (A_{280\text{ nm}} - 0.05A_{650\text{ nm}})/170,000$ } in the assay system was investigated by using the Cy5-labeled anti-T3 antibody. As shown in Fig. 3, the signal and the S_{max}/S_0 ratio (defined as the ratio of signal at 0.01 ng/ml to that at 100 ng/ml of T3, since the signals below 0.01 ng/ml and above 100 ng/ml are almost unchanged) are obviously increased with the increase of the concentration of Cy5-labeled anti-T3 antibody. This can be explained that the amount of immune complex of Cy5-labeled antibody-DTBTA- Eu^{3+} -labeled T3-BSA is increased with the increase of the concentration of Cy5-labeled anti-T3 antibody in the homogenous competitive immune reaction. Considering both the using amount of antibody and the S_{max}/S_0 ratio, the effect of higher concentration of Cy5-labeled antibody was not determined because the increase of S_{max}/S_0 ratio with the increase of Cy5-labeled antibody concentration from 3.6 to 5.9 nM is not very remarkable (the S_{max}/S_0 ratios are 1.6, 2.0, 2.5 and 2.7 for four concentrations of Cy5-labeled antibody, respectively), and 5.9 nM of Cy5-labeled antibody was used in the following assays.

The effect of labeling ratio of DTBTA- Eu^{3+} -labeled T3-BSA in the assay system has been investigated. As shown in Fig. 4, the signals and S_{max}/S_0 ratio are increased with the decrease of the labeling ratio from 22 to 4.0. This phenomenon

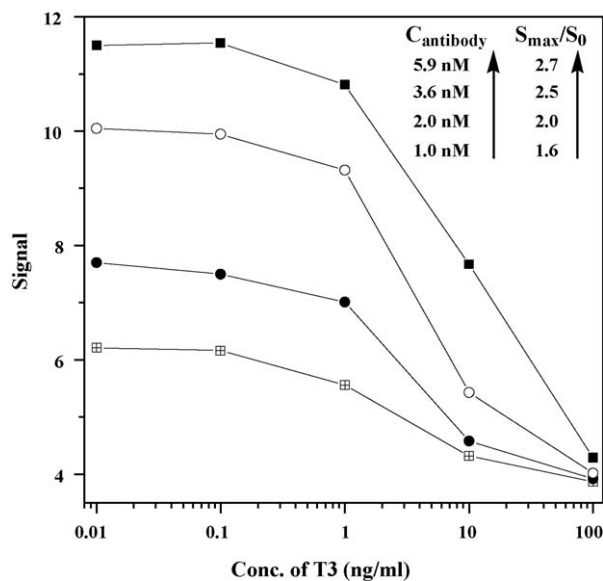


Fig. 3. The influence of the Cy5-labeled anti-T3 antibody concentration on the T3 assay. The DTBTA-Eu³⁺-labeled T3-BSA with the concentration of 11 nM and labeling ratio of 6.5 was used for the measurements.

is caused by the fact that the increase of labeling ratio of the Eu³⁺ complex-labeled T3-BSA in the assay solution causes the obvious increase of emission intensity at 615 nm, while the increase of emission intensity at 665 nm is small, and therefore the $I_{665\text{ nm}}/I_{615\text{ nm}}$ becomes small with the increase of the labeling ratio. Actually, only the Eu³⁺ label molecules closest to Cy5 label in the immune complex are contributive to the FRET, and the others in distant positions contribute to the background [17].

The effects of reaction time and temperature on the assay have also been investigated. As shown in Fig. 5, the assay is strongly

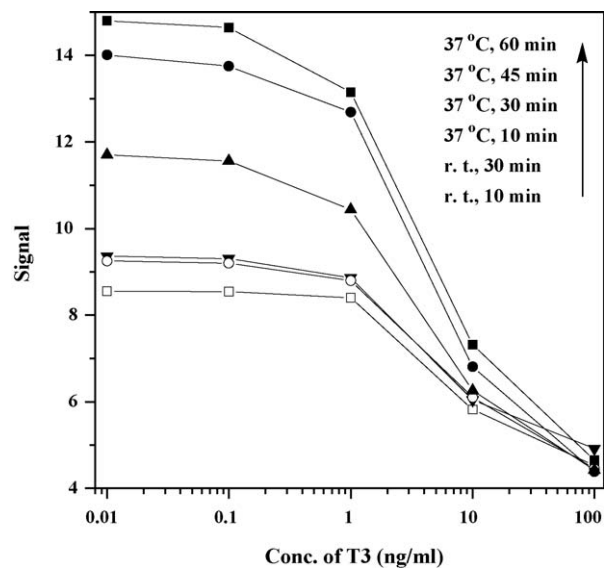


Fig. 5. The influence of the reaction time and temperature on the T3 assay.

affected by the reaction time and temperature, and a higher reaction temperature, 37 °C, is beneficial for increasing the S_{\max}/S_0 ratio and shortening the assay time. At 37 °C, the S_{\max}/S_0 ratio is increased with the increase of reaction time from 10 to 45 min, and which does not increase with the further increase of reaction time (the S_{\max}/S_0 ratios for 10, 30, 45 and 60 min reactions are 2.08, 2.65, 3.19 and 3.18, respectively). These results obviously indicate that the assay conditions, reaction at 37 °C for 45 min, are optimal for the sample detection.

3.3. Analysis of T3 in human serum samples

The calibration curve of homogenous TR-FIA for T3 is shown in Fig. 6. The detection limit, defined as the concentration corre-

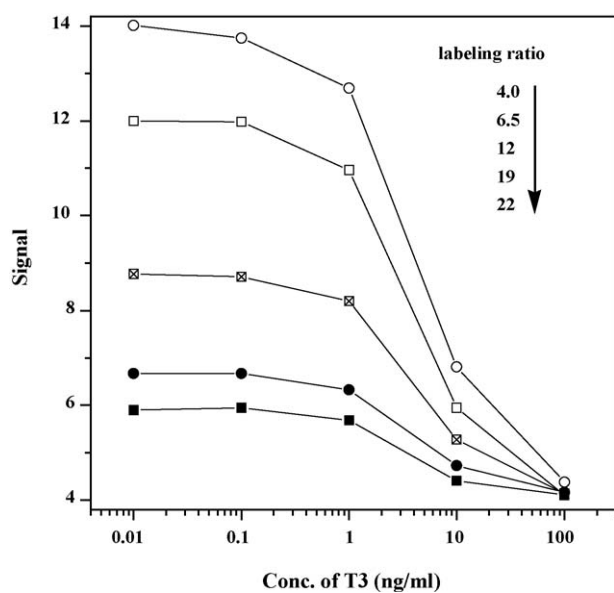


Fig. 4. The influence of the labeling ratio of DTBTA-Eu³⁺-labeled T3-BSA on the T3 assay. The Cy5-labeled antibody of 5.9 nM was used for the measurements.

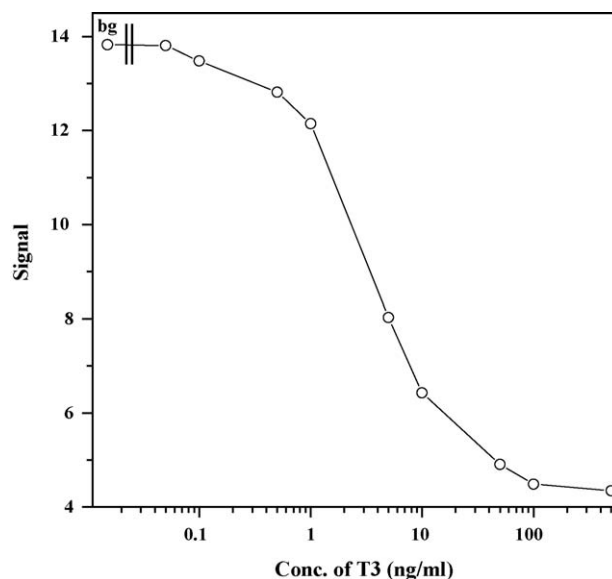


Fig. 6. Calibration curve of homogeneous TR-FIA for T3 in human sera; bg, background.

Table 1
Analytical precision and recovery of T3 added to human serum samples

Added (ng/ml)	Found (ng/ml)	Recovery (%)	Coefficient variation (%) ($n = 6$)
Sample 1	0.66	–	0.71
2.50	3.11	98.0	1.88
4.00	4.03	84.3	1.32
Sample 2	0.40	–	1.35
2.50	3.00	104.0	1.56
4.00	3.67	81.8	1.14
Sample 3	0.54	–	1.36
2.50	2.98	97.6	1.95
4.00	3.77	80.8	1.55
Sample 4	0.49	–	1.96
2.50	2.58	83.6	1.30
4.00	4.91	110.5	1.25

sponding to 3 S.D. (standard deviation) of the background signal, is 0.26 ng/ml. This detection limit is similar to those of RIA [3,4], electrochemiluminescent immunoassay [8] and homogeneous enzyme immunoassay [2] methods, and indicates that the present homogeneous TR-FIA method has an enough high sensitivity for the determination of T3 in human serum samples. The dynamic range of the present method is up to ~ 100 ng/ml. Compared with the heterogeneous immunoassay methods, the present method has the advantages of rapidity, simplicity and high reliability since the solid-phase carrier and B/F separation (separation of bound reagent and free reagent) steps usually used in heterogeneous immunoassay method are not necessary.

To evaluate the precision and accuracy of the assay, the recovery and coefficient variation of standard T3 added to human serum samples were measured six times. As shown in Table 1, the coefficient variations for 12 assay results are all less than 2%, and recoveries are in the range of 80–110%. These results show that the analytical precision and accuracy of the present method

are good enough for the application of T3 assay in human serum samples.

To evaluate the correlation of the present method with other established methods, the T3 concentrations in 30 human serum samples were determined with both the present method and a clinical used RIA method. Correlation of the two methods is shown in Fig. 7. The correlation coefficient is 0.989 with the correlation equation of $y = 1.028x - 0.043$, where y are the results of RIA method, x the results of the present method. This result indicates that the present method is highly reliable.

4. Conclusion

In the present work, a homogenous TR-FIA method based on the FRET using a newly synthesized Eu^{3+} complex DTBTA- Eu^{3+} and an organic fluorescence dye Cy5 as the donor–acceptor pair has been developed, and used for the determination of T3 in human serum samples. As a homogeneous immunoassay method, the advantages of simplicity and rapidity make the method particularly useful for a high-throughput determination. The results of TR-FIA for T3 show that the method is highly reliable and has an enough high sensitivity for determination of T3 in human serum samples with good precision and accuracy. It is expected that the new homogenous TR-FIA system could be extended to the determinations of other bioactive molecules, such as hormones, peptides and drugs.

Acknowledgements

The present work was supported by the National Natural Science Foundation of China (Nos. 20175027, 20575069).

References

- [1] R. Bunevičius, G. Kažanavičius, R. Žalinkevičius, A.J. Prange, New Engl. J. Med. 340 (1999) 424.
- [2] C.D. Karapitta, T.G. Sotirioudis, A. Papadimitriou, A. Xenakis, Clin. Chem. 47 (2001) 569.
- [3] I.J. Chopra, R.S. Ho, R. Lam, J. Lab. Clin. Med. 80 (1972) 729.
- [4] P.S. Petrou, S.E. Kakabakos, M.A. Koupparis, I. Christofidis, J. Immunoassay 19 (1998) 271.
- [5] W. Groskopf, S. Hsu, L. Sohn, Clin. Chem. 34 (1988) 1210.
- [6] Q. Le, M. Ka, L. Chiu, B. Toivola, Clin. Chem. 42 (Suppl.) (1996) 156.
- [7] S. Dayal, K. Arnold, A. Aziz, B. Monfiston, A. Kaiser, W. Hemans, M. Sylvestre, N. Patel, Clin. Chem. 46 (Suppl.) (2000) A122.
- [8] M. Sanchez-Carbayo, M. Mauri, R. Alfayete, C. Miralles, F. Soria, Clin. Biochem. 32 (1999) 395.
- [9] E.P. Diamandis, T.K. Christopoulos, Anal. Chem. 62 (1990) 1149A.
- [10] J. Yuan, K. Matsumoto, H. Kimura, Anal. Chem. 70 (1998) 596.
- [11] I. Hemmilä, V.-M. Mikkala, Crit. Rev. Clin. Lab. Sci. 38 (2001) 441.
- [12] J. Yuan, G. Wang, K. Majima, K. Matsumoto, Anal. Chem. 73 (2001) 1869.
- [13] Z. Ye, M. Tan, G. Wang, J. Yuan, Talanta 65 (2005) 206.
- [14] G. Mathis, Clin. Chem. 39 (1993) 1953.
- [15] G. Mathis, F. Socquet, M. Viguier, B. Darbouret, Anticancer Res. 17 (1997) 3011.

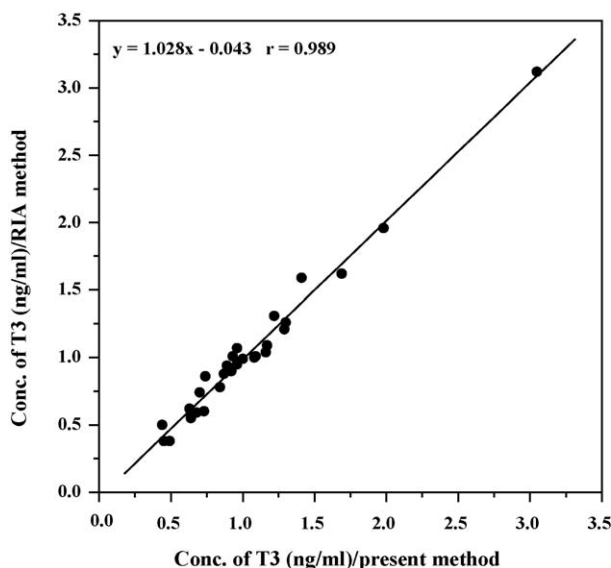


Fig. 7. Correlation between the present method and RIA method for the measurement of T3 in 30 human serum samples.

- [16] K. Stenroos, P. Hurskainen, S. Eriksson, I. Hemmilä, K. Blomberg, C. Lindqvist, *Cytokine* 10 (1998) 495.
- [17] K. Blomberg, P. Hurskainen, I. Hemmilä, *Clin. Chem.* 45 (1999) 855.
- [18] S. Sueda, J. Yuan, K. Matsumoto, *Bioconjug. Chem.* 11 (2000) 827.
- [19] G. Wang, J. Yuan, K. Matsumoto, Z. Hu, *Talanta* 55 (2001) 1119.
- [20] S. Sueda, J. Yuan, K. Matsumoto, *Bioconjug. Chem.* 13 (2002) 800.
- [21] M.A. Bacigalupo, A. Ius, R. Longhi, G. Meroni, *Talanta* 61 (2003) 539.
- [22] P. Lin, J.-J. Feng, H. Zheng, H.-H. Yang, J.-G. Xu, *Talanta* 65 (2005) 430.
- [23] K. Matsumoto, J. Yuan, G. Wang, M. Tan, European Patent 1,489,418 (2004).

A simple and sensitive chromium speciation procedure by hyphenating flow injection on-line preconcentration with catalytic spectrophotometry

Han Cui^a, Ronghuan He^b, Jianhua Wang^{a,*}

^a Research Center for Analytical Sciences, Box 332, Northeastern University, Shenyang 110004, China

^b Department of Chemistry, Box 332, Northeastern University, Shenyang 110004, China

Received 17 October 2005; received in revised form 19 December 2005; accepted 22 December 2005

Available online 10 February 2006

Abstract

A high sensitive chromium speciation procedure based on spectrophotometric detection was developed by coupling flow injection on-line preconcentration with a catalytic indicator reaction. Chromium(VI) is retained on a mini-column packed with polystyrene anion exchange resin (strong basic 717 resin), which was afterwards eluted with a small volume of NaNO₃ solution. The eluted Cr(VI) is then directed to catalyze the decoloration of alizarin cyanine green (ACG) in the presence of bromate as oxidizing reagent, and the absorbance change is proportional to the concentration of Cr(VI). With a sampling volume of 12 ml and a loading time of 120 s, an enrichment factor of 26.5 was achieved for the preconcentration. The most distinct feature of this procedure is characterized by its overall detection limit, i.e., 50 ng l⁻¹, which is much superior to those achieved by FAAS, and comparable to those obtained by inductively coupled plasma mass spectrometry (ICPMS) and electrothermal atomic absorption spectrometry (ETAAS). The procedure was validated with a certified reference material. It was also applied to the speciation of chromium in a series of surface water samples.

© 2006 Elsevier B.V. All rights reserved.

Keywords: Flow injection on-line preconcentration; Bromate-alizarin cyanine green (ACG) catalytic spectrometry; Chromium speciation

1. Introduction

The large amount of waste disposal has resulted in serious environmental pollution over the last decades. Among various pollution sources, heavy metals tend to cause a series of risks, including carcinogenic effects to human health, ecological threats and extinction of species [1–3]. Studies have shown that the carcinogenesis induced by certain toxic metals could be further enhanced or inhibited through their interactions with other metals, which processes depend strongly on the chemical forms of the metals [3]. Nowadays, the growing awareness of the strong dependence of the toxicity of heavy metals upon their chemical forms has led to an increasing interest in metal speciation analysis.

Among various analytical protocols devoted to metal speciation, the most attractive approaches are obviously the ones

with an appropriate separation procedure coupled to mass spectrometry. HPLC and capillary electrophoresis (CE) have shown obvious advantages in metal speciation analysis [4,5], attributed to their excellent separation capabilities. Coupling of these separation techniques to mass spectrometry provide most important speciation techniques, including their interface with ICPMS [6–8] and electrospray ionization mass spectrometry (ESI-MS) [9,10].

The hyphenation of chromatographic separation protocols with mass spectrometry offer the most promising approach for metal speciation, which makes it much easier to facilitate many of the sophisticated speciation tasks [11]. Yet, for some specific purposes, e.g., the speciation of inorganic species of some biologically interested heavy metals in routine laboratories, such as Cr(III)/Cr(VI), the aforementioned complicated hyphenation systems are frequently restricted, owing to the high cost for acquiring the instruments as well as their running expenses. Thus, simple instrumentation is preferential in this case, provided that the sensitivity of detection is sufficient for the speciation purpose.

* Corresponding author. Tel.: +86 83688944; fax: +86 83676698.
E-mail address: jianhua@jrz@mail.edu.cn (J. Wang).

We hereby report a simple spectrophotometric procedure for the speciation of inorganic chromium by hyphenation of flow injection on-line preconcentration with catalytic decoloration of ACG oxidized by bromate with Cr(VI) as the catalyst. This hyphenation system incorporating very simple instrumentation, while provides a favorable detection limit for Cr(VI).

2. Experimental

2.1. Instrumentation

A FIA-3110 flow injection system (Titan Instruments Co., Beijing) equipped with a injection valve and two peristaltic pumps was employed for the preconcentration of Cr(VI). Fig. 1 shows the flow manifold. All the tubes used were 0.5 mm i.d. PTFE tubing.

A T6 UV–vis spectrophotometer with a 20 μ l flow cell (Beijing Purkinje General Instrument Co. Ltd.) was employed to monitor the decoloration of ACG oxidized by bromate. The working wavelength was set at 610 nm.

2.2. Reagents

All the reagents used were of the highest purity available but at least of analytical reagent grade, and deionized water of 18 M Ω cm⁻¹ was used throughout.

Chromium(VI) working standard solutions were prepared by step-wise dilution of a 1000 mg l⁻¹ stock solution.

A KBrO₃ solution (4.8×10^{-3} mol l⁻¹) was prepared by dissolving appropriate amount of KBrO₃ (A.R., Shenyang Dongling Fine Chemicals, China) in deionized water.

An ACG solution (5.0×10^{-4} mol l⁻¹) was prepared by dissolving 0.1556 g of ACG (A.R., Shanghai Chemicals Co.) in 5 ml of water. The solution was then diluted to 500 ml with 5.2% (v/v) H₃PO₄ (A.R., Tianjin Tianhe Chemicals).

A NaNO₃ solution (0.8 mol l⁻¹) was prepared by dissolving 34 g of NaNO₃ (A.R., Shanghai Chemicals Co.) in 500 ml of water.

Other chemicals used were: HCl (G.R., Tianjin Yaohua Chemicals Co., China), NaOH (G.R., Beijing Beihua Fine

Chemicals), AgNO₃ (G.R., Shanghai Chemicals Co.), PbO₂ (A.R., Shanghai Chemicals Co.), MnO₂ (A.R., Shanghai Chemicals Co.).

2.3. Pretreatment of resin beads and column packing

In order to increase the retention capacity of the column, the used 717# anion exchange resin beads (bead size 300–1200 μ m) were grinded, and particles of ca. 150 μ m in diameter were collected by using a mesh filter.

The beads were then washed thoroughly by introducing a series of washing/stirring procedure (30 min for each), including HCl (1 mol l⁻¹), NaOH (1 mol l⁻¹), HCl (1 mol l⁻¹). After each washing step, a thorough rinsing with deionized water was followed until the acidity of the water approached pH 7.

A 20 mm (length) \times 2 mm (diameter) mini-column was packed by using certain amount of resin beads, both ends of the column were blocked with glass wool.

2.4. Principles of the analysis

In acidic medium, the main chemical forms of trace Cr(VI) in aqueous solution are H₂CrO₄, HCrO₄⁻, CrO₄²⁻ and Cr₂O₇²⁻, while the forms of Cr(III) are mainly Cr³⁺, CrOH²⁺ and Cr(OH)₂⁺. Although there might be Cr(OH)₄⁻ in basic solution, it is readily feasible to separate Cr(III) and Cr(VI) species with anion exchange resin by controlling the acidity of the solution. The use of anion exchange also facilitates preconcentration of Cr(VI).

Cr(VI) was found to be an excellent catalyst for the decoloration reaction of ACG with bromate as the oxidizing reagent. The catalytic reaction significantly enhanced the detection limit of the catalyst, Cr(VI). Thus, this hyphenation system provides a promising approach for improving detection capabilities of trace species.

2.5. Sample pretreatment

The present procedure was applied to the speciation of chromium in surface water samples, including lake water, river

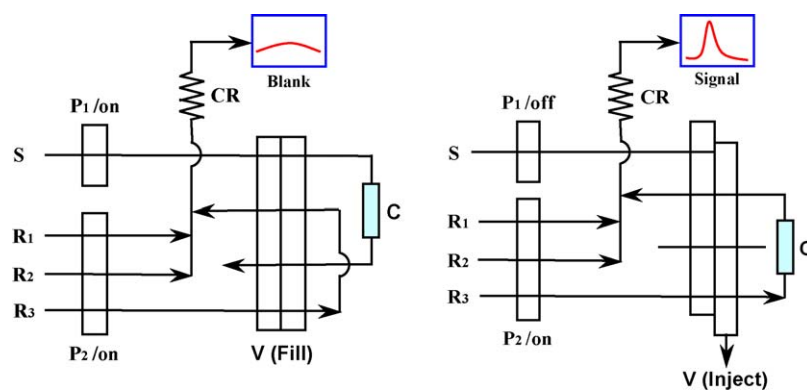


Fig. 1. The manifold of flow injection anion exchange preconcentration system hyphenated with BrO₃⁻–ACG decoloration reaction catalyzed with Cr(VI). CR: catalytic reaction coil; C: mini-column; S: sample; R₁: ACG; R₂: KBrO₃; R₃: NaNO₃; blank: read out in the absence of Cr(VI); signal: read out in the presence of Cr(VI).

water, rain water and tap water. All the water samples, except for tap water, were determined after filtration without any further treatment.

2.6. Operating procedure

As illustrated in Fig. 1 (fill), sample solution was delivered by peristaltic pump P₁ to pass through the anion exchange resin packed mini-column. Cr(VI) in sample solution was retained on the surface of the column while sample matrix components were directed to waste. At the same time, the solutions of BrO₃[−], ACG, and NaNO₃ were directed by the peristaltic pump P₂ to meet and flow through the decoloration reaction coil and the spectrophotometer to record the blank signal of the decoloration reaction in the absence of catalyst. The injection valve (IV) was afterward switched to *inject* position as illustrated in Fig. 1 (inject), P₂ was actuated and the elution of the retained Cr(VI) was facilitated by pumping NaNO₃ solution to flow through the column in an opposite direction. The eluate was further directed downstream to meet the BrO₃[−] and ACG solutions and catalyze the decoloration reaction. The signal related to the decoloration reaction in the presence of catalyst is thus recorded spectrophotometrically at the wavelength of 610 nm.

Cr(VI) concentration was derived from the above measurements, while total amount of chromium was obtained by oxidizing Cr(III) to Cr(VI) with appropriate oxidizing agent (see Section 3.5), and the Cr(III) was given by subtraction.

3. Results and discussion

3.1. Variables during the preconcentration stage

3.1.1. Sample acidity

It is known that Cr(VI) has various forms in aqueous solution, i.e., H₂CrO₄, HCrO₄[−], CrO₄^{2−} and Cr₂O₇^{2−}. The behaviors of the first three forms are similar to a binary acid, while Cr₂O₇^{2−} is a dimer, its distribution depends not only on the acidity, but also on its concentration. It is thus obvious that the acidity of the sample solution should be adjusted and controlled properly in order to facilitate the retention of Cr(VI). The experiments indicated that Cr(VI) was only partially retained by anion exchange column within the range of pH < 4, attributed to the existence of H₂CrO₄. Quantitative adsorption of Cr(VI) can only be achieved within the range of pH > 4 (Fig. 2). Although virtually a plateau was observed within the range of pH > 4, considering that in basic medium certain amount of Cr(III) converted to Cr(OH)₄[−], which might be retained and interfere with the determination of Cr(VI), the acidity of the sample solution was thus pre-adjusted to pH 5.

3.1.2. Loading flow rate and preconcentration time

In order to choose an appropriate sample loading flow rate, the kinetic property of the sorbent as well as the flow impedance created in the mini-column should be considered. The experimental results showed that by employing a fixed sample volume of 12 ml, quantitative adsorption of Cr(VI) could be achieved by employing a loading flow rate less than 6.0 ml min^{−1}, while

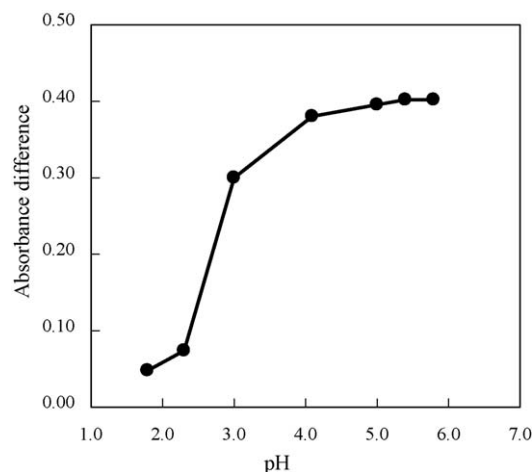


Fig. 2. The effect of acidity in the preconcentration stage. Preconcentration: 12 ml sample; loading flow rate 6.0 ml min^{−1}; eluent (NaNO₃) concentration/volume/flow rate: 0.8 mol l^{−1}/0.43 ml/1.3 ml min^{−1}; 5.0 μg l^{−1} Cr(VI). Catalytic reaction: 5.0 × 10^{−4} mol l^{−1} ACG; 4.8 × 10^{−3} mol l^{−1} KBrO₃; 5.2% (v/v) H₃PO₄; reaction temperature 90 °C; reaction time 240 s.

afterward a significant drop of the signal was recorded when exceeding this value until 12 ml min^{−1}. For further experiments, a sample loading flow rate of 6.0 ml min^{−1} was employed.

The overall sensitivity could be further improved by simply increasing the sample loading time or the sample volume, provided that break-through of the mini-column was not reached. Considering that the sensitivity of this procedure was sufficiently high for chromium speciation analysis in surface water samples encountered in this study, a sample volume of 12 ml was employed, corresponding to a sample loading time of 120 s.

3.1.3. The eluent and its concentration, volume and elution flow rate

The electrostatic interaction between anions and anion exchange resin depends on both the charge and size of the anion, thus the affinity of the column surface for various anions differ significantly with different anion forms. In order to select an appropriate eluent and effectively elute the analyte, this affinity should be considered. In addition, the eluate should have no interfering effect on the ensuing catalytic reaction. For this purpose, a series of potential eluents, including Na₂SO₄, H₂SO₄, KI, NaNO₃, HNO₃, KBr and NaCl, were examined. The experimental results indicated that NaNO₃ is most suitable for this purpose and it was thus employed for further experiments.

For a permanent column, an appropriate concentration and volume of the eluent should be chosen in order to obtain a complete elution of the retained Cr(VI), and at the same time facilitate the ensuing catalytic reaction under an optimal conditions. Thus, the effect of both NaNO₃ concentration within 0.2–1.0 mol l^{−1} as well as its corresponding volume for the elution of Cr(VI) were investigated. The results indicated that a higher signal was obtained by using 0.8 mol l^{−1} NaNO₃, and 430 μl of which sufficed the complete elution of the retained Cr(VI) within the concentration range encountered in the present study. For the ensuing experiments, 430 μl of 0.8 mol l^{−1} NaNO₃ was employed.

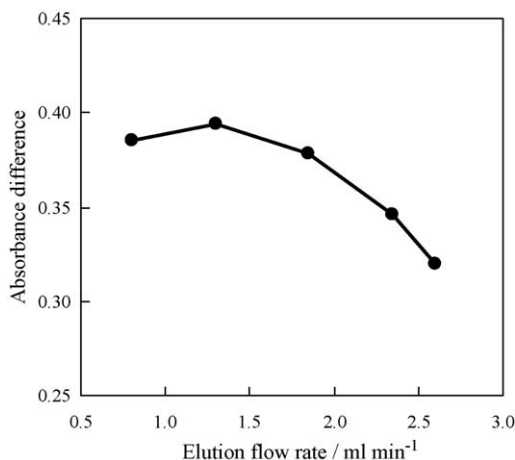


Fig. 3. The effect of elution flow rate. Preconcentration: 12 ml sample; sample acidity pH 5; loading flow rate 6.0 ml min^{-1} ; eluent (NaNO_3) concentration/volume: $0.8 \text{ mol l}^{-1}/0.43 \text{ ml}$; $5.0 \mu\text{g l}^{-1}$ Cr(VI). Catalytic reaction: $5.0 \times 10^{-4} \text{ mol l}^{-1}$ ACG; $4.8 \times 10^{-3} \text{ mol l}^{-1}$ KBrO_3 ; 5.2% (v/v) H_3PO_4 ; reaction temperature 90°C ; reaction time 240 s.

The experiments have shown that by employing a fixed volume of NaNO_3 , the elution flow rate within $0.8\text{--}2.6 \text{ ml min}^{-1}$ was found to significantly affect the elution efficiency of the retained Cr(VI), as illustrated in Fig. 3. It is obvious that lower flow rates less than 1.3 ml min^{-1} facilitated the complete elution, but a longer elution time caused increased dispersion of the eluate zone and thus deteriorated the catalytic efficiency of Cr(VI). After 1.3 ml min^{-1} , the increase of elution flow rate resulted in significant decline of the recorded signal attributed to partial elution of the retained Cr(VI). As a compromise, an elution flow rate of 1.3 ml min^{-1} was adopted for further investigations.

3.2. Variables during the catalytic reaction stage

3.2.1. The catalytic reaction system

One of the most critical issue in the hyphenation of on-line preconcentration system with catalytic indicator reaction is that the target analyte in the preconcentration stage should be an effective catalyst for the ensuing catalytic indicator reaction. In the case of Cr(VI), it has significant catalytic effect on the decoloration of ACG oxidized by bromate with detection by spectrophotometry.

3.2.2. The acidity for the catalytic reaction

The decoloration of ACG oxidized by bromate is preferentially performed in acidic medium. A series of acids were examined for this purpose. It indicated that when HCl was used for adjusting the acidity of the decoloration reaction, the non-catalytic decoloration of ACG was significantly accelerated in the absence of Cr(VI), i.e., the blank signal was considerably enhanced and the absorbance difference was minimized. On the contrast, H_2SO_4 inhibited the catalytic decoloration of the dye, and the absorbance difference was also drastically reduced. While in the acidic medium of H_3PO_4 , there is virtually no decoloration of ACG and a very low blank signal was recorded, while significant catalytic effect of Cr(VI) was observed and

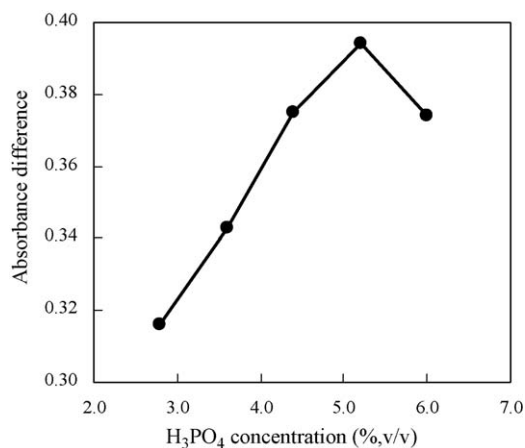


Fig. 4. The effect of H_3PO_4 concentration in the catalytic reaction stage. Preconcentration: 12 ml sample; sample acidity pH 5; loading flow rate 6.0 ml min^{-1} ; eluent (NaNO_3) concentration/volume/flow rate: $0.8 \text{ mol l}^{-1}/0.43 \text{ ml}/1.3 \text{ ml min}^{-1}$; $5.0 \mu\text{g l}^{-1}$ Cr(VI). Catalytic reaction: $5.0 \times 10^{-4} \text{ mol l}^{-1}$ ACG; $4.8 \times 10^{-3} \text{ mol l}^{-1}$ KBrO_3 ; reaction temperature 90°C ; reaction time 240 s.

the absorbance difference was magnified. Further investigations showed that an increase of the absorbance difference was recorded with increase of H_3PO_4 concentration up to 5.2% (v/v), while afterwards a remarkable decline of the signal was observed when exceeding this concentration, as illustrated in Fig. 4. For the ensuing investigations, a H_3PO_4 concentration of 5.2% (v/v) was employed.

3.2.3. The concentrations of oxidizing reagent and the dye

Generally, oxidizing decoloration reactions of organic dyes in the presence of an appropriate catalyst depend strongly on the concentrations of both oxidizing reagent and dye. In the present reaction system, the concentrations of both bromate and ACG should be carefully optimized in order to improve the detection sensitivity. Experiments showed that by fixing the concentration of ACG, a significant increment of the absorbance difference was recorded with the increase of bromate concentration in the range 1.2×10^{-3} to $4.8 \times 10^{-3} \text{ mol l}^{-1}$, afterwards a plateau was observed with further increase of the bromate concentration up to $7.2 \times 10^{-3} \text{ mol l}^{-1}$ (Fig. 5). A bromate concentration of $4.8 \times 10^{-3} \text{ mol l}^{-1}$ was selected.

With a fixed concentration of bromate, the increase of ACG concentration from 0.5×10^{-4} to $5.5 \times 10^{-4} \text{ mol l}^{-1}$ resulted in a steep increase of decoloration. Although a further increase of the concentration gave rise to an even higher absorbance difference, the obtained precision was significantly deteriorated, i.e., 2.0% R.S.D. at $5.0 \times 10^{-4} \text{ mol l}^{-1}$, while 6.2% R.S.D. at $5.5 \times 10^{-4} \text{ mol l}^{-1}$. As a compromise, the ACG concentration was selected as $5.0 \times 10^{-4} \text{ mol l}^{-1}$.

3.2.4. The catalytic reaction temperature and stopped flow time

The reaction temperature usually has significant effect on the catalytic indicator reaction. This is also hold true for the present case. Fig. 6 illustrated the influence of temperature on the catalytic decoloration of ACG oxidized by bromate. It is

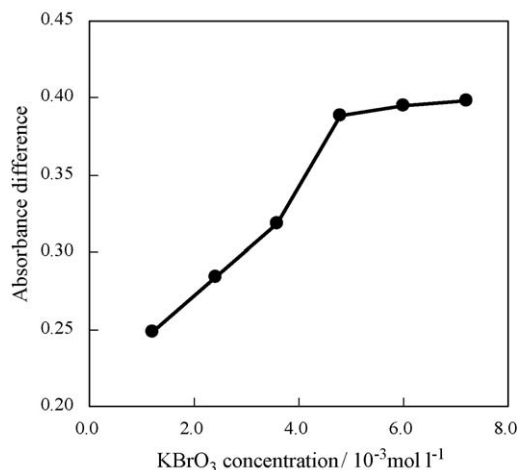


Fig. 5. The effect of KBrO₃ concentration in the catalytic reaction stage. Preconcentration: 12 ml sample; sample acidity pH 5; loading flow rate 6.0 ml min⁻¹; eluent (NaNO₃) concentration/volume/flow rate: 0.8 mol l⁻¹/0.43 ml/1.3 ml min⁻¹; 5.0 μg l⁻¹ Cr(VI). Catalytic reaction: 5.0 × 10⁻⁴ mol l⁻¹ ACG; 5.2% (v/v) H₃PO₄; reaction temperature 90 °C; reaction time 240 s.

obvious that the decoloration was remarkably enhanced with the increase of reaction temperature. The absorbance difference reached a maximum at 90 °C and remain virtually unchanged or showed a slight decline with further increase of the temperature. This is attributed to the fact that at a higher temperature, both the catalytic reaction and non-catalytic reaction or blank reaction were accelerated, which resulted in a slight decrease of the absorbance difference. For the ensuing studies, a temperature of 90 °C was selected.

Catalytic reactions based on the decoloration of organic dyes are usually slow ones, it is thus necessary to adopt stopped flow technique in order to improve the detection sensitivity. The experiments showed that the absorbance difference of the decoloration of ACG increased linearly with the increase of stopped flow time up to 420 s. Further increase of the reaction time gave

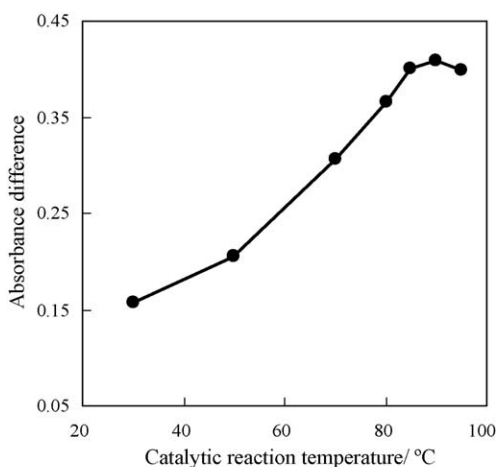


Fig. 6. The effect of catalytic reaction temperature. Preconcentration: 12 ml sample; sample acidity pH 5; loading flow rate 6.0 ml min⁻¹; eluent (NaNO₃) concentration/volume/flow rate: 0.8 mol l⁻¹/0.43 ml/1.3 ml min⁻¹; 5.0 μg l⁻¹ Cr(VI). Catalytic reaction: 5.0 × 10⁻⁴ mol l⁻¹ ACG; 4.8 × 10⁻³ mol l⁻¹ KBrO₃; 5.2% (v/v) H₃PO₄; reaction time 240 s.

rise to a decline of the absorbance difference, which is attributed to the dispersion of the reaction zones. Practically, a longer stopped flow time and a higher sensitivity sacrifice the sample throughput. As a compromise, a stopped flow time of 240 s was chosen.

3.3. Interferences

The potential interfering effects of some foreign species were tested with the present procedure. At a Cr(VI) concentration of 5.0 μg l⁻¹ and within a ±5% error range, no interfering effects were observed in the presence of metal species at concentration levels frequently encountered in environmental samples, especially for surface water samples. The tolerance limits for some of the anions: SO₄²⁻ (5 × 10⁴-fold), HCO₃⁻ (10⁴-fold), CO₃²⁻, ClO₃⁻, IO₃⁻ (1000-fold), F⁻ (500-fold), Cl⁻ (35-fold), Br⁻ (10-fold), I⁻ (5-fold), SO₃²⁻, S₂O₃²⁻ and NO₂⁻ (1-fold). It is obvious that Cl⁻, Br⁻, I⁻, SO₃²⁻, S₂O₃²⁻ and NO₂⁻ are potentially interferents for the determination of Cr(VI), and their removal from the sample solution is highly required. The elimination of interfering species was demonstrated in Section 3.5.

3.4. Performance and validation of the procedure

Under the aforementioned optimal conditions, the performance data obtained for the hyphenation of flow injection on-line anion exchange preconcentration of Cr(VI) with catalytic decoloration reaction of BrO₃⁻–ACG for Cr(VI) determination were summarized in Table 1. With a sample loading volume of 12 ml, an enrichment factor of 26.5 was obtained for the preconcentration stage, along with a retention efficiency of 95.4%. It is worth mentioning that the overall detection limit of the system for Cr(VI), i.e., 0.05 μg l⁻¹ by defining it as three times the blank standard deviation (3σ), was comparable to those obtained with detection by ICPMS and ETAAS, while the instrumentation employed herein is most simple and convenient.

A comparison of the detection limit and precision of the present procedure with some of the reported ones based on ETAAS, ICPMS, FAAS were summarized in Table 2. It is obvious that the sensitivity of the present protocol is much superior to those achieved with detection by FAAS [12–14]. Furthermore, it is also comparable to those of the published procedures with detection by ETAAS and/or ICPMS [15–22].

Table 1

Analytical performance of on-line anion exchange preconcentration hyphenated with Cr(VI) catalyzed BrO₃⁻–ACG decoloration reaction for Cr(VI) determination

Sample volume	12 ml
Linear calibration range	0.2–6.0 μg l ⁻¹
Regression equation	$A = 0.0742C_{\text{Cr(VI)}} + 0.0174$
Correlation coefficient	0.9994
Enrichment factor	26.5
Detection limit (3σ, n = 11)	50 ng l ⁻¹
R.S.D. (1.0 μg l ⁻¹ , n = 11)	2.1%
Retention efficiency	95.4%
Sampling frequency	10 h ⁻¹

Table 2

The detection limit for Cr(VI) and precision of the present procedure versus some of the reported data based on atomic spectrometry

Methods/samples analyzed	LOD ($\mu\text{g l}^{-1}$)	%R.S.D. ($\mu\text{g l}^{-1}$)	Reference
FI-FAAS: SPE on modified silica gel (tap/well/lake water)	2.3	3 (100)	[12]
FI-FAAS: SPE on PTFE surface (water, marine sediment)	0.8	3.2 (20)	[13]
SI-FAAS: SPE on activated alumina (sewage water)	42	10 (2000)	[14]
ETAAS (water)	0.67		[15]
ETAAS (mineral water)	0.005		[16]
ETAAS: extraction on Amberlite LA-2 (wastewater, sludge)	0.45	7.2 (2)	[17]
ETAAS: SPE on Diaion HP-2MG resin (mineral water)	0.03	5 (5.6)	[18]
ICPMS (wastewaters)	0.15		[19]
HPLC-ICPMS (surface water)	5.5	8	[20]
ICPMS (river and reservoir water)	0.06	<10	[21]
FI-ICPMS: SPE on chelating resin (sea water)	0.02	1.9	[22]
This procedure (surface waters)	0.05	2.1 (1.0)	

SI: sequential injection, FI: flow injection, SPE: solid phase extraction.

Table 3

The determination of Cr(VI) in a certified reference material (GBW08608) and chromium speciation in surface water samples ($n=3$)

Samples	Cr(VI) certified ($\mu\text{g l}^{-1}$)	Cr(VI) found ($\mu\text{g l}^{-1}$)	Cr(III) found ($\mu\text{g l}^{-1}$)	Cr(VI) spiked ($\mu\text{g l}^{-1}$)	Recovery (%)
GBW08608	31.4 \pm 2.0	29.8 \pm 1.6			
River water		37.2 \pm 2.6	78.3 \pm 6.3	100.0	98
Lake water		22.5 \pm 3.1	15.9 \pm 1.2	40.0	95
Rain water		2.5 \pm 0.5	3.7 \pm 0.2	5.0	103
Tap water		3.5 \pm 0.6	3.1 \pm 0.2	5.0	98

The procedure was validated using a certified reference material, i.e., GBW08608 (Trace elements in water). The obtained result was summarized in Table 3 showing agreement between the obtained and the certified values.

3.5. Real sample analysis

It can be seen obviously from Section 3.3 that the tolerance limits for $\text{S}_2\text{O}_3^{2-}$, SO_3^{2-} and NO_2^- are too low to avoid their interfering effects without sample pretreatment. In addition, the contents of Cl^- , Br^- and I^- in general surface water samples are also more than enough to interfere the preconcentration and subsequent determination of Cr(VI). Therefore, the elimination of these species before analysis is highly desired. For this purpose, 0.15 g of MnO_2 was employed as oxidizing agent to remove the interfering effects from $\text{S}_2\text{O}_3^{2-}$, SO_3^{2-} and NO_2^- in 50 ml of water sample. The potential of E^0 ($\text{MnO}_2\text{--Mn}^{2+}$) is 1.208 V (acidic medium), which is lower than that of E^0 ($\text{Cr}_2\text{O}_7^{2-}\text{--Cr}^{3+}$), i.e., 1.33 V. Thus, $\text{S}_2\text{O}_3^{2-}$, SO_3^{2-} and NO_2^- can easily be oxidized into no interfering SO_4^{2-} and NO_3^- , while Cr(III) was not oxidized at all. The residue MnO_2 was filtered and about 0.1 g of AgNO_3 was afterwards added in order to get rid of the Cl^- , Br^- and I^- by forming precipitate. After filtration, the water sample is suitable for Cr(VI) determination.

In order to convert Cr(III) to Cr(VI), PbO_2 was employed as the oxidizing agent. Considering the higher potential of E^0 ($\text{PbO}_2\text{--Pb}^{2+}$), i.e., 1.46 V in acidic medium, Cr(III) can be readily converted to Cr(VI). At the same time, the aforementioned interfering effects arising from $\text{S}_2\text{O}_3^{2-}$, SO_3^{2-} and NO_2^- were eliminated. The operation include addition of 0.15 g of PbO_2

into the water sample pre-adjusted to $\text{pH} < 2.5$, and the mixture was stirred for 30 min at 85°C . The solution was then filtered, and 0.1 g of AgNO_3 was added in order to precipitate the Cl^- , Br^- and I^- anion. After filtration, the total amount of chromium was determined by using the established procedure.

The obtained results were listed in Table 3.

4. Conclusions

In order to develop a practical procedure for chromium speciation in surface water samples by using simple instrumentation, flow injection on-line anion exchange preconcentration was hyphenated with catalytic decoloration reaction of an organic dye (ACG) with Cr(VI) as the catalyst. One of the most distinct feature of this procedure is characterized by its favorable detection limit, which has been improved by both preconcentration and catalytic magnification, it is not only much superior to those achieved with detection by FAAS, but also comparable to those obtained with detection by ETAAS and ICPMS.

Acknowledgements

The authors are indebted to the financial support from the National Natural Science Foundation of China (NSFC-20375007), the key project for scientific research from the Ministry of Education, China (105056), the Natural Science Foundation of Liaoning Province (20042011), the SRFDP program (20050145026), and the China Postdoctoral Science Foundation.

References

- [1] M.A. White, E. Sabbioni, *Sci. Tot. Environ.* 216 (1998) 253.
- [2] T. Barkay, H. Pritchard, *Microbiol. Sci.* 5 (1988) 165.
- [3] N.D. Hadjiliadis, *Cytotoxic, Mutagenic and Carcinogenic Potential of Heavy Metals Related to Human Environment*, Kluwer Academic Publishers, Dordrecht, The Netherlands, 1996.
- [4] J. Szpunar, *Analyst* 125 (2000) 963.
- [5] B. Michalke, *Fresenius J. Anal. Chem.* 354 (1996) 557.
- [6] B. Michalke, H. Witte, P. Schramel, *J. Anal. Atom. Spectrom.* 16 (2001) 593.
- [7] N. Miekeley, T.R.C. Pereira, E.A. Casartelli, C. Almeida, M. de FB Carvalho, *Spectrochim. Acta, Part B* 60 (2005) 633.
- [8] B. Michalke, *J. Chromatogr. A* 1050 (2004) 69.
- [9] O. Schramel, B. Michalke, A. Kettrup, *Fresenius J. Anal. Chem.* 363 (1999) 452.
- [10] A.L. Rosen, G.M. Hieftje, *Spectrochim. Acta, Part B* 59 (2004) 135.
- [11] M. Leermakers, W. Baeyens, M. De Gieter, B. Smedts, C. Meert, H.C. De Bisschop, R. Morabito, Ph. Quevauviller, *Trend. Anal. Chem.* 25 (1) (2006) 1–10.
- [12] H.F. Maltez, E. Carasek, *Talanta* 65 (2005) 537.
- [13] A.N. Anthemidis, G.A. Zachariadis, J.-S. Kougoulis, J.A. Stratis, *Talanta* 57 (2002) 15.
- [14] M.J. Marques, A. Morales-Rubio, A. Salvador, M. de la Guardia, *Talanta* 53 (2001) 1229.
- [15] M.I.C. Monteiro, A.K. Avila, R. Neumann, *Anal. Chim. Acta* 428 (2001) 265.
- [16] Y. He, M.L. Cervera, A. Pastor, M. de la Guardia, *Anal. Chim. Acta* 447 (2001) 135.
- [17] A.S. Stasinakis, N.S. Thomaidis, T.D. Lekkas, *Anal. Chim. Acta* 478 (2003) 119.
- [18] J. Chwastowska, W. Skwara, E. Sterlinska, L. Pszonicki, *Talanta* 66 (2005) 1345.
- [19] M.V.B. Krishna, K. Chandrasekaran, S.V. Rao, D. Karunasagar, J. Arunachalam, *Talanta* 65 (2005) 135.
- [20] A.F. Roig-Navarro, Y. Martinez-Bravo, F.J. Lopez, F. Hernandez, *J. Chromatogr. A* 912 (2001) 319.
- [21] B. Wen, X.-Q. Shan, J. Lian, *Talanta* 56 (2002) 681.
- [22] S. Hirata, K. Honda, O. Shikino, N. Maekawa, M. Aihara, *Spectrochim. Acta, Part B* 55 (2000) 1087.

Structural study of oriental lacquer films during the hardening process

Noriyasu Niimura^{a,*}, Tetsuo Miyakoshi^b

^a International Technical and Training Center, JEOL DATUM Ltd., 1156 Nakagami-cho Akishima-shi, Tokyo 196-0022, Japan

^b Department of Industrial Chemistry, Meiji University, Higashimita Tama-ku, Kawasaki-shi 214-8571, Japan

Received 3 October 2005; received in revised form 14 December 2005; accepted 16 December 2005

Available online 24 January 2006

Abstract

Oriental lacquer is the natural resin obtained by tapping lac trees. It hardens into a tough and insoluble film. The extreme hardness and insolubility are some of the most important functions, which are required for industrial coating materials. In this study, two kinds of oriental lacquer films, traditionally named Kiurushi (raw urushi) and Kuromeurushi produced by two different pretreatments, were analyzed during hardening with Fourier transform infrared spectroscopy (FT-IR), thermogravimetry/differential thermal analysis–mass spectrometry (TG/DTA–MS) and pyrolysis–gas chromatography/mass spectrometry (Py–GC/MS) to investigate their functional expression process. Typical functional groups of the lacquer films were detected by FT-IR. The TG/DTA–MS curves clarified that the thermal degradation of the lacquer films gradually began at around 200 °C, and reached the fastest rate at 400–500 °C. Apparently, FT-IR and TG/DTA–MS could not reveal any difference between the films. On the other hand, Py–GC/MS revealed differences between the films in the peak area ratios of 3-pentadecenylcatechol to 3-pentadecylcatechol and 3-pentadecadienylcatechol to 3-pentadecylcatechol. The ratios of Kiurushi lacquer film were higher than those of Kuromeurushi lacquer film. Both ratios, furthermore, decreased during hardening due to polymerization of the alkenylcatechols into an urushiol polymer skeleton comprising nucleus–side chain and side chain–side chain cross-linkages with 3-pentadecylcatechol at the terminal. The present results suggest that the reaction rate of these cross-linkages in Kuromeurushi lacquer film is faster than that in Kiurushi lacquer film. A good correlation was found between the peak area ratios obtained by Py–GC/MS and hardness obtained by pencil hardening testing. Oriental lacquer expresses the functions – an extreme hardness and insolubility – accelerating the nucleus–side chain and side chain–side chain cross-linkages. Furthermore, it has become clear that the traditional treatments called Nayashi and Kurome effectively accelerate the hardening rate by activating the cross-linkages.

© 2005 Elsevier B.V. All rights reserved.

Keywords: Structural study; Oriental lacquer film; Natural resin; Cross-linkage; Py–GC/MS; FT-IR; TG/DTA–MS

1. Introduction

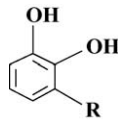
Natural resin has been used as adhesives, coating and painting materials, and so on for a long time. Nowadays, plastics are mostly used instead of the natural resin. However, it has been realized that plastics cause environmental problems such as dioxin, sick house syndrome and so on in this century. Furthermore, it has been warned that petroleum resources could be exhausted. Development of substitutes for plastics, which cause no environmental problem and are made from renewable resources for global sustainability without depletion of scarce resources, has been desired. In response to this desire, the development of biomimetic polymers has been studied. As an example, cardanol polymers have been developed [1]. These

polymers cause no environmental problem and are made from cashew nut shell liquid, which is oozed from cashew nut shells. Along this line, the synthesis of artificial urushis, which are modeled after natural resins, has been studied [2].

In this situation, we have studied the structure and the process of functional expression of natural resin films [3–6]. Based on these studies, we have developed functional coating films produced from biomasses [7–9]. We have applied various analytical methods to these studies with newly developed analytical techniques [10–13]. For example, an angle-resolved measurements using X-ray photoelectron spectroscopy (XPS) has been applied to surface structural analysis of oriental lacquer films to investigate the process of functional expressions [14,15]. The oriental lacquer is the sap obtained by tapping lac trees, specifically *Rhus vernicifera* (China, Korea and Japan) [16]. The sap is a latex material composed of urushiol (60–65%), water (20–25%), plant gum (5–7%), glycoprotein (2–5%) and laccase enzyme (1%) [17]. The composition of the urushiol has been investigated using

* Corresponding author. Tel.: +81 42 542 5502; fax: +81 42 541 9513.
E-mail address: niimura@jeol.co.jp (N. Niimura).

Table 1
The components of urushiol

	R	MW	%
	C ₁₅ H ₃₁	320	4.5
	8(Z)-C ₇ H ₁₄ CH=CHC ₆ H ₁₃	318	15.0
	10(Z)-C ₉ H ₁₈ CH=CHC ₄ H ₉	318	1.5
	8(Z),11(E)-C ₇ H ₁₄ CH=CHCH ₂ CH=CHC ₃ H ₇	316	4.4
	8(Z),11(Z)-C ₇ H ₁₄ CH=CHCH ₂ CH=CHC ₃ H ₇	316	6.5
	8(Z),11(E),13(E)-C ₇ H ₁₄ CH=CHCH ₂ CH=CHCH=CHCH ₃	314	1.7
	8(Z),11(E),13(Z)-C ₇ H ₁₄ CH=CHCH ₂ CH=CHCH=CHCH ₃	314	55.4
	8(Z),11(E),14-C ₇ H ₁₄ CH=CHCH ₂ CH=CHCH ₂ CH=CH ₂	314	7.4
	10(Z)-C ₉ H ₁₈ CH=CHC ₆ H ₁₃	346	1.5
	8(Z),11(Z)-C ₇ H ₁₄ CH=CHCH ₂ CH=CHC ₅ H ₁₁	344	1.8

gel permeation chromatography (GPC), high performance liquid chromatography (HPLC) and nuclear magnetic resonance (NMR) spectroscopy [18,19]. The components of urushiol are shown in Table 1. It was reported that the dimerization of urushiol proceeds through laccase-catalyzed C–C coupling [20,21]. However, many other kinds of reactions are presumed to occur during the film-making process. By angle-resolved measurements using XPS, we have found that the surface of the oriental lacquer films are rich in plant gum, which acts as a barrier against oxygen diffusion, and that the top surface is covered with urushiol, whose catechol rings are oriented to retard the radical chain reactions. These surface structures are responsible for high durability of the lacquer film. Furthermore, using pyrolysis–gas chromatography/mass spectrometry (Py–GC/MS) to investigate the molecular structure of the urushiol polymers, we have clarified that the urushiol polymers consist of nucleus–side chain and side chain–side chain cross-linkages [22–25]. The oriental lacquer is extremely hard and insoluble. These functions must be attributed to these cross-linkages.

In this study, we investigated structural changes of two kinds of oriental lacquer films during the hardening process to clarify the expression process of these functions. One lacquer film was treated by the traditional Nayashi and Kurome methods [26], which had been believed to promote the hardening reaction and improve the quality of the lacquer film, but the other film was not treated by these methods. The process of the functional expression of oriental lacquer films has been studied by comparing the Py–GC/MS results of these lacquer films.

2. Experimental

2.1. Sample

Two types of lacquer films – Kiurushi (raw urushi) and Kuromeurushi – were prepared as samples in this study. The former was produced by coating the sap of Chinese lacquer trees at Chengkou in the Hubei Province of China on glass plates without any pretreatment, while the latter with the traditional pretreatment called Nayashi and Kurome [26]. The sap was purchased from Tohtyu-Urushi-Ten (Osaka, Japan). The water concentration of the sap was 25%. Nayashi and Kurome processing was carried out in our laboratory as follows: the sap of 20 g was

stirred in an open vessel (bottom diameter: 80 mm; capacity: 100 ml) at room temperature for 1.5 h, and the temperature was then increased from 20 to 30 °C for 2 h until the water concentration was reduced to 3%. The both films were kept in a humidity-controlled chamber with relative humidity of 70% at 20 °C for two weeks. They were then removed from the chamber and left to dry in open air at room temperature for various times from 4 to 60 days. The thickness of lacquer films was 76 µm.

2.2. Pencil hardness testing

Scratch hardness of the sample films was measured with the pencil hardness testing with a pencil hardness tester: C-221 type (Yoshimitsu Seiki Co. Ltd.) with different pencils of various hardness (B-5H) [27]. The hardness obtained by this testing is expressed as 6H, 5H, . . . , 2H, H, F, HB, B, 2B, . . . , 5B, 6B in the order from the hardest to the softest, based on the pencil hardness.

2.3. Fourier transform infrared (FT-IR) spectroscopy

FT-IR spectra of sample films were obtained using a KBr pellet technique with an FT-IR spectrometer: JIR-6500 (JEOL Ltd.). To prepare the KBr pellets, each sample film of 2 mg was ground together with FT-IR grade KBr of 200 mg for 2 min. The FT-IR was operated at a resolution of 2 cm^{−1} and the collection time was 25 s (16 scans).

2.4. Thermogravimetry/differential thermal analysis–mass spectrometry (TG/DTA–MS)

TG/DTA–MS measurements were performed with a thermogravimetry/differential thermal analyzer TG/DTA 6300 (Seiko Instruments Inc.) and a mass spectrometer JMS-K9 (JEOL Ltd.). A sample film of 0.5 mg was placed in a furnace of the analyzer which was programmed to raise the temperature at a constant rate of 30 °C/min in a range from 50 to 900 °C. Helium was used for a carrier gas at a flow rate of 100 ml/min in the TG/DT analyzer. A part of the flow with a reduced rate of 2 ml/min at a capillary interface tube by a splitter was introduced into the mass spectrometer. Evolved gases ionized using an electron ionization at 70 eV were analyzed with the mass spectrometer.

2.5. Pyrolysis–gas chromatography/mass spectrometry (Py–GC/MS)

Py–GC/MS was carried out with a vertical microfurnace-type pyrolyzer: PY-2010D (Frontier Lab.), a gas chromatograph: Agilent 6890 (Agilent Ltd.) and a mass spectrometer: JMS-K9 (JEOL Ltd.). A sample film of 0.5 mg was placed in a platinum sample cup, which was set at the top of the pyrolyzer kept at room temperature. The sample cup was inserted into a furnace at 400 °C, followed by heating a gas chromatograph oven, which was programmed to raise the temperature at a constant rate of 20 °C/min in a range from 40 to 330 °C. Helium was used as a carrier gas at a flow rate of 50 ml/min in the pyrolyzer, which was reduced to 1 ml/min with a splitter at the capillary column in the gas chromatograph. A stainless steel capillary column with an inner diameter of 0.25 mm and a length of 30 m coated with 0.25 μ m thick Ultra Alloy PY-2 – methylsilicone 100% – was used for separation. Ionization method of the mass spectrometer was electron ionization with an ionization energy of 70 eV.

3. Results and discussion

3.1. Pencil hardness testing

The hardness of the two types of lacquer films is shown as a function of drying time from 4 to 60 days in Table 2. After 4 day drying, the shortest drying time, Kiurushi shows the hardness of F, while Kuromeurushi shows that of 4H. The hardness

Table 2

Results of pencil hardness testing

Drying time (days)	4	14	30	60
Kiurushi	F	H	2H	5H
Kuromeurushi	4H	4H	4H	5H

of Kiurushi gradually increases with drying time from F to 5H after 60 day drying. In contrast, that of Kuromeurushi shows rather high hardness of 4H after the shortest drying time and slightly increases to 5H after 60 day drying, the longest drying time, which is the same as that of Kiurushi. The observed hardness in this table clearly shows that the traditional pretreatment of Nayashi and Kurome accelerates the hardening rate of the lacquer film.

3.2. FT-IR measurements

FT-IR spectra of the two types of lacquer films, Kiurushi and Kuromeurushi, after 4 day drying are shown in Fig. 1. Overall patterns of these two spectra are quite similar to each other. Eight main absorption peaks are observed in these spectra. They are designated as 1–8, as shown in Fig. 1. Based on these peaks, five functional groups are identified as follows—OH: 3407 cm^{-1} (1) and 1272 cm^{-1} (7); C–H: 3013 cm^{-1} (2), 2926 cm^{-1} (3), 2853 cm^{-1} (4) and 1455 cm^{-1} (6); C=O: 1621 cm^{-1} (5); Ph: about 1500 and 1600 cm^{-1} ; conjugated triene: 993 cm^{-1} (8). The OH functional group is attributed to urushiol, but C=O and

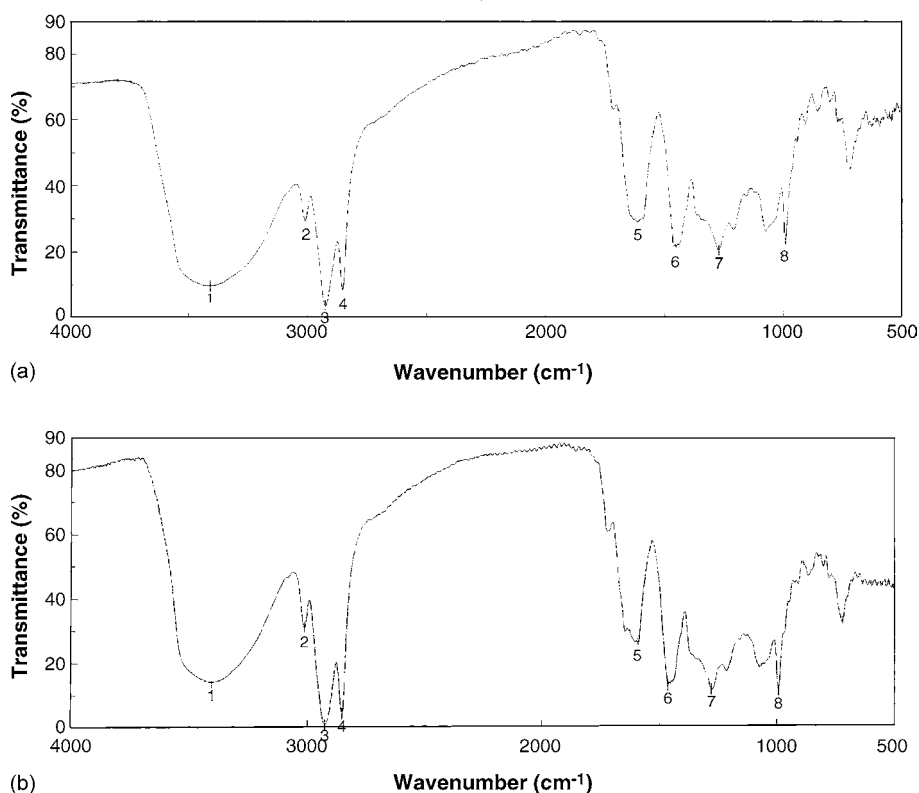


Fig. 1. FT-IR spectra of the lacquer films after 4 day drying. (a) Kiurushi and (b) Kuromeurushi. OH: (1) 3407 cm^{-1} , (7) 1272 cm^{-1} , C–H: (2) 3013 cm^{-1} , (3) 2926 cm^{-1} , (4) 2853 cm^{-1} , (6) 1455 cm^{-1} , C=O: (5) 1621 cm^{-1} , Ph: about 1500 and 1600 cm^{-1} , conjugated triene, (8) 993 cm^{-1} .

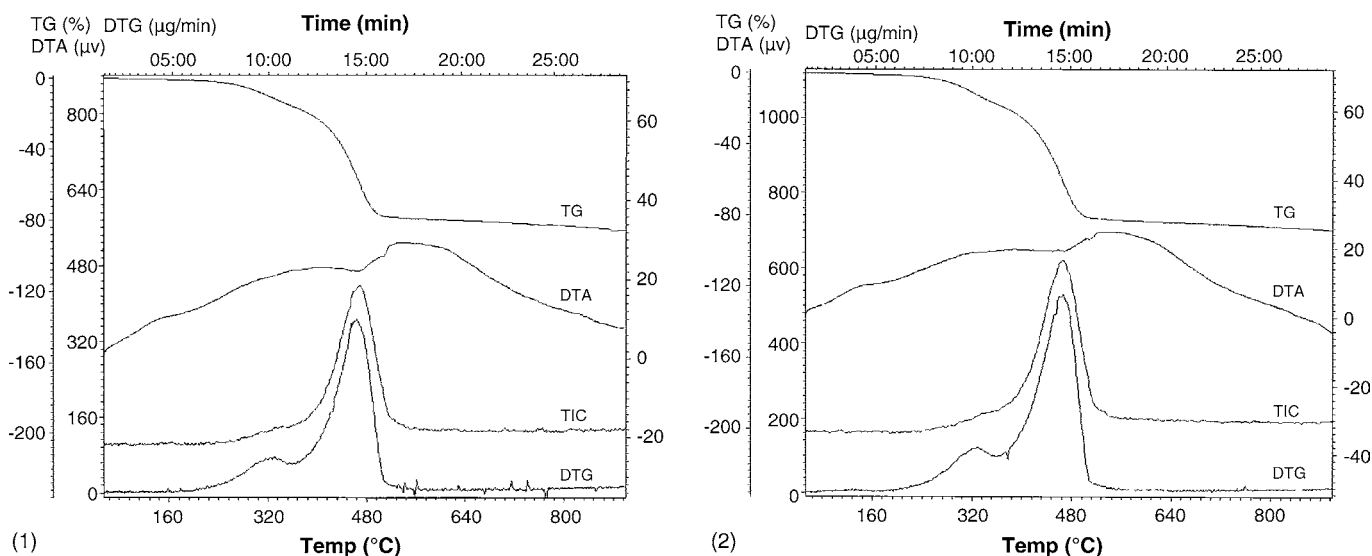


Fig. 2. TG, DTA, DTG curves and TIC of the lacquer films after 4 day drying: (1) Kiurushi and (2) Kuromeurushi.

conjugated triene functional groups do not exist in the urushiol. It has been reported that the peak intensity of C=O and conjugated triene functional groups increases with the progress of urushiol polymerization [28], thus these functional groups are attributed to the oxidative polymerization of urushiol.

Although the pencil hardness of these two types of films are substantially different as shown in Table 2, only a slight difference between these films is observed even in the intensities of peaks 5 and 8 so that a higher peak resolution for FT-IR spectra is needed to correlate the FT-IR spectra with the pencil hardness.

3.3. TG/DTA–MS measurements

TG, DTA and DTG curves and TIC of respective lacquer films after 4 day drying are shown in Fig. 2. No distinct difference was observed in the three curves and TIC of the two types of lacquer films. The TG and DTA curves indicate that the thermal degradation of the lacquer films gradually begins at around 200 °C, and the degradation rate becomes fastest at 400–500 °C. The TIC and DTG curves confirm the above results showing peaks at 470 °C. These peaks were attributed to evolved gas during the thermal degradation.

Previously, we reported that the pyrolysis products of glycoprotein are detected from the lacquer film by the pyrolysis at 200 °C. Alkylcatechols and alkenylcatechols are observed as the thermally decomposed components from the terminal alkyl- and alkenylcatechol-side chains of the lacquer film by the pyrolysis at 300 °C. Alkylphenols and alkenylphenols are detected as the pyrolysis products of the nucleus–side chain C–O coupling urushiol polymer, which is the main component of the lacquer film, by the pyrolysis at 500 °C [22].

In this study, the gases evolved at around 200, 300 and 500 °C must be attributed to these steps of degradations. We tried to confirm the detection of these components by identifying each mass spectrum, but it was difficult, because the spectra were very complicated. The evolved gases consisted of mixed compounds. Chromatographic methods are needed to identify these gases.

3.4. Py–GC/MS measurements

Fig. 3 shows TICs and mass chromatograms (m/z 320, 318, 316, 314) of the two types of lacquer films after 4 day drying. Peaks 1–3 were detected at retention times of 13.98, 13.90 and 13.62 min in the mass chromatograms (m/z 320, 318 and 316, respectively), but no peak was detected at retention time of around 13 min in the mass chromatograms (m/z 314). If 3-pentadecatrienylcatechol (MW 314), which is urushiol monomer, is produced by the pyrolysis, a peak should be detected at retention time of around 13 min in the mass chromatograms (m/z 314) [7]. Peaks 1–3 were identified as 3-pentadecylcatechol (MW 320), 3-pentadecenylcatechol (MW 318) and 3-pentadecadienylcatechol (MW 316) based on the mass spectra. The mass spectrum of peak 1 is shown in Fig. 4. The molecular ion peak was detected at m/z 320. The base ion peak at m/z 123 was a typical fragment ion peak of an alkylcatechol. These pyrolyzed products are urushiol monomers, which are produced from the terminal groups of urushiol polymers [6]. Pyrolysis mechanism of the terminal groups is shown in Fig. 5. The reaction rate of the nucleus–side chain C–C coupling depends on the degree of unsaturation of the side chain. The reaction rate of the nucleus–trienyl side chain C–C coupling is the fastest and that of the nucleus–dienyl side chain C–C coupling is the second fastest. That of the nucleus–monoeryl side chain C–C coupling is third, while that of the nucleus–unsaturated side chain C–C coupling is the slowest [3,5]. Therefore, it is assumed that the terminal groups consist of more saturated urushiols and monoeryl urushiols than dienyl urushiols and trienyl urushiols at the end of the hardening process.

To confirm the above assumption, the areas of the respective peaks identified as 3-pentadecylcatechol, 3-pentadecenylcatechol, 3-pentadecadienylcatechol and 3-pentadecatrienylcatechol were measured after 4, 17, 38 and 60 day drying. 3-Pentadecatrienylcatechol was not detected after 4 day drying as shown in Fig. 3. Since the reaction rate of the nucleus–trienyl side chain C–C coupling is the fastest, 3-pentadecatrienylcatechol

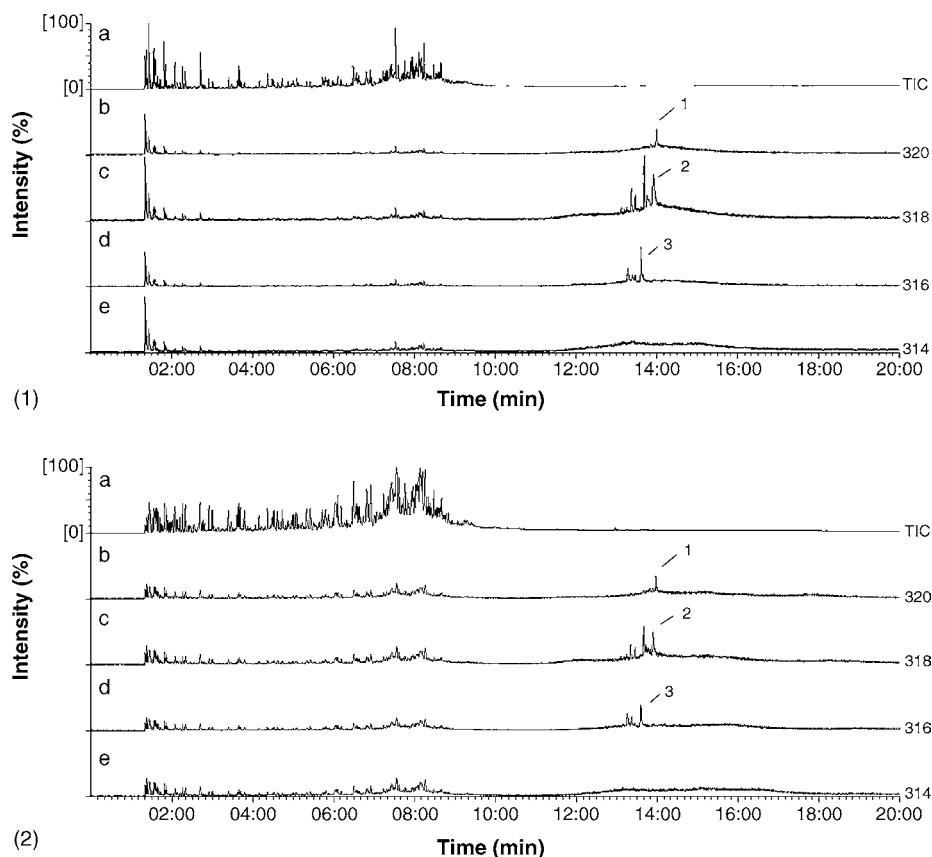


Fig. 3. TICs and mass chromatograms of Kiurushi (1) and Kuromeurushi (2) lacquer films after 4 day drying: (a) TIC; (b) mass chromatogram (m/z 320), 1:3-pentadecylcatechol (MW 320); (c) mass chromatogram (m/z 318), 2:3-pentadecenylcatechol (MW 318); (d) mass chromatogram (m/z 316), 3:3-pentadecadienylcatechol (MW 316); (e) mass chromatogram (m/z 314).

has already been taken into the skeleton of urushiol polymer after 4 day drying. 3-Pentadecylcatechol, 3-pentadecenylcatechol and 3-pentadecadienylcatechol were detected in the respective analyses. The peak areas of 3-pentadecenylcatechol and 3-pentadecadienylcatechol significantly decreased with the

increase in drying time. These peak areas of the two lacquer films after 60 day drying were the lowest. The rate of decrease in their peak areas was compared between Kiurushi and Kuromeurushi lacquer films. Fig. 6 shows a comparison of the peak area ratios of 3-pentadecenylcatechol to

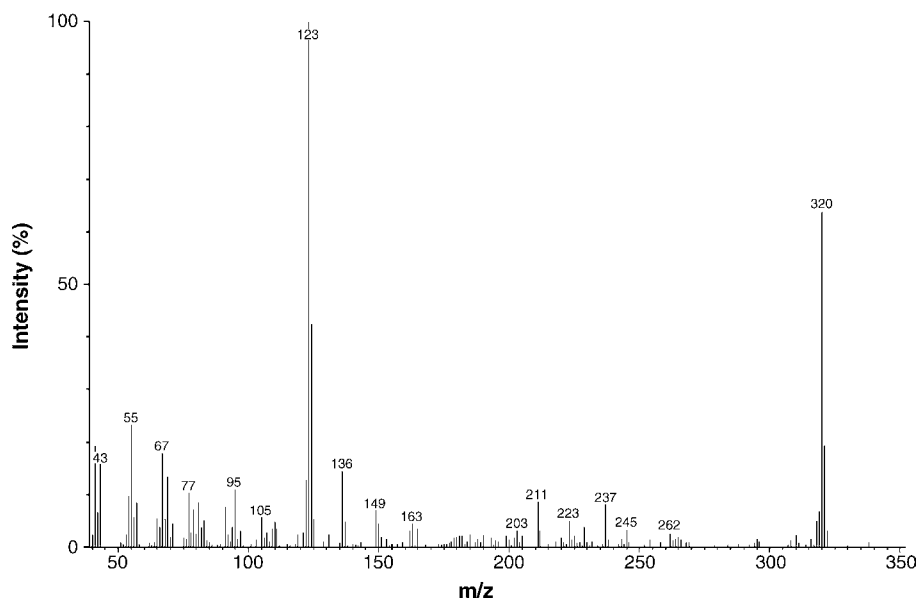


Fig. 4. Mass spectrum of peak 1 is shown in this figure: 3-pentadecylcatechol.

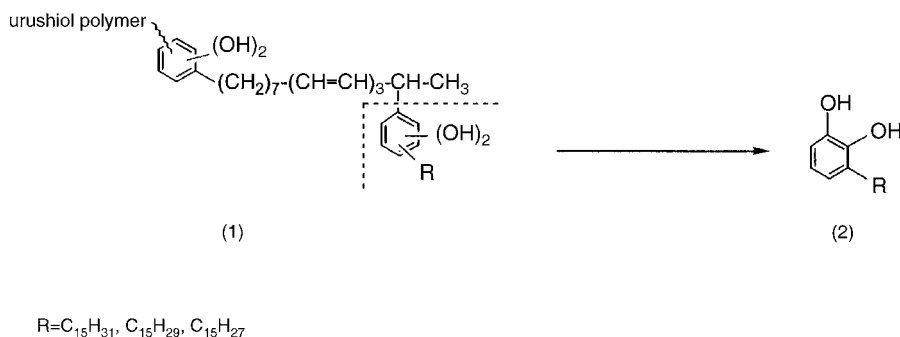


Fig. 5. Pyrolysis mechanism of urushiol polymer: (1) urushiol polymer and (2) 3-alkylcatechol.

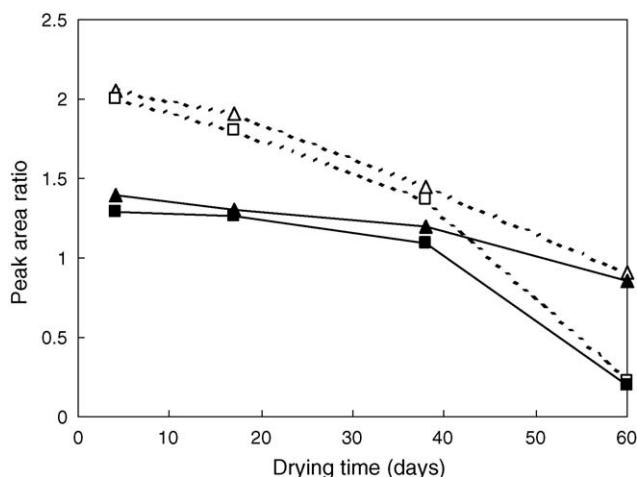


Fig. 6. Peak area ratios of 3-pentadecenylcatechol to 3-pentadecylcatechol and 3-pentadecadienylcatechol to 3-pentadecylcatechol between Kiurushi and Kuromeurushi: (Δ) 3-pentadecenylcatechol/3-pentadecylcatechol of Kiurushi; (▲) 3-pentadecenylcatechol/3-pentadecylcatechol of Kuromeurushi; (□) 3-pentadecadienylcatechol/3-pentadecylcatechol of Kiurushi; (■) 3-pentadecadienylcatechol/3-pentadecylcatechol of Kuromeurushi.

3-pentadecylcatechol and of 3-pentadecadienylcatechol to 3-pentadecylcatechol between Kiurushi and Kuromeurushi lacquer films. All the peak area ratios decreased with the increase in drying time. Comparing the two lacquer films, both 3-pentadecenylcatechol/3-pentadecylcatechol ratio and 3-pentadecadienylcatechol/3-pentadecylcatechol ratio of Kiurushi lacquer film were higher than those of Kuromeurushi lacquer film. These ratios of Kiurushi lacquer film were, furthermore, much higher than those of Kuromeurushi lacquer film after 4 day drying. However, these ratios of Kiurushi lacquer film were almost the same as those of Kuromeurushi lacquer film after 60 day drying. These results have a good correlation with those of the pencil hardness testing. Kuromeurushi lacquer film with pencil hardness 4H was much harder than Kiurushi lacquer film with pencil hardness F after 4 day drying. The harder lacquer film has the lower 3-pentadecenylcatechol/3-pentadecylcatechol ratio and 3-pentadecadienylcatechol/3-pentadecylcatechol ratio, while the softer lacquer film has higher ratios. These ratios of the two lacquer films were almost the same value after 60 day drying, because their pencil hardness was the same value of 5H. The ratios significantly indicate the hardness of the lacquer films.

4. Conclusions

Two kinds of oriental lacquer films, which were produced with two different drying methods, were analyzed during the hardening process using FT-IR, TG/MS and Py-GC/MS. FT-IR and TG/MS analyses could not reveal any difference between the films. On the other hand, the peak area ratios of 3-pentadecenylcatechol to 3-pentadecylcatechol and 3-pentadecadienylcatechol to 3-pentadecylcatechol, which were obtained by Py-GC/MS, were different between the films. The ratios of Kiurushi lacquer film were higher than those of Kuromeurushi lacquer film. Furthermore, both ratios decreased during the hardening process, because 3-pentadecenylcatechol and 3-pentadecadienylcatechol polymerize into urushiol polymer skeleton producing a nucleus-side chain cross-linkage, and 3-pentadecylcatechol terminates the polymerization. These results suggest that the reaction rate of nucleus-side chain cross-linkage on Kuromeurushi lacquer film is faster than that on Kiurushi lacquer film. These Py-GC/MS results also indicated a good correlation with the hardness obtained by pencil hardening testing. Oriental lacquer expresses some of the most important functions for industrial use, such as an extreme hardness and insolubility, accelerating the nucleus-side chain and side chain-side chain cross-linkages. Furthermore, it has become clear that the traditional treatments called Nayashi and Kurome effectively accelerate the hardening rate by activating the cross-linkages.

It is important to investigate the process of functional expression in material science. Studying the functional expression process effectively promotes development of new functional materials. We hope this study leads to the successful development of new functional coating materials – modified oriental lacquer film, which is one of biomimetic polymers – made from renewable resources for future generations.

References

- [1] R. Ikeda, H. Tanaka, H. Uyama, S. Kobayashi, *Polym. J.* 32 (2000) 589.
- [2] R. Ikeda, H. Tanaka, H. Oyabu, H. Uyama, S. Kobayashi, *Bull. Chem. Soc. Jpn.* 74 (2001) 1067.
- [3] N. Niimura, T. Miyakoshi, J. Onodera, T. Higuchi, *J. Anal. Appl. Pyrolysis* 37 (1996) 199.
- [4] N. Niimura, T. Miyakoshi, J. Onodera, T. Higuchi, *Rapid Commun. Mass Spectrom.* 10 (1996) 719.

- [5] N. Niimura, N. Kishi, T. Miyakoshi, *J. Mass Spectrom. Soc. Jpn.* 51 (2003) 229.
- [6] N. Niimura, T. Miyakoshi, *J. Mass Spectrom. Soc. Jpn.* 51 (2003) 439.
- [7] N. Niimura, Y. Kamiya, T. Sato, I. Katano, T. Miyakoshi, *J. Jpn. Oil Chem. Soc.* 47 (1998) 171.
- [8] N. Niimura, T. Miyakoshi, *Int. J. Polym. Anal. Charact.* 8 (2003) 47.
- [9] N. Niimura, T. Miyakoshi, *Tosou Kougaku* 33 (1998) 338.
- [10] N. Niimura, T. Miyakoshi, *Tosou Kougaku* 33 (1998) 166.
- [11] N. Niimura, T. Miyakoshi, J. Onodera, T. Higuchi, *Int. J. Polym. Anal. Charact.* 4 (1998) 309.
- [12] N. Niimura, T. Miyakoshi, *Surf. Interface Anal.* 29 (2000) 381.
- [13] N. Niimura, T. Miyakoshi, Y. Iijima, *Anal. Sci. Suppl.* 17 (2001) i155.
- [14] N. Niimura, Y. Iijima, T. Miyakoshi, *Bunseki Kagaku* 42 (1993) 605.
- [15] N. Niimura, Y. Iijima, T. Miyakoshi, *Surf. Interface Anal.* 24 (1996) 237.
- [16] K. Nagase, *Tosou to Toryo* 337 (1981) 66.
- [17] J. Kumanotani, K. Inoue, M. Achiwa, L.W. Chen, *Polym. Sci. Technol.* 33 (1986) 163.
- [18] Y. Yamauchi, R. Oshima, J. Kumanotani, *J. Chromatogr.* 243 (1982) 71.
- [19] J. Bartus, W.J. Simonsick, C. Garner, T. Nishiura, T. Kitayama, K. Hatada, O. Vogel, *Polym. J.* 26 (1994) 67.
- [20] J. Kumanotani, S. Tanaka, T. Matsui, *Proceedings of the 12th International Conference on Organic Coatings Science and Technology*, 1986, p. 195.
- [21] J. Kumanotani, *Zairyou Kagaku* 19 (1982) 88.
- [22] N. Niimura, T. Miyakoshi, J. Onodera, T. Higuchi, *Nihon Kagaku Kaishi* 9 (1995) 724.
- [23] N. Niimura, T. Miyakoshi, *Tosou Kougaku* 33 (1998) 204.
- [24] N. Niimura, T. Miyakoshi, *Tosou Kougaku* 33 (1998) 252.
- [25] N. Niimura, T. Miyakoshi, *Tosou Kougaku* 33 (1998) 296.
- [26] K. Taneda, *Mokuzai Kougyou* 40 (1985) 10.
- [27] P.R. Guevin Jr., *J. Coat. Technol.* 67 (1995) 61.
- [28] T. Kenjou, *Toso to Toryo* 44 (1988) 69.

Simultaneous residue monitoring of four tetracycline antibiotics in fish muscle by in-tube solid-phase microextraction coupled with high-performance liquid chromatography

Yi Wen, Ying Wang, Yu-Qi Feng*

Department of Chemistry, Wuhan University, Wuhan 430072, PR China

Received 25 September 2005; received in revised form 30 November 2005; accepted 30 November 2005

Available online 6 January 2006

Abstract

An on-line simple and rapid method for the simultaneous determination of tetracycline (TC), oxytetracycline (OTC), chlortetracycline (CTC) and doxycycline (DC) residues in fish muscle was developed by coupling in-tube solid-phase microextraction (SPME) to high-performance liquid chromatography (HPLC) with a photodiode array detector. Biocompatible poly (methacrylic acid–ethylene glycol dimethacrylate) monolithic capillary was selected as the extraction medium, and no precipitating protein and removing fat steps were required prior to extraction. In order to optimize the extraction of these compounds, several in-tube SPME parameters were investigated. Simply performed by extracting with 0.01 M EDTA–MacIlvaine buffer solution (pH 4.0) and centrifugation, the sample then could be directly injected into the device for extraction. The limits of detection of tetracycline, oxytetracycline, chlortetracycline and doxycycline were calculated to be 22, 16, 30 and 21 ng/g, respectively. The calibration curves showed linearity in the range of 100–10,000 ng/g with a linear coefficient R^2 value above 0.9980. Excellent method reproducibility was found by intra- and inter-day precisions, yielding the R.S.D.s less than 4.22% and 5.71%, respectively.

© 2005 Elsevier B.V. All rights reserved.

Keywords: Tetracycline antibiotics; Fish; In-tube SPME–HPLC; Poly (methacrylic acid–ethylene glycol dimethacrylate) monolithic capillary

1. Introduction

Tetracyclines (TCs) represent a class of antibacterial compounds. Due to their broad antibacterial spectrum and economic advantages, TCs have been commonly used in both veterinary medicine and in aquaculture for the purpose of prevention and treatment of disease. However, the widespread use of them could lead to TC residues in animal-producing food. And the antibiotics in food consumed for long periods can cause problems regarding the spread of drug-resistant microorganisms [1]. To ensure food safety for the consumers, several authorities around the world have established the maximum residue limit (MRL) for the tetracycline group in various tissues including fish muscle. European Union [2] and China [3] both set maximum residue limit of 100 ng/g in muscle for all species. The U.S. Food and Drug Administration has also set MRL of 2 µg/g for tetracy-

cline (TC), oxytetracycline (OTC), and chlortetracycline (CTC) in animal muscle [4].

Therefore, residue monitoring of TCs plays an important role to guarantee the safety of food. Microbiological assays are the most commonly used for the measurement of TCs in foods, but these methods are complicated, time-consuming, semiquantitative measurements and lack specificity [5]. On the other hand, the high-performance liquid chromatography (HPLC) method, due to its high selectivity, sensitivity and precision, has been given much attention in this field. Coupled to UV detection, HPLC has been successfully applied to determine several TC residues in fish [6–18]. To get higher sensitivity, HPLC-fluorescence [19–21] and LC–MS methods [22] were also utilized for this work. When using HPLC method, sampling and sample preparation steps are the most crucial and time-consuming for the analyzing the compounds of interest in complex matrices such as food samples. As TCs can complex with metal ions and bind with proteins [23], an effective organic or inorganic agent is demanded to extract TCs from fish muscle samples with high extraction efficiency. A mild

* Corresponding author. Tel.: +86 27 87867564; fax: +86 27 68754067.
E-mail address: yqfeng@public.wh.hb.cn (Y.-Q. Feng).

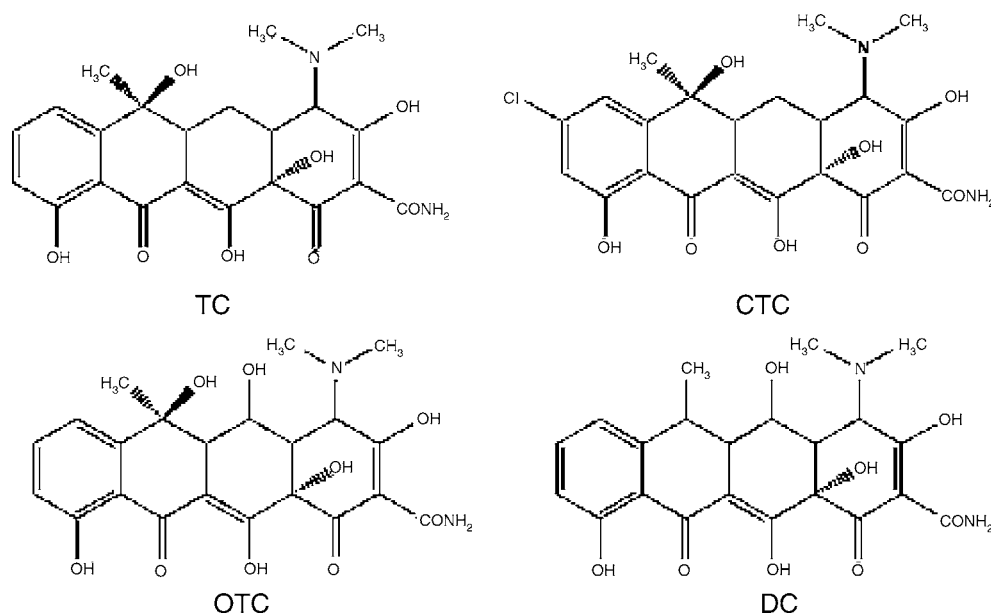


Fig. 1. Chemical structures of four tetracycline antibiotics.

acid solvent containing EDTA, such as 0.1 MEDTA–MacIlvaine buffer (pH 4.0) [6,11,12,14,15,19–22], was widespread accepted as the extractant. Furthermore, extraction strategies, such as solid-phase extraction (SPE) [7–16,19–22] and matrix solid-phase dispersion (MSPD) [17], have been widely employed to achieve cleanup and concentration simultaneously for the determination of TC residues in fish. However, these two methods possess time-consuming multi-step processes that include extraction, elution, evaporation and sample reconstitution steps. To achieve simple and rapid analysis, Coyne developed a one-step high-performance liquid chromatography method for the determination of oxytetracycline in fish muscle [6]. But this method required additional precipitation of proteins step. Ueno also presented a one-step HPLC method, which sample preparation was performed by extracting with 90% methanol containing EDTA, centrifugation and filtration [18]. However, the congealing of the fish muscle around the Ultra-turrax blade resulted in a lengthy cleaning procedure between each sample homogenization [6].

Another one promising sample preparation technique is in-tube solid-phase microextraction (SPME), a solvent-free extraction method invented by Pawliszyn in 1997 [24]. In-tube SPME integrates sample extraction, concentration and introduction into one single step, and thus overcomes the above drawbacks of SPE and MSPD techniques. In addition, coupled to HPLC, on-line analysis is successfully accomplished. So it not only shortens analysis time, but also provides better accuracy, precision and sensitivity than those off-line methods.

The objective of this study was to develop and validate an in-tube SPME–HPLC method for the rapid, simple and simultaneous determination of four widely used tetracycline antibiotic (Fig. 1) residues in fish muscle. A poly (methacrylic acid–ethylene glycol dimethacrylate) monolithic capillary column was selected as the extraction medium, which has successfully been used in the analysis of drugs in biological fluids

[25–27]. Due to the biocompatibility of the extraction phase, no requirement of protein-precipitating and fat-removing steps were achieved.

2. Experimental

2.1. Chemicals and reagents

The ethylene glycol dimethacrylate (EGDMA) was purchased from Acros (Sweden). The methacrylic acid (MAA), 2,2'-azobis (2-methylpropionitrile) (AIBN), dodecanol and toluene were obtained from Shanghai Chemical Co. Ltd. (Shanghai, China) and were of analytical reagent grade. Double distilled water was used for all experiments.

Tetracycline, oxytetracycline, chlortetracycline and doxycycline (DC) were purchased from National Institute for the Control of Pharmaceutical and Biological Products (Beijing, China). A mixed stock solution of all standards was prepared in methanol at a concentration of 1 mg/mL and stored at 4 °C in the dark. With the standard solution, the sample solution was spiked to the concentration for experiments.

2.2. In-tube SPME–HPLC device

A poly (MAA–EGDMA) monolithic capillary column (15 cm × 0.25 mm, i.d.) was used as extraction medium, and was prepared by in situ polymerization method described previously [25].

The schematic diagram of the in-tube SPME–HPLC system used for the study is illustrated in Fig. 2 [25]. The whole device consisted of a pre-extraction segment and an analytical segment. In the present paper, the pre-extraction segment included a six-port valve (valve 1), a Shimadzu LC-10AT pump (pump A) (Shimadzu, Tokyo, Japan) and a PEEK tube (0.762 mm i.d., 0.7 mL total volume); the analytical segment was composed of

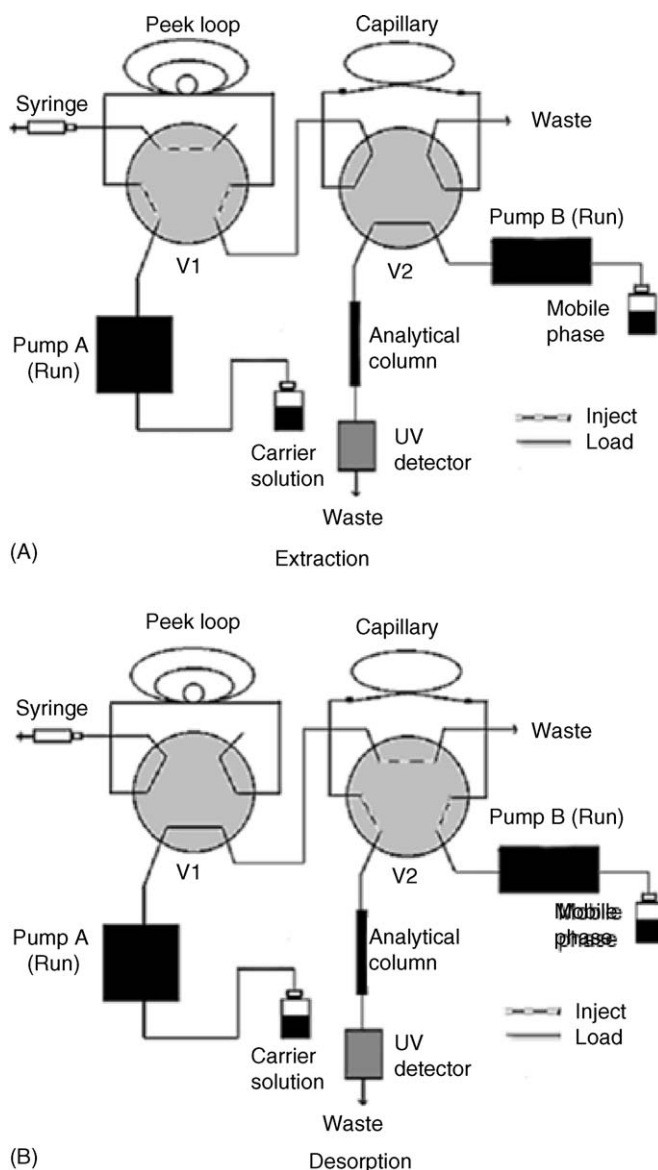


Fig. 2. Construction of in-tube SPME-HPLC device.

an Agilent 1100 series HPLC system (Agilent Technologies, Palo Alto, CA, USA), which included a quaternary pump (pump B), a micro-vacuum degasser, a six-port valve (valve 2) and a photodiode array detector (PAD). Connecting Valve 1 and Valve 2 with a PEEK tube, on-line extraction, desorption and introduction was achieved. The procedure of this device has been described in detail in our previous reports [25].

2.3. Chromatography

The instrument used for the study has been described in the above section, which is not discussed here again. The analytical column was 250 mm × 4.6 mm, i.d., packed with Kromasil ODS (5 μm), which was purchased from Eka Chemicals (Bohus, Sweden). The optimized mobile phase for desorption and separation was 20% methanol–20% acetonitrile–60% 0.02 mol/L oxalic acid solution (pH 3.0), and the flow rate was kept at

0.8 mL/min. The PAD wavelength was set at 355 nm for all the four analytes.

Extraction flow rate and desorption flow rate in the present experiment were 0.04 mL/min and 0.02 mL/min, respectively.

2.4. Preparation of fish samples

The sample used was the edible muscle of crucian. Analyte-free whole fish was filleted, the skin and bones removed. And the obtained fish muscle was kept frozen until analysis. 1 g of sample was spiked with known variable amounts of TCs. 10 mL of 0.01 M EDTA in MacIlvaine buffer solution (pH 4.0) was added and pureed with a hand-held food mixer for 10 min. Then the sample was kept at 4 °C for 30 min in the dark. Finally, the sample was centrifuged at 12,000 rpm for 5 min and the supernatant was readily employed for the further extraction step. Blank fish sample was prepared as the same as above steps only without the compound-spiked step.

2.5. Method validation

Several criteria were used to evaluate the developed method, such as sensitivity, linearity, reproducibility and stability.

The sensitivity of the method was evaluated by the limit of detection (LOD) and limit of quantification (LOQ). LOD and LOQ for these four compounds in fish samples were determined at a concentration where signal to noise ratios were equal to 3 and 10 under our HPLC–UV detector conditions, respectively.

The linearity of the method was evaluated by the correlation coefficients (R^2) of the calibration curves. Linearity of each compound was determined with seven concentration levels.

The reproducibility of the method was determined by the intra-day and inter-day precisions. The intra-day and inter-day R.S.D.s were investigated with the low, medium and high concentrations, respectively, according to the calibration curve ranges. Five extraction of a mixture sample solution over a day gave the intra-day R.S.D.s. The inter-day precision was determined by extracting a mixture sample solution that has been independently prepared for continuous three days.

The stability of the method was evaluated by investigating the changes of capillary column backpressure and extraction efficiency over two months during this study.

3. Results and discussion

3.1. HPLC separation and in-tube SPME desorption

Tetracycline antibiotics can adsorb on the silanol group in a reversed phase column [23], so they are inclined to appear as tailing peaks and affect quantification. Therefore, several acids added to the mobile phase to avoid their adsorption on RP columns were reported, such as phosphoric, citric and tartaric acids. However, only a mobile phase containing oxalic acid (pH 2.0–3.0) enabled no tailing peaks of the TCs [23].

Optimization of the mobile phase for HPLC separation of the four compounds was accomplished by investigating various volume ratios of 0.02 mol/L oxalic acid solution (pH 3.0) and

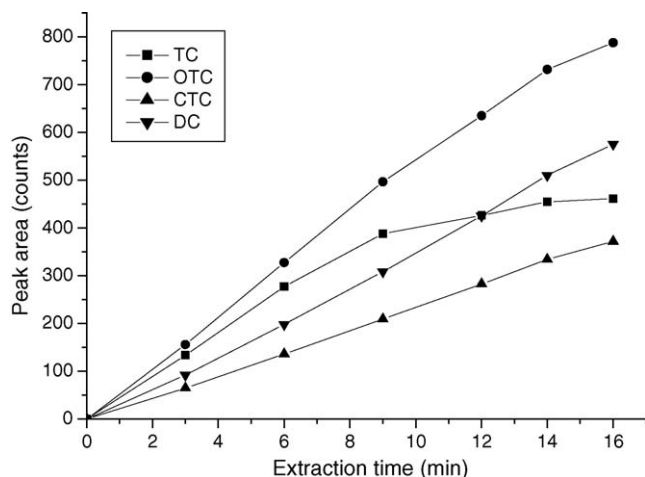


Fig. 3. In-tube SPME–HPLC extraction time profiles of four tetracycline antibiotics. TCs were spiked at 1 $\mu\text{g/mL}$ in water. Carrier solution was double-distilled water. SPME and HPLC conditions were outlined in Section 2.

organic phase. Good separation (resolution = 1.5) was achieved with a mobile phase composition of 20% methanol–20% acetonitrile–60% 0.02 mol/L oxalic acid solution (pH 3.0).

The optimized mobile phase was also used to elute the extracted TCs from the poly (MAA–EGDMA) monolithic capillary column. The desorption time was optimized in the range of 3–6 min. Results showed that the four analytes could be completely eluted from the capillary after 6 min, and little carryover was found. Therefore, a desorption time of 6 min was selected.

3.2. Optimization of in-tube SPME conditions

Several parameters such as extraction time and pH value of sample matrix were investigated in this paper, which had influence on the extraction efficiency for in-tube SPME [28].

The extraction time profiles of four tetracycline antibiotics were monitored by increasing sampling time for a 1 $\mu\text{g/mL}$ standard solution. The flow rate of the carrier solution was kept at 0.04 mL/min, and the sampling time was increased from 3 min to 16 min, corresponding to 120–640 μL of sampling volume. As shown in Fig. 3, the amounts of four compounds extracted (presented as the peak areas) increased greatly and rapidly when the extraction time rose from 3 to 9 min. Increasing extraction time beyond this point did not result in a proportional increase in the extracted amount for tetracycline, while the extraction equilibrium profiles for other three compounds were not obtained even after 16 min of sampling time. To achieve sufficient analysis sensitivity for all the four compounds, 16 min of extraction time was selected for the analysis of fish samples.

The effect of sample pH on the extraction efficiency of these four compounds by in-tube SPME was examined using several buffer solutions. As shown in Fig. 4, higher extraction efficiencies for all the four analytes were obtained in acid buffer solutions, and an obvious decrease was found when the pH above 5.5. The $\text{pK}_{\text{a}1}$ and $\text{pK}_{\text{a}2}$ of these four tetracycline antibiotics are in the range of 7.5–8.0 and 8.9–9.6, respectively [29]. On the other hand, the acidic polymer networks of this extraction phase could be deprotonated and possess negative charge at higher pH

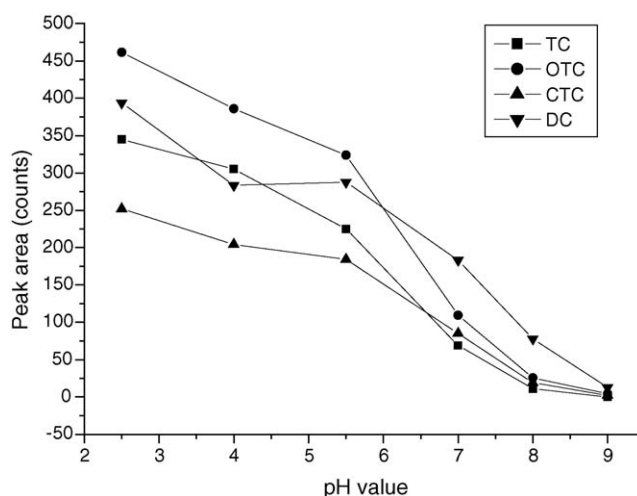


Fig. 4. Optimization of pH of the sample matrix. Sample solutions consisted of four tetracycline antibiotics spiked at 1 $\mu\text{g/mL}$, with 0.02 mol/L phosphate buffers at pH 2.5–7.0 and with 0.02 mol/L Tris–HCl buffers at pH 8.0–9.0. Carrier solution was double distilled water. Extraction time was 5 min. Other SPME and HPLC conditions were outlined in Section 2.

value. Hence, the repulsive interaction of homogeneous charges between the target compounds and extraction phase could be present, resulting in decrease of extraction efficiency. On the other hand, the existence of ion-exchange interaction at lower pH value leads to increase in the extraction efficiency. The optimum extraction efficiency could be obtained at pH 2.5 of buffer solution. However, tetracycline antibiotics are unstable under strong acid conditions and apt to form reversible epimers under pH 3.0 [30]. Therefore, to maintain the feasible analysis of tetracycline antibiotics in fish samples, the sample matrix was adjusted to pH 4.0.

Furthermore, the effect of acetonitrile content in sample solutions on extraction was also investigated. As shown in Fig. 5, the extracted amounts of tetracycline and oxytetracycline decreased with the increase of acetonitrile content in the solution, and those of chlortetracycline and doxycycline decreased greatly when acetonitrile content in the solution exceeded 5%. Therefore, acetonitrile content in sample solutions during the extraction was limited at 5% (v/v).

3.3. Method performance

Under the above-optimized conditions (no acetonitrile content in sample solution), Fig. 6 shows the typical chromatograms of four compounds obtained by in-tube SPME–HPLC and direct injection into the LC column. Great enhancement of the peak height obtained by in-tube SPME can be obviously found, indicating that a notable decrease in the limit of detection could be achieved by in-tube SPME. Table 1 shows the limits of detection (LOD) of four compounds obtained by direct injection and in-tube SPME, respectively.

According to the theory of in-tube SPME, the extraction efficiencies of tetracycline, oxytetracycline, chlortetracycline and doxycycline were calculated to be 28.8%, 40.8%, 68.1% and

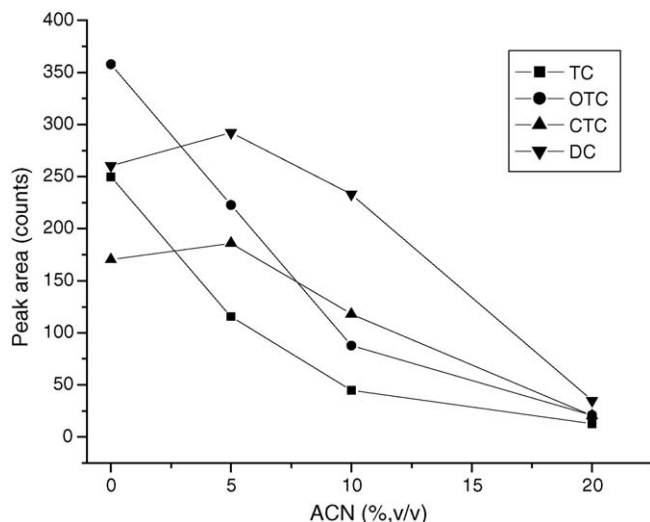


Fig. 5. Effect of acetonitrile content in sample solutions on the extraction for four TCs. TCs were spiked at 1 $\mu\text{g/mL}$ using a mixture solution of 0.02 mol/L Na_2HPO_4 buffer solution (pH 4.0) and acetonitrile in different ratios. Carrier solution was 0.02 mol/L Na_2HPO_4 buffer solution (pH 4.0). Extraction time was 5 min. Other SPME and HPLC conditions were outlined in Section 2.

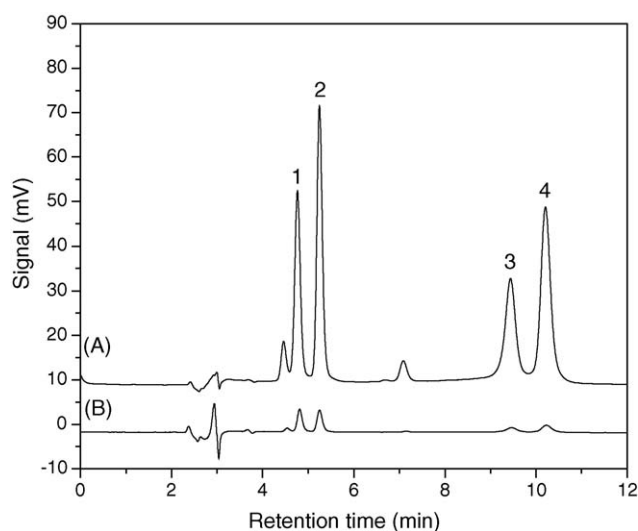


Fig. 6. HPLC chromatograms of four TCs obtained by in-tube SPME-HPLC (A) and direct injection of the standard sample (B). TCs were spiked at 1 $\mu\text{g/mL}$ in 0.02 mol/L Na_2HPO_4 buffer solution (pH 4.0). The volume for direct injection was 20 μL . Carrier solution was 0.02 mol/L Na_2HPO_4 buffer solution (pH 4.0). Extraction time was 16 min. Other SPME and HPLC conditions were outlined in Section 2. Peaks: 1, Tetracycline; 2, oxytetracycline; 3, chlortetracycline and 4, doxycycline.

Table 1
The limits of detection of TCs by direct injection and in-tube SPME

Method	Limits of detection (ng/mL)			
	TC	OTC	CTC	DC
Direct injection	12	12	62	40
In-tube SPME	1.4	1.0	2.5	1.5

Table 2

The limits of detection of TCs using two different extractants

Extractant	Limit of detection (ng/g)			
	TC	OTC	CTC	DC
0.01 M EDTA–MacIlvaine buffer (pH 4.0)	22	16	30	21
Acetonitrile	69	52	68	34

75.9%, respectively. In comparison with the existing open tubular capillary for in-tube SPME [31–34], this monolithic capillary showed higher extraction efficiency. This is mainly due to the greatly increased ratio of the surface area of extraction phase contacted with sample solution to the volume of sample solution.

3.4. Analysis of four TCs in fish muscle

The developed method provided a simple and rapid sample preparation procedure, which required no organic solvent to precipitate proteins and remove fats prior to extraction. This poly (MAA–EGDMA) monolithic material is a kind of polymer sorbent that possesses polar group, carboxyl acid group, in the hydrophobic bone structure [25,35]. And thus, while the target compounds are adsorbed onto the extraction phase via hydrophobic interaction, irreversible adsorption of proteins and fats does not occur due to the presence of acid group available in the structure of extraction phase under the acidic condition.

The comparison of two extractants for extracting TCs from fish muscle samples were investigated. The first one was 0.01 M EDTA–MacIlvaine buffer (pH 4.0) solution; and the extraction procedure was outlined in Section 2. The second one was the organic extractant, acetonitrile. To 1 g of sample, 0.5 mL of acetonitrile was added and pureed with a hand-held food mixer for 10 min. Then 9.5 mL of 0.02 mol/L Na_2HPO_4 buffer solution (pH 4.0) was added to the above sample. Finally, the sample was centrifuged at 12,000 rpm for 5 min and the supernatant liquid was employed to further extraction step. As shown in Table 2, 0.01 M EDTA–MacIlvaine buffer (pH 4.0) offered the lower limit of detection, so it was selected for the subsequent experiments.

Fig. 7 shows the typical chromatograms obtained by in-tube SPME of fish samples. A blank fish sample was extracted in the same way (Fig. 7B). No significant interference from fish components was observed. And thus quantification of the four compounds could be successfully achieved.

Table 3

Linearity and sensitivity characteristics of four TCs by in-tube SPME

Compound	Regression line			LOD (ng/g)	LOQ (ng/g)
	Slope	Intercept	R^2 values		
TC	0.0170	4.6182	0.9980	22	73
OTC	0.0232	3.9660	0.9982	16	53
CTC	0.0250	1.9943	0.9988	30	100
DC	0.0510	0.1022	0.9994	21	70

Concentration range: 100–10,000 ng/g. Number of data points: 7 points.

Table 4

Intra- and inter-batch precisions of four TCs by in-tube SPME

Compound	Intra-batch precision (R.S.D.%; $n = 5$)			Inter-batch precision (R.S.D.%; $n = 3$)		
	Low (100 ng/g)	Medium (1000 ng/g)	High (10,000 ng/g)	Low (100 ng/mL)	Medium (1000 ng/mL)	High (10,000 ng/mL)
TC	2.34	1.22	0.57	3.60	3.99	4.34
OTC	3.21	1.24	1.09	5.09	4.63	4.84
CTC	4.22	3.20	3.11	3.17	4.24	5.71
DC	3.50	0.77	2.05	4.22	5.09	4.23

Fish samples were spiked over a range of 100–10,000 ng/g with these four TCs. As shown in Table 3, satisfactory regression coefficients for the calibration curves were obtained. Data of the limits of detection and quantification are also included in Table 3. The LODs of tetracycline, oxytetracycline, chlortetracycline and doxycycline were all far lower than the maximum residue limit (100 ng/g).

The intra-day and inter-day precisions of the method were evaluated at three concentrations over the linear dynamic range (low, medium, high). Data are included in Table 4. The intra-day precisions for all compounds were less than 4.22%. The inter-day precision proved to be less than 5.71%.

Moreover, the monolithic capillary showed high stability since no significant changes, such as capillary column back-pressure and extraction efficiency, were found in its extractions over two months during this study.

3.5. Application to real samples

The effectiveness of this method was checked by analyzing fish muscle from the fish, which were orally medicated with a daily dose of 100 mg/kg oxytetracycline for four days. As shown in Fig. 8(A), the peak of oxytetracycline was detected and there was no interfering peak in the resulting chromatogram.

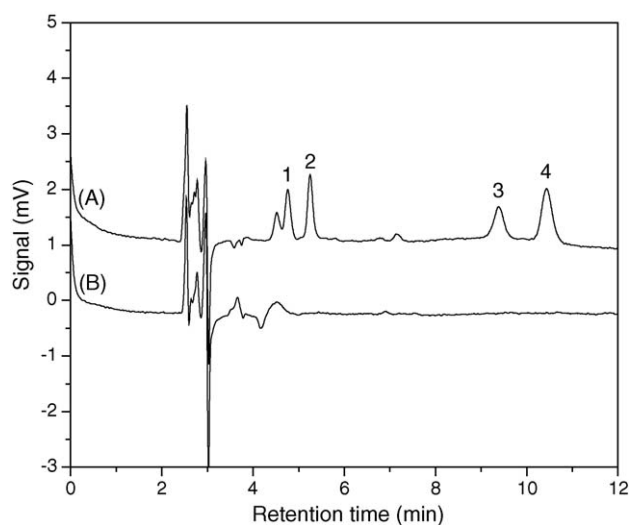


Fig. 7. HPLC chromatograms of four TCs obtained by in-tube SPME–HPLC from spiked fish muscle sample (A) and blank fish muscle sample (B). Sample solution consisted of four compounds spiked at 300 ng/g. Extraction time was 16 min. Carrier solution was 0.02 mol/L Na_2HPO_4 buffer solution (pH 4.0). Other SPME and HPLC conditions were outlined in the Section 2. Peaks: 1, tetracycline; 2, oxytetracycline; 3, chlortetracycline and 4, doxycycline.

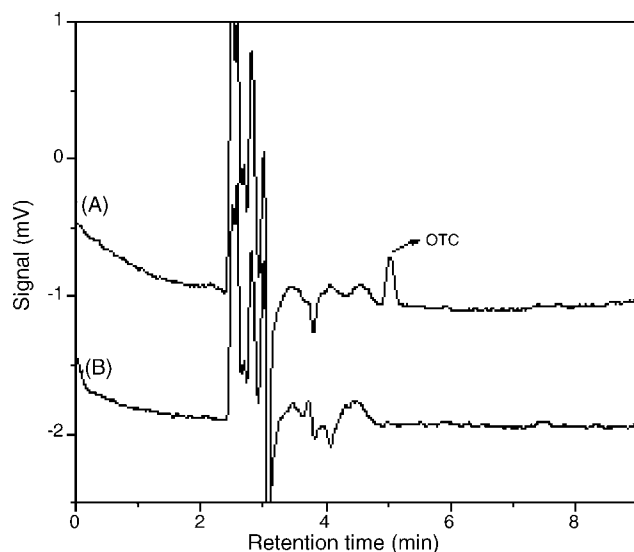


Fig. 8. HPLC chromatograms obtained by in-tube SPME–HPLC from fish orally medicated with a daily dose of 100 mg/kg oxytetracycline for four days (A) and analyte-free fish sample (B). SPME and HPLC conditions were as the same as Fig. 7.

4. Conclusions

The developed procedure provided a rapid, simple, precise and sensitive method for the simultaneous determination of tetracycline, oxytetracycline, chlortetracycline and doxycycline residues in fish muscle. On-line analysis was easily realized by coupling in-tube SPME to HPLC. The biocompatibility of the poly (MAA–EGDMA) monolithic material brought no requirement to precipitate proteins and remove fats, and thus no such additional steps were required. In addition, the in-tube SPME–HPLC method proved to be a sensitive and selective technique, allowing simultaneous monitoring of four commonly applied tetracycline antibiotics in fish muscle at a level under the maximum residue limit. Therefore, the proposed method will be useful and practical in the residue monitoring and studying pharmacokinetics of tetracycline, oxytetracycline, chlortetracycline and doxycycline in fish muscle.

Acknowledgements

This work was partly supported by grants from the National Natural Science Foundation of China (grant no. 20275029) and the Excellent Young Teachers Program of MOE, China.

References

- [1] S.B. Levy, *J. Food Protect.* 50 (1987) 616.
- [2] Commission Regulation no. 2377/90, *Off. J. Eur. Commun.*, 18 August 1990, no. L224.
- [3] The maximum residue limit of veterinary drugs in edible animal food established by Ministry of Agriculture of People's Republic of China, *Chin. J. Vet. Drug* 37 (2003) 15.
- [4] U.S. Code of Federal Regulations, Title 21, Part 556, Sections 150, 500, and 720, U.S. Government Printing Office, Washington DC, 2003 (Chapter 1).
- [5] J. Kurittu, S. Lonnberg, M. Virta, M. Karp, *J. Food Protect.* 63 (2000) 953.
- [6] R. Coyne, O. Bergh, O.B. Samuelsen, *J. Chromatogr. B* 810 (2004) 325.
- [7] Y. Onji, M. Uno, K. Tanigawa, *J. Assoc. Off. Anal. Chem.* 67 (1984) 1135.
- [8] M. Horie, Y. Hoshino, N. Nose, H. Iwasaki, H. Nakazawa, *Eisei Kagaku* 31 (1985) 371.
- [9] I. Nordlander, H. Johnsson, B. Osterdahl, *Food Addit. Contam.* 4 (1987) 291.
- [10] A. Rogstad, V. Hormazabal, M. Yndestad, *J. Liq. Chromatogr.* 11 (1988) 2337.
- [11] H. Björklund, *J. Chromatogr.* 432 (1988) 381.
- [12] J.R. Meinertz, G.R. Stehly, W.H. Gingerich, *J. AOAC Int.* 81 (1998) 702.
- [13] R.G. Aoyama, K.M. McErlane, H. Erber, *J. Chromatogr.* 588 (1991) 181.
- [14] V.M. Moretti, G.L. Maggi, A. Albertini, F. Bellagamba, U. Luzzana, G. Serrini, F. Valfré, *Analyst* 119 (1994) 2749.
- [15] M. Touraki, P. Rigas, P. Pergandas, C. Kastritsis, *J. Chromatogr. B* 663 (1995) 167.
- [16] W.X. Du, M.R. Maeshall, W.B. Wheeler, M. Mathew, D. Gatlin, S.D. Rawles, D.H. Xu, W.A. Rodgers, C.I. Wei, *J. Food Sci.* 60 (1995) 1220.
- [17] A.R. Long, L.C. Hsieh, M.S. Malbrough, C.R. Short, S.A. Barker, *J. Assoc. Off. Anal. Chem.* 73 (1990) 864.
- [18] R. Ueno, T. Aoki, *Fish Pathol.* 30 (1995) 239.
- [19] A.L. Pena, C.M. Lino, M.I.N. Silveira, *J. AOAC Int.* 86 (2003) 925.
- [20] H.S. Rupp, C.R. Anderson, *J. AOAC Int.* 88 (2005) 505.
- [21] K. Fujita, K. Ito, E. Araki, K. Tanno, M. Murayama, Y. Saito, *J. Food Hyg. Soc. Jpn.* 38 (1997) 12.
- [22] H. Nakazawa, S. Ino, K. Kato, T. Watanabe, Y. Ito, H. Oka, *J. Chromatogr. B* 732 (1999) 55.
- [23] H. Oka, Y. Ito, H. Matsumoto, *J. Chromatogr. A* 882 (2000) 109.
- [24] R. Eisert, J. Pawliszyn, *Anal. Chem.* 69 (1997) 3140.
- [25] Y. Fan, Y.Q. Feng, S.L. Da, Z.G. Shi, *Anal. Chim. Acta* 523 (2004) 251.
- [26] Y. Fan, Y.Q. Feng, S.L. Da, X.P. Gao, *Analyst* 129 (2004) 1065.
- [27] Y. Wen, Y. Fan, M. Zhang, Y.Q. Feng, *Anal. Bioanal. Chem.* 382 (2005) 204.
- [28] H. Kataoka, *Curr. Pharmaceut. Analysis* 1 (2005) 65.
- [29] Z. Qiang, C. Adams, *Water Res.* 38 (2004) 2874.
- [30] L.A. Mitscher (Ed.), *The Chemistry of the Tetracycline Antibiotics*, first ed., Marcel Dekker, New York, 1978, p. 123.
- [31] J.C. Wu, J. Pawliszyn, *Anal. Chem.* 73 (2001) 55.
- [32] J.C. Wu, C. Tragas, H. Lord, J. Pawliszyn, *J. Chromatogr. A* 976 (2002) 357.
- [33] W.M. Mullett, K. Levsen, J. Borlak, J.C. Wu, J. Pawliszyn, *Anal. Chem.* 74 (2002) 1695.
- [34] J.C. Wu, J. Pawliszyn, *J. Chromatogr. A* 909 (2001) 37.
- [35] N.A. Peppas, P. Bures, W. Leobandung, H. Ichikawa, *J. Pharm. Biopharm.* 50 (2000) 27.

A selective optical chemical sensor for 2,6-dinitrophenol based on fluorescence quenching of a novel functional polymer

Xu Wang, Hui Zeng, Lixia Zhao, Jin-Ming Lin*

State Key Laboratory of Environmental Chemistry and Ecotoxicology, Research Center for Eco-Environmental Sciences,
Chinese Academy of Sciences, P.O. Box 2871, Beijing 100085, China

Received 25 September 2005; received in revised form 31 December 2005; accepted 4 January 2006

Available online 13 February 2006

Abstract

A bifurcated optical fiber based chemical sensor for continuous monitoring of 2,6-dinitrophenol (2,6-DNP) has been proposed based on the reversible chemical reaction between a novel functional poly(vinyl chloride) (PVC) as the sensing material and the analytes. The functional PVC (FPVC), containing a fluorescent curcumin moiety, was synthesized by the nucleophilic substitution of a fraction of the chlorine atoms bound to the PVC backbone by curcumin. When plasticized in a membrane of 5 μm thickness, FPVC extracts 2,6-DNP from aqueous solution into the bulk membrane phase and reacts with the analyte to form a complex with low fluorescence efficiency through hydrogen bonding. Formation of the complex gave a significant fluorescence quenching which is suitable for signalling the occurrence of the host–guest interaction. At pH 3.50, the sensor exhibits a dynamic detection range from 2.5×10^{-6} to $7.0 \times 10^{-3} \text{ mol L}^{-1}$ with a limit of detection of $1.0 \times 10^{-6} \text{ mol L}^{-1}$. As 2,6-DNP can provide an optimal space geometry matches to the formation of hydrogen bonds, the sensor shows excellent selectivity for 2,6-DNP over other nitrophenols. The forward and reverse response time (t_{95}) of the sensor both was within 1 min. The repeatability, reproducibility, and lifetime of the sensor were also satisfied. The sensor was applied to determine 2,6-DNP in water samples successfully.

© 2006 Elsevier B.V. All rights reserved.

Keywords: Optical chemical sensor; 2,6-Dinitrophenol; Fluorescence quenching; Functional polymer

1. Introduction

In recent years, the ever-increasing number of organic toxic compounds being detected in human environment has risen concern about the contamination of environment resources. Among various toxic compounds, nitrophenols are widely presented and persistent in the environment, especially in waters [1,2]. They have great potential toxicities of carcinogenesis, teratogenesis, and mutagenesis such that are considered to be hazardous wastes and priority toxic pollutants by U.S. Environmental Protection Agency (EPA) [3]. 2,6-Dinitrophenol (2,6-DNP) is one of the six possible dinitro phenol forms used in the synthesis of dyes, picric acid, picramic acid, wood preservatives, diaminophenoldihydrochloride (a photographic developer), explosives, and insecticides [4]. A few literatures about the determination of 2,6-DNP are focused on conventional chromatographic meth-

ods [5–7], which suffer from various disadvantages such as discontinuity, time consumption, analyte destruction, and high running cost. Thus there is still a significant demanding for the fabrication of a new optical fiber chemical sensor for 2,6-DNP, since the user-friendly optochemical sensors can offer advantages in terms of no sample pretreatment, small size, low cost, and quick signal transmission. The determination using an optical sensor can be performed through immobilizing the sensing materials on a solid-state support to form a chemically recognized membrane which was connected with a transducer device. Since nitrophenols are known to be good electron acceptors and quenchers, the quenching effect of nitrophenols on some fluorescent substances have been used to fabricate optical sensors for nitrophenols [8–10].

In the recent years, polymers have gained tremendous recognition in the field of artificial sensor in the goal of gaining better selectivity and fast measurement [11,12]. But as one of the most widely used polymers, PVC was mainly used as the plasticized matrices for the dispersion of sensing molecules within it and the modified PVC was rarely used to behave a sensing substance.

* Corresponding author. Fax: +86 10 62841953.

E-mail address: jmlin@mail.rcees.ac.cn (J.-M. Lin).

Fortunately, the studies on the functionalization of PVC through nucleophilic substitution have been carried out [13–15]. These functional PVC (FPVC) have been successfully applied to prepare surfactant-selective electrode [13], reduce plasticizer migration [14], and construct novel biomaterials [15].

This paper describes our efforts focused on developing a solid-state chemical sensor for 2,6-DNP in water using a novel FPVC as the sensing substance. The FPVC was synthesized by the nucleophilic substitution reaction on PVC backbone with curcumin. The design of the approach consists of electron-donating curcumin moiety as a 2,6-DNP-bonding site as well as a fluorescence site, where the hydrogen bonding is responsible for the quenching of the fluorescence emission of curcumin moiety. The sensing characteristics of the proposed sensor were investigated. The steric effect or spatial matching occurred between host and guest was proved to be the primary factor that dominated the complex formation. FPVC was readily used as the sensing substance in an optic fiber based chemical sensor for 2,6-DNP. Compared with the physically embedded curcumin membrane with PVC as the matrixes, the proposed FPVC-based membrane showed markedly better sensing performance in terms of sensitivity, selectivity, response time, and lifetime. The proposed sensor was used to determine 2,6-DNP in water samples satisfactorily. To our best knowledge, the functionally substituted polymer based fluorescence sensor was rarely reported.

2. Experimental

2.1. Apparatus

^1H NMR spectra were recorded on an ARX-400 (Bruker, 400 MHz, Germany) spectrometer in $\text{DMSO}-d_6$ with tetramethylsilane as internal standard. Infrared spectra were obtained from a NEXUS 670-FT-IR (Thermo Nicolet Corporation, Massachusetts, USA) spectrophotometer with KBr disk. Elemental analysis was performed on a Flash EA 1112 elemental analyzer (Thermoquest, Italy). A Dektak 8 surface profiler (Digital Instruments, California, USA) was used to determine the film thickness by scanning the edge of a small scratch that was applied to the sensing membrane that was coated to a circular quartz plate. UV–visible measurements were performed on a Shimadzu UV-2401 UV–visible spectrophotometer (Shimadzu, Kyoto, Japan). All fluorescence measurements were carried out on a Hitachi F-2500 fluorescence spectrometer (Hitachi, Tokyo, Japan) with excitation and emission slits set at 5 and 10 nm, respectively. A homemade PTFE flow cell and a bifurcated optical fiber (50 + 50 quartz fibers, diameter 6 mm and length 1.2 m) were used for the sensing measurements (Fig. 1). The quartz plate with the sensing membrane on it was mounted in the flow cell. The membrane side is facing the cell chamber with the circulating sample solution sweeping over the membrane driven by a peristaltic pump (Lange Instruments, Baoding, China). The opposite side of the quartz plate tightly matching the common end of the optical fiber. Data processing was performed on a Pentium III computer with software of Sigma plot. For pH measurements, an Orion Model 828 pH meter (Massachusetts, USA) was used. A spin-on device [12] was used to prepare the membrane.

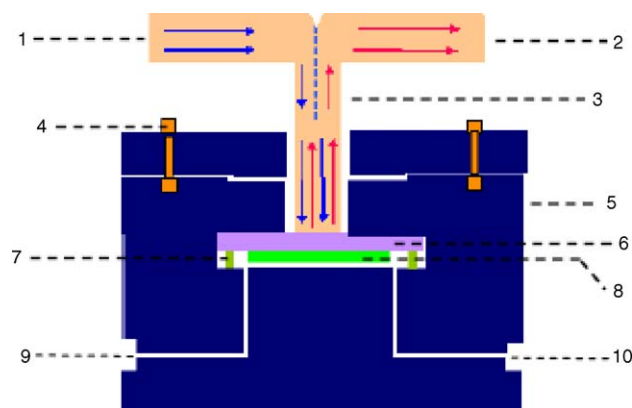


Fig. 1. Schematic diagram of the flow cell arrangement: (1) excitation light, (2) signal light, (3) bifurcated optical fiber, (4) screw cap, (5) cell body, (6) quartz glass slide, (7) O silicon ring, (8) sensing membrane, (9) sample inlet, and (10) sample outlet.

2.2. Chemicals

Analytical reagent grade chemicals were used unless indicated otherwise. The following reagents were used for FPVC synthesis and membrane preparation: high molecular weight PVC was purchased from Sigma (St. Louis, USA). Curcumin was from Shanghai Chemical Factory (Shanghai, China). Hexadecyltrimethyl ammonium bromide (CTAB), tetrahydrofuran (THF), tributyl phosphate (TBP), diisooctyl sebacate (DOS), and dioctyl phthalate (DOP) were obtained from Beijing Chemical Factory (Beijing, China).

2,6-DNP, *o*-nitrophenol (*o*-NP), *m*-nitrophenol (*m*-NP), *p*-nitrophenol (*p*-NP), 2,4-dinitrophenol (2,4-DNP), 2,4,6-trinitrophenol (2,4,6-TNP), and other phenols used were from Beijing Chemical Factory (Beijing, China). The stock solutions of nitrophenols were prepared by dissolving the appropriate amount of each sample in methanol. Working solutions were prepared by successive dilution of the stock solutions with 0.1 M sodium acetate–hydrochloric acid buffer solution of pH 3.50. The ultra high purity deionized water used in the experiment was obtained from Easypure water purification system with a 0.2 μm fiber filter (Barnstead, USA).

2.3. Substitution reaction of PVC with curcumin

0.5 g curcumin (1.36 mmol) was added to a 40 mL sodium carbonate–sodium bicarbonate buffer solution (0.1 mol L^{-1} , pH 10.0) at room temperature and stirred for 20 min. Then a 50 mL THF solution of PVC resin (2 g, 0.01 mmol) was added. The resulting red brown solution was heated and stirred for 30 min at 50 $^{\circ}\text{C}$, after which, calculated amount (0.1 g, 0.27 mmol) of CTAB as phase-transfer catalyst was added dropwise. After stirring the mixture at 80 $^{\circ}\text{C}$ for 5 h, THF was removed under reduced pressure. A brown color precipitate developed immediately. The products were collected by filtration, subjected to mild sonication in a bath type sonicator for 3 min to remove any surface adhering reactants, and then dried in an air oven at 80 $^{\circ}\text{C}$ to constant weight. Product: ^1H NMR [16,17] (400 MHz, $\text{DMSO}-d_6$) 2.23–2.34 ppm (br m, 20H, methylene protons of

–[CH₂–CHCl]_n–), 4.34–4.45 ppm (br m, 10H, methyne protons of –[CH₂–CHCl]_n–), 9.65 ppm (s, 2H, hydroxy H of benzene ring), 7.14–7.56 ppm (m, 6H, *ortho*- and *meta*-H of the substituted benzene ring), 6.74–6.83 ppm (m, 4H, –HC=CH– double bond H), 6.06 ppm (s, 1H, hydroxy H of enol form of curcumin moiety), 3.82 ppm (s, 6H, methoxy-H); FT-IR (KBr disk) 2910, 2850, 1430, 1250, 964, 768, 690, 636, 611 cm^{–1} (C–C and C–H stretching vibrations of PVC), 611, 636, 690, 768 cm^{–1} (stretching vibrations of C–Cl) [18,19], 845 cm^{–1} (adjoining hydrogens at benzene ring), 1590 cm^{–1} (benzene ring skeleton vibration), 1620 cm^{–1} (–C=C– stretching vibration of benzene ring), 3640 cm^{–1} (C–O–H stretching vibration); UV spectra λ_{max} (THF): 426 nm.

2.4. Preparation of sensing membrane

The sensing membrane solution was prepared by dissolving a mixture of 50 mg of FPVC and 200 mg of TBP in 2 mL of freshly distilled THF. A circular quartz plate of 25 mm diameter was mounted on the spin-on device and then rotated at a frequency of 800 rpm. Using a syringe, 0.2 mL of the membrane solution was sprayed to the center of the plate. After a spinning time of 4 s, a membrane of 5 μm thickness, which was determined by the surface profiler [20], was then coated on the quartz plate. The membrane was stored in buffer solution when not used.

2.5. Measurement procedure

Two arms of the bifurcated optical fiber were fixed in the detecting chamber of the spectrofluorimeter to carry the excitation and emission light. The fluorescence measurements were carried out at the maximum excitation wavelength of 460 nm and the maximum emission wavelength of 503 nm. The sample solution was fed through the detecting chamber of the flow cell by the peristaltic pump at a rate of 2.0 mL min^{–1}. After each measurement, the flow cell was washed with blank buffer solution until the fluorescence intensity of the sensor reached the original blank value.

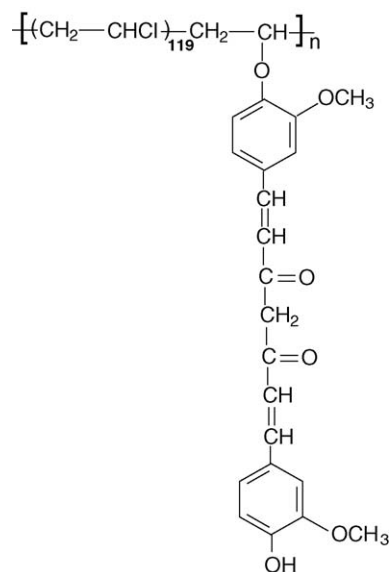
3. Results and discussion

3.1. Elemental analysis

The elemental analysis presents us the C% of PVC and FPVC with 38.57% and 39.82%, respectively, from which a 1:120 number ratio of curcumin molecules to –[CH₂CHCl]– units in FPVC was calculated, which corresponds to about 4.5% covalently bound curcumin in 1 g of FPVC. According to the molar absorptivity of curcumin at 423 nm (151.8 cm^{–1} mg^{–1} mL) in THF, 1 g of the novel polymer contains 4.0 % of curcumin [21].

3.2. pK_a determination

In order to testify the formation of FPVC, the absorption spectra at various acidities of the polymer were studied and its pK_a was determined according to reported method [22]. The pK_a of FPVC, characterized by a difference of those two values of curcumin reported (8.05 ± 0.05, 10.41 ± 0.05) [23], has only



Scheme 1. The molecular structure of novel FPVC.

one value and was calculated to be 10.72. The results indicated that PVC was nucleophilic attacked by one hydroxyl group of curcumin and curcumin was attached to the backbone of the polymer, which was consistent with the conclusion obtained from ¹H NMR spectra, FT-IR spectra and elemental analysis. Thus the molecular structure of FPVC was drawn and shown in Scheme 1.

Since FPVC was found to show excellent membrane formability with plasticizers, there was no need to use PVC as matrixes in the fabrication of sensing membrane.

3.3. Optical properties of FPVC

The absorption spectra (not shown here) of FPVC (λ_{max} = 426 nm) in sensing membrane redshifted 3 nm compared with curcumin in tributyl phosphate plasticized PVC membrane (λ_{max} = 423 nm). The reason for this perhaps was the electron-donating effect experienced by curcumin moiety produced through adjacent electron-offering alkyl backbone of the polymer, which decreased the electronic energy level of curcumin.

Fig. 2 shows the fluorescence spectra of the sensing membrane exposed to a solution containing different concentrations of 2,6-DNP, which are recorded at λ_{ex} = 460 nm, λ_{em} = 503 nm. Owing to the conjugated double bond system and the high mobility of its π-electrons, curcumin moiety exhibits fluorescence emission at 503 nm when excited by 460 nm radiation. From Fig. 2, one can see that the fluorescence intensities of the sensing membrane decrease with increase of the concentration of 2,6-DNP, which constitutes the basis for the determination of 2,6-DNP with the optical fiber sensor proposed in this paper.

3.4. Optimization of membrane compositions

Since plasticization can increase the mobility of polymer segments to improve the rate of guest extraction into and diffusion

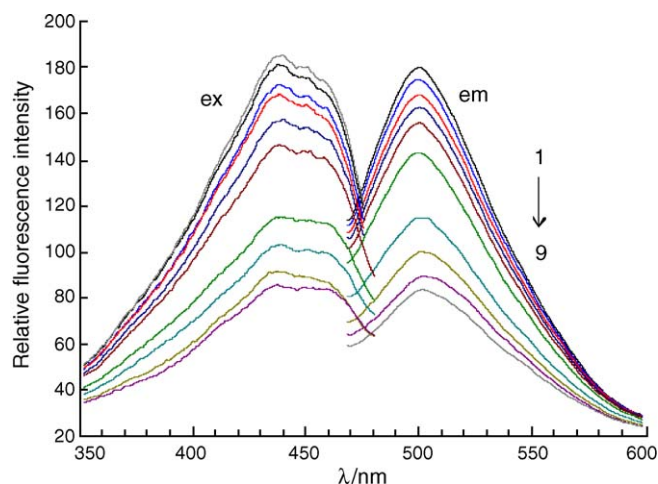


Fig. 2. Fluorescence spectra of the sensing membrane in the presence of different concentrations of 2,6-DNP at pH 3.50: (1) 0; (2) 1.0×10^{-6} ; (3) 5.0×10^{-6} ; (4) 1.0×10^{-5} ; (5) 5.0×10^{-5} ; (6) 1.0×10^{-4} ; (7) 5.0×10^{-4} ; (8) 1.0×10^{-3} ; (9) 5.0×10^{-3} ; (10) $8.0 \times 10^{-3} \text{ mol L}^{-1}$ ($\lambda_{\text{ex}} = 460 \text{ nm}$, $\lambda_{\text{em}} = 503 \text{ nm}$).

throughout the film [24], as well as increase the workability, flexibility, and distensibility of the film, several membrane compositions were investigated by selecting appropriate plasticizers and varying the ratio of plasticizers to FPVC. A sensing membrane made of different plasticizers, such as tributyl phosphate (TBP), diisooctyl sebacate (DOS), and dioctyl phthalate (DOP) were prepared. Membranes consisting of TBP show the best response to 2,6-DNP and the longest lifetime. When the amount of FPVC for immobilizing was 50 mg, the optimal amount of TBP was found to be 200 mg (Table 1).

3.5. Characteristics of the optical membrane

3.5.1. Determination of the complex ratio and the equilibrium constant

Based on an operation principle reported [25], the relationship between response parameter, α , and 2,6-DNP concentration [G_{aq}] can be represented as

$$\frac{\alpha^n}{1 - \alpha} = \frac{1}{nKC_{\text{H}}^{n-1}[G_{\text{aq}}]^m} \quad (1)$$

where m and n are the complexing number of 2,6-DNP and FPVC, respectively. C_{H} and K refer to the total amount of

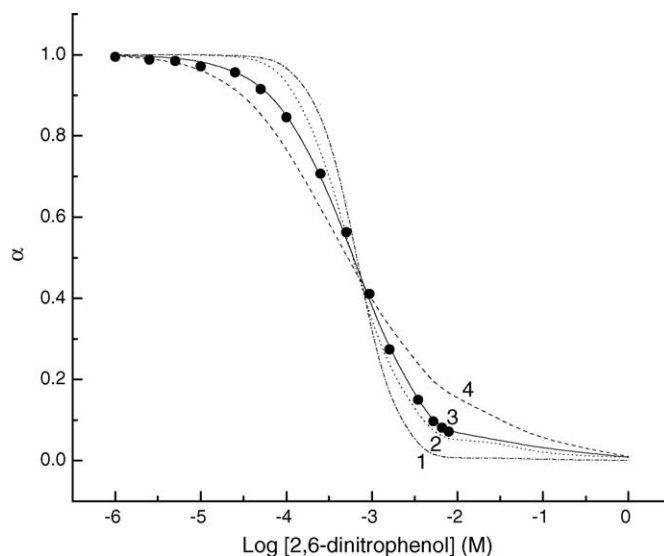


Fig. 3. Response parameter values (α) at 460/503 nm as a function of the logarithm of 2,6-DNP concentration at pH 3.50. Theoretical response of 2,6-DNP as predicted by Eq. (1). The experimental data were fitted to the equation with the different complex ratios and equilibrium constant: (1) $n:m = 1:2$, $K = 7.7 \times 10^5$; (2) $n:m = 2:2$, $K = 1.2 \times 10^6$; (3) $n:m = 1:1$, $K = 2.0 \times 10^3$ (best fit); (4) $n:m = 2:1$, $K = 2.2 \times 10^6$ (●●) experimentally observed data points).

FPVC in membrane and the overall equilibrium constant, respectively. Eq. (1) is the basis of the quantitative determination of 2,6-DNP in aqueous solution by using the proposed sensor. The experimental data were fitted to Eq. (1) by changing the ratio of n to m and adjusting the overall equilibrium constant, K . Fig. 3 shows the fitted curves that represents the experimental data for 2,6-DNP. The curve referring to the 1:1 complex ratio and $K = 2.0 \times 10^3$ is the best one fitted to the experimental data (Fig. 3, solid line 3). The best-fitting curve can serve as the calibration curve for the determination of 2,6-DNP.

3.5.2. Effect of pH and flow rate

The effect of solution pH and flow rate on α and response time, t , was investigated over a wide pH range from 2.0 to 12.0 and flow rate range from 0.5 to 4.5 mL min^{-1} in the presence of $5.0 \times 10^{-5} \text{ mol L}^{-1}$ 2,6-DNP. The blank fluorescence of the sensing membrane itself was found to be independent of pH from 2.0 to 10.5. Solutions at pH > 10.8 caused FPVC to be dissolved

Table 1

Composition of the membrane cocktail and the response behavior of the sensing membrane at pH 3.50^a

Membrane number	Plasticizer (mg)	Working range (mol L^{-1})	Detection limit ^b (mol L^{-1})	Lifetime ^c (times)
1	DOS, 200	7.8×10^{-5} to 3.7×10^{-3}	2.5×10^{-5}	80
2	DOP, 200	9.8×10^{-5} to 1.1×10^{-3}	3.6×10^{-5}	100
3	TBP, 100	3.4×10^{-6} to 8.5×10^{-3}	2.0×10^{-6}	100
4	TBP, 200	2.5×10^{-6} to 7.0×10^{-3}	1.0×10^{-6}	>250
5	TBP, 300	4.0×10^{-6} to 4.0×10^{-3}	1.3×10^{-6}	150

^a Each membrane cocktail contains 50 mg of FPVC and the listed amount of plasticizer, which were diluted to 2 mL with fresh distilled THF.

^b The detection limit was defined as $\alpha = 0.99$.

^c The lifetime was defined as the usage times of the sensing membrane that produced fluorescence signal changes less than 5% [31].

out from the PVC membrane because of its pK_a of 10.72. Since the pK_a of 2,6-DNP is approximately 3.68 [26], the ionization of 2,6-DNP was inhibited at $pH < 4.2$ and α remained a constant. The extent of 2,6-DNP ionization was increased at $pH > 4.2$ so that the ability to form complex with FPVC was weakened and α gradually increased. In the tested pH range, t increased only from 46 to 48 s with increasing pH . So 0.1 mol L^{-1} sodium acetate–hydrochloric acid buffer solution was used to adjust solution pH at 3.50. The flow rate had almost no effect on α and α remained a constant with variation of the flow rate. The response time t was apparently influenced by the flow rate with a variation from 53 to 45 s when the flow rate was increased from 0.5 to 4.5 mL min^{-1} , which was resulted from increasing of the renew rate of the sensing membrane interface and will strengthen the migration process of 2,6-DNP from the aqueous solution to the membrane phase. In order to avoid the leakage of the sensing substance in the membrane at high flow rate, a flow rate of 2.0 mL min^{-1} was finally selected as a compromise among response time and membrane stability.

3.5.3. Dynamic response behavior

With the optimum conditions, the sensor exhibits a dynamic detection range from 2.5×10^{-6} to $7.0 \times 10^{-3} \text{ mol L}^{-1}$ ($0.05 < \alpha < 0.95$) [27] and limit of detection of $1.0 \times 10^{-6} \text{ mol L}^{-1}$. The response behavior of the sensor to 2,6-DNP was shown in Fig. 4. As can be seen, under the optimum conditions, the forward response time (going from lower to higher 2,6-DNP concentrations), t_{95} (time needed for 95% of the total signal change to occur) was within 1 min, whereas the time for the reverse response was in the range of 1 min over the entire concentration range. Thus the proposed sensor was independent of the order of concentration change, and it was quite reversible and no noticeable hysteresis effect was observed, which indicated that the migration rate of the analyte in the dynamic process was fast [28].

Clearly, both the polymer cavity size and the binding strength can affect the diffusion rate of analytes in a polymer film

[29]. Larger cavities and weaker polymer–analyte interactions will result in faster diffusion. Linking curcumin moieties to the backbone of polymer made the cavities generated between adjacent polymers are sufficiently large enough to allow rapid and facile diffusion of small analyte molecules, to the entity of polymer, and simultaneously, the supramolecular recognition interaction between the electron-rich polymer and the electron-deficient analyte was quiet reversible, all of which were responsible for the distinctly fast response of the sensing membrane.

3.5.4. Repeatability and reproducibility

The sensor repeatability and reproducibility were calculated according to the definition by Alabbas et al. [30]. The R.S.D. for repeatability of the sensor for the measurement of 2,6-DNP concentration of $5.0 \times 10^{-5} \text{ mol L}^{-1}$ and $5.0 \times 10^{-6} \text{ mol L}^{-1}$ was calculated to be 1.2% and 1.1%, respectively. On the other hand, the reproducibility was found to have a R.S.D. value of 3.0% for 2,6-DNP concentration of $5.0 \times 10^{-5} \text{ mol L}^{-1}$ and 4.1% for 2,6-DNP concentration of $5.0 \times 10^{-6} \text{ mol L}^{-1}$.

3.5.5. Lifetime

The stability of the sensor was tested by recording the fluorescence intensity of $5.0 \times 10^{-5} \text{ mol L}^{-1}$ 2,6-DNP over a period of 8 h for 50 measurements. A relative standard deviation of the fluorescence reading of 1.0% was recorded. No decrease of the fluorescence intensity of the membrane was observed after a continuous 150 measurement. The sensing membrane exhibited neither bleaching of the fluorophore, chemical decomposition, nor peeling-off of the polymer layer from the glass support for a period of longer than 5 months when stored in buffer solution in the dark at room temperature. The increase of the stability and lifetime of the sensor was resulted from its effective protection from backbone of PVC.

3.5.6. Selectivity

To define the response of the sensor to other nitrophenols, different concentrations of 2,6-DNP, *o*-NP, *m*-NP, *p*-NP, 2,4-DNP, and 2,4,6-TNP solutions were pumped to the flow cell separately and the fluorescence intensity was recorded. In Fig. 5, the response parameter, α , at pH 3.50, are plotted as functions of the concentrations logarithms of 2,6-DNP and other nitrophenols. The curve fittings for the experimental points were calculated by assuming a 1:1 complex ratio. The optical selectivity coefficients, $\log K^{\text{opt}}$ values [31] are summarized in Table 2. From Fig. 5 and Table 2, we can see that the response of the sensor toward nitrophenols decreases in the order of $2,6\text{-DNP} \gg 2,4\text{-DNP} > p\text{-NP} > m\text{-NP} > o\text{-NP} > 2,4,6\text{-TNP}$.

The effects of other potential interferences such as phenols except for nitrophenols, amines, organic acids, alcohols, and some ions were tested for their possible co-occurrences in environmental or industrial samples with 2,6-DNP. The tolerance limit is set as the concentration of interferences that produces a relative error of less than $\pm 5\%$ in the apparent recovery of $5.0 \times 10^{-5} \text{ mol L}^{-1}$ 2,6-DNP. The results are summarized in

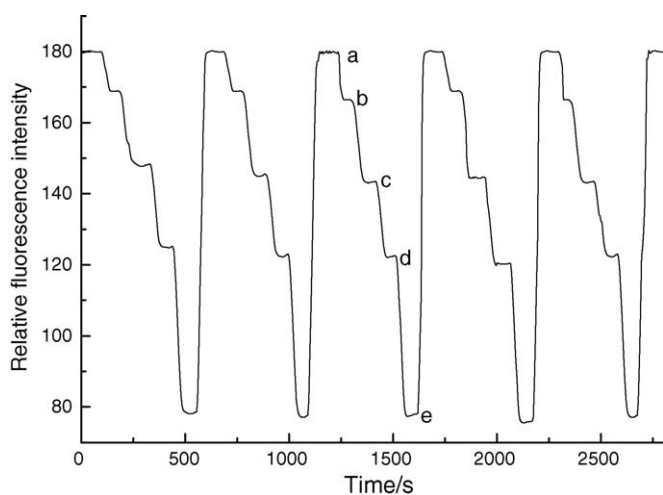


Fig. 4. The time-dependent response of the sensor. The sensor is alternatively exposed to (b) 2.5×10^{-6} , (c) 1.0×10^{-4} , (d) 1.0×10^{-3} , and (e) $8.0 \times 10^{-3} \text{ mol L}^{-1}$ 2,6-DNP solutions with (a) blank solution in between.

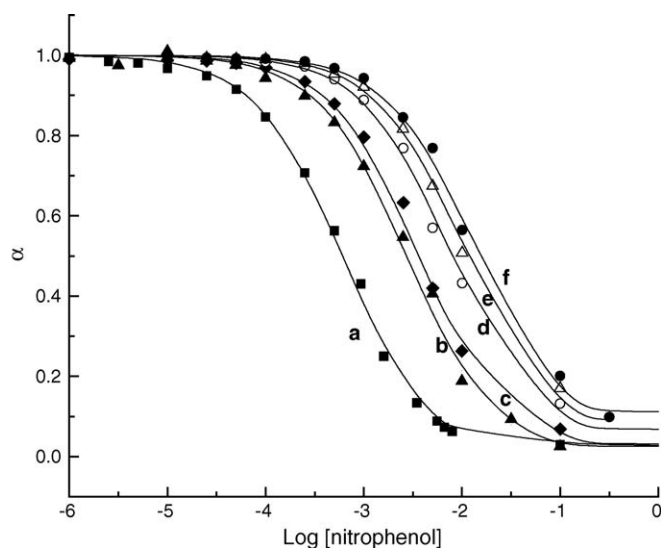


Fig. 5. Response function of the sensing membrane on exposure to various aqueous solutions of nitrophenols measured at pH 3.50 and at an excitation wavelength of 460 nm and an emission wavelength of 503 nm: (a) 2,6-DNP; (b) 2,4-DNP; (c) *p*-NP; (d) *m*-NP; (e) *o*-NP; (f) 2,4,6-TNP. The solid lines were calculated according to Eq. (1).

Table 3. As can be seen, many possibly coexisting substances in environmental water showed no remarkable interference for the determination of 2,6-DNP even at high concentration. The limiting water solubility of the tested phenols precluded their higher concentration interference determination. The most serious interference come from $\text{Cr}_2\text{O}_7^{2-}$ and MnO_4^- , which were anionic oxidants with color and can be eliminated through a column packed with anionic-exchange resins.

In order to clarify the specific sensing properties of the proposed sensor, the comparison of the sensing characteristics in determining 2,6-DNP between the proposed curcumin substituted PVC sensor and a curcumin embedded sensor was carried out under the same experimental conditions, even though the latter was reported to show high selectivity to *o*-nitrophenol [10]. The results were shown in Table 4. As can be seen, the proposed sensor exhibited apparent advantages over the embedded sensor in terms of sensitivity, selectivity, response time, and lifetime, which almost covers the whole scope of sensor characteristics. The results also reconfirmed the nucleophilic substitution of PVC by curcumin and the distinct sensing ability of FPVC.

Table 2

Association constants (K) and selectivity coefficients ($\log K^{\text{opt}}$) of the sensing membrane for other nitrophenols in comparison to 2,6-DNP at pH 3.50

Interfering agent	K (mol L^{-1})	$\log K^{\text{opt}}$
2,6-DNP	2.0×10^3	0
2,4-DNP	7.3×10^2	−1.14
<i>p</i> -NP	4.4×10^2	−1.23
<i>m</i> -NP	3.1×10^2	−1.61
<i>o</i> -NP	1.9×10^2	−1.81
2,4,6-TNP	0.42×10^2	−1.92

Table 3

Effect of different phenols and possible interference on the determination of 0.05 mM 2,6-DNP in pH 3.50 buffer solution

Interference	Tolerance limit (molar ratio)	Fluorescence variation
Phenols		
Pyrocatechol, resorcinol	300	+
<i>m</i> -Cresol, 2,6-xyleneol	250	+
Phenol, <i>o</i> -cresol, hydroquinone	200	+
<i>p</i> -Cresol	180	+
2,4-Xyleneol, 2-naphthol, pyrogallol	150	+
2,4,6-Trinitrophenol		—
<i>p</i> -Chlorophenol, 2,4-dichlorophenol, 2,6-dichlorophenol, 1-naphthol	120	+
2,4,6-Trichlorophenol		—
Salicylic acid	100	—
<i>o</i> -Nitrophenol	80	—
<i>m</i> -Nitrophenol, <i>p</i> -nitrophenol	60	—
2,4-Dinitrophenol	50	—
Cationic ions		
Na^+ , K^+ , NH_4^+ , Ag^+ , Mn^{2+} , Ni^{2+} , Mg^{2+} , Ca^{2+} , Sr^{2+} , Ba^{2+} , Zn^{2+} , Fe^{2+} , Cu^{2+} , Cd^{2+} , Pb^{2+} , Hg^{2+} , Al^{3+} , Fe^{3+} , Co^{2+} , Cl^{3+}	1000	a
	200	—
Anionic ions		
F^- , Cl^- , Br^- , I^- , NO_3^- , NO_2^- , ClO_3^- , BrO_3^- , HCOO^- , CH_3COO^- , IO_4^- , S^{2-} , SO_4^{2-} , SO_3^{2-} , $\text{S}_2\text{O}_3^{2-}$, SiO_3^{2-} , CO_3^{2-} , $\text{C}_2\text{O}_4^{2-}$, MoO_4^{2-} , PO_4^{3-} , AsO_4^{3-} , $\text{Cr}_2\text{O}_7^{2-}$, MnO_4^-	1000	a
	15	—
	8	—
Organic acids		
Formic acid, propionic acid, <i>n</i> -butyric acid, succinic acid, tartaric acid, citric acid, lactic acid, <i>p</i> -toluenesulfonic acid, <i>p</i> -phthalic acid, DL-malic acid	1000	a
Others		
Glucose, boric acid, urea	1000	a
Aniline, humic acid	100	—

—, Fluorescence decrease; +, fluorescence increase.

^a No interference.

Table 4

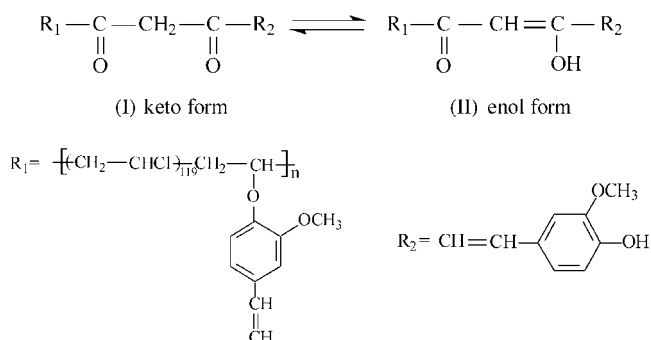
Comparison of sensing characteristics between the two sensors for 2,6-DNP determination

Sensors	The proposed sensor	The curcumin embedded sensor
Membrane matrices	No matrices	PVC
Sensing substances	Curcumin substituted PVC	Curcumin
Dynamic range (mol L^{-1})	2.5×10^{-6} to 7.0×10^{-3}	8.0×10^{-4} to 1.0×10^{-3}
Detection limit (mol L^{-1})	1.0×10^{-6}	6.0×10^{-4}
Response time (t_{95}) (s)	50	100
Lifetime ^a (%)	0	20

^a Fluorescence intensity decrease percent after a continuous 200 measurements.

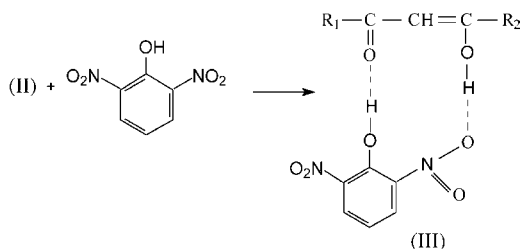
3.6. Sensing mechanism

Suppose that the curcumin moiety in FPVC remains the keto–enol tautomeric equilibrium of curcumin molecule [32], i.e.,



So it is possible for hydroxyl or carbonyl groups to form associated complexes by the means of hydrogen bond with some compounds containing hydroxyl or nitro group.

As the stoichiometric ratio of the tested nitrophenols to FPVC was proved to be 1:1 and 2,6-DNP exists mainly in the molecular form at pH 3.50, it seems that the hydroxyl and nitro-groups in 2,6-DNP simultaneously associate with the carbonyl and hydroxyl groups of enol form of FPVC through hydrogen bond to form non-fluorescent ground state complex, i.e.,



The formation of the cyclic structure III causes the fluorescence quenching of FPVC.

The 2,6-DNP selectivity of this sensing membrane was based on the ability difference between 2,6-DNP and other nitrophenols in forming the cyclic non-fluorescent complex with FPVC through hydrogen bonding. Two factors, including the steric hindrance and acidity of nitrophenols, must be considered. The steric hindrance, or spatial matching effect, was predominated by the cavity size of polymer and the molecular structure of the analyte. The ionisation constant ($\text{p}K_{\text{a}}$) was the indicator for acidity of nitrophenols, which was summarized in Table 5. As can be seen from Table 5, under the experimental pH, the tested nitrophenols were all in their molecular form except 2,4,6-TNP. The solution pH of 3.50 deprotonated its phenolic hydroxy group and it is mainly in the anion form such that inclined to stay in the solution and not to diffuse into the membrane phase. In addition, the steric hindrance experienced by 2,4,6-TNP because of its three-dimensional molecular structure [35] may also block its migration into the membrane phase and react with the sensing materials. So FPVC showed the smallest response to 2,4,6-TNP. *o*-NP was very much more intramolecularly hydrogen bonded than other nitrophenols [36], which may form a unfavorable molecular structure for its effective interaction with FPVC to

Table 5

Ionisation constant ($\text{p}K_{\text{a}}$) of tested nitrophenols

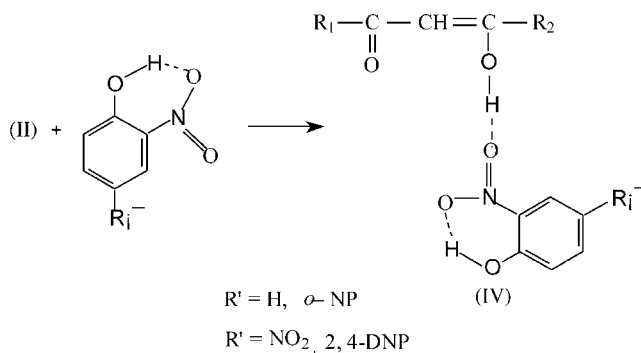
Nitrophenols	$\text{p}K_{\text{a}}$
<i>o</i> -NP	7.23 ^a
<i>m</i> -NP	8.39 ^a
<i>p</i> -NP	7.15 ^a
2,4-DNP	4.09 ^a
2,6-DNP	3.68 ^b
2,4,6-TNP	0.71 ^c

^a Data taken from [33].

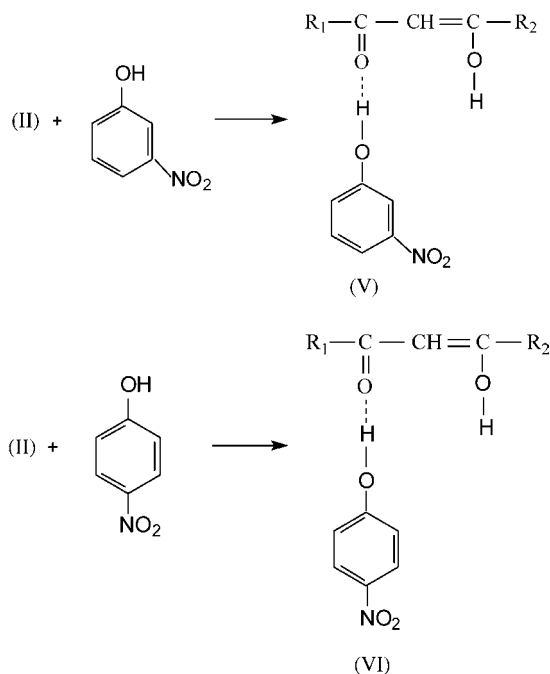
^b Data taken from [26].

^c Data taken from [34].

form the non-fluorescent complex. The similar phenomenon also occurred to 2,4-DNP, i.e.,



It is apparent that the 3- and 4-position nitro groups in *m*- and *p*-NP may offer disadvantageous configuration for their effective interaction with FPVC through hydrogen bond and their response was relatively small.



It can be seen that the spatial adaptability between the analytes and sensing substance showed the dominating effect on their effective interaction in the proposed chemical sensor. 2,6-DNP possesses a most spatially matching structure for its migra-

Table 6
Analytical results for 2,6-DNP in water samples ($n=5$)

Sample	Nitrophenols added (10^{-5} mol L $^{-1}$)	2,6-DNP found (10^{-5} mol L $^{-1}$)		Recovery (%)	
		Proposed sensor	HPLC method [7]	Proposed sensor	HPLC method [7]
Tap water 1	<i>o</i> -NP, 0.2; <i>m</i> -NP, 0.15; <i>p</i> -NP, 0.3; 2,4-DNP, 0.15; 2,6-DNP, 0.2; 2,4,6-TNP, 0.1	0.21 ± 0.01	0.20 ± 0.01	105	100
Tap water 2	<i>o</i> -NP, 0.3; <i>m</i> -NP, 0.15; <i>p</i> -NP, 0.3; 2,4-DNP, 0.15; 2,6-DNP, 0.3; 2,4,6-TNP, 0.1	0.32 ± 0.02	0.31 ± 0.01	107	103
River water 1	<i>o</i> -NP, 1.0; <i>m</i> -NP, 1.5; <i>p</i> -NP, 1.0; 2,4-DNP, 1.5; 2,6-DNP, 5.0; 2,4,6-TNP, 1.5	4.7 ± 0.2	4.8 ± 0.1	94	96
River water 2	<i>o</i> -NP, 1.0; <i>m</i> -NP, 1.0; <i>p</i> -NP, 0.8; 2,4-DNP, 1.2; 2,6-DNP, 1.0; 2,4,6-TNP, 0.8	1.1 ± 0.2	1.1 ± 0.2	110	110

tion through the polymer cavity and approach the fluorophore to form a supramolecular complex.

3.7. Preliminary analytical application

The proposed sensor was applied to the determination of 2,6-DNP in tap and river water samples in the presence of other nitrophenols. River water samples were first acidified by sulphuric acid to pH 3.50, then filtered through a 0.45- μ m filter membrane (Ya Dong Nuclear Grade Resins Co. Ltd., Shanghai Institute of Pharmaceutical Industry, Shanghai, China) and a column packed with anionic-exchange resin (Amberlite IRA-400, USA), successively. Tap water samples were acidified to pH 3.50 and analyzed without any pretreatment. All the water samples were spiked with nitrophenols at different concentration levels and then analyzed. The results obtained for 2,6-DNP determination were also compared with those obtained by HPLC method [7] and were shown in Table 6. We can see that the results were satisfactory. The present sensor may be useful for the determination of 2,6-DNP in real samples.

4. Conclusions

A novel functional polymer has been successfully synthesized by the nucleophilic substitution of a fraction of the chlorine atoms bound to the PVC backbone by curcumin. The polymer was applied to fabricate an optical fiber chemical sensor for the determination of 2,6-DNP simply, quickly, and selectively. The fluorescence signal variation was very reversible and was proportional to 2,6-DNP concentration. As 2,6-DNP can provide an optimal space geometry matches to the formation of a cyclic complex with low fluorescence efficiency, the sensor shows excellent selectivity for 2,6-DNP. The response time, repeatability, and lifetime of the sensor were also satisfied. The study results enabled better understanding of the interaction between functional polymer and the analytes and prove useful in the future development of high-quality chemical sensors for on line environmental monitoring.

Acknowledgements

The authors gratefully acknowledge financial support of the National Science Fund for Distinguished Young Scholars of

China (No. 20125514), National Natural Science Foundation of China (No. 20437020, 50273046) and Major Research Program of Chinese Academy of Sciences (KZCX3-SW-432).

References

- [1] D.M. Nevskaja, E. Castillejos-Lopez, V. Muñoz, A. Guerrero-Ruiz, *Environ. Sci. Technol.* 38 (2004) 5786.
- [2] M.L. Davi, F. Gnudi, *Water Res.* 33 (1999) 3213.
- [3] U.S., Environmental Protection Agency (EPA), National Recommended Water Quality Criteria, 2004.
- [4] B. Swarnalatha, Y. Anjaneyulu, *J. Mol. Catal. A: Chem.* 223 (2004) 161.
- [5] R. Belloli, B. Barletta, E. Bolzacchini, S. Meinardi, M. Orlandi, B. Rindone, *J. Chromatogr. A* 846 (1999) 277.
- [6] D. Kaniasky, E. Krčmová, V. Madajová, M. Masár, J. Marák, F.I. Onuska, *J. Chromatogr. A* 772 (1997) 327.
- [7] H. Roseboom, C.J. Berkhoff, J.I.J. Wammes, R.C.C. Wegman, *J. Chromatogr.* 208 (1981) 331.
- [8] H. Sohn, R.M. Calhoun, M.J. Sailor, W.C. Trogler, *Angew. Chem. Int. Ed.* 40 (2001) 2104.
- [9] X. Yang, C.G. Niu, G.L. Shen, R.Q. Yu, *Analyst* 126 (2001) 349.
- [10] Y. Wang, K.M. Wang, G.L. Shen, R.Q. Yu, *Talanta* 44 (1997) 1319.
- [11] B. Adhikari, S. Majumdar, *Prog. Polym. Sci.* 29 (2004) 699.
- [12] A. Mirmohseni, A. Oladegaragoze, *Sens. Actuators B* 102 (2004) 261.
- [13] I. Varga, R. Mészáros, Z. Szakács, T. Gilányi, *Langmuir* 21 (2005) 6154.
- [14] S. Lakshmi, A. Jayakrishnan, *Polymer* 39 (1998) 151.
- [15] S. Lakshmi, A. Jayakrishnan, *Biomaterials* 23 (2002) 4855.
- [16] P.V.C. Rao, V.K. Kaushik, I.S. Bhardwaj, *Eur. Polym. J.* 31 (1995) 341.
- [17] M. Rogestadt, T. Hjertberg, *Macromolecules* 26 (1993) 60.
- [18] J.L. Koenig, M.K. Antoon, *J. Polym. Sci.: Polym. Phys. Ed.* 15 (1977) 1379.
- [19] D. Fabbri, D. Tartari, C. Trombini, *Anal. Chim. Acta* 413 (2000) 3.
- [20] F. Sittner, B. Enders, W. Ensinger, *Thin Solid Films* 459 (2004) 233.
- [21] T. Rosatzin, P. Holý, K. Seiler, B. Rusterholz, W. Simon, *Anal. Chem.* 64 (1992) 2029.
- [22] N.U. Perišić-Janjić, A.A. Muk, V.D. Canic, *Anal. Chem.* 45 (1973) 798.
- [23] S.V. Jovanovic, S. Steenken, C.W. Boone, M.G. Simic, *J. Am. Chem. Soc.* 121 (1999) 9677.
- [24] J. Crank, G.S. Park, *Diffusion in Polymers*, Academic Press, London, 1968, p. 21.
- [25] X.B. Zhang, C.C. Guo, Z.Z. Li, G.L. Shen, R.Q. Yu, *Anal. Chem.* 74 (2002) 821.
- [26] G. Nalecz-Jawecki, J. Sawicki, *Chemosphere* 52 (2003) 249.
- [27] M.M.F. Choi, X.J. Wu, Y.R. Li, *Anal. Chem.* 71 (1999) 1342.
- [28] D.S. Blair, L.W. Burgess, A.M. Brodsky, *Anal. Chem.* 69 (1997) 2238.
- [29] J.S. Yang, T.M. Swager, *J. Am. Chem. Soc.* 120 (1998) 11864.

- [30] S.H. Alabbas, D.C. Ashworth, R. Narayanaswamy, *Anal. Proc.* 26 (1989) 373.
- [31] R.H. Yang, K.A. Li, F. Liu, N. Li, F.L. Zhao, W.H. Chan, *Anal. Chem.* 75 (2003) 3908.
- [32] G. Litwinienko, K.U. Ingold, *J. Org. Chem.* 69 (2004) 5888.
- [33] M. Czaja, A. Kozak, M. Makowski, L. Chmurzynski, *J. Chem. Thermodyn.* 35 (2003) 1645.
- [34] S.G. Dmitrienko, E.N. Myshak, L.N. Pyatkova, *Talanta* 49 (1999) 309.
- [35] M.H. Abraham, C.M. Du, J.A. Platts, *J. Org. Chem.* 65 (2000) 7114.
- [36] B. Müller, M.R. Heal, *J. Phys. Chem. A* 106 (2002) 5120.

Ion-exclusion/adsorption chromatography of dimethylsulfoxide and its derivatives for the evaluation to quality-test of TiO₂-photocatalyst in water

Masanobu Mori^{a,*}, Kazuhiko Tanaka^b, Hiroshi Taoda^c,
Mikaru Ikedo^d, Hideyuki Itabashi^a

^a Department of Chemistry, Faculty of Engineering, Gunma University, 1-5-1 Tenjin-cho, Kiryu, Gunma 376-8515, Japan

^b Graduate School for International Development and Cooperation, Hiroshima University, 1-5-1 Kagamiyama, Higashi-Hiroshima 739-8529, Japan

^c National Institute of Advanced Industrial Science and Technology, 110 Nishiibarara-cho, Seto 489-0884, Japan

^d Engineering of Graduate School, Chubu University, 1200 Matsumoto-cho, Kasugai, Japan

Received 31 October 2005; received in revised form 8 January 2006; accepted 1 February 2006

Available online 6 March 2006

Abstract

Ion-exclusion/adsorption chromatography of dimethylsulfoxide (DMSO) and its derivatives, i.e., methanesulfinic acid (MSI), methanesulfonic acid (MSA) and sulfuric acid (SA), was developed in order to clear the decomposition mechanism of DMSO on quality-test of TiO₂-photocatalyst in water. The separation was achieved by the adsorption effect for DMSO and ion-exclusion effect for MSI, MSA and SA under optimum conditions, using a weakly acidic cation-exchange resin column with 20 mM succinic acid as the eluent. In this system, DMSO and MSI with UV at 195 nm and MSA and SA with conductivity detection were consecutively determined by single injection and single separation column. This method was used to monitor the artificial decomposition of DMSO induced by a photocatalyst. The concentration of DMSO by active oxygens (e.g., OH radical) generated from surface of photocatalyst was found to be decreased through the stoichiometric reaction in the order of MSI, MSA and SA.

© 2006 Elsevier B.V. All rights reserved.

Keywords: Ion-exclusion; Adsorption; Chromatography; Photocatalyst; Dimethylsulfoxide; Active oxygen

1. Introduction

Recently, TiO₂-photocatalyst has been expected as one of several promising advanced oxidation technologies for environmental remediation in purification of air- and water-quality. They can effectively decompose and removal many pollutants by active oxygens, e.g., OH radical, hydrogen peroxide, generated from the surface of the photocatalysts with light irradiation [1–9]. Therefore, TiO₂-photocatalyst-coated materials have been numerously developed by many researchers, as a result, the photocatalytic-coated products (tile, floor, wall, road, glass, etc.) have been commercialized. However, the establishments of quality-test for photocatalytic materials in air or water phases were insufficient, though it has been required in order to confirm their purification performances and to obtain the reliance for consumers.

In our laboratory, the standardization of evaluation method for TiO₂-photocatalytic materials in water phase has been progressed in terms of the establishment of photocatalytic reaction system, the selection of testing-sample and the effective monitoring method.

Previously, we used methyleneblue (MB) as a testing-sample concerning the quality-test of TiO₂-photocatalyst in water [10], because it has been widely used in the fields of self-cleaning, and defense of dirt or germ. The monitoring method was to observe the decrease of the maximum adsorption coefficient of MB (650–660 nm) using spectrophotometer. However, MB is often adsorbed to the photocatalytic materials even under non-irradiation when a hydrophobic material, e.g., silica-gel, is used as the matrix in order to fix photocatalytic powder. Therefore, it was difficult to judge only from the decrease of the MB concentration which it is by adsorption to the matrices of photocatalytic materials or by real photodecomposition with UV-irradiation.

In this study, dimethylsulfoxide (DMSO) was used as one of the testing-sample. DMSO is an organic solvent, which is colorless, highly hygroscopic, thermally and chemically stable, and

* Corresponding author. Tel.: +81 277 30 1271; fax: +81 277 30 1271.
E-mail address: m_mori@chem.gunma-u.ac.jp (M. Mori).

has strong solvency for both organic and inorganic compounds. It has been widely used in the manufacture of electronics, polymers, dyes, membranes, etc. In nature, DMSO is an intermediate in the global sulfur cycle produced from photo-oxidation of dimethylsulfide (DMS), methanesulfinic acid (MSI), methanesulfonic acid (MSA) and sulfuric acid (SA) [11]. DMSO has been known also as a scavenger that it can indirectly determine active oxygens such as OH radical generated during a biological reaction [12]. The oxidative decomposition of DMSO with the active oxygen is stoichiometric reaction to MSI, MSA and SA. From these reasons, DMSO can be expected to be a useful testing-sample that can evaluate activity of the photocatalyst with irradiation of UV-ray.

Ion-exclusion/adsorption chromatography was used simultaneously to determine the decomposition of DMSO and the formation of the MSI, MSA and SA by a photocatalyst. This can separate the acid anions and neutral compounds by an acidic cation-exchange resin with an acid as an eluent [13–15]. The succinic acid was used as an eluent, because of the rapid conditioning time until obtaining the stable conductometric baseline and the low background level [15]. DMSO and MSI were detected by UV at 195 nm, due to the low conductometric response. In contrast, acid anions such MSA and SA were detected by conductivity.

In this work, we report for development of a rapid and simple method for the separation and determination of DMSO, MSI, MSA and SA using ion-exclusion/adsorption chromatography with succinic acid; and its application to the evaluation of the artificial decomposition of DMSO by a photocatalytic material.

2. Experimental

2.1. Ion-exclusion chromatographic system

The ion chromatograph (Tokyo, Japan) consisted of Tosoh LC-8020-Model II chromatographic data processor, DP-8020 dual pump operated at flow rate of 0.6 ml/min, SD-8022 on-line degasser, CO-8020 column oven operated at 40 °C, CM 8020 conductivity detector and UV 8020 spectrophotometric detector. Fig. 1 shows the schematic illustration of the present ion chromatographic method. The injection volume was 100 μ l. A separation column in this study was a polymethacrylate-based weakly acidic cation-exchange resin in the H⁺-form,

Tosoh TSKgel Super IC-A/C-0.1 packed with 3 μ m particle and 0.1 mequiv./ml cation-exchange capacity (150 mm \times 6 mm i.d.). The guard column was a polymethacrylate-based weakly acidic cation-exchange resin in the H⁺-form, Tosoh TSKguardcolumn Super IC-A/C-0.1 packed with 3 μ m particle and 0.1 meq/ml cation-exchange capacity (2.0 mm \times 4.6 mm i.d.). The columns were equilibrated with an eluent for 30 min before the chromatographic run.

All reagents were of analytical reagent-grade, purchased from Wako (Osaka, Japan) and the preparation of the standard solutions was dissolved with distilled and deionized water as necessary.

2.2. Photocatalytic reaction system

Acryl-resin based photocatalytic oxidation reactor (290 mm \times 108 mm \times 110 mm) in this system is lay out and assembled as shown in Fig. 2. The tested TiO₂-photocatalyst-coated materials are put into photocatalyst area (110 mm \times 110 mm \times 50 mm) of the reactor. The turbulent pieces are inserted before and after the photocatalyst area in order to increase the contact between testing-solution and the photocatalytic materials.

DMSO, which was prepared with distilled-deionized water, was used as the test sample in the evaluation method of TiO₂-photocatalyst. A 500-ml solution containing DMSO was poured into the photocatalytic reactor. The pH of testing-solution was measured using the portable-type pH meter (TOA Portable pH meter HM-14P, Tokyo, Japan).

An anatase-type TiO₂-glass beads BL2.5DX coating 1 μ m thickness of TiO₂ on a 2.5 mm \varnothing of silica-glass bead was purchased from Photocatalytic Materials Inc. (Aichi, Japan). Fifty grams of photocatalyst-coated beads were used at one experiment. The UV-irradiation to TiO₂-photocatalyst was carried out by the UV-light source, which is a commercial BLB light (National-FL20S-BLB lamp) with spectral peak around 350 nm. The photocatalyst was irradiated at room temperature for 1 h before pouring the testing-solution. The solution in the reactor was circulated by peristaltic pump (Cole-Parmer Master Flex 7518-10) at 500 ml/min of flow rate. A 10 ml sample solution during photocatalytic reaction was collected at every 60 min. The concentrations of DMSO and its products in the solution were determined by the ion-exclusion/adsorption chromatography established in this study.

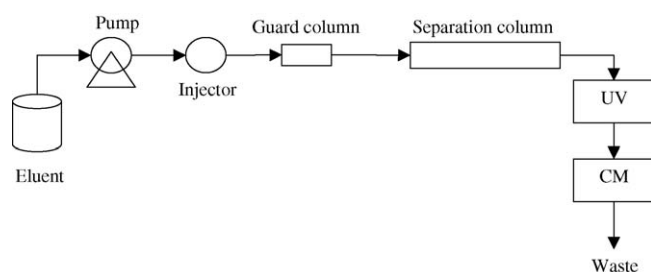


Fig. 1. Schematic illustration of the present ion-exclusion/adsorption chromatography.

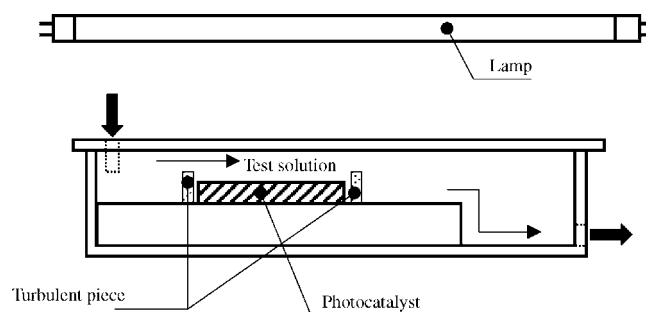


Fig. 2. Schematic illustration of the present photocatalytic reaction system.

3. Results and discussion

3.1. Ion-exclusion/adsorption chromatography of DMSO and its derivatives

Ion-exclusion/adsorption chromatography of DMSO and its derivatives using a weakly acidic cation-exchange resin in the H^+ -form with succinic acid as the eluent was optimized in terms of the retention times and the peak resolutions of each analytes with UV and conductivity detections.

The retention of organic solvent such as DMSO was decreased with increasing the concentration of succinic acid in the eluent, because it is mainly governed by the adsorption effect to the cation-exchange stationary phase [16]. In contrast, the retentions of fully ionized acids such as MSI, MSA and SA were increased with increasing concentration of the succinic acid. This is because the acids are penetrated to the stationary phase with the neutralized carboxyl-functional groups by increasing hydrogen ion in the eluent [15].

The background conductance level was increased with increasing the concentration of succinic acid in the eluent (e.g., 5 to 30 mM: 62 to 449 $\mu S/cm$). Since the increase of the succinic acid concentration gave the decrease of the conductivity response of the acids, the lowest possible concentration of succinic acid was required to obtain the sensitive detection. As a result, the optimum concentration of succinic acid was concluded to be 20 mM, which was 397 $\mu S/cm$ of background level, by considering the above factors.

Fig. 3 shows a typical chromatogram of DMSO and its derivatives under the optimum ion-exclusion/adsorption chromatographic conditions.

3.2. Analytical performance

Peak areas of DMSO, MSI, MSA and SA under the optimal conditions were, respectively, plotted against their different concentrations. The calibration graphs obtained were linear in the ranges of the concentration of 0.01–10 ppm for all analytes ($r^2 = 0.9961$ – 0.9998). Detection limits at $S/N = 3$ by injecting 0.1 ppm for each sample were DMSO = 15 ppb, and MSI = 6.2 ppb with UV at 195 nm, and MSI = 20.7 ppb, MSA = 9.0 ppb and SA = 3.1 ppb with conductivity. Although MSI could be detected by both UV and conductivity detections, the detection and determination in the photodecomposition process were carried out by UV in terms of the detection limits. In the 10th repeated chromatographic runs, the relative standard deviations of peak areas and retention times for 0.1 ppm analytes were 0.32–2.12 and 0.10–1.3%, respectively.

3.3. Photooxidation of DMSO by anatase-type TiO_2

Photooxidation process of DMSO by anatase-type TiO_2 -coated glass beads in water was investigated by using the photocatalytic reaction system developed in this study. The testing-solution with 10 ppm DMSO was poured to the reactor, and the circulating time was for 10 h. Under the non-irradiation of UV-ray, there was no adsorption of 10 ppm DMSO to the pho-

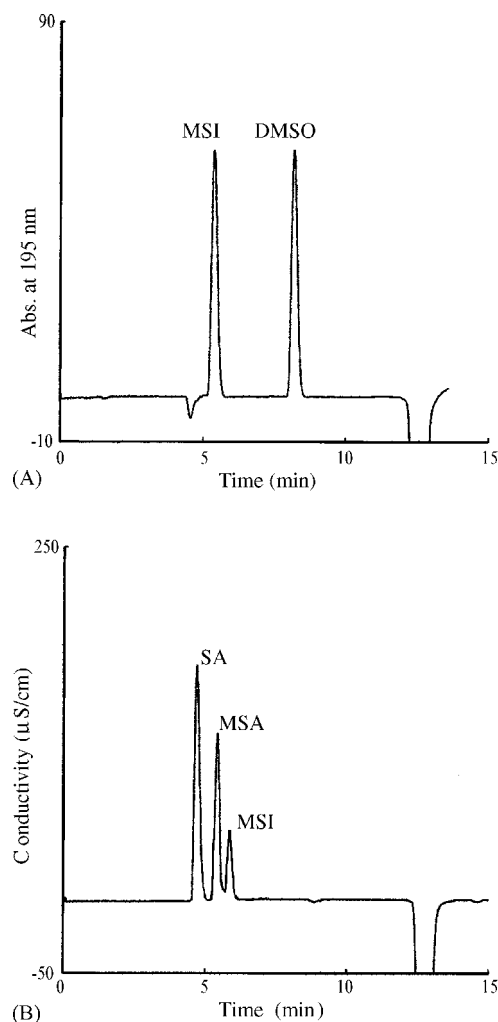


Fig. 3. Ion-exclusion/adsorption chromatogram of DMSO and its derivatives. Ion chromatographic conditions: eluent: 20 mM succinic acid; detection: (A) UV at 195 nm and (B) conductivity; separation column: TSKgel Super IC-A/C packed with a weakly acidic cation-exchange resin in the H^+ -form (150 mm \times 6 mm i.d.); guard column: TSKguardcolumn Super IC-A/C-0.1 packed with a weakly acidic cation-exchange resin in the H^+ -form (2.0 mm \times 4.6 mm i.d.); flow rate: 0.6 ml/min; column oven: 40 $^{\circ}C$; injection volume: 100 μl . Sample concentrations: 10 ppm DMSO, and 5 ppm MSI, MSA and SA.

tocatalyst beads during the observation for 10 h. Additionally, the concentration of DMSO in the reactor without photocatalyst was not changed by UV-irradiation for 10 h since it is thermally stable.

Fig. 4 shows a typical peak profile of DMSO remained and its intermediate products in the test sample solution by the TiO_2 -coated glass beads with UV-irradiation for 4 h, under the present ion-exclusion/adsorption chromatographic conditions. The DMSO remained was gradually decreased with time-dependence of UV-irradiation, in contrast the intermediates was produced in order of MSI, MSA and SA with the irradiation time. Fig. 5 shows the changes in the concentrations of sulfur atom in DMSO remained and the intermediate products formed by the TiO_2 -coated glass beads with UV-irradiation for 10 h. DMSO was rapidly oxidized to MSA through MSI from 1 to 4 h irradiation of UV-ray. Intermediate MSI was suddenly increased

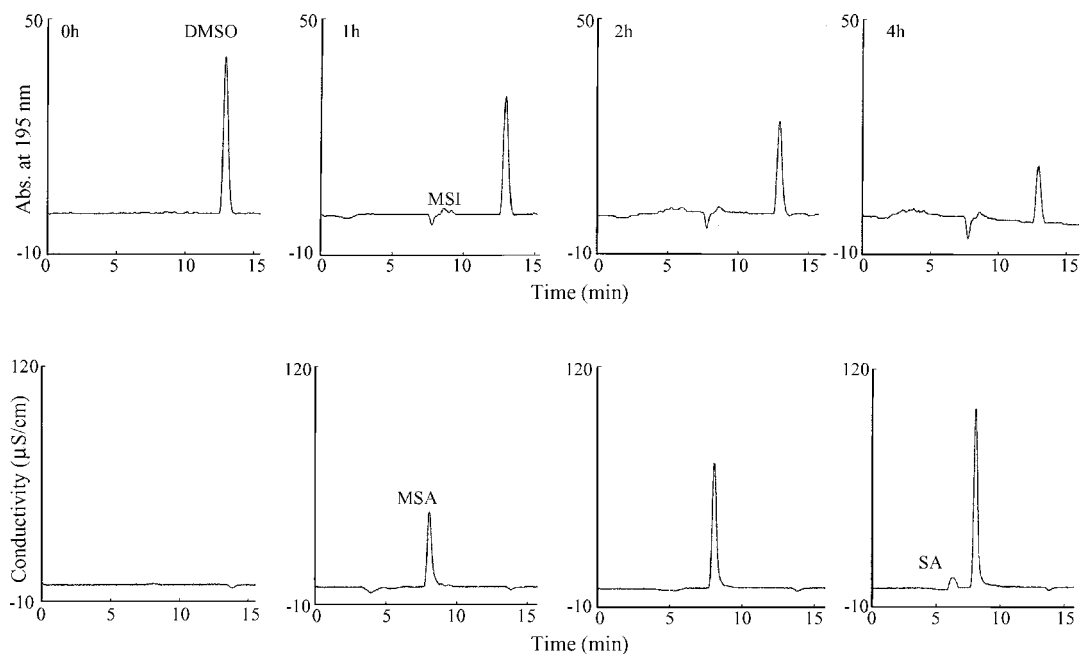


Fig. 4. Peak profiles of DMSO decomposed and the products formed by TiO₂-photocatalyst with UV-irradiations. Ion chromatographic conditions: same as in Fig. 3. Photocatalytic conditions: photocatalyst: anatase-type TiO₂-coated glass beads (50 g); flow rate: 500 ml/min; test sample: 10 ppm DMSO; UV-strength: 2 mW/cm².

during 1 h irradiation, and MSA was rapidly increased with decreasing MSI from 1 to 3 h. Moreover, the concentration of SA was increased when the MSA concentration was begun to decrease after irradiations for 3 h. Consequently, DMSO was finally decomposed to MSA and SA after UV-irradiations for 10 h, and the pH values were decreased from 6.5 to 4.0 due to the increase of acids such as MSA and SA. Here, the reaction between anatase-type TiO₂ and DMSO was selective since there were no photooxidation of DMSO and change of the pH values when using the rutile-type TiO₂-coated and non-coated glass beads.

The relationship between the decrease of DMSO and the formation of MSI, MSA and SA was a stoichiometric reaction

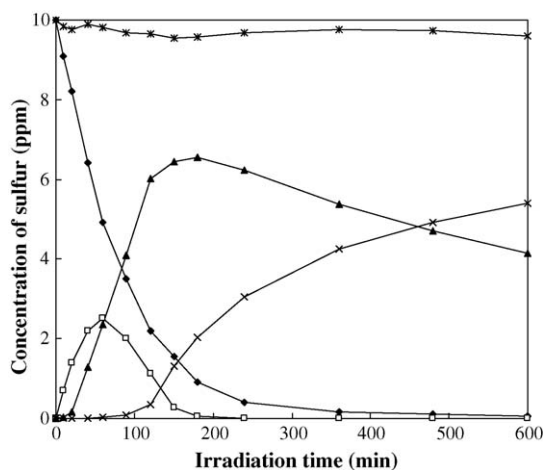


Fig. 5. Changes of sulfur atom concentrations in the DMSO and its decomposed products with and without UV-irradiation. Ion chromatographic and photocatalytic conditions: same as in Figs. 3 and 4, respectively. Plot's identities: (◆) DMSO; (□) MSI; (▲) MSA; (×) SA and (*) total of sulfur atom.

through the material balance of sulfur atom of them as shown in Fig. 5. In addition, the decomposition of DMSO by the TiO₂-coated beads was expected to be proceeded with a sequential demethylation in order of MSI, MSA and SA. This reaction would be related to active oxygen generated from surface of photocatalyst by UV-ray. The photocatalytic oxidative pathway of DMSO with active oxygen, for example OH radical, in the aqueous phase is predicted as follows:

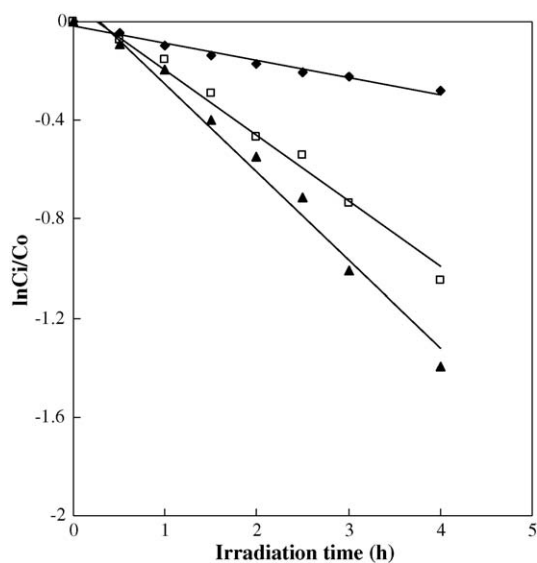
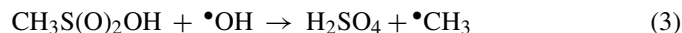
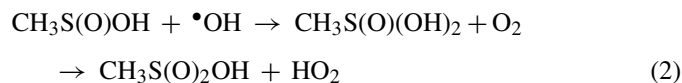


Fig. 6. Changes in relative concentration of DMSO remained in the solution with irradiation time of UV for 4 h. Ion chromatographic and photocatalytic conditions: same as in Figs. 3 and 4, respectively. Plot's identities: (▲) 1 ppm DMSO; (□) 10 ppm DMSO; (◇) 100 ppm DMSO.



Moreover, influence of different initial concentrations of DMSO solutions 1, 10 and 100 ppm, was investigated. Fig. 6 shows the relative concentration of DMSO remained in the solution C/C_0 plotted in logarithmic scale as a function of irradiation time of UV for each DMSO solution. The lower initial concentration of DMSO was found to be the higher photodecomposition rate. This implied that the decomposition rate of DMSO by the photocatalyst was related to the initial concentration.

4. Conclusion

Simultaneous determination of DMSO and its derivatives could be achieved by ion-exclusion/adsorption chromatography on a weakly acidic cation-exchange resin column with a succinic acid eluent. This method was applicable to the evaluation method on quality-test of TiO_2 -photocatalytic materials in water, using the exclusive photocatalytic reactor established in this study. Also, DMSO was found to obtain the stoichiometric decomposition by active oxygen generated from surface of TiO_2 . The evaluation for quality-test of photocatalytic materials with various matrices such as tile, filter and gel will be the subject of future work.

References

- [1] Y. Ohko, I. Ando, C. Niwa, T. Tatsuma, T. Yamamura, T. Nakashima, Y. Kubota, A. Fijishima, *Environ. Sci. Technol.* 35 (2001) 2365.
- [2] V. Maurino, C. Minero, E. Pelizzetti, M. Vincenti, *Colloids Surf. A: Physicochem. Eng. Aspects* 151 (1999) 329.
- [3] E. Pelizzetti, C. Minero, V. Maurino, V. Carlin, E. Pramauro, O. Zerbini, M.L. Tosato, *Environ. Sci. Technol.* 24 (1990) 1559.
- [4] S. Kim, W. Choi, *Environ. Sci. Technol.* 36 (2002) 2019.
- [5] N. Serpone, J. Martin, S. Horikoshi, H. Hidaka, J. Photochem. Photobiol. A: Chem. 169 (2004) 234.
- [6] S. Kim, W. Choi, *J. Phys. Chem. B* 106 (2002) 13311.
- [7] M. Toyoda, T. Tsumura, Y. Nanbu, M. Omura, M. Inagaki, *J. Jpn. Soc. Water Environ.* 126 (2003) 209.
- [8] B. Tryba, A.W. Morawski, M. Inagaki, *Appl. Catal. B: Environ.* 41 (2003) 427.
- [9] G.K.-C. Low, S.R. McEvoy, R.W. Matthew, *Chemosphere* 19 (1989) 1611.
- [10] M. Mori, H. Taoda, Q. Xu, M. Ikeda, W. Hu, K. Tanaka, *Ind. Water (in Japanese)* 541 (2003) 19.
- [11] M.D. Bentley, I.B. Douglass, J.A. Lacadie, D.R. Whittier, *J. Air Pollut. Control Assoc.* 22 (1972) 359.
- [12] R. Bruck, H. Aeed, H. Shirin, Z. Matas, L. Zaidel, Y. Avni, Z. Halpern, *J. Hepatol.* 31 (1999) 27.
- [13] T. Nakazato, H. Tao, T. Taniguchi, K. Isshiki, *Talanta* 58 (2002) 121.
- [14] M.J. Hemmings, E.A. Jones, *Talanta* 38 (1991) 151.
- [15] K. Tanaka, J.S. Fritz, *J. Chromatogr.* 409 (1987) 271.
- [16] M. Mori, K. Tanaka, M.I.H. Helaleh, Q. Xu, M. Ikeda, Y. Ogura, S. Sato, W. Hu, K. Hasebe, P.R. Haddad, *J. Chromatogr. A* 997 (2003) 219.

Ion-exclusion chromatography with the direct UV detection of non-absorbing inorganic cations using an anion-exchange conversion column in the iodide-form

Masanobu Mori^{a,*}, Hideyuki Itabashi^a, Mikaru Ikedo^b, Kazuhiko Tanaka^c

^a Faculty of Engineering, Gunma University, 1-5-1, Tenjin-cho, Kiryu, Gunma 376-8515, Japan

^b Graduate School of Engineering, Chubu University, Kasugai, Aichi 487-8501, Japan

^c Graduate School for International Development and Cooperation, Hiroshima University, 1-5-1 Kagamiyama, Higashi-Hiroshima 739-8529, Japan

Received 27 September 2005; received in revised form 10 January 2006; accepted 30 January 2006

Available online 10 March 2006

Abstract

An ion-exclusion chromatographic method for the direct UV detection of non-absorbing inorganic cations such as sodium (Na^+), ammonium (NH_4^+) and hydrazine (N_2H_5^+) ions was developed by connecting an anion-exchange column in the I^- -form after the separation column. For example, NH_4^+ is converted to a UV-absorbing molecule, NH_4I , by the anion-exchange column in the I^- -form after the ion-exclusion separation on anion-exchange column in the OH^- -form with water eluent. As a result, the direct UV detection of Na^+ , NH_4^+ and N_2H_5^+ could be successfully obtained as well as the well-resolved separation. The calibration graphs of the analyte cations detected with UV at 230 nm were linear in the range of 0.001–5.0 mM. The detection limits at $S/N=3$ of the cations were below 0.1 μM . This method was applied to real water analysis, the determination of NH_4^+ in river and rain waters, or that of N_2H_5^+ in boiler water, with the satisfactory results. This could be applied also to low- or non-absorbing anions such as fluoride or hydrogencarbonate ions by the combination of a weakly acidic cation-exchange resin in the H^+ -form as the separation column and the anion-exchange conversion column.

© 2006 Elsevier B.V. All rights reserved.

Keywords: UV detection; Ammonium ion; Hydrazine ion; Ion-exclusion chromatography; Anion-exchange; Water analysis

1. Introduction

Ion-exclusion chromatography has been the one of convenient way to determine weakly basic cations such as ammonium ion (NH_4^+) or weakly acidic anions such as hydrogencarbonate ion (HCO_3^-) [1–5]. The separations are obtained using an anion-exchange resin column in the OH^- -form for the cations and a cation-exchange resin column in the H^+ -form for the anions only with water eluent, due to the penetration effect to the stationary phase. Conductivity has been commonly used as the detection method. However, the responses of partially ionized species such as NH_4^+ ($\text{p}K_b=4.75$) and HCO_3^- ($\text{p}K_a=6.34$) are low due to the low limiting equivalent ionic conductance [6].

The spectrophotometric detector (e.g., UV detector) can simply monitor ion species alternating to conductivity, since it

can selectively change by changing the wavelength monitored. Commonly, the analyte ions monitored by UV detector are UV-absorbing ions such as nitrate or iodide ions at the wide wavelength. For non-UV-absorbing ions, the indirect detection and/or postcolumn derivatization with subsequent UV measurement has been considered to be the common detection method [7]. In indirect UV-detection, the eluent having absorbance in the UV spectral region is used for the detection of non-absorbing analyte ions [8–10]. A decrease of the signal is resulted in when a sample peak is eluted. However, this method is generally used only in cases where the separation and detection conditions have been carefully worked out. In the postcolumn method, the ideal color-forming reagent is used in order to react with a large number of metal ions or inorganic anions. Basically, the color-forming reagents used after ion chromatographic separations are aromatic dyes such as arenazo III [11] or 4-(2-pyridylazo)-resorsinol (PAR) [12] for metal ions, and chelate reagents such as ferric perchlorate [11] or ethylenediaminetetraacetic acid (EDTA) [13] for anions. The eluent concentration

* Corresponding author. Tel.: +81 277 30 1271; fax: +81 277 30 1271.
E-mail address: m_mori@chem.gunma-u.ac.jp (M. Mori).

is high to get the stable reactions with analyte ions. Thus, the use of too high concentration of eluent must be taken care not to derive the overload of background absorption.

In this study, as novel UV detection method, an ion-exclusion chromatography with direct UV-detection of non-absorbing weak bases such as NH_4^+ and N_2H_5^+ was examined using anion-exchange resin in the UV-absorbing anion form connected after the separation column. A strongly acidic anion-exchange column in the I^- -form was used as a conversion column, in terms of well-reproducible anion-exchange reaction for the analytes better than the other forms, e.g., NO_3^- , Br^- , or CrO_4^{2-} -form. For example, NH_4^+ (i.e., NH_4OH) separated from other cations by a basic anion-exchange resin in the OH^- -form is converted to UV-absorbing NH_4I by the conversion column in the I^- -form. The eluent used in this system is only water without any special color-forming reagents.

We report for direct UV detections of NH_4^+ and N_2H_5^+ on the present ion-exclusion chromatography and its application to real water analysis. As an additional experiment, this system was tested also for several anions such as fluoride (F^-) or hydrogen-carbonate (HCO_3^-) ions using cation-exchange resin column in the H^+ -form as separation column.

2. Experimental

2.1. Apparatus

The ion chromatograph consisted of Tosoh LC-8020 Model-II chromatographic data processor, DP-8020 dual pump operated at flow rate of 1 ml/min, SD-8022 on-line degasser, CO-8020 column oven operated at 40 °C and UV-8020 UV-vis absorption detector. The injection volume was 100 μl .

2.2. Reagents

All reagents were of analytical reagent-grade, purchased from Wako (Osaka, Japan) and dissolved in distilled and deionized water for the preparation of standard solutions. Appropriate amounts of analytes at the concentration of 0.1 M each were diluted with water as necessary.

2.3. Columns

A separation column for inorganic cations used in this study was a polymethacrylate-based weakly basic anion-exchange resin in the OH^- -form, TSKgel DEAE-5PW (7.5 mm i.d. \times 150 mm; 10 μm -particle; 0.1 mequiv./ml-capacity). A separation column for inorganic anions was a polymethacrylate-based weakly acidic cation-exchange resin in the H^+ -form, TSKgel Super IC-A/C (7.8 mm i.d. \times 150 mm; 3 μm -particle; 0.2 mequiv./ml-capacity). A conversion column was a polystyrene-divinylbenzene-based strongly basic anion-exchange resin in the I^- -form, TSKgel SAX (4.6 mm i.d. \times 50 mm; 5 μm -particle; 1.0 mequiv./ml-capacity). The wavelength was 230 nm, which is around maximum absorbance coefficient of I^- . The columns were separately conditioned by passing through NaOH to a weakly basic anion-exchange resin

in the OH^- -form, and HI to a weakly acidic cation-exchange resin in the H^+ -form and a strongly basic anion-exchange resin in the I^- -form for 30 min. After the conditionings, all columns were equilibrated with water eluent for 30 min before chromatographic runs.

3. Results and discussion

3.1. Ion-exclusion chromatography with direct UV detection of non-absorbing cations

When a 100 μl sample containing NaCl, NH_4Cl , and $\text{N}_2\text{H}_5\text{Cl}$ (0.1 mM for each) was injected to a weakly basic anion-exchange resin in the OH^- -form with water eluent, they were converted to NaOH, NH_4OH and $\text{N}_2\text{H}_5\text{OH}$ passing through the column. Basically, their responses with UV detection were not observed due to their very low absorption coefficients, as shown in Fig. 1A. In order to obtain the direct UV detection of the cations, a strongly basic anion-exchange column in the I^- -form (conversion column) was inserted between the separation column and the UV detector. Fig. 1B shows the ion-exclusion chromatogram of the NaI, NH_4I and $\text{N}_2\text{H}_5\text{I}$ converted by the conversion column. The direct UV detections of the analytes were achieved as well as the well-resolved separation. In addition, this system was applicable also to the direct UV detection of alkaline metal earth metal cations such as Ca^{2+} and Mg^{2+} . However, the peaks were overlapped with those of alkali metal cations such as Na^+ and K^+ .

The peak areas of Na^+ , NH_4^+ and N_2H_5^+ were plotted on their various concentrations, and all of them were linear in the wide range of 0.001–5.0 mM. The correlation coefficients (r^2) were 0.9994 for Na^+ , 0.9996 for NH_4^+ and 0.9993 for N_2H_5^+ . As summarized in Table 1, the detection limits at S/N=3 by this system with UV were superior to those by the previous system with conductivity, which convert from low conductivity

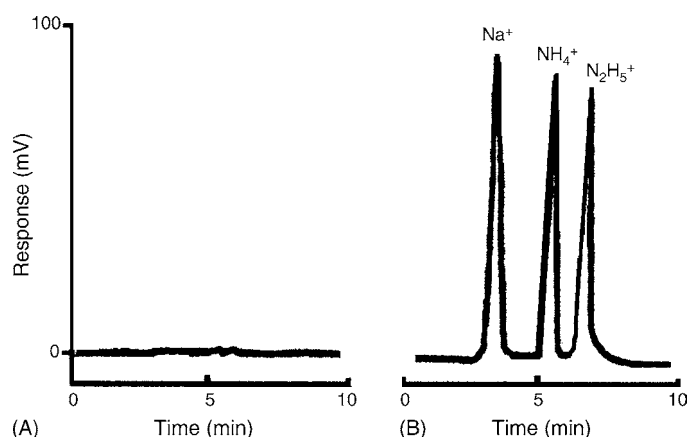


Fig. 1. Ion-exclusion chromatograms of some cations with and without the anion-exchange conversion column in the I^- -form. Separation column: a polymethacrylate-based weakly basic anion-exchange resin column in the OH^- -form; conversion column: a polystyrene-divinylbenzene strongly basic anion-exchange resin in the I^- -form; sequence of column: A = the separation column; B = A + the conversion column; injected sample: a mixture of NaCl, NH_4Cl and $\text{N}_2\text{H}_5\text{Cl}$ (0.1 mM for each); eluent: distilled and deionized water (1 min/ml); detector: UV at 230 nm; injection volume: 100 μl .

Table 1
Detection limits of analyte cations at signal to noise of 3 in this proposed system^a

Cations	Detection limits (μM)	
	UV at 230 nm	Conductivity ^b
Na^+	0.007	—
NH_4^+	0.012	0.031
N_2H_5^+	0.008	0.019

^a Sequence of columns was the same as in Fig. 1B, and other conditions as in Fig. 1.

^b Experimental conditions in ion-exchange enhancement system with conductivity were described in Ref. [14].

Table 2
Relative standard deviations of the retention times and peak areas of the analyte cations ($1 \mu\text{M}$ for each) on the 100th-repeated chromatographic runs in this proposed system^a

Cations	Retention time (%)	Peak area (%)
Na^+	0.20	0.53
NH_4^+	0.25	0.89
N_2H_5^+	0.41	1.06

^a Sequence of columns was the same as in Fig. 1B, and other conditions as in Fig. 1.

response of weak bases to high conductivity response of strong acids by a sequence of one separation column and two ion-exchange enhancement columns [14]. This would be because the background noise level with the UV at 230 nm was lower than that with the conductivity.

The durability of the sequence of columns on the 100-times repeated chromatographic runs was investigated on the proposed ion-exclusion chromatography. The results were very stable without the regenerations of the columns, and the relative standard deviations were pretty good as summarized in Table 2.

3.2. Application to several real water samples

As the application to real water analysis, NH_4^+ in rain and river water samples and N_2H_5^+ in boiler water sample were, respectively, determined by the present ion-exclusion chromatography. As shown in Fig. 2, NH_4^+ and N_2H_5^+ from other

Table 3
Determinations of NH_4^+ and N_2H_5^+ in several real water samples by the proposed system^a

Samples	Analyte	Concentration (μM)	Added (μM)	Recovery (%)
Rainwater 1	NH_4^+	471	100	92.3
Rainwater 2	NH_4^+	129	100	103
Lake water	NH_4^+	8.12	10.0	96.0
River water (upstream)	NH_4^+	50.3	10.0	93.0
River water (downstream)	NH_4^+	431	100	101.9
Seawater ^b	NH_4^+	32.5	50.0	98.0
Boiler water	NH_4^+	1.21	1.00	92.2
	N_2H_5^+	0.54	1.00	98.7

^a Sequence of columns was the same as in Fig. 1B, and other conditions as in Fig. 1.

^b Seawater sample was diluted to 20-fold by water. The other samples were injected without the dilution.

cations (e.g., Na^+ , K^+ , Ca^{2+} , and Mg^{2+}) coexisted in the real water samples could be selectively separated without any difficulties. Especially, sub- μM level of N_2H_5^+ added to control pH of boiler water could be successfully achieved by this method. Table 3 summarizes the analytical results of NH_4^+ and N_2H_5^+ in several real water samples including lake water, seawater and tap water. The recoveries in the addition of 1–100 μM NH_4^+ and N_2H_5^+ into the real water samples were ranged of 92.0–103%.

3.3. Ion-exclusion chromatography with direct UV detection of non-absorbing anions

As another application of this study, several non-absorbing inorganic anions, e.g., F^- or HCO_3^- , were tested using a weakly acidic cation-exchange resin column in the H^+ -form and the anion-exchange conversion column in the I^- -form. A 100 μl sample containing NaCl , NaNO_3 , NaNO_2 , NaF and NaHCO_3 (0.1 mM each) was injected to the column system. The anions eluted with water were converted to HCl , HNO_3 , HNO_2 , HF and H_2CO_3 on the weakly acidic cation-exchange column in the H^+ -form, and were separated depending on the penetrations to the stationary phase. At the present stage, HCl , HF and H_2CO_3 were

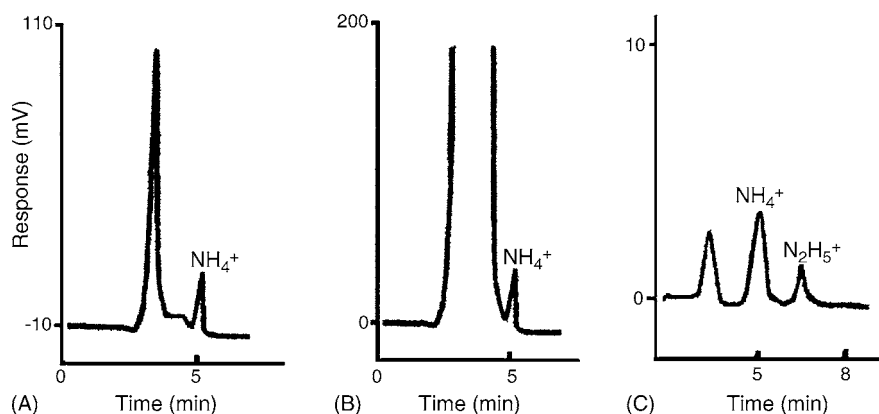


Fig. 2. Ion-exclusion chromatograms of NH_4^+ and N_2H_5^+ in (A) rainwater, (B) river water, and (C) boiler water. Sequence of column: the separation column + the conversion column, and other experimental conditions were the same as in Fig. 1.

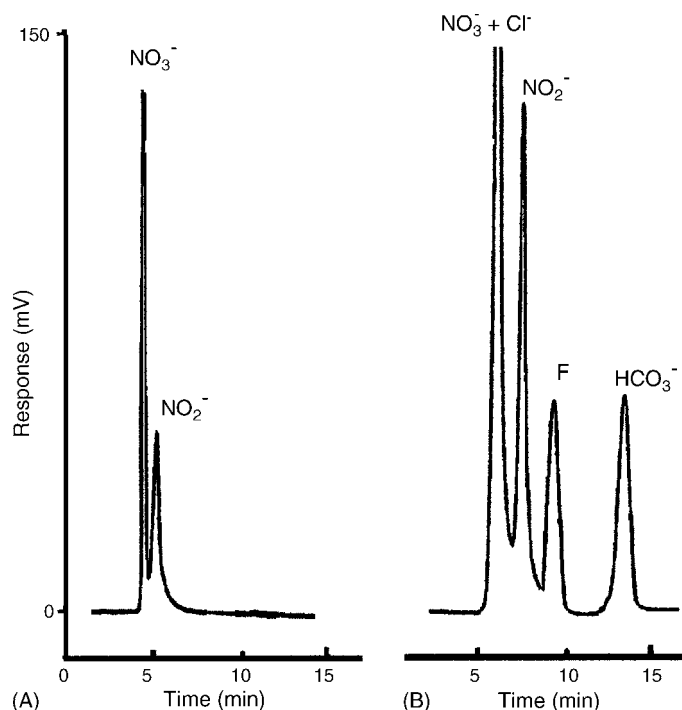


Fig. 3. Ion-exclusion chromatograms of some anions with and without the conversion column. Separation column: a polymethacrylate-based weakly acidic cation-exchange resin column in the H^+ -form; conversion column: a polystyrene-divinylbenzene strongly basic anion-exchange resin in the I^- -form; sequence of column: A = the separation column; B = A + the conversion column; sample: a mixture of NaCl , NaNO_3 , NaNO_2 , NaF and NaHCO_3 (0.1 mM for each); eluent: water (1 min/ml); detector: UV at 230 nm; injection volume: 100 μl .

not detected with UV at 230 nm, while HNO_3 and HNO_2 were directly detected as shown in Fig. 3A.

When the conversion column in the I^- -form was inserted between the separation column and UV detector, the direct detection of Cl^- , F^- and HCO_3^- were obtained converting into HI by the anion-exchange reaction with I^- , as shown in Fig. 3B. This method was possible to obtain the direct UV detection for strong acid anions such as SO_4^{2-} and PO_4^{3-} , though the peaks were interfered by that of Cl^- and NO_3^- due to their similar retentions to stationary phase. Also, the peak of UV-absorbing NO_2^- was increased by converting to HI by this column system

because of higher adsorption coefficient of I^- at 230 nm than that of NO_2^- .

The peak areas on the different concentrations of Cl^- , F^- and HCO_3^- injected to the ion-exclusion chromatographic system were linear in the range of 0.01–2 mM. The correlation coefficients (r^2) were 0.9996 for Cl^- , 0.9992 for F^- and 0.9991 for HCO_3^- . The detection limits ($\text{S/N} = 3$) were 0.41 μM for Cl^- , 0.65 μM for F^- and 0.52 μM for HCO_3^- . This ion-exclusion chromatographic system for anions will be applied to actual water samples after the further investigations.

4. Conclusions

The ion-exclusion chromatography with direct UV detection could be obtained, respectively, for the non-absorbing cations and anions by connecting the anion-exchange resin column in the I^- -form after the separation column. This may spread the possibility of ion chromatographic field, because this is simply obtained by two columns and water eluent, providing the calibration linearity in the wide range of sample concentrations.

References

- [1] P.R. Haddad, F. Hao, B.K. Glod, J. Chromatogr. 671 (1994) 3.
- [2] K. Tanaka, R. Kurokawa, R. Nakashima, J.S. Fritz, Bunseki Kagaku 37 (1988) 99 (in Japanese).
- [3] M. Mori, K. Tanaka, M.I.H. Helaleh, Q. Xu, M. Ikeda, Y. Ogura, S. Sato, W. Hu, K. Hasebe, P.R. Haddad, J. Chromatogr. A 997 (2003) 219.
- [4] K. Tanaka, T. Ishizuka, H. Sunahara, J. Chromatogr. 174 (1979) 153.
- [5] K. Tanaka, J.S. Fritz, Anal. Chem. 59 (1987) 708.
- [6] R.S. Robinson, R.H. Stokes (Eds.), Electrolyte Solutions Revised, 2nd ed. Revised, Butterworths, London, 1965.
- [7] J.S. Fritz, D.T. Gjerde (Eds.), Ion Chromatography, 3rd ed., Wiley-VCH, Weinheim, 2000, pp. 66–69.
- [8] M. Denkert, L. HacEzell, G. Schill, E. Sjogren, J. Chromatogr. 218 (1981) 31.
- [9] H. Small, T.E. Miller, Anal. Chem. 54 (1982) 462.
- [10] R.A. Cochrane, D.E. Hillman, J. Chromatogr. 241 (1982) 392.
- [11] T. Imanari, S. Tanabe, T. Toida, T. Kawanishi, J. Chromatogr. 250 (1982) 55.
- [12] J.S. Fritz, J.N. Story, Anal. Chem. 46 (1974) 825.
- [13] A.W. Fitchett, A. Woodruff, LC 1 (1983) 48.
- [14] M. Mori, K. Tanaka, Q. Xu, M. Ikeda, H. Taoda, W. Hu, J. Chromatogr. A 1039 (2004) 135.

Gas chromatographic analysis and aerosol mass spectrometer measurement of diesel exhaust particles composition

Kenichi Akiyama*

Japan Automobile Research Institute, Karima, Tsukuba-shi Ibaraki 305-0822, Japan

Received 31 October 2005; received in revised form 8 February 2006; accepted 13 February 2006

Available online 27 March 2006

Abstract

Aerosol particles have important effects on human health, climate, regional visibility, and the deposition of acidic and toxic substances. The aerosols also have significant pharmaceutical and industrial applications. Trials of gas chromatographic analysis of extracts composition of diesel exhaust particles and aerosol mass spectrometer measurement of diesel exhaust particles composition are introduced in this paper. Usually, organic fraction of automotive exhaust particles are concentrated to 1 mL by Kuderna-Danish concentrator after extracted into dichloromethane by soxhlet extraction. Then, these extracts are analyzed by GC/MS. In the extracts from the diesel exhaust particles, there are over several thousands of components, for example paraffinic hydrocarbons, aromatics, oxygenates and other hydrocarbons.

© 2006 Elsevier B.V. All rights reserved.

Keywords: Gas chromatography; Diesel exhaust; Aerosol; Ultra fine particles; Fuel; Lubricant oil; Speciation; Aerosol mass spectrometer; Semi-volatile

1. Introduction

Atmospheric aerosols and particulate matter (PM) from a wide variety of emission sources are receiving increasing attention because of their influence on human health [1], visibility, acid deposition, and global climate [2]. These measurements are conventionally performed by recording PM mass. The ambient standards are written in terms of mass concentrations, and emission regulations are based on mass. However, in order to understand better the nature of the mobile source contribution to ambient PM, many research groups are currently extending their investigations to include speciation of particles in automotive exhaust.

Progress in understanding and mitigating these problems is limited by the ability of existing instruments to provide real-time, size-resolved, quantitative measurements of aerosol mass and chemical composition [3]. A number of measurement techniques possessing some of the required aerosol analysis capabilities have emerged recently. Real-time aerosol mass spectrometers aiming to provide information on chemical composition of particle ensembles or individual particles. Most

of these instruments also provide information on particle size. A recent review of aerosol measurements by McMurry [3] states that “these mass spectrometers are, arguably, the most significant development in aerosol measurement in the past 20 years.

Trials of gas chromatographic analysis of extracts composition of diesel exhaust particles and aerosol mass spectrometer measurement of diesel exhaust particles composition are introduced in this paper.

2. Materials and methods

2.1. Gas chromatographic analysis

Organic fraction of automotive exhaust particles are concentrated to 1 mL by Kuderna-Danish concentrator after extracted into dichloromethane (special grade) by 24 h soxhlet extraction [4]. These extracts are analyzed by GC/MS.

GC separation was carried out using a Hewlett Packard 6890 GC System and mass detection was carried out using a Hewlett Packard 5973 MS System. Data were acquired and processed on a Hewlett Packard kayak computer using the ChemStation software. DB-5MS (30 m × 0.25 mm I.D. × 0.5 µm film thickness) was used for separation column. The oven temperature was held at 40 °C for 3 min and then programmed at 20 °C min⁻¹ to 100 °C, and at 8 °C min⁻¹ to 300 °C, and at 2 °C min⁻¹ to 320 °C

* Tel.: +81 298 56 1111; fax: +81 298 56 1134.

E-mail address: kaki@jari.or.jp.

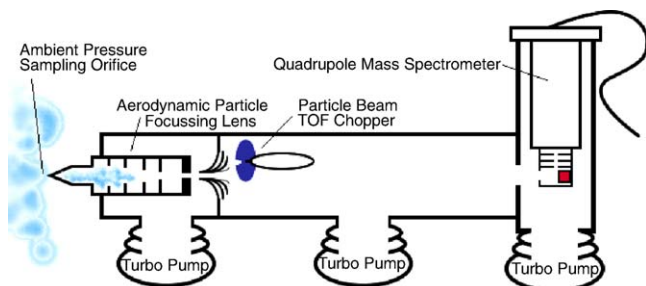


Fig. 1. Schematic of the aerodyne aerosol mass spectrometer (AMS).

and hold. Flow rate of helium was 1 mL min^{-1} , splitless injector was 320°C and interface of MS was 280°C .

2.2. Aerosol mass spectrometer

An aerosol mass spectrometer (AMS) developed at Aerodyne Research, which has been designed to provide real-time quantitative information on particle size-resolved mass loadings for volatile and semi-volatile chemical components present in/on ambient aerosol particles [5]. In its present configuration, the AMS cannot detect refractory aerosol components such as sea salt, soil dust, and elemental carbon. A schematic of the AMS is presented in Fig. 1.

The AMS consists of three main parts: an aerosol inlet [6,7], a particle sizing chamber, and a particle composition detection section. The different sections are separated by small apertures and differentially pumped. A computational fluid dynamics simulation of the AMS inlet system shows nearly 100% transmission efficiency to the detector for particles in the aerodynamic diameter range 70–500 nm, and shows substantial transmission for particles in the 20–70 and 500–2.5 μm ranges for spherical particles. Irregularly shaped particles may have lower transmission efficiencies [5]. Size-dependent particle velocities created by expansion into vacuum are used to determine particle size through a particle time-of-flight measurement. The focused particle beam is modulated by a rotating wheel chopper operating at about 100 Hz. Time-resolved particle detection after a known flight distance gives the particle velocity from which the particle aerodynamic diameter is obtained. Detection is performed by directing the particle beam onto a resistively heated, roughened surface under high vacuum. On this surface, the volatile and semi-volatile components in/on the particles flash vaporize. The vaporization source is integrally coupled to an electron impact ionizer at the entrance of a quadrupole mass spectrometer. When the quadrupole is tuned to a representative m/z , bursts of ions are produced that are averaged to produce a size-resolved mass distribution.

3. Result and discussion

3.1. Gas chromatographic analysis

Fig. 2 shows typical two types of total ion chromatogram (TIC)s of the extracts from diesel exhaust particulate matter. Fig. 3 shows typical TIC of boiled diesel fuel (diesel fuel

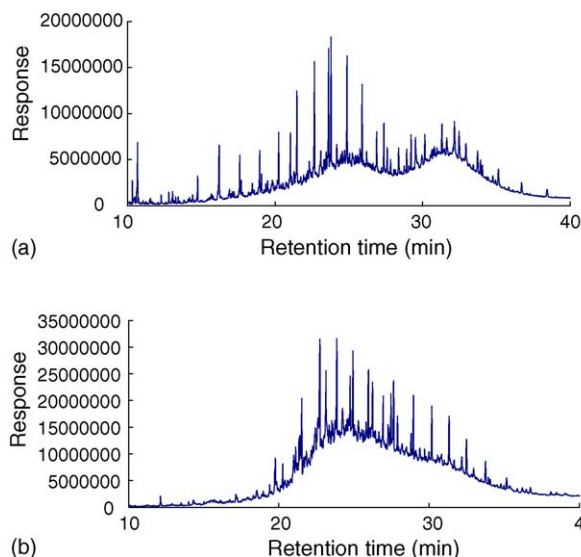


Fig. 2. Typical TIC examples of diesel exhaust particle extract: (a) one of the typical TIC of diesel exhaust particle extract (type 1); (b) one of the typical TIC of diesel exhaust particle extract (type 2).

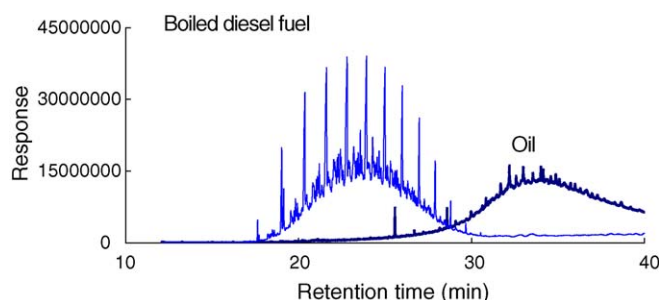


Fig. 3. Typical TIC of boiled diesel fuel and lubricant oil.

removed of low boiling point hydrocarbons) and lubricant oil. Composition of the extract shown in Fig. 2(a) is mixture of boiled fuel and lubricant oil, and composition resulted in Fig. 2(b) seems to mainly composed of boiled fuel and small amount of lubricant oil is exist in this extract. It is thought that this difference depends on type of engine and driving cycle. Extract resulted in Fig. 2(a) and (b) are named type 1 and type 2. There are many peaks on these chromatograms. Fig. 4 shows mass chromatogram of $m/z=99$ in the type 1 extracts that shows the presence of compounds including $\text{C}_7\text{H}_{15}^+$ hydrocarbons. This mass chromatogram of $m/z=99$ shows almost paraffin

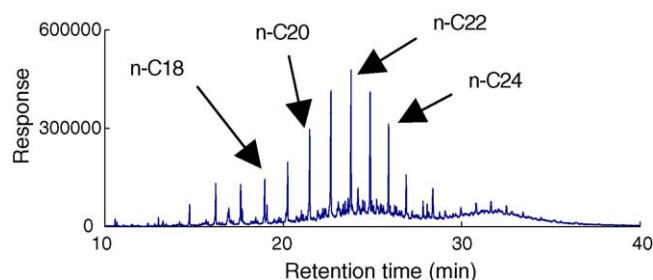


Fig. 4. Typical mass chromatogram ($m/z=99:\text{C}_7\text{H}_{15}^+$) of diesel exhaust particle extract.

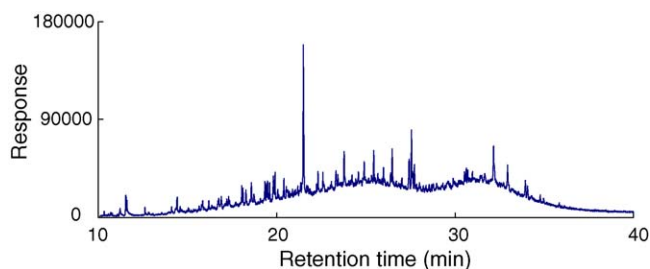


Fig. 5. Typical mass chromatogram ($m/z = 91$: $C_7H_7^+$) of type 1 diesel exhaust particles extract.

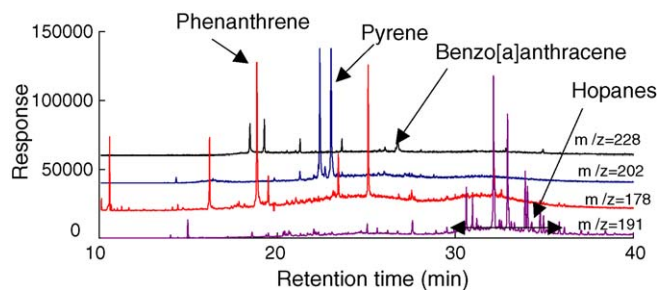


Fig. 6. Typical mass chromatogram ($m/z = 191$: Hopanes, $m/z = 178$, 202, 228: PAHs) of type 1 diesel exhaust particles extract.

hydrocarbons and a part of high boiling point area (right side of chromatogram) is not only paraffin hydrocarbons, include C_7 alkyl hydrocarbons chain and some oxygenate compounds. Sharp and large peaks on this chromatogram is normal paraffin hydrocarbons for example octadecane, eicosane, etc. and small peaks are seems to be naphthenes and branched chain hydrocarbons. Fig. 5 shows mass chromatogram of $m/z = 91$ in the type 1 extract that indicated compounds including $C_7H_7^+$ hydrocarbons, which are due to 1-ring aromatic hydrocarbons and some oxygenated aromatics include $C_7H_7^+$ hydrocarbons. Fig. 6 shows mass chromatograms of $m/z = 191$, 178, 202 and 228, these mass chromatograms indicate hopanes ($m/z = 191$) and molecular ion of poly nuclear aromatic hydrocarbons (PAHs, $m/z = 178$, 202, 228) of type 1 extract. Hopanes are well known for tracer components of lubricant oil. Mass chromatogram of $m/z = 178$ is typical molecular ion of phenanthrene and anthracene, mass chromatogram of $m/z = 202$ is typical molecular ion of fluoranthene and pyrene and mass chromatogram of $m/z = 228$ is typical molecular ion of Benzo[a]anthracene and chrysene.

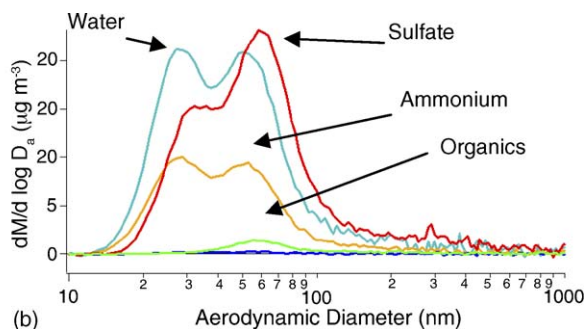
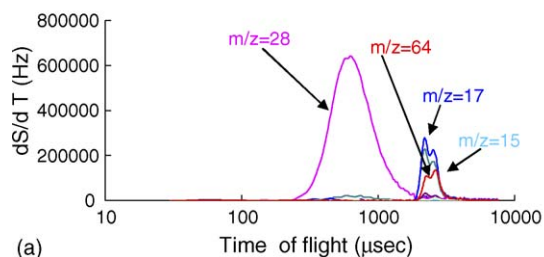


Fig. 7. Example of particle size conversion: (a) raw measurement result of particles by AMS; (b) calculated result of particle size dependent distribution.

Table 1
Speciation of test vehicle

Diesel passenger car		
Exhaust gas regulation	Year	1998
Overall width	mm	1800
Overall height	mm	1770
Overall length	mm	4655
Vehicle weight	kg	1850
Seating capacity	Number	5
Gross vehicle weight	kg	2125
Engine cylinder arrangement	Number	4
Engine total displacement	L	2982
Engine maximum torque	kW/rpm	N125/3400
Engine maximum power	N m/rpm	270/4400
Exhaust gas measurement		OCC, EGR
Millage	km	37403

These ions corresponding to molecule ions of PAHs are generated not only PAHs but also another heavy components.

These results show a part of extracted components in diesel exhaust particles. It is thought that diesel exhaust particles extract include several thousand of components.

3.2. Result of aerosol mass spectrometer measurement

3.2.1. Result of aerosol mass spectrometer measurement

Fig. 7 shows typical measurement result of AMS. Fig. 7(a) described raw analytical result of automotive exhaust particles by AMS (the horizontal axis: flight time of particles, the vertical axis: intensity of signal of each m/z ion). Particles of diesel exhaust are concentrated and most of gas phase are removed in the aerodynamic lens. Remaining gas phase of diesel exhaust arrive at detector of the AMS first. Fig. 7(b) shows an example of particle semi-volatile chemical components size distribution of diesel exhaust, after conversion from flight time of particles to particle size and signal of each ions to weight.

3.2.2. Particle size dependent distribution of semi-volatile chemical components in the diesel exhaust

Particle size dependent distribution of semi-volatile chemical components in the diesel exhaust was examined. In this test, the diesel vehicle of 3000 ml displacement (Table 1) and diesel fuel (S:28 ppm) were used. Measurement interval of the AMS was every 12 s. Fig. 8 shows typical particle size dependent

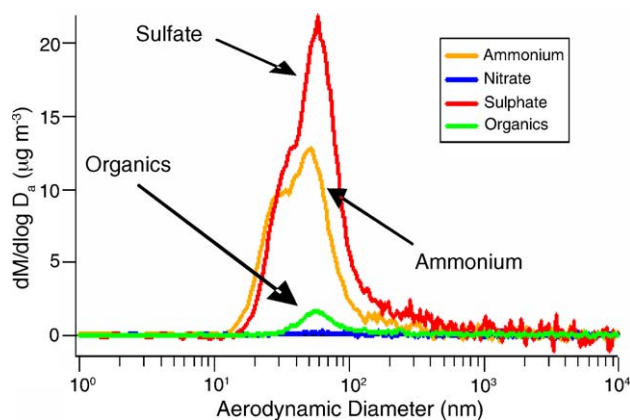


Fig. 8. Semi-volatile particle components in the diesel exhaust particles (high load driving condition).

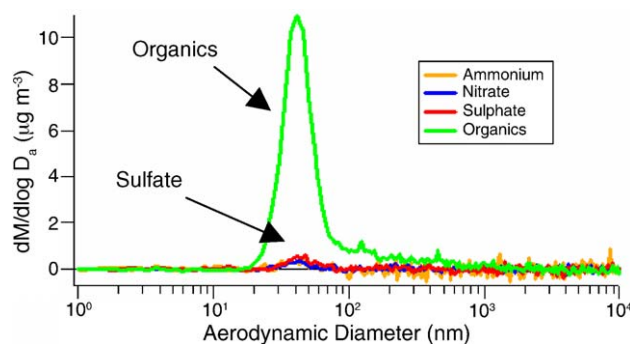


Fig. 9. Semi-volatile particle components in the particles (low load driving condition).

distribution of semi-volatile chemical components in the diesel exhaust at 2200 rpm and 6% gradient condition. In this result, sulfate and ammonium were distributed highest on 50 nm particle size, furthermore, there was another peaks of those species at about 30 nm particle size. In this result, main components of semi-volatile chemical components in the diesel exhaust at high load driving condition was sulfate. Feasibility of the present of sulfate in such amount is high, because concentration of sulfate is relatively high and there are a few interfering fragment ions for $m/z=48$ and 64 coming from other components, although reliability of ammonium quantity is low, because there

are some interference to $m/z=17$ which is used for quantify ammonium, but $m/z=17$ is not only coming from ammonium, but also another components such as water which gives $m/z=17$ fragment ion. Fig. 9 shows typical particle size distribution of semi-volatile chemical components in the diesel exhaust at idling condition. In this result, organics are main components, and distributed highest particle size is at 30–40 nm. This pattern is perfectly different from particle composition of high load driving condition.

4. Conclusions

When using gas chromatographic analysis, extracts from diesel exhaust particulate matter consist mainly of diesel fuel and lubricant oil. These ratio depended on type of engine and driving cycle. It is thought that diesel exhaust particles contain several thousand of components.

The AMS has been applied to obtain the information on the size and chemical composition of semi-volatile species in automobile exhaust particles. Mass spectrum, mass concentration, and size and chemically resolved mass distribution data were obtained. The major components observed on the diesel exhaust particles were sulfate and organics when high load condition and idling, respectively.

Acknowledgments

The authors are grateful to Dr. Akio Shimono of Sanyu plant service co. and Dr. Douglas Worsnop of the Aerodyne research for the ongoing collaboration that has greatly helped the development and testing of the AMS.

References

- [1] D.W. Dockery, et al., N. Engl. J. Med. 329–324 (1993) 1753–1759.
- [2] J.H. Seinfeld, et al., Atmospheric Chemistry and Physics: from Air Pollution to Climate Change, John Wiley, New York, 1998.
- [3] P.H. McMurry, Atmos. Environ. 34 (12–14) (2000) 1959–1999.
- [4] K. Akiyama, Jpn. Soc. Atmos. Environ. 35–36 (2000) A73–A84.
- [5] J.T. Jayne, et al., Aerosol Sci. Technol. 33 (1–2) (2000) 49–70.
- [6] B.Y.H. Liu, et al., Aerosol Sci. Technol. 22 (1995) 293–313; B.Y.H. Liu, et al., Aerosol Sci. Technol. 22 (1995) 314–324.
- [7] X. Zhang, et al., Aerosol Sci. Technol. 36 (2002) 617–631.

An application of EGA–MS with skimmer interface to pyrolysis behavior of DHTAM, an antibacterial and antifungal material with thermostability

Takahisa Tsugoshi^{a,*}, Sachiko Nakagi^a, Fumihiko Ohashi^b, Koji Watari^a

^a Advanced Sintering Technology Group, Advanced Manufacturing Research Institute,
National Institute of Advanced Industrial Science and Technology (AIST), Japan

^b Mesoporous Ceramics Research Group, Materials Research Institute for Sustainable Development,
National Institute of Advanced Industrial Science and Technology (AIST), Japan

Received 11 November 2005; received in revised form 17 January 2006; accepted 24 January 2006

Abstract

An application of evolved gas analysis–mass spectrometry (EGA–MS) with skimmer interface was carried out to investigate the pyrolysis mechanism of an antibacterial and antifungal material that is expected with thermostability. The skimmer interface between a furnace and a vacuum chamber with a mass spectrometer transmitted the gaseous species, which were trapped by a general capillary interface. As a result, it became clear that the thermostability of antimicrobial activity was limited by the heat resistance of the coordinate bond between nitrogen and silver in the silver chelate.

© 2006 Elsevier B.V. All rights reserved.

Keywords: Evolved gas analysis; Mass spectrometry; Skimmer interface; Pyrolysis; Thermostability; Antibacterial; Antifungal

1. Introduction

It is well-known antibacterial and antifungal activities of material have been required, depending on the demand of a comfortable and hygienic life style. Therefore montmorillonite (Mont), intercalated by silver cations, has received attention because of its strong antibacterial activity. However when the aqueous sol is allowed to stand under sunshine, the silver cations between the Mont layers are easily reduced to metallic silver particles, leading to a lowering of antibacterial activity and a change in color from pale blue to black [1]. This reduction has been successfully suppressed by the use of silver chelate instead of silver cation [2,3]. This technique was further extended to prepare an agent with both strong antibacterial and antifungal activities. For example, Mont intercalated by: (i) silver chelate

of 2-(4-thiazolyl)-benzimidazole which has strong antifungal activity, and (ii) the quaternary ammonium cation which has strong antibacterial activity, has been prepared [4]. There is potential for this intercalation technique, using Mont as a host material, to reveal an antimicrobial agent with high thermostability. Ohashi and Oya have investigated the thermostability of Mont intercalated using silver chelate and quaternary ammonium [5]. However analysis of the evolved gaseous species has not been carried out because the gaseous species were adsorptive.

In this study, the evolved gas analysis has been focused as an application of the EGA–MS instrument with skimmer interface [6], since the interface has a property with less adsorption of the gaseous species, which are the analyzed target.

2. Experimental

2.1. Sample preparation [5,7]

The purified montmorillonite (Mont; trade name: Kunipia-F, Kunimine Industries Co. Ltd.) was used as a host mate-

* Corresponding author. Present address: Reference Material System Division, National Metrology Institute of Japan, National Institute of Advanced Industrial Science and Technology (AIST), 1-1-1 Umezono, Tsukuba 305-8563, Japan. Tel.: +81 29 861 4023; fax: +81 29 861 4125.

E-mail address: tsugoshi.takahisa@aist.go.jp (T. Tsugoshi).

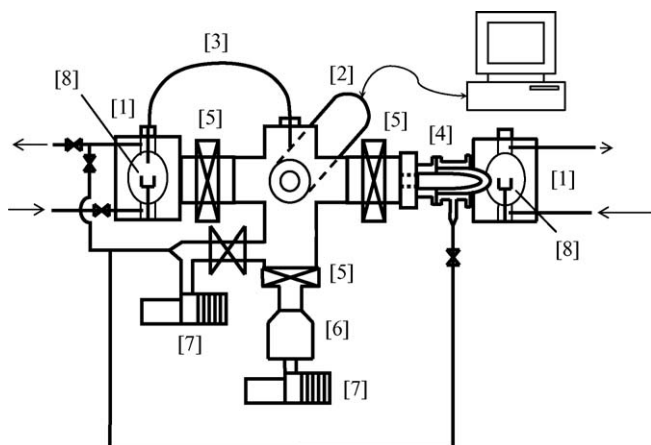


Fig. 1. Schematic diagram of the instrumental model EGA-MS instrument. (1) Furnace, (2) Q-MS, (3) capillary interface, (4) skimmer interface, (5) gate valve, (6) turbo molecular pump, (7) rotary pump, and (8) sample.

rial, of which the cation-exchange capacity (CEC) was 115 mequiv./100 g. The theoretical chemical formula was $\text{Na}^{0.66+}((\text{Al}_{3.34}\text{Mg}_{0.66})\text{Si}_8\text{O}_{20}(\text{OH})_4)^{0.66-}$. An aqueous dispersion of Mont sol (content 3 wt.%) was prepared. To intercalate the antibacterial reagents interlayer space, each of *n*-dodecyltrimethyl ammonium chloride (Dode; $\text{C}_{12}\text{H}_{25}\text{N}(\text{CH}_3)_3\text{Cl}$, m.p. 246 °C, Tokyo Chemical Industry Co. Ltd.) and hexadecylpyridinium chloride (Hexa; $\text{C}_{16}\text{H}_{33}\text{N}(\text{CH}_3)_2\text{Cl} \cdot \text{H}_2\text{O}$, m.p. 77–83 °C) dissolved in deionized water as 40% and 30% of CEC, respectively, was added to the aqueous dispersion, which led to the Dode/Hexa/Mont compound.

The mixing of silver nitrate (AgNO_3 , 99.8%, Wako Pure Chemical Industry Co. Ltd.) solution of CEC 30% and 2-(4-thiazolyl)-benzimidazole (TBZ; $\text{C}_{10}\text{H}_7\text{N}_3\text{S}$, m.p. 296–303 °C, decomposition temperature 700 °C, Tokyo Chemical Industry Co. Ltd.) methanol solution of CEC 60% offered to synthesize a silver-TBZ chelate which was $\text{Ag}(\text{TBZ})_2$, and added to the rinsed-out Dode/Hexa/Mont compound under stirring. After the product was rinsed out with deionized water, it was freeze-dried. The final product, namely the powdered clay-organic complex,

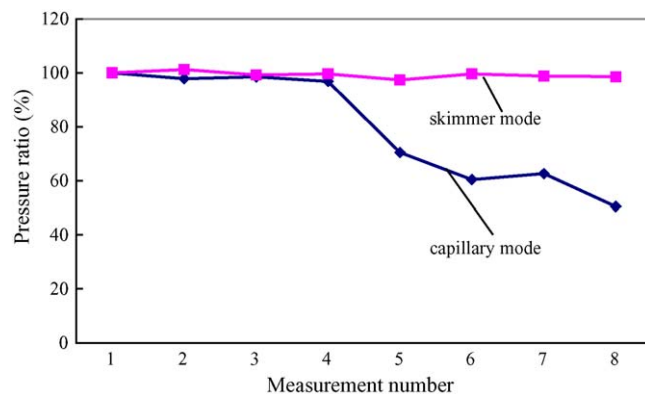


Fig. 3. Ratio of pressure in vacuum chamber against measurement number.

was determined as Dode/Hexa/(TBZ)₂Ag/Mont (DHTAM) with X-ray diffraction [5,7].

2.2. Apparatus and measurement conditions

The EGA-MS instrument has been constructed with two gold image furnaces (MR-39H, ULVAC-Riko) and a quadrupole mass spectrometer (M-400QA-M, ANELVA) as shown in Fig. 1. In capillary-interface mode, the two devices are connected with a fused-silica capillary coated with polyimide. Its length and inner-diameter are 700 and 0.10 mm, respectively. The pathway of gaseous species has been heated at 200 °C. The carrier gas is high-purity helium, plumbed with a liquid nitrogen pool to trap traces of water and other impurities. In the other skimmer-interface mode, two conic quartz tubes with orifices connected the two devices at atmospheric pressure or under a vacuum. Since the carrier gas used is also high-purity helium, the evolved gaseous species with higher masses are enriched after the second orifice, consequently as a principle of a jet separator, due to differences in the diffusion velocity. The quartz tube is with no special heating, except due to infrared from the furnace lamp and radiant heat from the sample respectively. In fact, the image furnaces of the capillary and skimmer modes have differed subtly. While a single lamp type has been used in capillary mode, a

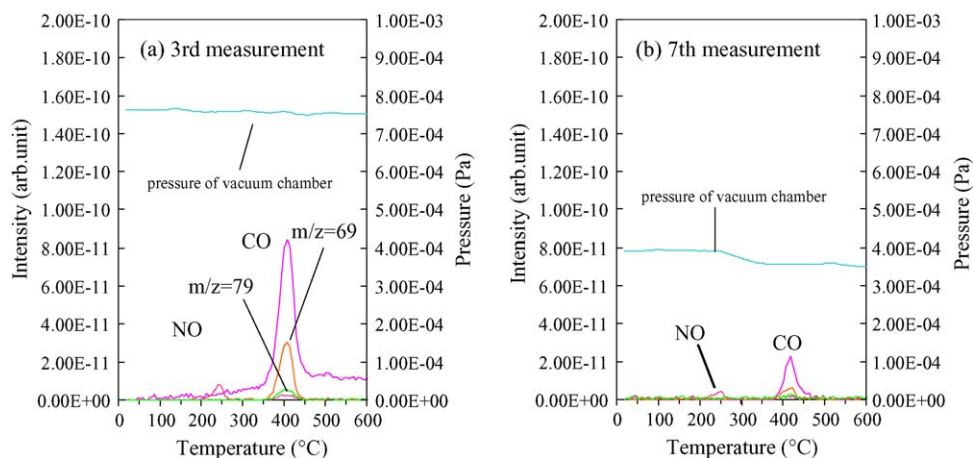


Fig. 2. Comparison of peak intensity and vacuum pressure of 3rd (a) and 7th (b) measurements as repeatability of measurement.

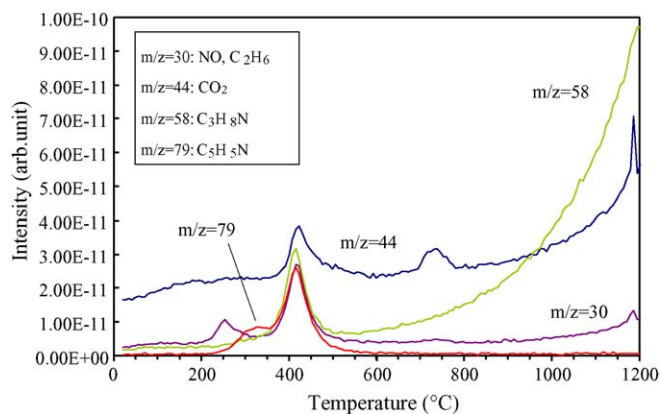
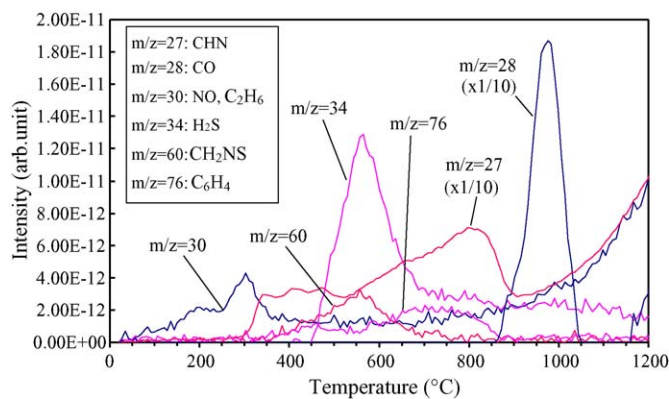


Fig. 4. EGA-MS curves obtained from DHTAM.

Fig. 5. EGA-MS curves obtained from (TBZ)₂Ag/Mont.

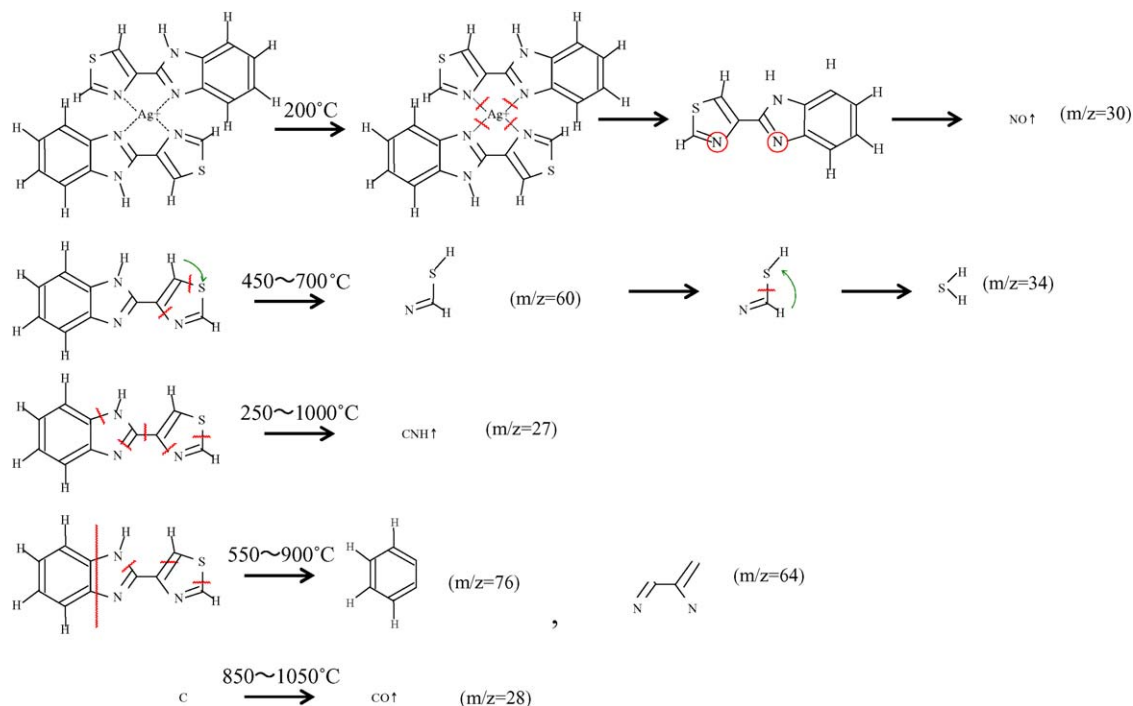
double-lamp type has been used in skimmer mode, because we were afraid the skimmer would create shadow and thus lower its maximum temperature.

3. Results and discussion

3.1. Comparison of the interfaces

As a simulation of the general apparatus, the measurements of the capillary-interface mode were carried out for DHTAM. During checking of the repeatability, the sensitivity decreased. Fig. 2 shows a comparison of the sensitivity and the vacuum chamber pressure with the mass spectrometer. For example, at the 3rd measurement (Fig. 2(a)), the evolution of CO, NO and the other hydrocarbons (e.g., $m/z = 69$ and 79) were detected reflecting pyrolysis. Of course similar data were obtained from the 1st

and 2nd measurements. After a series of several measurements, e.g., at the 7th measurement, the peak intensities and pressure in vacuum chamber decreased (Fig. 2(b)). The peak intensity of CO decreased to about 25% at the 3rd measurement. Fig. 3 shows the pressure ratio dependence against the measurement number when it took 100% for the vacuum pressure of the 1st measurement. The capillary interface stopped transmitting the gaseous species following repeated measurement, meaning the adsorbed species on the capillary inner wall blocked the transmission of the gaseous species via this capillary from a furnace to a vacuum chamber with a mass spectrometer. On the other hand, the result as shown in Fig. 3 proved that the skimmer interface had no such block problem for gaseous transmission. In other words, this problem should be the reason why the general commercial instrument as TG-MS encountered a failure for this measurement. Therefore all subsequent measurements were carried out in skimmer interface mode.



Scheme 1. Pyrolysis reaction of Ag-TBZ chelate intercalated between Mont layers.

3.2. Pyrolysis behavior

Fig. 4 shows the EGA–MS curves obtained from DHTAM. At first a small peak of $m/z=30$ was detected at about 250 °C. The evolved gas was due to nitrogen monoxide (NO) because the other possibility of C_2H_6 was denied by the non-detection of the main fragment ion of $m/z=28$. The main peak on each EGA curve was obtained at about 400 °C. This peak should be due to the pyrolysis of organic compounds, since the peaks of $m/z=30$, 44, 58 and 79 can be tentatively assigned as C_2H_6 , CO_2 , C_3H_8N and C_5H_5N , respectively. The other fragment ions also indicated the EGA peak, due to the pyrolysis of organic substances such as quaternary ammonium salts including an alkyl chain. The remaining carbon in the interlayer space caused the CO_2 ($m/z=44$) evolution at about 730 °C.

As a reference to interpret the pyrolysis behavior, a complex of $(TBZ)_2Ag/Mont$ was also analyzed (Fig. 5). The NO ($m/z=30$) evolution was obtained from about 200 °C; even though the temperature of the peak-top is about 300 °C. It coincided with a report indicating that silver particles (20–40 nm) were observed with TEM after 200 °C heating [7]. It means the structure of silver-TBZ chelate had decomposed since the coordinate bond between N and Ag was broken. Subsequently, thermal decomposition in the form of the evolution of CHN ($m/z=27$) was observed. At 560 °C, gaseous species with sulfur such as H_2S ($m/z=34$) and CH_2NS ($m/z=60$) were found to evolve. The C_6H_4 gas ($m/z=76$), according to the benzene

structure, was detected broadly between about 400 and 850 °C. The evolution of CO ($m/z=28$) at 980 °C was due to the remaining carbon between the Mont layers. The pyrolysis mechanism is described in Scheme 1.

4. Conclusion

This study demonstrated an application of the EGA–MS technique with a skimmer interface. This instrument with the skimmer interface can successfully perform the evolved gas analysis, even though the capillary interface, generally speaking, cannot do so because of its adsorption of the evolved gaseous species. Therefore the pyrolysis mechanism became well understood for the montmorillonite intercalated with silver chelate and quaternary ammonium cation such as the antibacterial and antifungal material that is expected with high thermostability, i.e., the strength of the coordinate bond limited the heat resistance of the antimicrobial activity.

References

- [1] A. Oya, T. Banse, F. Ohashi, S. Otani, Appl. Clay Sci. 6 (1992) 135.
- [2] F. Ohashi, A. Oya, Appl. Clay Sci. 6 (1992) 301.
- [3] F. Ohashi, A. Oya, J. Mater. Sci. 27 (1992) 5027.
- [4] F. Ohashi, A. Oya, Antibact. Antifung. Agents 21 (1993) 591.
- [5] F. Ohashi, A. Oya, J. Mater. Sci. 31 (1996) 3407.
- [6] T. Tsugoshi, M. Furukawa, M. Ohashi, Y. Iida, J. Therm. Anal. Calorim. 64 (2001) 1127.
- [7] F. Ohashi, A. Oya, Nendo-Kagaku 37 (1997) 58.

Evolved gas analysis with skimmer interface and ion attachment mass spectrometry for burnout monitoring of organic additives in ceramic processing

Takahisa Tsugoshi*, Nanaka Ito, Takaaki Nagaoka, Koji Watari

*Advanced Sintering Technology Group, Advanced Manufacturing Research Institute,
National Institute of Advanced Industrial Science and Technology (AIST), Japan*

Received 11 November 2005; received in revised form 17 January 2006; accepted 24 January 2006

Abstract

A monitoring of the individual pyrolysis of mixed polymer as a binder for ceramic processing was carried out as an application of evolved gas analysis-mass spectrometry (EGA-MS) with a skimmer interface and ion attachment mass spectrometry (IAMS). It could detect characteristic species evolved by the pyrolysis of the organic additives, according to the instrumental advantages as the transmission of the gaseous species with no transformation by the skimmer interface and complete soft ionization for gaseous species by IAMS technique. Further, the pyrolysis behavior of blended polymers as a binder could be monitored individually as EGA curves of characteristic species evolved by the pyrolyses.

© 2006 Elsevier B.V. All rights reserved.

Keywords: Evolved gas analysis, EGA; Mass spectrometry; Skimmer interface; Pyrolysis; Ion attachment mass spectrometry, IAMS; Binder; Monitoring

1. Introduction

Sintering aids for ceramics are usually organic materials, such as polyvinyl alcohol (PVA), latex, methylcellulose (MC), and starch, which are used as binders, because ceramic starting powders do not themselves harden when mixed with water [1–5]. The role of a binder is to provide green strength so that a green body can be formed and will retain its desired shape before heating. For better property of the green body, a blended binder between two or more species has been used [6,7]. In all instances, these organic additives are pyrolyzed during the firing and sintering processes. Their pyrolysis behavior is important in improving the conditions for the process and the properties of the final product. It is also important from the viewpoint of environmental protection because some organic materials emit harmful species during pyrolysis. The analysis of the gaseous species that are evolved during pyrolysis in order to elucidate the pyrolysis behavior usually requires evolved gas analysis-mass spectrometry (EGA-MS), better known as thermogravimetry-

mass spectrometry (TG-MS). However, the usual method for EGA-MS has problems in relation to in situ monitoring of the pyrolysis process, because fragmentation resulting from ionization complicates the mass spectrum; e.g., different organic species can produce identical fragment ions.

In this study, IAMS was applied to EGA-MS for in situ monitoring of the pyrolysis behavior of a blended ceramic additive with PVA and MC. The peaks in the IAMS spectrum were expected to be due solely to fragments produced by pyrolysis and not by ionization. A technique of this kind is required because although gas chromatography (GC) is an excellent technique for analyzing gaseous species, it cannot readily be applied to in situ monitoring inside a heated furnace or to on-site monitoring to control the process.

2. Experimental

2.1. Analytical instrumentation

All IAMS measurements were carried out with a prototype apparatus (Fig. 1) consisting of a gold image furnace based on TPD type R (Rigaku Corporation) and an IAMS instrument (L-241G-IA; Canon ANELVA Technix Corporation), as previously

* Corresponding author. Present address: 1-1-1 Umezono, Tsukuba 305-8563, Japan. Tel.: +81 29 861 4023; fax: +81 29 861 4125.

E-mail address: tsugoshi.takahisa@aist.go.jp (T. Tsugoshi).

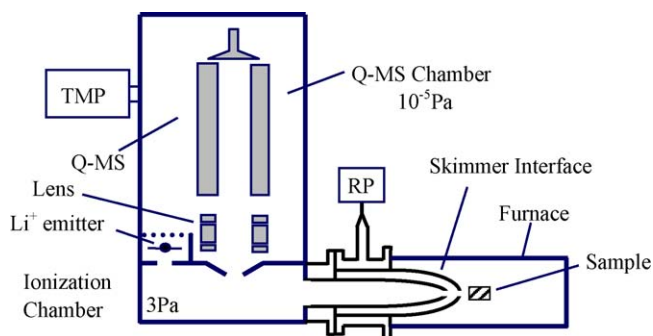


Fig. 1. Schematic diagram of the prototype instrument TIAS-254 with skimmer interface and IAMS.

reported [8]. The skimmer interface connected the furnace as atmospheric pressure, and the ionization chamber under vacuum. During the measurement, the carrier gas helium flowed into the furnace at a heating rate of $20\text{ }^{\circ}\text{C min}^{-1}$.

2.2. Sample preparation

The specimens were raw materials for alumina ceramics. PVA (PVA500, Completely Hydrolyzed, Mw 400–600; WAKO), MC (Methyl Cellulose 15CP; WAKO), and their blended mixtures were used as a binder for alumina powder (TMDAR [$\alpha\text{-Al}_2\text{O}_3$]; Taimei Chemicals) to provide green bodies. The preparation of the analytical samples was performed as follows: for an MC binder sample, alumina powder (4 g) and a stirred mixture of MC (7.2 g) and H_2O (100 ml) were mixed and dried; for a PVA binder sample, alumina powder (4 g) and a stirred mixture of PVA (4 g) and H_2O (20 ml) were mixed and dried; for blend-binder samples, 0.2 and 0.6 g of each polymer were portioned and mixed with alumina powder (4 g) and H_2O (2 ml) to give the (MC:PVA = 25:75, 75:25) analytes. Further MC:PVA = 50:50 analyte was obtained from portion of 0.4 g of each polymer.

3. Results and discussion

In the spectrum of IAMS, all peaks are with 7 amu higher than the molecular weight because Li^+ ion with 7 amu is attached as a result of the ionization principle. For example, a mass peak with 25 amu means H_2O having a molecular weight of 18 amu.

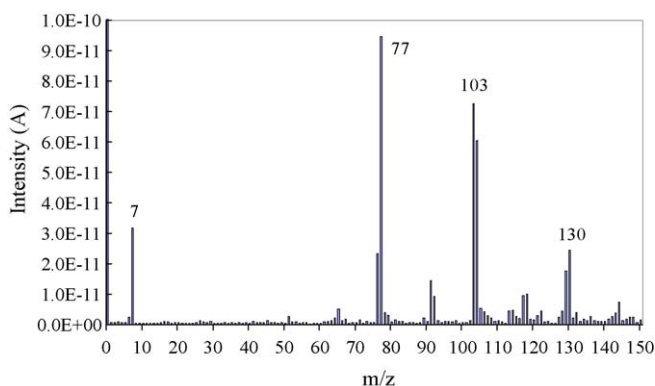


Fig. 2. IAMS spectrum of evolved species from a PVA sample at pyrolysis.

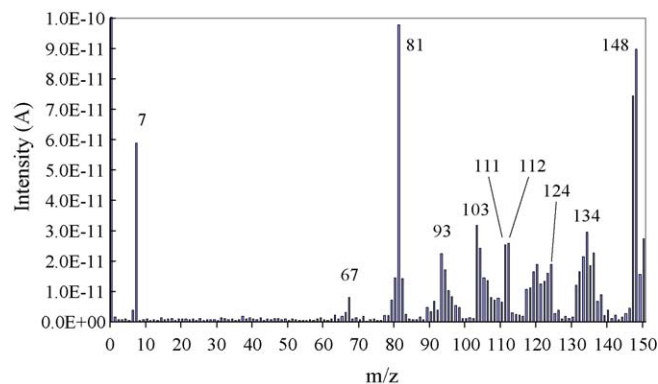


Fig. 3. IAMS spectrum of evolved species from an MC sample at pyrolysis.

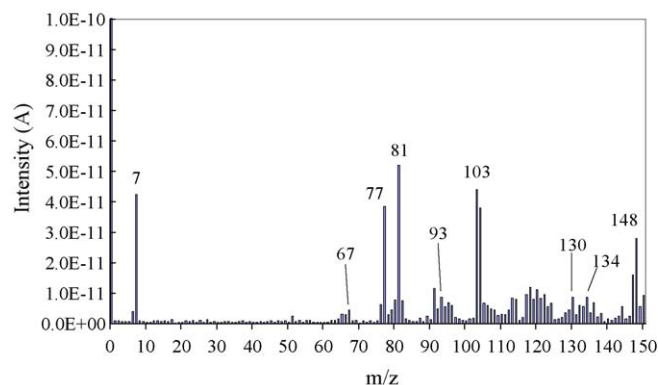


Fig. 4. IAMS spectrum of evolved species from a PVA:MC = 50:50 sample at pyrolysis.

From the sample containing PVA as the binder, crotonaldehyde ($M_w = 70$; $m/z = 77$), which is detected also with GC-MS, was obtained in the mass spectrum at about $270\text{ }^{\circ}\text{C}$ during the pyrolysis of the PVA, as shown in Fig. 2. Other characteristic species

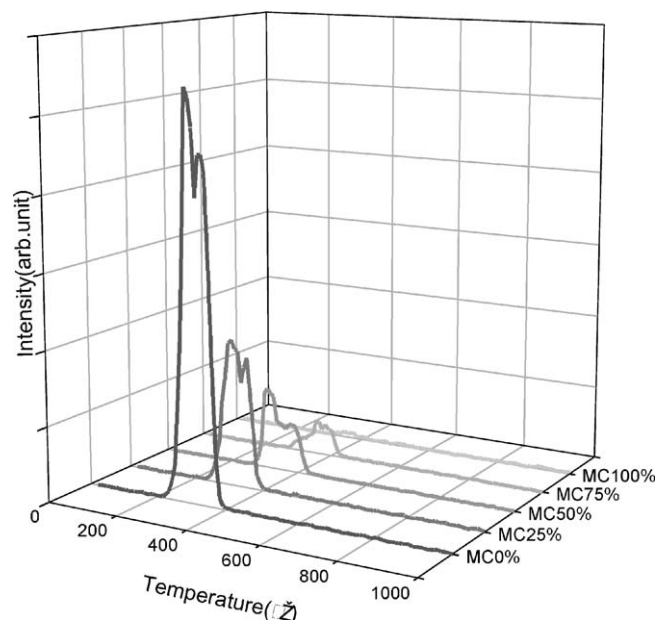


Fig. 5. EGA curves of $m/z = 77$ as a PVA indicator.

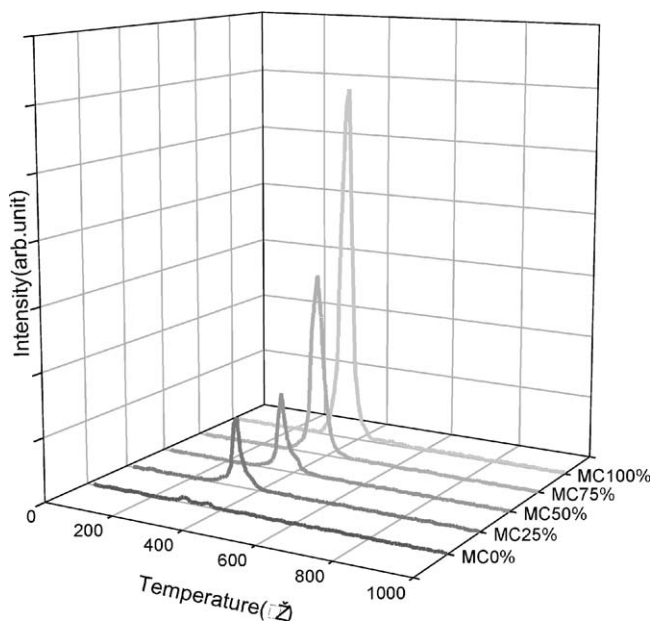


Fig. 6. EGA curves of $m/z = 81$ as an MC indicator.

with 103 and 130 m/z were detected, though their identifications are not yet clear. The peak of 7 m/z was due to the Li^+ ion being the ionization source. Fig. 3 shows a mass spectrum obtained from the sample containing MC as the binder. Also, the characteristic species from MC with 67, 81, 93, 103, 111, 112, 120, 124, 134, and 148 m/z were detected during its pyrolysis. On the other hand, the spectrum obtained from a mixed sample of PVA (50%) and MC (50%) shown in Fig. 4 was almost estimated to coincide on the spectrum synthesized from PVA and MC spectra. It may mean that less interaction exists during their pyrolyses.

To monitor the pyrolysis behavior, we focused on the EGA curves at about $m/z = 77$ and 81 as indicators of PVA and MC,

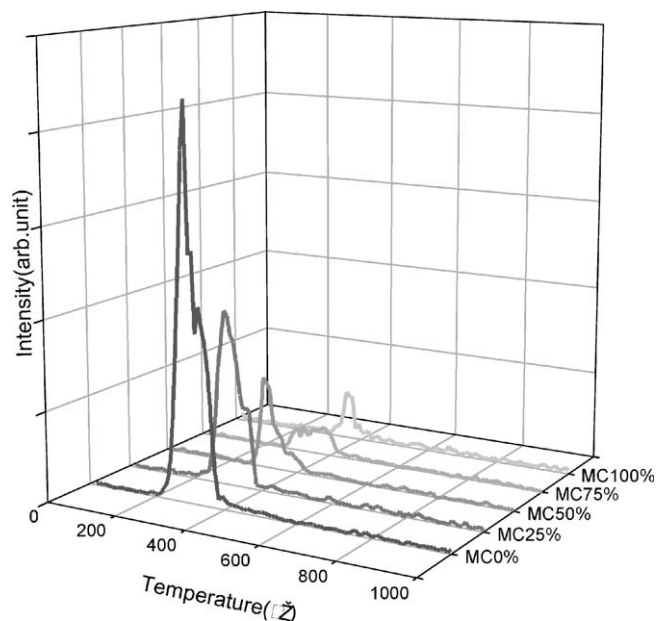


Fig. 8. EGA curves of $m/z = 130$ as a major peak in the spectrum from PVA.

respectively, whose mass peaks are independent of each other. Fig. 5 shows the EGA curves when $m/z = 77$, reflecting the pyrolysis behavior of PVA. The intensity is normalized by binder weight in the samples. As pyrolysis behavior, the EGA curves indicated a two-step thermal decomposition. The peak intensity reflected the PVA ratio of in the each binder. On the other hand, the EGA curves of $m/z = 81$, which is expected to indicate MC pyrolysis, reflected the MC ratio, as shown in Fig. 6, even though neither indicator offered a linearity between the mixed ratio and the intensity.

Figs. 7 and 8 show the EGA curve comparisons versus the mixture ratio by the other characteristic peaks in the mass spectra. Even though both the 103 m/z and the 130 m/z seemed

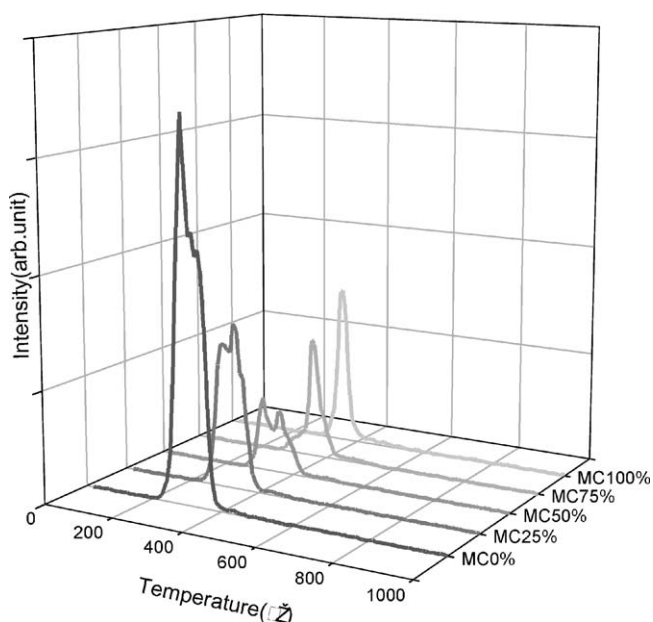


Fig. 7. EGA curves of $m/z = 103$ as a major peak in the spectrum from PVA.

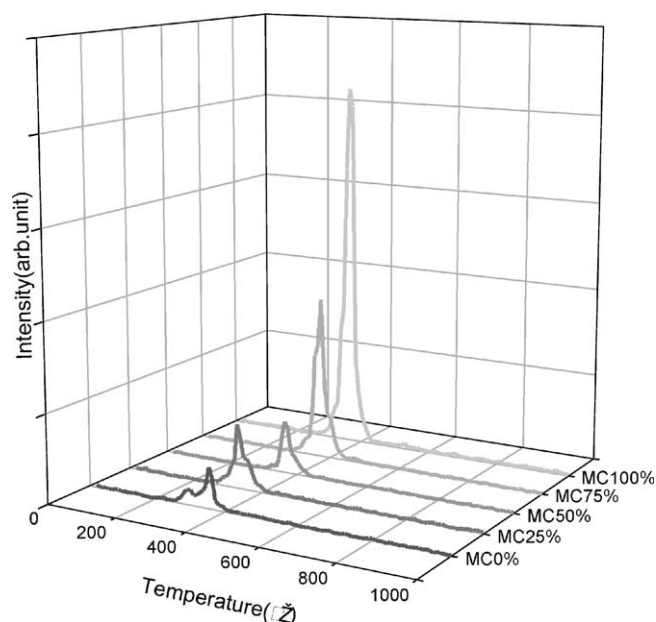


Fig. 9. EGA curves of $m/z = 148$ as a major peak in the spectrum from MC.

distinctive to PVA, the sample without PVA (MC 100%) offers the EGA peak during the binder pyrolysis. It means that these evolved species cannot be an indicator to monitor PVA pyrolysis. Also, in regard to MC the 148 m/z peak seemed characteristic as the evolved species during the MC pyrolysis; however, it too cannot be an indicator to monitor MC pyrolysis. Fig. 9 shows the EGA peaks detected from the sample only with PVA (MC 0%).

4. Conclusion

The new EGA-MS that has a skimmer interface and IAMS possibly offers unique data on hot gaseous species that have evolved from pyrolyzed organic substances. Furthermore, it is useful to the individual monitoring of the pyrolysis behavior of an organic mixture as a blended binder used for ceramic processing. However, a correlation between the peak intensity and the ratio of mixtures should be established for fine monitoring, including quantitative information.

Acknowledgement

This study was supported by a “matching fund” of AIST with NGK INSULATORS, LTD. The fund is on a 50–50 collaboration basis and is entitled “Research and Development of Low Environmental Load Processes”.

References

- [1] J.J. Benbow, E.W. Oxley, J. Bridgwater Chem. Eng. Sci. 42 (1987) 2151.
- [2] A. Kristoffersson, E. Carlström, J. Eur. Ceram. Soc. 17 (1997) 289.
- [3] A. Kristoffersson, E. Roncari, C. Galassi, J. Eur. Ceram. Soc. 18 (1998) 2123.
- [4] C.B. Sawyer, J.S. Reed, J. Am. Ceram. Soc. 84 (2001) 1241.
- [5] O. Lyckfeldt, J.M.F. Ferreira, J. Eur. Ceram. Soc. 18 (1998) 131.
- [6] K.J. Voorhees, S.F. Baugh, D.N. Stevenson, Thermochim. Acta 274 (1996) 187.
- [7] S. Baklouti, J. Bouaziz, T. Chartier, J.-F. Baumard, J. Eur. Ceram. Soc. 21 (2001) 1087.
- [8] T. Tsugoshi, T. Nagaoka, K. Hino, T. Arii, M. Inoue, Y. Shiokawa, K. Watari, J. Therm. Anal. Calorim. 80 (2005) 787.

Rapid determination of bromide in seawater samples by capillary ion chromatography using monolithic silica columns modified with cetyltrimethylammonium ion

Atsushi Suzuki, Lee Wah Lim, Toshiya Hiroi, Toyohide Takeuchi *

Department of Chemistry, Faculty of Engineering, Gifu University, 1-1 Yanagido, Gifu 501-1193, Japan

Received 31 October 2005; accepted 22 December 2005

Available online 20 March 2006

Abstract

Monolithic silica capillary columns dynamically modified with quaternary ammonium ions were evaluated for the determination of bromide in seawater samples. A quaternary ammonium ion such as cetyltrimethylammonium ion was dynamically introduced onto monolithic silica surfaces. The first layer of the modifier was introduced by electrostatic interaction, whereas the second layer was introduced by hydrophobic interaction. The latter layer worked as the anion-exchange sites. The modified monolithic silica capillary columns could be used for rapid separation of inorganic anions. Separation of authentic mixture of five anions was achieved within a few minutes. The addition of small amount of the modifier in the eluent improved the repeatability of the retention time. Seawater samples could be directly injected onto the prepared capillary columns, and bromide could be determined to be 63 mg/L.

© 2006 Elsevier B.V. All rights reserved.

Keywords: Ion chromatography; Monolithic silica capillary columns; Cetyltrimethylammonium ion; Bromide; Seawater

1. Introduction

Because of lower separation impedance, monolithic silica capillary columns have a potential to achieve higher column efficiency than conventional packed columns. The monolithic silica columns possess unique pore structures and permeability, viz., μm order of through pore and silica domain [1–6]. The μm order of through pore structure increases the permeability, allowing longer column lengths, whereas the μm order of the silica domain size maintains its higher efficiency. So far, reversed-phase stationary phases have mostly been developed for monolithic silica columns, whereas few stationary phases have been developed for ion chromatography.

Determination of trace ions contained in seawater is one of the most difficult task in ion chromatography owing to the effect of matrix ions. Low-capacity anion-exchange columns, as well as C18 reversed-phase columns coated with cetyltrimethylammonium ion in water–methanol mixtures, have been applied to the determination of iodine species in seawater [7]. Ito [8] has used a

semi-microcolumn packed with styrene-divinylbenzene copolymer and a mobile phase including 0.03 M sodium perchlorate, 0.5 M sodium chloride and 5 mM sodium phosphate buffer, for the determination of trace iodide in seawater. Ito et al. [9] also reported the determination of nitrite and nitrate in seawater samples using conventional-size monolithic ODS columns coated with cetyltrimethylammonium ion. An electrostatic ion chromatographic method for rapid and direct determination of iodide in seawater has also been reported where a reversed-phase C18 packed column modified with Zwittergent-3–14 micelles, and an eluent comprising an aqueous solution containing 0.2 mM sodium perchlorate and 0.3 mM Zwittergent-3–14 are used [10]. It is also reported that reversed-phase C30 stationary phase coated with poly(ethylene glycol) allows the direct injection of seawater samples for the determination of iodide and thiocyanate [11,12].

It is well-known that silica gel columns dynamically modified with a quaternary ammonium ion such as cetyltrimethylammonium ion can work as the stationary phase for anions [13]. These columns can be prepared by just passing an aqueous solution containing cetyltrimethylammonium ion into the column. This type of the stationary phase can be easily applied to monolithic silica columns.

* Corresponding author. Tel.: +81 58 293 2806; fax: +81 58 293 2806.
E-mail address: takeuchi@apchem.gifu-u.ac.jp (T. Takeuchi).

The present paper describes the preparation of monolithic silica capillary columns dynamically modified with a quaternary ammonium ion and their application to the rapid determination of bromide in seawater samples.

2. Experimental

2.1. Apparatus

Eluent was supplied by applying the pressure from a nitrogen gas cylinder or by using a Model MF2 Microfeeder (Azumadenki Kogyo, Tokyo, Japan) equipped with a 0.5-mL MSGAN050 gas-tight syringe (Ito, Fuji, Japan). In the former case the eluent was filled in a 0.8-mL loop attached with a Model 7000 6-way switching valve (Rheodyne, Cotati, CA, USA). Sample was loaded by using a CN4-4344-.02 nanovolume sample injector with an injection volume of 20 nL (VICI_{AG}, Schenkon, Switzerland) without split. A model CE-1570 UV/VIS Detector (Jasco, Tokyo, Japan) was used, and analytes were visualized by on-column detection.

2.2. Reagents

Acetonitrile and distilled water were of HPLC grade and obtained from Wako Pure Chemical Industries (Osaka, Japan). Other reagents were of reagent grade and were obtained from Wako Pure Chemical Industries, unless otherwise noted. The reagents were used as received. Tetramethoxysilane (TMOS) was purchased from Tokyo Chemical Industry (Tokyo, Japan). Cetyltrimethylammonium bromide (Cetrimide) and cetyltrimethylammonium chloride (CTAC) were purchased from Nacalai Tesque (Kyoto, Japan) and Wako Pure Chemical Industries, respectively. PEG 10,000 was purchased from Sigma–Aldrich Japan (Tokyo, Japan).

2.3. Preparation of monolithic capillary columns

Monolithic silica was in situ prepared in fused-silica capillary with 0.1 mm i.d. according to the sol–gel method previously reported [14]. Fused-silica capillary tubes with 0.1 mm i.d. (GL Sciences, Tokyo, Japan) were treated with 1 M sodium hydroxide at 60 °C for 2 h, followed by washing with 1 M hydrochloric acid and methanol. The fused-silica capillary tubes were then dried at 120 °C in a stream of nitrogen for 30 min. Sol–gel solution was prepared by dissolving 0.53 g of PEG 10,000 in a mixture of 2 mL of TMOS and 5 mL of 0.01 M acetic acid, followed by agitation in an ice water-bath for 40 min. The solution was then degassed under vacuum for 10 min before filling the solution into the above pretreated capillary. The fused-silica capillary tubes filled with the sol–gel solution were kept at 40 °C for 20 h, and nitrogen was passed to remove the reagent from the column after the reaction, followed by washing with water and 0.1 M ammonia aqueous solution. The monolithic silica capillary columns were then filled with 0.1 M ammonia aqueous solution and kept at 60 °C for 45 h, followed by washing with 60% ethanol aqueous solution. The capillary columns were finally heated at 330 °C for 5 h. A 0.5 mL volume of aqueous

solution of 3 mM Cetrimide or CTAC was passed into the prepared monolithic capillary column at a flow rate of 0.69 $\mu\text{L}/\text{min}$ to prepare the stationary phase for anion-exchange chromatography.

3. Results and discussion

3.1. Effect of modification condition on the retention of analyte ions

Effect of the concentration of Cetrimide as the modifier on the retention of analyte anions was examined. A 0.5 mL volume of aqueous solution of Cetrimide with different concentration, 1, 3 or 5 mM, was passed into each monolithic silica capillary column (200 mm \times 0.1 mm i.d.) at a flow rate of 0.69 $\mu\text{L}/\text{min}$ before the measurements. The eluent was aqueous solution of 50 mM sodium chloride containing no cetyltrimethylammonium ion and supplied at constant inlet pressure, 0.5 MPa. Fig. 1 shows the chromatograms obtained by the columns modified with different-concentration Cetrimide solutions. The retention times observed in Fig. 1 were nearly the same, but the retention factor increased with increasing Cetrimide concentration, e.g., the retention factors (k) of nitrate were 4.0, 6.8 and 7.0 for 1, 3- and 5-mM Cetrimide, respectively. Since the difference in the retention factor was not very different for the modification with 3- and 5-mM Cetrimide aqueous solutions, 3 mM Cetrimide solution was employed in the following experiments.

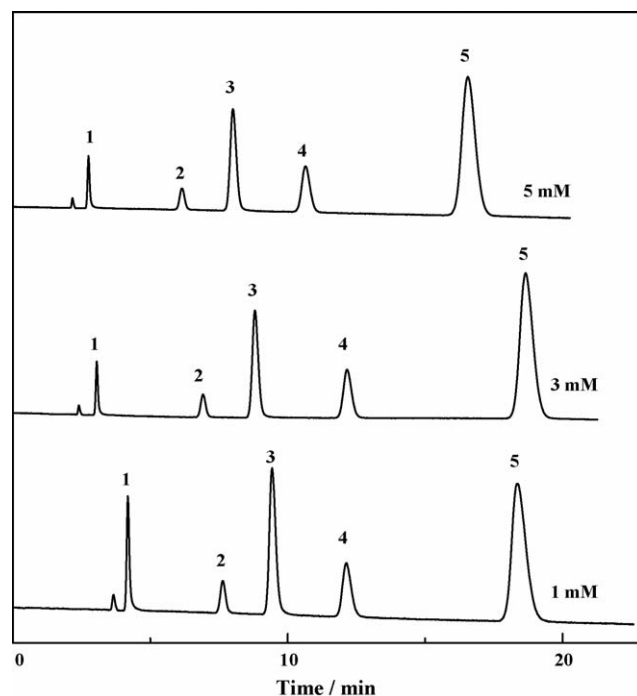


Fig. 1. Effect of the concentration of Cetrimide as the modifier on the retention of anions. Column: monolithic silica capillary column (200 mm \times 0.1 mm i.d.) modified with Cetrimide. Modification condition: 0.5 mL of aqueous solution of 1-, 3- or 5-mM Cetrimide was supplied into each capillary at 0.69 $\mu\text{L}/\text{min}$. Eluent: 50 mM sodium chloride aqueous solution. Inlet pressure: 0.5 MPa. Wavelength of UV detection: 210 nm. Analyte: 0.5 mM each of iodate (1), bromate (2), nitrite (3), bromide (4) and nitrate (5).

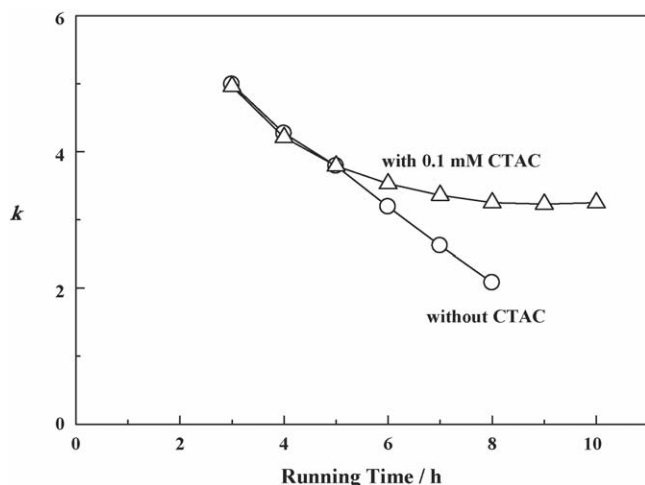


Fig. 2. Stability of monolithic silica capillary column modified with cetyltrimethylammonium ion. Column: monolithic silica capillary column modified with Cetrimide (200 mm \times 0.1 mm i.d.). Eluent: 50 mM sodium chloride solution with or without CTAC. Flow-rate: 2.1 μ L/min. Wavelength of UV detection: 210 nm. Analyte: 0.5 mM nitrate. Injection volume: 20 nL.

The retention factor of nitrate increased with increasing the volume of the Cetrimide solution passed into the capillary column. For example, the capillary was modified with 3 mM Cetrimide at 0.69 μ L/min, the retention factor of nitrate was 3.8 and 6.4 for 6- and 12-h modification, respectively. Considering these results, capillary was modified with Cetrimide or CTAC for 12 h in the following experiments.

3.2. Effect of eluent concentration

Effects of the concentration of the eluent concentration on the retention factor of the analyte anions were examined by using sodium chloride and sodium sulfate as the eluent. Linear relationships between $\log k$ and the eluent concentration were observed for both eluent in the region between 50 and 200 mM. The slopes of the linear curves observed for monovalent analyte anions were 1.0–1.1 and 0.37–0.45 for sodium chloride and sodium sulfate as the eluent, respectively. These values were nearly the same as the corresponding theoretical values 1 and 0.5, respectively. In other words, ion exchange is involved in the retention of the analyte anions on the present stationary phase.

In order to apply the present stationary phase to the determination of bromide in seawater samples, the eluent concentration should be increased to around 500 mM so that effects of matrix ions can be minimized. The present stationary phase still retained bromide when such a higher concentration eluent was used.

3.3. Stability of the stationary phase

The stability of a prepared modified monolithic silica capillary column (200 mm \times 0.1 mm i.d.) was examined by using 50 mM sodium chloride as the eluent. Fig. 2 shows the results for the column dynamically modified with cetyltrimethylammonium ion. It can be seen from the figure that the retention factor of nitrate decreases with running time when the eluent contained

no CTAC. On the contrary, the retention factor of nitrate for the eluent containing 0.1 mM also decreased but it converged on some value. CTAC is superior to Cetrimide in terms of the background in case cetyltrimethylammonium ion is added in the eluent since chloride is more transparent at lower wavelengths than bromide.

In addition, the addition of 0.1 mM CTAC in the eluent did not deteriorate the resolution of the analytes. Nearly the same results were observed for higher eluent concentration, e.g., 500 mM sodium chloride.

Monolithic silica capillary columns possess higher permeability compared with common densely packed columns. This means that rapid separation on monolithic capillary columns can be done at lower inlet pressures. Fig. 3 demonstrates a rapid separation of five anions on a CTAC-modified monolithic capillary column at a flow rate of 11.1 μ L/min. It can be seen that the separation of five anions is completed within 1 min. The inlet pressure under the operating conditions in Fig. 3 is estimated to be ca. 5.3 MPa.

3.4. Validation

The operating condition for the determination of bromide in seawater sample was validated, where 40-cm column was employed in order to improve the resolution. Table 1 shows the repeatability of retention time and peak signals using 500 mM sodium chloride containing 0.1 mM CTAC as the eluent. The relative standard deviation (R.S.D.) values for six successive measurements were less than 0.61% for the retention time, whereas those for the peak height and peak area were less than 3.5%.

The detection limit and the determination limit for bromide under the conditions in Table 1 were 4.5 and 15 mg/L, respectively. The peak height was linear to the bromide con-

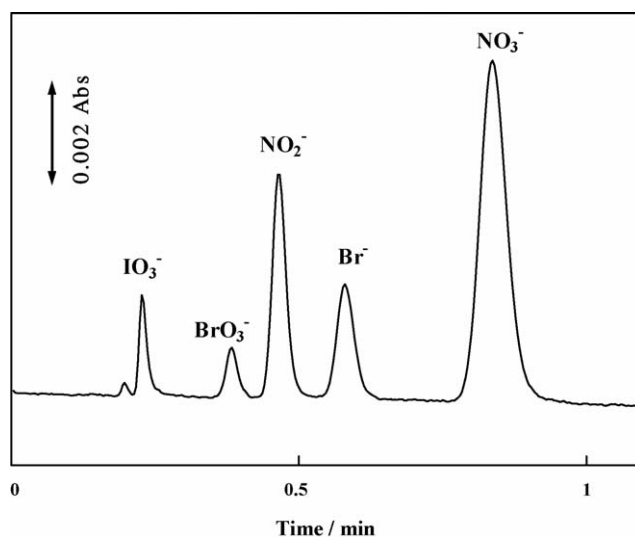


Fig. 3. Rapid separation of five anions on a monolithic silica capillary column modified with cetyltrimethylammonium ion. Eluent: 50 mM sodium chloride solution with 0.1 mM CTAC. Flow-rate: 11.1 μ L/min. Analytes: 0.5 mM each of iodate, bromate, nitrite, bromide and nitrate. Other operating conditions are the same as in Fig. 2.

Table 1
Repeatability of retention time, peak area and peak height

	R.S.D., % (<i>n</i> = 6)			
	Bromate	Nitrite	Bromide	Nitrate
Retention time	0.61	0.54	0.40	0.00
Peak area	2.4	1.0	2.9	3.4
Peak height	2.8	1.8	3.5	3.2

Column: monolithic silica capillary column (400 mm × 0.1 mm i.d.) modified with cetyltrimethylammonium ion. Eluent: 500 mM sodium chloride containing 0.1 mM CTAC. Flow-rate: 5.6 µL/min. Wavelength of UV detection: 210 nm. Analyte: 0.5 mM each of bromate, nitrite, bromide and nitrate. Injection volume: 20 nL.

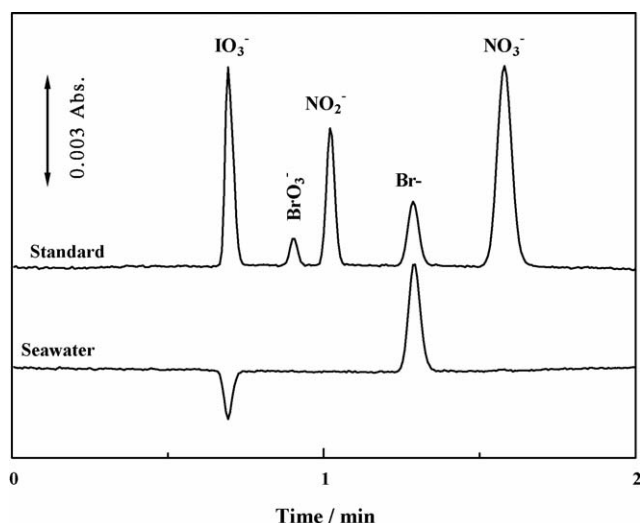


Fig. 4. Separation of authentic mixture of five anions and bromide in a seawater sample on a monolithic silica capillary column modified with cetyltrimethylammonium ion. Column: 400 mm × 0.1 mm i.d. Eluent: 500 mM sodium chloride containing 0.1 mM CTAC. Flow rate: 5.6 µL/min. Injection volume: 20 nL. Samples: 0.5 mM each for the upper trace; seawater for the lower trace. Wavelength of UV detection: 210 nm.

centration up to 2 mM with the correlation factor of 0.9999 (r^2).

3.5. Determination of bromide in seawater samples

Fig. 4 demonstrates the separation of an authentic mixture of five anions and bromide in a seawater sample on a monolithic silica capillary column modified with CTAC. It can be seen that the retention time of bromide for the seawater sample is the same as for the standard sample. This indicates that the matrix ions' effects are negligible for the present separation

system. The concentration of bromide in the seawater sample was determined to be 63 mg/L (0.79 mM). In addition, the seawater sample was filtrated with a 0.45-µm membrane filter before injection. Unfortunately, the present detection sensitivity is not satisfactory because of on-column detection. The sensitivity should be improved so as to determine trace anions such as nitrite, nitrate and iodide contained in seawater.

4. Conclusion

It was proved that monolithic silica capillary columns just modified with cetyltrimethylammonium ion retained anions and allowed the determination of bromide in seawater without tedious pretreatments. The stability of the retention time of analyte anions could be improved by adding 0.1 mM CTAC in the eluent. Monolithic silica capillary columns achieved rapid separation at lower inlet pressures.

Acknowledgements

This work was partially supported by the Ministry of Education, Culture, Sports, Science and Technology, Grant-in-Aid for Scientific Research (C), No. 16550071, 2005.

References

- [1] N. Tanaka, H. Kobayashi, H. Nakanishi, H. Minakuchi, N. Ishizuka, Anal. Chem. 73 (2001) 420A.
- [2] N. Tanaka, H. Nagayama, H. Kobayashi, T. Ikegami, K. Hosoya, N. Ishizuka, H. Minakuchi, K. Nakanishi, K. Cabrera, D. Lubda, J. High Resolut. Chromatogr. 23 (2000) 111.
- [3] C. Fujimoto, J. High Resolut. Chromatogr. 23 (2000) 89.
- [4] N. Ishizuka, H. Minakuchi, K. Nakanishi, N. Soga, H. Nagayama, K. Hosoya, N. Tanaka, Anal. Chem. 72 (2000) 1275.
- [5] J.D. Hayes, A. Malik, Anal. Chem. 72 (2000) 4090.
- [6] M. Motokawa, H. Kobayashi, N. Ishizuka, H. Minakuchi, K. Nakanishi, H. Jinnai, K. Hosoya, T. Ikegami, N. Tanaka, J. Chromatogr. A 961 (2002) 53.
- [7] K. Ito, E. Shoto, H. Sunahara, J. Chromatogr. 549 (1991) 265.
- [8] K. Ito, J. Chromatogr. A 830 (1999) 211.
- [9] K. Ito, Y. Takayama, N. Makabe, R. Mitsui, T. Hirokawa, J. Chromatogr. A 1083 (2005) 63.
- [10] W. Hu, P.-J. Yang, K. Hasebe, P.R. Haddad, K. Tanaka, J. Chromatogr. A 956 (2002) 103.
- [11] L. Rong, T. Takeuchi, J. Chromatogr. A 1042 (2004) 131.
- [12] L. Rong, L.W. Lim, T. Takeuchi, Chromatographia 61 (2005) 371.
- [13] T. Takeuchi, E.S. Yeung, J. Chromatogr. 370 (1986) 83.
- [14] T. Takeuchi, S. Tatsumi, S. Masuoka, K. Hirose, H. Uzu, J.-Y. Jin, C. Fujimoto, K. Ohta, K.-P. Lee, J.-J. Ryoo, S.-H. Choi, J. Chromatogr. A 1021 (2003) 55.

The use of trichloroacetic acid imprinted polymer coated quartz crystal microbalance as a screening method for determination of haloacetic acids in drinking water

Roongnapa Suedee^{a,*}, Wimon Intakong^a, Franz L. Dickert^b

^a Molecular Recognition Materials Research Unit, Department of Pharmaceutical Chemistry, Faculty of Pharmaceutical Sciences, Prince of Songkla University, Hatyai, Songkla 90112, Thailand

^b Institute of Analytical Chemistry, Vienna University, Währinger Straße 38, A-1090 Vienna, Austria

Received 6 March 2006; received in revised form 5 April 2006; accepted 6 April 2006

Available online 9 June 2006

Abstract

An alternative screening method for haloacetic acids (HAAs) disinfection by-products in drinking water is described. The method is based on the use of piezoelectric quartz crystal microbalance (QCM) transducing system, where the electrode is coated with a trichloroacetic acid-molecularly imprinted polymer (TCAA-MIP). This MIP comprises a crosslinked poly(ethyleneglycoldimethacrylate-*co*-4-vinylpyridine). The coated QCM is able to specifically detect the analytes in water samples in terms of the mass change in relation to acid–base interactions of the analytes with the MIP. The TCAA-MIP coated QCM showed high specificity for the determination of TCAA in aqueous solutions containing inorganic anions, but its sensitivity reduced in water samples containing hydrochloric acid due to a mass loss at the sensor surface. Cross-reactivity studies with HAA analogs (dichloro-, monochloro-, tribromo-, dibromo-, and monobromo-acetic acids) and non-structurally related TCAA molecules (acetic acid and malonic acid) indicated that recognition of the structurally related TCAA compounds by the TCAA-MIP-based QCM is due to a carboxylic acid functional group, and probably involves a combination of both size and shape selectivity. The total response time of sensor is in the order of 10 min. The achieved limits of detection for HAAs (20–50 $\mu\text{g l}^{-1}$) are at present higher than the actual concentrations found in real-life samples, but below the guidelines for the maximum permissible levels (60 $\mu\text{g l}^{-1}$ for mixed HAAs). Recovery studies with drinking water samples spiked with TCAA or spiked with mixtures of HAAs revealed the reproducibility and precision of the method. The present work has demonstrated that the proposed assay can be a fast, reliable and inexpensive screening method for HAA contaminants in water samples, but further refinement is required to improve the limits of detection.

© 2006 Elsevier B.V. All rights reserved.

Keywords: Haloacetic acids; Disinfection by-products; Molecularly imprinted polymer; Quartz crystal microbalance

1. Introduction

Chlorination, the most widely used disinfection process for drinking water, produces two classes of disinfection by-products (DBPs); trihalomethanes and haloacetic acids [1,2]. After trihalomethanes, haloacetic acids (HAAs) which include the following nine compounds: monochloroacetic acid (MCAA), dichloroacetic acid (DCAA), trichloroacetic acid (TCAA), monobromoacetic acid (MBAA), dibromoacetic acid (DBAA), tribromoacetic acid (TBAA), bromochloroacetic acid (BCAA), dichlorobromoacetic acid (DCBAA), and dibromochloroacetic

acid (DBCBA), represent the second most abundant DBP species in chlorinated drinking water. HAA disinfection by-products are usually present in water as a complex mixture, with a large proportion of DCAA and TCAA [3]. They are of great concern to public health, owing to their potential carcinogenic [4] and mutagenic effects [5]. Several previous DBP studies have focused mainly on the ingestion route of exposure to THMs, and to date THMs are monitored regularly in drinking water [6–8], whilst the presence of HAAs in water was rather disregarded. Evidence for the widespread occurrence of HAAs in environmental waters around the world is increasing [9–10]. Additionally, it is now clear that levels of THMs are not considered to be a good indicator of the levels of HAAs [11]. Recently, however, potential health risks to humans from long term exposure to particular HAAs has led to increased efforts to monitor

* Corresponding author. Tel.: +66 74 288862; fax: +66 74 428239.
E-mail address: roongnapa.s@psu.ac.th (R. Suedee).

and reduce their concentration in drinking waters [12]. Since determination of HAAs is quite a new environmental concern, few references are available dealing with development of liquid chromatographic methods for their analysis. The standard methods for determination of HAAs (such as ion chromatography, GC–ECD, GC–MS) are time consuming, complicated and costly for routine analysis of drinking water. A fast, simple and inexpensive analysis method is needed in order to complement these established sophisticated analytical techniques. The primary aim of the current study is to investigate the development of such a technique, with a view to eventually developing an on-line rapid screening method.

Electrochemical detection has been recognized as a useful method for organic acid analysis. However this technique cannot be used for monitoring HAA concentrations directly in water [13,14]. Although several non-crosslinked conducting polymers, such as poly(pyrrole) [15] or poly(vinyl chloride) incorporating the selective molecule such as polyoxyanion macrocyclics [16], have been used as a tool for the detection of organic ions in electrochemical analysis systems, none of these have shown sufficient specificity for the analytes. Recently, a conductometric sensor specific to the group of haloacetic acids (HAAs) has been developed by our research group [17]. The detection system of this sensor was based on molecular recognition of the analytes by a polymer prepared by a molecular-imprinting polymerization technique with a transduction of polyvinyl chloride membrane support. Molecularly imprinted polymers (MIPs), which recognize target molecules with size and shape-complementary cavities are becoming an important class of sensing materials due to their molecular recognition ability and good stability [18]. These artificial receptors have been incorporated in several transducing systems, such as electrochemical, piezoelectric and optical [19–22].

During the last decade, the introduction of polymer selectivity by the molecular imprinting technique has been made mostly with crosslinked polymers rather than non-crosslinked polymers. The reason is that the former polymers give greater stability and certainty of recognition. The most commonly used crosslinking monomer, ethylene glycol dimethacrylate (EDMA), has potential for molecular-imprinted polymer synthesis of organic compounds since it gives high molecular recognition to the polymer with good stability of the layer. However the EDMA polymer is hydrophobic and inert, and it is not therefore attractive to polar molecules of the analytes. Crosslinking polymerization of EDMA monomer with 4-vinyl pyridine (VPD) functional monomer is capable of generating an electrically conducting polymer [23] that would be advantageous, since the VPD monomer will not only form the reception site in MIP matrix but also make EDMA crosslink to be electrically active. This increases the attraction capability of the MIP produced, and perhaps improves the mechanical properties and processibility of the layer on electrode, due to the increased polarity of polymer. In addition to this, trichloroacetic acid (TCAA), which was chosen as the print molecule for this work, can be used as a doping agent.

By making use of the molecular-imprinting polymerisation technique, with appropriate modulation of the polymer composi-

tion, the recognition material engineered should be able to detect TCAA and structurally similar compounds directly in drinking water. The current study was designed to show that by using the TCAA-imprinted polymer coated quartz crystal microbalance (TCAA-MIP-QCM), it would be possible to specifically detect the group of HAAs in water, using mass-sensitive measurements. In this study, we have successfully synthesized TCAA-imprinted polymer of crosslinked poly(VPD-co-EDMA) as a spin-coated film at gold electrode surfaces, and evaluated its interaction with six commonly occurring HAAs, i.e., TCAA, DCAA, MCAA, TBAA, DBAA and MBAA, on QCM-based assay protocol. Since piezoelectric QCM, which is a well-known mass detection method, offers simplicity and low cost for chemical analysis, this assay method was chosen for the current study. Unspecific conductivity effects would be minimized by a dual QCM electrode comprising of multi-electrode structures on a single piezo-crystal with larger electrode diameters in contact with the liquid phase and two time smaller electrodes facing the gas-phase, according to techniques previously described in the literatures [24,25].

2. Experimental

2.1. Chemicals and materials

Ethylene glycol dimethacrylate (EDMA), 4-vinylpyridine (VPD) and malonic acid were obtained from Aldrich Chemical Company (Milwaukee, WI, USA). 2,2'-Azobis(isobutyronitrile) (AIBN) was purchased from Janssen Chimica (Geel, Belgium). Trichloroacetic acid (TCAA) was purchased from Merck K.G. (Darmstadt, Germany). Dichloroacetic acid (DCAA), monochloroacetic acid (MCAA), dibromoacetic acid (DBAA), monobromoacetic acid (MBAA) and tribromoacetic acid (TBAA) were obtained from Fluka Chemie AG (Buchs, Switzerland). All chemicals for preparing buffer solution were analytical grade and were obtained from Merck (Darmstadt, Germany). All solvents were analytical grades and dried with molecular sieves prior to use.

2.2. Immobilisation of polymer on QCM electrode

To prepare the QCM electrode, a dual QCM-pattern designed as described in a previous study [24] was sequentially screen-printed on each side of 10 MHz AT-cut quartz disc (15 mm diameter), using the gold screen-printing technique. The electrode facing the aqueous phase had a diameter of 4.5 mm with 2.5 mm electrode on the gas-phase side. The thickness of the gold electrode layer on each side of the quartz crystal after sintering was determined by scratching with a needle and measuring depth of the scratches using an AFM (Digital Instruments Inc., Santa Barbara, CA) with a Nanotec Electronica WSxM scanning probe microscopy software version 3.0 Beta 8.1, which this was found to be about 180 nm.

The procedure for immobilisation of MIP on electrodes was as follows: 14 mg of TCAA (0.08 mmol), 34 mg of VPD (0.32 mmol), 200 mg of EDMA (1.0 mmol) and 9 mg of AIBN (0.05 mmol) were dissolved in 1 ml of acetonitrile. Then, the

solution was purged with a stream of nitrogen gas for 1 min and pre-polymerisation was carried out at 65 °C for 1 min in a water-bath. The non-imprinted polymer (NIP) was prepared in the same manner as the MIP, but in the absence of the TCAA template. A crystal was spin-coated with 10 μ l of the MIP solution onto the center of the surface of the analytical electrode with a rotation speed of 3000 rpm, following by spin-coating of 10 μ l of the NIP solution at the reference electrode. Subsequently, the blank quartz was placed in a chamber flushed with nitrogen gas for 1 min. Polymerisation was carried out at 70 °C for 18 h in a hot-air oven. After the immobilizing process, the electrode was washed with five portions of 100 ml de-ionised water to remove the template molecules. For removing the templates absorbed in the recognition sites, a washing process in deionized water needed for at least 3 h. Finally, the electrode was dried in air for overnight. The thickness of the MIP coated films was inspected using an AFM method that was similar to the method employed for measuring of the gold layer onto electrodes.

2.3. Fabrication of the sensor device

The QCM constructed with a coated TCAA-MIP and a coated corresponding NIP gold electrode was mounted in a flow-cell with a volume of 250 μ l and placed in a thermostat at 25 °C. A home-built oscillator circuit and a self-programmed frequency read-out were used with a processing software. The oscillator frequency was measured by means of an HP 53131A frequency counter. The response of the oscillator circuit were checked by means of a HP 8572C network analyser (Hewlett Packard, Germany) to obtain data relating to acoustic damping and frequency

shifts. The sensor experiments were performed using a flow system with a flow rate of 2 ml/min. Before making a measurement, the sensor was stabilized by running 200 ml de-ionised water through the cell for 3 h. One hundred milliliters of a series of standard solutions of TCAA and analogs were run through the cell separately. The frequency of both TCAA-MIP-QCM and the corresponding NIP-based QCM was recorded as parallel until a stable frequency was obtained. The water samples were analysed under the same condition as that used for the standard solutions. For the sample measurement using the sensor, the response of sensor exposed to a solution of the analyte was reported as frequency shift response ($-\Delta F$) which was the difference value of frequency shift of MIP electrode and frequency shift of NIP electrode. All measurements were performed in triplicate.

3. Results and discussion

3.1. Performance of the TCAA-MIP-QCM

Piezoelectric quartz crystal microbalance is well known as a remarkably sensitive mass detection method. Recently the use of MIPs coated onto piezoelectric QCM sensing system has attracted increase attention [19,20]. Normally, the integration of MIP into a piezoelectric QCM sensor requires thin or ultra-thin MIP films (nanometres) on the transducer surface. This can be achieved in several ways; in situ electro-polymerisation; surface coating (direct or spin coating) [26]; physical entrapment of MIP particles into gel [27]; or chemical coupling of the MIP [28]. For this work the spin-coating method was used for immobilising MIP onto the QCM electrode.

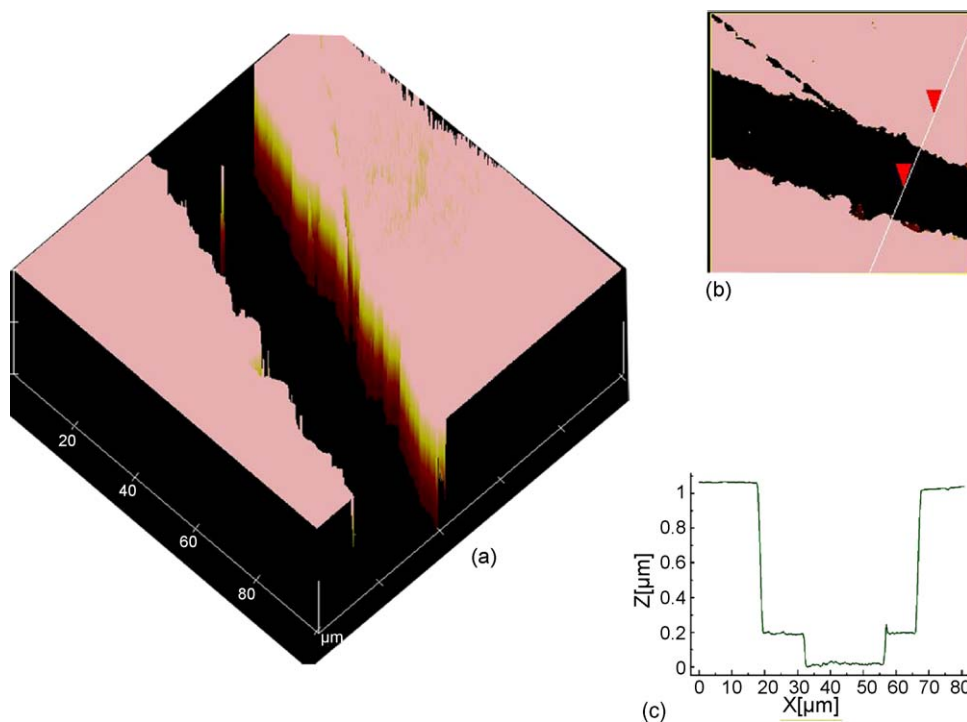


Fig. 1. (a) AFM 3D topography; (b) AFM of a cross-section of a scratch on a 20 kHz-MIP layer, and the measured depth of the polymer layer of 870 nm which is shown on (c) the plot of depth (z) vs. width (x) generated using Nanotec Electrónica WSxM scanning probe microscopy software version 3.0 Beta 8.1. Scan rate of 1000 Hz is used.

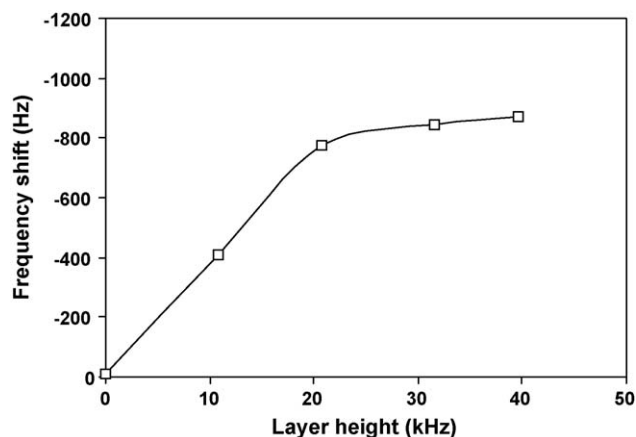


Fig. 2. The effect of imprinted layer height on frequency shift of the TCAA-imprinted coated QCM exposed to TCAA at concentration level of $100 \mu\text{g l}^{-1}$.

The TCAA-imprinted polymer matrix from crosslinked poly(VPD-co-EDMA) have been produced by copolymerisation of VPD functional monomer and EDMA crosslinker in the presence of TCAA template in acetonitrile at the optimised TCAA/VPD/EDMA mole ratio (1:4:12). This polymer constitution did not only give high molecular recognition, i.e. the frequency shift response to 100 mg l^{-1} of TCAA was the highest comparing to that of the other TCAA/VPD/EDMA mole ratios; 1:2:12, 1:6:12, 1:8:12, 1:4:10, 1:4:15 and 1:4:18, but also provided a film on gold electrode surfaces with good stability in terms of adhesion. The low relative standard deviation (2.4%, $n=4$) indicates good and reproducible coating. Viscosity, conductivity and pressure fluctuations were compensated for measurements with a coated NIP gold electrode as the reference electrode. The recorded Δf before and after MIP immobilization was found to be $0.0196 \pm 0.0004 \text{ Hz}$, which corresponds to about 800 nm according to the Sauerbrey equation [29]:

$$\Delta f = \frac{f_0^2 \Delta m}{N \rho_q A}$$

where f_0 is the fundamental frequency of the crystal, N the modulus of quartz (167 kHz cm), ρ_q the quartz density (2.648 g cm^{-3}), and A is the piezoelectrically active. The film thickness obtained by the QCM was in good agreement with that measured by the AFM method (Fig. 1).

A preliminary evaluation of the various layer heights for bulk effects in TCAA-imprinted polymer of crosslinked poly(VPD-co-EDMA) prepared at 1:4:12 TCAA/VPD/EDMA molar ratio was performed by QCM measurement. The frequency shift of the different heights of imprinted layer in the range 0–40 kHz (or 0–1580 nm as measured by an AFM method), showed a different frequency shift of the imprinted layer to 100 mg l^{-1} (ppm) TCAA solution, as seen in Fig. 2. The frequency shift of sensor greatly increased at initial layer-heights of the MIP and started to level off after 20 kHz layer-height. The compensated sensor response with a 800 nm-thickness (or 20 kHz-height) of the MIP layer for 100 mg l^{-1} TCAA solution is about 800 Hz. A measurement of noise of 6 Hz allows a detection limit for TCAA

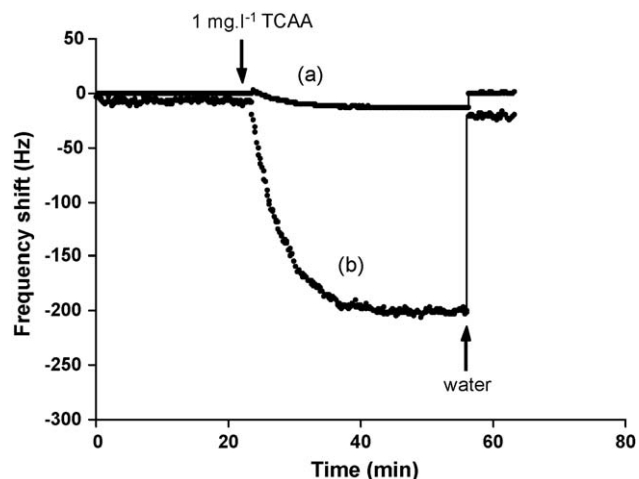


Fig. 3. Signal response of the QCM sensor with (a) NIP- and (b) MIP-coated electrode to TCAA at concentration level of 1 mg l^{-1} .

of about $54 \mu\text{g l}^{-1}$ (ppb), with a signal-to-noise ratio of 3:1. A steady response with the sensor was found within 20 min.

The effect of swelling of the MIP film on the sensor response was also investigated. The results revealed that the frequency response obtained using a 24 h-hydrated polymer (9.965 Hz) is similar to the frequency response using from the dry polymer (9.967 Hz) when measured in air after evaporation of water. In general, EDMA generates an imprinted polymer that is compact, inert and highly stable with respect to rigidity of polymer structure. The negligible change in signal response of the sensor after hydration of the MIP suggests that the imprinted structure produced by the EDMA-based polymer is very stable.

Several buffer solutions (pH 1, 4 and 7 buffers) were tested as background solutions for the QCM measurements. The frequency changes of the MIP-based QCM for 10 mg l^{-1} TCAA concentration were 482, 105, 210 and 374 Hz, respectively, when measured in de-ionised water, 0.2M HCl-KCl buffer pH 1, 0.2M phosphate buffer pH 4 and 0.2M phosphate buffer pH 7 running solution. Hence, de-ionised water was employed as background solution for studying the interaction of TCAA-MIP-QCM with HAAs in water samples, since it afforded the highest sensor response.

3.2. The efficiency of TCAA-MIP coated QCM

3.2.1. Recognition of the template by the TCAA-MIP-QCM

The signal response of the QCM sensor with MIP and non-imprinted polymer-coatings when exposed to a solution of TCAA at a concentration of 1 mg l^{-1} is presented in Fig. 3. The TCAA solution causes a decrease in the frequency shift of the MIP sensor, and this effect is completely reversible after washing with pure water. In contrast, the effect of the TCAA solution on the frequency signal of the NIP-based sensor is very slight. These results indicate that TCAA-imprinted polymer coated onto QCM electrode affords a highly specific and significantly strong signal response to the template in water. The mass change of the MIP film when exposed to TCAA solution is presumably due to the change in the mass of the polymer as tem-

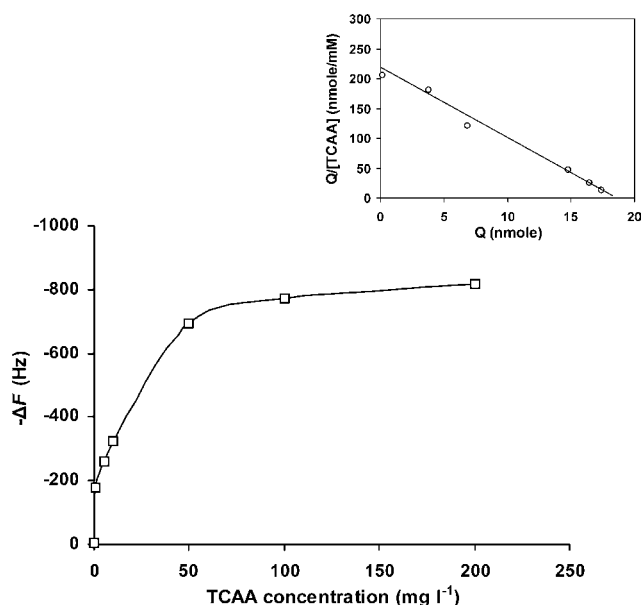


Fig. 4. Effect of different concentration of TCAA (0–200 mg l⁻¹) on the frequency shift response of the TCAA-MIP-QCM. Top right is Scatchard plot that is relative to concentration dependence of the sensor.

plate can insert itself into the imprint within the polymer matrix. The main force of binding between the MIP and TCAA in water solution might be expected to derive from acid–base interaction between the carboxylate anion and vinylpyridinium cation of the MIP. In addition the results demonstrated that dissociation of TCAA at the imprinted sites is possible in de-ionised water.

The effect of electrolytes (HCl, NaCl, KCl, K₂HPO₄ and KH₂PO₄) on the signal response of the QCM sensor was studied. The signal responses of the MIP-coated QCM sensor for the water solution containing inorganic substances (as individual) at a concentration of 0.1 mM were measured under the optimized conditions. The polymer gave positive frequency shifts with 0.1 mM HCl ($\Delta F = +40$). In contrast, frequency shifts of the MIP to 0.1 mM KCl, K₂HPO₄ or KH₂PO₄ in water solution were negligible (<10 Hz). The positive frequency shift towards HCl of the MIP-based QCM electrode can be explained by a mass loss effect on the sensor surface due to the lighter ion protons [30]. These results demonstrated that TCAA-imprinted crosslinked poly(VPD-co-EDMA) coated QCM is very sensitive towards the inorganic acid, hydrochloric acid, and this is likely to limit the application of this sensor for the assay of HAAs in water samples containing hydrochloric acid. However the sensor is not affected by Na, K cation and Cl, HPO₄ and H₂PO₄ anions at concentrations below 0.1 mM.

As can be seen from Fig. 4, the TCAA-MIP-QCM gives frequency shift responses correspondingly to the increasing repeated concentrations of TCAA in water. The response of the TCAA-MIP-QCM reaches a plateau at the higher concentration (>100 mg l⁻¹) of TCAA, suggesting a saturation of recognition sites in the imprinted polymer with the template molecules. The adsorption behaviour of the MIP film fabricated in the sensor can be fitted to the Langmuir isotherm. Accordingly, Scatchard analysis was used to estimate the binding parameters of the polymers. The Scatchard equation is as follows:

Table 1

Binding constant (K_a), site population (Q_{\max}) and cross-reactivity related to TCAA (CR) of the TCAA-MIP-QCM responding to TCAA and analogs ($n = 3$)

Substrate	K_a (mM ⁻¹)	Q_{\max} (nmol)	CR ^a (%)
TCAA	10.6	18.9	100
DCAA	7.0	14.1	80
MCAA	4.0	13.2	66
TBAA	6.4	13.8	84
DBAA	5.1	14.1	84
MBAA	4.3	13.2	83
Acetic acid	2.5	10.6	18
Malonic acid	2.2	12.6	20

^a CR is the ratio of the frequency shift measured at EC₅₀ for analog to that of TCAA. EC₅₀ is the analyte concentration for which HAA binding to MIP is inhibited by 50%.

$Q/[TCAA] = (Q_{\max} - Q)/K_D$, where Q is the amount of TCAA bound to the polymer, Q_{\max} the apparent maximum number of binding sites, K_D the equilibrium dissociation constant, and $[TCAA]$ represents the equilibrium concentration of TCAA. K_D and Q_{\max} were determined from the slope of the straight line and the intercept of the Scatchard plot, and the binding constant (K_a) value was obtained from the reciprocal of the K_D value. Plot of $Q/[TCAA]$ versus Q (see Fig. 4, top right) yielded a straight line with a dissociation constant value (K_d) of 0.094 mM ($K_a = 10.60$ mM⁻¹) and the Q_{\max} value of 18.9 nmol.

The recognition range of the TCAA-MIP-QCM was examined using five structurally related TCAA compounds such as DCAA, MCAA, TBAA, DBAA and MBAA and two non-related TCAA compounds (non-haloacetic acids) such as acetic acid and malonic acid as the substrates. For this purpose, the K_a and Q_{\max} of TCAA-MIP-QCM responding for analogs were determined. The results are collected in Table 1. The results revealed that five HAA analogs have high capability of locating in the TCAA-imprinted cavity compare to both non-haloacetic acids (acetic acid and malonic acid), but their degree of fitting is lower than that of the TCAA template. The specificity of the TCAA-MIP-QCM for each analog was evaluated by measuring the cross-reactivity (CR) (i.e. is the ratio of the frequency shift measured at EC₅₀ (see Section 3.2.2) for analog to that of TCAA). The results are shown in Table 1. As can be seen, CR value of the template was higher than that of other five HAA analogs. Also, there is some cross-reactivity of the TCAA-MIP-QCM with the non-haloacetic acids, malonic acid and acetic acid, but much lower degree than that obtained with HAA analogs. The selectivity profile of the TCAA-MIP-QCM for HAAs and non-haloacetic acids was in order as TCAA > DCAA > TBAA > DBAA > MBAA > MCAA > malonic acid > acetic acid. From the selectivity profile obtained, it seems that the tri- or di-substituted HAAs cross-react more than the mono-substituted HAAs, while the cross-reactivity of chloro-HAA and bromo-HAA analogs with the same degree of halogen substitution is not different. Thus, the recognition of the analogs of TCAA by the TCAA-MIP-QCM is due to a carboxylic group, and that this involves a combination of both size and shape selectivity. It appears that TCAA-MIP-QCM gives %CR value higher than 80% for four out of six HAAs (e.g.

Table 2

Analytical characteristics of the TCAA-MIP-QCM in the QCM-based assay when the QCM-based assay is conducted for a HAA(s) concentration ranging from 0.1 to 100 mg l⁻¹ in de-ionised water (*n* = 3)

Compound	Equation	<i>R</i> ²	EC ₅₀ (mg l ⁻¹)
TCAA	$-\Delta F = -326.47 \log(C) - 102.4$	0.984	4.5
DCAA	$-\Delta F = -318.72 \log(C) + 109.8$	0.990	15
MCAA	$-\Delta F = -289.75 \log(C) + 148.7$	0.997	19
TBAA	$-\Delta F = -312.83 \log(C) + 119.6$	0.986	20
DBAA	$-\Delta F = -316.47 \log(C) + 140.8$	0.992	23
MBAA	$-\Delta F = -292.7 \log(C) + 144.5$	0.996	25
Six HAAs ^a	$-\Delta F = -559.40 \log(C) + 321.7$	0.996	4.5

^a Refers to TCAA, DCAA, MCAA, TBAA, DBAA and MBAA altogether.

DCAA, TBAA, DBAA and MBAA), and CR value between 70% and 60% for one out of six HAAs (e.g. MCAA) and CR value about 20% for non-haloacetic acids, malonic acid and acetic acid. This result suggests that there could be a possibility of inter-anionic competitions for recapture in TCAA binding sites. The mechanism for determination trace HAAs of the TCAA-MIP-QCM electrode may involve in the cooperation and competition of favorable structures of polymer–salt complexes formed between TCAA-MIP and six HAA anions [31]. It is possible that HAAs have similar capability of attaining charge balance in the polyion salts and/or similar supramolecular arrangement within the complex as TCAA, but that TCAA has preference over the HAAs in terms of re-binding.

3.2.2. Analytical characteristics of the TCAA-MIP-QCM in the QCM-based assay of HAAs

Analytical characteristics of the TCAA-MIP-QCM in the QCM-based assay of HAA were examined with a HAA concentration ranging from 0.1 to 100 mg l⁻¹ in de-ionised water. The mathematic data are shown in Table 2. The calibration curves constructed from the frequency shift parameter ($-\Delta F$) dependency provided reasonable results for analysis of TCAA and other five HAA analogs (see Fig. 5). There was a linear relation-

ship between frequency shift responses of the sensor against the logarithm of concentrations ($\log C$) of TCAA and analogs (individually) and the mixture of total six HAAs, *R*² value > 0.98 with the equation shown for each analyte in Table 2. The measured EC₅₀ value is 4.5 mg l⁻¹ for TCAA and about 20 mg l⁻¹ for the other five HAAs (see Table 2), calculated as the analyte concentration for which HAA binding to MIP is inhibited by 50%. The limits of detection (LOD) according to 3*S*_b/*m* criterion, where *m* is the linear calibration and *S*_b estimated as the standard deviation of the signal response for HAAs, were between 20 and 60 µg l⁻¹ for the various HAAs (see the precise value for each compound in Table 3). Detection limits of TCAA and DCAA were in the mid to low µg l⁻¹ range. The WHO has a guideline value for DCAA (50 µg l⁻¹) and TCAA (200 µg l⁻¹) [32], i.e. water samples must not contain these HAAs at concentration above these values. TCAA-MIP-QCM can therefore detect and measure DCAA or TCAA at concentrations below the maximum permitted concentrations. Moreover, the LOD values obtained for TCAA or DBAA analyses were lower than those in the literature using conductivity or amperometry methods (with incorporation of liquid chromatography analysis system) [16], see Table 3. The LOD values for MCAA or DBAA analyses were also lower than those in previous reports using HPLC–UV methods [16]. When compared with the membrane sensor, using a TCAA-imprinted polymer-deposited polyvinyl chloride membrane of a previous study [17], detection limits of HAAs with the QCM sensor were not improved (see Table 3).

For a mixture of HAAs in water samples, the proposed method can be used only for assay of total HAA. The US

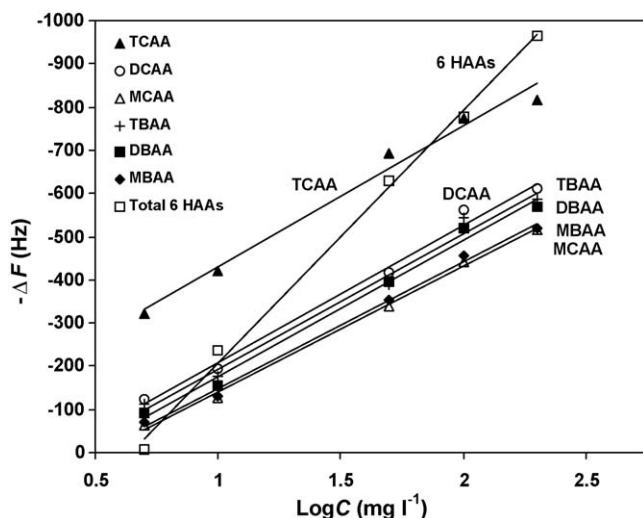


Fig. 5. The calibration plot of frequency shift parameter ($-\Delta F$) vs. added HAA(s) for the TCAA-MIP-QCM in the QCM-based assay of HAAs. Each point represents the average of three independent measurements.

Table 3

Comparison of µg l⁻¹ detection limits obtained for the analysis of haloacetic acids by the QCM and several other published methods

Analyte	QCM ^a	Membrane sensor ^{b,a}	UV ^{c,d}	Conductivity ^{c,d}	Amperometry ^{c,d}
TCAA	50.0	1.0	5.10	80.0	100.0
DCAA	60.0	4.2	8.0	16.0	10.0
MCAA	35.0	4.2	70.0	8.0	1.00
TBAA	26.0	0.2	–	–	–
DBAA	20.0	0.5	90.0	30.0	100.0
MBAA	30.0	5.0	–	–	–

^a An on-line method.

^b Cited from Ref. [17].

^c Cited from Ref. [16].

^d Used in the conjunction with liquid chromatography.

Table 4

Analysis data for HAAs spiked in two brands of commercial bottled water and a municipal tap water with home filtration system by the QCM-based assay

Compound/spiked concentration	Measured ^a , $\mu\text{g l}^{-1}$ after adding HAAs (% recovery)		
	Bottled water from supermarket	Bottled water from local supplier	Municipal tap water ^b
TCAA 0.1 mg l^{-1}	103 \pm 0.9	97 \pm 5.3	104 \pm 1.3
TCAA 10 mg l^{-1}	102 \pm 1.4	99 \pm 1.5	102 \pm 2.9
Total six HAAs ^c 0.12 mg l^{-1} (0.02 mg l^{-1} each)	102 \pm 2.6	99 \pm 1.9	103 \pm 5.4
Total six HAAs ^c 12 mg l^{-1} (2 mg l^{-1} each)	101 \pm 1.4	99 \pm 1.3	97 \pm 1.7

^a Expected concentrations are amounts added plus the amounts already present in the water sample (mean \pm R.S.D., $n = 3$).^b With home filtration system.^c Total six HAAs refers to TCAA, DCAA, MCAA, TBAA, DBAA and MBAA altogether.

Environmental Protection Agency (USEPA) has set a maximum contaminant level of 60 g l^{-1} for the five commonly occurring acids namely TCAA, DCAA, MCAA, DBAA and MBAA in the Stage 1 of the disinfection by-product regulation [33]. The specific sensitivity and selectivity apparent with the six HAAs indicates the possibility of using the TCAA-MIP-QCM as an analysis tool for measuring concentrations of HAA mixtures in drinking water samples. The stability of the TCAA-MIP-QCM is good, in that its analytical performance is unaffected after being stored for more than 1 month at room temperature. The advantages of the method developed in this work are the ease of the automation of the sensor system, the low cost per unit of sensor device as well as the potential to manufacture the sensor on an industrial scale.

3.3. Analysis of drinking water samples

The QCM-based assay has been applied to the group analysis of HAAs in real-life samples. Two brands of commercial bottled water obtained either from a supermarket or local supplier and a municipal tap water with home filtration system were subjected to analysis by this method. Measurement of HAAs by the LLE-GC-ECD method is recommended by the USEPA [34], and assay of samples by this method revealed only TCAA in the samples at concentration levels of 0.8, 1.0 and $1.1 \mu\text{g l}^{-1}$ contained in the bottled-water sample from a supermarket, the bottled-water sample from a local supplier and municipal tap water with home filtration system, respectively. Hence the HAA contents in the water samples were below the detection limit of the sensor described in this present study.

Recovery studies of HAA analyses by the QCM sensor were carried out with the samples after spiking with two different amounts of TCAA standard solution (0.1 and 10 mg l^{-1}) or with the mixtures of six HAAs standard solution (0.02 and 2 mg l^{-1} of each, total 0.12 and 12 mg l^{-1} , respectively). A calibration curve was prepared by dissolving TCAA in de-ionised water to attain the solutions having TCAA (or total six HAAs) concentration between 0.01 and 50 mg l^{-1} and compared to that measured for TCAA alone or the mixture of six HAAs in spiked samples. The analysis data for HAA in spiked water samples by the QCM method are summarized in Table 4. As can be seen, recoveries range between 97% and 104% and %R.S.D. values less than 5.3% were achieved. The result demonstrates the reproducibility

and precision of the assay with the sensor for the analysis of HAAs in drinking water samples.

4. Conclusions

It has been shown that TCAA-MIP-QCM can specially detect the group of HAAs in drinking water, using mass-sensitive measurements. The selectivity of the QCM to HAA analogs is satisfactory. Also, the analytical dynamic range for six HAAs (trichloro-, dichloro-, monochloro-, tribromo-, dibromo-, and monobromo-acetic acids) is large. The limits of detection of HAAs are at present higher than concentrations commonly found in actual drinking water samples, but are well below the maximum permissible levels of HAAs ($60 \mu\text{g l}^{-1}$) in water sample. However, further refinement will undoubtedly improve the limit of detection. It can therefore be concluded that the assay with TCAA-MIP-QCM can be used as a screening method of drinking waters contaminated with HAAs. The proposed method offers fast and cheap measurements.

Acknowledgements

Financial support from the 2005 PSU Collaborative Research Fund of Prince of Songkla University is gratefully acknowledged. The authors would like to thank Prof. L.A. Damani for his useful comments.

References

- [1] S.D. Faust, O.M. Aly, Chemistry of Water Treatment, 2nd ed., Ann Arbor Press, Ann Arbor, MI, 1998.
- [2] D.A. Reckhow, P.C. Singer, R.L. Malcolm, Environ. Sci. Technol. 24 (1990) 1655.
- [3] W. Chen, C. Weisel, J. Am. Water Works Assoc. 90 (1998) 151.
- [4] F.J. Bove, M.C. Fulcomer, J.B. Klotz, J. Esmart, E.M. Dufficy, J.E. Savrin, Am. J. Epidemiol. 141 (1995) 850.
- [5] J.M. Wright, J. Schwartz, D.W. Dockery, Environ. Health Perspect. 112 (2004) 920.
- [6] M.J. Nieuwenhuijsen, M.B. Toledano, N.E. Eaton, P. Elliott, J. Fawell, Occup. Environ. Med. 57 (2000) 73.
- [7] J. Gibbons, S. Laha, Environ. Pollut. 106 (1999) 425.
- [8] M.J. Nieuwenhuijsen, M.B. Toledano, P. Elliott, J. Expo. Anal. Environ. Epidemiol. 10 (2000) 586.
- [9] L.K. Simpson, K.P. Hayes, Water Res. 32 (1998) 1522.
- [10] N.K. Kristiansen, K.T. Aune, M. Froshaug, G. Becher, E. Lundanes, Water Res. 30 (1996) 2155.

- [11] UKDWI, Final Report for Phase 1. Contractor: Metcalf & Eddy Ltd. UKDWI, London, 2002.
- [12] E. Malliarou, C. Collins, N. Graham, M.J. Nieuwenhuijsen, *Water Res.* 39 (2005) 2722.
- [13] B. Paull, L. Barron, *J. Chromatogr. A* 1046 (2004) 1.
- [14] D. Martinez, J. Farre, F. Borrell, M. Calull, J. Ruana, A. Colom, *J. Chromatogr. A* 808 (1998) 229.
- [15] P. Akhtar, C.O. Too, G.G. Wallace, *Anal. Chim. Acta* 341 (1997) 141.
- [16] D. Zielinska, I. Poels, M. Pietraszkiewicz, J. Radecki, H.J. Geise, L.J. Nagels, *J. Chromatogr. A* 915 (2001) 25.
- [17] R. Suedee, T. Srichana, C. Sangpagai, C. Tunthana, P. Vanichapichat, *Anal. Chim. Acta* 504 (2004) 89.
- [18] G. Wulff, Polymer assisted molecular recognition: the current understanding of the molecular imprinting procedure, in: U. Pandit (Ed.), *Bioorganic Chemistry in Healthcare and Technology*, Plenum Press, New York, 1991.
- [19] F.L. Dickert, O. Hayden, *TrAC Anal. Chem.* 18 (1999) 192.
- [20] K. Yano, I. Karube, *TrAC Anal. Chem.* 18 (1999) 199.
- [21] S. Al-Kindy, R. Badia, J.L. Suarez-Rodriguez, M.E. Diaz-Garcia, *Crit. Rev. Anal. Chem.* 30 (2000) 291.
- [22] S.A. Piletsky, E.V. Piletskaya, A.V. Elgersma, K. Yano, I. Karube, *Biosens. Bioelectron.* 10 (1995) 959.
- [23] C.K. Kwan, H. Wei, *Electrical Transport in Solids with Particular Reference to Organic Semiconductors*, Pergamon Press, Oxford, England, 1981.
- [24] F.L. Dickert, K. Halikias, O. Hayden, L. Piu, R. Sikorski, *Sens. Actuators B* 76 (2001) 295.
- [25] G.C. Dunham, N.H. Benson, D. Petelenz, J. Janata, *Anal. Chem.* 67 (1995) 267.
- [26] K. Haupt, N. Krzysztof, K. Wlodzimierz, *Anal. Commun.* 36 (1999) 391.
- [27] C.J. Percival, S. Stanley, A. Braithwaite, M.I. Newton, G. McHale, *Analyst* 127 (2002) 1024.
- [28] B.S. Ebarvia, C.A. Binag, F. Sevilla III, *Talanta* 66 (2005) 145.
- [29] M. Zougagh, A. Rios, M. Valcarcel, *Anal. Chim. Acta* 539 (2005) 117.
- [30] R. Borngreber, J. Hartmann, R. Lucklum, S. Rösler, P. Hauptmann, *Sens. Actuators B* 65 (2000) 273.
- [31] H.M. Yamamoto, J.-I. Yamaura, R. Kato, *J. Am. Chem. Soc.* 120 (1998) 5905.
- [32] WHO, *Guidelines for Drinking-Water Quality. Recommendations*, 3rd ed., 2004.
- [33] USEPA, U.S. Environmental Protection Agency, *Disinfectants and disinfection by products; final rule*, Federal Register 63 (1998) 69478.
- [34] USEPA, *Method 552.3, Environmental Monitoring and System Laboratory*, Cincinnati, OH, 2003.

A simple and sensitive method of nonaqueous capillary electrophoresis with laser-induced native fluorescence detection for the analysis of chelerythrine and sanguinarine in Chinese herbal medicines

Qian Liu, Yingju Liu, Manli Guo, Xubiao Luo, Shouzhao Yao*

State Key Laboratory of Chemo/Biosensing and Chemometrics, College of Chemistry and Chemical Engineering, Hunan University, Changsha 410082, PR China

Received 15 January 2006; received in revised form 15 February 2006; accepted 19 February 2006

Available online 11 April 2006

Abstract

Laser-induced fluorescence (LIF) is a highly sensitive detection method for capillary electrophoresis (CE). However, it usually requires analyte to be derivatized, unless the wavelength of native fluorescence of analyte matches the laser's. That limits its application in drug analysis. In this work, we introduced a rapid, simple and sensitive method of nonaqueous capillary electrophoresis with laser-induced native fluorescence (NACE–LIF) detection for the analysis of chelerythrine and sanguinarine for the first time. As these two alkaloids have some native fluorescence, they were directly detected using a commercially available Ar⁺ laser without troublesome fluorescent derivatization. The fluorescence was enhanced by nonaqueous media. Compared with previously reported UV detection method, lower limit of detection (LOD) is achieved thanks to the high sensitivity of LIF detection (2.0 ng/mL for chelerythrine and 6.3 ng/mL for sanguinarine). Moreover, with NACE, the baseline separation of these alkaloids is finished within 3.5 min. This method is successfully applied to determine the contents of chelerythrine and sanguinarine in *Macleaya cordata* (Willd.) R. Br. and *Chelidonium majus* L.

© 2006 Elsevier B.V. All rights reserved.

Keywords: Chelerythrine; Sanguinarine; Chinese herbal medicine; Nonaqueous capillary electrophoresis; Laser-induced native fluorescence

1. Introduction

Laser-induced fluorescence (LIF) is one of the most sensitive detection methods of capillary electrophoresis (CE), whose limit of detection (LOD) can easily reach attomole to zeptomole levels and even single molecule [1]. Generally, to reach maximum sensitivity, the fluorescence wavelength of analyte is required to match that of the laser. However, there are only a few wavelengths provided by commercially available lasers, such as He–Ne laser (544, 593 and 633 nm), He–Cd laser (320 and 442 nm) and Ar ion laser (275 and 488 nm) [2]. Most drugs lack native fluorescence, or lack a suitable laser to induce their native fluorescence. Therefore, it becomes a common trend to chemically derivatize the drugs with a fluorescent label to make them detectable. But fluorescent derivatization is usually time-consuming due to the slow kinetics of the derivatization reaction

[3]. And lots of drugs including most alkaloids can still not be derivatized well due to the lack of a reaction group or proper fluorescent label. Especially for drug analysis in plants, derivatization is not a wise choice due to the complicated matrix of ingredients. These drawbacks greatly limit the application of LIF detection. However, in our work, we found that although the native fluorescence of some drugs does not perfectly match the laser's wavelength, very low LOD can still be achieved due to the high sensitivity of LIF detection, for instance, chelerythrine and sanguinarine. Properly utilizing the native fluorescence of the analyte can avoid the troublesome fluorescent derivatization.

Chelerythrine and sanguinarine (Fig. 1), the most important members of quaternary benzo[c]phenanthridinium alkaloids, always coexist in plants such as Chinese herbal medicine *Macleaya cordata* (Willd.) R. Br. and *Chelidonium majus* L. They exhibit various bioactivities such as anti-inflammatory [4], antitumor [5], SH-enzymes inhibition [6] and antiplatelet effect [7]. While they also show enormous toxicity when being used at relatively high concentration [8]. To better exploit and safely

* Corresponding author. Fax: +86 731 8821848.

E-mail address: szyao@hnu.cn (S. Yao).

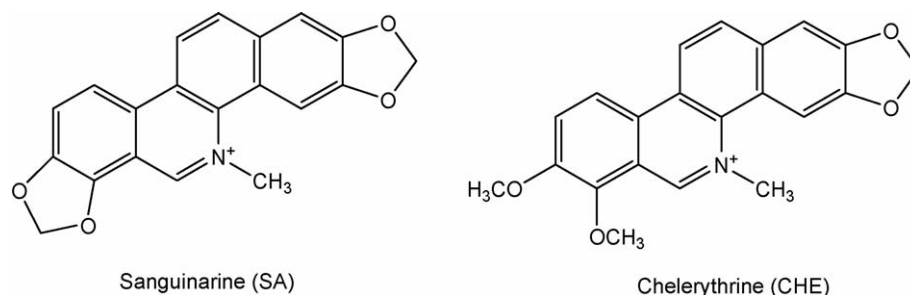


Fig. 1. Structures of chelerythrine (CHE) and sanguinarine (SA).

utilize these plants, several methods have been developed to analyze chelerythrine and sanguinarine in plants [9–12]. Fluorescence detection [13] and electrospray mass spectrometry (ESI-MS) [14] have been coupled to high-performance liquid chromatography (HPLC) to determine sanguinarine and chelerythrine, which were sensitive but uneconomical and rather time-consuming. CE with UV detection has also been applied to analyze these alkaloids [15,16], and study their acid–base properties [17] and interactions with molecules containing mercapto group [18,19]. However, UV detection cannot offer a satisfactory sensitivity without preconcentration. To our best knowledge, there have been no reports about the analysis of these alkaloids using CE–LIF due to the lack of a proper fluorescent label or detector. In addition, owing to its high resolving power and short analysis time, nonaqueous capillary electrophoresis (NACE) has been widely used as an attractive method for the analysis of active ingredient in plants. Therefore, in this work, we introduced a rapid, simple and sensitive method of NACE with LIF detection for the analysis of chelerythrine and sanguinarine in Chinese herbal medicine skillfully using the native fluorescence of these alkaloids for the first time.

2. Materials and methods

2.1. Apparatus

CE was performed on a Beckman P/ACE MDQ capillary electrophoresis system (Beckman Instruments, Fullerton, CA, USA) with 488 nm Ar⁺ laser module controlled by 32 Karat software. A fused-silica capillary (Yongnian Photoconductive Fiber Factory, Hebei, China) of 30 cm (20 cm to the detector) \times 75 μ m i.d. was used for separation. The virgin capillary was conditioned by rinsing with 0.1 M NaOH for 10 min, water for 2 min, and then buffer for 5 min. Before each run, the capillary was rinsed with buffer for 3 min. The buffer was renewed after every five runs to ensure good reproducibility. Samples were injected from the anode end of the capillary with a pressure of 0.5 psi for 5 s. The capillary was thermostated at 25 °C. All solutions were filtered through a 0.22 μ m pore size membrane filter before use.

The fluorescence spectra were recorded using a Hitachi module F-4500 fluorescence spectrophotometer. The excitation wavelength was fixed at 488 nm, and the emission wavelength scanned from 500 to 700 nm.

2.2. Reagents

Chelerythrine and sanguinarine were obtained from Chemistry and Chemical Engineering College, Hunan Normal University (Changsha, China). Ammonium acetate and acetic acid were purchased from Antai Ltd. (Changsha, China). Methanol was from Merck Co. (Darmstadt, Germany) and acetonitrile (ACN) was from Tedia Co. (Fairfield, OH, USA). *M. cordata* (Willd.) R. Br. and *C. majus* L. were purchased from the National Institute for the Control of Pharmaceutical and Biological Products (Beijing, China). All reagents were of analytical grade.

2.3. Sample preparation

Stock solutions of chelerythrine and sanguinarine (1000 mg/L) were prepared in methanol. Solutions of lower concentration were prepared by dilution of the stock solutions with the proper running buffer. The running buffer solutions were prepared by mixing 2.0 mL of 200 mM ammonium acetate, 0.5 mL acetic acid and 5.0 mL ACN in a 10 mL volumetric flask and then being diluted to volume with methanol.

The powdered total grass (1.0 g) of *M. cordata* (Willd.) R. Br. and *C. majus* L. were extracted with 10.0 mL methanol for 30 min in an ultrasonic bath. After centrifugation, the extract was collected and the residues were extracted for another two times. The extracts were combined together and then diluted to 50 mL with methanol as stock solution. When injected into the capillary, 0.1 mL stock solutions were diluted to 1.0 mL with the proper running buffer as sample solutions.

3. Results and discussion

3.1. Fluorescence emission spectra of chelerythrine and sanguinarine

The fluorescence emission spectra of chelerythrine and sanguinarine were firstly investigated to estimate the feasibility of this method. The $\lambda_{\text{ex}}/\lambda_{\text{em}}$ (maximum excitation and emission wavelength) of chelerythrine and sanguinarine are 294/407 and 299/408 nm, respectively. To reach maximum sensitivity, the $\lambda_{\text{ex}}/\lambda_{\text{em}}$ of analyte should match that of detector [20]. However, there are no commercially available lasers that can offer such wavelengths, and these alkaloids are difficult to derivatized

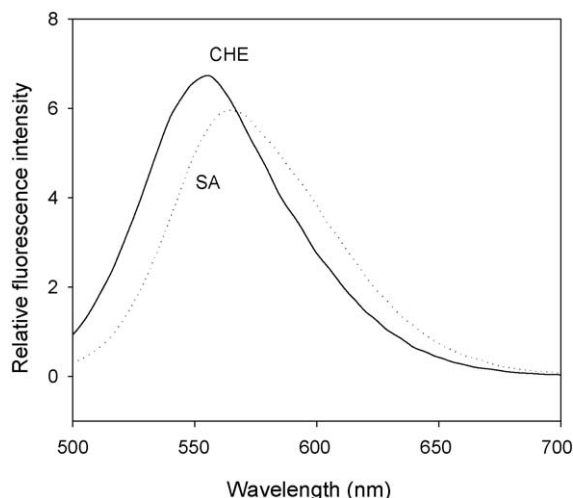


Fig. 2. Fluorescence emission spectra of chelerythrine and sanguinarine in the running buffer. Analyte concentration: 25 $\mu\text{g/mL}$; excitation wavelength: 488 nm; scan rate: 2400 nm/min.

either. As a result, there has been no report about their analysis by CE–LIF. In our work, we found that chelerythrine and sanguinarine can produce fluorescence at 520 nm when being excited at 488 nm. So it is possible to use a 488 nm Ar^+ laser to detect them in CE. As shown in Fig. 2, chelerythrine and sanguinarine exhibit two bands around 556 and 564 nm when being excited at 488 nm, respectively. Their relative fluorescence intensity at 520 nm, i.e., the detection wavelength of the working Ar^+ laser, is also sufficiently high. Due to the high sensitivity of LIF detection, even a tiny fluorescence can be easily detected in CE. Therefore, although the wavelength of native fluorescence of these alkaloids does not perfectly match that of the detector, we try to directly detect them without fluorescent derivatization in CE–LIF.

3.2. Fluorescence in different solvents and electrolytes

To select a suitable BGE solvent, the fluorescence of chelerythrine and sanguinarine in several organic solvents was investigated, such as methanol (MeOH), ACN, ethanol (EtOH), *N,N*-dimethylformamide (DMF) and dimethylsulfoxide (DMSO). It was found that the most intensive fluorescence can be obtained in methanol. Considering that adding dipolar aprotic ACN into amphiprotic methanol is particularly favorable to shorten analysis time and achieve high selectivity by adjustment of BGE composition in NACE [21,22], we try to use methanol containing ACN as the BGE solvent. Therefore, we further investigated the fluorescence intensity of the analytes in the methanol containing different concentrations of ACN. It is found that more fluorescence can be obtained in pure methanol or ACN than in the mixture. That may be related to the co-solvent effect. The detailed optimization of ACN concentration will be discussed in the following CE experiments.

Then, we investigated the fluorescence intensity of the analytes in the presence of different electrolytes used mostly in CE, including ammonium acetate, borax and tris(hydroxymethyl)

aminomethane (Tris). Phosphate is excluded due to its poor solubility in methanol or ACN. The analytes were dissolved in methanol solution containing 50 mM electrolyte, and then the relative fluorescence intensity was determined. It was found that the fluorescence of chelerythrine is the most intensive in acetate solution, while sanguinarine fluoresces strongest in borax solution. Considering that ammonium acetate has the best compatibility and excellent solubility in methanol, it is adopted.

3.3. Optimization of NACE and LIF detection conditions

3.3.1. Effect of ACN concentration

The effect of ACN concentration was firstly investigated. Pure methanol or ACN are excluded, because pure methanol will result in long separation time due to the low dielectric constant-to-viscosity ratio, while pure ACN will cause low solubility of ammonium acetate. It was observed that the migration time decreases with the increase of the ACN concentration due to the increase of dielectric constant-to-viscosity ratio. However, at the concentration of >50% (v/v), the migration time changes slightly. Moreover, ACN at high concentration may cause low peak intensity and current breakdown during the separation due to bubble formation in running buffer [23]. Therefore, 50% (v/v) ACN is selected.

3.3.2. Effect of pH^*

It is general knowledge that the pH in NACE is different from that in aqueous CE. In practice, the pH in nonaqueous media is usually measured by using an all-aqueous pH-meter consisting of aqueous calibration buffer and aqueous reference electrode filling solution [24]. This resulted pH value is called apparent pH (pH^*). In this work, the pH of BGE was adjusted by acetic acid, and the pH^* was used to indicate the buffer pH. As shown in Fig. 3, with the decrease of pH^* from 8.3 to 5.6, the migration time decreases while the peak intensity increases dramatically. Simultaneously, the peak shape becomes better and the peak broadening is diminishing. Obviously, the pH of BGE greatly affects the separation performance mainly due to its modification of electroosmotic flow (EOF). At the pH^* smaller than 5.6, the migration time and peak intensity alter slightly. Therefore, pH^* 5.6 is adopted as the optimum.

3.3.3. Effect of ammonium acetate concentration

As electrolyte greatly affects the separation parameters such as Joule heating, running current and mobility of analyte, the effect of ammonium acetate concentration on the mobility and peak intensity of the analytes was investigated from 10 to 60 mM. It was observed that migration time increases with the increase of ammonium acetate concentration due to the increase of ionic strength that hinders the analytes transferring in the capillary. While the peak intensity of the analytes increases significantly with the increase of electrolyte concentration, mainly due to the suppression of adsorption of the analytes on the capillary wall. To compromise between shorter analysis time and stronger detection signal, 40 mM is selected as the appropriate electrolyte concentration.

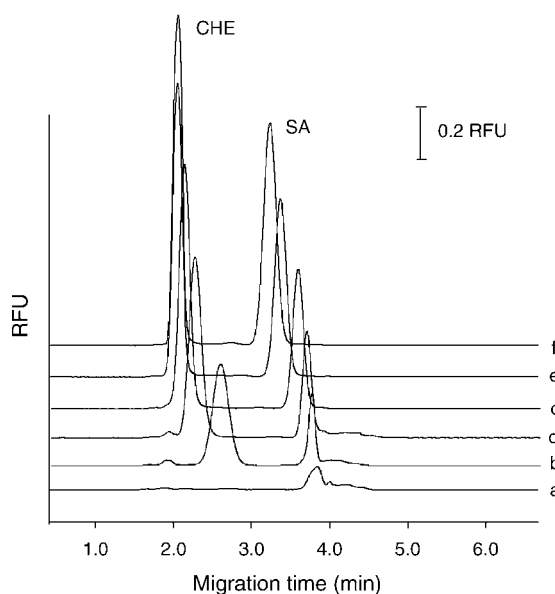


Fig. 3. Effect of pH on the separation of chelerythrine and sanguinarine. Buffer: 40 mM ammonium acetate + 50% (v/v) ACN (pH^{*} 8.3 (a), 6.7 (b), 6.3 (c), 6.0 (d), 5.8 (e) and 5.6 (f)); separation capillary: uncoated fused-silica of 30.0 cm (20.0 cm to the detector) \times 75 μ m i.d.; applied voltage: 10 kV; cartridge temperature: 25.0 $^{\circ}$ C; injection: 0.5 psi for 5 s. RFU, relative fluorescence intensity unit.

3.3.4. Effect of applied voltage

The effects of applied voltage on the mobility and running current were also investigated in the range of 6–13 kV. Higher applied voltage results in shorter migration time as expected. At the same time, the running current increases linearly with the increase of applied voltage, which will produce more Joule heat during the separation. To obtain shorter analysis time and better stability, 10 kV applied voltage is adopted.

Accordingly, when the buffer consists of 40 mM ammonium acetate and 50% (v/v) ACN in methanol (pH^{*} 5.6), and the applied voltage is 10 kV, the separation shows the best performance. A typical electropherogram for a standard mixed solution

of chelerythrine and sanguinarine under the optimum conditions is shown in Fig. 4A. The baseline separation is completed within 3.5 min.

3.4. Linearity, reproducibility and LOD

The linearity and LOD of chelerythrine and sanguinarine are listed in Table 1. Over extensive concentration ranges, the peak area of analyte shows excellent linear behavior with the concentration. The relative standard deviations (R.S.D., $n=5$) of the migration time and the peak area are 0.55 and 0.60% for chelerythrine, and 1.19 and 1.45% for sanguinarine, respectively.

3.5. Comparison with other methods

Table 2 shows the performance of other four methods on these alkaloids. NACE–LIF shows a total superiority in sensitivity and linearity over HPLC–UV [12] and CE–UV [16]. Much lower LOD and wider linear range can be obtained by LIF detection than UV detection. HPLC–fluorescence detection [13] and HPLC–ESI–MS [14] are somewhat more sensitive than NACE–LIF, but NACE–LIF is much more rapid, and its consumption of materials is much lower. In addition, in HPLC and aqueous CE methods, the peaks of chelerythrine and sanguinarine are often tailed and their peak shapes are not symmetrical. NACE can greatly improve the peak shapes due to its suppression of hydrolysis of the analytes.

3.6. Interference of other substances

To better study the selectivity of this method, much possible interference of other substances on the determination of chelerythrine and sanguinarine was investigated. These substances include some alkaloids, vitamins and flavonoids. The interferent of 0.1 mg/mL is added into the standard mixed sample of chelerythrine and sanguinarine, and then runs for 5 min under above optimum conditions. The interference factor α is defined

Table 1
Results of regression analysis on calibration curves and detection limits

Analyte	Regression equation, $Y = a + bC^a$	Correlation coefficient	Linearity range (ng/mL)	LOD (ng/mL) ^b
Chelerythrine	$Y = 3.278 \times 10^4 + 91.66C$	0.9998	$25-5 \times 10^4$	2.0
Sanguinarine	$Y = 2.307 \times 10^4 + 79.26C$	0.9999	$50-5 \times 10^4$	6.3

^a Y and C stand for the peak area and the concentration (ng/mL) of the analyte, respectively.

^b The LOD was defined as the concentration where the signal-to-noise ratio was 3.

Table 2
Linearity and LOD obtained for chelerythrine and sanguinarine by other methods

Method	Linear range		LOD		Analysis time (min)
	Chelerythrine	Sanguinarine	Chelerythrine	Sanguinarine	
HPLC–UV [12]	–	0.01–1.0 mg/g	–	5 μ g/g	≈ 6
HPLC–fluorescence detection [13]	–	10^{-8} to 10^{-5} M	–	3 nM	≈ 16
HPLC–ESI–MS [14]	3.75–750 ng/mL	5.25–1050 ng/mL	1.11 ng/mL	1.60 ng/mL	≈ 8
CE–UV [16]	20–500 μ M	20–500 μ M	2.4 μ M	3.0 μ M	≈ 5

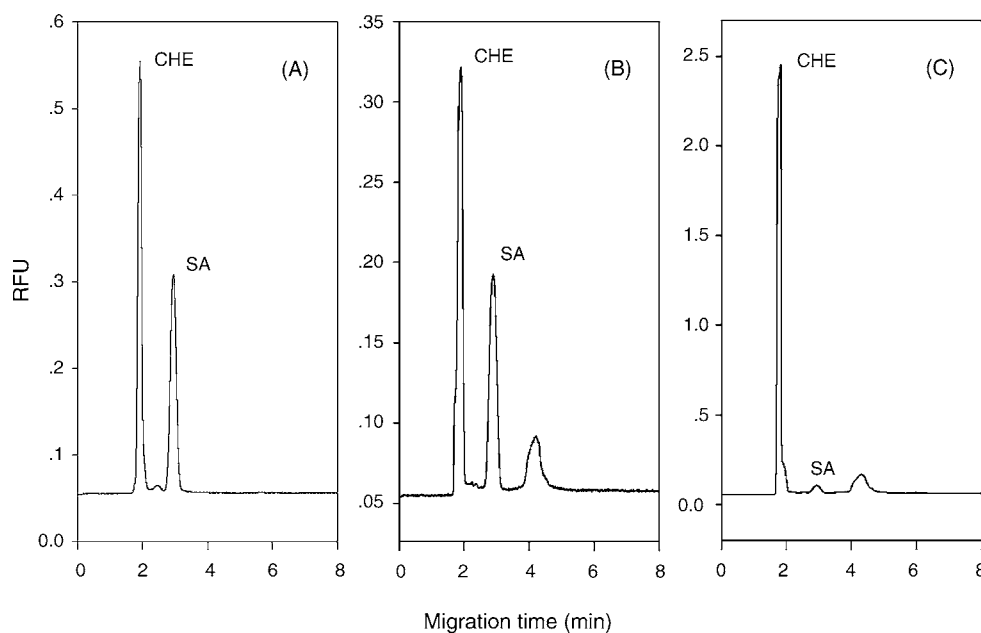


Fig. 4. Electropherograms of standard mixed solution and real samples: (A) standard mixed solution; (B) *Macleaya cordata* (Willd.) R. Br.; (C) *Chelidonium majus* L. Buffer: 40 mM ammonium acetate + 50% (v/v) ACN (pH^{*} 5.6); current: 32.5 μ A; other conditions as in Fig. 3.

as follows [25]:

$$\alpha = \frac{\Delta t}{t}$$

where Δt is the difference of migration time between analyte and interferent and t is the migration time of analyte. The α_1 and α_2 stand for the interference factors of chelerythrine and sanguinarine, respectively. It was found that no peak was observed for the most tested substances, such as thiamine, ascorbic acid, nicotinamide, coumarin, hesperidin, aconitine, anisodamine, brucine, geniposide and choline. For the substances such as quercetin, berberine and cinchonine, the values of α_1 and α_2 are in the range of 0.079–0.994 and 0.055–0.388, respectively. Obviously, there is no significant interference caused by these substances,

indicating that the selectivity of this method is excellent in this work.

3.7. Application and recovery

The typical electropherograms of *M. cordata* (Willd.) R. Br. and *C. majus* L. sample are shown in Fig. 4B and C. The peaks are identified by comparison with previously obtained migration times and using standard addition method. Generally, due to the complicated matrix of ingredients in Chinese herbal medicine, fluorescent derivatization may bring interference and unknown peaks. This method utilizes the native fluorescence of the analytes and requires no derivatization, which eliminates lots of potential interference. As shown in Fig. 4B and C, few unknown

Table 3
Determination of the recovery for this method ($n = 3$)

Sample	Base value (μg/mL)	Quantity added (μg/mL)	Quantity found (μg/mL)	Mean recovery (%)
<i>Macleaya cordata</i> (Willd.) R. Br.				
Chelerythrine	2.59	10.0	12.4 ± 0.6	97.7 ± 4.2
		5.0	7.5 ± 0.3	
		2.5	4.9 ± 0.2	
Sanguinarine	2.49	10.0	12.9 ± 0.5	99.3 ± 2.9
		5.0	7.4 ± 0.2	
		2.5	4.8 ± 0.1	
<i>Chelidonium majus</i> L.				
Chelerythrine	25.3	25.0	53.0 ± 2.3	101.7 ± 3.1
		10.0	35.6 ± 0.6	
		5.0	30.0 ± 0.9	
Sanguinarine	0.69	1.00	1.64 ± 0.09	94.2 ± 4.8
		0.50	1.12 ± 0.07	
		0.25	0.86 ± 0.03	

peaks can be found in the electropherograms due to the good selectivity of this method.

The contents of chelerythrine and sanguinarine found in these Chinese herbal medicines are 129.6 ± 4.52 and 124.7 ± 3.51 mg/kg for *M. cordata* (Willd.) R. Br., and 1266.7 ± 7.14 and 34.3 ± 4.01 mg/kg for *C. majus* L., respectively. To evaluate the accuracy of this method, the recovery was studied by previously reported means [21,26]. Shortly, chelerythrine and sanguinarine standard solutions of different concentrations were added into the samples, and then were analyzed using the proposed method. Results are listed in Table 3. From it we can find that the results are satisfactory.

4. Conclusion

A rapid and sensitive NACE–LIF method was proposed for the simultaneous determination of chelerythrine and sanguinarine in Chinese herbal medicines. This method skillfully utilizes the native fluorescence of the analytes and requires no fluorescent derivatization. Although the fluorescence wavelength of the analytes does not perfectly match that of detector, very low LOD can still be achieved without any preconcentration steps due to the high sensitivity of LIF detection. Moreover, the fluorescence of the analytes can be enhanced in nonaqueous media. This method was successfully applied to the analysis of Chinese herbal medicine *M. cordata* (Willd.) R. Br. and *C. majus* L. Results show that it is a simple, high-efficient and economical method for the analysis of these alkaloids. This paper also proposes a new idea for CE analysis of drugs that fluoresces to some degree. Even though the native fluorescence of some drugs does not perfectly match the laser's wavelength, LIF detection can still be successfully used.

Acknowledgements

This work was supported by the Research Fund for the Doctoral Program of Higher Education (No. 20030523017) and the National Natural Science Foundation of China (No. 20335020).

References

- [1] Y.H. Lee, R.G. Maus, B.W. Smith, J.D. Winefordner, Anal. Chem. 66 (1994) 4142–4149.
- [2] Y.W. Lin, T.C. Chiu, H.T. Chang, J. Chromatogr. B 793 (2003) 37–48.
- [3] S.K. Lau, F. Zaccardo, M. Little, P. Banks, J. Chromatogr. A 809 (1998) 203–210.
- [4] J. Lenfeld, M. Kroutil, E. Maršálek, J. Slavík, V. Preininger, V. Šimánek, Planta Med. 43 (1981) 161–165.
- [5] M.L. Colombo, E. Bosio, Pharmacol. Res. 33 (1996) 127–134.
- [6] J.M. Herbert, J.M. Augereau, J. Gleye, J.P. Maffrand, Biochem. Biophys. Res. Commun. 172 (1990) 993–999.
- [7] D. Walterová, J. Ulrichová, I. Válka, J. Vičar, C. Vavrečková, E. Táborská, R.J. Harkrader, D.L. Meyer, H. Černá, V. Šimánek, Acta Univ. Palacki Olomuc Fac. Med. 139 (1995) 7–16.
- [8] M. Das, S.K. Khanna, Crit. Rev. Toxicol. 27 (1997) 273–297.
- [9] P. Balderstone, S.F. Dyke, J. Chromatogr. 132 (1977) 359–362.
- [10] D. Walterová, Z. Stránský, V. Preininger, V. Šimánek, Electrophoresis 6 (1985) 128–132.
- [11] C. Bugatti, M.L. Colombo, F. Tomè, J. Chromatogr. 393 (1987) 312–316.
- [12] S. Husain, R. Narsimha, R.N. Rao, J. Chromatogr. A 863 (1999) 123–126.
- [13] P. Kosina, J. Ševčík, M. Modrianský, A. Gavenda, P. Bednář, P. Barták, D. Walterová, J. Ulrichová, J. Sep. Sci. 26 (2003) 679–685.
- [14] X. Luo, B. Chen, S. Yao, Chromatographia 60 (2004) 347–351.
- [15] H. Stuppner, M. Ganzer, J. Chromatogr. A 717 (1995) 271–277.
- [16] J. Ševčík, J. Vičar, J. Ulrichová, I. Válka, K. Lemr, V. Šimánek, J. Chromatogr. A 866 (2000) 293–298.
- [17] M. Vlčková, P. Barták, V. Kubáň, J. Chromatogr. A 1040 (2004) 141–145.
- [18] R. Vespalec, P. Barták, V. Šimánek, M. Vlčková, J. Chromatogr. B 797 (2003) 357–366.
- [19] P. Barták, V. Šimánek, M. Vlčková, J. Ulrichová, R. Vespalec, J. Phys. Org. Chem. 16 (2003) 803–810.
- [20] X. Páez, L. Hernández, Biopharm. Drug Dispos. 22 (2001) 273–289.
- [21] Y. Li, S. Qi, X. Chen, Z. Hu, Electrophoresis 25 (2004) 3003–3009.
- [22] M.-L. Riekkola, Electrophoresis 23 (2002) 3865–3883.
- [23] Y. Li, S. Qi, X. Guo, Z. Hu, Talanta 65 (2005) 15–20.
- [24] S.P. Porras, E. Kenndler, J. Chromatogr. A 1037 (2004) 455–465.
- [25] S. Liu, Y. Liu, J. Li, M. Guo, W. Pan, S. Yao, Talanta 69 (2006) 154–159.
- [26] S. Cherkaoui, K. Bekkouche, P. Christen, J.L. Veuthey, J. Chromatogr. A 922 (2001) 321–328.

Short communication

Purification and determination of stachyose in Chinese artichoke (*Stachys Sieboldii* Miq.) by high-performance liquid chromatography with evaporative light scattering detection

Junfa Yin^a, Gengliang Yang^{a,b,*}, Sumin Wang^b, Yi Chen^a^a Beijing National Laboratory for Molecular Sciences, Laboratory of Analytical Chemistry for Life Science, Institute of Chemistry, Chinese Academy of Sciences, Beijing 100080, China^b College of Pharmacy, Hebei University, Baoding 071002, China

Received 12 January 2006; received in revised form 10 March 2006; accepted 13 March 2006

Available online 18 April 2006

Abstract

A high-performance liquid chromatography (HPLC) method with evaporative light scattering detection (ELSD) was applied for simultaneous determination of stachyose, sucrose and raffinose in Chinese artichoke (*Stachys Sieboldii* Miq.). Carbohydrates were separated on a Bondapak NH₂ column using a ternary solvent mixture of methanol–acetonitrile–water (55:25:20, v/v/v) as mobile phase. Two different crafts (method 1 and method 2) for extraction and purification of stachyose in Chinese artichoke tubers were detailed and evaluated. Method 1 can meet the purpose of quantification and method 2 is appropriate for the purpose of purification. The content of stachyose in dry tubers was determined to be 236.0 mg/g (from method 1) and the purity of the extracted stachyose flour was calculated to be 87.34% (from method 2), respectively. The analytical method fulfills all the standard requirements of linearity, accuracy and precision. Therefore, it is suitable for purification and routine quantification of stachyose in Chinese artichoke.

© 2006 Elsevier B.V. All rights reserved.

Keywords: Stachyose; Chinese artichoke (*Stachys Sieboldii* Miq.); Evaporative light scattering detection (ELSD); Carbohydrates

1. Introduction

Stachyose, a tetrasaccharide consisting of two galactoses, a glucose and a fructose, can reportedly stimulate the growth of bifidobacteria in the human intestine and protect the function of organs eliminating harmful substances [1,2]. Since it cannot be digested nor absorbed, stachyose is also regarded as a potential substitute for sugar for diabetes patients. Foods and herbs containing oligosaccharides (such as raffinose and stachyose) are approved as the special health care foods in many countries. Stachyose is the main storage oligosaccharide in the tubers of the Chinese artichoke (*Stachys Sieboldii* Miq.). As good sources of oligosaccharides, proteins, and water-soluble vitamins, Chinese artichoke makes a major contribution to human nutrition.

Generally, carbohydrates lack chromophoric and fluorophoric groups which were necessary for UV and fluorescence

detection. Therefore, determination of stachyose by HPLC or capillary electrophoresis (CE) method suffers from disturbances of solvents and the impurities, due to the low-wavelength UV adsorption (approximately 190 nm) of stachyose. The conventional methods for the determination of stachyose in many grain legumes and food products involve the separations on ion-exchange, reverse-phase and porous graphitized carbon stationary phases or fused silica capillary with refractive index (RI) and electrochemical detectors (ECD) [3–12]. However, it has many disadvantages for RI detection such as lacking sensitivity and selectivity, depending on temperature and flow rate, and incompatibility with gradient elution [10,13]. Similarly, ECD detection is much dependent on the conditions such as composition and flow rate of mobile phase and temperature.

The evaporative light scattering detector (ELSD) is not plagued by these limitations. Since the detection is based on the universal ability of particles to cause photon scattering, ELSD can detect most compounds less volatile than the mobile phase, not relying on the optical properties of the analytes [10–19]. Furthermore, for this kind of mass detector, baseline drift caused by

* Corresponding author. Tel.: +86 10 82627290; fax: +86 10 62559373.
E-mail address: glyang@iccas.ac.cn (G. Yang).

mobile phase and temperature effects can be avoided. In terms of these merits, HPLC–ELSD has been proposed to be good protocols for screening carbohydrates in real samples such as plants, foods and drink products [10,13,20,21].

This paper describes the simultaneous determination of stachyose, sucrose and raffinose in Chinese artichoke by HPLC–ELSD method. Two different crafts for extraction and purification of stachyose in the tubers of the Chinese artichoke were designed and evaluated.

2. Experimental

2.1. Reagent and standard solutions

Analytical grade stachyose, sucrose and raffinose (all contents >99%) were purchased from Sigma–Aldrich (Missouri, USA). The dried powder of Chinese artichoke tubers was donated by Anguo Pharmaceutical Inc. (Baoding, China). Anion-exchange resin (D900) and cation-exchange resin (D152) were purchase from Bon Chemical Inc. (Cangzhou, China). HPLC-grade methanol and acetonitrile were purchased from Fisher (New Jersey, USA). DI water was prepared from a Millipore system (resistivity 18.2 MΩ cm).

Stock standard solutions of stachyose, sucrose and raffinose at a concentration of 2.0 mg/mL were prepared in DI water and stored at 4 °C in the refrigerator. Working standard solutions were prepared as needed by appropriate dilution of the stock solutions in water. All sample solutions were filtered through a 0.45 μm Millipore membrane filter before use.

2.2. Apparatus

The chromatographic system consists of a PU-1580 pump (JASCO, Japan), a SEDEX-75 evaporative light scattering detector (SEDERE, France), and a Rheodyne 7725i injector equipped with a 20-μL loop. A CS501-SP thermostat (Sida Experimentation Apparatus, China) was used to control the analytical temperature. Data processing was carried out with a HW2000 chromatography workstation (Qianpu Software, China).

2.3. Extraction and purification

The crushed tubers of Chinese artichoke were ground into powder. Two different extraction and purification methods were designed according to the reported oligosaccharide extraction procedure [10,22–24].

2.3.1. Method 1

Dried powder (5.0 g) was put into 50 mL of chloroform and then heated to reflux for 2 h. Solvent was removed by filtration and the defatted powdered residue was then extracted with 50 mL sodium carbonate aqueous solution (0.1 M) twice at a 60 °C bath for 4 h. The extracts were collected and combined. After that, 1 mL of trichloroacetic acid (TCA) was added to this combined extract, following stirred at room temperature for 1 h. The extract was kept in a refrigerator overnight to allow the deposition of proteins and other organic colloids. After centrifugal

sedimentation (3000 rpm), the supernatant fluid was collected and then was concentrated to 25 mL by reduced pressure distillation. Four volumes of ice-cold acetone were added to the culture supernatant, and carbohydrates were precipitated at 4 °C for 12 h. Off-white flour of the carbohydrates was obtained by filtration and then dried in a vacuum oven at 60 °C overnight. For HPLC analysis, 5.0 mg of the resulting dry flour was dissolved into 10.0 mL water and then stored in a refrigerator at 4 °C. This sample was labeled *Sample 1*.

2.3.2. Method 2

Dried powder (5.0 g) of Chinese artichoke tubers was directly extracted with 50 mL calcium hydroxide aqueous solution (0.20 M) twice for each 4 h. The extracts were combined and then neutralized with oxalic acid. After centrifugal sedimentation (3000 rpm), the supernatant flowed through active carbon column (50 cm × 2.0 cm i.d.). The outflow solution was concentrated to 25 mL and then loaded on a D900 anion-exchange resin column (100 cm × 3.6 cm i.d.). Selective washing solutions such as methanol, series of methanol–water (volume proportion from 95:5 to 85:15) were employed so that most matrixes and some uninterested carbohydrates could be eluted into the waste rinses. Then the analytes were eluted with 50 mL × 4 methanol–HCl aqueous solutions (75:25), which pH ranged from 6.4 to 3.2. These eluted fragments were concentrated and then loaded onto D152 cation-exchange resin column (100 cm × 3.6 cm i.d.) and sequentially eluted with methanol–water (50:50). The eluents were combined and then concentrated to 25 mL by reduced pressure distillation. Off-white powder of the carbohydrates was obtained by adding mixture of methanol and ethanol, filtration and drying in sequence, being similar to method 1. Finally, 5.0 mg of the resulting dry flour was dissolved into 10.0 mL water and stored in a refrigerator for further analysis. This sample was labeled as *Sample 2*.

2.4. HPLC analysis

Performance characteristics (i.e. precision, calibration curve, detection limit and accuracy) of the proposed method were measured on HPLC using a Bondapak NH₂ column (300 mm × 3.9 mm i.d., 5 μm, Waters, USA) with 10 μL-sample injections at 30 °C. A ternary solvent mixture of methanol–acetonitrile–water (55:25:20, v/v/v) was used as mobile phase and measurements were performed at a flow rate of 1.0 mL/min. ELSD used nitrogen as nebulizing gas at a flow rate 4.0 mL/min, and the temperature of drift tube was fixed at 40 °C. Retention factors were calculated from the equation $k = (t_R - t_0)/t_0$, where t_R is the retention time of retained analytes and t_0 is the retention time of the void marker (0.1 mg/mL NaCl).

3. Results and discussion

3.1. HPLC analysis

The content of water in mobile phase showed a great effect on the retention of the carbohydrates. Retention times of the carbohydrates were decreased with the increase of water in the

mobile phase. Decrease of water in mobile phase could get longer retention times of the carbohydrates, but the peaks in the chromatogram became broad and asymmetric when the content of water was below 10% (v/v). By testing several solvent systems, a ternary solvent mixture methanol–acetonitrile–water (55:25:20, v/v/v) with a flow rate of 1.0 mL/min was selected, which the retention times were 6.6 min for sucrose, 8.4 min for raffinose and 13.5 min for stachyose, respectively. To be mentioned, when column temperature or mobile phase changed within a small range, the baseline still remained flat and stable and the responses of the carbohydrates were not obviously influenced. Thus on-line RI detection, which would lead to a fluctuant baseline and varied responses at the same conditions.

Under the selected conditions, 10 μ L of the standard mixed solution and purified extracts obtained by methods 1 and 2 (i.e. Samples 1 and 2) were individually injected into the HPLC system at a temperature of 30 °C. Fig. 1(A) represented the chromatograms of stachyose, sucrose and raffinose in a standard mixture (0.2 mg/mL for each sugar). Results indicated that the Bondapak NH₂ column could provide good separation of stachyose, sucrose and raffinose from the extracts eluted within

15 min, and no other interfering peaks presented near the analyte peaks. The retention factors were 5.68 for stachyose, 2.34 for sucrose and 3.15 for raffinose, respectively.

Fig. 1(B and C) represented the chromatograms of Samples 1 and 2, which were obtained from different extraction and purification methods. According to the relationship in double logarithmic of peak areas versus sample concentrations, the contents of the sugars in dry tubers of Chinese artichoke could be calculated. The content of stachyose in the dry tubers and the purity in the extracted flour were 236.0 mg/g and 58.55% for Sample 1, and 194.6 mg/g and 87.34% for Sample 2, respectively.

3.2. Method development and validation

The proposed HPLC–ELSD method showed good sensitivities and linear responses to the studied carbohydrates, which were good enough to quantify them.

Calibration curves were obtained by injecting each working standard solution (10 μ L) of stachyose (0.05, 0.1, 0.2, 0.5, 0.8 and 1.0 mg/mL), sucrose (0.02, 0.05, 0.1, 0.2 and 0.5 mg/mL)

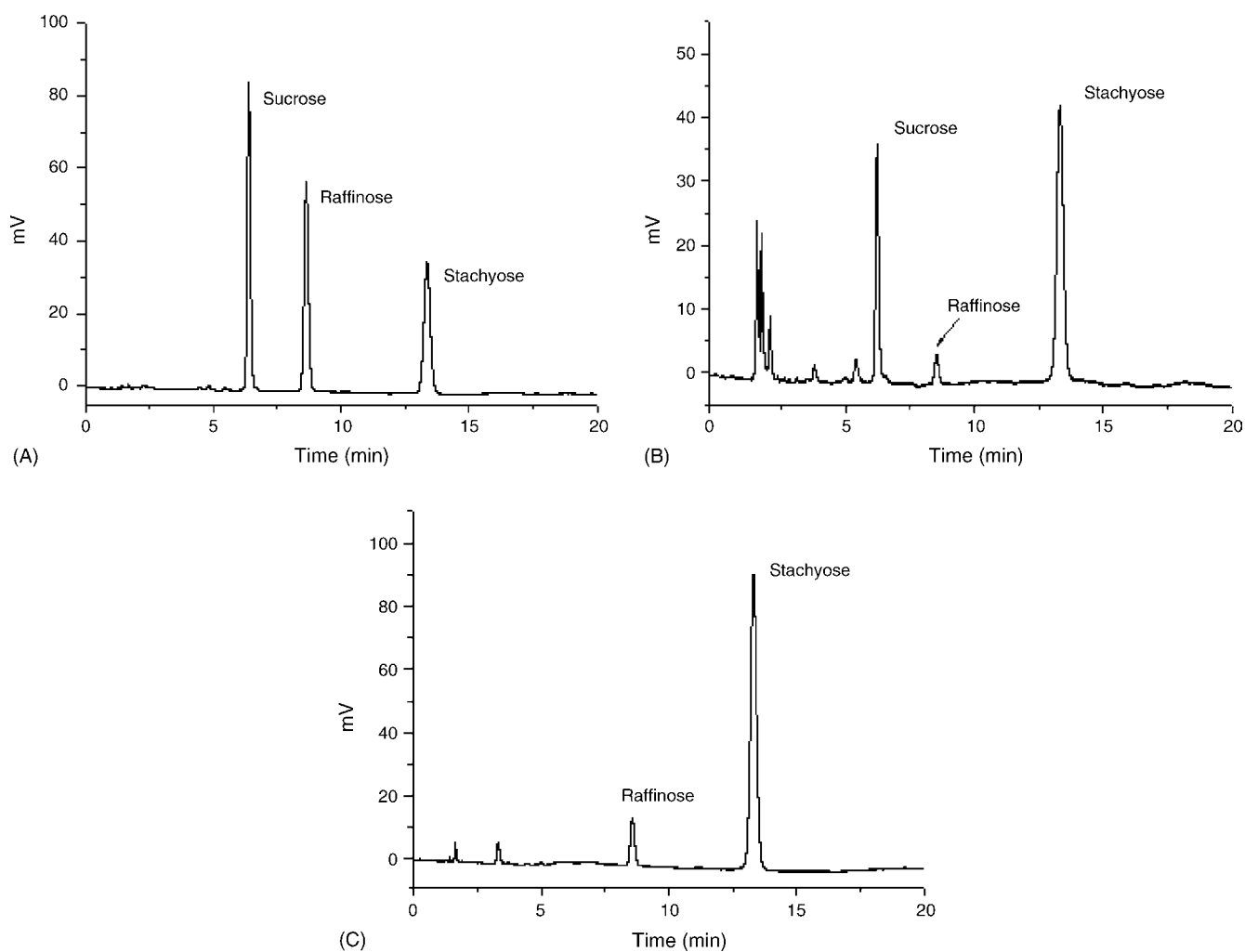


Fig. 1. Chromatogram of (A) standard mixture of stachyose, sucrose and raffinose (0.2 mg/mL for each sugar), (B) Sample 1 and (C) Sample 2. HPLC conditions: column, Bondapak NH₂ column (300 mm \times 3.9 mm i.d., 5 μ m, Waters, USA); mobile phase, methanol–acetonitrile–water (55:25:20); flow rate, 1.0 mL/min; temperature, 30 °C. ELSD used nitrogen as nebulizing gas at a flow rate 4.0 mL/min, and the temperature of drift tube was fixed at 40 °C.

Table 1
Performance characteristics of the proposed method

Analytes	Linearity range (μg)	Correlation coefficient	LOD (μg)	LOQ (μg)	Precision (R.S.D.%, $n = 5$)	
					Intra-day	Inter-day
Stachyose	0.51–10.16	0.9995	0.10	0.25	1.42	1.78
Sucrose	0.20–5.08	0.9986	0.04	0.10	1.76	2.24
Raffinose	0.20–8.04	0.9992	0.06	0.15	1.06	1.29

and raffinose (0.02, 0.05, 0.1, 0.2, 0.5 and 0.8 mg/mL) in triplicate. The linearity was evaluated based on the correlations between the logarithm of peak areas and the logarithm of concentrations of the analytes. The results were summarized in Table 1. The limits of detection (LOD, $S/N = 3$) and quantification (LOQ, $S/N = 10$) for stachyose, sucrose and raffinose were calculated experimentally from serial dilution. LOD were 0.10, 0.04 and 0.06 μg and LOQ were 0.25, 0.10 and 0.15 μg , respectively, for stachyose, sucrose and raffinose. This revealed that the employed ELSD was sensitive enough to these carbohydrates.

The precision of injection was demonstrated by replicative injections ($n = 5$) of the known concentration solutions (typically 0.20 mg/mL) of each sugar. The mean values for precision were 0.96% R.S.D. (relative standard deviation) for stachyose, 1.27% R.S.D. for sucrose and 0.83% R.S.D. for raffinose. Intra- and inter-day precisions were determined by analysis of the average amounts of the sugars in Sample 1. R.S.D. values ranged from 1.06 to 1.76 for intra-day precision and 1.29 to 2.24 for inter-day precision.

The accuracy of the method was determined by investigating the recovery of stachyose at three levels, i.e. 80, 100 and 120% of the known amount (29.4 mg), by spiking it with the standard stachyose. The recoveries of stachyose were found to be between 94.8 and 99.2%, and the average R.S.D. was below 2.4% (Table 2).

Maltose, xylose, rhamnose, galactose and fructose were tested for verifying the specificity of the proposed method. Results indicated that those carbohydrates had no interferences on the quantification of stachyose, sucrose and raffinose.

3.3. Evaluation of the extraction and purification methods

Extraction may involve removal of one or more unwanted components in either a single step or multiple steps. Removal of undesirable components is essential for optimal utilization of Chinese artichoke as human food and enhanced nutritional quality. A number of different processing methods have been put forward to that and, the most conventional being soaking,

Table 2
Recovery of stachyose by spiking method

Back ground (mg)	Added (mg)	Found (mg)	Average recovery (%)	R.S.D. (%)
29.4	23.5	50.1 \pm 0.42	94.8	1.73
29.4	29.4	58.3 \pm 0.26	99.2	0.58
29.4	35.2	63.5 \pm 0.88	98.4	2.34

Table 3
The contents and purities of the sugars determined by methods 1 and 2

Samples	Content (mg/g)			Purity of stachyose (%)
	Stachyose	Sucrose	Raffinose	
Sample 1	236.0	88.6	12.4	58.55
Sample 2	194.6	–	42.0	87.34

boiling, germination, and fermentation. In this study, two crafts were designed and employed to extract and purify the stachyose.

With regard to effects of two different extraction and purification methods, there were significant differences in the values of both content and purity of the sugars. For instance, the content of stachyose in the dry tubers and the purity in the extracted flour were 23.60 mg/g and 58.55% for method 1, and 19.46 mg/g and 87.34% for method 2, respectively. Firstly, Fig. 1 and Table 3 showed that sucrose was abundant in Sample 1, indicating there must correspondingly exist abundant sucrose in Chinese artichoke tubers, however, it disappeared in Sample 2. It was more likely that sucrose has been removed into the waste rinses in the course of selective washing procedures for the two ion-exchange resin columns. Furthermore, in method 1, the powder of the plant tubers was defatted by refluxing with chloroform, following proteins, pecans and other organic colloids were partly removed by addition of trichloroacetic acid. The carbohydrates were not lost during the treat process due to their indissolubility to methanol and no adsorption losses. However, in method 2, both an active carbon column and two ion-exchange resin columns were employed. Inevitably, the adsorption loss of raffinose and stachyose to some extent was resulted. So the contents of oligosaccharides in Sample 1 were more than those of Sample 2. On the other hand, the soluble impurities in the extract could be removed by the sorbents packed in columns so that the purities of the raffinose and stachyose in Sample 2 were significantly enhanced.

Therefore, the two designed methods could cater for different desires: method 1 was suited for determination and method 2 was suited for purification of stachyose in the Chinese artichoke.

4. Conclusion

Two extraction and purification procedures were performed and evaluated, indicating that different methods could cater for different purposes: determination or purification of carbohydrates in Chinese artichoke. The proposed HPLC–ELSD method was simple and reliable and appropriate for simultaneous deter-

mination of stachyose, sucrose and raffinose in the tubers of Chinese artichoke (*Stachys Sieboldii* Miq.)

Acknowledgements

This work is supported by “BaiRen Project” of Chinese Academy of Sciences, the National Natural Science Foundation of China (grant nos. 20375010, 20435030) and the Excellent Teacher Program of China Education Ministry.

References

- [1] M. Xiao, K. Tanaka, X. Qian, K. Yamamoto, H. Kumagai, *Biotech. Lett.* 22 (2000) 747.
- [2] P. Scalabrini, M. Rossi, P. Spettoli, D. Matteuzzi, *Int. J. Food Microbiol.* 39 (1998) 213.
- [3] E. Landberg, A. Lundblad, P. Pahlsson, *J. Chromatogr. A* 814 (1998) 97.
- [4] T.R. Cataldi, G. Margiotta, L. Iasi, B. Di Chio, C. Xiloyannis, S.A. Bufo, *Anal. Chem.* 72 (2000) 3902.
- [5] S. Thurl, B. Muller-Werner, G. Sawatzki, *Anal. Biochem.* 235 (1996) 202.
- [6] F. Kvasnicka, R. Ahmadova-Vavrousova, J. Frias, K.R. Price, P. Kadlec, *J. Liq. Chromatogr. Relat. Technol.* 19 (1996) 135.
- [7] I.M. Knudsen, *J. Sci. Food Agric.* 37 (1986) 560.
- [8] M. Muzquiz, C. Burbano, G. Ayet, M.M. Pedrosa, C. Cuadrado, *Biotechnol. Agron. Soc. Environ.* 3 (1999) 210.
- [9] B.L. Wong, K.L. Baggett, A.H. Rye, *Can. J. Bot.* 81 (2003) 780.
- [10] Z. El-Rassi (Ed.), *Carbohydrate Analysis by Modern Chromatography and Electrophoresis*, vol. 66, 2nd ed., Elsevier, Amsterdam, *J. Chromatogr. Libr. Ser.*, 2002.
- [11] F. D'Eramo, J.M. Marioli, A.H. Arevalo, L.E. Sereno, *Talanta* 61 (2003) 341.
- [12] H.L. Lee, S.C. Chen, *Talanta* 64 (2004) 210.
- [13] L.C. Nogueira, F. Silva, I.M.P.L.V.O. Ferreira, L.C. Trugo, *J. Chromatogr. A* 1065 (2005) 207.
- [14] B. Herbreteau, V. Villette, M. Lafosse, M. Dreux, *Fresenius J. Anal. Chem.* 351 (1995) 246.
- [15] B. Herbreteau, M. Lafosse, L. Morin-Allory, M. Dreux, *Anal. Chim. Acta* 267 (1992) 147.
- [16] I. Clarot, A. Regazzeti, N. Auzeil, F. Laadani, M. Citton, P. Netter, A. Nicolas, *J. Chromatogr. A* 1087 (2005) 236.
- [17] A.M. van Nederkassel, V. Vijverman, D.L. Massart, Y. Vander Heyden, *J. Chromatogr. A* 1085 (2005) 230.
- [18] R. Jacquet, P. Favetta, C. Elfakir, M. Lafosse, *J. Chromatogr. A* 1083 (2005) 106.
- [19] X.-Y. Chai, S.-L. Li, P. Li, *J. Chromatogr. A* 1070 (2005) 43.
- [20] A. Antonopoulos, P. Favetta, M. Lafosse, W. Helbert, *J. Chromatogr. A* 1059 (2004) 83.
- [21] N. Kasai, H. Ikehara, *J. Agric. Food Chem.* 53 (2005) 4245.
- [22] J. Fang, *Chin. Pharm. Bull.* 19 (1984) 46.
- [23] J.C. Onweluzo, H.P. Ramesh, R.N. Tharanathan, *Carbohydr. Polym.* 47 (2002) 253.
- [24] P. Ghosh, P. Ghosal, S. Thakur, P. Lerouge, C. Loutelier-Bourhis, A. Driouich, B. Ray, *Food Chem.* 90 (2005) 719.

Determination of polyphenolic compounds in wastewater olive oil by gas chromatography–mass spectrometry

A. Zafra^a, M.J.B. Juárez^b, R. Blanc^a,
A. Navalón^a, J. González^b, J.L. Vilchez^{a,*}

^a Research Group of Analytical Chemistry and Life Sciences, Department of Analytical Chemistry,
University of Granada, Avda. Fuentenueva s/n, E-18071 Granada, Spain

^b Research Group of Environmental Microbiology, Institute of Water Research, University of Granada, E-18071 Granada, Spain

Received 18 October 2005; received in revised form 15 December 2005; accepted 16 December 2005

Available online 7 February 2006

Abstract

A simple and sensitive method for the determination of 21 polyphenolic compounds in wastewater from olive oil production plants is proposed. The method involves a liquid–liquid microextraction (LLME) procedure with ethyl acetate followed by a silylation step. Identification and quantification have been performed by gas chromatography–mass spectrometry (GC–MS). MS measurements were carried out using selected ion monitoring mode (SIM). α -Naftol was used as internal standard. The proposed method was applied to the determination of these compounds in wastewater from an olive oil production factory in Jaén (Spain) at concentration levels ranging from 1.0 to 75.0 $\mu\text{g ml}^{-1}$ for each compound. The autodegradation process by own microbiota in samples collected in three different points of the factory was also studied. The method was validated by a recovery assay with spiked samples.

© 2006 Elsevier B.V. All rights reserved.

Keywords: Wastewater olive oil (WOO); Polyphenols; Antioxidants; Liquid–liquid microextraction (LLME); Silylation; Gas chromatography–mass spectrometry (GC–MS)

1. Introduction

In the last years a large amount of scientific studies have demonstrated the healthy properties of olive oil. Virgin olive oil is a fundamental ingredient of the Mediterranean diet and, over the past few years, its diffusion and consumption has spread remarkably outside the Mediterranean basin [1]. The incidence of cancer and heart disease is considerably lower within this geographical area compared to the rest of Europe. The scientific studies have linked these health benefits increasing olive oil consumption [2,3].

However, during production of olive oil, a high organic content water is generated as a by-product of mechanical extraction. This waste, that contains powerful contaminants, is called commonly wastewater olive oil (WOO). The residue is a complex mixture of water, sugars, nitrogenous substances, organic acids,

pectins, mucilages and tannins, lipids and inorganic substances. All of them have poor biodegradability and high phytotoxicity due to the presence of a large amount of phenolic compounds (PCs), free fatty acids and inorganic salts (mainly potassium salts) [4]. Although the fruit variety and the production process employed in the manufacture of the olive oil have a significant impact on the amount and composition of the residue, polar compounds, as phenolic, end up into the waste in extraction process, rendering this by-product a potential source of harm [5,6].

In the last years it has been demonstrated that these compounds are strong natural antioxidants and they have in vitro biological activities [7,8]. This has attracted considerable attention and stimulated research on its potential role as a preservative in foods or cosmetics [9–11]. Therefore, it is of crucial importance to know the phenolic composition of the residue in order to propose analytical methodologies to check polyphenol contents into this matrix. The classical method for total polyphenols quantification is a colorimetric procedure using the Folin-Ciocalteu reagent [6]. In recent years, it has been shown that the new methodologies provided for the separation and

* Corresponding author. Tel.: +34 958 243326; fax: +34 958 243328.
E-mail address: jvilchez@ugr.es (J.L. Vilchez).

quantitative determination of individual PCs by either gas chromatography (GC) or liquid chromatography (LC) are much more satisfactory [10–14].

In complex matrices as WWOO the key to the PCs determination is the preliminary sample processing, which requires a previous separation of the phenolic fraction from the other constituents present in the samples. Liquid–liquid microextraction (LLME) is essentially a simultaneous extraction and concentration procedure suitable for the analysis of a wide range of organic trace compounds in water, and it has been selected for this purpose [15,16]. The principle of LLME is the mixture of a large volume of aqueous sample with a very small volume of organic solvent that previous stirring, separation and drying can be directly analysed without any further treatment. It can be easily performed with basic equipment and low manpower. Inconveniences arising from large solvent volumes and interference from solid phase extraction materials are avoided. Furthermore, LLME offers the possibility of lowering the cost and time needed for the analysis. In addition, the use of micro methods in which the amount of organic solvents is very small reduces damage to the environment.

Here, a new analytical method based on application of gas chromatography coupled mass spectrometry (GC–MS) with a LLME step for the determination of 21 phenolic compounds is proposed. The analytical performance of the method has been established and the method has been applied to the study of degradation of these compounds in WWOO from different points in an olive oil plant from Jaén (Spain).

2. Experimental

2.1. Apparatus and software

Gas chromatographic analysis was performed using an Agilent 6890 Series GS System (Agilent Technologies, Wilmington, DE, USA) gas chromatograph fitted with a splitless injector for a low background HP-5MS fused silica capillary column (60 m \times 0.25 mm i.d. \times 0.25 μ m film thickness) supplied by Agilent. A silanized injector liner split/splitless (2 mm i.d.) was used. Detection was carried out with a 5973 mass-selective single quadrupole detector (Agilent Technologies). The GC–MS operation control and the data process were carried out by ChemStation software package (Agilent Technologies).

The injector temperature was 250 °C. The oven temperature was held at 90 °C for 1 min, then increased to 220 °C at a heating rate of 6 °C min^{−1}, then to 290 °C at 10 °C min^{−1} and held for 1.23 min and finally to 310 °C at a rate of 40 °C min^{−1} and the temperature was held for 7.5 min. The total run time was 38.5 min. The detector temperature was 280 °C.

The carrier gas used was helium (purity 99.999%) at a flow rate of 1.0 ml min^{−1}. The samples were injected in the splitless mode and the splitter was opened after 5 min (delay time). The sample volume in the direct injection mode was 1 μ l.

The conditions for electron impact ionization (EI) were an ion energy of 70 eV and the mass range scanned was 140–465 *m/z*. The MS was tuned everyday to *m/z* 69, 219 and 502 with per-

fluorotributylamine (PFTBA) as a calibration standard. Single ion monitoring (SIM) acquisition mode (dwell time 100 ms/ion) was used.

2.2. Reagents

All reagents were of analytical reagent grade unless stated otherwise. Water was purified with a Milli-Q plus system (Millipore, Bedford, MA, USA).

Stock solutions of polyphenols (Sigma, St. Louis, MO, USA) containing 1000 μ g ml^{−1} were prepared in absolute ethanol 99% (v/v) (Panreac, Barcelona, Spain). The solutions were stored in glass dark bottles at 4 °C, remaining stable for at least 3 months. These solutions were used to spike blank samples.

A standard solution of 1000 μ g ml^{−1} of α -naftol (Sigma) in ethanol was used as internal standard after adequate dilution to a final concentration of 50 μ g ml^{−1} in samples. A mixture of *N*,*o*-bis(trimethylsilyl)trifluoroacetamide (BSTFA) and pyridine (Sigma) in ethyl acetate was used as the silylation reagent.

2.3. Sample treatment

2.3.1. Natural samples

WWOO samples were collected from an olive oil production plant in Jaén (Spain) and stored in 1000 ml low density polypropylene airtight containers at −20 °C until use. Samples were picked up in three different points in the olive oil production plant: centrifugation, wastewater pool where the residue is definitively placed and in a third place called “alpechinera” located inside the factory. Samples were also diluted with pure water to 60 and 20% (v/v) in order to compare the degradation of polyphenolic compounds after and before dilution.

2.3.2. Blank samples

Samples free of analytes were obtained by degradation of total phenols by using microorganisms as described by Amhajji et al. [17]. The blank samples appear to be completely free of interesting analytes. They were sterilized at 0.5 atm for 30 min in order to remove microorganisms and to avoid autodegradation by WWOO own microbiota being finally stored in 1000 ml low density polypropylene airtight containers at 4 °C until use.

2.4. Analytical procedure

Two millilitres of sample previously acidified (pH 3) and spiked with a 50 μ g ml^{−1} of α -naftol was transferred to a separatory funnel. The sample was saturated with NaCl and 0.5 ml of ethyl acetate was added. The mixture was mechanically shaken for 1 min at room-temperature and the organic phase was allowed to drip into a glass funnel filled with anhydrous sodium sulfate to dehydrate it. The extraction was repeated twice and organic phases were all mixed. Next, the sample was evaporated to near dryness under nitrogen and transferred to a 200 μ l microvial. After evaporation to dryness under nitrogen, the vial was stoppered because silyl derivatives tend to be sensitive to moisture. Fifty microlitres of BSTFA–pyridine–ethyl acetate

(4:1:5, v/v/v) was added and the mixture was mechanically shaken for 2 min at room-temperature. At this point the samples were ready to be injected into the gas chromatograph–mass spectrometer.

Moisture is a major competitor of phenolic hydroxyl groups during derivatization with the mixture BSTFA–pyridine and can produce low recoveries. To avoid the problem all reagents used in silylation were previously dried adding anhydrous sodium sulphate. It was checked that the silylated compounds were stable at room-temperature and in the darkness for at least 1 week.

3. Results and discussion

3.1. Liquid–liquid microextraction procedure

Quantitative extraction of phenolic compounds in natural matrices is difficult. Therefore, tests of recovery were carried out to ensure effectiveness of the extraction procedure of phenolic compounds from matrix. A LLME procedure was selected as appropriate for analyte extraction.

The pH influence of the medium in the extraction efficiency of polyphenols was studied. It was observed that the extraction efficiency is maximum for acid pH values. This behaviour could be attributed to a drop in the extraction efficiency of compound because the dissociated form remains in aqueous phase. Therefore, compounds extractions were carried out at pH 3 adding hydrochloric acid solution.

Organic extracting solvent ethyl ether, *n*-hexane, dichloromethane, trichloromethane and ethyl acetate were tested. Due to the good recovery obtained for all compounds and the lower boiling point for solvent removing, ethyl acetate was selected as the most adequate extracting agent.

The volume of organic solvent to be used and the ionic strength of the medium were also optimised. Saturation with sodium chloride and 0.5 ml of solvent bring near us the optimum values obtained for all compounds.

3.2. Derivatization of the analytes

A comparison between different combinations of derivatization agents was carried out. Pure BSTFA, BSTFA with 1% TMCS (v/v), BSTFA diluted in ethyl acetate and in the presence of pyridine were tested. The best results were obtained by using a mixture of BSTFA and pyridine (4:1, v/v).

The optimisation of the derivatization method was carried out by applying the experimental design methodology. The effect of varying the concentration of BSTFA/pyridine, temperature and reaction time was tested on the analytical response corresponding to a mixture of selected polyphenols. The three factors were simultaneously optimised by application of a 2³ central composite design plus face centred (with three centred points). Considering the results obtained from the established response surface, the following optima values were found: a mixture of 20:5:25 (v/v/v) BSTFA–pyridine–ethyl acetate coupled to a reaction time of 2 min at room-temperature is enough to get an adequate derivatization. The application of experi-

Table 1
SIM mode for phenolic compounds

Compound	RT (min)	<i>m/z</i>
<i>p</i> -Vanillin	19.377	224 + 209 + 194
α -Naftol	19.678	185 + 201 + 216
Tyrosol	19.944	282 + 267 + 193 + 179
3-Hydroxyphenyl acetic acid	20.641	296 + 281 + 252 + 164 + 147
Protocetic aldehyde	21.055	282 + 267 + 193 + 165
<i>p</i> -Hydroxybenzoic acid	21.037	282 + 267 + 223 + 193
Vanillol	21.166	298 + 209 + 179
<i>p</i> -Hydroxyphenyl acetic acid	21.260	296 + 281 + 252 + 179
Syringic aldehyde	22.513	254 + 239 + 224 + 195
di-Hydroxyphenyl ethanol	23.434	370 + 267 + 193 + 179
<i>p</i> -Hydroxyphenyl propionic acid	23.469	310 + 295 + 192 + 179
Vanillic acid	23.480	312 + 297 + 282 + 267 + 253 + 223
Protocetic acid	24.323	370 + 355 + 311 + 193
3,4,5-Trimetoxibenzoic acid	24.432	284 + 269 + 225 + 195
Syringic acid	25.494	342 + 327 + 312 + 297 + 253
<i>p</i> -Coumaric acid	26.177	308 + 293 + 279 + 219
Gallic acid	26.215	458 + 459 + 443 + 444 + 281
Ferulic acid	28.025	338 + 323 + 308 + 293
Esculetin	28.300	395 + 322 + 307
Caffeic acid	28.482	396 + 381 + 219 + 191
Sinapic acid	29.632	368 + 353 + 338 + 323
Epicatechine	35.660	368 + 369 + 370 + 356 + 357

mental designs was carried out using the Statgraphics software package [18].

3.3. Analytical characteristics of the method

Calibration model for the GC–MS method was built by injecting 1 μ l of different standard solutions at concentrations ranging from 1.0 to 75.0 μ g ml^{−1}. This also allowed the establishment of the retention time and the mass fragmentation of each compound. Table 1 shows the most important fragments for each one used for SIM mode.

Analytical performance was established according to the Analytical Methods Committee [19], the *lack-of-fit* test was applied to two replicates and three injections of each standard. The results for the intercept (*a*), slope (*b*), correlation coefficient (*R*²) and probability level of the *lack-of-fit* test, *P*_{lof} (%), are summarised in Table 2. Thus, the data yield shows good linearity within the stated ranges. The precision, determined as relative standard deviation (R.S.D.), was measured for an amount of 25 μ g ml^{−1} in each analyte by performing 10 independent determinations.

Limits of detection were calculated in order to determine analytes present in real samples. In this paper criteria for method performance have been proposed that include the decision limit, *CC* _{α} , and the detection capability, *CC* _{β} [20]. The decision limit, *CC* _{α} , is the limit from which it can be decided that a sample is contaminated with an error probability of α . The detection capability, *CC* _{β} , is the smallest content of the analyte that may be detected, identified and/or quantified in a sample with an error

Table 2
Analytical and statistical parameters

	<i>n</i>	<i>a</i>	<i>S_a</i>	<i>b</i> (ml μg ⁻¹)	<i>S_b</i> (ml μg ⁻¹)	<i>R</i> ² (%)	<i>S_{y/x}</i>	LDR (μg ml ⁻¹)	CC _α (μg ml ⁻¹)	CC _β (μg ml ⁻¹)	R.S.D. (%)	<i>P</i> _{lof} (%)
<i>p</i> -Vanillin	7	9.0 × 10 ⁻⁵	4.8 × 10 ⁻³	8.8 × 10 ⁻³	1.2 × 10 ⁻⁴	99.8	8.0 × 10 ⁻³	2.0–75.0	1.3	2.1	3.5	96.4
Tyrosol	7	2.5 × 10 ⁻²	9.9 × 10 ⁻³	1.4 × 10 ⁻²	2.6 × 10 ⁻⁴	99.7	1.7 × 10 ⁻²	2.0–75.0	1.6	2.7	3.1	28.5
3-Hydroxyphenyl acetic acid	7	8.3 × 10 ⁻⁵	8.9 × 10 ⁻³	7.3 × 10 ⁻³	2.3 × 10 ⁻⁴	99.3	1.5 × 10 ⁻²	0.5–75.0	0.3	0.5	3.9	46.2
Protocatechic aldehyde	7	1.9 × 10 ⁻⁵	7.5 × 10 ⁻³	8.5 × 10 ⁻³	2.0 × 10 ⁻⁴	99.6	1.3 × 10 ⁻²	0.5–75.0	0.2	0.3	3.2	70.4
<i>p</i> -Hydroxybenzoic acid	7	3.3 × 10 ⁻⁵	3.0 × 10 ⁻²	2.9 × 10 ⁻²	7.8 × 10 ⁻⁴	99.5	5.0 × 10 ⁻²	4.0–75.0	2.4	4.0	3.5	65.1
Vanillol	7	5.5 × 10 ⁻³	7.1 × 10 ⁻³	1.3 × 10 ⁻²	1.8 × 10 ⁻⁴	99.8	1.2 × 10 ⁻²	2.0–75.0	1.3	2.1	3.0	85.3
<i>p</i> -Hydroxyphenyl acetic acid	7	3.7 × 10 ⁻⁵	2.8 × 10 ⁻³	6.0 × 10 ⁻³	7.3 × 10 ⁻⁵	99.9	4.7 × 10 ⁻³	2.0–75.0	1.1	1.8	2.9	92.2
Syringic aldehyde	7	1.7 × 10 ⁻⁴	3.5 × 10 ⁻³	9.1 × 10 ⁻³	9.1 × 10 ⁻⁵	99.9	5.9 × 10 ⁻³	2.0–75.0	0.9	1.5	3.5	94.2
di-Hydroxyphenyl ethanol	7	1.4 × 10 ⁻⁵	1.1 × 10 ⁻²	2.5 × 10 ⁻²	2.8 × 10 ⁻⁴	99.9	1.8 × 10 ⁻²	2.0–75.0	1.0	1.7	2.5	49.4
<i>p</i> -Hydroxyphenyl propionic acid	7	5.6 × 10 ⁻⁵	2.9 × 10 ⁻³	5.8 × 10 ⁻³	7.5 × 10 ⁻⁵	99.9	4.8 × 10 ⁻³	2.0–75.0	1.2	1.9	2.6	87.1
Vanillic acid	7	3.7 × 10 ⁻³	4.9 × 10 ⁻³	1.2 × 10 ⁻²	1.3 × 10 ⁻⁴	99.9	8.3 × 10 ⁻³	2.0–75.0	1.0	1.6	2.2	97.0
Protocatechic acid	7	2.8 × 10 ⁻⁵	9.9 × 10 ⁻³	1.8 × 10 ⁻²	2.6 × 10 ⁻⁴	99.8	1.6 × 10 ⁻²	2.0–75.0	1.3	2.1	3.6	86.3
3,4,5-Trimetoxi benzoic acid	7	4.0 × 10 ⁻⁴	5.5 × 10 ⁻³	8.7 × 10 ⁻³	1.4 × 10 ⁻⁴	99.8	9.3 × 10 ⁻³	2.0–75.0	1.5	2.4	2.4	69.3
Syringic acid	7	1.8 × 10 ⁻⁴	7.1 × 10 ⁻³	1.6 × 10 ⁻²	1.8 × 10 ⁻⁴	99.9	1.2 × 10 ⁻²	2.0–75.0	1.0	1.7	1.8	67.9
<i>p</i> -Coumaric acid	7	5.6 × 10 ⁻⁴	4.3 × 10 ⁻³	1.0 × 10 ⁻³	1.1 × 10 ⁻⁴	99.9	7.2 × 10 ⁻³	2.0–75.0	1.0	1.6	3.1	82.6
Gallic acid	7	4.5 × 10 ⁻²	1.7 × 10 ⁻³	3.4 × 10 ⁻³	4.3 × 10 ⁻⁴	99.9	2.8 × 10 ⁻²	2.0–75.0	1.2	1.9	2.9	90.9
Ferulic acid	7	6.9 × 10 ⁻⁴	5.8 × 10 ⁻³	1.2 × 10 ⁻²	1.5 × 10 ⁻⁴	99.9	9.7 × 10 ⁻³	2.0–75.0	1.1	1.8	3.2	86.8
Esculetine	7	5.2 × 10 ⁻⁵	7.1 × 10 ⁻³	1.0 × 10 ⁻²	1.9 × 10 ⁻⁴	99.8	1.2 × 10 ⁻²	3.0–75.0	1.7	2.7	1.7	56.0
Caffeic acid	7	2.2 × 10 ⁻⁴	2.0 × 10 ⁻²	2.8 × 10 ⁻²	5.2 × 10 ⁻⁴	99.7	3.3 × 10 ⁻²	3.0–75.0	1.7	2.7	3.3	85.0
Sinapic acid	7	4.3 × 10 ⁻⁶	1.1 × 10 ⁻²	1.3 × 10 ⁻²	2.8 × 10 ⁻⁴	99.7	1.8 × 10 ⁻²	3.0–75.0	2.0	3.2	2.5	96.7
Epicatechine	7	7.1 × 10 ⁻⁴	1.8 × 10 ⁻²	2.8 × 10 ⁻²	4.7 × 10 ⁻⁴	99.8	3.1 × 10 ⁻²	3.0–75.0	1.5	2.5	3.6	99.6

n: number of measurements; *a*: intercept; *S_a*: intercept standard deviation; *b*: slope; *S_b*: slope standard deviation; *R*: determination coefficient; LDR: linear dynamic range; CC_{α,0.05}: decision limit; CC_{β,0.05}: detection capability; R.S.D.: relative standard deviation; *S_{y/x}*: regression standard deviation; *P*_{lof}: *P*-value for lack-of-fit test.

Table 3
Recovery assay for polyphenolic compounds in spiked wastewater olive oil

Compound	Added (μg ml ⁻¹)	<i>R</i> ^a (%)	Added (μg ml ⁻¹)	<i>R</i> ^a (%)	Added (μg ml ⁻¹)	<i>R</i> ^a (%)
<i>p</i> -Vanillin	10.0	96.5	25.0	98.5	50.0	96.5
Tyrosol	10.0	104.5	25.0	96.2	50.0	99.2
3-Hydroxyphenylacetic acid	10.0	94.2	25.0	98.5	50.0	95.3
Protocatechic aldehyde	10.0	99.6	25.0	99.1	50.0	102.3
<i>p</i> -Hydroxybenzoic acid	10.0	102.3	25.0	94.2	50.0	104.2
Vanillol	10.0	96.3	25.0	103.2	50.0	99.5
<i>p</i> -Hydroxyphenylacetic acid	10.0	105.0	25.0	102.5	50.0	98.5
Syringic aldehyde	10.0	98.3	25.0	98.3	50.0	97.6
di-Hydroxyphenylethanol	10.0	96.3	25.0	99.1	50.0	102.3
<i>p</i> -Hydroxyphenylpropionic acid	10.0	105.6	25.0	97.7	50.0	104.6
Vanillic acid	10.0	94.3	25.0	95.8	50.0	95.8
Protocatechic acid	10.0	98.3	25.0	94.6	50.0	96.4
3,4,5-Trimetoxibenzoic acid	10.0	95.6	25.0	96.2	50.0	97.5
Syringic acid	10.0	95.3	25.0	101.2	50.0	96.2
<i>p</i> -Coumaric acid	10.0	104.9	25.0	104.3	50.0	99.1
Gallic acid	10.0	97.2	25.0	98.5	50.0	95.1
Ferulic acid	10.0	96.2	25.0	94.9	50.0	98.2
Esculetine	10.0	98.5	25.0	97.8	50.0	99.3
Caffeic acid	10.0	96.3	25.0	101.9	50.0	95.3
Sinapic acid	10.0	98.2	25.0	103.6	50.0	94.5
Epicatechine	10.0	103.5	25.0	99.2	50.0	102.6

^a Mean of three determinations.

probability of β . Decision limit and detection capacity which are better adjusted to a statistical evaluation are implemented. Thus, CC_α ($\alpha = 5\%$) and CC_β ($\beta = 5\%$) were calculated and the results obtained are also summarised in Table 2.

3.4. Application of the method to natural samples

A recovery assay with spiked samples was carried out. The recovery values for three replicate samples at three concentration levels of each compound are shown in Table 3.

The concentration of each phenolic compound was determined by direct interpolation in the standard calibration curve within their linear dynamic range. Recoveries are close to 100% in all cases.

The method was applied to the determination of the analytes in diluted and non-diluted natural wastewater olive oil samples collected from the olive oil factory in Jaén (Spain). The degradation of these compounds by WWO own microbiota after incubation for a week at 30 °C and 150 rpm was also studied. Physical parameters as pH, density and conductivity were controlled in the process and chemical and biological oxygen demands were determined too. A representative chromatogram of a sample is depicted in Fig. 1. Table 4 shows the evolution of found polyphenol concentrations in analysed samples.

As it is shown in Table 4, sample dilution does not seem to be related with improving degradation of polyphenolic compounds present in WWO. Moreover, a high variability in degradation percentages of each compound in the samples picked up at different points has been found. This behaviour could be accounted for the different composition of microbiota in the sampling points. Finally, compounds as caffeic or *p*-coumaric acids are 100% degraded in any experimental condition while compounds as tyrosol or 2-dihydroxyphenylethanol presents in higher concentration in WWO show lower degradation percentages.

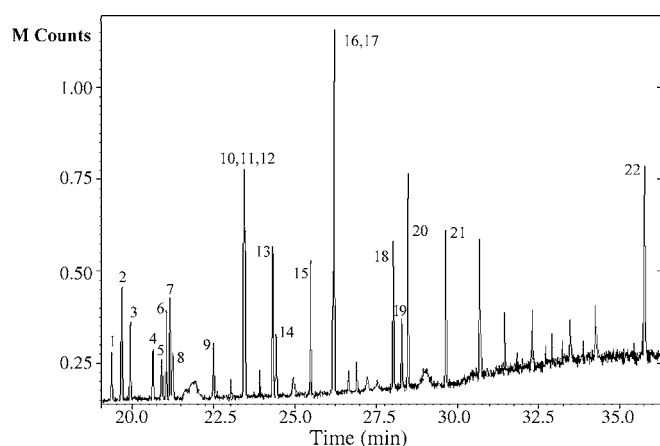


Fig. 1. Representative chromatogram of a wastewater olive oil sample spiked with $25 \mu\text{g ml}^{-1}$ of each analyte and the internal standard: (1) *p*-vanillin, (2) α -naftol (internal standard), (3) tyrosol, (4) 3-hydroxyphenylacetic acid, (5) protocatecic aldehyde, (6) *p*-hydroxybenzoic acid, (7) vanillol, (8) *p*-hydroxyphenylacetic acid, (9) syringic aldehyde, (10) di-hydroxyphenyl ethanol, (11) *p*-hydroxyphenylpropionic acid, (12) vanillic acid, (13) protocatecic acid, (14) 3,4,5-trimethoxybenzoic acid, (15) syringic acid, (16) *p*-coumaric acid, (17) gallic acid, (18) ferulic acid, (19) esculetine, (20) caffeic acid, (21) sinapic acid and (22) epicatechine.

Table 4

Polyphenolic compounds degradation in wastewater olive oil

	Centrifuge	"Alpechinera"	Pool
Degradation without dilution (%) [*]			
Tyrosol	66.7	22.6	44.5
<i>p</i> -Hydroxybenzoic acid	82.0	100.0	52.5
<i>p</i> -Hydroxyphenylacetic acid	85.5	100.0	100.0
<i>p</i> -Hydroxyphenylpropionic acid	55.0	57.7	65.0
Vanillic acid	53.1	63.8	65.5
di-Hydroxyphenylethanol	66.5	58.7	43.3
Protocatecic acid	76.1	10.4	55.2
<i>p</i> -Coumaric acid	100.0	100.0	100.0
Caffeic acid	100.0	100.0	100.0
Degradation diluted 60% (%) [*]			
Tyrosol	66.5	12.8	1.4
<i>p</i> -Hydroxybenzoic acid	78.1	31.2	35.5
<i>p</i> -Hydroxyphenylacetic acid	83.5	100.0	76.8
<i>p</i> -Hydroxyphenylpropionic acid	41.2	45.7	48.9
Vanillic acid	48.8	100.0	33.6
di-Hydroxyphenylethanol	58.9	62.8	6.6
Protocatecic acid	9.4	100.0	50.1
<i>p</i> -Coumaric acid	100.0	100.0	100.0
Caffeic acid	100.0	100.0	100.0
Degradation diluted 20% (%) [*]			
Tyrosol	44.8	0.0	97.0
<i>p</i> -Hydroxybenzoic acid	46.0	100.0	15.9
<i>p</i> -Hydroxyphenylacetic acid	7.7	100.0	56.6
<i>p</i> -hydroxyphenylpropionic acid	16.4	42.2	60.9
Vanillic acid	100.0	100.0	28.1
di-Hydroxyphenylethanol	2.3	8.5	68.6
Protocatecic acid	100.0	100.0	100.0
<i>p</i> -Coumaric acid	100.0	100.0	100.0
Caffeic acid	100.0	100.0	100.0

^{*} Mean of three determinations.

4. Conclusions

A simple and low cost method for the simultaneous determination of 21 polyphenolic compounds in wastewater olive oil samples is proposed. A liquid–liquid microextraction procedure is used in conjunction with a silyl derivatization for the analysis of the compounds by gas chromatography–mass spectrometry. The method has been applied to samples from different sources and consequently, with different composition. The appropriate sample collection and conservation in conjunction with a previous centrifugation allows good recovery values in all cases as demonstrated by the validation procedure employed.

References

- [1] M. Bonoli, M. Montanucci, T.G. Toshi, G. Lercker, J. Chromatogr. A 1011 (2003) 163.
- [2] A. Keys, C. Aravanis, F.S.P. Van Buchem, H. Blackburn, R. Buzina, B.S. Djorjevic, Lancet 2 (1981) 58.
- [3] M. Gerber, in: M.J. Hill, A. Giacosa, C.P.G. Caygill (Eds.), Epidemiology of Diet and Cancer, Ellis Horwood, Chichester, UK, 1994, pp. 263–275.
- [4] L. Ceccon, D. Saccú, G. Procida, S. Cardinali, J. AOAC Int. 84 (2001) 1739.
- [5] V. Sciancalepore, G. De Stefano, P. Piacquadio, R. Sciancalepore, Ing. Ambientale 24 (1995) 627.

- [6] N. Mulinacci, A. Romani, C. Galardi, P. Pinelli, C. Giaccnerini, F. Vincieri, *J. Agric. Food Chem.* 49 (2001) 3509.
- [7] E. Ragazzi, G. Veronese, *J. Chromatogr.* 77 (1973) 369.
- [8] R.W. Owen, R. Haubner, W. Mier, A. Giacosa, W.E. Hull, B. Spiegelhalder, H. Bartsch, *Food Chem. Toxicol.* 41 (2003) 703.
- [9] J.A. Vinson, X. Su, L. Zubik, P. Bose, *J. Agric. Food Chem.* 49 (2001) 5315.
- [10] J.B. Harborne, in: J.B. Harborne (Ed.), *Phytochemical Methods, A Guide to Modern Techniques of Plant Analysis*, Chapman and Hall, London, UK, 1973 (Chapter 2).
- [11] J.M. Schulz, K. Herrman, *J. Chromatogr.* 195 (1980) 85–94.
- [12] M. Saitta, S. Lo Curto, F. Salvo, G. Di Bella, G. Dugo, *Anal. Chim. Acta* 466 (2002) 335.
- [13] R. Tsao, R. Yang, J.C. Young, H. Zhu, *J. Agric. Food Chem.* 51 (2003) 6347.
- [14] T.L. Potter, T. Carpenter, R. Putnam, K. Reddy, J.M. Clark, *J. Agric. Food Chem.* 39 (1991) 2184.
- [15] R. Heyer, A. Zapf, H.J. Stan, *Fresenius J. Anal. Chem.* 351 (1995) 752.
- [16] J.L. Vilchez, P. Espinosa, F.J. Arrebola, A. González-Casado, *Anal. Sci.* 13 (1997) 817.
- [17] A. Amhajji, M.H. El-Jalil, M. Faid, J.L. Vassel, M. El-Yachoui, *Grasas Aceites* 51 (2000) 400.
- [18] Statgraphics, Version Plus 5.0, Statistical Graphics Corporation and Manugistics Inc., Rockville, MA, USA, 2000.
- [19] Analytical Methods Committee, *Analyst* 119 (1994) 2363.
- [20] Commission Decision Laying Down Performance Criteria for the Analytical Methods to be used for Certain Substances and Residues Thereof in Live Animals and Animal Products According to Council Directive 96/23/EC, Draft SANCO/1805/2000 Rev. 1, 2000.

A flow-injection chemiluminescence method for the determination of some estrogens by enhancement of luminol–hydrogen peroxide–tetrasulfonated manganese phthalocyanine reaction

Lun Wang*, Ping Yang, Yongxin Li*, Changqin Zhu

College of Chemistry and Materials Science, Anhui Normal University, Wuhu 24100, PR China

Received 4 October 2005; received in revised form 19 December 2005; accepted 19 December 2005

Available online 7 February 2006

Abstract

A novel flow-injection chemiluminescence (FI-CL) method for the determination of estrogens is proposed, based upon its enhancing effect on the CL reaction of luminol with hydrogen peroxide catalyzed by tetrasulfonated manganese phthalocyanine (MnTSPc) in alkaline solution. Under the selected experimental conditions, a linear relationship was obtained between the CL intensity and the concentration of estrone in the range of 1.0×10^{-7} to 1.0×10^{-6} mol/l, estradiol in the range of 9.0×10^{-8} to 1.0×10^{-6} mol/l and estriol in the range of 3.0×10^{-7} to 2.0×10^{-6} mol/l, respectively. The detection limits were 5.1×10^{-8} mol/l for estrone, 7.2×10^{-9} mol/l for estradiol and 6.5×10^{-8} mol/l for estriol with a relative standard deviation of 2.8% for 5.0×10^{-7} mol/l estrone, 2.4% for 1.0×10^{-7} mol/l estradiol, and 3.1% for 7.0×10^{-7} mol/l estriol ($n = 11$). This method has been applied to the determination of estrogen in pharmaceutical injections and tap water with satisfactory results.

© 2006 Elsevier B.V. All rights reserved.

Keywords: Flow injection; Chemiluminescence (CL); Estrogens; Tetrasulfonated manganese phthalocyanine (MnTSPc)

1. Introduction

Estradiol, estrone and estriol are three main natural estrogenic hormones in the human body. In the past years, they had been used widely as some regulatory factors preventing the aging substance in women and remedies related to women diseases. Since these estrogens were found in low concentration [1]. Some analytical procedures which have low detection limits are required to determine estrogens. Several analytical methods have been reported for the determination of estrogens, including gas chromatography–mass spectrometry (GC–MS), high performance liquid chromatography (HPLC), HPLC–MS, solid-phase extraction–enzyme-linked immunosorbent, immunoassay based on ELISA, and electrochemical method [2–11].

Although most of these methods are specific, their applications were limited due to the high commercial price and insufficient sensitivity. Chemiluminescence (CL) has received much attention as an attractive detection method for analyti-

cal application because of its low detection limit, wide working range, relatively cheap apparatus, and reagents [12]. In 1986, Van den Berg et al. developed the CL immunochemical detection after HPLC technique for estrogenic hormones [13]. Zhao and Lin exploited a microplate magnetic CL enzyme immunoassay for rapid and high throughput analysis of estradiol in water samples [14]. Tanaka et al. used bridge-heterologous CL enzyme-linked immunosorbent assay of estriol 3-sulfate in pregnancy plasma [15]. Xie and co-workers gave a potassium permanganate–formaldehyde CL system for the determination of dienestrol, diethylstilbestrol, and hexestrol [16]. Hence CL has become a novel interesting method for the determination of some estrogens.

Till date, the CL reaction of luminol with hydrogen peroxide catalyzed by all kinds of mimetic enzymes has received high attention in biochemistry and clinical chemistry [17–19]. Horseradish peroxidase has been used as enzyme catalyst in CL reactions for a long time, but it was unstable and expensive. So researchers focused their interest on metal–complex mimetic enzymes such as metalloporphyrin. Now these metal mimetic enzymes have been applied widely in electrocatalysis field, fluorescence analysis and CL analysis. Metallophthalocyanine has analogical structure to metalloporphyrin, and it also

* Corresponding authors. Tel.: +86 553 3869302; fax: +86 553 3869303.

E-mail addresses: wanglun@mail.ahnu.edu.cn (L. Wang), liyongxin@hotmail.com (Y. Li).

shows strongly catalytic activities as mimetic enzyme in fields like electroreduction on the surface of electrodes [20,21], production and oxidation of small organic molecules [22–24], and fluorescence analysis [25,26]. In 1990, Hara and Tsukagoshi firstly developed the application of metallophthalocyanine compounds as catalysts in CL reaction between luminol and H_2O_2 for determination of biological constituents [27] and then metallophthalocyanine has been used for a wide range of applications in CL [28,29]. Recently, Wang et al. have established a CL method for measuring diethylstilbestrol using tetrasulfonated cobalt phthalocyanine to catalyst luminol– H_2O_2 system [30]. However, to our knowledge, the analytical application of CL method combined with metallophthalocyanine for the assay of estrogens has not been explored in great detail. In this work, tetrasulfonated manganese phthalocyanine (MnTSPc) was used as a mimic enzyme to catalyze the CL reaction of luminol and hydrogen peroxide, and estrogens could greatly enhance this CL emission in alkaline solution. Moreover, the degree of the enhancement depends on the concentration of estrogens. Thus, combined with a flow-injection system, a novel CL method was presented for the determination of estrogens. This method was applied for the determination of total estrogens in pharmaceutical formulations and tap water with satisfactory results. The possible CL reaction mechanism was also discussed.

2. Experimental

2.1. Reagents and solutions

Tetrasulfonated manganese phthalocyanine was synthesized and purified as previously described [31]. The product was identified by polyamide thin layer chromatography and by its UV–vis and IR spectra. The stock solution was prepared by dissolving 0.046 g of MnTSPc in 500 ml of water, giving a molar concentration of 1.0×10^{-3} mol/l.

Estrogens and luminol were purchased from Sigma (St. Louis, MO, USA) and used without further purification. Dissolving 0.443 g of luminol in 0.10 mol/l NaOH solution, a stock standard solution of 0.025 mol/l was obtained. A working standard solution of luminol was prepared by diluting the stock solution with 0.1 mol/l Na_2HPO_4 –NaOH buffer solution (pH 10.1). Stock solutions of estrone, estradiol and estriol were firstly dissolved using several drops of 0.01 mol/l NaOH solution and the working standard solution was diluted with water.

H_2O_2 (30%, w/w) was commercially available and the stock solution (2% H_2O_2) was standardized by titration with a standard solution of KMnO_4 .

All the reagents were of analytical grade and the water used was doubly distilled.

2.2. Apparatus

All CL measurements were performed with the IFFM-D mode flow-injection chemiluminescence (FI-CL) analysis system (Xi'an Remax Company, Xi'an, China). It has two peristaltic pumps and an injection system synchronized by a micropro-

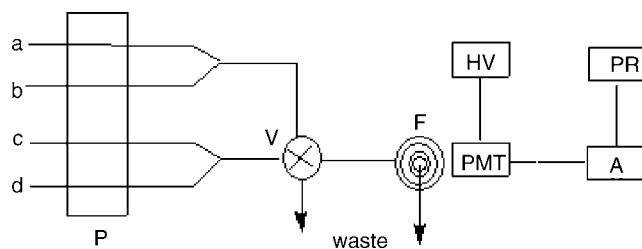


Fig. 1. Schematic diagram of the flow-injection system: (a) estrogen (or sample) solution; (b) carrier solution (water); (c) luminol and MnTSPc solution; (d) H_2O_2 solution; P, peristaltic pump; V, six-way injection valve; F, flow-cell; PMT, photomultiplier tube; A, amplifier; PR, printer; HV, negative voltage.

cessor. All the reactor coils were made of Teflon tubing. The flow-cell was a glass tube (i.d. 0.5 mm) connected with a selected high sensitivity, low noise photomultiplier tube. Light measurement data (I_{CL}) were transferred to a computer automatically. Data acquisition and treatment were used with REMAX software running under Windows 98.

CL spectrum was recorded with a Hitachi F-4500 spectrofluorimeter (Tokyo, Japan) combined with a flow-injection system.

2.3. Procedures

MnTSPc (0.1 ml , 1.0×10^{-4} mol/l) solution and luminol (0.1 ml , 4.0×10^{-4} mol/l) solution were placed in a 10 ml calibrated tube, then diluted with water to the mark and mixed thoroughly. A schematic diagram of the flow-injection chemiluminescence system is shown in Fig. 1. One peristaltic pump (two channels) was used to carry estrogen (or sample solution) and carrier solution (water), and another pump (two channels) was used to carry H_2O_2 solution and luminol/MnTSPc solution, respectively. The pumps were started with the 2.7 ml/min flow rate until a stable baseline was recorded. Injection was operated using a six-way injection valve fitted with a $150 \mu\text{l}$ sample loop. Then $150 \mu\text{l}$ estrogen (or sample) solution was injected into the stream of the luminol/MnTSPc and hydrogen peroxide solution and reached a flow cell to produce the CL intensity signal.

The concentration of estrogen was quantified by the maximum CL intensity.

3. Results and discussion

3.1. Enhancement effect of estrogens on luminol CL reaction

The CL reaction system of luminol and hydrogen peroxide has been extensively studied, and this CL reaction can be catalyzed by many metal ions and metal compounds. It was confirmed that the excited state of 3-aminophthalate was an emitter [32,33]. Kinetic profiles of luminol CL reaction catalyzed by MnTSPc in the presence and absence of estrone are shown in Fig. 2. It can be seen that in the absence of estrone, the oxidation of luminol by hydrogen peroxide catalyzed by MnTSPc is relatively a slow reaction process, and the CL intensity is relatively weak. However, when estrone was added into

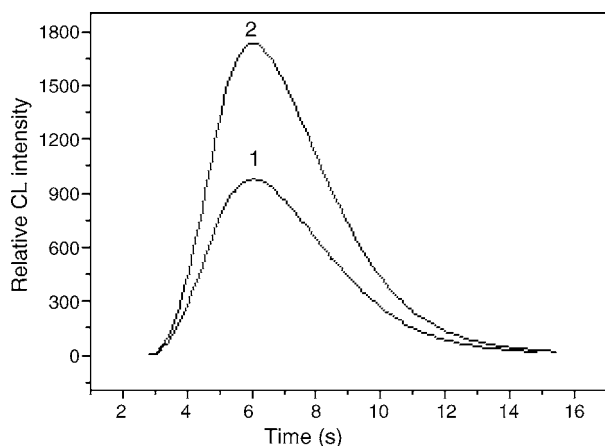


Fig. 2. Time course of the kinetic profiles of the luminol CL reaction catalyzed by MnTSPc in the absence (1) and presence (2) of 1.0×10^{-6} mol/l estrone. Conditions: luminol, 4.0×10^{-6} mol/l; H_2O_2 , 1.5×10^{-2} mol/l; MnTSPc, 1.0×10^{-6} mol/l; pH, 10.1; flow rate, 2.7 ml/min.

the luminol–hydrogen peroxide–MnTSPc CL system, the CL intensity increased markedly. The similar phenomena could be observed for estradiol and estriol.

In order to explore the possible mechanism of this CL enhancing phenomena, the following experiments were performed. Firstly, the CL spectrum was drawn using an F-4500 model spectrofluorimeter combined with a flow-injection system, whose light entrance slot was shut. The obtained CL spectrum is shown in Fig. 3. As can be seen, the maximum emission wavelength of the luminol–hydrogen peroxide or luminol–estrone–hydrogen peroxide CL system catalyzed by MnTSPc was located at 425 nm, only the relative CL intensity increased when estrone was added (Fig. 3, curve 2). Thus, we can deduce that the excited state of 3-aminophthalate is the possible emission species. Next, UV–visible absorption spectra of estrone, luminol and MnTSPc were obtained, as depicted in Fig. 4. It can be seen that estrone had a notable absorption peak at about 295 nm, MnTSPc had an

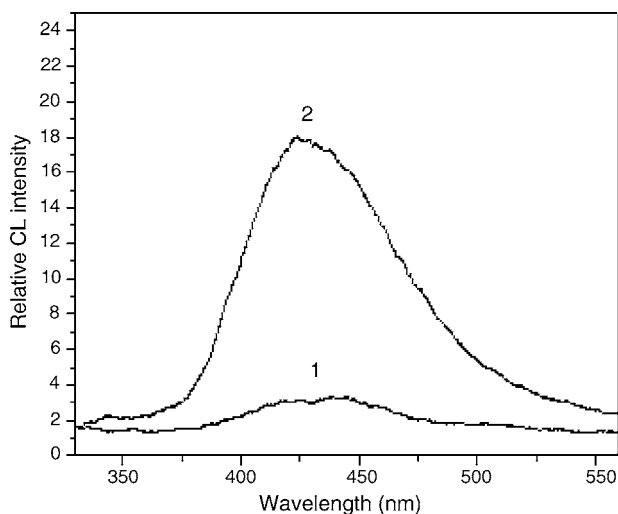


Fig. 3. CL spectrum of luminol and hydrogen peroxide catalyzed by MnTSPc in the absence (1) and presence (2) of 1.0×10^{-6} mol/l estrone. Conditions: luminol, 4.0×10^{-6} mol/l; H_2O_2 , 1.5×10^{-2} mol/l; MnTSPc, 1.0×10^{-6} mol/l; pH, 10.1; flow rate, 2.7 ml/min.

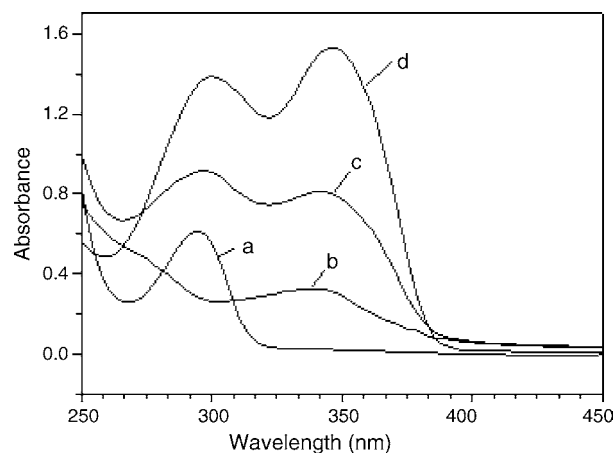


Fig. 4. UV–visible absorption spectrum of: (a) 1.0×10^{-6} mol/l estrone; (b) 1.0×10^{-6} mol/l MnTSPc; (c) 4.0×10^{-6} mol/l luminol; (d) a + b + c.

absorption peak at about 345 nm, and luminol had two distinct absorption peaks at 296 and 346 nm, respectively. The absorption spectrum of the mixture system was approximately the sum of these three individual spectra, which implied that no complex was formed between the species. Consequently, it appears that the reaction product generating CL is to be attributed to 3-aminophthalate ions, the oxidation product of luminol, and not to the estrone analyte as such. Hydrogen peroxide can oxidize estrogen and produce energy that induces the transition of oxidized estrogen from its ground state to excited electronic state. When the excited oxidized estrogen molecule returns to the ground state, it could transfer energy to the ground state of 3-aminophthalate ions, and form more excited 3-aminophthalate ions, the more excited 3-aminophthalate ions return to the ground state with enhanced CL phenomena. Therefore, the enhanced CL mechanism of the reaction may be attributed to the following reactions though more evidence is not available (Scheme 1).

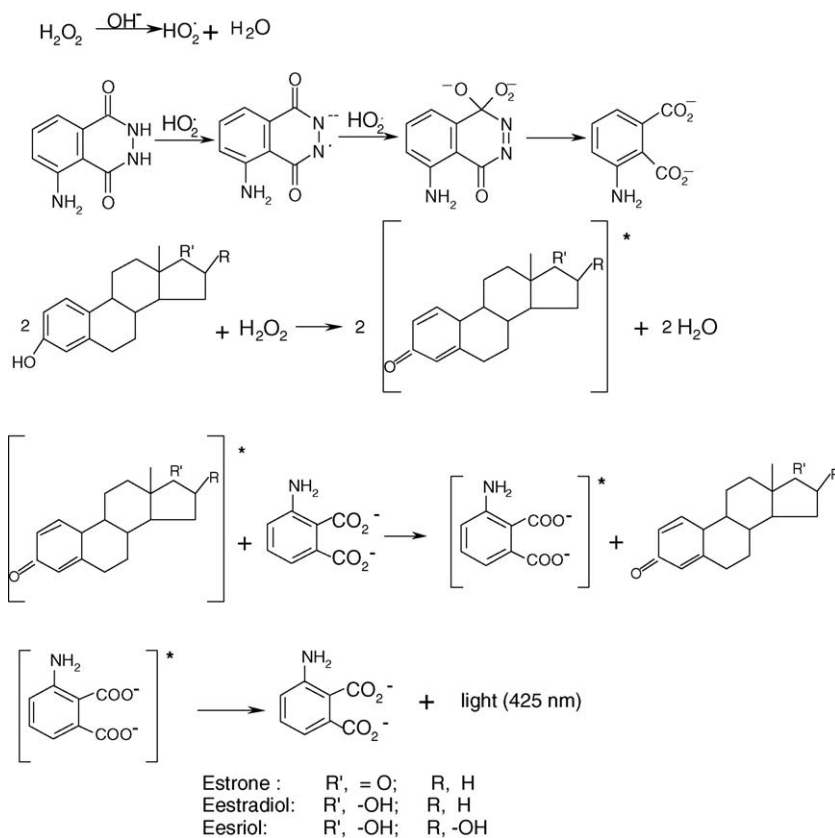
3.2. Optimum conditions of CL reaction

3.2.1. Effect of pH

The pH played an important role in MnTSPc catalyzed luminol– H_2O_2 CL reaction. Fig. 5 illustrates the results of pH optimization. The CL intensity increased slowly from 9.0 to 10.0 and the maximum CL intensity was obtained at pH 10.1. Above pH 10.1, the CL intensity reduced probably because of the instability of estrogens in strong basic solution. Thus, a pH of 10.1 (0.1 mol/l Na_2HPO_4 – NaOH buffer solution) was chosen as optimum for further experiments.

3.2.2. Effect of luminol concentration

The effect of the concentration of luminol was examined in the range of 1.0×10^{-6} to 7×10^{-6} mol/l. The results showed that the CL intensity increases with an increase of luminol concentration from 1.0×10^{-6} to 4.0×10^{-6} mol/l and decreases when the concentration is higher than 4.0×10^{-6} mol/l. Therefore, the concentration of luminol solution was adjusted to 4.0×10^{-6} mol/l.



Scheme 1.

3.2.3. Effect of H_2O_2 concentration

The effect of hydrogen peroxide concentrations on relative CL intensity was studied in the range of 3.3×10^{-3} to 3.3×10^{-2} mol/l. At a lower concentration of hydrogen peroxide, the signal increases gradually, and the maximum CL intensity occurs at 1.5×10^{-2} mol/l. Over this concentration, poor relative CL intensity was observed. Thus, 1.5×10^{-2} mol/l hydrogen peroxide was chosen as the optimum concentration in this study.

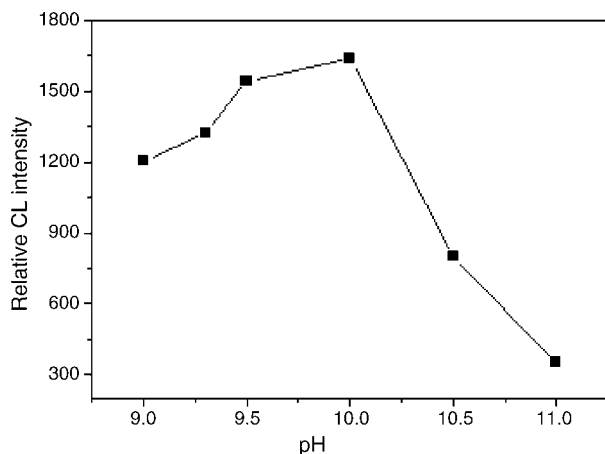


Fig. 5. Effect of pH on relative CL intensity. Conditions: estrone, 1.0×10^{-6} mol/l; luminol, 4.0×10^{-6} mol/l; H_2O_2 , 1.5×10^{-2} mol/l; MnTSPc, 1.0×10^{-6} mol/l; flow rate, 2.7 ml/min.

3.2.4. Effect of MnTSPc concentration

When the concentration of MnTSPc was in the range 5.0×10^{-7} to 2.0×10^{-6} mol/l, the CL intensity of the system was highest and fairly constant. When the concentration of MnTSPc exceeded 3.0×10^{-6} mol/l, the background intensity increased remarkably. Therefore, in our experiment, a 1.0×10^{-6} mol/l MnTSPc was recommended.

3.2.5. Effect of flow rate

In this work, we also studied the effect of flow rate. Although the CL intensity increases with increasing flow rate, the signal of background also increases significantly. A flow rate of 2.7 ml/min was recommended in order to reduce the consumption of reagents and to improve the detection limit.

3.3. Analytical parameters

Under the optimized experimental conditions and by use of the manifold depicted in Fig. 1, the calibration curves of the relative CL intensity versus concentration were constructed for estrone, estradiol and estriol. The linear ranges, linear regression equation, correlation coefficients and the detection limit are displayed in Table 1. The determination of sample could be finished in 40 s, including sampling and washing at a flow rate of 2.7 ml/min. Fig. 6 gives the linear effect of estrone over the range 1.0×10^{-7} to 1.0×10^{-6} mol/l. The reproducibility of the proposed CL method for the assay of estrogens was evaluated by performing 11 repeated injections of estrogens. The relative

Table 1
Linear relationship of CL intensity with the concentration of estrogens

Agents	Linear ranges (mol/l)	Linear regression equation (C , $\mu\text{mol/l}$)	Correlation coefficient	Detection limit ($S/N = 3$ mol/l)
Estrone	1.0×10^{-7} to 1.0×10^{-6}	$\Delta I_{\text{CL}} = 1072.6 + 933.1C$	0.9996	5.1×10^{-8}
Estradiol	9.0×10^{-8} to 1.0×10^{-6}	$\Delta I_{\text{CL}} = 1922.5 + 732.5C$	0.9968	7.2×10^{-9}
Estriol	3.0×10^{-7} to 2.0×10^{-6}	$\Delta I_{\text{CL}} = 1331.4 + 247.2C$	0.9902	6.5×10^{-8}

Table 2
Effect of foreign substances on the determination of 6.0×10^{-7} mol/l estrone under the optimum conditions

Interference added	Concentration	Relative error (%)
Na^+ , Cl^-	38.4 $\mu\text{g/ml}$	−1.3
K^+ , Cl^-	38.4 $\mu\text{g/ml}$	+2.5
K^+ , SO_4^{2-}	38.4 $\mu\text{g/ml}$	+1.1
Glucose	3.84 $\mu\text{g/ml}$	−2.3
Ethanol	3.84 $\mu\text{g/ml}$	−1.4
Uric acid	3.84 $\mu\text{g/ml}$	+3.7
Ca^{2+} , SO_4^{2-}	3.84 $\mu\text{g/ml}$	+1.4
Mg^{2+} , Cl^-	3.84 $\mu\text{g/ml}$	+3.5
Sucrose	192 ng/ml	−1.3
Dextrin	192 ng/ml	−2.0
Fructose	192 ng/ml	−1.9
Lactose	192 ng/ml	−1.6
Ascorbic acid	3.84 ng/ml	−7.3
Cu^{2+}	3.84 ng/ml	+4.2
Co^{2+}	3.84 ng/ml	−4.9
Mn^{2+}	3.84 ng/ml	−7.2
Fe^{3+}	3.84 ng/ml	−2.0
Zn^{2+}	3.84 ng/ml	−4.3

standard deviation was 2.8% for 5.0×10^{-7} mol/l estrone, 2.4% for 1.0×10^{-7} mol/l estradiol, and 3.1% for 7.0×10^{-7} mol/l estriol, respectively.

3.4. Interferences

The interference of foreign substances was investigated under the optimized conditions by analyzing a standard solution of

Table 3
Determination of estradiol in pharmaceutical tablets ($n = 5$)

Estradiol added (mol/l)	Labeled value ^a (mol/l)	Found value (mol/l)	Recovery (%)	R.S.D. (%)
0.00	5.25×10^{-5}	4.91×10^{-5}	—	2.5
2.63×10^{-5}	—	7.36×10^{-5}	93.5	1.9
5.25×10^{-5}	—	9.96×10^{-5}	96.2	2.1

^a Per tablet in 100 ml solution.

Table 4
Determination of estrogens in tap water samples^a ($n = 5$)

Sample	Initially present (mol/l)	Added (mol/l)	Found (mol/l)	Recovery (%)	R.S.D. (%)
Estrone	0.00	5.00×10^{-7}	4.98×10^{-7}	99.6	2.3
		9.00×10^{-7}	9.02×10^{-7}	100.3	1.4
Estradiol	0.00	5.00×10^{-7}	5.05×10^{-7}	101.2	1.9
		9.00×10^{-7}	8.87×10^{-7}	98.5	2.8
Estriol	0.00	5.00×10^{-7}	4.96×10^{-7}	99.2	2.4
		1.00×10^{-6}	9.79×10^{-7}	97.6	1.8

^a Wuhu, China.

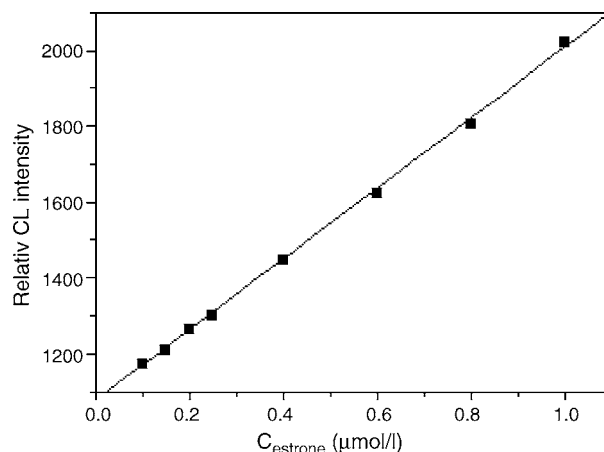


Fig. 6. The relation between relative CL intensity and concentration of estrone. Conditions: H_2O_2 , 1.5×10^{-2} mol/l; luminol, 4.0×10^{-6} mol/l; MnTSPc, 1.0×10^{-6} mol/l; pH, 10.1; flow rate, 2.7 ml/min.

6.0×10^{-7} mol/l estrone and the results are listed in Table 2. It can be seen from above that some metal ions and ascorbic acid could interfere with the determination of estrogens to a significant extent. Hence these species effect should be considered when a real sample is analyzed.

3.5. Samples analysis

A commercially available pharmaceutical tablet was chosen for testing the proposed method. Ten tablets of estradiol were

firstly weighed and pulverized, then diluted to the mark in a volumetric flask using 0.1 mol/l $\text{Na}_2\text{HPO}_4\text{--NaOH}$ buffer (pH 10.1). The determination procedures of samples were the same as that of estradiol standard solution described in above CL method. The results are listed in Table 3. As can be seen, an acceptable correlation was found between the claimed values and the results obtained by the proposed method.

The proposed method was also applied to the determination of estrogen residues in the tap water samples. The results obtained are listed in Table 4 which shows that this CL method could be used for the determination of trace estrogens in water, but the samples need to be treated before the determination of estrogens.

4. Conclusions

A flow-injection CL method has been established for the determination of estrone, estradiol and estriol based on the enhancement of luminol–hydrogen peroxide CL system catalyzed by MnTSPc. The method has the merits of high sensitivity, wide linear ranges and a short analytical time. The enhanced effect of estrogens on CL intensity is attributed to the synergistic effect of the product of estrogens with hydrogen peroxide on luminol's CL reaction. Thus, it provides a new principle and alternative method for the detection of estrogens and extends the analytical application of luminol CL system catalyzed by the mimic enzyme.

Acknowledgements

This work was financially supported by the key teachers of Anhui Province, National Natural Science Foundation of China, and Natural Science Foundation of Educational Commission of Anhui Province.

References

- [1] E.J. Routledge, D. Shbahan, C. Desbrow, M. Waldock, J.P. Sumpter, *Environ. Sci. Technol.* 32 (1998) 1559.
- [2] C. Desbrow, E.J. Routledge, G.C. Brighty, J.P. Sumpter, M. Waldock, *Environ. Sci. Technol.* 32 (1998) 1549.
- [3] M. Torigai, Y. Ishii, S. Yun, T. Hashiba, *J. Environ. Chem.* 10 (2001) 595.
- [4] C.H. Huang, D.L. Sedlak, *Environ. Toxicol. Chem.* 20 (2001) 133.
- [5] J.K. Fawell, D. Sheahan, H.A. James, M. Hurst, S. Scott, *Water Res.* 35 (2001) 1240.
- [6] J.F. Zhao, Y.C. Wang, M.X. Zhang, Y.X. Li, W.B. Chang, *Chin. J. Anal. Chem.* 31 (2003) 129.
- [7] Z. Li, S. Wang, N. Alice Lee, R.D. Allan, I.R. Kennedy, *Anal. Chim. Acta* 503 (2004) 171.
- [8] N.M. Czekala, J.E. Meier, B.L. Lasley, *Zool. Biol.* 5 (1986) 1.
- [9] J.V. Lee, C.S. Whaling, B. Lusley, P. Marcer, *Zool. Biol.* 74 (1995) 97.
- [10] G.P. Jin, X.Q. Lin, *Electrochim. Acta* 50 (2005) 3556.
- [11] S. Armstrong, Z.F. Miao, F.I. Rowell, Z. Ali, *Anal. Chim. Acta* 444 (2001) 79.
- [12] K. Robrads, P.J. Worsfold, *Anal. Chim. Acta* 266 (1992) 147.
- [13] R.H. Van den Berg, E.H.J.M. Jansen, G. Zomer, C. Enkeluier-Willemsen, R. Bothmiedema, R.W. Stephany, *J. Chromatogr.* 360 (1986) 449.
- [14] L.X. Zhao, J.M. Lin, *J. Biotechnol.* 118 (2005) 177.
- [15] T. Tanaka, M. Yanagi, A. Kubodera, *Steroids* 63 (1998) 516.
- [16] S. Liao, X. Wu, Z. Xie, *Anal. Chim. Acta* 537 (2005) 189.
- [17] W.G. Wood, S.B. Pad (Eds.), *Immunoassay Technology*, vol. 1, DeGruyter, Berlin, New York, 1985, p. 105.
- [18] G.H. Thorpe, L.J. Kricka, *Methods Enzymol.* 133 (1986) 331.
- [19] J.P. Gosling, *Clin. Chim.* 36 (1990) 1408.
- [20] N. Chebotareva, T.J. Nyokong, *Appl. Electrochem.* 27 (1997) 975.
- [21] J. Wang, *Anal. Lett.* 29 (1996) 1575.
- [22] R. Raja, P. Ratnasamy, *Appl. Catal. A* 158 (1997) 27.
- [23] R.F. Parton, P.E. Neys, P.A. Jacobs, R.C. Sosa, *J. Catal.* 164 (1996) 341.
- [24] Y.X. Qi, G.J. Wang, W.D. Zhang, X.K. Ye, *Chem. J. Chin. Univ.* 16 (1995) 791.
- [25] Q.Y. Chen, D.H. Li, Q.Z. Zhu, H. Zheng, J.G. Xu, *Anal. Chim. Acta* 381 (1999) 175.
- [26] C.Q. Zhu, D.H. Li, H. Zheng, Q.Z. Zhu, Q.Y. Chen, J.G. Xu, *Anal. Sci.* 16 (2000) 253.
- [27] T. Hara, K. Tsukagoshi, *Anal. Sci.* 6 (1990) 797.
- [28] Y.X. Li, C.Q. Zhu, L. Wang, M.G. Li, F. Gao, L.Y. Wang, Y.W. Zhu, *Anal. Lett.* 34 (2001) 1841.
- [29] Y.X. Li, D.H. Zhao, C.Q. Zhu, L. Wang, J.G. Xu, *Anal. Bioanal. Chem.* 374 (2002) 395.
- [30] J. Wang, H.Z. Ye, Z. Jiang, N.S. Chen, J.L. Huang, *Anal. Chim. Acta* 508 (2004) 171.
- [31] J. Weber, J.H. Bush, *Inorg. Chem.* 4 (1965) 469.
- [32] E.H. White, M.M. Bursey, *J. Am. Chem. Soc.* 86 (1964) 941.
- [33] Y. Li, C. Zhu, L. Wang, *Microchim. Acta* 150 (2005) 95.

Talanta

The International Journal of Pure and Applied Analytical Chemistry

Editors-in-Chief

Professor G.D. Christian, University of Washington, Department of Chemistry, 36 Bagely Hall, P.O. Box 351700, Seattle, WA 98195-1700, U.S.A.

Professor J.-M. Kauffmann, Université Libre de Bruxelles, Institut de Pharmacie, Campus de la Plaine, C.P. 205/6, Boulevard du Triomphe, B-1050 Bruxelles, Belgium

Associate Editors

Professor J.-H. Wang, Research Center for Analytical Sciences, Northeastern University, Box 332, Shenyang 110004, China

Professor J.L. Burguera, Los Andes University, IVAQUIM, Faculty of Sciences, P.O. Box 542, 5101-A Mérida, Venezuela.

Assistant Editors

Dr R.E. Synovec, Department of Chemistry, University of Washington, Box 351700, Seattle, WA 98195-1700, U.S.A.

Professor J.-C. Vire, Université Libre de Bruxelles, Institut de Pharmacie, Campus de la Plaine, C.P. 205/6, Boulevard du Triomphe, B-1050 Bruxelles, Belgium

Talanta

R. Apak (Istanbul, Turkey)
L.G. Bachas (Lexington, KY, U.S.A.)
E. Bakker (Auburn, AL, U.S.A.)
D. Barceló (Barcelona, Spain)
K. Booksh (Tempe, AZ, U.S.A.)
C.M.A. Brett (Coimbra, Portugal)
Yi. Chen (Beijing, China)
R. Compton (Oxford, U.K.)
S. Cosnier (Grenoble, France)
P.K. Dasgupta (Lubbock, TX, U.S.A.)
D. Diamond (Dublin, Ireland)
G.A. Eiceman (Las Cruces, NM, U.S.A.)
M.-R. Fuh (Taipei, Taiwan)
K. Grupdán (Chaing Mai, Thailand)

V.K. Gupta (Roorkee, India)
A. Gustavo González (Sevilla, Spain)
I. Gutz (Sao Paulo, Brazil)
E.H. Hansen (Lyngby, Denmark)
P. de B. Harrington (OH, U.S.A.)
W.L. Hinze (Winston-Salem, NC, U.S.A.)
A. Ivaska (Turku, Finland)
B. Karlberg (Stockholm, Sweden)
U. Karst (Enschede, The Netherlands)
R. Lobinski (Pau, France)
C.A. Lucy (Edmonton, AB, Canada)
M.D. Luque de Castro (Cordoba, Spain)
I.D. McKelvie (Victoria, Australia)
E. Morosonova (Moscow, Russia)

J.-M. Pingarrón (Madrid, Spain)
E. Pretsch (Zürich, Switzerland)
W. Schuhmann (Bochum, Germany)
M. Shamsipur (Kermanshah, Iran)
K. Suzuki (Yokohama, Japan)
D.L. Tsalev (Sofia, Bulgaria)
Y. Umezawa (Tokyo, Japan)
K. Vytras (Pardubice, Czech Republic)
B. Walczak (Katowice, Poland)
R. von Wandruszka (Moscow, U.S.A.)
J. Wang (Tempe, AZ, U.S.A.)
J.D. Winefordner (Gainesville, U.S.A.)
Xiu-Ping Yan (Tianjin, China)
E.A.G. Zagatto (Piracicaba, SP, Brazil)

Copyright © 2006 Elsevier B.V. All rights reserved

Publication information: *Talanta* (ISSN 0039-9140). For 2006, volumes 68–70 are scheduled for publication. Subscription prices are available upon request from the Publisher or from the Regional Sales Office nearest you or from this journal's website (<http://www.elsevier.com/locate/talanta>). Further information is available on this journal and other Elsevier products through Elsevier's website: (<http://www.elsevier.com>). Subscriptions are accepted on a prepaid basis only and are entered on a calendar year basis. Issues are sent by standard mail (surface within Europe, air delivery outside Europe). Priority rates are available upon request. Claims for missing issues should be made within six months of the date of dispatch.

Orders, claims, and journal enquiries: please contact the Customer Service Department at the Regional Sales Office nearest you:

Orlando: Elsevier, Customer Service Department, 6277 Sea Harbor Drive, Orlando, FL 32887-4800, USA; phone: (+1) (877) 8397126 [toll free number for US customers], or (+1) (407) 3454020 [customers outside US]; fax: (+1) (407) 3631354; e-mail: usjcs@elsevier.com

Amsterdam: Elsevier, Customer Service Department, PO Box 211, 1000 AE Amsterdam, The Netherlands; phone: (+31) (20) 4853757; fax: (+31) (20) 4853432; e-mail: nlinfo-f@elsevier.com

Tokyo: Elsevier, Customer Service Department, 4F Higashi-Azabu, 1-Chome Bldg, 1-9-15 Higashi-Azabu, Minato-ku, Tokyo 106-0044, Japan; phone: (+81) (3) 5561 5037; fax: (+81) (3) 5561 5047; e-mail: jp.info@elsevier.com

Singapore: Elsevier, Customer Service Department, 3 Killiney Road, #08-01 Winsland House I, Singapore 239519; phone: (+65) 63490222; fax: (+65) 67331510; e-mail: asiainfo@elsevier.com

USA mailing notice: *Talanta* (ISSN 0039-9140) is published monthly by Elsevier B.V. (P.O. Box 211, 1000 AE Amsterdam, The Netherlands). Annual subscription price in the USA US\$ 3,628 (valid in North, Central and South America), including air speed delivery. Application to mail at periodical postage rate is pending at Jamaica, NY 11431.

USA POSTMASTER: Send address changes to *Talanta*, Publications Expediting Inc., 200 Meacham Avenue, Elmont, NY 11003.

AIRFREIGHT AND MAILING in the USA by Publications Expediting Inc., 200 Meacham Avenue, Elmont, NY 11003.

Talanta

The International Journal of Pure and Applied Analytical Chemistry

Editors-in-Chief

Professor G.D. Christian, University of Washington, Department of Chemistry, 36 Bagely Hall, P.O. Box 351700, Seattle, WA 98195-1700, U.S.A.

Professor J.-M. Kauffmann, Université Libre de Bruxelles, Institut de Pharmacie, Campus de la Plaine, C.P. 205/6, Boulevard du Triomphe, B-1050 Bruxelles, Belgium

Associate Editors

Professor J.-H. Wang, Research Center for Analytical Sciences, Northeastern University, Box 332, Shenyang 110004, China

Professor J.L. Burguera, Los Andes University, IVAQUIM, Faculty of Sciences, P.O. Box 542, 5101-A Mérida, Venezuela

Assistant Editors

Dr R.E. Synovec, Department of Chemistry, University of Washington, Box 351700, Seattle, WA 98195-1700, U.S.A.

Professor J.-C. Vire, Université Libre de Bruxelles, Institut de Pharmacie, Campus de la Plaine, C.P. 205/6, Boulevard du Triomphe, B-1050 Bruxelles, Belgium

Advisory Board

Chairman: Professor J.D. Winefordner, Gainesville, FL, U.S.A.

Talanta

R. Apak (Istanbul, Turkey)

L.G. Bachas (Lexington, KY, U.S.A.)

E. Bakker (Auburn, AL, U.S.A.)

D. Barcelo (Barcelona, Spain)

K. Booksh (Tempe, AZ, U.S.A.)

C.M.A. Brett (Coimbra, Portugal)

Yi. Chen (Beijing, China)

R. Compton (Oxford U.K.)

S. Cosnier (Grenoble, France)

P.K. Dasgupta (Lubbock, TX, U.S.A.)

D. Diamond (Dublin, Ireland)

G.A. Eiceman (Las Cruces, NM, U.S.A.)

M.-R. Fuh (Taipei, Taiwan)

K. Grupdan (Chaing Mai, Thailand)

V. K. Gupta (Roorkee, India)

A. G. Gustavo-Gonzales (Sevilla, Spain)

I. Gutz (Sao Paulo, Brazil)

E.H. Hansen (Lyngby, Denmark)

P. de B. Harrington (OH, U.S.A.)

W.L. Hinze (Winston-Salem, NC, U.S.A.)

A. Ivaska (Turku, Finland)

B. Karlberg (Stockholm, Sweden)

U. Karst (Enschede, The Netherlands)

R. Lobinski (Pau, France)

C.A. Lucy (Edmonton, AB, Canada)

M.D. Luque de Castro (Cordoba, Spain)

I.D. McKelvie (Victoria, Australia)

E. Morosonova (Moscow, Russia)

J.-M. Pingarron (Madrid, Spain)

E. Pretsch (Zürich, Switzerland)

W. Schuhmann (Bochum, Germany)

M. Shamsipur (Kermanshah, Iran)

K. Suzuki (Yokohama, Japan)

D.L. Tsalev (Sofia, Bulgaria)

Y. Umezawa (Tokyo, Japan)

K. Vytras (Pardubice, Czech Republic)

B. Walczak (Katowice, Poland)

R. von Wandruszka (Moscow, U.S.A.)

J. Wang (Tempe, AZ, U.S.A.)

J.D. Winefordner (Gainesville, U.S.A.)

Xiu-Ping Yan (Tianjin, China)

E.A.G. Zagatto (Piracicaba, SP, Brazil)

Volume 70 (2006)



ELSEVIER Amsterdam – Boston – Jena – London – New York – Oxford – Paris – Philadelphia – San Diego – St. Louis